# Modelling Lymphangioleiomyomatosis (LAM) Using Two-dimensional and Three-dimensional *in vitro* co-culture systems

***Arundhati Vinaychandra Dongre BPharm., MSc.***

Thesis submitted to the University of Nottingham for the Degree of

Doctor of Philosophy

June 2017



***This thesis is dedicated to my grandparents, Aji and Ajoba this one's for you.***

## Abstract

### Background:

Lymphangioleiomyomatosis (LAM) is a rare progressive neoplastic cystic lung disease that primarily affects women of child bearing age leading to lung destruction, respiratory failure and death. Thought to be a consequence of dysregulated protease expression, cells of unknown origin accumulate in the lung, often forming clusters or nodules of cells with both melanocytic and smooth muscle properties. Some of these cells, known as LAM cells, have bi-allelic mutations in *TSC2* resulting in constitutive mTOR activation. However LAM nodules are heterogeneous structures and genotyping analyses suggest that cells without LOH for *TSC2* including wild-type fibroblasts are also common within LAM nodules.

### Hypotheses and aims:

We hypothesise that LAM cells recruit wild-type fibroblasts and modify their properties to generate a permissive microenvironment, akin to a tumour stroma including the production and activation of matrix-degrading proteases which contribute to the destruction of the lung parenchyma. This study has therefore deigned *in vitro* co-culture models with an aim to study the expression patterns and activation of proteases in a LAM lung leading to matrix destruction. Another aim was also to characterise transcriptional differences normal human lung fibroblasts (NHLFs) and LAM-associated fibroblasts (LAFs) and to investigate changes in their gene expression when cultured together with a model LAM cell line, 621-101 angiomyolipoma cells which were derived from a LAM patient and have bi-allelic loss of TSC2.

### Methods:

In vitro 2-dimensional (2D) and 3-dimensionalD (3D) co-culture models were designed and validated using fibroblasts characterised and isolated from 4 LAM lung donors, now termed LAFs, and 621-101 cells. The 3D

extracellular matrix (ECM) incorporated the two cell types in a 10:1 ratio embedded in a basement membrane extract (BME) mimicking the lung matrix. An organotypic spheroid model was also developed incorporating both cell types thereby mimicking a LAM nodule. 6 LAM lung and 3 normal lung tissue donors were screened for candidate proteases in LAM pathology using qRT-PCR and identified upregulated proteases which may contribute to a role in LAM pathology. These findings were verified in the 2D and 3D in vitro models as well as ex vivo tissue using a variety of immunostaining techniques, activity assays and ELISA. Lastly, commercially bought NHLF (n=3) and LAF (n=3) were cultured in the presence or absence of 621-101 cells in the 2D Boyden chamber co-culture model. LAF and NHLF RNA was analysed using Affymetrix Human Genome U133 Plus 2.0 Arrays and Genomics Suite and Pathway (Partek). Findings were validated by multiplex assay and immunohistochemistry in 2D and 3D *in vitro* models and tissue respectively. Inflammatory cell migration and function was examined in co-culture model and LAM tissue.

**Results:**

The 3D BME model showed that $TSC2^{-/-}$ 621-101 cells and fibroblasts spontaneously form aggregates and clump together akin to a LAM nodule. The two cell types exhibited strong heterotypic cell-cell adhesive forces and resulted in strictly spherical spheroids. The 3D models designed all showed expression of markers of LAM nodules thereby representing LAM nodules in a dish.

Of 30 proteases screened, *cathepsin K* gene expression was increased almost 15-fold in LAM lung compared to normal tissue and was also found to be elevated in 3D BME model. Cathepsin K in LAM tissue was expressed in the LAM nodules associated with cysts and was expressed exclusively by fibroblasts in the 3D spheroid model. As cathepsin K requires low pH for activity it was determined if LAFs and $TSC2^{-/-}$ cells can acidify the extracellular space. $TSC2^{-/-}$ cells but not LAFs decreased extracellular pH, over 24 hours and pH values <7 were associated with increased cathepsin

K activity in co-cultures. TSC2$^{-/-}$ cells expressed membrane transporters associated with extra-cellular acidification and inhibitors of the sodium bicarbonate co-transporters, carbonic anhydrases and mTOR reduced the pH gradient and decreased CTSK activity in co-cultures.

Transcriptomic analysis using the 2D co-culture model showed 148 genes were significantly altered in both NHLF and LAF by 621-101 cells. Soluble factors from 621-101 cells induce pro-inflammatory transcriptional changes in both NHLFs and LAFs and pathway analysis showed enhanced chemokine signalling which highlighted stimulation of mainly the C-X-C motif chemokines and chemokine receptor signalling. The analysis identified 6 C-X-C motif chemokines all possessing a cognate receptor. The gene and protein expression of these chemokines was validated in the in vitro models and in ex vivo LAM lung tissue.

**Conclusions:**

The in vitro models are versatile and mimic the LAM lung nodule and environment. A potent matrix degrading protease possibly playing a role in LAM has been identified and using the in vitro models a possible mechanism of activation of CTSK resulting from a synergistic relationship between TSC2$^{-/-}$ cells and LAFs has been demonstrated. Also, soluble factors from the TSC2$^{-/-}$ LAM cell line elicit changes in gene expression in co-cultured fibroblasts. Chemokine signalling is associated with cell migration; elevated chemokine expression may be associated with the recruitment of inflammatory cells to the LAM nodule. The identification of these mechanisms and pathways opens up new avenues for therapeutic interventions in LAM.

## Publications

**Dongre A**, Clements D, Fisher AJ, Johnson SR. Cathepsin K in Lymphangioleiomyomatosis: LAM Cell-Fibroblast Interactions Enhance Protease Activity by Extracellular Acidification. *Am J Pathol. In Press.*

Clements D, **Dongre A,** Krymskaya VP, Johnson SR. Wild type mesenchymal cells contribute to the lung pathology of lymphangioleiomyomatosis. *PloS One*. 2015 May; 10(5):e0126025. doi: 10.1371/journal.pone.0126025.

Rogers NK, Clements D, **Dongre A**, Harrison TW, Shaw D, Johnson SR. Extra-cellular matrix proteins induce matrix metalloproteinase-1 (MMP-1) activity and increase airway smooth muscle contraction in asthma. *PLoS One.* 2014 9(2):e90565. doi: 10.1371/journal.pone.0090565.

### Abstracts

**Dongre A,** Clements D & Johnson SR. TSC2-null Cell-Fibroblast Interactions Enhance Protease Activity by Extracellular Acidification in Lymphangioleiomyomatosis (LAM). *Poster discussion at the American Thoracic Society Annual Conference, Washington DC, May 19-24 2017*

**Dongre A,** Clements D & Johnson SR. Expression and Activity of Cathepsin K in Lymphangioleiomyomatosis (LAM). *Poster presented at the American Thoracic Society Annual Conference, San Francisco, California, May 13-18 2016*

**Dongre A,** Clements D et al. Cell-cell communication in lymphangioleiomyomatosis: microarray analysis shows induction of chemokines and fibroblast growth factors in LAM associated fibroblasts. *Poster discussion at the American Thoracic Society Annual Conference, San Francisco, California, May 13-18 2016*

Dongre A, Clements D & Johnson SR. Modelling Lymphangioleiomyomatosis (LAM) in 2D and 3D Co-culture Systems. *Poster presented at the American Thoracic Society Annual Conference, Denver, Colorado, May 15-20 2015*

**Oral communications**

**Dongre A,** Clements D et al. Cell-Cell Communication in Lymphangioleiomyomatosis. *Oral presentation at the Joint Respiratory Research Day, 3rd May 2017*

**Dongre A,** Clements D & Johnson SR. Expression and Activity of Cathepsin K in Lymphangioleiomyomatosis. *Oral presentation at the Joint Respiratory Research Day, 4th May 2016*

**Acknowledgments**

*This thesis would not have been possible without the help and support of several people. Firstly, my greatest thank you goes to my supervisors Professor Simon Johnson and Dr Debbie Clements. I am grateful to Professor Johnson for giving me the immense opportunity to embark on this PhD and for allowing me freedom to explore my own ideas. I am thankful to Dr Clements for her constant support, encouragement, positivity and for helping me develop the skills necessary to a scientist.*

*A special thank you to all the LAM patients who have donated to this study and to my funding body, LAM Action UK. This study would never have been possible without them. I would like to thank Professor Sean May, Dr Marcos Castellanos-Uribe and the team at NASC for performing the microarray analysis for this study and for lending their patience and expertise in teaching me the analytical techniques.*

*I must thank the team at Respiratory Medicine, QMC for providing such a friendly working environment. I would like to thank Drs Ivonne Siebeke and Brendan Mallia-Milanes for their friendship, encouragement and critical advice. A special thank you goes to Sangita Bhaker, Chris Philp and Sarath Channavajjhala for being great friends and making work such an enjoyable experience.*

*An immense thank you goes to my mum, Tanuja, to whom I owe everything, you always believed in me and never once let me compromise despite all the hardships. Thank you to my brother, Abhishek for supporting me no matter what and always putting a smile on my face. Thank you to my grandparents to whom I dedicate this thesis, for your unconditional love. Thank you Nitin mama and Nanda mami, for being my second parents and supporting my education, to you I owe a great deal. Thank you to Gauri mavshi and Sandeep kaka for giving me my first career break. Thank you to my mother-in-law, to have supported me and fed me endlessly with nutritious home food throughout my PhD. Lastly, but definitely not least, a big thank you to my husband, Yamitraj Patel for*

*unquestionably supporting me through thick and thin and for reminding me, no matter what there is always a silver lining. I cannot imagine my life without you all. You truly make me complete.*

# Contents

ABSTRACT ..... III

PUBLICATIONS ..... VI

ACKNOWLEDGMENTS ..... VIII

LIST OF FIGURES ..... XX

LIST OF TABLES ..... XXV

ABBREVIATIONS ..... XXVIII

1 CHAPTER 1: LYMPHANGIOLEIOMYOMATOSIS (LAM): AN INTRODUCTION ..... 1

**1.1 Lymphangioleiomyomatosis (LAM) ..... 1**

1.1.1 Definition ..... 1

1.1.2 Background, Epidemiology and Importance ..... 1

**1.2 Clinical presentation, symptoms and diagnosis ..... 3**

**1.3 TSC-LAM and Sporadic LAM ..... 7**

1.3.1 TSC-LAM ..... 7

1.3.2 Sporadic LAM ..... 10

**1.4 Genetics of LAM and the mTOR pathway ..... 12**

1.4.1 mTORC1 ..... 17

1.4.1.1 Upstream regulators of mTORC1 ..... 17

1.4.1.2 Downstream processes of mTORC1 ..... 18

1.4.2 mTORC2 ..... 20

**1.5 Current theories on pathogenesis of LAM ..... 22**

**1.6 Current treatments for LAM ..... 26**

1.6.1 Hormone Therapy ..... 26

1.6.2 mTOR inhibitors ..... 27

1.6.3 Matrix metalloproteinase inhibitors ..... 30

**1.7 LAM lesions and the LAM lung phenotype ..... 31**

**1.8 Fibroblasts ..... 34**

**1.9 Current models for LAM ..... 39**

1.9.1 Animal models ..... 39

1.9.2 Tumour homograft and xenograft models ..... 41

1.9.3 Cellular LAM models ..... 42

**1.10 In vitro disease models ..... 45**

1.10.1 Co-culture models ..... 46

1.10.2 3-dimensional scaffold based models ..... 50

1.10.3 Spheroid-based models ..... 55

**1.11 The Extracellular Matrix of the lung ..... 62**

**1.12 ECM turnover – A focus on Cathepsins ..... 63**

1.12.1 Cysteine cathepsins ..... 66

**1.13 Cathepsin K ..... 71**

1.13.1 Gene organisation and regulation ..... 71

1.13.2 Activation and cellular distribution ..... 73

1.13.3 Physiological role of cathepsin K ..... 74

1.13.4 Cathepsin K and lung diseases ..... 77
1.13.5 Inhibitors of cathepsin K ..... 78

**1.14 Protease-mediated cystic lung destruction in LAM ..... 81**

**1.15 Hypotheses ..... 85**

**1.16 Aims ..... 85**

2 CHAPTER 2: MATERIALS AND METHODS ..... 86

**2.1 Materials ..... 86**

2.1.1 Plastic ware ..... 86
2.1.2 Cell Culture Reagents ..... 86
2.1.3 Antibodies ..... 86
2.1.4 Inhibitors and drug compounds ..... 89

**2.2 Mammalian cell and tissue culture techniques ..... 91**

2.2.1 Primary Cells and Cell Lines ..... 91
2.2.2 Patient cohort and tissue samples ..... 92
2.2.3 Primary cell isolation and culture ..... 92
2.2.4 Thawing and sub-culturing cells ..... 95
2.2.5 Cryopreservation of cells ..... 96
2.2.6 Standard method for cell culture experiments ..... 97
2.2.7 Standard method for explant tissue culture ..... 97
2.2.8 Labelling cells with CellTracker™ Dyes ..... 98
2.2.9 MTT Reduction assay ..... 98
2.2.10 AlamarBlue® assay ..... 99

**2.3 Quantification of gene expression ..... 100**

2.3.1 Tissue homogenisation ..... 100
2.3.2 Total ribonucleic acid (RNA) extraction ..... 101
2.3.3 Complementary DNA (cDNA) synthesis ..... 102
2.3.4 Quantitative real-time polymerase chain reaction (qRT-PCR) ..... 103

**2.4 Histology and Cytology ..... 106**
2.4.1 Haematoxylin and Eosin staining ..... 106
2.4.2 Chromogenic Immunohistochemistry (IHC) ..... 106
2.4.3 Fluorescent Immunohistochemistry (IHC-Fr) ..... 108
2.4.4 Immunofluorescence ..... 109

**2.5 Protein determination ..... 110**
2.5.1 Bio-Plex® Multiplex Immunoassay ..... 110
2.5.2 Proteome profiler™ Human Protease array ..... 112

**2.6 Microscopy and Image analyses ..... 113**
2.6.1 Microscopy and imaging ..... 113
2.6.2 Densitometry analysis ..... 113

**2.7 Statistical Analyses ..... 114**
2.7.1 Analysis of variance ..... 114
2.7.2 Linear regression and correlation analysis ..... 115

3 CHAPTER 3: *IN VITRO* MODELLING OF LYMPHANGIOLEIOMYOMATOSIS ..... 116

**3.1 Introduction ..... 116**
3.1.1 Background ..... 116
3.1.2 Aims & Objectives ..... 118

**3.2 Methods ..... 119**

3.2.1 Embedding Cells in Extracellular Matrix (ECM Gel) ..... 119
3.2.2 Embedding Cells in Culturex® Basement Membrane Extract (BME) Gel ..... 120
3.2.3 Spheroid (LAM Spheroid) Culture ..... 120
3.2.4 Organoid (LAMosphere) Culture ..... 121
3.2.5 Measuring Spheroid and Organoid Size ..... 122
3.2.6 Embedding Spheroids and Organoids ..... 122

**3.3 Results ..... 125**

3.3.1 Characterisation of Isolated Fibroblast-Like Cells via Immunofluorescent Detection of Fibroblast Markers ..... 126
3.3.2 Extracellular Matrix (ECM) Gel as a Three Dimensional Scaffold ..... 131
3.3.2.1 Determining Appropriate Cell Number and Ratio ..... 131
3.3.2.2 Selection of the Appropriate Type of ECM Gel for 3D LAM Model Using Appropriate Cell Number and Cell Ratio ..... 134
3.3.3 Culturex® Basement Membrane Extract (BME) Gel as a Three Dimensional Scaffold ..... 136
3.3.4 Assessment of Cellular Metabolic Activity via MTT Reduction Assay ..... 139
3.3.5 Measuring Cell Viability Using Alamarblue® Viability Assay ..... 140
3.3.6 Gene Expression of Markers of A LAM Nodule and Fibroblast Specific Markers in the 3D BME Model ..... 141
3.3.7 Protein Expression of Markers of a LAM Nodule and Fibroblast Specific Markers in the 3D BME Model ..... 143
3.3.8 Generation of Multicellular Co-Culture Spheroids - LAM Spheroids ..... 145
3.3.8.1 Selection of Appropriate Technique for Spheroid Formation ..... 145
3.3.8.2 Determining Optimum Cell Number for LAM Spheroids ..... 149
3.3.9 Expression of Fibroblast and Melanocytic Markers in LAM Spheroids ..... 155
3.3.10 Generation of LAM Lung Organoids – Tissue Derived LAMospheres ..... 157
3.3.11 Expression of LAM-Specific Markers in LAMospheres ..... 160

**3.4 Discussion ..... 162**

**3.5 Conclusion ..... 170**

4 CHAPTER 4: PROTEASE PROFILE FOR LAM: THE EXPRESSION AND ACTIVITY OF CATHEPSIN K ..... 171

**4.1 Introduction ..... 171**

4.1.1 Background ..... 171

4.1.2 Aims & Objectives ..... 174

**4.2 Methods ..... 175**

4.2.1 Proteome Profiler – Protease Array ..... 175

4.2.2 Double Chromogenic and Fluorescent Immunohistochemistry ..... 176

4.2.3 Measurement of pH ..... 177

4.2.4 Intracellular Cathepsin K Activity – Magic Red® ..... 177

4.2.5 Extracellular Cathepsin K activity assay ..... 178

4.2.6 Cathepsin K ELISA ..... 179

**4.3 Results ..... 181**

4.3.1 Literature Search and q RT-PCR Screen for Proteases Overexpressed in LAM ..... 182

4.3.2 Expression of Proteases in 2-Dimensional and 3-Dimensional Cell Cultures ..... 189

4.3.3 Protein expression of proteases in non-contact Boyden chamber LAF and 621-101 cell cultures191

4.3.4 Cathepsin K Expression in *Ex Vivo* LAM Lung Tissue ..... 196

4.3.5 Cathepsin K Expression is Associated with LAM Nodules ..... 199

4.3.6 Effect of β-Estradiol (E2) and Rapamycin on CTSK Expression ..... 201

4.3.7 Expression of Cathepsin K (CTSK) in Cultured Cells ..... 203

4.3.8 Cathepsin K Expression in LAM Spheroids and LAMospheres ..... 206

4.3.9 Magic Red® – Intracellular Cathepsin K Activity ..... 208
4.3.10 Association of Cathepsin K with Fibroblast-like Spindle-shaped cells in LAM nodules 210
4.3.11 Extracellular Cathepsin K Activity ..... 213
4.3.12 Cell viability at low pH ..... 215
4.3.13 Acidification of Tissue Culture Medium by 621-101 Cells ..... 216
4.3.14 Expression of Membrane Proton Pumps and Transporters in 621-101 Cells ..... 218
4.3.15 Expression of Membrane Pumps and Transporters in LAM Lung Tissue ..... 220
4.3.16 Inhibition of Membrane Pumps and Transporters in 621-101 Cells ..... 223
4.3.17 Effect of Inhibition of Membrane Pumps and Transporters on Cathepsin K Activity ..... 226
4.3.18 Effect of Inhibition of Membrane Pumps and Transporters on Cell Viability ..... 231
4.3.19 Cathepsin K Activity Relates To Total Cathepsin K Expression in Cultured Cells ..... 233

**4.4 Discussion ..... 236**

**4.5 Conclusion ..... 247**

5 CHAPTER 5: COMPARATIVE TRANSCRIPTIONAL PROFILING OF LAFS AND NHLFS 248

**5.1 Introduction ..... 248**

5.1.1 Background ..... 248
5.1.2 Aims and Objectives ..... 251

**5.2 Methods ..... 252**

5.2.1 Boyden Chamber Transwell® Culture ..... 252
5.2.2 Chemotactic Mast Cell Migration Assay ..... 253
5.2.3 Assessment of RNA Integrity Number (RIN) ..... 254
5.2.4 Labelling, Hybridisation and Generation of Transcriptional Expression Array using the Affymetrix U 133 Plus 2.0 GeneChip™ ..... 255

5.2.5 Measurement of Chemokine Protein Expression Using Bio-Plex® Multiplex Immunoassay 257

5.2.6 Immune Cell Detection and Cell Counts ..... 258

**5.3 Results ..... 260**

5.3.1 Experimental Design and Assessment of RNA Quality ..... 261

5.3.2 Normalisation of Data and Post-Import Quality Assessment / Quality Control (QA/QC) Reports Using Partek® Genomics Suite™ 6.6 ..... 263

5.3.3 Assigning Sample Attributes and Principal Component Analysis Identifying Outliers and Overlapping Variables ..... 265

5.3.4 Differentially Expressed Genes and Sources of Variation ..... 269

5.3.4.1 LAF Co-Culture vs. LAF Mono-Culture ..... 270

5.3.4.2 NHLF Co-Culture vs. NHLF Mono-Culture ..... 273

5.3.5 Visualising Differentially Expressed Genes by Hierarchical Clustering ..... 275

5.3.6 Comparing Gene Lists Using Venn Diagrams ..... 279

5.3.7 Analysis of Genetic Networks within the Acquired Lists Using Gene Ontology Enrichment Analysis283

5.3.8 Pathway Analysis Using Partek Pathway™ ..... 286

5.3.9 Visualisation of Distribution of Selected Gene Intensities Using Dot Plots and Box and Whiskers Plots ..... 293

5.3.10 Quantitative Real-Time PCR (qRT-PCR) Validation of Selected Gene Targets in LAFs and NHLFs 299

5.3.11 Effect of β-estradiol (E2) on Gene Expression of Chemokines ..... 303

5.3.12 Validation of Protein Expression of Selected Chemokines in LAFs ..... 305

5.3.13 Effect of E2 and Rapamycin on 621-101 Cell Chemokine Expression ..... 308

5.3.14 Measuring Protein Expression of Selected Chemokines in *Ex Vivo* LAM Lung Tissue via Bio-Plex® Multiplex Immunoassay System and Immunohistochemistry ..... 311

5.3.15 Expression of Selected Chemokines in 3D Culture Model – LAM Spheroids ..... 315

5.3.16 Expression of C-X-C Motif Chemokine Receptor 2 (CXCR2) in LAM ..... 320

5.3.17 Presence of Immune Cells in LAM Lung ..... 323

5.3.18 Chemotactic Directional Migration of Mast Cells – Boyden Chamber Transwell® Migration Assay ..... 328

**5.4 Discussion ..... 330**

**5.5 Conclusion ..... 344**

6 CHAPTER 6: GENERAL DISCUSSION ..... 344

**6.1 General Overview ..... 344**

**6.2 *In Vitro* Models ..... 346**

**6.3 Activated Fibroblast Phenotype in LAM ..... 347**

**6.4 Recruitment of Mast cells ..... 348**

**6.5 Acidification of the LAM Nodule Microenvironment ..... 350**

**6.6 Cathepsin K and Inflammation ..... 351**

**6.7 Clinical applications of findings ..... 353**

**6.8 Strengths and weaknesses ..... 355**

**6.9 Final conclusion ..... 357**

7 CHAPTER 7: FUTURE WORK ..... 358

**7.1 Preclinical *in vivo* studies ..... 358**

**7.2 Establishing the proteolytic role of cathepsin K and the Warburg effect using *in vitro* models 358**

**7.3 Tailoring 2D and 3D *in vitro* models to LAM ..... 359**

**7.4 Identifying mechanisms of cell recruitment ..... 360**

8 APPENDIX ..... 361

**8.1 Appendix I: Isotype controls ..... 361**

9 BIBLIOGRAPHY ..... 363

# List of Figures

**FIGURE 1.1 SCHEMATIC REPRESENTATION OF THE STRUCTURE OF THE TWO PROTEINS ENCODED BY TSC1 (HAMARTIN) AND TSC2 (TUBERIN).**. ..... 13

**FIGURE 1.2 DIAGRAMATIC ILLUSTRATION OF THE MTORC1 AND MTORC2 COMPLEXES.**. ..... 16

**FIGURE 1.3 THE M TOR PATHWAY.** ..... 21

**FIGURE 1.4 PROPOSED MECHANISMS OF LAM PATHOGENESIS.** ..... 25

**FIGURE 1.5 DIAGRAMMATIC ILLUSTRATION OF NON-ACTIVATED AND ACTIVATED FIBROBLASTS.**. 35

**FIGURE 1.6 ILLUSTRATION OF A CO-CULTURE AND ITS ADVANTAGES.** ..... 47

**FIGURE 1.7 DIAGRAMMATIC ILLUSTRATION OF TRANSWELL-BASED CO-CULTURE MODELS.** ..... 49

**FIGURE 1.8 THE EFFECT OF PHYSICAL ENVIRONMENT ON CELL STRUCTURE.** ..... *51*

**FIGURE 1.9 3D ECM GEL CO-CULTURE-BASED MODEL.** ..... 54

**FIGURE 1.10 STEPS IN THE FORMATION OF SPHEROID-BASED MODELS.** ..... 61

**FIGURE 1.11 SCHEMATIC REPSRESENTATION OF PROTEASE DOMAINS OF CYSTEINE CATHEPSINS AND EXAMPLE RIBBON STRUCTURE.** ..... 68

**FIGURE 1.12 SURFACE POTENTIAL OF CATHEPSIN K.** ..... 72

**FIGURE 2.1 COLLAGENASE DIGEST OF LAM LUNG TISSUE.** ..... 95

**FIGURE 3.2.1 SPHEROID MOULD AND AGAROSE EMBEDDING OF SPHEROIDS.** ..... 124

**FIGURE 3.3.1 IMAGES OF NHLFS AND FIBROBLAST-LIKE CELLS (FLCS) SHOWING PRESENCE OF FIBROBLAST MARKERS.** ..... 127

**FIGURE 3.3.2 IMMUNOFLUORESCENT IMAGES SHOWING ASMA EXPRESSION IN NHLFS, FLCS AND NORMAL AIRWAY SMOOTH MUSCLE (NORMAL ASM) CELLS.** ..... 129

**FIGURE 3.3.3 OPTIMISATION OF CELL NUMBER AND RATIO FOR 3D CO-CULTURE MODEL.** ..... 131

**FIGURE 3.3.4 CELLS IN CO-CULTURE AND MONO-CULTURE EMBEDDED IN ECM GEL.** ..... 134

**FIGURE 3.3.5 NHLFS AND LAFS IN CO-CULTURE AND MONO-CULTURE EMBEDDED IN BME GEL.** 136

**FIGURE 3.3.6 LAFS IN CO-CULTURE WITH 621-101 CELLS.**. ..... 138

**FIGURE 3.3.7 MTT REDUCTION ASSAY PERFORMED SHOWING SURVIVAL CO-CULTURE OF MODEL OVER 7 DAYS.** ..... 139

**FIGURE 3.3.8 ALAMARBLUE® ASSAY PERFORMED SHOWING SURVIVAL CO-CULTURE OF MODEL OVER 7 DAYS.** ..... 140

**FIGURE 3.3.9 EXPRESSION OF MARKERS OF FIBROBLASTS AND MELANOCYTIC CELLS IN NHLF AND LAF 3D BME MODELS.**. ..... 141

**FIGURE 3.3.10 LAF AND NHLF CO-CULTURES SHOWING PRESENCE OF LAM NODULE-SPECIFIC MARKERS.** ..... 143

**FIGURE 3.3.11 DIAGRAMMATIC ILLUSTRATION OF GENERATION OF SPHEROIDS USING LIPIDURE-COAT ULTRA-LOW ATTACHMENT U-BOTTOM PLATE.** ..... 146

**FIGURE 3.3.12 REPRESENTATIVE BRIGHTFIELD IMAGES OF LAM SPHEROIDS GENERATED USING LIPIDURE-COAT® ULA 96-WELL U-BOTTOMED PLATES.** ..... 147

**FIGURE 3.3.13 DETERMINING APPROPRIATE CELL DENSITY FOR LAM SPHEROIDS.** ..... 149

**FIGURE 3.3.14 REPRESENTATIVE IMAGES OF LAM SPHEROIDS AT DIFFERENT CELL NUMBERS.** ..... 152

**FIGURE 3.3.15 HISTOMORPHOLOGY OF LAM SPHEROIDS GENERATED.** ..... 155

**FIGURE 3.3.16 DIAGRAMATIC REPRESENTATION OF GENERATION OF LAM TISSUE-DERIVED LAMOSPHERES FROM TRANSPLANT LUNG TISSUE.** ..... 158

**FIGURE 3.3.17 REPRESENTATIVE BRIGHTFIELD IMAGES OF LAMOSPHERES GENERATED.** ..... 159

**FIGURE 3.3.18 EXPRESSION OF LAM SPECIFIC MARKERS IN LAMOSPHERES.** ..... 160

**FIGURE 4.3.1 RELATIVE GENE EXPRESSION FOR LAM SPECIFIC MARKERS IN HUMAN LAM AND CONTROL LUNG TISSUE.** ..... 185

**FIGURE 4.3.2 RELATIVE PROTEASE GENE EXPRESSION IN HUMAN LAM AND CONTROL LUNGS.** ..... 187

**FIGURE 4.3.3 RELATIVE PROTEASE GENE EXPRESSION IN LAF AND 621-101 CELL 2D AND 3D CULTURES.** . ..... 189

**FIGURE 4.3.4 PROTEIN EXPRESSION OF PROTEASES IN LAF AND 621-101 CELL CO-CULTURES AND MONO-CULTURES.** ..... 192

**FIGURE 4.3.5 CATHEPSIN K EXPRESSION WITHIN LAM LUNG NODULES.** ..... 197

**FIGURE 4.3.6 EXPRESSION OF CATHEPSIN K IN LAM.**. ..... 199

**FIGURE 4.3.7 CATHEPSIN K GENE EXPRESSION IN EX VIVO LAM LUNG TISSUE.** ..... 201

**FIGURE 4.3.8 CATHEPSIN K EXPRESSION IN FIBROBLASTS AND 621-101 CELLS.** ..... 203

**FIGURE 4.3.9 IMMUNOFLUORESCENT DETECTION OF CATHEPSIN K.** ..... 204

**FIGURE 4.3.10 IMMUNOHISTOCHEMICAL EXPRESSION OF CATHEPSIN K IN LAM SPHEROIDS AND LAMOSPHERES.** ..... 206

**FIGURE 4.3.11 INTRACELLULAR ACTIVITY OF CATHEPSIN K MEASURED USING THE MAGIC RED® SUBSTRATE.** ..... 208

**FIGURE 4.3.12 IMMUNOFLUORESCENT (IHC-FR) CO-LOCALISATION OF FIBROBLAST SPECIFIC PROTEIN (FSP) AND CATHEPSIN K IN LAM LUNG NODULES.** ..... 210

**FIGURE 4.3.13 CHROMOGENIC IMMUNOHISTOCHEMICAL CO-LOCALISATION OF FIBROBLAST SPECIFIC PROTEIN (FSP) AND CATHEPSIN K IN LAM LUNG NODULES.** ..... 212

**FIGURE 4.3.14 EXTRACELLULAR CATHEPSIN K ACTIVITY IS PH DEPENDANT.** ..... 214

**FIGURE 4.3.15 LAFS AND 621-101 CELLS SURVIVE AT LOW PH.** ..... 215

**FIGURE 4.3.16 EXTRACELLULAR PH REDUCTION BY 621-101 CELLS.** ..... 216

**FIGURE 4.3.17 621-101 CELLS RAPIDLY REDUCED CELL CULTURE MEDIUM PH.** ..... 217

**FIGURE 4.3.18 EXPRESSION OF MEMBRANE PUMPS AND TRANSPORTERS IN 621-101 CELLS.** ..... 219

**FIGURE 4.3.19 EXPRESSION OF $H^+$ ION TRANSPORTERS IN LAM LUNG TISSUE.** ..... 220

**FIGURE 4.3.20 EXPRESSION OF CAIX AND SLC4A4 IN EX VIVO LAM LUNG TISSUE.** ..... 222

**FIGURE 4.3.21 MEMBRANE PUMP AND TRANSPORTER INHIBITION IN 621-101 CELLS.** ..... 224

**FIGURE 4.3.22 *24* HOUR INHIBITION OF MEMBRANE PUMPS AND TRANSPORTERS IN 621-101 CELLS.** ..... 225

**FIGURE 4.3.23 INHIBITION OF MEMBRANE PUMPS AND TRANSPORTERS AND THEIR EFFECT ON CTSK ACTIVITY IN LAFS AND 621-101 CELLS.** ..... 227

**FIGURE 4.3.24 INHIBITION OF MEMBRANE PUMPS AND TRANSPORTERS AND THEIR EFFECT ON CTSK ACTIVITY IN LAF/621-101 CO-CULTURES.** ..... 229

**FIGURE 4.3.25 CELL VIABILITY MEASURED AFTER INHIBITION OF MEMBRANE PUMPS AND TRANSPORTERS IN LAFS AND 621-101 CELLS.** ..... 231

**FIGURE 4.3.26 TOTAL CATHEPSIN K PROTEIN MEASURED IN LAFS AND 621-101 CELLS AFTER INHIBITION OF MEMBRANE PUMPS AND TRANSPORTERS.**.....234

**FIGURE 5.2.1 DIAGRAMMATIC REPRESENTATION OF ASSAY WORKFLOW FOR AMPLIFICATION AND LABELLING PROCESS.** .....256

**FIGURE 5.3.1 DIAGRAMMATIC REPRESENTATION OF EXPERIMENTAL DESIGN AND QUALITY ASSESSMENT OF ISOLATED RNA.**. .....261

**FIGURE 5.3.2 SCHEMATIC REPRESENTATION OF NORMALISATION PARAMETERS APPLIED AND POST-IMPORT QA/QC REPORT.**.....263

**FIGURE 5.3.3 SCHEMATIC REPRESENTATION OF ATTRIBUTES ASSIGNED TO SAMPLES.** .....265

**FIGURE 5.3.4 PRINCIPAL COMPONENT ANALYSIS (PCA).**. .....267

**FIGURE 5.3.5 HIERARCHICAL CLUSTERING OF ALL DIFFERENTIALLY EXPRESSED TRANSCRIPTS IN CO-CULTURE VS. MONO-CULTURE COMPARISON.**.....277

**FIGURE 5.3.6 VENN DIAGRAM COMPARING INDIVIDUAL LISTS; LAF CO-CULTURE VS LAF MONO-CULTURE AND NHLF CO-CULTURE VS NHLF MONO-CULTURE.**. .....279

**FIGURE 5.3.7 GO ENRICHMENT ANALYSIS PERFORMED ON THE LIST OBTAINED FROM THE VENN DIAGRAM COMPARISON OF LAF CO-CULTURE VS. LAF MONO-CULTURE VS. NHLF CO-CULTURE VS. NHLF MONO-CULTURE.**.....284

**FIGURE 5.3.8 DIAGRAMMATIC ILLUSTRATION OF THE TOP 2 MOST ENRICHED PATHWAYS FROM THE COMPARISON LIST GENERATED BY PARTEK PATHWAY™.** .....290

**FIGURE 5.3.9 DOT AND BOX AND WHISKERS PLOTS SHOWING DISTRIBUTION OF GENES INTENSITIES OF SELECTED TARGETS IN LAFS.** .....294

**FIGURE 5.3.10 DOT AND BOX AND WHISKERS PLOTS SHOWING DISTRIBUTION OF GENES INTENSITIES OF SELECTED TARGETS IN NHLFS.** .....297

**FIGURE 5.3.11 INITIAL QRT-PCR VALIDATION OF SELECTED CHEMOKINE TARGETS IN LAFS AND NHLFS.** . .....300

**FIGURE 5.3.12 SPEARMANS'S CORRELATIONS BETWEEN FOLD-CHANGE OBTAINED FOR GENE OF INTEREST ASSESSED BY RMA AND QRT-PCR.**.....302

**FIGURE 5.3.13 SECOND GENE EXPRESSION ANALYSIS: EFFECT OF B-ESTRADIOL ON EXPRESSION OF CHEMOKINES IN LAFS AND NHLFS.** ..... 303

**FIGURE 5.3.14 PROTEIN EXPRESSION OF SELECTED CHEMOKINES ASSESSED BY BIO-PLEX® MULTIPLEX IMMUNOASSAY SYSTEM.**. ..... 305

**FIGURE 5.3.15 EXPRESSION OF CHEMOKINES IN LAF CO-CULTURE, LAF MONO-CULTURE AND 621-101 CELL MONO-CULTURE ASSESSED BY BIO-PLEX® MULTIPLEX IMMUNOASSAY SYSTEM.**.. 308

**FIGURE 5.3.16 EXPRESSION OF SELECTED CHEMOKINES IN TREATED LAM LUNG TISSUE ASSESSED BY BIO-PLEX® MULTIPLEX IMMUNOASSAY SYSTEM.** ..... 311

**FIGURE 5.3.17 CHEMOKINE EXPRESSION IN LAM NODULES.**. ..... 313

**FIGURE 5.3.18 EXPRESSION OF SELECTED CHEMOKINES IN 3D LAM SPHEROID MODEL ASSESSED BY BIO-PLEX® MULTIPLEX IMMUNOASSAY SYSTEM.** ..... 315

**FIGURE 5.3.19 EXPRESSION OF C-X-C CHEMOKINES IN LAM SPHEROIDS ASSESSED VIA IMMUNOHISTOCHEMISTRY.** ..... 317

**FIGURE 5.3.20 QRT-PCR ANALYSIS FOR THE EXPRESSION OF CXCR2 IN LAFS AND 621-101 CELLS.** 320

**FIGURE 5.3.21 IMMUNOHISTOCHEMICAL DETECTION OF CXCR2 IN LAM LUNG TISSUE.** ..... 322

**FIGURE 5.3.22 EXPRESSION OF MARKERS OF IMMUNE CELLS IN LAM NODULES IN EARLY AND LATE LAM PATIENTS.** ..... 325

**FIGURE 5.3.23 NUMBER OF IMMUNE CELLS PER $MM^2$ IDENTIFIED BY SPECIFIC MARKERS.** ..... 327

**FIGURE 5.3.24 CHEMOTACTIC MIGRATION OF HMC-1 CELLS TOWARDS LAFS AND 621-101 CELLS IN CO-CULTURE AND MONO-CULTURE.** ..... 329

# List of Tables

**TABLE 1.1 PROTEINS COMPRISING THE MTORC1/2 COMPLEXES AND THEIR FUNCTION.** .....15

**TABLE 1.2 UPSTREAM REGULATORS OF MTORC1.**.....18

**TABLE 1.3 CLINICAL TRIALS FOR LAM CONDUCTED USING RAPAMYCIN AND ITS ANALOGUES WITH VARYING OUTCOMES. TRIAL INFORMATION OBTAINED FROM (CLINICALTRIALS.GOV)** .....29

**TABLE 1.4 METASTATIC MECHANISMS IN LAM.**.....33

**TABLE 1.5 TSC1$^{+/-}$ MOUSE MODELS GENERATED.**.....41

**TABLE 1.6 BROAD CLASSIFICATION OF IN VITRO MODELS.**.....46

**TABLE 1.7 METHODS USED TO GENERATE SPHEROID-BASED MODELS.**.....56

**TABLE 1.8 TISSUE AND CELLULAR LOCALISATION AND ECM SUBSTRATES OF KNOWN CATHEPSINS.** .....65

**TABLE 1.9 INHIBITORS OF CATHEPSIN K WITH STRUCTURES AND THEIR VARIOUS STAGES OF DEVELOPMENT.** .....80

**TABLE 2.1 LIST OF PRIMARY ANTIBODIES USED FOR IMMUNOHISTOCHEMISTRY AND IMMUNOFLUORESCENCE WHICH RESPECTIVE DILUTIONS AND SUPPLIERS.**.....88

**TABLE 2.2 LIST OF ISOTYPE CONTROLS USED FOR IMMUNOHISTOCHEMISTRY AND IMMUNOFLUORESCENCE WHICH RESPECTIVE HOST SPECIES AND SUPPLIERS.** .....89

**TABLE 2.3 LIST OF SECONDARY ANTIBODIES USED FOR IMMUNOHISTOCHEMISTRY AND IMMUNOFLUORESCENCE WHICH RESPECTIVE DILUTIONS AND SUPPLIERS.**.....89

**TABLE 2.4 LIST OF INHIBITORS USED LISTED WITH THE WORKING CONCENTRATIONS USED.**.....90

**TABLE 2.5 PRIMARY CELL AND COMMERCIAL CELL TYPES USED IN THIS STUDY WITH THEIR METHOD OF DERIVATION.**.....92

**TABLE 2.6 CDNA MASTERMIX**.....102

**TABLE 2.7 CDNA SYNTHESIS CYCLING CONDITIONS**.....103

**TABLE 2.8 QRT-PCR MASTERMIX (A) AND CYCLING CONDITIONS (B)**.....104

**TABLE 2.9 RANKS AND CORRESPONDING LOCATIONS OF PREDESIGNED KICQ START PRIMERS** ...105

**TABLE 3.3.1 ADVANTAGES AND DISADVANTAGES OF CULTUREX® BME1 GEL AND ECM GEL** .....138

**TABLE 3.4.1 ADVANTAGES AND DISADVANTAGES OF THREE 3D LAM MODELS DESIGNED.**.....169

**TABLE 4.3.1 LIST OF 30 PROTEASES ELEVATED IN OR EXPRESSED IN LAM, OTHER INTERSTITIAL AND AIRWAY LUNG DISEASES SELECTED FOR SCREENING IN LAM LUNG TISSUE.**.....184

**TABLE 4.3.2 SIGNIFICANT PROTEASE GENE EXPRESSION COMPARISONS BETWEEN 2D AND 3D CULTURES.** .....190

**TABLE 5.2.1 EXTRACTED LAF AND NHLF RNA DESIGNATED WITH SAMPLE NAMES FOR EASE OF USE IN FURTHER ANALYSES.** .....255

**TABLE 5.2.2 BEAD REGIONS AND FIRST STANDARD VALUES (PG/ML) FOR CHEMOKINE ANALYTES SET FOR BIO-PLEX 100,200 MACHINE.**.....258

**TABLE 5.2.3 PRIMARY ANTIBODIES USED TO IDENTIFY IMMUNE CELLS IN LAM LUNG NODULES** .259

**TABLE 5.3.1 SAMPLES INCLUDED IN EACH COMPARISON LIST WITH APPROPRIATE ATTRIBUTE.**..266

**TABLE 5.3.2 ANOVA FACTORS DESIGNATED FOR EACH COMPARISON LIST TO GENERATE INITIAL LIST OF TRANSCRIPTS.**.....269

**TABLE 5.3.3 TOP 41 DIFFERENTIALLY EXPRESSED TRANSCRIPTS BETWEEN LAF CO-CULTURE AND LAF MONO-CULTURE.** .....272

**TABLE 5.3.4 TOP 41 DIFFERENTIALLY EXPRESSED TRANSCRIPTS BETWEEN NHLF CO-CULTURE AND NHLF MONO-CULTURE.**.....275

**TABLE 5.3.5 24 OUT OF THE 148 DIFFERENTIALLY EXPRESSED IN BOTH FIBROBLASTS WHEN CO-CULTURED** .....281

**TABLE 5.3.6 TOP 10 ENRICHED GO FUNCTIONS ANNOTATED TO TRANSCRIPTS ON COMPARISON OF LAF CO-CULTURE VS. LAF MONO-CULTURE VS NHLF CO-CULTURE VS. NHLF MONO-CULTURE.** .....286

**TABLE 5.3.7 PATHWAY ANALYSIS OF 148 COMMONLY SHARED TRANSCRIPTS BETWEEN LAF CO-CULTURE VS. LAF MONO-CULTURE AND NHLF CO-CULTURE VS. NHLF MONO-CULTURE.** ....287

**TABLE 5.3.8 SPECIFIC GENES FROM LIST INVOLVED IN DIFFERENT HIGHLY ENRICHED PATHWAYS.** .....292

**TABLE 5.3.9 FOLD CHANGE INCREASE OF CHEMOKINE EXPRESSION IN LAF AND NHLF CO-CULTURE COMPARED TO MONO-CULTURE.** ..... 301

## Abbreviations

| | |
|---|---|
| 2D/3D | 2-dimensional / 3-dimensional |
| ADAM | A Disintegrin and Metalloproteinase |
| AFC | Amino-4-Trifluoromethyl Coumarin |
| AML | Angiomyolipoma |
| AMPK | Adenosine Monophosphate-Activated Protein Kinase |
| ANOVA | Analysis of Variance |
| AP-1 | Activator Protein 1 |
| ASM | Airway Smooth Muscle Cells |
| Atg13 | Autophagy-related Gene 13 |
| BHD | Birt Hogg Dube |
| BME | Basement Membrane Extract |
| BP1 | Building Protein 1 |
| BSA | Bovine Serum Albumin |
| CA | Carbonic Anhydrase |
| CAF | Cancer-associated Fibroblast |
| CCR | C-C chemokine receptor type |
| CD | Cluster Differentiation |
| cDNA | Complementary DNA |
| CMCS | Co-culture Multicellular Spheroids |
| COPD | Chronic Obstructive Pulmonary Disease |
| CT | Computed Tomography |
| CTX/NTX | C-terminal telopeptide / N-terminal telopeptide |
| CX3CR | CX3C chemokine receptor |

| | |
|---|---|
| CXCL | C-X-C motif ligand |
| CXCR | C-X-C chemokine receptor type |
| DAPI | 4', 6-diamidino-2-phenylindole |
| DEPC | Diethyl Pyrocarbonate |
| DEPTOR | DEP Domain Containing mTOR-Interacting Protein |
| DES | Desmin |
| $DL_{CO}$ | Diffusing Capacity for Carbon Monoxide |
| DMEM | Dulbecco's Modified Eagle Medium |
| DMEM/F-12 | Dulbecco's Modified Eagle Medium/Nutrient Mixture F-12 |
| DNA | Deoxyribonucleic acid |
| dNTP | Deoxyribose Nucleotide Triphosphate |
| DPBS | Dulbecco's Phosphate Buffered Saline |
| DTT | Dithiothreitol |
| E2 | β-estradiol |
| EBP | Elastin Binding Protein |
| ECM | Extracellular Matrix |
| EDTA | Ethylenediaminetetraacetic acid |
| EGF | Epidermal Growth Factor |
| EHS | Engelbreth-Holm Swarm |
| eIF4E | Eukaryotic Translation Inititation Factor 4E |
| ELISA | Enzyme-linked Immunosorbent Assay |
| EMT | Epithelial-mesenchymal Transition |
| EMT | Epithelial-mesenchymal Transition |
| EpCAM | Epithelial Cell Adhesion Molecule |
| ERK1/2 | Extracellular-signal-regulated Kinase 1/2 |

| | |
|---|---|
| ERM | Ezrin-Radixin-Moesin |
| ERS | European Respiratory Society |
| ERα/β | Oestrogen Receptor α/β |
| FAPα | Fibroblast Activation Protein |
| FCS | Foetal Calf Serum |
| FCS | Foetal Calf Serum |
| FDR | False Discovery Rate |
| FEV 1 | Foreced Expiratory Volume in One Second |
| FFPE | Formalin-fixed paraffin-embedded |
| FGF | Fibroblast Growth Factor |
| FGM | Fibroblast Growth Medium |
| FIP200 | Focal Adhesion Kinase Family-interacting Protein of 200kDa |
| FLC | Fibroblast-like cells |
| FSP | Fibroblast Surface Protein |
| FVC | Forced Vital Capacity |
| GAG | Glycosaminoglycans |
| GAP | GTpase-Activating Protein |
| GAPDH | Glyceraldehyde 3-phosphate dehydrogenase |
| GO | Gene Ontology |
| GSK3-β | Glycogen Synthase Kinase 3β |
| HGF | Hepatocyte Growth Factor |
| HIER | Heat Induced Epitope Retrieval |
| HIF-1α/2α | Hypoxia-inducible Factor 1-alpha / 2-alpha |
| HMB-45 | Homatropine Methylbromide 45 |
| HMC-1 | Human Mast Cell Line-1 |

| | |
|---|---|
| IFNγ | Interferon gamma |
| IGF1 | Insulin-like Growth Factor 1 |
| IHC | Immunohistochemistry |
| IKKβ | Inhibitor of Nuclear Factor Kappa-B Kinase Subunit Beta |
| IL | Interleukin |
| IMDM | Iscove's Modified Dulbecco's Medium |
| IPF | Idiopathic Pulmonary Fibrosis |
| KEGG | Kyoto Encyclopaedia of Genes and Genomes |
| LAF | LAM-associated Fibroblast |
| LAM | Lymphangioleiomyomatosis |
| LEC | Lymphatic Endothelial Cells |
| LIP | Lymphocytic Interstitial Pneumonitis |
| LOH | Loss of Heterozygosity |
| M6PR | Mannose-6-phosphate Receptor |
| MAPK | Mitogen-activated Protein Kinase |
| MCT | Monocarboxylate Transporter |
| MCTS | Multicellular Tumour Spheroid Models |
| MEF | Mouse Embryonic fibroblasts |
| MITF | Microphthalmia-associated Transcription Factor |
| MLST8 | Mammalian Lethal with Sec-13 |
| MMP | Matrix Metalloproteinases |
| mRNA | Messenger RNA |
| mTOR | Mechanistic Target of Rapamycin |
| mTORC1/2 | Mechanistic Target of Rapamycin Complex 1/2 |

| | |
|---|---|
| MTT | 3-(4,5-Dimethylthiazol-2-Yl)-2,5-Diphenyltetrazolium Bromide |
| NF-κB | Nuclear Factor Kappa-Light-Chain-Enhancer of Activated B Cells |
| NHLF | Normal Human Lung Fibroblast |
| OD | Optical Density |
| OMS | Organotypic Multicellular Spheroid |
| PAI | Plasminogen Activator Inhibitor |
| PBS | Phosphate Buffered Saline |
| PCA | Principal Component Analysis |
| PCNA | Proliferating Cell Nuclear Antigen |
| PDGF | Platelet-derived Growth Factor |
| PEComa | Perivascular Epithelioid Cell Tumour |
| PGC1α | PPARγ Coactivator 1α |
| $pH_e$ | Extracellular pH |
| $pH_i$ | Intracellular pH |
| PI3K | Phosphoinositide 3-Kinase |
| PKC-α | Protein Kinase C-α |
| PMT | Photomultiplier tube |
| PPARγ | Peroxisome Proliferator-Activator-γ |
| PRAS40 | Proline-rich Akt Substrate 40kDa |
| PTEN | Phosphatase and Tensin Homolog |
| qRT-PCR | Quantitative Real Time Polymerase Chain Reaction |
| RANK | Receptor Activator of NF-κB |
| REDD1 | Regulation of DNA Damage Response 1 |
| Rheb | Ras Homolog Enriched in Brain |

| | |
|---|---|
| RIN | RNA Integrity Number |
| RMA | Robust Multi-array Average |
| RNA | Ribonucleic acid |
| ROS | Reactive Oxygen Species |
| RSK1 | Ribosomal S6 Kinase |
| RT | Room temperature |
| S LAM | Sporadic Lymphangioleiomyomatosis |
| S6K1 | S6 Kinase 1 |
| SA-PE | Streptavidin-phycoerythrin |
| SDF-1 | Stromal Cell-derived Factor 1 |
| SGK1 | Serum And Glucocorticoid-induced Protein Kinase 1 |
| SREBP1/2 | Sterol Regulatory Element Binding Protein ½ |
| SRF | Serum Response Factor |
| SSc | Systemic Sclerosis |
| TDTs | Tissue-derived Tumour Spheres |
| TGFβ | Transforming Growth Factor-β |
| TIMP | Tissue Inhibitor of Metalloproteinases |
| TNFα | Tumour Necrosis Factor-α |
| TSC | Tuberous Sclerosis Complex |
| TSC1/2 | Tuberous Sclerosis Complex ½ |
| ULA | Ultra-low attachment |
| ULK1 | Unc-51-like Kinase 1 |
| uPA | Urokinase-type Plasminogen Activator |
| VEGF-D | Vascular Endothelial Growth Factor |
| VEGFR | Vascular Endothelial Growth Factor Receptor |

| | |
|---|---|
| VIM | Vimentin |
| WHO | World Health Organisation |
| YY1 | Ying-Yang 1 |
| αSMA | α-Smooth Muscle Actin |

# 1 CHAPTER 1: Lymphangioleiomyomatosis (LAM): An Introduction

## 1.1 Lymphangioleiomyomatosis (LAM)

### 1.1.1 Definition

Lymphangioleiomyomatosis is a rare and possibly fatal genetic disease that affects the lungs, axial lymphatics and kidneys. It is characterised by a gradual infiltration of proliferating smooth muscle cells in the affected areas, known as lesions, which lead to the development of cysts within the lung parenchyma. Chiefly occurring in the kidneys, angiomyolipomas, which are benign mesenchymal tumours are also a characteristic feature of LAM. LAM can be associated with tuberous sclerosis complex (TSC-LAM) or can occur in isolation (sporadic LAM) (Johnson, 2004).

### 1.1.2 Background, Epidemiology and Importance

Lymphangioleiomyomatosis (LAM) is a rare disorder that almost exclusively progresses in women and affects multiple organs leading to cystic lungs and eventually, respiratory failure (Oprescu et al., 2013, Ryu et al., 2006). An estimated 210,000 to 290,000 patients worldwide are affected by LAM today. The first known recorded case of LAM was in 1918 (Lutembacher, 1918) with a major series of cases being reported from USA (Chu et al., 1999), South-East Asia (Kitaichi et al., 1995), the UK (Wahedna, 1994) and France (Urban et al., 1999) in the 1990s. Studies conducted in France on a female population aged between 20-69 in 1997

and on the total population of UK in 2000 estimated about 2.6 cases/million women (Urban et al., 1999) and 1/1.1 million of the UK population (Johnson and Tattersfield, 2000) respectively. An increasing interest in LAM thereafter, initiated the establishment of patient registries and groups resulting in an exponential increase in LAM research (Harknett et al., 2011).

Procuring prevalence figures for rare diseases like LAM is difficult since many patients remain undiagnosed or misdiagnosed (Harknett et al., 2011). At diagnosis, LAM may be confused with other conditions such as emphysema, Langerhans cell histiocytosis since the disease may not always have a 'classical appearance' (Johnson, 2004). Moreover, the rarity of pulmonary diseases such as LAM, leads to patients being seen by physicians working outside their area of expertise. In the UK only an estimated 0.6-1.3% of the total LAM population are seen by most respiratory physicians, thereby making them unable to build up expertise in the management and diagnosis of the disease (Johnson, 2010). In 2010, Johnson and colleagues laid down ERS guidelines for the correct diagnosis and categorisation of LAM into 1) Definite LAM, 2) Probable LAM and 3) Possible LAM based on HRCT, clinical history and disease presentation (Johnson, 2010). Application of these guidelines to a study conducted by Chang et al on a national cohort left only 30% of the patients without a 'definite diagnosis', with a further reduction to 20% when measurement of serum biomarker vascular endothelial growth factor D (VEGF-D) (Chang et al., 2012).

LAM, although rare affects all races and ethnicities. In a survey carried out by the LAM foundation, of the 480 LAM patients screened 90% were Caucasians, 3.5% Asians, 3% African-Americans, and 2% Hispanics. Although LAM has been described to occur almost exclusively in women, radiological and histological findings have confirmed LAM in 5 reported cases in men (Aubry et al., 2000, Kim et al., 2003b, Ryu et al., 2006).

A rare disease such as LAM is defined as one that can affect less than 5 in 10,000 of the general population and about 7% of the population, at some point will be affected by a rare disease. Although the number of people individually affected by such diseases is low, collectively these diseases are not rare. About 3.5 million people in the UK are or will be affected by a rare disease (2014). Therefore, much research is still needed to fully understand and treat this rare condition.

### 1.2 Clinical presentation, symptoms and diagnosis

LAM was initially thought to fatally affect premenopausal women of childbearing age with a lung transplant as the only option (Orkin et al., 1977). Subsequent clinical studies have painted a more complete picture. With the data obtained from patients in the database of the US LAM Foundation and LAM Action in the UK a large survey (n=328) conducted found that more women over the age of 40 are being diagnosed with LAM, with the result the mean age of diagnosis is continually shifting from the current 30 years of age (Cohen et al., 2005, Harari et al., 2015). Initially given a 10 year prognosis, LAM patients can now survive for more than

15-20 years, nevertheless LAM is a chronic and debilitating neoplastic disease with no efficient treatment (Hammes and Krymskaya, 2013, Kleinman et al., 1982). The pulmonary symptoms in LAM serve to dictate the clinical course, the most common features being pneumothorax, progressive dyspnoea and chylous pleural effusions. Other symptoms include cough, haemoptysis and chyloptysis. Dyspnoea results in airflow obstruction, with the lung parenchyma being replaced by large cysts filled with air (Johnson, 2004, Urban et al., 1999, Chu et al., 1999, Kitaichi et al., 1995, Taylor et al., 1990). Recurrent pneumothorax is a significant contributor to morbidity in LAM which occurs in approximately two thirds of patients (Johnson, 2004).

Extrapulmonary manifestations include lymphadenopathy, large cystic lymphatic masses (termed lymphangioleiomyomas) and chylous abdominal collections (Matsui et al., 2000c, Avila et al., 2000). Computed tomography (CT) scans show a large population of LAM patients have been found to have a co-existing benign tumour of smooth muscle, blood vessels and fat, termed angiomyolipoma (AML), mainly occurring in the kidneys (Astrinidis et al., 2000, Maziak et al., 1996, Johnson, 2004). Patients with LAM show a distinctive radiologic finding of thin-walled cysts disseminated throughout the lung parenchyma (Glasgow et al., 2010). These cystic lesions result in a loss of lung function and airway obstruction thereafter which is sometimes partly reversible with the use of a bronchodilator (Taveira-DaSilva et al., 2001).

The aggressiveness of the disease depends on the rate at which the lung function declines in patients (Taveira-DaSilva et al., 2001). In a study carried out by Johnson and Tattersfield on 43 female patients, the average rate of change in FEV1 was 118±21 ml/year and $DL_{CO}$ was 0.905±0.26 ml/min/mmHg/year (Johnson and Tattersfield, 1999). The decline in FEV1 of pre- and post-menopausal women in this study group was found to be 170 ml/year and 86 ml/year respectively (Johnson and Tattersfield, 1999). Through these findings it is evident that since LAM progress exclusively in women compared to men, oestrogen may have a significant role in disease progression. A study involving 15 women diagnosed with LAM during their pregnancy reported not only a worse obstetric outcome but also 66.7% of these women suffered from breathlessness, pneumothorax or chylothorax, as compared to those diagnosed before or after pregnancy. This clearly shows that pregnancy exacerbates LAM symptoms suggesting that oestrogen promotes LAM (Cohen et al., 2009).

Women with LAM have been treated with oophorectomy, however Taylor et al reported out of a total of 16 patients who underwent oophorectomy for the treatment of LAM, 25% had stable LAM and in 69% of patients, the disease had worsened (Taylor et al., 1990). Oophorectomy did not have any survival advantage nor did anti-oestrogen tamoxifen treatment in 9 patients studied (Taylor et al., 1990). Johnson and Tattersfield observed that in patients treated with progesterone, reductions in FEV1 were not significantly smaller than the untreated patients (Johnson and Tattersfield, 1999). Although a significant decrease in $DL_{CO}$ was observed between

progesterone treated and untreated patients, the two groups were not matched (Johnson and Tattersfield, 1999). Change in the route of administration of progesterone to intramuscular also did not show any significant decline in FEV1 or $DL_{CO}$ when compared to a matched untreated patient group (Taveira-DaSilva et al., 2004). Thus, removing the endogenous oestrogen or administration of anti-oestrogen therapy does not show any evidence in halting the progression of this predominantly premenopausal disease.

The gold standard in the diagnosis of LAM still remains a lung biopsy. According to the European Respiratory Society (ERS) guidelines a consensus was reached that a firm diagnosis can be made by a lung biopsy and a characteristic or compatible high resolution CT showing innate lung cysts and/or an angiomyolipoma (kidney), a chylous collection and compatible clinical history (Johnson et al., 2010). Pathologic features of a definite diagnosis show LAM lesions identified by cysts and nodules of LAM cells. Two subpopulations make up a LAM cell population: spindle-shaped smooth muscle-like cells, expressing smooth muscle specific proteins such as α-actin, desmin and vimentin and perivascular epitheloid-like cells, presumed to be 'LAM cells', expressing glycoprotein gp100, a melanoma cell and immature melanocyte marker (Johnson et al., 2010, Harari, 2011). These histologic features along with a positive immunohistochemical staining for α-actin, desmin and HMB45, immunoreacts with gp100, are now efficient along with CT scanning and

patient history in making an effective diagnosis of LAM (Johnson et al., 2010).

Although a biopsy is required in making a confirmed diagnosis of LAM, a shift towards a more non-invasive diagnostic strategy has been recently considered. This involves examination of tell-tale signs for TSC, Birt–Hogg–Dubé syndrome (BHD) and lymphocytic interstitial pneumonitis (LIP) and ruling out the latter two which are often confused with LAM, a CT of the abdomen to identify the presence of an AML and checking for lymphatic abnormalities such as lymphadenopathy, lymphangioleiomyomas, or chylous ascites. Elevated levels of a serum biomarker, vascular endothelial growth factor D (VEGF-D) have been found to be elevated in most women with LAM and a serum level of greater than 800pg/ml can be used to differentiate LAM from other cystic lung diseases thereby reducing the need for a lung biopsy (Benton et al., 2014).

## 1.3 TSC-LAM and Sporadic LAM

Lymphangioleiomyomatosis can occur in women sporadically (sporadic LAM or S-LAM) or in conjunction with Tuberous Sclerosis Complex (TSC, TSC-LAM) (Astrinidis et al., 2000).

### 1.3.1 TSC-LAM

Characterised by tumour-like lesions in multiple organs, called hamartomas, TSC is an inherited autosomal dominant disorder caused by loss of function mutations in either the *TSC1* or *TSC2* genes (Yates, 2006).

The most commonly occurring tumours include subependymal giant cell astrocytomas, facial angiofibromas, cardiac rhabdomyomas and renal angiomyolipomas (Astrinidis et al., 2000, Henske, 2003) Loss of heterozygosity (LOH) in either of the two genes of the TSC, *TSC1* located on chromosome band *9q34* (van Slegtenhorst et al., 1998) and *TSC2* located on chromosome band *16p13* (European Chromosome 16 Tuberous Sclerosis, 1993) cause the disease. The *TSC1* gene identified in 1997 (van Slegtenhorst et al., 1997) codes for a 130kDa protein hamartin whereas the *TSC2* gene isolated in 1993 (European Chromosome 16 Tuberous Sclerosis, 1993) codes for a 200kDa protein tuberin. TSC can occur both sporadically (about 60%) or can be inherited as a germline mutation of either gene from mother to offspring (Sampson and Harris, 1994, Slingerland et al., 1989). In TSC associated LAM however, majority of the mutations are seen on *TSC2* gene which also causes more severe manifestations than the *TSC1* mutation. In a study conducted by Kwiatkowski et al on a cohort of 224 women, 60% with a sporadic *TSC2* mutation showed a higher frequency of renal AMLs as compared to 31% with a sporadic *TSC1* mutation (Dabora et al., 2001).

A high occurrence of LAM in women with TSC has been reported which gives rise to the fact that this subgroup of patients are at a risk of developing pulmonary LAM (Moss et al., 2001a). Currently an estimated 20% of women at 18 years have TSC associated LAM and lung cysts are seen in about 10% of men with TSC (Benton et al., 2014, Noel et al., 1992). A recent investigation of a TSC-LAM patient cohort identified age

as a crucial risk factor for the development of LAM in women with TSC. Data from this study showed that women over 40 years of age had a higher prevalence (81%) of this cystic lung disease as compared to those between 30-40 years (58%) (Cudzilo et al., 2013, Benton et al., 2014). After renal disease and brain tumours, LAM was the third most common cause of death in patients with TSC (Castro et al., 1995).

Renal angiomyolipomas (AML) occur in 80% of TSC patients are seen in most patients with TSC-LAM (Rakowski et al., 2006, Dabora et al., 2001). Cells of patients with TSC-LAM are known to exhibit a LOH that indicates inactivation of the wild type *TSC2* allele which gives rise to the conclusion that the Knudson 'two-hit' hypothesis can be used to explain the pathogenesis of TSC-LAM (Yu et al., 2001, Knudson, 2001). Genetic analysis of the three distinct components of an AML comprising of dysplastic vessels, smooth muscle cells and fat, from TSC-LAM patients has shown that all these components arise from a common progenitor cell (Niida et al., 2001, Karbowniczek et al., 2003). Moreover, a recent genetic analysis revealed 7 out of 8 AMLs associated with TSC examined carried a *TSC2* and not *TSC1* mutation which is in keeping with the pathogenesis of TSC-LAM (Qin et al., 2011).

### 1.3.2 Sporadic LAM

In 1937, Von Stössell reported the first case of a LAM patient who did not have TSC (von Stossel, 1937). Over time it was evident that this less prevalent form of LAM without underlying TSC occurs sporadically and is termed as sporadic LAM or S-LAM (Henske and McCormack, 2012). The occurrence of S-LAM is rarer than TSC-LAM and affects about 10,000 patients globally (Harknett et al., 2011). Extrapulmonary manifestations observed in TSC such as renal angiomyolipomas, axial lymphadenopathy and abdominal lymphangiomyomas are also seen in S-LAM (Ryu et al., 2006) and sporadic LAM has been reported in only one karyotypically normal male (Seidl et al., 2002). Sporadic LAM is reported to be more severe than TSC-LAM and also progresses faster (Ryu et al., 2006, Cohen et al., 2005).

Renal AMLs occur in approximately 50% of S-LAM patients, and unlike in TSC, S-LAM patients present with single, unilateral and asymptomatic AMLs (Avila et al., 2007). Occurrence of LAM sporadically suggested that women with S-LAM could have somatic TSC2 mutations (Carsillo et al., 2000). TSC-LAM and S-LAM present with similar lung and renal manifestations, and studies have revealed 54% of the AMLs from women with S-LAM showed a LOH on the chromosome band *16p13* of the *TSC2* gene and no LOH in the *TCS1* gene, indicating that S-LAM is more likely caused by *TSC2* mutations (Smolarek et al., 1998). Somatic nature of *TSC2* mutations was confirmed in S-LAM as mutational analysis of the surrounding normal lung and kidney tissue did not show any mutation

(Carsillo et al., 2000). Pulmonary LAM cells from the patient tissue samples, identified by smooth muscle actin staining, isolated using laser capture microdissection, were also found to carry the same LOH in the *16p13* region of *TSC2* suggesting that the Knudson two-hit tumour suppressor gene model applies to both the AML cells and LAM cells from S-LAM patients (Carsillo et al., 2000, Knudson, 2001). *TSC1* LOH has not been detected in any of the AMLs (Carsillo et al., 2000).

## 1.4 Genetics of LAM and the mTOR pathway

Tuberin a highly evolutionarily conserved protein that activates GTPase, is encoded by *TSC2* (Manning et al., 2002). It is ubiquitously expressed, is a tumour suppressor, is 198kDa and is located on chromosome 16 (European Chromosome 16 Tuberous Sclerosis, 1993). The 1784 amino acid tuberin consists of a leucine zipper motif, two small coiled-coil domains and a small region similar with GTPase-activating protein (GAP) (Figure 1.1) (European Chromosome 16 Tuberous Sclerosis, 1993, Rubinfeld et al., 1991, Rubinfeld et al., 1992). The protein bears a region of homology with the Rap1 GTPase-activating protein (Rap1GAP) and has multiple phosphorylation sites for the serine-threonine kinase, protein kinase B (Akt/PKB) (European Chromosome 16 Tuberous Sclerosis, 1993, Maheshwar et al., 1996, Manning et al., 2002).

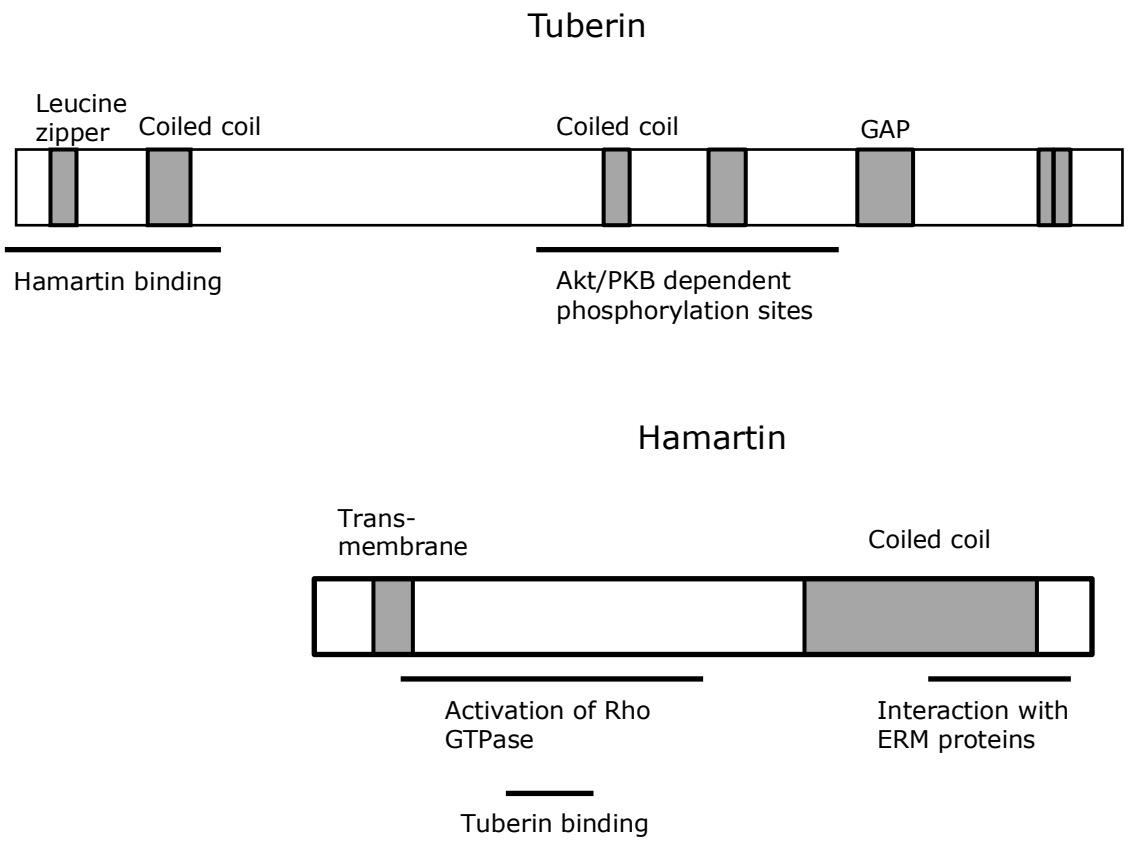



**Figure 1.1** ***Schematic representation of the structure of the two proteins encoded by TSC1 (hamartin) and TSC2 (tuberin).*** *Tuberin contains a GAP (GTPase activating protein) domain, hamartin-binding site and multiple Akt/PKB phosphorylation sites. Hamartin is smaller and contains Rho GAP and tuberin-binding domain.*

Hamartin, the protein encoded by the *TSC1* gene heterodimerises with tuberin and is essential for its function (Plank et al., 1998). It has a molecular weight of 130kDa and is located on chromosome 9 of the *TSC1* gene (van Slegtenhorst et al., 1997). The protein is smaller than tuberin and consists of a potential transmembrane domain towards the N-terminus and a coiled-coil domain towards the C-terminus (van Slegtenhorst et al., 1997). Hamartin also contains, additionally, Rho GTPase-activating (GAP), tuberin binding and ezrin-radixin-moesin (ERM) family binding domains (Lamb et al., 2000). Binding of tuberin to hamartin occurs via the N-terminus (Figure 1.1) (van Slegtenhorst et al., 1998, Plank et al., 1998).

Since the loss of function of either *TSC1* or *TSC2* is implicated in TSC-LAM and S-LAM, it suggested that the proteins encoded by the two genes are functionally related. Immunohistochemical studies show that in vivo hamartin and tuberin co-localise (Johnson et al., 1999, Murthy et al., 2001, Johnson et al., 2001) and also coimmunoprecipitate from cell lines and primary cells with either hamartin or tuberin anti-sera (Catania et al., 2001, van Slegtenhorst et al., 1998). It is the coiled-coil domain of hamartin that drives the heterodimerisation forming large insoluble complexes *in vitro* and as soon as hamartin is synthesised, tuberin binds to it and prevents self-aggregation of hamartin suggesting that it acts as a molecular chaperone (Nellist et al., 1999).

mTOR (mammalian target of rapamycin) is a serine/threonine protein kinase, sensitive to rapamycin treatment, that is atypical and belongs to the phosphoinositide 3-kinase (PI3K)-related kinase family. mTOR consists of two separate complexes namely, mTOR complex 1 (mTORC1) and 2 (mTORC2) which are formed via its interaction with several proteins (Table 1.1) (Laplante and Sabatini, 2012) which in turn control several anabolic and catabolic processes in cells (Kristof, 2010). The mTORC1 and mTORC2 complexes consist of six and seven proteins respectively. Regulatory-associated protein of mammalian target of rapamycin (raptor) (Hara et al., 2002, Kim et al., 2002)and proline-rich Akt substrate 40kDa (PRAS40) (Sancak et al., 2010, Thedieck et al., 2007, Wang et al., 2007) are exclusive to the mTORC1 complex (Figure 1.2 (a)), whereas rapamycin-insensitive companion of mTOR (rictor) (Jacinto et al., 2004, Sarbassov et

al., 2004), mammalian stress-activated map kinase-interacting protein 1 (mSin1) (Frias et al., 2006) and protein observed with rictor 1 and 2 (protor1/2) (Pearce et al., 2007, Thedieck et al., 2007) are only seen in the mTORC2 complex (Figure 1.2 (b)). The two complexes, however, share a common mTOR subunit, mammalian lethal with sec-13 (mLST8) (Jacinto et al., 2004, Kim et al., 2003a), DEP domain containing mTOR-interacting protein (DEPTOR) (Peterson et al., 2009) and the Tti1/Tel2 complex (Kaizuka et al., 2010). The functions of these proteins are discussed in Table 1.1

| **m TORC1** | **m TORC2** |
|---|---|
| **mTOR** – serine/threonine kinase | **m TOR** – serine/threonine kinase |
| **raptor** - scaffold protein overseeing assembly, localisation and substrate binding of mTORC1 | **rictor** – scaffold protein overseeing the assembly and substrate binding of mTORC2 |
| **pras40** - mTORC1 inhibitor | **mSin1** – scaffold protein overseeing the assembly of mTORC2 and its interaction with SGK1 |
| **deptor** - mTOR inhibitor | **protor1/2** – increase mTORC2-mediated activation of SGK1 |
| **m LST8** – unknown function | **deptor** – mTOR inhibitor |
| **Tti1/Tel2** – scaffold protein overseeing the assembly and stability of mTORC1 | **mLST8** – essential for mTORC2 activity |
| | **Tti1/Tel2** – scaffold protein overseeing the assembly and stability of mTORC2 |

**Table 1.1** ***Proteins comprising the mTORC1/2 complexes and their function.*** *Adapted from (Laplante and Sabatini, 2012) Laplante and Sabatini 2012*

Effects of rapamycin on the mTOR pathway are quite complicated and not yet fully understood however one of its mechanisms of action could be via the binding of intracellular 12kDa FK506-binding protein (FKBP12) protein to mTORC1 and not mTORC2 of the mTOR complex (Sabatini et al., 1994, Brown et al., 1994). It is suggested that this binding might contribute to

compromised structural integrity (Kim et al., 2002, Yip et al., 2010) and decreased activity of the kinase domain (Brown et al., 1994, Burnett et al., 1998) of mTORC1, which is acutely sensitive to rapamycin, nonetheless, it is still unclear as to how the formation of the FKBP12-rapamycin complex occurs.

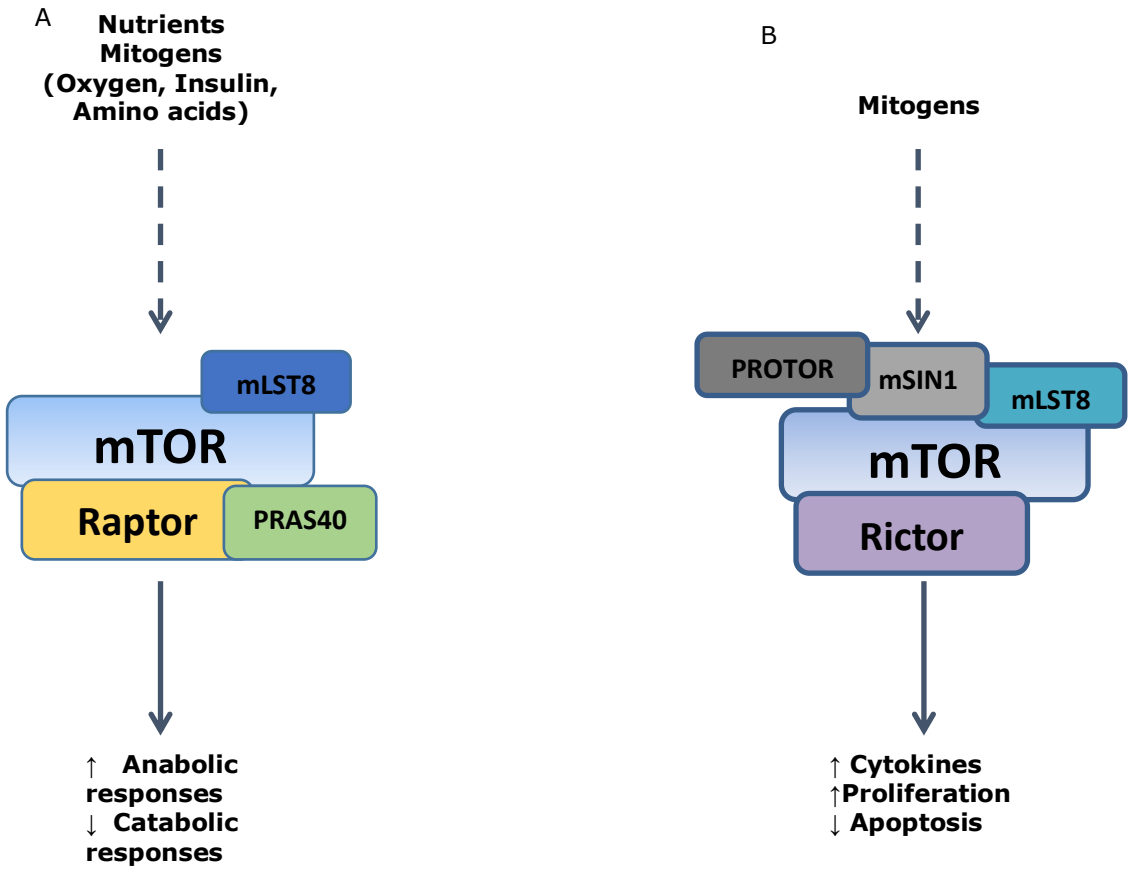



**Figure 1.2** ***Diagramatic illustration of the mTORC1 and mTORC2 complexes.*** *(A) mTORC1 and (B) mTORC2 consisting of their adaptor proteins. The presence of nutrients or mitogens elicits different downstream responses by the two complexes.*

### 1.4.1 mTORC1

The better characterised mTORC1 of the mTOR complex is sensitive to various intracellular and extracellular signals such as growth factors, stress, amino acids, oxygen and energy status. In the presence of these stimuli, the heterodimer comprising of hamartin (also referred to as TSC1) and tuberin (also referred to as TSC2), an upstream regulator of mTORC1 (Inoki et al., 2002), function as a GTPase-activating protein (GAP) for the Ras homolog enriched in brain (Rheb). As a Rheb GAP, the heterodimer complex negatively regulates mTORC1 by converting Rheb from its active GTP bound state to the inactive GDP form (Inoki et al., 2003a, Tee et al., 2003, Inoki et al., 2002, Garami et al., 2003). Although the GAP domain is present only in tuberin and evidence of mutations in the GAP domain have resulted in inability of TSC1/2 complex to fully inactivate Rheb; mutations of hamartin still clinically present tuberous sclerosis of a lesser severity (Dabora et al., 2001, Nellist et al., 2005). Growth factors such as insulin and insulin-like growth factor 1 (IGF1) are other upstream signals transmitted via TSC1/2 that regulate activity of mTORC1 via stimulation of the PI3K and Ras pathways (Inoki et al., 2002, Manning et al., 2002, Potter et al., 2002). Several other upstream regulators, listed in Table 1.2, impinge on mTORC1 via TSC1/2 and regulate its downstream activity.

#### 1.4.1.1 Upstream regulators of mTORC1

The upstream regulators of mTORC1 are enlisted in Table 1.2.

| Pathway | Effector kinase | Mechanism of action |
|---|---|---|
| PI3K and Ras pathways | Protein kinase B (Akt/PKB), extracellular-signal-regulated kinase 1/2 (ERK1/2) and ribosomal S6 kinase (RSK1) | Inactivate TSC1/2 complex by phosphorylation and thus activate mTORC1 (Inoki et al., 2002, Ma et al., 2005, Potter et al., 2002) |
| TNFα signalling pathway | Inhibitor of nuclear factor kappa-B kinase subunit beta (IKKβ) | Inhibition of TSC1/2 through phosphorylation of TSC1 thereby activating mTORC1 (Lee et al., 2007) |
| Wnt signalling pathway | Inhibits glycogen synthase kinase 3β (GSK3-β) | Activation of mTORC1 via un-phosphorylation of TSC2 thus causing inhibition of TSC1/2 (Inoki et al., 2006) |
| Hypoxia and DNA damage | Adenosine monophosphate-activated protein kinase (AMPK) | Phosphorylates TSC2, increasing its GAP activity and inactivates mTORC1 (Inoki et al., 2003b) |
| | Regulation of DNA damage response 1 (REDD1) | Releases TSC2 from inhibitory proteins thereby activating TSC1/2 and inactivating mTORC1 (DeYoung et al., 2008) |
| DNA damage | Induces expression of Tsc2 and phosphatase and tensin homolog deleted on chromosome 10 (Pten) | Downregulation of PI3K-mediated mTORC1 activity and activates AMPK (Feng et al., 2005, Stambolic et al., 2001) |

**Table 1.2** ***Upstream regulators of mTORC1.*** *Effector kinases involved in pathways upstream of mTORC1 activate or inactivate TSC1/2 complex via its phosphorylation at several sites on either tuberin or hamartin thus regulating mTORC1 activity in normal cells.*

#### 1.4.1.2 Downstream processes of mTORC1

mTORC1 is a regulator of several cellular anabolic and catabolic processes including, protein synthesis, lipid synthesis, cholesterol synthesis, cellular metabolism and autophagy (Figure 1.3).

Protein synthesis is the most well documented downstream process that is regulated by mTORC1 wherein, mTORC1 activates protein synthesis by

directly phosphorylating the translational regulators eukaryotic translation initiation factor 4E (eIF4E), binding protein 1 (4E-BP1) and S6 kinase 1 (S6K1) (Ma and Blenis, 2009, Hay and Sonenberg, 2004, Gingras et al., 2001). S6K1 is a regulator of cell size, protein translation and cell proliferation (Holz, 2012) which is activated through various effectors via mTORC1 that leads to mRNA biogenesis, initiation of translation and elongation (Tang et al., 2001, Wang et al., 2001). Phosphorylation of 4E-BP1 occurs via mTOR on four sites, two of which are sensitive to rapamycin (Choo et al., 2008).

Inhibition of mTORC1 with rapamycin leads to changes in mRNA levels of metabolic enzymes involved in glycolysis, amino acid, sterol, lipid and nucleotide metabolism (Peng et al., 2002). In response to insulin, mTORC1 acts through the sterol regulatory element binding protein 1/2 (SREBP1/2) by converting its inactive form localised in the endoplasmic reticulum to the active form which travels to the nucleus and activates transcription of genes that control fatty acid and cholesterol synthesis (Duvel et al., 2010, Porstmann et al., 2008). Induction of lipid synthesis by mTORC1 occurs via activation of SREBP-1 through S6K1 and via the activation of peroxisome proliferator-activator-γ (PPARγ), a major regulator of adipogenesis (Li et al., 2011, Wang et al., 2011, Kim and Chen, 2004, Zhang et al., 2009).

Cellular metabolism is another important process positively controlled by mTORC1 since inhibition of mTORC1 reduces mitochondrial membrane potential, oxygen consumption and ATP production (Schieke et al., 2006).

Studies have shown that inhibition of mTORC1 decreases glycolysis which normally activates the transcription and translation of hypoxia inducible factor 1α (HIF1α) increasing glycolytic flux (Figure 1.3) (Duvel et al., 2010, Hudson et al., 2002, Zhong et al., 2000). Cunningham and colleagues also reported that mTORC1 enables the interaction of PPARγ coactivator 1α (PGC1α) and transcription factor Ying-Yang 1 (YY1) which in turn increases mitochondrial DNA content and oxidative function (Cunningham et al., 2007).

Besides the enlisted anabolic functions of mTORC1; mTORC1 also negatively regulates the self-degradative process in cells, autophagy. Nutrient starvation, oxidative stress and infection causes upregulation of autophagy, required for the recycling of damaged organelles and general cellular housekeeping (Codogno and Meijer, 2005). In a nutrient-dependent manner, mTORC1 regulates autophagy by directly phosphorylating ULK1 and Atg13 from the UKL1/Atg13/FIP200 complex, in turn supressing it (Ganley et al., 2009, Hosokawa et al., 2009).

### 1.4.2 mTORC2

Not much is known about the function, upstream signals and downstream targets of mTORC2, however as originally thought (Jacinto et al., 2004, Sarbassov et al., 2004), mTORC2 is not completely insensitive to rapamycin since chronic rapamycin treatment does reduce mTORC2 signalling by supressing its assembly in certain cell types (Sarbassov et al., 2006). Active mTORC2 is important for cell survival, metabolism,

proliferation and cytoskeletal organisation (Figure 1.3). Phosphorylation activates mTORC2 which in turn controls several kinases including Akt, regulating cellular metabolism, survival, apoptosis, growth and proliferation (Sarbassov et al., 2005, Garcia-Martinez and Alessi, 2008); serum and glucocorticoid-induced protein kinase 1 (SGK1) (Garcia-Martinez and Alessi, 2008), controlling ion transport and growth in cells and protein kinase C-α (PKC-α), responsible for cytoskeletal organisation (Jacinto et al., 2004, Sarbassov et al., 2004).

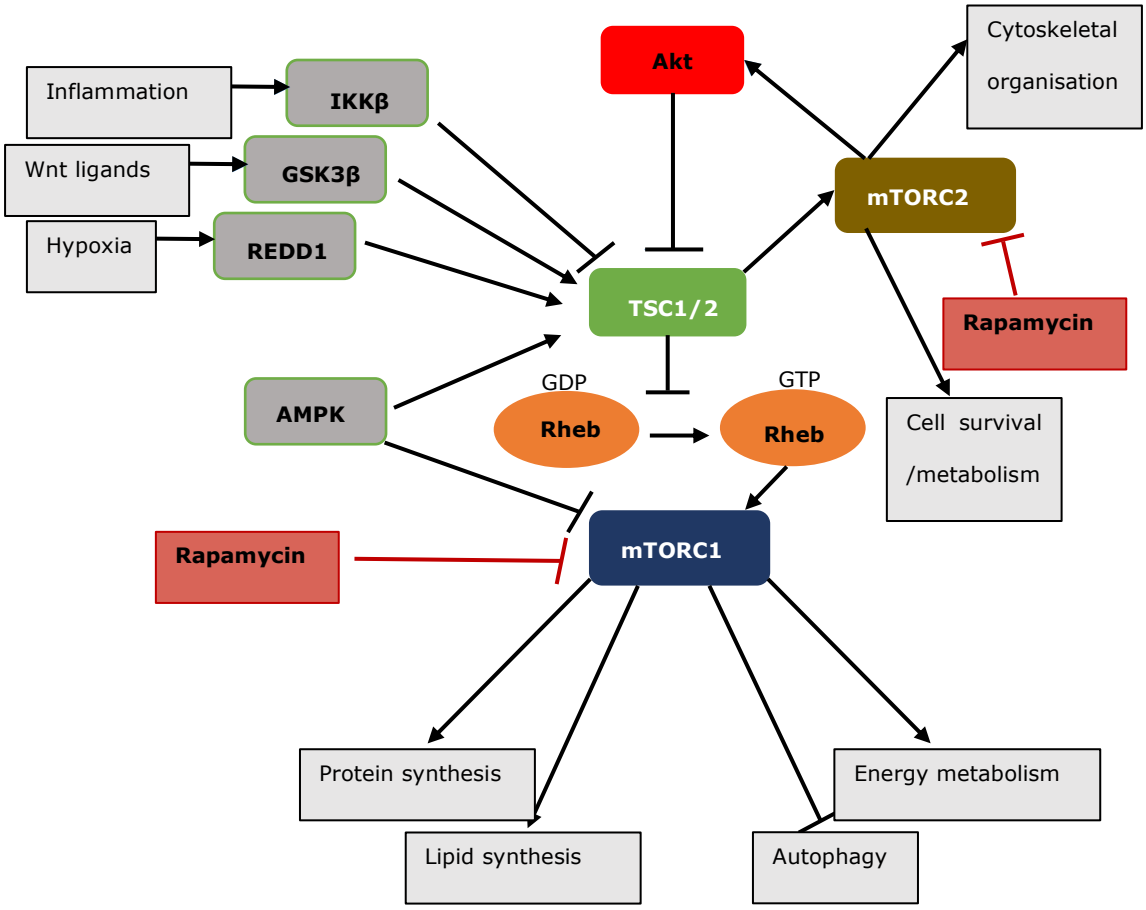



**Figure 1.3** ***The m TOR pathway.*** *Activation of mTORC1 leads to protein and lipid synthesis and thereby cell growth and proliferation whereas activation of mTORC2 results in phosphorylation of Akt. Inflammation, growth factors and hypoxia affect the status of the TSC1/2 complex. mTORC1 is acutely sensitive to inhibition by rapamycin while mTORC2 is inhibited after prolonged exposure.*

## 1.5 Current theories on pathogenesis of LAM

LAM has now been classified as a low-grade malignant neoplasm by the World Health Organisation (WHO) and is listed as a neoplasm similar to PEComas (Chottanapund et al., 2013). The notion that LAM cells are malignant comes from the fact that when transplant lungs from male donors were donated to female LAM patients the recipient's LAM cells had invaded the donor lungs (Karbowniczek et al., 2003, Rozenchan et al., 2009). Furthermore, LAM cell clusters consisting of LAM cell aggregates covered by lymphatic endothelial cells have been detected in blood and chylous fluid and *TSC2* null LAM cells were identified in body fluids of more than 90% of patients (Mitani et al., 2009).

mTOR pathway dysregulation results in abnormal proliferation of LAM cells. Hamartin and tuberin, the two proteins encoded by *TSC1* and *TSC2* genes regulate the intracellular serine/threonine kinase mTOR signalling pathway which in turn regulates cell size, proliferation and survival (Laplante and Sabatini, 2012). The loss of tuberin results in the accumulation of active Rheb-GTP which results in stimulation of mTOR, phosphorylation of S6 kinase and eukaryotic initiation factor 4E-binding protein resulting in increased translation, cell size and proliferation (Shekhar et al., 2001).

Oestrogen has been a suspect in the pathogenesis of LAM as it occurs almost exclusively in women (McCormack, 2008). Moreover, cells within the LAM lung nodules and AMLs express oestrogen and progesterone receptors (Logginidou et al., 2000), LAM first occurs at a premenopausal age (Benton et al., 2014) and pulmonary symptoms of LAM worsen during

pregnancy (Cohen et al., 2009). Although the exact role of oestrogen in the pathogenesis of LAM is yet to be determined, in vitro and animal data have shown that proliferation of the *TSC2 null* rat ELT3 cells and human AML *TSC2 null* cells is elevated in the presence of oestrogen and so is the growth of subcutaneous tumours in animal models of TSC (Yu et al., 2004, Yu et al., 2009, Glassberg et al., 2008).

One of the hypothesis of cyst formation in LAM is that the proliferating cells produce collagen and elastic fibre degrading proteases leading to cystic lesions (Henske and McCormack, 2012). This may result from elevated matrix metalloproteinase (MMP) activity in the lungs. LAM nodules have been shown to express MMPs-2, -9, -1, -13, -14 and reduced levels of MMP inhibitor tissue inhibitor of metalloproteinases 3 (TIMP3) (Matsui et al., 2000a, Zhe et al., 2003, Ludwig et al., 2013). Expression of cathepsin K has also been detected in LAM nodules which together with MMPs could lead to degradation of collagen and elastic fibres (Chilosi et al., 2009). Thus an imbalance between such proteases and their endogenous inhibitors could contribute to destruction of lung parenchyma (Goncharova et al., 2012) (Figure 1.4).

Elevated serum VEGF-D levels have been associated with the severity of lung disease and lymphatic spaces are present in LAM lung nodules (Young et al., 2013b, Radzikowska et al., 2015, Chang et al., 2012). Moreover, expression of vascular endothelial growth factor receptor 3 (VEGFR-3) and other lymphatic markers have also been detected in LAM lung nodules. Thus it was proposed that disorganised lymphangiogenesis could result in

formation of cysts (Henske and McCormack, 2012, Booth et al., 2012, Davis et al., 2013) (Figure 1.4).

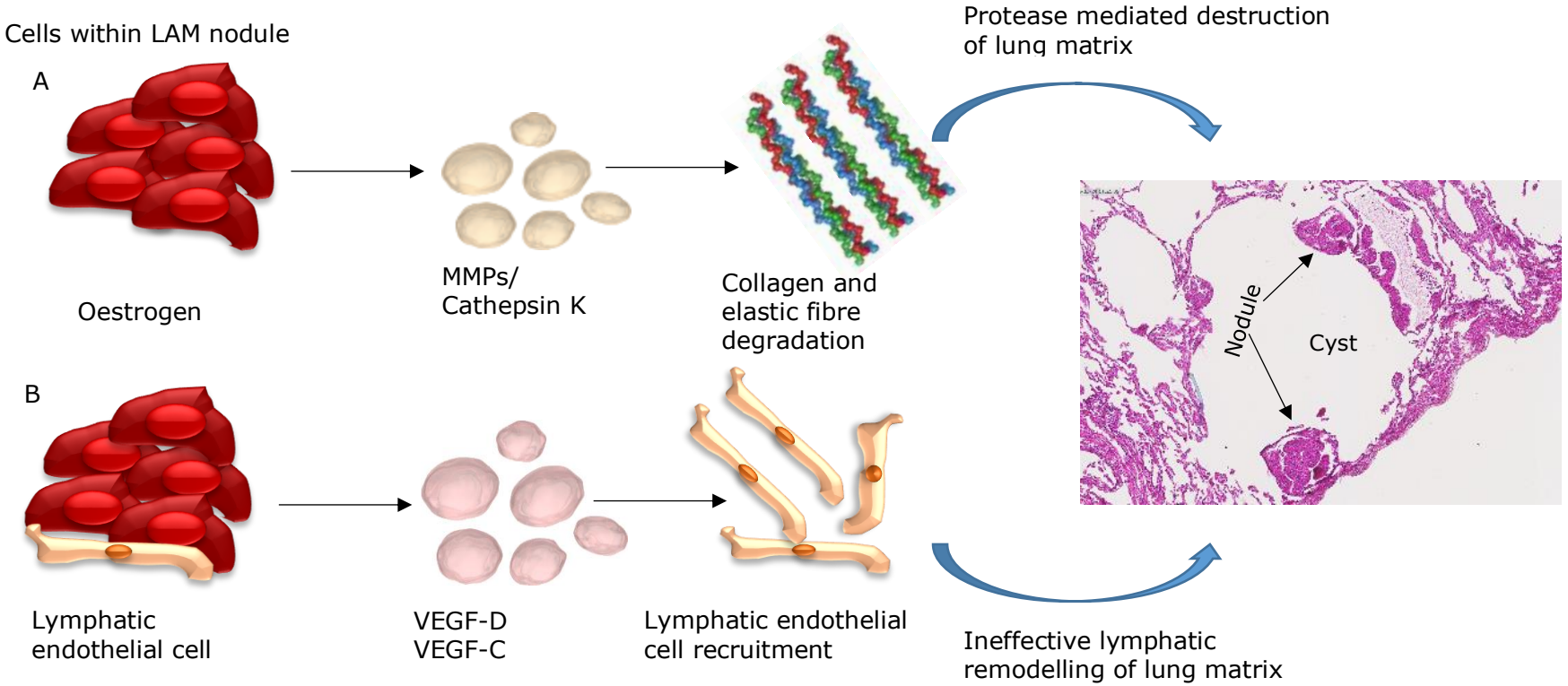



**Figure 1.4** ***Proposed mechanisms of LAM pathogenesis.*** *Diagrammatic illustration of mechanisms of cyst formation in LAM lung. Oestrogen is ubiquitious as LAM occurs mainly in women. (A) Cells wihtin LAM nodules secrete proteases including MMPs and cathepsin K which can degrade extracellular matrix thereby leading to airspace enlargement. (B) Cells within LAM nodule express lymphangiogenic growth factors VEGF-D and VEGF-C thereby recruiting lymphatic endothelial cells driving the formation of lymphatic chanes distorting the lung architecture.*

## 1.6 Current treatments for LAM

### 1.6.1 Hormone Therapy

Commonly prescribed hormone regimens for patients with rapidly progressing LAM are 400mg monthly intramuscular injection or a daily oral dose of medroxyprogesterone at 10mg to 20mg (Johnson, 2006). However commonly occurring side effects of progesterone including bloating, fluid retention and nausea can be severe enough to stop treatment. Recently two studies have shown no benefit in lung function decline and a significant reduction in the rate of $DL_{CO}$ in the treated patients compared to the untreated (Taveira-DaSilva et al., 2004, Johnson and Tattersfield, 1999). Progesterone treatment may be associated with the occurrence of meningiomas in LAM (Moss et al., 2001b).

Bilateral oophorectomy and ovarian irradiation which were the generally used anti-oestrogen therapy options are no longer recommended since the long-term benefits of these treatments is unknown. Moreover, the risk of cardiovascular disease and osteoporosis was elevated in light of these treatments (Johnson, 2006). Tamoxifen, a partial oestrogen receptor antagonist and used as an anti-oestrogen therapy, seems to exacerbate the disease in some patients (Ryu et al., 2006). Gonadotropin-releasing hormone agonists have also been used, however their benefits remain uncertain (Desurmont et al., 1996). An analogue of the gonadotropin-releasing hormone, triptorelin, examined by Harari et al in 11 LAM patients did not show amelioration in the decline in lung function or disease progression, instead it had a detrimental effect on bone mineral content (Harari et al., 2008). TRAIL (Trial of Aromatase Inhibition in LAM) recent

clinical trial undertaken with post-menopausal women receiving an aromatase inhibitor, letrozole (Francis X McCormack, P.I., Cincinnati, OH, USA), on the basis that in post-menopausal women aromatase inhibitors can supress endogenous oestrogen secreted from the adrenal glands (Riemsma et al., 2010). However, there is still a need for much research and clinical trials of pre-menopausal women, the main targets of LAM.

### 1.6.2 mTOR inhibitors

Treatment with rapamycin (Sirolimus) and its analogues are now the treatment of choice for LAM patients suffering from the severe form of the disease (McCormack et al., 2011). The rationale for initial clinical trials of sirolimus was based on the fact that the upstream TSC1/2 complex negatively regulates mTOR (Tee et al., 2002) and that cell size and number is regulated by downstream targets , p70 S6 and 4E-BP1 (Tee et al., 2002, Goncharova et al., 2002). An immunosuppressant, sirolimus forms a complex with FKBP-12 and acutely inhibits mTORC1 whereas mTORC2 is inhibited only after prolonged use (Sarbassov et al., 2006, Zeng et al., 2007, Foster, 2009, Toschi et al., 2009). Patients with TSC or sporadic LAM having AMLs showed a decrease in tumour size by half when treated with sirolimus for a year while some other patients showed an improvement in lung function (Bissler et al., 2008). Treatment withdrawal however, causes the tumours to regain size and some reports have suggested that sirolimus inhibits rather than improve lung function (Davies et al., 2008). Thus

treatment with sirolimus does not have uniform outcomes with every patient.

Several LAM clinical trials using sirolimus were undertaken with differing end points. These are listed in Table 1.3

| Name of trial | Desired end point | Patient criteria | Outcome | Conclusion |
|---|---|---|---|---|
| **CAST** (The Cincinnati Angiomyolipoma Sirolimus Trial) | Proof of principle trial to determine if sirolimus could reduce size of AMLs (Bissler et al., 2008) | Renal tumours ≥1cm treated for 1 year with sirolimus and 2nd year off therapy | AML volume decreased by 50%; FEV1 and FVC increased by 10% and 15%. However off therapy AML size returned; FEV1 and FVC above baseline | No conclusions on the efficacy of sirolimus in LAM |
| **TESSTAL** (Trial of the Efficacy and Safety of Sirolimus for Renal Angiomyolipomas in patients with TSC and Sporadic LAM) (Davies et al., 2008) | Decrease in size of AML in LAM patients | Men and women with AML of at least 2cm diameter having TSC or sporadic LAM | Did not show any definite trend towards improvement | Inconclusive |
| **RAD001 angiomyolipoma Trial** (Phase I/II) | Size reduction in AML | Patients between 18-25 years; AML should be ≥1cm | Patients will be considered responders if their AML volume decreases by 30% or more from baseline and if their AML decreases by 75% or more. | Study completed but no results are available |
| **Long term follow up for RAD001** therapy of AML in TSC and LAM patients | Inhibition of growth of AML and regression | Patients between 18-35 years; AML should be ≥1cm | Tolerance to RAD001 was studied and reduction of AML per year treatment was measured | Study completed but no results are available |

| | | | | |
|---|---|---|---|---|
| **Sirolimus Therapy for AML in TSC and Sporadic LAM(Davies et al., 2011)** | Primary outcome, change in the size of renal AMLs measured by MRI; Secondary outcome, safety, neurocognitive and pulmonary function | Patients aged 18 to 65 and should have had at least one renal AML of 2cm diameter or more | 50% of AMLs responded to treatment. 41 out of 48 AMLs were smaller than baseline measurements | Study showed regression of AML in patients receiving drug for 2 years |
| **EXIST-2** (Efficacy and safety of RAD001 in patients with AML associated with TSC or sporadic LAM) (Phase III) | Primary outcome is time to AML progression measured by MRI; secondary outcome includes changes in skin lesions, renal function and biomarkers | Patients must be 18 years and over and have an AML of at least 3cm in diameter | 42% of patients with AMLs responded to treatment; time to AML progression, was statistically significantly longer in patients on everolimus | Everolimus, a rapalog, reduced AML volume with an acceptable safety profile, making it a potential treatment for AML associated with tuberous sclerosis (Bissler et al., 2013) |
| **MILES** (The Multicentre International LAM Efficacy of Sirolimus Trial) (Phase III) | Improvement in lung function (FEV1) and whether benefits of sirolimus outweigh risks | Patients should be 18 years or older, have a definite diagnosis with a VEGF-D level of at least 800pg/ml and a FEV1 of 70% or less | VEGF-D levels reduced at 6 and 12 months in treated group compared to placebo; 65% patients showed improvement in FEV1 at 12 months | Serum VEGF-D could be a possible marker of severity of LAM disease and could inform the risk-benefit analysis of sirolimus therapy (Young et al., 2013a). |

**Table 1.3** ***Clinical trials for LAM conducted using rapamycin and its analogues with varying outcomes. Trial information obtained from (ClinicalTrials.gov)***

Synergistic inhibition of mTORC1 using sirolimus and the MAPK pathway has been reported to be more efficient in inhibiting proliferation of $Tsc2^{-/-}$ cells in mice (Mi et al., 2009). Rheb inhibition by the Ras inhibitor farnesyl-thiosalicylic acid inhibits proliferation and migration of $Tsc2^{-/-}$ ELT3 cells and reduces growth of tumours *in vivo* by reducing Rheb and Rheb-GTP. This suggests that Rheb is a possible alternative target in inhibiting the mTOR pathway (Makovski et al., 2012).

### 1.6.3 Matrix metalloproteinase inhibitors

Primarily a tetracycline antibiotic, doxycycline has been shown to inhibit MMPs outside of its antimicrobial activity (Hanemaaijer et al., 1998) and in some cells it directly inhibits catalytic activity of MMPs or activation of pro-MMPs resulting in diminished or loss of enzymatic activity (Smith et al., 1996). MMPs are present within LAM lesions and may play an important role in causing cystic lung destruction making them a potential therapeutic target (Matsui et al., 2000a, Ji, 2006).

Decreased urinary levels of MMPs with an improvement in lung function was reported in one patient with LAM being treated with doxycycline (Moses et al., 2006). Pimenta et al reported a decrease in serum levels of MMP2 and 9 in 34 patients being treated with doxycycline (100mg/day) for 6 months (Pimenta et al., 2011). In a recent clinical trial undertaken by Prof Simon Johnson, Nottingham, UK 23 female LAM patients were randomised to doxycycline, 100mg/day for 3 months followed by 200mg/day for 21 months or matched placebo. The main endpoint of this

study was improvement in lung function of treated patients compared to placebo. Although urine levels of MMP9 were significantly decreased, there was no improvement in FEV1 decline between the two patient groups with the drug having no effect on FVC as well thus making it unlikely that doxycycline has any beneficial effect in LAM (Chang et al., 2014).

## 1.7 LAM lesions and the LAM lung phenotype

Lesions in the LAM lung consist of nodules or clusters of LAM cells surrounded by cystic lesions and lymphatics. Within these nodules, LAM cells develop as spindle-shaped – proliferative and express α-smooth muscle actin (αSMA), vimentin, desmin, proliferating cell nuclear antigen (PCNA) and Ki-67; or epitheloid cells – expressing smooth muscle antigens along with melanoma makers, namely, gp100, MART-1, CD63 and PNL2 (Zhe and Schuger, 2004, Hoon et al., 1994). Origins of LAM cells are unknown, however although they express immunophenotypically distinct markers it is possible they originate from a common progenitor having a possible neural crest origin due to the expression of melanocytic markers (Henske and McCormack, 2012). In many cases LAM cells also express oestrogen and progesterone receptors and can be termed as a perivascular epithelial cell or PEC (Martignoni et al., 2010, Juvet et al., 2007).

Proliferative hyperplastic type II pneumocytes coat the LAM nodules and appear to have apical microvilli and cytoplasmic projections (Matsui et al., 2000d). Lymphatic endothelial cells (LEC) also present in the nodule were first identified by their expression of VEGFR-3 and podoplanin. These LECs are seen lining the lymphatic channels and surrounding LAM cell clusters

(Kumasaka et al., 2005). Presence of mast cells in the nodules was also detected by expression of c-Kit, highly expressed by mast cells (Edwards et al., 2005).

It has been a challenge trying to isolate and successfully grow LAM cells from explants of lung tissue obtained at the time of transplant or from biopsies. All of the approaches have failed to yield a homogenous population of LAM cells showing LOH at the *TSC2* locus, thus yielding a mixed population of cells with and without the genetic features of LAM cells (Darling et al., 2010). Pacheco-Rodriguez et al found that CD44v6, a product of alternative splicing of CD44 was only expressed in the sub-population of cells associated with LOH of the TSC2 gene in the nodule (Pacheco-Rodriguez et al., 2007). This class I transmembrane glycoprotein associated with tumour metastasis (Heider et al., 2004) enabled sorting of the TSC2 null cell population, however, the antibody used for isolation also prompts cells death, preventing efforts to grow a pure population. However, a recent study conducted by Ando et al designed a fluorescence-activated cell sorting-based method for isolating LAM cells from LAM-affected lung tissue. Using a combination of antibodies including epithelial cell adhesion molecule (EpCAM), podoplanin, CD34 and CD90 they were able to identify HMB45 positive cells possessing a *TSC2* LOH. These cells were viable and amenable to subsequent cell culture and were believed to be LEC-like (Ando et al., 2016).

Akin to cancer cells, LAM cells also express chemokines and their receptors with an increased expression of C-X-C chemokine receptor type 4 (CXCR4)

detected in LAM tissue and in AML cells derived from LAM patients (Clements et al., 2010). Expression of C-C chemokine receptor type 3 (CCR3) (chemotaxis), CX3C chemokine receptor 1 (CX3CR1), CXCR4 (homing to lungs) and CXCR6 (proliferation) was found on AML cells and LAM tissue. Ligands for these receptors result in the phosphorylation of Akt and MAPK in turn promoting the mTOR pathway. Moreover, CXCL12, the only known ligand for CXCR4, was found to be expressed in type II pneumocytes surrounding LAM nodules in the lung and vascular endothelial cells in AMLs suggesting that it may act as a chemoattractant for circulating LAM cells (Clements et al., 2010). Metastatic attributes of LAM cells are enlisted in Table 1.4

| **Mutations or markers in LAM cells** | **Mechanisms** |
|---|---|
| Loss of heterozygosity of TSC2 | Activation of mTOR pathway causing increased cell growth and proliferation (Carsillo et al., 2000, Yu et al., 2001) |
| Oestrogen receptor (ERα) | Promotes cell proliferation, lung colonisation and MMP activation (Yu et al., 2009) |
| Chemokines and receptors | Increased migration, homing and stromal and LAM cell interactions (Clements et al., 2010, Pacheco-Rodriguez and Moss, 2010) |
| Matrix metalloproteinases | Enable invasion of LAM cells by degradation of extracellular matrix (Yu and Henske, 2010) |
| CD44v6 | Inhibition of apoptosis by binding to Fas ligand (Pacheco-Rodriguez et al., 2007) |
| CD9 | Invasiveness, adhesion and cell interactions (Cai et al., 2010) |

**Table 1.4** ***Metastatic mechanisms in LAM.*** *Adapted from Grzegorek et al 2013*

## 1.8 Fibroblasts

Fibroblasts are a type of mesenchymal cell and are an integral part of the most important tissue that holds the human body together – connective tissue. The connective tissue consists of a vast extracellular matrix (ECM) interspersed with fibroblasts which are responsible for the production of ECM structural proteins Fibroblasts are ubiquitious, elongated cells with extended cell processes showing a spindle-like shape and are often identified based on their distinct shape (Son et al., 2006). Nevertheless, they remain poorly defined in molecular terms and a limiting factor to studying fibroblasts is the lack of a reliable and specific molecular marker. Despite this fact, a panel of site-specific markers can be used to identify a fibroblast phenotype which include vimentin, α smooth muscle actin (αSMA), fibroblast activation protein (FAPα), fibroblast surface protein (FSP), desmin and cluster differentiation 90 (CD90) (Kalluri and Zeisberg, 2006).

Pulmonary fibroblasts are usually present in the adventitia of vascular structure and airways. Fibroblasts are chemotactic and can be recruited in response to cytokines which is well characterised in the wound healing response. The source of these fibroblasts has given rise to a few theories but the most accepted one is that a bone-marrow derived mesenchymal progenitor known as the fibrocyte gives rise to new populations of fibroblasts (Bellini and Mattoli, 2007). A terminally undifferentiated cell, fibroblasts have the potential of being activated and can differentiate into other mesenchymal cells such as the myofibroblasts (Schmitt-Gräff et al., 1994). Myofibroblasts are mainly found in disease and are thought to

differentiate from resident fibroblasts or epithelial cells via epithelial-mesenchymal transition (EMT) (Hynes, 2009, Cirri and Chiarugi, 2011). The myofibroblast phenotype is the result of the appropriate stimulus and is characterised by the expression of αSMA (presence of aligned actin fibres), contractile and having a greater rate of ECM synthesis (Ogawa et al., 2006, Phan, 2008). However, there is evidence to suggest that on withdrawal of the stimulus, myofibroblasts can lose their stress fibres and switch back into fibroblasts (Wicks et al., 2006). This suggests that both fibroblasts and myofibroblasts can be in existence at any given time (Figure 1.5).

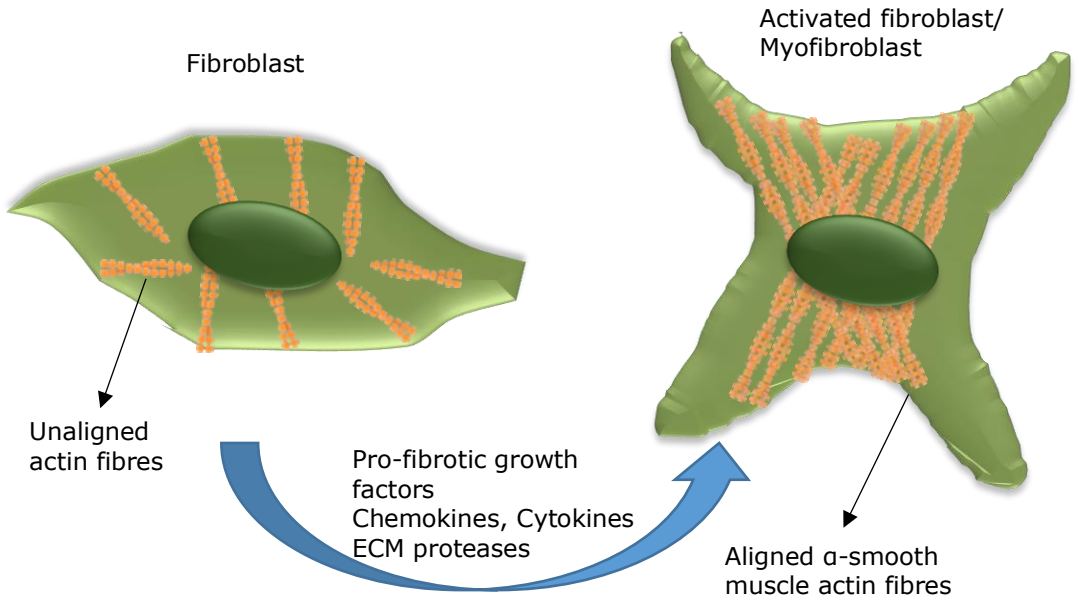



**Figure 1.5** ***Diagrammatic illustration of non-activated and activated fibroblasts.*** *Non-activated fibroblasts have a prominent cytoskeleton with unaligned intermediate actin fibres. Upon the right pro-fibrotic stimulus fibroblasts become activated and similar to myofibroblasts are often characterised by their expression of αSMA.*

Fibroblasts and their phenotypes play several other important roles in health and disease. Fibroblasts are mainly responsible for ECM turnover and the same fibroblasts that produce the ECM are also responsible for matrix degradation (Kendall and Feghali-Bostwick, 2014). Several matrix degrading proteases such as matrix metalloproteinases (MMPs), cysteine proteases (cathepsins) and serine proteases are expressed by fibroblasts which highlights their vital role in maintaining an ECM homeostasis (Chang et al., 2002, Eck et al., 2009). Via the expression of proteases, fibroblasts play a key role in normal wound healing and in diseases such as idiopathic pulmonary fibrosis (IPF) (Zeidan et al., 2010) and systemic sclerosis (SSc) (Hatherell et al., 2011). Fibroblasts isolated from sites of wound healing and fibrosis are 'activated' a phenomenon which can be induced by transforming growth factor-β (TGFβ). Once the wound is healed, the number of activated fibroblasts reduce and the non-activated fibroblast phenotype returns. However, similar to fibroblasts associated with IPF, fibroblasts within a tumour stroma perpetually remain in an activated state. These fibroblasts acquire a highly proliferative modified phenotype similar to that of myofibroblasts and produce increased levels of ECM-degrading proteases and are known as cancer-associated fibroblasts (CAFs) (Kalluri and Zeisberg, 2006, Zeisberg et al., 2000).

Several paracrine signalling factors such as platelet-derived growth factor (PDGF), TGFβ, interleukin 6 (IL-6) and 13 (IL-13), fibroblast growth factor (FGF) and tumour necrosis factor alpha (TNFα) to name a few, that enable the activation of fibroblasts (Kendall and Feghali-Bostwick, 2014). Activated fibroblasts and CAFs show an elevated secretion of MMPs such

as MMPs-2, -3, -9, -13 and -14 some of which serve to activate other MMPs enabling remodelling of the ECM (Camp et al., 2011, Hutchinson and Kirk, 2011, Knight and Przyborski, 2015). Several cysteine cathepsin proteases are known to be expressed by CAFs and activated fibroblasts in various disease conditions. For example, cathepsins K and S are elevated in synovial fibroblasts from rheumatoid and osteoarthritis patients and there is evidence to suggest that cathepsin K is involved in joint destruction in these patients (Hou et al.). Cathepsin K has been implicated in ECM degradation in lung fibrosis (Buhling et al., 2004b) and cathepsins K, L and S are elevated in pulmonary emphysema (Cheema et al., 2003). CAFs can capture released proteases thus enabling ECM digestion and invasion (Masson et al., 2011). Besides MMPs and cysteine proteases, CAFs associated with breast and colon cancer also express urokinase-type plasminogen activator (uPA) and its receptor uPAR, which are responsible for the activation of plasminogen to plasmin (Edmondson et al., 2014)

Activated fibroblasts secrete elevated levels of transforming growth factor beta 1 (TGFβ1), interleukin 1β, interleukin 33, C-X-C motif and C-C motif chemokines thereby playing a role in inflammation and immune cell recruitment (Miki et al., 2012, Blom et al., 2016, Holt et al., 2010). C-X-C motif chemokine 12 (CXCL12) or stromal cell-derived factor 1 (SDF-1) secreted by CAFs promotes tumour growth by inducing angiogenesis and enhancing proliferation of cancer cells (Orimo et al., 2005). The expression of CXCL12 is also responsible for the recruitment of fibroblasts towards the corresponding receptors C-X-C motif chemokine receptor type 4 and 7

usually expressed by cancer cells (De Wever and Mareel, 2003, Suzuki et al., 2004).

Thus, via the expression of several proteases and pro-inflammatory factors the activated fibroblast phenotypes serve three main purposes: (1) direct degradation of ECM associated with disease progression (2) cleavage of other ECM degrading proteases, growth factors, pro-inflammatory factors among others and (3) aiding immune cell recruitment and infiltration and providing a profibrotic stimulus (Holliday et al., 2009, Sethi et al., 2002).

## 1.9 Current models for LAM

### 1.9.1 Animal models

*Eker Rat model*

First described in 1954 by Reidar Eker as an autosomal dominant hereditary model of predisposition to renal adenomas and carcinoma, the Eker rat with genotype *Tsc2*$^{Ek/+}$ causes cystadenoma lesions in the kidney that develop early at 4 months of age (Eker, 1954, Eker et al., 1981). A small percentage of these tumours turn malignant and occasionally metastasize to lungs, pancreas and liver. Despite the occurrence of these tumours in the kidneys, the main organ involved in AMLs in TSC and LAM patients, there is no pathological relationship between the cystadenomas and AMLs. Eker rats also develop pituitary adenomas, uterine leiomyomas and leiomyosarcomas (Yeung et al., 1994, Everitt et al., 1992). The model fits the Knudson two-hit hypothesis and LOH occurs with the loss of the wild-type allele which is seen in the renal adenomas, uterine leiomyomas and pituitary adenomas occurring in the rat (Yeung et al., 1995).

Oophorectomy can supress the commonly occurring uterine leiomyomas (Walker et al., 2001) and although ELT3 is a frequently used cell line in TSC and LAM studies isolated from a uterine leiomyoma from the Eker rat, TSC and LAM patients do not develop uterine leiomyomas (Walker et al., 2003). Markers of mTORC1 activation including phospho-S6 and p70S6K are expressed in the renal tumours, consistent with the LOH on the *Tsc2* locus, which are inhibited with a marked decrease in proliferation when treated with rapamycin (Kenerson et al., 2002). Ultrasound imaging of the

renal cystadenomas also showed a decrease in tumour volume when treated with rapamycin. However the main cause of death in these rats was the pituitary adenoma (Kenerson et al., 2005).

*TSC$^{+/-}$ mouse models*

Targeting different coding exons of *Tsc2*, three different knockout alleles of *Tsc2* have been reported with the first two being phenotypically identical (Kwiatkowski, 2010). These *Tsc$^{+/-}$* mice, like the Eker rat, develop renal cystadenomas at 6-12 months of age, which grow throughout their life and about 5-10% develop metastatic disease by 18 months. Liver hemangiomas are a characteristic feature of these Tsc2$^{+/-}$ mice consisting of endothelial and smooth muscle proliferative cells which develop by 18 months of age and can rupture leading to death (Kobayashi et al., 1999). Both renal cystadenomas and liver hemangiomas show LOH in keeping with second hit loss of the wild-type allele (Onda et al., 1999). Increased VEGF levels are noted in both kidney tumours and serum from the Tsc2$^{+/-}$ mice which are increased due to both mTOR-dependent and mTOR-independent pathways (El-Hashemite et al., 2003). Tsc1$^{+/-}$ mouse models have also been developed, but since mainly TSC2 mutations are noted in LAM they are not used as frequently. Tsc1$^{+/-}$ mouse models are enlisted in Table 1.5.

| Gene | Allele name | Main characteristics of animals |
|---|---|---|
| Tsc1 | -,Kwiatkowski | Renal cystadenomas, liver hemangiomas(Kwiatkowski et al., 2002) |
| Tsc1 | -,Hino | Renal cystadenomas, liver hemangiomas(Kobayashi et al., 2001) |
| Tsc1 | -,Cheadle | Renal cystadenomas, liver hemangiomas, reduced survival and kidney cancer in some strains(Wilson et al., 2005) |

**Table 1.5** ***Tsc1$^{+/-}$ mouse models generated.*** *Adapted from Kwiatkowski 2010.*

### 1.9.2 Tumour homograft and xenograft models

Clements et al had successfully generated an animal tumour xenograft model by twice passaging SV7$^{tert}$ AML cells into nude mice resulting in reproducible tumours that expressed ERβ, increased expression of extracellular matrix and smooth muscle related proteins and phosphorylated S6K1. The tumours however did not express the angiomyolipoma marker HMB-45. Although this model is not fully accurate to LAM, it makes a useful tool for screening drugs (Clements et al., 2009). Another homograft model developed recently by Krymskaya et al used Tsc2 null mouse kidney cells twice passaged which show mTORC1 activation, increased proliferation, migration, invasiveness and α-smooth muscle expression similar to LAM cells. Treatment of the mice with a combination of rapamycin and simvastatin resulted in prevention of alveolar airspace enlargement which was seen in vehicle only treated mice and simvastatin treatment alone prevents lesion growth and induces apoptosis (Goncharova et al., 2012). Although this model is not an exact replica of the human LAM disease, it is similar to the disease in many ways.

### 1.9.3 Cellular LAM models

Cellular models for LAM have till date been cells carrying a LOH or allelic imbalance for TSC2. Efforts have been made to isolate LAM lung cells from tissue which have resulted in cells that are positive for HMB-45 and show increased VEGF levels (Black et al., 2005) or cells that are αSMA positive and show hyperphosphorylation of p70S6 and S6 (Goncharova et al., 2008), however it has not been possible to obtain a homogenous population of cells showing LOH on TSC2 and expressing the typical markers of a LAM cell in vivo.

As it was not possible to isolate true 'LAM cells' from the lung researchers then turned their sights to cell derived from angiomyolipomas (AMLs) Arbiser et al produced a stable cell line obtained by sequentially introducing SV40 large T antigen and human telomerase into tumour cells from an AML derived from a sporadic LAM patient. These cells phenotypically resembled human AML cells with regards to microphthalmia-associated transcription factor (MITF) expression, however the cells did not show any mutations in the TSC1 or TSC2 genes (Arbiser et al., 2001). The $SV7^{tert}$ AML cells were deposited on the American Type Culture Collection (ATCC CRL-2461, Manassas, VA) and have been used since mainly in tumour xenograft models (Chang et al., 2010, Clements et al., 2010, Clements et al., 2009).

Cell lines from human AML tissue associated with TSC or LAM patients were then successfully isolated. Smooth muscle-like cells isolated by Lesma et al showed a TSC2 LOH, a lack of tuberin expression and the expression of epidermal growth factor (EGF) and insulin-like growth factor 1 (IGF-1) on

their surface. Studies found that anti-EGFR antibody inhibited proliferation and survivin treatment inhibited apoptosis thus revealing potential drug targets (Lesma et al., 2005, Lesma et al., 2008, Carelli et al., 2007).

A primary culture of cells was isolated from a LAM-associated renal angiomyolipoma in another study. Both TSC2 alleles in this cell line are inactivated through a missense change from DNA sequence G mutant to A at position 1832 of the TSC2 gene along with a loss of heterozygosity. The cells express oestrogen receptor α, oestrogen receptor β and androgen receptor and exposure of these cells to oestradiol and tamoxifen promotes growth (Yu et al., 2004). The described cells are known as 621-101 cells and since their generation, are the most widely used human model cell line for LAM today and have also been used extensively in the current study conducted as a model LAM cell line. Siroky et al, as a part of their studies immortalised the 621-101 cells by transfection of HPV E6/E7 (pLXSN hTERT-hyg). These immortalised cells were then transfected with empty vector (pcDNA3.1) or cDNA corresponding to the TSC2 open reading frame (pcDNA3.1 TSC2-zeo). The resultant cell lines were then called 621-102 ($TSC2^{+/-}$ cells) and 621-103 ($TSC2^{+/+}$ cells).

$TSC2^{-/-}$ cells derived from rodent models have also been developed and are widely used. Similar to the previously described cell lines these cells lack either TSC1 or TSC2 and as a result recapitulate the signalling defect caused by the loss of TSC2 in LAM cells. These cells have therefore been used in several preclinical studies. Mouse embryonic fibroblasts (MEFs) have been isolated from both TSC1 and TSC2 knockout mice despite the

fact that germline activation of both alleles of TSC1 and TSC2 genes in mice is embryonic lethal. Interestingly establishment of TSC2-null MEF lines requires the inactivation of p53 possibly because abrogation of p53 function prevents senescence and/or induces immortalisation of TSC deficiency (Onda et al., 1999, Zhang et al., 2003). Similar to cells arising from TSC-deficient animals and LAM lesions, TSC-null MEFs exhibit upregulation of m TORC1 signalling.

Perhaps the most widely used animal derived cell line is derived from tumours that arose in the Eker rat model described in section 1.9.1. Heterozygous for TSC2 these animals develop tumours in the kidney (renal cell carcinoma, RCC) (Kobayashi et al., 1995, Walker et al., 1992), uterus (uterine leiomyoma) (Everitt et al., 1995) and other areas including spleen and highly vascular areas of the skin which are a source for multiple cell lines (Yeung et al., 1995). One of the most often utilised surrogate cell lines for LAM are the proliferative smooth muscle cell lines isolated from the uterine leiomyomas of the Eker rat, known as the ELT cell lines (Howe et al., 1995). These cells lines are proliferative, TSC2-null, have constitutively active m TORC1 signalling, express oestrogen and progesterone receptors and retain their hormone responsiveness (Hodges et al., 2002).

Reflecting the LAM cell phenotype in vitro, both TSC1 and TSC2 deficient cell lines exhibit upregulation of m TORC1 signalling and growth of these cell lines along with their elevated S6K and S6 phosphorylation, characteristic of dysregulated m TORC1 signalling, is inhibited by

rapamycin and its analogues. These cell lines have therefore been used as surrogate models for LAM cell in preclinical studies for LAM.

## 1.10 In vitro disease models

In vitro cell culture has always been a reliable method for understanding the specific cellular mechanisms in a disease and to screen drug compounds at an early stage. While animal models can capture the complexity of a living system, a clear visualisation of individual steps is challenging and extracting mechanistic data can be difficult. Moreover, animal models may not fully recapitulate the relevant disease entirely and as most models used are rodents, a species difference adds another level of difficulty to the study. In contrast, in vitro models may have a reduced physiological relevance but at the same time allow control of most experimental variables and quantitative analysis is permissible (Katt et al., 2016, Doke and Dhawale, 2015). Often, in vitro models provide preliminary information which can then be used to design an experiment in vivo and in many cases animal testing has been replaced entirely by in vitro cell culture tests (Xu et al., 2000). Various types of cell-based in vitro models have been developed to study various aspects of diseases such as cancer and different lung diseases. These are described in Table 1.6.

| Model type | Study phenomena |
|---|---|
| Co-culture models | Transwell-based models<br>• Cell-cell communication<br>• Migration<br>• Invasion |

| | |
|---|---|
| | • Matrix remodelling<br>• Air-liquid interface<br>• Immune interactions (paracrine signalling)<br><br>Direct contact models<br>• Cell-cell communication<br>• Matrix remodelling<br>• Immune interactions (juxtacrine signalling) |
| 3D scaffold-based models | • Cell-cell communication<br>• Cell-ECM communication<br>• Matrix remodelling<br>• Invasion, angiogenesis |
| Spheroid-based models | • Growth/proliferation<br>• Invasion, angiogenesis<br>• Matrix remodelling<br>• Drug screening<br>• Nutrient/oxygen gradient |
| Ex vivo tissue models | • Invasion<br>• Growth/proliferation<br>• Drug screening |

**Table 1.6** ***Broad classification of in vitro models.*** *In vitro models can be broadly classified co-culture, 3D scaffold-based, spheroid-based and ex vivo models. Different aspects of a disease can be studied with different models (Katt et al., 2016).*

### 1.10.1 Co-culture models

Recently co-culture systems have become of particular interest to researchers. The impetus for using such a model is to study natural interactions between one or more cell populations or improving culturing success for certain populations (Figure 1.6). In principle, a co-culture model is a set-up in which two or more different populations of cells are grown with some degree of contact between them. Highly relevant for research, co-culture models provide a more representative human in vivo-like tissue model than animal models and allow the study of cell-cell interactions. On occasion, certain cell populations cannot be easily mono-cultured however the presence of another cell population can improve the culturing success or cell behaviour (Moir et al., 2011).In cancer biology co-culture models have been used to examine immune interactions and

evaluation of mesenchymal-stromal interactions which can highlight new pathways involved in the disease pathology (Mathur et al., 1977, Glace et al., 2009). Knowledge of these interactions and pathways involved have proven to be an invaluable tool as previously, rigorous testing for function and safety in terms of cell-cell interactions had to be carried out with subsequent optimisation process (Prizant et al., 2013, Ando et al., 2016)

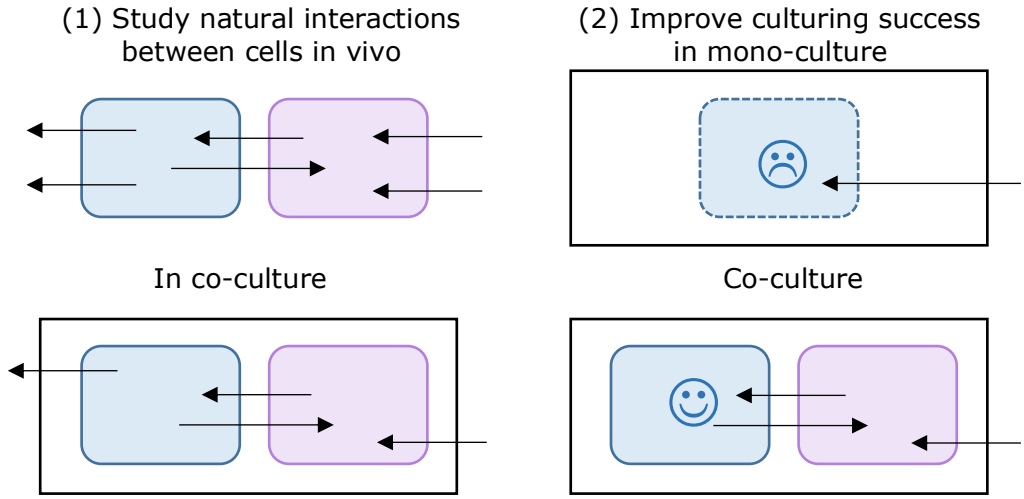



**Figure 1.6** ***Illustration of a co-culture and its advantages.*** *Co-cultures are advantageous for studying in vivo interactions between cells and improving growth conditions for certain cells.*

While designing a co-culture model for a particular disease there are several variables to be considered. A co-culture consisting of a large number of cell types can increase the possibility of complex reaction pathways useful to identify but this can vastly complicate experimental procedure and subsequent quantification of results. In fact, more than three cell populations could lead to unmanageable complexity leading to unpredictability and instability. Therefore most studies have incorporated utmost two cell populations to avoid further complications (Zeidan et al., 2010). Although there are few studies done using three cell populations,

some studies have suggested that larger number of cell populations may not always be advantageous, for example, comparison of mono-, bi-, and tri- culture models of the blood-brain barrier found that a bi-culture performed best in regards to maintaining a barrier function (Hatherell et al., 2011).

Another controlling variable is the degree of separation between the cell populations. Depending on the experimental requirements cell populations within a co-culture could be in indirect (partially separated) or direct (mixed) contact. The appropriate population separation method needs to be carefully chosen ensuring relevance to the ultimate application of the co-culture. Indirect co-cultures enable paracrine signalling allowing for the exchange of soluble factors from one cell type to another while also allowing the user to separate the different cell types for subsequent analysis (Figure 1.7 (a)). This type of a system can be achieved by separating cells using a semi-permeable membrane. Transwell-based models are an example of such a system where one cell type is cultured in the upper chamber on a semi-permeable membrane with a 0.4μm pore size while the other cell type is cultured in the lower chamber. This type of technique allows for cell-cell communication while also allowing separation of the two cell types for subsequent quantification (Goers et al., 2014). Indirect co-cultures using Transwell-based models are used routinely in cancer studies (Heneweer et al., 2005, Miki et al., 2012), to study immune cell responses on other cells such as fibroblasts (Holt et al., 2010) and to model various lung diseases where an air-liquid interface is required (Blom et al., 2016, Adamson et al., 2011). Transwell-based models also known

as Boyden chamber assays can also be used to assess cell migration (Figure 1.7 (b)). These assays incorporate a porous membrane usually between 3 and 12μm and a pore size appropriate to cell size is chosen. Cells undergoing migration are placed in the upper chamber and are allowed to migrate vertically through the pores towards the lower chamber containing an attractant or another cell type. Transwell-based migration assays were first developed to analyse chemotactic responses of leukocytes (Boyden, 1962). However, now they are not only used in measuring immune cell chemotactic migration but also migration of stromal cells to cancer cells (Mognetti et al., 2013) and have also been used to track the chemotactic migration of fibroblasts towards CXCL12 in studying the recruitment of these cells to the LAM nodule (Clements et al., 2015).

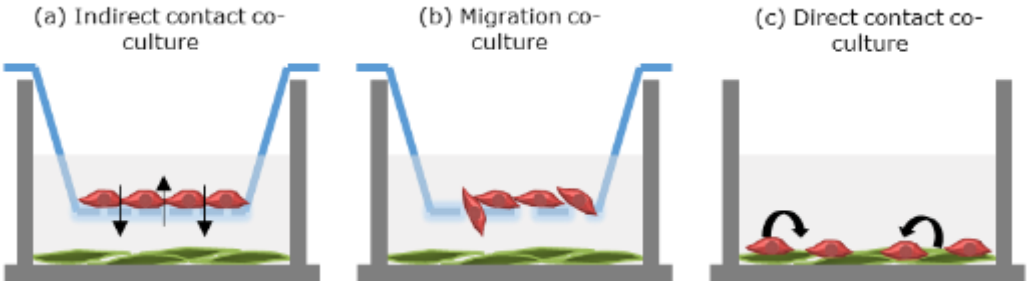



**Figure 1.7** ***Diagrammatic illustration of Transwell-based co-culture models.*** *Figure shows (a) Indirect contact co-culture, (b) Transwell-based migration assay co-culture and (c) direct contact co-culture.*

Cell-cell contact has been reported to play an important role in the pathogenesis of diseases. Invasion of cancer cells occurs via the actions of adhesion molecules such as N-cadherin (De Wever and Mareel, 2003) and proteases such as extracellular matrix metalloproteinase inducer (EMMPRIN) and matrix metalloproteinase 14 (MMP-14) (Suzuki et al.,

2004) which is a result of cellular contact between stromal fibroblasts and cancer cells. This type of a system therefore allows the exchange of juxtacrine signals between cells thereby creating a more in vivo-like environment for modelling a disease. All cell populations within a direct contact co-culture must be maintained under symmetrical conditions and therefore a vast amount of optimisation is required during model design (Goers et al., 2014). Direct contact co-cultures of breast cancer cells and fibroblasts when compared to the indirect contact co-cultures showed that the former had a broader transcriptional response and highlighted more signalling pathways than the latter (Camp et al., 2011). However, the direct contact methodology has various technical difficulties and it is not possible to decipher exactly which responses belong to each cell type and therefore indirect contact co-cultures are often used (Miki et al., 2012).

### 1.10.2 3-dimensional scaffold based models

It has been postulated that the cellular microenvironment profoundly influences cell behaviour, phenotype and evolution. Cells within an organ are not an island, instead they take cues from their environment and also from each other via the environment (Bissell, 1981). 2-dimensional (2D) monolayer culturing completely lacks this aspect and can therefore not provide cells with the appropriate stimuli when designing a disease model in vitro. For example, 2D culture of immortalised tumour lines as models for cancer has resulted in a 95% drug failure rate (Hutchinson and Kirk, 2011). Moreover, cells grown in 3-dimensional (3D) culture have shown better viability, morphology, differentiation, response to stimuli and cell-

cell communication compared to cells in 2D (Ravi et al., 2015). Cells grown in 2D or 3D can be visualised is each of the three dimensions (X, Y and Z) (Figure 1.8). When grown in a 2D monolayer, the overall height of cells is usually fixed whereas in 3D, the height can be adjusted depending on the 3D methodology used and can be built up to form multi-layered tissue like structures. Therefore, creating a third dimension is considered as a practical alternative when modelling a disease in vitro (Knight and Przyborski, 2015).

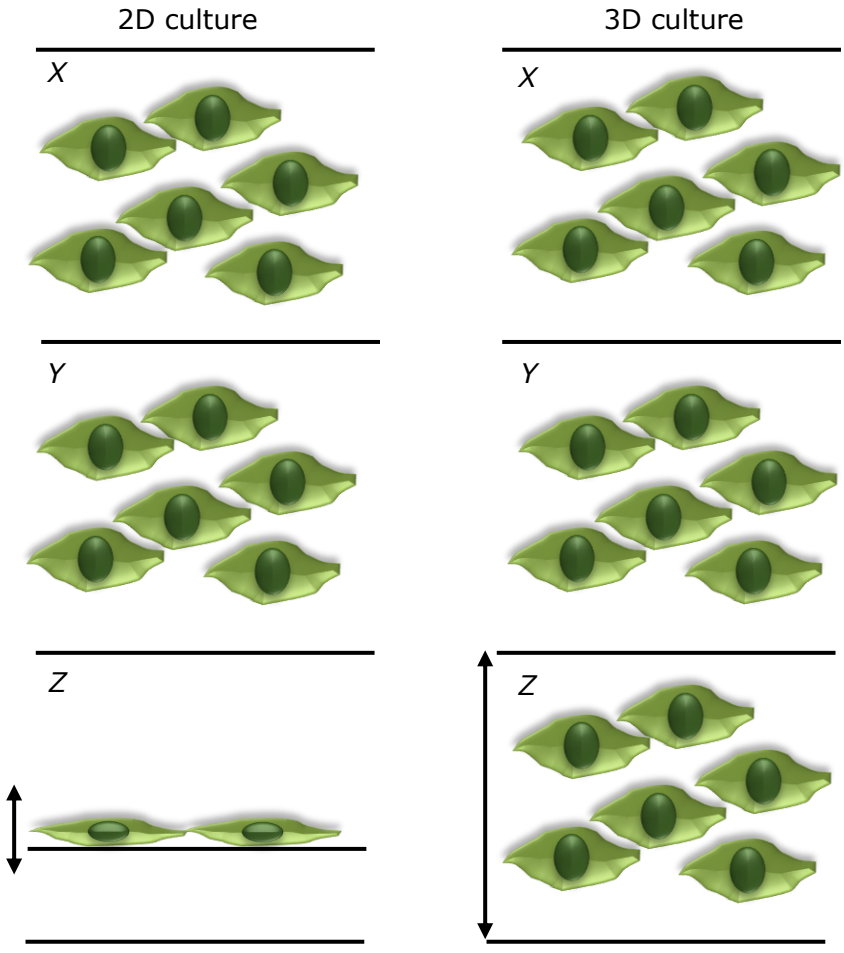



***Figure 1.8 The effect of physical environment on cell structure.*** *Diagrammatic illustration of cell morphology in each of the three dimensions, X,Y and Z where X and Y symbolise length and width of a cell whereas Z described height.*

When grown in 3D culture systems, cells can form aggregates within a matrix which is not possible in 2D monolayer culture. Cells in these aggregates closely mimic cell-cell and cell-ECM interactions found in vivo and also exhibit cell morphology resembling its natural shape in tissue (Edmondson et al., 2014). Several natural and synthetic scaffolds including metals and glass were subsequently developed for this purpose.

Due to the existence of a dynamic reciprocity between the ECM and the cells embedded therein the most widely used scaffold is natural extracellular matrix (Weigelt et al., 2014). Collagen gel scaffolds are commonly used as they are cytocompatible, easily assemble into hydrogels and are stable for encapsulation. One of the few studies describing an in vitro 3D collagen hydrogel model for breast cancer using three different cell types: luminal epithelial cells, myoepithelial cells and stromal fibroblasts showed that the different cell types had organised themselves just like in vivo (Holliday et al., 2009). Collagen hydrogels are also used to study wound healing and remodelling in asthma where fibroblast or airway smooth muscle cell mediated contraction of the hydrogels is a measure of either integrin binding or matrix remodelling (Rogers et al., 2014, Sethi et al., 2002).

The most commonly used natural ECM that allows encapsulation of both non-malignant and malignant cells is a basement membrane (BM) gel derived from Engelbreth-Holm-Swarm (EHS) tumours (Orkin et al., 1977). A liquid at 4°C the extract can be mixed with cells and when heated, the aggregation of proteins forms a gel at 37°C. These extracts like the EHS

tumour are rich in ECM proteins consisting mainly of laminin, collagen IV, heparin sulphate proteoglycans which provide both structural and signal transduction functions (Kleinman et al., 1982). In addition to this, BM gel preparations also consist of several growth factors including FGF, EGF, TGF-β, IGF-1 and PDGF. The most commonly used BM preparations are Matrigel™ (BD Biosciences) and Culturex® BME (Trevigen) both of which are available as a soluble extract. The Culturex® BME gel is also available also with reduced growth factors which allows for defining growth factor requirements for different cells (Benton et al., 2014). The basement membrane extract (BME) gel can promote differentiation however, differentiation response depends on the cell types (Kleinman and Martin, 2005). While normal cells can exhibit a decrease in proliferation and an increase in differentiation in Matrigel, malignant cells such as MCF-7 cells can grow rapidly and metastatic breast cancer cell lines such as MDA-MB-231 appear stellate and will invade and degrade BME. Cell morphology in BME can therefore be used to predict the progression of malignant diseases (Benton et al., 2011).

Although the combination of BM gel and co-culture based models is still bourgeoning these models show great promise in recapitulating diseases (Figure 1.9). Access to primary human tissue can be limited for routine culture and immortalised cell lines alone do not fully represent the entirety of the disease. Therefore co-culturing disease cell lines with primary cells using BME gel models not only represents a more in vivo-like state but also prolongs the lifetime of primary cells in many cases (Weigelt et al., 2014). 3D BME gel co-culture models consisting of fibroblasts with breast

cancer cells, immune cells or adipocytes have demonstrated a reciprocal communication between ECM and the cells in co-culture (Noel et al., 1992, Seidl et al., 2002, Chottanapund et al., 2013, Rozenchan et al., 2009). Tumour-associated fibroblasts when cultured with cancer cells in Matrigel contribute to tumour invasiveness via the production of ECM degrading proteases (Shekhar et al., 2001). Moreover, growth factors in the BME/Matrigel preparations enhance the appropriate microenvironment. Colon cancer cells acquired a more invasive phenotype in 3D BME gel supplemented with EGF. However this effect was reversible when the factors were removed providing evidence that growth factors tethered to the ECM play an important role in the progression of colon cancer (Ludwig et al., 2013). Thus co-culture in 3D can become a powerful tool that allows the design of multicellular in vitro models to recapitulate and better understand cellular signalling mechanisms in vivo.

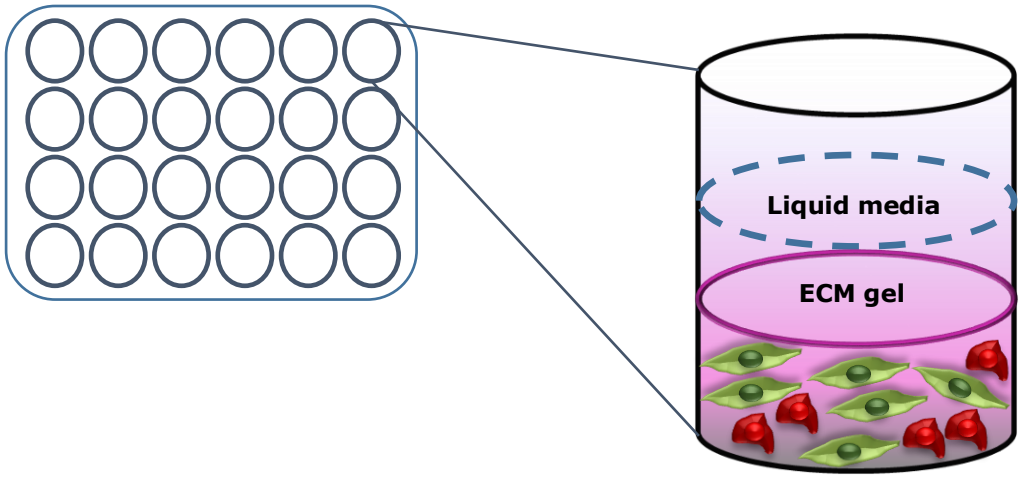



**Figure 1.9 3D *ECM gel co-culture-based model.*** *Illustration of cells in co-culture embedded in an ECM gel (BME/Matrigel). Cells are mixed and evenly distributed in the ECM gel where they arranged themselves in a manner similar to in vivo. ECM gels when set at 37°C are usually overlaid with liquid medium to prevent drying out of gels.*

### 1.10.3 Spheroid-based models

Multicellular tumour spheroid models (MCTS) were first developed by Sutherland and colleagues mainly using cancer cell lines cultured under non-adherent conditions (Sutherland, 1970, Sutherland et al., 1971). A decade later, Bjerkvig and colleagues introduced a new spherical model obtained via simple cutting of cancer tissue referred to as the organotypic multicellular spheroid (OMS) which had the closest resemblance to tumours in vivo (Bjerkvig et al., 1990). Since then other types of spheroid models have been developed that share very little with the first MCTS models apart from their 3D morphology. Recently, tissue-derived tumour spheres (TDTs) that are obtained by the partial dissociation of tumour tissue have been developed. TDTs allow maintenance of cell-cell contact and have since been used extensively in cancer studies (Weiswald et al., 2013, Young et al., 2013c, Kondo et al., 2011). Broadly speaking, spheroid-based models can now be classified into four main groups.

| Spheroid-based model | Source | Culture condition | Formation time |
|---|---|---|---|
| Multicellular tumour spheroids (MCTS) | Single or multi-cell suspension from permanent cell lines and/or primary cells | • Low-attachment plastic<br>• Medium with FCS | 1-7 days |
| Tumourospheres | Single cell suspension from permanent cell lines, tumour tissue or blood | • Serum-free medium with EGF and FGF-2<br>• Low-attachment plastic<br>• Potential preliminary cell sorting | 5-7 days until 1-2 months |
| Organotypic multicellular spheroids | Cut and minced tumour tissue | • Medium with FCS and non-essential amino acids<br>• Non-adherent conditions | 2-5 days until 12-18 days |
| Tissue-derived tumour spheres | Partially mechanically or enzymatically dissociated tumour tissue | • Medium with FCS or serum-free medium with EGF and FGF-2<br>• Culture-treated plastic then non-adherent conditions | 1-3 days |

**Table 1.7** ***Methods used to generate spheroid-based models.*** *Table adapted from and original references in (Weiswald et al., 2015) EGF: Epidermal growth factor; FGF-2 fibroblast growth factor 2.*

*Multicellular tumour spheroids (MCTS)*

MCTS are generated scaffold-free in conventional foetal calf serum (FCS)-supplemented medium. Usually generated from a single cell type in non-adherent or low-attachment culture plates, co-culture MCTS consisting of or two or more cell types have subsequently been generated (Kunz-Schughart et al., 2001) (Figure 1.10 (a)). MCTS often originate from cell lines but are now being generated from tissue derived primary cells, nevertheless, not all cell types are able to generate compact MCTS. Compact spheroids are formed only when the homotypic or heterotypic

cell-cell adhesive forces are strong failing which loose aggregates of cells that can easily detach and disintegrate are formed (Friedrich et al., 2009). Therefore various methods used to generate MCTS rely on one main principle: to provide conditions in which the adhesive forces between cells are greater than those for the substrate they are plated on thereby promoting cell-cell adhesion leading to well-rounded spherically structured MCTS (Weiswald et al., 2015).

A popular method incorporated for the generation of MCTS is the liquid overlay technique. This technique is easy maintaining cells in suspension on a non-adherent surface allowing aggregation of cells into varying size spheroids. Cells are typically placed on tissue culture plastic coated with a thin layer of substrates such as agar, agarose or polyHEMA (Dangles et al., 1997, Dangles-Marie et al., 2007). This prevents cells from adhering to the culture plastic thus promoting cell aggregation and compaction (Figure 1.10 (a)). More recently, multi-well ultra-low attachment U-bottom or V-bottom culture plates with a polystyrene surface offer low-adhesion properties for the generation of spheroids using this technique. The shape of the well encourages the formation of a single, centrally located MCTS of homogenous size per well. Spheroids grown on ultra-low attachment plates exhibit a more compact structure than those grown on agar-coated plates and a probability for automation makes this technique ideal for high-throughput screening (Vinci et al., 2012, Friedrich et al., 2009). Despite the fact that the liquid overlay method provides the right conditions for spheroid formation, not all primary cells or permanent cell lines are capable for forming compact spheroids. Nevertheless, if it is essential to obtain

spheroids using difficult cell types, the addition of BME or Matrigel may be necessary. However such spheroids are artificial and the alterations in growth, expression profile and behaviour of the cells must be monitored well.

The use of heterotypic MCTS is rapidly increasing in cancer studies as these take into account the presence of non-cancerous cells in tumour tissue. The most frequently studied cellular interactions using this model are typically those between cancer cells and fibroblasts with the latter being the most abundant cell type in the cancer stroma. The resulting MCTS generated known as mixed MCTS are a closer representation of conditions in vivo. For example, lung cancer cells co-cultured with fibroblasts showed resistance to Erbtiux treatment by upregulating fibroblast-derived hepatocyte growth factor receptor (HGFR) expression and activation. These data are analogous with clinical treatment of lung cancer patients that show a positive response only with treated with both hepatocyte growth factor (HGF) and epidermal growth factor receptor (EGFR) inhibitors (Majety et al., 2015). Tri-culture spheroid models consisting of cancer cells, fibroblasts and immune cells such as macrophages have also been developed which indicate the influence of intercellular interactions on stroma formation and maintenance and are also important in studying immune cell migration into spheroids and their activation (Rama-Esendagli et al., 2014, Konur et al., 1996).

Depending on the cell type, MCTS can be generated to attain a maximum diameter of 1 to 3mm in diameter (Haji-Karim, 1978). Spheroid cultures

can begin to develop oxygen and nutrient gradients at diameters between 200 and 500μm and those above 600μm in diameter tend to develop a necrotic core in long-term culture. The spheroid then turns into an outer layer of proliferating cells, an inner layer of quiescent cells with the core being necrotic. Hypoxia is of importance in diseases characterised by tumours of proliferating cells as it can lead to numerous indirect effects by modulating expression patterns for example of hypoxia-inducible factor 1-alpha (HIF-1α) regulated genes. Development of secondary necroses has to be determined as per the intended application. For this reason several studies only culture MCTS over a short period before the experimental end-point (Hirschhaeuser et al., 2010, Friedrich et al., 2009).

*Tissue-derived tumour spheres (TDTs)*

Obtained from the partial enzymatic or mechanical dissociation of tissue, TDTs were first used to study colon cancer and were referred to as colospheres. These were generated by finely cutting the tissue sample, then crushing and cultivating the resulting pieces in a cell culture-treated flask (Figure 1.10 (b)). Colospheres were then formed in 1 day after cell remodelling and compaction. Using this technique, around 50% of colorectal tumour samples yielded TDTs. These TDTs can be kept for 2 weeks in culture in non-adherent conditions and can also be cryopreserved as whole structures in freezing medium (Weiswald et al., 2013, Weiswald et al., 2009). Other TDTs obtained from cancer tissues were obtained after incubation with a digestive enzyme and formed using Matrigel (Kondo et

al., 2011). Almost exclusively formed from the dissociation of tumour tissues, TDTs are now used in various cancer studies and have been shown to have E-cadherin-mediated cell-cell interactions. Due to their strong cell-cell interactions, TDTs escape anoikis and remain viable for weeks in culture (Morales and Alpaugh, 2009, Ye et al., 2013). Several TDTs have been shown to mimic the parent tissue in terms of histological characteristics, gene expression profiles, mutations and metastatic properties. This type of similarity cannot be found in the MCTS. Moreover, compared to the proliferative cell lines in MCTS, only fractions of proliferating cells are observed in TDTs which is similar to that seen in vivo (Morales and Alpaugh, 2009, Young et al., 2013c). Although the TDTs are the most relevant form or 3D model, the problems associated with this technique are the availability of tissue, guarantee and uniformity of the TDTs obtained and preservation sub-culture of TDTs which may not be possible with all types of diseased tissue (Hirschhaeuser et al., 2010).

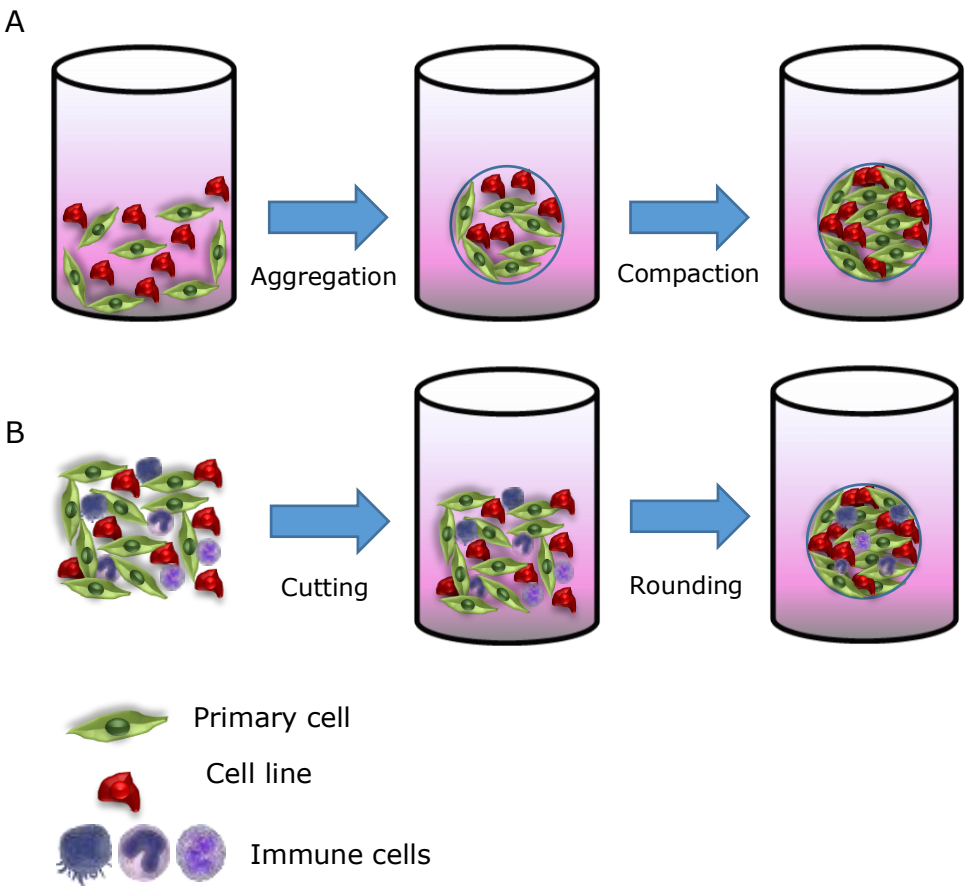



**Figure 1.10** ***Steps in the formation of spheroid-based models.*** *Figure shows (A) MCTS obtained after aggregation and compaction of a co-culture cell suspension cultured in non-adherent conditions. (B) TDTs generated via partial dissociation of tissue formed after compaction and remodelling.*

## 1.11 The Extracellular Matrix of the lung

The physiology and morphology of the lung is a result of the amalgamation of the interactions between pulmonary cells and the encompassing ECM. The ECM is tissue-specific and is a macromolecular structure which primarily provides structural support to the surrounding tissue and is essential for normal organ function. In addition to providing support, the ECM can also affect cell shape and function. A variety of cellular responses including adhesion and differentiation, formation of focal contacts and stress fibres, stimulation of proliferation and migration, induction of polarity and gene expression, alterations in metastatic activity, and outgrowth of cell processes are also elicited by the underlying matrix (Dunsmore and Rannels, 1996). The ECM proteins can also sequester growth factors such as EGF, FGF as well as other signalling molecules such as TGF-β thereby influencing cell behaviour (Bonnans et al., 2014). This pleiotropic aspect of ECM function depends on the ever-changing structure of ECM and on the levels of synthesis and degradation of its components whereby diverse cellular behaviours can be regulated (Lu et al., 2011).

The lung ECM is typically divided into to two sections, namely, the basement membranes which are thin specialised layers that support the epithelial and endothelial cells and the interstitial spaces which form the parenchyma of the lung. The lung interstitium houses the resident lung fibroblasts, the most commonly identified cell type that is mainly responsible for ECM turnover (White, 2015).

The term ‘matrisome’ was coined by Haynes and Naba to define a list of all proteins consisting of any given matrix and a larger list of all their associated modifying molecules. The lung parenchyma primarily consists of collagens, elastins, glycoproteins and proteoglycans and the basement membrane comprises of mainly type IV collagens, laminin, nidogen and perlecan. Besides theses the ECM also consists of growth factors or signalling molecules and ECM modifying or stabilising enzymes (Hynes and Naba, 2012).

## 1.12 ECM turnover – A focus on Cathepsins

The ECM is a very dynamic environment wherein radical remodelling occurs during developmental process as well as during regular adult bodily functions such as remodelling of the bone or mammary gland (Fukumoto and Yamada, 2005, Page-McCaw et al., 2007). The dynamics result from changes in ECM composition possibly due to the altered synthesis or degradation of one or more of its components. Therefore in normal conditions, the ECM dynamics are a tightly regulated and the cross talk between cells and the ECM enables the striking of a delicate balance between ECM synthesis, stabilisation and degradation by modifying enzymes. However, it is when this well-oiled ship becomes corrupted the ECM dynamics become deregulated leading to various human diseases including cancer (Lu et al., 2011). ECM remodelling is carried out usually by the cleavage or removal of one or more of the ECM components. This work is usually carried out by the ECM modifying enzymes, the proteases. It is a well-known fact that in other interstitial lung diseases such as

chronic obstructive pulmonary disease (COPD), parenchymal destruction is associated with an imbalance in protease and anti-protease activity (Greene and McElvaney, 2009). Taking lessons from what we know about the pathogenesis of COPD, it has been proposed by several researchers that similar mechanisms exist in LAM. The largest class of human proteases is the matrix metalloproteases (MMP) followed by serine, cysteine, threonine and aspartic proteases.

The term cathepsin, derived from ancient Greek meaning 'to digest', was first coined in 1929 by Richard Willstätter and Eugen Bamann (Willstätter and Bamann, 1929). Initially described as lysosomal intracellular hydrolases, cathepsins are a class of globular proteases that are now also known to have an extracellular function. Denoted by the abbreviation 'CTS' followed by a distinct alphabet denoting the different members, the cathepsin family consists of more than a dozen members classified based on their structure and catalytic type. Cathepsins (CTS) B, C (also known as cathepsin J and dipeptidyl-peptidase 1), F, H, L, K (also known as cathepsin O2), O, S, V (also known as cathepsin L2), W, and X (also known as cathepsin Z/P) are cysteine proteases of the papain family which form a part of the largest and the most intensely studied class of cathepsins. Cathepsins (CTS) A and G are serine carboxy peptidases whereas cathepsins (CTS) D and E are aspartic proteases (Kuester et al., 2008). The different cathepsins and their tissue localisations are listed in Table 1.8.

| Cathepsin | Subtype | Expressed tissue | ECM protein substrate (if known) |
|---|---|---|---|
| A | Serine | Platelets, primary human antigen presenting cell, testis and epididymis | |
| B | Cysteine | macrophages, hepatocytes, renal tubules, all endocrine organs | Proteoglycan, aggrecan, collagens type II IV, IX, X, XI, fibronectin, osteocalcin, laminin, osteonectin |
| C | Cysteine | Ubiquitous | Dipeptide esters, amides, amilides and beta-naphtylamides |
| D | Aspartic | Eccrine sweat, extracellular matrix and synovial fluid of cartilage | Osteonectin, laminin, fibronectin |
| E | Aspartic | Immune system | |
| F | Cysteine | Antigen presenting cells | |
| G | Serine | Polymorphonuclear leukocyte | Elastin |
| H | Cysteine | Ubiquitous | Osteocalcin |
| L | Cysteine | Ubiquitous | Proteoglycan, aggrecan, collagens type I, II, IX, XI, elastin, fibronectin, laminin, osteocalcin |
| K | Cysteine | Bone, ovary, heart, placenta, lung, skeletal muscle, colon and small intestine | Aggrecan, collagens type I and II, elastin, osteonectin |
| O | Cysteine | Ubiquitous | |
| S | Cysteine | Spleen and professional antigen-presenting cells | Aggrecan, collagen, elastin, fibronectin, osteocalcin |
| V | Cysteine | Thymus and testis, corneal epithelium | Elastin |
| W | Cysteine | T-lymphocytes | |
| X | Cysteine | Immune system | |
| Z | Cysteine | Widely expressed in tissues | |

**Table 1.8** ***Tissue and cellular localisation and ECM substrates of known cathepsins.*** *Several properties of cysteine cathepsins shown including their type, cell and tissue localisation and ECM substrate specificity. Original reference can be found within (Brömme and Wilson, 2011, Tan et al., 2013).*

### 1.12.1 Cysteine cathepsins

Cysteine cathepsins also known as papain-like thiol proteases are the largest family of cathepsins consisting of 11 members. Expression of the cysteine cathepsins can either be ubiquitous or tissue and cell specific. Cathepsins B, L, C, O, and H are found in a wide range of cells and tissue signifying that these enzymes may be involved in normal matrix protein turnover. In contrast, cathepsins S, K, V, F and W, show a more restricted cell and tissue distribution suggesting specific roles for these proteases (Lecaille et al., 2002). Expressed highly in macrophages, dendritic cells and/or thymic cortical epithelial cells, cathepsins S, F and V are involved in antigen processing and presentation (Riese and Chapman, 2000, Shi et al., 2000). Expressed by immune-related cells, cathepsin C also processes varied precursor proteins including the serine proteases such as granzyme zymogens (Pham and Ley, 1999). $CD8^+$ lymphocytes and natural killer cells specifically express cathepsin W, however its exact function in unknown (Linnevers et al., 1997). Expression of cathepsin V is restricted to thymus and testis (Bromme et al., 1999). Cathepsin K is highly expressed in osteoclasts, synovial fibroblasts and epithelial cells. Of all the matrix-degrading enzymes, cathepsin K is the only protease to play an essential role in normal bone resorption.

*Structure and regulation of cathepsin activity*

Papain-like cysteine proteases are comprised of a signal peptide, a propeptide and a catalytic domain. In their structure, two domains, left (L-) formed by three α-helices and right (R-) which has a β-barrel structure form a papain-like fold which is a characteristic feature of cysteine cathepsins. A cleft between the two domains houses the two active-site residues, Cys25 (cysteine) and His159 (histidine) (Figure 1.11 (b) and (c)) (Fonovic and Turk, 2014). Responsible for translocation into the endoplasmic reticulum during mRNA translation the signal peptides are typically 10 and 20 amino acids in length. Propeptides are of a variable length ranging between 36 amino acids in cathepsin X and 251 amino acids in cathepsin F (Figure 1.11 (a)) (Wiederanders et al., 2003). The propeptide functions as a scaffold for protein folding of the catalytic domain, acts as a chaperone for the transport of the proenzyme to the endosomal/lysosomal compartment and acts as a high-affinity reversible inhibitor preventing the premature activation of the catalytic domain. The catalytic domains contain between 214 and 260 amino acids and are highly conserved active sites containing a cysteine, a histidine and an asparagine residue (Mellor et al., 1993).

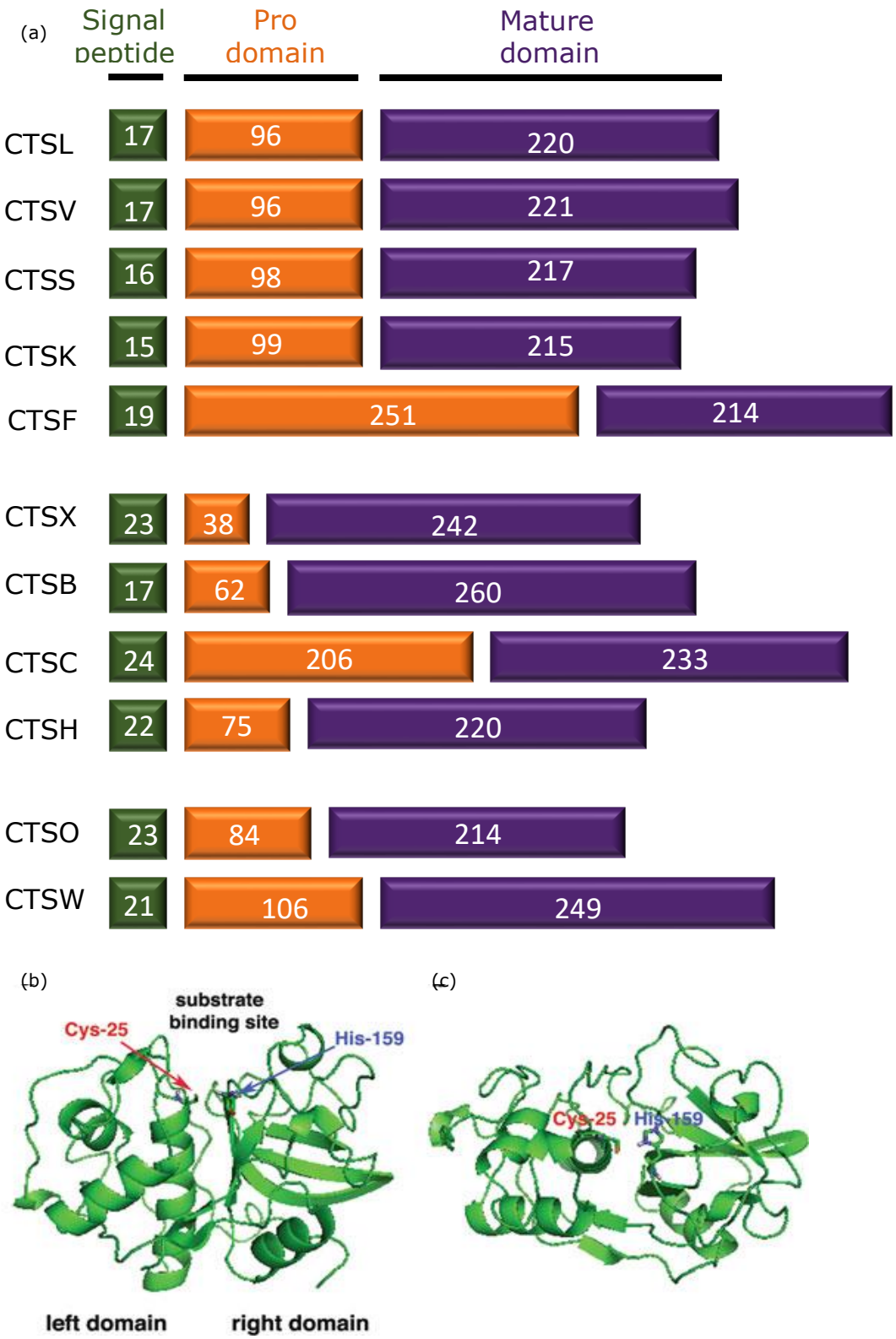



**Figure 1.11** ***Schematic repsresentation of protease domains of cysteine cathepsins and example ribbon structure.*** *Panel A shows Cysteine cathepsins expressed as polypeptides containting a signal peptide, a propeptide and a catalytic domain. Different domain lengths for different cathepsins are depicted. The propeptide is cleaved in an acidic environmant resulting in a fully active catalytic domain. Panel B shows the ribbon structure of cysteine cathepsins, cathepsin K showing the L and R domain and*

*C shows the top view of cathepsin K showing the catalytic diad. Figure courtesy of (Brömme and Wilson, 2011).*

Optimal activity of cathepsins requires a reducing and slightly acidic milieu which exists in lysosomes. Cathepsins are typically synthesized as preproenzymes which can undergo an N-terminal signal peptide cleavage. On removal of the signal peptide, the propeptide targets the lysosome using a specific mannose-6-phosphate receptor (M6PR) pathway simultaneously acting as an inhibitor to prevent inappropriate proteolytic activity (Saftig and Klumperman, 2009, Schroder et al., 2010). Mature proteolytically active cathepsins are then released on removal of the N-terminal propeptide a process which can be catalysed by different proteases including cathepsins such as cathepsin D and other cysteine cathepsins under acidic conditions (Nissler et al., 1998, Wiederanders et al., 2003, Nishimura et al., 1989). Several cathepsins including cathepsins B, H, L, S and K can undergo autocatalytic activation at low pH which takes place due to a chain reaction initiated by an initial mature molecule catalysing a procathepsin molecule which when activated in turn cleaves another procathepsin molecule and so on (Caglic et al., 2007).

Therefore, requirement of acidic conditions for optimal activity and a general instability of cysteine cathepsins at neutral pH are believed to protect the cell and limit unwanted proteolysis. However, certain physiological and pathological conditions can coerce cathepsins to translocate to the cell surface and be released into the extracellular space in either the mature active form or in the proenzyme form to be further

activated. This suggested that cathepsins are active also under less favourable conditions (Reiser et al., 2010). However, if mechanisms to prevent unwarranted proteolytic activity fail, activity of secreted cysteine cathepsins is additionally regulated by the endogenous inhibitors such as stefins, cystatins and kininogens, serpins and alpha$_2$ macroglobulins that provide an added level of safety (Boris et al., 2002). Cysteine cathepsins play a physiological role in health and various disease conditions.

## 1.13 Cathepsin K

One of the most potent known human collagen-elastin degrading protease cathepsin K was identified by several different groups and cathepsin K gene was first cloned from rabbit osteoclasts. Formerly known as cathepsin OC-2, over the years human cathepsin K has also been referred to as cathepsin O, cathepsin X and cathepsin O2 (Shi et al., 1995, Bromme et al., 1996, Inaoka et al., 1995). Believed initially to be expressed in human osteoclasts alone, cathepsin K expression has now been found in several other cell types.

### 1.13.1 Gene organisation and regulation

Located on chromosome 1q21 with 8 exons and 7 introns human cathepsin K like human cathepsin S is encoded by a single-copy gene of approximately 12.1 kb genomic DNA (Rood et al., 1997). Cathepsin K bears a similar homology to cathepsins L, S and V with approximately 60% amino acid sequence identity (Chauhan et al., 1993). Similar to cathepsins L, S and V, cathepsin K consists of a characteristically-shaped active groove confirmation but unlike the other cathepsins has highly-positive charged basic residues that allow for allosteric accommodation of negatively-charged glycosaminoglycans (GAGs) (Figure 1.12). This facilitates the formation of high molecular weight complexes of cathepsin K and GAGs which participate in the formation of a unique collagenolytically active complex that is necessary for unwinding of triple

helical collagens at multiple locations, an activity which is unparalleled among human collagenases (Li et al., 2004, Novinec et al., 2010).

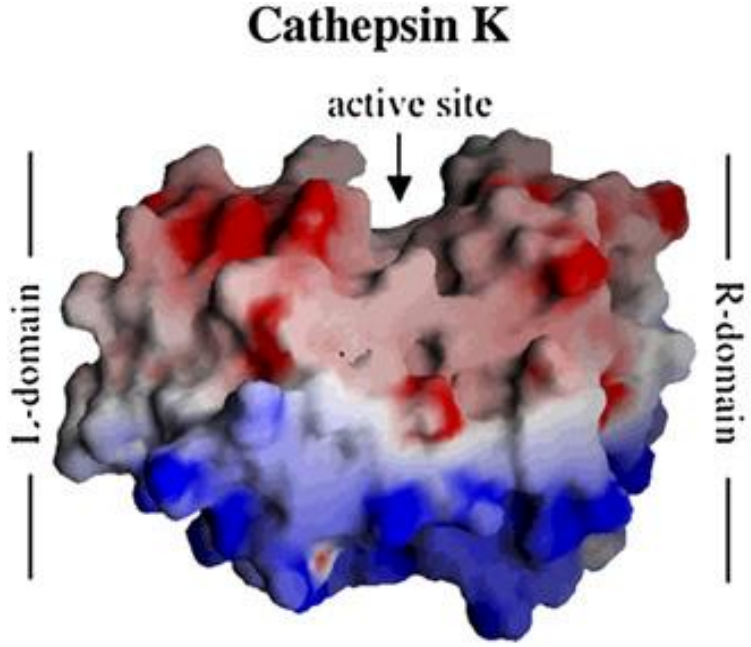



**Figure 1.12** ***Surface potential of cathepsin K.*** *negative potential regions are coloured red which depict glycosaminoglycan binding whereas areas of positive potential as coloured blue. Figure courtesy of (Lecaille et al., 2008).*

Transcriptional initiation of the cathepsin K gene may be enhanced by several transcription regulatory elements including activator protein 1 (AP-1), Microphthalmia-associated transcription factor (Mitf), Transcription factor E3 (TFE3), Transcription factor PU.1 (PU.1) among a few others (Lecaille et al., 2008). The receptor activator of NF-κB ligand (RANKL) plays a crucial role in osteoclast differentiation and activation. RANKL produced by osteoblasts and stromal cells, bind to its cytoplasmic receptor RANK (receptor activator of NF-κB) (Yasuda et al., 1998, Shalhoub et al., 1999). During osteoclast differentiation, transcription factors PU.1 and Mitf can both regulate specific genes in response to colony stimulating factor 1 (CSF-1) and RANKL signalling. Pro-inflammatory cytokine, TNF-α which

belongs to the same superfamily of ligands as RANKL also stimulates cathepsin K mRNA expression in pre-osteoclasts and rheumatoid synoviocytes (Hsu et al., 1999, Hou et al., 2002). Cathepsin K synthesis in macrophages and smooth muscle cells is stimulated by other pro-inflammatory cytokines such as interferon gamma (IFNγ) and interleukins 6 (IL-6) and 13 (IL-13) (Wang et al., 2000, Zheng et al., 2000, Ebisui et al., 1995). Retinoic acid, vitamin D, prostaglandinE2, fibroblast growth factor-2, insulin-like growth factor-1 and various hormones such as parathyroid hormone, thyroid hormone and particularly oestrogen are also indirect regulators of cathepsin K expression (Troen, 2006)

### 1.13.2 Activation and cellular distribution

Cathepsin K is synthesised as a 37kDa inactive zymogen, which is transported from the endoplasmic reticulum to the lysosomal compartment via the M6PR pathway (Rieman et al., 2001). Removal of the propeptide and subsequent activation of cathepsin K can be catalysed by other cathepsins such as cathepsin D (Nishimura et al., 1988) or in low pH conditions and/or in the presence of glycosaminoglycans (McQueney et al., 1997). A soluble protein, cathepsin K can be secreted from certain cells as a glycosylated proform which can be activated extracellularly. Moreover, heparin sulphate can anchor cathepsin K to the cell membrane thereby increasing its activity at neutral pH (Almeida et al., 2001).

Human cathepsin K was predominantly thought to be expressed by multinucleated osteoclasts where activation of this protease is best

documented. Here, cathepsin K is activated at the ruffled border of the cells where the pH is as low as 4.0 and is secreted into the extracellular environment in the resorption lacunae enabling it to degrade type I collagen which is essential for physiological bone remodelling (Everts et al., 2006). It was only when fibroblasts treated with cathepsin K inhibitors were found to contain large amounts of phagocytosed but undigested collagen fibrils within their cytoplasm, the predominant role of cathepsin K in collagen degradation became apparent (van Noorden and Everts, 1991, Hou et al.). Cathepsin K is expressed in skin fibroblasts where it plays a role in homeostasis of the dermal ECM during wound healing and inflammation (Quintanilla-Dieck et al., 2009). Cartilage degradation results from cathepsin K expressed by synovial fibroblasts and chondrocytes (Kafienah et al., 1998). Cathepsin K also plays a role in lung matrix homeostasis in cultures of pulmonary fibroblasts and adult lung airway epithelium (Buhling et al., 2004b). Aortic smooth muscle cells (Sukhova et al., 1998), macrophages (Punturieri et al., 2000), bronchoalveolar lavage fluids (Serveau-Avesque et al., 2006) also express cathepsin K and are proposed to play a role in extracellular remodelling.

### 1.13.3 Physiological role of cathepsin K

Cathepsin K is crucial for bone remodelling. Predominantly expressed in osteoclasts, cathepsin K is responsible for 98% of total cysteine protease and MMP collagenase activity required for bone remodelling (Bromme et al., 1996, Shingleton et al., 1996). Cathepsin K is capable or degrading

type I collagen in its non-collagenous termini (N- and C- telopeptide regions) releasing cross-linked N- and C-telopeptides that can be detected in urine and serum as a measure of bone resorption (Atley et al., 2000). Cathepsin K is also involved in skeletal, heart, lung and intestinal development. Respiratory and gastrointestinal mucosae of human embryos are rich in cathepsin K. Here cathepsin K is believed to play a role in extracellular remodelling itself or by releasing ECM tethered enzymes (Buhling et al., 2004a, Haeckel et al., 1999). Cathepsin K is most potent in cleaving mature insoluble elastin compared to cathepsins S and L thereby playing an important role in remodelling the arterial wall notoriously resistant to proteolysis. Found in Sertoli cells of adult rat testes, cathepsin K has also been suggested to play a role in facilitating germ cell movement and spermiation (Anway et al., 2004).

Besides playing an important role in normal physiological functions, cathepsin K also plays a crucial role in the progression various diseases. Pycnodysostosis is a rare genetic disorder caused due to genetic defects in the cathepsin K gene. The disease is characterised by an impaired osteoclast function causing them to accumulate undigested collagen fibrils. This renders patients with brittle bones and results in osteosclerosis and short stature of patients and although the disease is not a life-threatening condition, frequent fractures, craniosynostosis, respiratory, sleep and dental problems result in significant patient suffering (Everts et al., 2003, Turan, 2014). Osteoporosis occurs when bone resorption exceeds bone formation. Several studies have shown that cathepsin K is involved in the pathogenesis of osteoporosis and Paget's disease as elevated cathepsin K

levels are found in the osteoclasts and serum from these patients. Thus inhibiting cathepsin K is thus an attractive therapeutic target for preventing of bone loss bone resorption disorders (Meier et al., 2006).

An imbalance between cathepsin K and its endogenous inhibitor leads to an increase in collagen activity leading to the breakdown of fibrillar type II collagen the major component of articular collagen. Osteoarthritis (OA) and rheumatoid arthritis (RA) both characterised by the progressive destruction of articular cartilage are caused by such an increase in cathepsin K activity. Synovial fibroblast-mediated degradation of type II collagen in cartilage has been linked to the increased activity of cathepsin K in OA and RA patients (Hou et al., 2002).

Cathepsin K has been extensively studied for its role in various cancers primarily for its role in tumour progression via ECM degradation as well as for its diagnostic potential and prognostic impact. An interplay between stromal cells such as fibroblasts and cancer cells aid tumour progression via cathepsin K-mediated degradation. Tissue expression of cathepsin K has been detected in bone sarcomas, breast, prostate, skin, thyroid carcinomas, head and neck cancer and melanoma and has been associated with aiding cancer progression via ECM degradation and enabling cancer cell invasion. On the other hand, expression in various PEComas has been useful in diagnosing them and distinguishing them from a majority of human cancer types reviewed in (Verbovsek et al., 2015).

### 1.13.4 Cathepsin K and lung diseases

Cathepsin K expression and activity has been reported in various lung diseases. Depending on the pathogenesis of the disease, this protease can have protective or destructive effects on disease progression. In diseases characterised by fibrosis, cathepsin K-mediated lung ECM digestion serves to protect against fibrosis by counteracting the increased matrix deposition. Buhling et al have previously shown that activated pulmonary fibroblasts express large amounts of cathepsin K. Elevated cathepsin K expression was detected in a bleomycin-induced lung fibrosis mouse model soon after bleomycin challenge. Moreover, cathepsin K driven, lung fibroblast-mediated collagen degradation has also been associated with pulmonary fibrosis and cathepsin K expression was upregulated in patients with this condition suggesting that this enzyme played a pivotal role in pulmonary fibrosis (Srivastava et al., 2008, Buhling et al., 2004b). Homogenates of silicotic lungs show increased cathepsin K activity than control lungs. Both proform and mature forms of cathepsin K have been in bronchoalveolar lavage fluid of patients suffering from chronic silicosis or sarcoidosis (Perdereau et al., 2006).

However, in lung diseases characterised by the destruction of matrix, increased cathepsin K activity can play a crucial role in lung ECM destruction and further progression of the disease. In the lungs, cathepsin K expressed by fibroblasts, smooth muscle cells and macrophages can also degrade elastin. Lungs of transgenic mice that mimic COPD, a chronic inflammatory lung disease characterised by proteolytic destruction of the lung ECM, have shown an increased production of not only MMPs but also

cathepsin K among other cysteine cathepsins (Zheng et al., 2000). Cysteine cathepsin K has been found to be extracellularly released from macrophages which is detected in emphysematous bronchoalveolar lavage fluids (Takeyabu et al., 1998). In guinea pigs exposed to cigarette smoke, inflammation and emphysematous changes have been associated with a decrease in collagen and elastin and a three-fold increase in cathepsin K activity in the lungs (Golovatch et al., 2009). This suggested that cathepsin K may contribute to the excessive degradation of collagen and elastin associated with emphysema. Intracellular and extracellular stromal cell proteolytic activity of cathepsin K also aids in cancer cell invasion in lung adenocarcinomas, squamous cell carcinoma and non-small-cell lung cancer (Naumnik et al., 2009, Rapa et al., 2006).

### 1.13.5 Inhibitors of cathepsin K

Natural endogenous inhibitors of cathepsin K are widely distributed in humans and belong mainly to the cystatin family. The cystatin family consists of three groups, stefins, cystatins and kininogens that are tight-binding competitive inhibitors of cysteine proteases. Widely distributed in almost all cells and tissues, stefin B protects cells against uncontrolled proteolysis by cathepsins and an imbalance between this endogenous inhibitor and cathepsins favours proteolysis. Resulting in intracellular inhibition, stefin B can help regulate bone resorption by blocking cathepsin K activity in osteoclasts (Laitala-Leinonen et al., 2006). Also, elevated stefin A and B levels in patients suffering from non-small-cell lung cancer

are associated with a higher chance of survival (Werle et al., 2006). Probably the best known extracellular inhibitor of cathepsin K activity, cystatin C is the tightest-binding inhibitor capable of inhibiting cathepsin K activity in the picomolar range ($K_i$=4.1pM) (Bromme et al., 1991). Changes in the balance between cystatin C and cathepsin K has been implicated in numerous pathological conditions such as fibrosarcoma (Kopitz et al., 2005), non-small-cell lung cancer (Werle et al., 2006) and atherosclerosis (Liu et al., 2004). Other endogenous inhibitors of cathepsin K include thyropins, serpins (serpin B3) and $\alpha_2$-macroglobulin.

Synthetic cathepsin K inhibitors were primarily designed as anti-resorptive drugs. Previous strategies to synthesize lipophilic and basic reversible synthetic inhibitors of cathepsin K led to off-target inhibition and lysosmotropism. Therefore, safer non-basic inhibitors that were potent and selective were synthesised. Several cathepsin K inhibitors are showing promising results and are currently at various phases of clinical development while a few others have been abandoned due to their side effects (Lecaille et al., 2008). The potency profiles of the various cathepsin K inhibitors are summarised in Table 1.9.

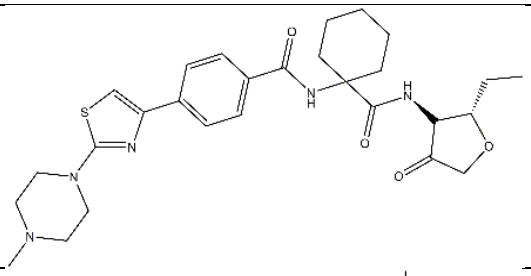
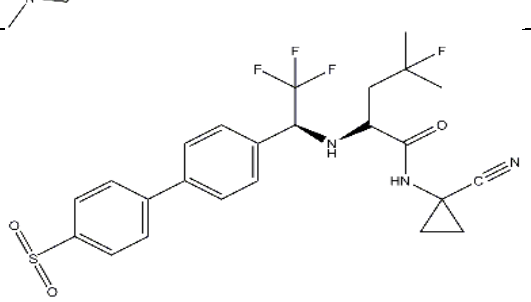
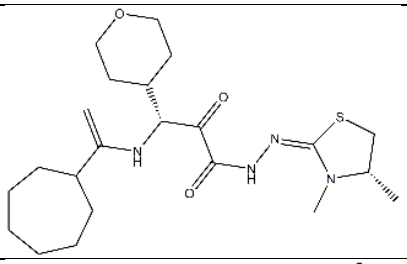
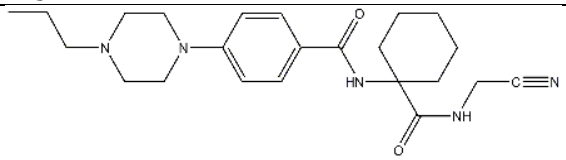
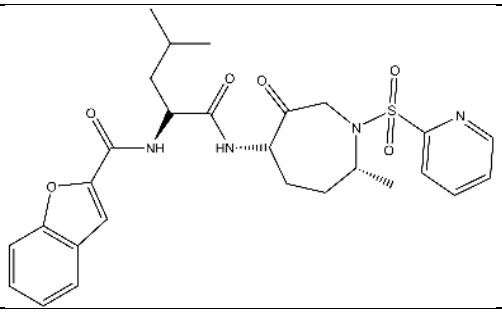
| Compound and status | Chemical Structure | Potency profile |
|---|---|---|
| MIV-711, Phase II (ongoing) |  | $IC_{50}$ (nM)<br>CTSK=2.5 |
| Odanacatib, Phase III (suspended) |  | $IC_{50}$ (nM)<br>CTSK=0.2<br>CTSB=1034<br>CTSL=2995<br>CTSS=60<br>CTSV=762<br>CTSF=795<br>(Gauthier et al., 2008) |
| ONO-5334, Phase III (discontinued) |  | $K_i$ (nM)<br>CTSK=0.10<br>CTSS=0.83<br>CTSL=1.7<br>CTSB=32<br>(Ochi et al., 2014) |
| Balicatib, Phase II (discontinued) |  | $IC_{50}$ (nM)<br>CTSK=2.7<br>CTSB=4800<br>CTSL=503<br>CTSS=65,000<br>(Bromme and Lecaille, 2009) |
| Relacatib, Phase I (discontinued) |  | $K_i$ (nM)<br>CTSK=0.041<br>CTSB=15<br>CTSL=0.068<br>CTSS=1.6<br>CTSV=0.053<br>(Kumar et al., 2007) |

**Table 1.9** ***Inhibitors of cathepsin K with structures and their various stages of development.***

## 1.14 Protease-mediated cystic lung destruction in LAM

LAM is characterised by an increased proliferation of abnormal smooth-muscle like cells along with cystic lung degradation. Microscopic and immunohistochemical analysis of open lung biopsies by Fukuda et al revealed emphysema-like changes in the areas of cell accumulation that showed degraded collagen and elastic fibres which were believed to be caused by an imbalance of proteases such as elastases (Fukuda et al., 1990). Changes in the organisation of elastin and collagen have been noted in the LAM lung and it is believed that these changes result in defects in lung function rather than just abnormal proliferating cells. The degradation and loss of elastin also correlated with an increase in matrix metalloproteinases (MMPs) particularly MMPs 2, 9, possessing an elastase activity, and 14 an MMP2 activator (Hayashi et al., 1997).

Recent studies have indicated that thickening of interstitial connective tissue is associated with alveolar wall destruction and ensuing development of cysts. Studies by Merrilees et al showed that LAM lung contained twice as much interstitial tissue as compared to normal lung with actin positive smooth muscle-like cells making up less than 24% of interstitial volume. The interstitium was strongly positive for matrix proteoglycans, versican and biglycan but no evidence of elastic fibres whereas the thickened areas of the interstitium contained disorganised elastic fibres suggesting a disrupted elastin deposition. Evidence of proteoglycan-induced shedding of elastin binding protein and inhibition of elastin fibre formation is also observed. Moreover, alveolar walls in the LAM lung show a strong versican staining but reduced elastin content

(Merrilees et al., 2004). All of these findings strongly suggest that ECM proteins play an important role in the remodelling seen in LAM lungs and it is the subsequent loss of ECM and formation of cystic lesions that leads to deterioration in lung function correlating to an impaired $DL_{CO}$ (Sobonya et al., 1985, Taveira-DaSilva et al., 2001).

Evidence of MMP overexpression, MMP inducer EMMPRIN and the endogenous inhibitors TIMP in LAM is clear. MMP-1 and MMP-2 are highly expressed in LAM lung tissue whereas MMP9 is elevated in serum from LAM patients (Pimenta et al., 2011, Odajima et al., 2009, Hayashi et al., 1997). Pro and active forms of MMP-9 but not MMP-2 were found in urine from LAM patients (Chang et al., 2014). Increased levels of MMP-2 have also been associated with loss of *TSC2* in animal models for LAM (Lee et al., 2010, Moir et al., 2011, Chang et al., 2010). Goncharova et al showed that MMP expression was induced by TSC2 null lesions in a mouse model characterised by airspace enlargement and alveolar destruction. MMPs-2, -3 and -9 were elevated in bronchoalveolar lavage fluid whereas MMPs-7, -8, -9 and -12 showed increased tissue expression compared to controls (Goncharova et al., 2012). Moderate to strong expression of MMP-14 is mainly found in the spindle shaped cells in LAM nodules and an immunohistochemical co-localisation of MMP-14 and MMP-2 expression is observed in the nodules (Matsui et al., 2000a). Increased levels of serum response factor (SRF) in mouse lung fibroblasts showed an upregulated expression of MMPs-2 and -14 while the MMP inhibitor TIMP-3 was downregulated (Zhe et al., 2003). Mild to moderate immunohistochemical expression of TIMPs-1 and -2 has been found mainly in spindle-shaped

cells in LAM nodules (Hayashi et al., 1997). Intense staining for EMMPRIN was found in LAM nodules and the expression was found to be co-localised with α smooth muscle actin and MMP-2 or MMP-9 in LAM nodules. EMMPRIN was also detected in increased levels in bronchoalveolar lavage fluid from LAM patients compared with controls (Odajima et al., 2010).

Elevated SRF in human lung fibroblasts also upregulated uPA while PAI-1 was downregulated. The same trend was observed in LAM lung tissue where LAM lesions showed stronger immunoreaction for uPA and absence of PAI-1 expression compared to surrounding normal lung parenchyma. Ultimately this results in activation of MMPs via uPA-mediated cleavage of plasminogen to plasmin (Zhe et al., 2005). Cathepsin K, a papain-like cysteine protease with a highest known collagen-elastin degrading activity (Bromme et al., 1996, Inaoka et al., 1995). This protease which is downstream of mTOR in osteoclasts, is strongly expressed in spindle-shaped and to a lesser extent epithelioid-shaped cells in LAM lesions (Chilosi et al., 2009). Evidently increased levels of proteases with an elastase and collagenase activity and decreased levels of the endogenous inhibitors (anti-proteases) in LAM tissues correlates with lung degradation, however, it is not entirely clear whether the degradation and subsequent cyst formation is due to the secreted proteases alone. Moreover, although the abovementioned studies have reported an upregulation of proteases in LAM lung, there is a lack of evidence of an increased proteolytic activity. Thus, investigating the transitory and durable expression of proteases along with their activation will lead to a better understanding of cystic

remodelling and will also lead to the discovery of novel therapeutic strategies for targeting these mechanisms.

## 1.15 Hypotheses

The lungs of LAM patients contain a clonal population of $TSC2^{-/-}$ LAM cells. These cells proliferate and recruit a larger population of wild type fibroblasts. The two populations synergise within LAM nodules and mutually support each other in the recruitment of other cell types and the production and activation of matrix degrading proteases which contribute to the destruction of the lung parenchyma. Further these processes are dependent upon factors downstream of LAM cell mTOR which represent targets for therapy.

By recapitulating these elements in a tissue culture system better models than the current animal models of LAM lung destruction can be generated.

## 1.16 Aims

- To develop relevant 2D and 3D in vitro cell culture models recapitulating in vivo LAM physiology.
- To determine the effect of LAM cell-fibroblast interactions on the production and activation of proteases leading to lung matrix destruction.
- To understand LAM cell and fibroblast crosstalk that leads to LAM nodule formation and subsequent lung destruction.
- To identify the key players involved with a view to finding novel drug targets for the treatment of cystic lung destruction associated with LAM.

# 2 CHAPTER 2: Materials and Methods

## 2.1 Materials

### 2.1.1 Plastic ware

Unless otherwise stated, all cell culture vessels and assay plates were obtained from Corning® Costar® UK Ltd, High Wycombe, UK.

### 2.1.2 Cell Culture Reagents

Dulbecco's Modified Eagle's medium (DMEM), Dulbecco's Modified Eagle's Medium 10x (10x DMEM), Antibiotic Antimycotic solution (100x), L-Glutamine solution, Folic acid and Dulbecco's Phosphate Buffered Saline (DPBS) were obtained from Sigma, Dorset, UK. Dulbecco's Modified Eagle Medium/Nutrient Mixture F-12 (DMEM/F-12), phenol red free medium and foetal calf serum (FCS) were obtained from Gibco, Life Technologies, Paisley, UK. Iscove's Modified Dulbecco's Medium (IMDM) with GlutaMAX™ was obtained from Fisher Scientific, Loughborough, UK.

### 2.1.3 Antibodies

*Primary antibodies*

| **Antigen** | **Dilution and application** | **Monoclonal /Polyclonal** | **Host** | **Isotype** | **Supplier and product code** |
|---|---|---|---|---|---|
| Fibroblast Surface Protein (FSP) Clone 1B10 | 1:50 (IF, IHC, IHC-Fr) | Monoclonal | Mouse | IgM | Sigma, Dorset, UK #F4771 |
| Cluster Differentiation | 1:100 (IF) | Monoclonal | Rabbit | IgG | Abcam, Cambridge, |

| | | | | | |
|---|---|---|---|---|---|
| 90 (CD90) Clone EPR3133 | | | | | UK #ab133350 |
| Fibroblast Activation Protein alpha (FAPα) | 1:100 (IF) | Polyclonal | Rabbit | IgG | Abcam, Cambridge, UK #ab28244 |
| Vimentin | 1:100 (IF) | Polyclonal | Rabbit | IgG | Proteintech, Manchester, UK # 10366-1-AP |
| Desmin | 1:100 (IF) | Polyclonal | Rabbit | IgG | Proteintech, Manchester, UK # 1652-1-AP |
| α Smooth Muscle Actin – Cy3 (αSMA-Cy3) Clone 1A4 | 1:200 (IF) | Monoclonal | Mouse | IgG2a | Sigma, Dorset, UK #C6198 |
| Proliferating cell nuclear antigen (PCNA) | 1:500 | Polyclonal | Rabbit | IgG | Abcam, Cambridge, UK #ab18197 |
| Melanoma associated antigen (PNL2) | 1:50 (IHC) | Monoclonal | Mouse | IgG1 | Zytomed, Berlin, Germany #MSK082 |
| Cathepsin K Clone 3F9 | 1:2000 (IHC); 1:100 (IF) | Monoclonal | Mouse | IgG | Abcam, Cambridge, UK #ab37259 |
| Cathepsin K | 1:1000 (IHC)<br><br>1:500 (IHC-Fr) | Polyclonal | Rabbit | IgG | Proteintech, Manchester, UK # 11239-1-AP |
| αSMA Clone 1A4 | 1:10,000 (IHC) | Monoclonal | Mouse | IgG2a | Sigma, Dorset, UK #A2547 |
| Carbonic anhydrase IX (CAIX) | 1:500 (IHC) | Polyclonal | Rabbit | IgG | Abcam, Cambridge, UK #ab15086 |
| Sodium Bicarbonate | 1:2000 (IHC) | Polyclonal | Rabbit | IgG | Abcam, Cambridge, |

| | | | | | |
|---|---|---|---|---|---|
| Cotransporter 1 (SLC4A4) | | | | | UK #ab187511 |
| C-X-C motif ligand 1 (CXCL1) | 1:500 | Polyclonal | Rabbit | IgG | Abcam, Cambridge, UK #ab8643 |
| C-X-C motif ligand 5 (CXCL5) | 1:50 | Polyclonal | Rabbit | Unknown | Abcam, Cambridge, UK #ab9802 |
| C-X-C motif ligand 6 (CXCL6) | 1:2000 | Polyclonal | Rabbit | IgG | Novus Biological, Abingdon, UK #NBP1-33078s |
| C-X-C motif ligand 8 (CXCL8) | 1:25 | Monoclonal | Mouse | IgG1 kappa | Abcam, Cambridge, UK #ab1867 |
| C-X-C motif receptor 2 (CXCR2) | 1:100 | Monoclonal | Mouse | IgG2A | R & D Systems, Abingdon, UK #MAB331 |

**Table 2.1** ***List of primary antibodies used for immunohistochemistry and immunofluorescence which respective dilutions and suppliers.***

*Isotype controls*

| **Antigen** | **Dilution** | **Monoclonal /Polyclonal** | **Host** | **Isotype** | **Supplier and product code** |
|---|---|---|---|---|---|
| Isotype | As required | Monoclonal | Mouse | IgM | Abcam, Cambridge, UK #ab18400 |
| Isotype | As required | Polyclonal | Rabbit | IgG | Invitrogen, Life Technologies, Paisley, UK #10500C |
| Isotype | As required | Monoclonal | Mouse | IgG | Vector Labs, Peterborough, UK #I-2000 |

| | | | | | |
|---|---|---|---|---|---|
| Isotype (Alexa Fluor® 488) | As required | Monoclonal | Mouse | IgG2a | Abcam, Cambridge, UK #ab171464 |

**Table 2.2** ***List of isotype controls used for immunohistochemistry and immunofluorescence which respective host species and suppliers.***

*Secondary antibodies*

| Primary antibody | Dilution and application | Conjugate | Host | Isotype | Supplier and product code |
|---|---|---|---|---|---|
| Anti-rabbit | Ready to use (IHC) | Horseradish peroxidase | Horse | IgG | Vector Labs, Peterborough, UK #MP-7401 |
| Anti-mouse | Ready to use (IHC) | Horseradish peroxidase | Horse | IgG | Vector Labs, Peterborough, UK #MP-7402 |
| Anti-rabbit | 2 drops/ml (IF, IHC-Fr) | Alexa Flour® 594 | Goat | IgG | Invitrogen, Life Technologies, Paisley, UK #R37117 |
| Anti-mouse | 2 drops/ml (IF, IHC-Fr) | Alexa Flour® 488 | Goat | IgG | Invitrogen, Life Technologies, Paisley, UK #R37120 |
| Anti-mouse | 1:250 (IHC) | Horseradish peroxidase | Goat | IgM | Sigma, Dorset, UK #A8786 |
| Anti-mouse | 1:100 (IF) | FITC | Goat | IgM | Sigma, Dorset, UK #F9259 |

**Table 2.3** ***List of secondary antibodies used for immunohistochemistry and immunofluorescence which respective dilutions and suppliers.***

### 2.1.4 Inhibitors and drug compounds

| Inhibitor | Target | Concentration used | Supplier and product code |
|---|---|---|---|
| L006235 | Cathepsin K | 100nM | Tocris, Biotechne, Bristol, UK #3066 |

| | | | |
|---|---|---|---|
| E64 | Cysteine proteases | 10μM | Tocris, Biotechne, Bristol, UK #5208 |
| CHC | Monocarboxylate transporters | 1mM | Tocris, Biotechne, Bristol, UK #5029 |
| S4 | Carbonic anhydrases IX and XII | 100μM | Tocris, Biotechne, Bristol, UK #5577 |
| Acetazolamide | Carbonic anhydrases | 1mM | Sigma, Dorset, UK #A6011 |
| BIX | Sodium $H^+$ exchanger 1 | 100nM | Tocris, Biotechne, Bristol, UK #5512 |
| S0859 | Sodium bicarbonate transporters | 50μM | Sigma, Dorset, UK #SML0638 |
| Concanamycin A | Vacuolar-type $H^+$-ATPases | 100nM | SantaCruz Biotech, Insight Biotech, Wembley, UK #sc-202111 |
| Rapamycin | mTOR | 10nM | Calbiochem, Merck, Hertfordshire #553211 |
| β-Estradiol | Oestrogen receptor agonist | 10nM | Sigma, Dorset, UK #E2758 |
| SB225002 | CXCR2 | 100nM | Selleck Chem, Stratech Sci, Suffolk, UK # S7651 |

**Table 2.4** ***List of inhibitors used listed with the working concentrations used*****.**

## 2.2 Mammalian cell and tissue culture techniques

### 2.2.1 Primary Cells and Cell Lines

| Cell Type | Cell ID | Derivation |
|---|---|---|
| Human Airway Smooth Muscle cells | HASM (D0501) | Extracted from human tracheal rings of non-asthmatic patients and characterised by >95% actin staining by immunofluorescence, by Dr. Bo Liu (Division of Respiratory Medicine, University Of Nottingham, UK) according to a previously described method (Bellini and Mattoli, 2007) |
| Normal Human Lung Fibroblasts | NHLF (0000343490) | Commercially bought primary fibroblasts isolated from normal lungs of a female pre-menopausal donor. Obtained from Lonza, Slough UK. |
| Human Pulmonary Fibroblasts | HPF (9102601.5) | Commercially bought primary fibroblasts isolated from normal lungs of a female pre-menopausal donor. Obtained from Promocell, Heidelberg, Germany. |
| Human lung fibroblasts | RS11010 | Derived by Nottingham University Hospital, BRU from normal lung regions of patient biopsies. |
| $TSC2^{-/-}$ cells | 621-101 cells | Human TSC-null cells isolated from an angiomyolipoma. Cells were isolated characterised by the lack of tuberin expression by Yu et al (Yu et al., 2004). These cells were a gift from Dr Elizabeth P. Henske (Harvard Medical School) |
| Human Mast Cell line-1 | HMC-1 cells | Human mast cell line-1 isolated from a patient with mast cell leukaemia were found to be phenotypically similar to human mast cells (Nilsson et al., 1994). these cells were a gift from Prof |

| | | |
|---|---|---|
| | | Peter Bradding, University of Leicester, UK |
| LAM Lung Derived Human Fibroblasts | NC0913 | LAM lung derived fibroblasts were isolated during this study by the author (Division of Respiratory Medicine, University of Nottingham, UK). Cells were isolated from transplant lung tissue, enzymatically digested and were characterised as described further in this thesis. |
| | HF0114 | |
| | NC0914 | |
| | HF1014 | |

**Table 2.5** ***Primary cell and commercial cell types used in this study with their method of derivation.***

### 2.2.2 Patient cohort and tissue samples

Women with LAM receiving clinical care at the UK LAM Centre, were enrolled in a comprehensive cohort study. Informed consent was obtained for the use of tissue taken as part of clinical care, including diagnostic biopsy or diseased LAM lung removed at the time of lung transplantation to be used for cell and tissue culture. LAM lung tissue removed at the time of transplantation was received from UK transplant centres and the National Disease Research Interchange (USA). The study has approval from the Nottingham research ethics committee (Ref. 13/EM/0264) and written informed consent was obtained from all patients.

### 2.2.3 Primary cell isolation and culture

Fresh LAM lung tissue from four donors obtained at the time of transplant was cut into approximately 1.2cm x 1.2cm pieces. Cut tissue was teased

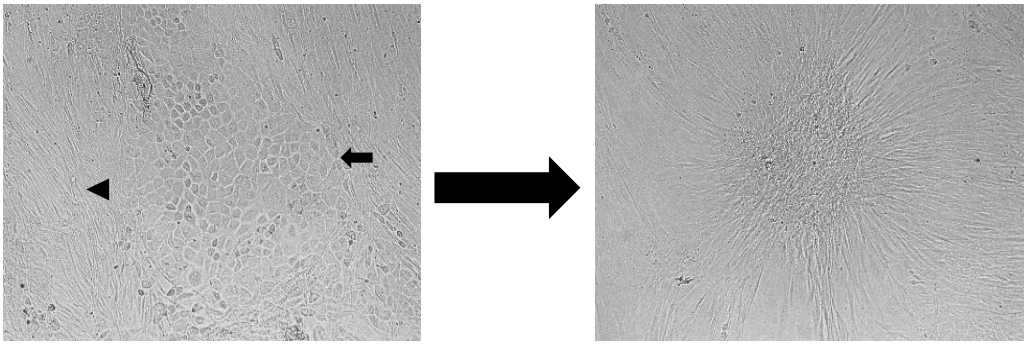
apart using a scalpel and needle making cuts in the tissue to aid dissociation. A 2mg/ml Collagenase (*Clostridium histolyticum, TypeII)* (Sigma, Dorset, UK) solution was prepared using in Dulbecco's Modified Eagle Medium/Nutrient Mixture F-12 (DMEM/F-12, Life Technologies, Paisley, UK) and tissue was submerged in medium and left in a standard humidified incubator at 37°C and 5% $CO_2$ for an overnight period. Digested tissue was then washed twice in media to get rid of debris. Dissociated cells were pelleted, resuspended in fresh DMEM/F-12 supplemented with 10% v/v foetal calf serum (FCS, Life Technologies, Paisley, UK) and x1 Antibiotic Antimycotic solution (Sigma, Dorset, UK), plated in 75$cm^2$ flasks and left to adhere overnight. Initial culture of the derived cell population yielded both spindle shaped and epitheliod adherent cells. Cells were subsequently sub-cultured which yielded a homogenous population of adherent proliferative fibroblast-like cells (FLC) from all donors.

Commercially bought normal human lung fibroblasts (NHLF, Lonza, Slough, UK) and human pulmonary fibroblasts (HPF, Promocell, Heidelberg, Germany) were recovered from frozen cryovials and initially seeded into 75$cm^2$ flasks containing Fibroblast Growth Medium (FGM) supplemented with basic fibroblast growth factor and 5µg/ml insulin (Promocell, Heidelberg, Germany). In order to wean fibroblasts off the FGM a 1:1 mixture of FGM and DMEM/F-12 was used in the subsequent culture after which media was replaced with DMEM/F-12 supplemented with 10% v/v FCS and x1 Antibiotic Antimycotic solution. Both NHLFs and HPFs will be collectively referred to as NHLFs from here on.

Human mast cell line-1 (HMC-1) was a generous gift from Prof Peter Bradding, University of Leicester, UK. These cells were cultured in Iscove's Modified Dulbecco's Medium (IMDM) with GlutaMAX™ (Fisher Scientific, Loughborough, UK) supplemented with 10% v/v FCS and x1 Antibiotic Antimycotic solution in a standard humidified incubator at 37°C and 5% CO2.

Human airway smooth muscle cells (HASM) were derived as described in Table 2.5 and were cultured in Dulbecco's Modified Eagle Medium (DMEM) (Sigma, Dorset, UK) supplemented with 10% v/v FCS and x1 Antibiotic Antimycotic solution in a standard humidified incubator at 37°C and 5% $CO_2$.

*TSC2 null* 621-101 cells were derived from a renal angiomyolipoma of a patient with sporadic LAM in a method described by Yu et. al (Yu et al., 2004) and were a gift from Prof Elizabeth P Henske (Harvard University) These cells were also cultured in DMEM/F-12 supplemented with 10% v/v FCS and x1 Antibiotic Antimycotic solution in a standard humidified incubator at 37°C and 5% $CO_2$.



Initial population of tissue digest

Fibroblast-like cells - subsequent culture

**Figure 2.1** ***Collagenase digest of LAM lung tissue.*** *Enzymatically digested LAM lung tissue initially yielded a mixed population of cells consisting of epitheloid-shaped cells (arrow) and spindle-shaped fibroblast-like cells (arrowhead). Subsequent culturing (P1 and onwards) resulted in a uniform population of proliferative spindle-shaped fibroblast-like cells.*

### 2.2.4 Thawing and sub-culturing cells

Liquid nitrogen frozen cryovials containing FLCs, NHLFs, 621-101 cells and HMC-1 cells were thawed by partial immersion in a water bath at 37°C. Once thawed, the cells were transferred to a universal tube containing 5-10 ml pre-warmed DMEM, DMEM/F-12 or IMDM supplemented with 10% FCS and x1 antibiotic and antimycotic solution (from here on referred to as complete medium) prior to being centrifuged. The supernatant was then aspirated and the resultant cell pellet was resuspended in 1ml complete medium and seeded in a 75cm$^2$ tissue culture flask containing 15ml complete medium.

FLCs and NHLFs once 90-100% confluent and 621-101 cells when 70% confluent were subjected to subculture. The latter do not contact inhibit and hence can overgrow and die if left to full confluency. After removing the existing medium the cell monolayer was detached by washing once with pre-warmed x1 Trypsin-EDTA solution (Sigma, Dorset, UK) and then

incubating for 2-5 minutes at 37°C and 5% $CO_2$. Cells were urged to detach with gentle tapping after which the cell suspension was transferred to a universal tube containing 5-10ml complete medium to inhibit trypsin activity. The cell were centrifuged, resultant supernatant aspirated and the cell pellet resuspended in 1ml complete medium. In the case of FLCs and NHLFs and the resultant cell solution was equally distributed between 4 75cm$^2$ tissue culture flasks whereas 621-101 cells were distributed between 10 75cm$^2$ tissue culture flasks.

Suspension cell line HMC-1 were observed for cell clusters. If the clusters increased in proportion to the area of the flask, the cell containing medium was aspirated into a universal tube and centrifuged. Resultant supernatant was discarded and the cell pellet was resuspended in 1ml complete medium. The cells were then distributed between 10 75cm$^2$ tissue culture flasks.

### 2.2.5 Cryopreservation of cells

Cells per 75cm$^2$ tissue culture flask were detached as described in section 2.2.4. The freezing medium consisting of 90% FCS and 10% dimethyl sulphoxide (DMSO, Sigma, Dorset, UK) was prepared and the resultant cell pellet was resuspended in it following which it was transferred to a cryovial. The cryovials were placed in -80°C for 24-48 hours and then transferred to liquid nitrogen for long term storage.

### 2.2.6 Standard method for cell culture experiments

FLCs, NHLFs and 621-101 cells were thawed and subcultured as described in section 2.2.4. Unless otherwise stated, prior to any experiments, cells were serum starved for an overnight period following which they were detached and counted using a Neubauer chamber haemocytometer. Cell were mixed in a 1:1 ratio with 0.4% trypan blue solution (Sigma, Dorset, UK) to account for dead cells prior to counting. Cells were counted as per the experimental conditions and were used only between passages 3 and 6. All of the experiments per donor were performed in triplicate or as six replicates and where necessary, the replicates were pooled.

### 2.2.7 Standard method for explant tissue culture

Whole lungs excised at the time of transplant were obtained from UK transplant centres. LAM lung tissue was thoroughly washed in DPBS followed by several washes of DMEM supplemented with x1 antibiotic and antimycotic solution (Sigma, Dorset, UK). Tissue from two donors was freshly cut into approximately 4mm x 4mm pieces from six different areas of the lung parenchyma. Each of the tissue explants were placed in each well of a 24-well tissue culture plate and three such plates were set up per donor. The tissue explants were allowed to equilibrate overnight in serum-free DMEM/F-12. The following day, tissue explants were treated with either vehicle (DMSO), 10nM β-estradiol, 10nM rapamycin or a combination of 10nM β-estradiol and 10nM rapamycin for 48 hours.

### 2.2.8 Labelling cells with CellTracker™ Dyes

CellTracker™ Dyes (Invitrogen, Life Technologies, Paisley, UK) were used to label cells in culture used in co-culture models in order to distinguish between two cell types. Medium was aspirated from cell monolayers cultured in 75cm$^2$ flasks. The medium was replaced with serum free DMEM/F-12 supplemented with 4nm CellTracker™ Green CMFDA dye (Invitrogen, Life Technologies, Paisley, UK) for fibroblasts and 4nm CellTracker™ Orange CMTMR dye (Invitrogen, Life Technologies, Paisley, UK) for 621-101 cells. Cells were then placed in the incubator for 30 minutes at 37°C and 5% $CO_2$ until the dye was incorporated by the cells. The dye containing medium was then aspirated and replaced with fresh serum free DMEM/F-12 for another 30 minutes. Following this the cells could be detached and used experimental procedures.

### 2.2.9 MTT Reduction assay

The 3-(4,5-Dimethylthiazol-2-Yl)-2,5-Diphenyltetrazolium Bromide or MTT colourimetric assay is used to evaluate cell viability. The conversion of tetrazolium salt MTT to formazan crystals requires cellular mitochondrial activity. As mitochondrial activity is constant for most viable cells, an increase or decrease in this activity is indicative in an increase or decrease in cells, hence the assay serves as a surrogate marker for cell number (van Meerloo et al., 2011).

A 0.5mg/ml MTT (Sigma Aldrich, Dorset, UK) solution was prepared using DMEM/F-12 phenol red free medium. On the designated experimental day,

the existing overlaying media was aspirated, cell monolayer was briefly washed with DPBS and depending on the culture vessel, replaced with 0.5 to 1ml of the freshly prepared MTT solution. The plate was returned to the incubator at 37°C and 5% $CO_2$ for 2-6 hours protected from direct light. The incubation time was determined depending on the cell density as sparse cultures required longer incubation times (Sieuwerts et al., 1995). Following incubation, MTT solution was gently aspirated and 0.5 to 1ml of isopropyl alcohol (propan-2-ol) solution was added to each well to solubilise the formazan crystals resulting in a purple coloured solution. The solution was resuspended and each sample was transferred as 100µl triplicates in a 96-well plate. A solvent only (isopropyl alcohol) blank was also set up and the absorbance as measured at 570nm with a background subtraction at 690nm using the Flexstation 3 Multi-Mode Microplate Reader (Molecular Devices, Berkshire, UK).

### 2.2.10 AlamarBlue® assay

Another marker for cell viability and proliferation, AlamarBlue® monitors the reducing environment of the living cell. Live cells maintain a reducing environment in their cytosol. The active ingredient resazurin is cell permeable which is converted to resorufin a pink coloured highly fluorescent under reducing conditions in the cells. Thus an increase or decrease in colour intensity or fluorescence is an indication of viable and proliferative cells (Rampersad, 2012, ThermoFisherScientific, 2008).

On the designated experimental day, 100µl of 10x alamarBlue solution (Thermo Scientific, Life Technologies, Paisley, UK) was added to the existing cell culture medium in each well resulting in a x1 final concentration. Appropriate experimental controls were also set up. Culture plates were then returned to the incubator at 37°C and 5% $CO_2$ for 4 hours protected from direct light. Following incubation, the resultant AlamarBlue sample and control solutions were transferred in triplicate to a black-walled 96-well plate and fluorescence was read using the Flexstation 3 Multi-Mode Microplate Reader (Molecular Devices, Berkshire, UK) at an excitation wavelength of 540nm and emission wavelength of 610nm.

## 2.3 Quantification of gene expression

### 2.3.1 Tissue homogenisation

Fresh LAM lung tissue obtained at the time of transplant was cut into 180 to 240mg pieces each from six different areas of the lung parenchyma and snap frozen. Optimal cutting temperature (OCT) embedded donated LAM lung tissue obtained from the National Disease Research Interchange (NDRI) was cut into 180 to 240mg pieces. 250µl per 40mg of fresh frozen and OCT embedded tissue of lysis buffer containing freshly added 2-mercaptoethanol (2-ME, Sigma, Dorset, UK) was added and the tissue was either manually homogenised using disposable polypropylene pestles (Sigma, Dorset, UK) or mechanically homogenised using an IKA-ultra-turrax® T25 (IKA, Oxford, UK) homogeniser. This was followed by shearing using a 19-gauge needle (Becton Dickson, Oxford, UK),

centrifuging for 10 minutes and filtering the supernatant using GenElute™ Filtration Columns (Sigma, Dorset, UK) to remove tissue debris. The flow through was retained and taken further for total RNA extraction.

### 2.3.2 Total ribonucleic acid (RNA) extraction

Total RNA was extracted using GenElute™ Mammalian Total RNA Miniprep Kit (Sigma, Dorset, UK) with an adapted protocol. A total of 250µl of lysis buffer solution with freshly added 2-mercaptoethanol for up to $5x10^6$ cells was added and the resulting solution was resuspended before harvesting with scraping followed by vortexing. The tissue lysate obtained after filtering as described (section 2.3.1) and cell lysate was then mixed with equal amount of 70% RNase-free ethanol which was mixed into the lysate by inversion and then loaded onto a GenElute™ binding column. The column was centrifuged at 14,000rpm for 1min at room temperature (RT) to bind RNA. This was followed by an on-column DNase I enzyme digest (Sigma, Dorset, UK) for the removal of contaminating genomic deoxyribonucleic acid (DNA). Column bound RNA was treated with 80µl of DNase I solution (10µl DNase I + 70µl DNase I buffer) for 15mins at RT before washing with 250µl of wash solution 1 followed by centrifugation (14,000rpm, 1min, RT). The column was washed a second time using 500µl of wash solution 2 followed by centrifugation (14,000rpm, 1min, RT). The addition of wash solution 2 was repeated followed by centrifugation at 14,000rpm for 2 mins at RT. The column was then centrifuged without adding any solution at 14,000rpm for 1 min at RT.

Lastly the binding column was transferred to a fresh tube, 30µl of elution solution was added followed by centrifugation at 10,000rpm for 2 mins at RT to yield RNA which was collected and immediately stored at -80°C.

### 2.3.3 Complementary DNA (cDNA) synthesis

cDNA synthesis was performed using the SuperScript® III First-Strand Synthesis System (Invitrogen, Life Technologies, Paisley, UK) alongside random hexamers (Invitrogen, Life Technologies, Paisley, UK). A modified double reaction was set up using a mastermix (Table 2.6) for each reaction. 500ng of RNA was used for each 26µl initial reaction. This was incubated at 65°C for 5 minutes, cooled for 1 minute on ice and then placed at RT.

| **Reagent** | **Volume per reaction (µl)** |
|---|---|
| Random hexamers (50ng/ml) | 4 |
| 5mN dNTP mixture | 4 |
| RNA | 500ng |
| DEPC water | As required |
| **Total** | **26µl** |
| 5x FS buffer | 8 |
| DTT(0.1M) | 4 |

**Table 2.6** ***cDNA mastermix***

The next master mix of 5x First Strand buffer and 0.1M dithiothreitol (DTT) was then added to the initial reaction. 2µl of SuperScript™ III Reverse Transcriptase (RT) (Invitrogen, Life Technologies, Paisley, UK) was added

to the +RT samples with 2µl of DEPC water added to the –RT samples. The samples were then placed in a thermocycler and cDNA synthesised using the program settings in Table 2.7.

| Temperature (°C) | Time (mins) |
|---|---|
| **25** | 10 |
| **42** | 60 |
| **72** | 15 |
| **4** | hold |

**Table 2.7 cDNA synthesis cycling conditions**

### 2.3.4 Quantitative real-time polymerase chain reaction (qRT-PCR)

Quantitative RT-PCR was performed to assess the relative abundance of gene transcripts using the Brilliant III Ultra-Fast SYBR® Green QPCR Master Mix (Agilent Technologies, Cheshire, UK). cDNA synthesised as described (section 2.3.3) was diluted 25-fold using DEPC water to account for the sensitivity of the reaction. A mastermix excluding the cDNA was then prepared as listed in Table 2.8 (a)

A

| Reagent | Volume per rection (µl) |
|---|---|
| 2x Brilliant III SYBR Green mastermix | 12.5 |
| Primer mix (5µm) | 1 |
| cDNA | 5 |
| DEPC water | 6.5 |
| **Total** | **25** |

B

| Temperature (°C) | Time | |
|---|---|---|
| 95 | 3mins | 40 cycles |
| 95 | 10secs | |
| 60 | 20secs | |
| 95 | 1min | |
| 55 | 30secs | |
| 95 | 30secs | |

**Table 2.8** ***qRT-PCR mastermix (A) and cycling conditions (B)***

20µl of mastermix per well and 5µl cDNA was added directly to each reaction in a 96-well reaction plate followed by secure sealing and briefly centrifuging before placing into a thermocycler. Reactions were run using the Mx3005P qPCR System and analysed with the MxPro Software (Agilent Technologies, Cheshire, UK). Predesigned and validated KiCq Start SYBR Green Primers (Sigma, Dorset, UK) were used which were selected on the basis of their rank and exon locations (Table 2.9)

| Rank | Location |
|---|---|
| 1 | The middle of one primer overlaps an exon splice site |
| 2 | The 5’ or 3’ end of one primer overlaps an exon splice site |
| 3 | The amplicon, but neither primer, overlaps an exon splice site |
| 4 | Primer overlap is not possible for various reasons, e.g. the gene has only one exon |

**Table 2.9** ***Ranks and corresponding locations of predesigned KiCq Start primers***

Reactions were performed in triplicate and PCR data was analysed using the comparative CT ($2^{-\Delta CT}$) method (Livak and Schmittgen, 2001) which provides normalisation to an endogenous reference in differing cDNA added to the reaction mixture. As total copy number is not a goal of these experiments, relative quantification is suitable as no standard curve is needed. Internal controls were validated to show that there was little variation of housekeeping gene expression with experimental protocols.

## 2.4 Histology and Cytology

### 2.4.1 Haematoxylin and Eosin staining

Formalin-fixed paraffin embedded tissue sections were dewaxed for 5 minutes in Histoclear (R.A. Lamb, Fisher Scientific, Loughborough, UK) and transferred to fresh Histoclear for a further 5 minutes. Slides were then rehydrated through a series of graded alcohols; 3 minutes each in 100%, 95%, 70% ethanol, then taken to deionised water ($dH_2O$) and then phosphate buffered saline (PBS). Slides were then transferred to a Coplin jar containing Mayer's Haematoxylin (Sigma, Dorset, UK) for 5 minutes to allow nuclear staining. Slides were rinsed in running tap water for 5 minutes after which they were transferred to a coplin jar containing Eosin (Sigma, Dorset, UK) for a further 5 minutes. Slides were then dehydrated back through the series of graded alcohols (70%, 95%, 100%), through to Histoclear and then mounted using VectaMount Permanent Mounting Medium (Vector Laboratories, Peterborough, UK) placing a coverslip lowered carefully over tissue, removing all air bubbles. Edges of the slide were then wiped and left to set for 24 hours at room temperature. Slides were imaged on Nikon Diaphot 300 Inverted Microscope (Nikon UK Limited, UK).

### 2.4.2 Chromogenic Immunohistochemistry (IHC)

Immunohistochemistry was performed on sections cut from FFPE wax blocks. Slides were dewaxed for 5 minutes in Histoclear followed by rehydration through the series of graded alcohols (100%, 95%, 70%),

through to $dH_2O$ and then PBS supplemented with 0.05% Tween 20 (Sigma, Dorset, UK) (PBST). Heat-induced epitope retrieval (HIER) was then performed using sodium citrate buffer solution, pH 6.0. The slides were then submerged in the buffer solution (pre-warmed in a microwave) placed in a Breville ITP181 steamer, heated to 100°C and incubated for 20 minutes. The steamer was then turned off and slides were left to cool for a further 20 minutes. Sections were then placed in PBST for a minute after which they were incubated with 3% aqueous hydrogen peroxide solution (Sigma, Dorset, UK) for 10 minutes to quench endogenous peroxidases. Sections were then rinsed in PBST and incubated with 2.5% horse serum (Vector Laboratories, Peterborough, UK) for 30 minutes at room temperature to block non-specific binding sites. Following this sections were incubated primary antibodies diluted in 2.5% horse serum and, unless otherwise stated, incubated overnight at 4°C. Sections were then washed 3 times in PBST for 10 minutes each followed by incubation with horseradish peroxidase conjugated secondary antibodies for 1 hour at room temperature. Washing was repeated as described above. Chromogenic detection was carried out using ImmPact DAB (diaminobenzidine) (Vector Laboratories, Peterborough, UK) prepared by adding 30µl of ImmPact DAB chromogen concentrate to 1ml of ImmPact DAB diluent. The resultant DAB working solution was applied on to tissue sections at incubated at room temperature for 2-5 minutes as optimised per antibody reaction. Sections were then rinsed in $dH_2O$ after which they were counterstained using Mayer's haematoxylin for 3 minutes at room temperature following by bluing under running tap water for 1 minute.

Slides were then taken to $dH_2O$ and subsequently dehydrated through the series of graded alcohols; 3 minutes each in 70%, 95% and 100% ethanol. Slides were then taken through to Histoclear, excess wiped carefully and tissue sections were mounted in VectaMount permanent mounting media (Vector Laboratories, Peterborough, UK) as described in section 2.4.1. Immunostained section images were acquired using a Nikon Diaphot 300 Inverted Microscope (Nikon UK Limited, UK) or a NanoZoomer (Hamamatsu Photonics, Hertfordshire, UK).

### 2.4.3 Fluorescent Immunohistochemistry (IHC-Fr)

Fluorescent immunohistochemistry was performed on FFPE tissue sections. Sections were dewaxed and subjected to HIER as described in section 2.4.2. The peroxidase block was omitted and sections were incubated with primary antibodies at 4°C overnight. The following day sections were washed as described (section 2.4.2) and incubated with fluorophore-conjugated secondary antibodies for 1 hour at room temperature. Sections were washed in PBST as described (section 2.4.2) followed by counterstaining with 4',6-diamidino-2-phenylindole (DAPI, Sigma, Dorset, UK) diluted 1:5000 using PBS for 10 minutes at room temperature. Excess PBS was carefully wiped off and sections were mounted using Fluorescent Mounting Medium (Dako UK Ltd, Ely, UK). Immunostained images were obtained using an Improvision spinning disc confocal microscope and Volocity 3D image analysis software V6.3 (Perkin Elmer, MA, USA).

### 2.4.4 Immunofluorescence

Immunofluorescence was performed on cells cultured in 8-well Nunc Lab-Tek II Chamber Slide System (Fisher Scientific, Loughborough, UK). Culture medium was aspirated, cells were washed 3 times for 5 minutes each with DPBS and then fixed using 4% formaldehyde solution (Sigma, Dorset, UK) overnight at 4°C. The following day, formaldehyde was aspirated and each well was washed 3 times with PBS. Cells were then permeabilised to expose the intracellular antigens by incubating with 0.15% Triton X-100 (Sigma, Dorset, UK) in PBS for 10 minutes followed by aspiration and washing 3 times with PBS. Cells were blocked with 10% goat serum (Sigma, Dorset, UK) in 1% bovine serum albumin (BSA) in PBS for 30 minutes at room temperature. Blocking agent was aspirated and fixed and permeabilised cells were then incubated with either primary antibodies or isotype controls diluted in blocking solution overnight at 4°C, unless otherwise stated (Table 2.1 and Table 2.2).

The following day primary antibodies were aspirated and wells were washed 3 times with PBS. Cells were then incubated with fluorophore conjugated secondary antibodies appropriately diluted (Table 2.3) with blocking agent for 1 hour at RT on a platform rocker, protected from light. The secondary antibodies were then aspirated and cells were washed 2 time with PBS. 4',6-diamidino-2-phenylindole (DAPI) (Sigma, Dorset, UK) at a stock concentration of 1mg/ml in $dH_2O$ was added to the last PBS wash at a working concentration of 0.2µg/ml to allow visualisation of the nuclei for 10 minutes at room temperature before aspirating. Chamber sections of the slides were removed, excess PBS was carefully wiped off

and slides were mounted by carefully placing a cover slip on each slide using Dako Fluorescent Mounting medium (Dako, Ely, UK). Images were obtained using the Improvision spinning disc confocal microscope using Volocity 3D image analysis software V6.3 (Perkin Elmer, MA, USA).

## 2.5 Protein determination

### 2.5.1 Bio-Plex® Multiplex Immunoassay

The Bio-Plex multiplex assay is a high-throughput multiplex bead array assay that is capable of quantifying large number of analytes. Coupled beads react with the analyte of interest within the samples and any unbound protein thereafter was washed off. A biotinylated detection antibody creates a sandwich complex and the final detection complex was formed by the addition of streptavidin-phycoerythrin (SA-PE) conjugate. Phycoerythrin fluoresces green and serves as a fluorescent indicator. The reader passes a red (635nm) laser to illuminate the fluorescent dyes within each bead to provide classification of beads and identification of the analyte. Simultaneously, a green (532nm) laser excites phycoerythrin generating a reporter signal. This is detected by a photomultiplier tube (PMT) and the Bio-Plex Manager™ software presents data as concentration (pg/ml) (Bio-Plex, 2017).

Bio-Plex Multiplex Immunoassay using a customised Bio-Plex® Pro Human Chemokine assay panel (Bio-Rad Laboratories, Watford, UK) was carried out as per manufacturer's instructions. In brief, supernatant samples were x2 diluted using DMEM/F-12 supplemented with 0.5% bovine serum

albumin (BSA). The standard was reconstituted and a fourfold standard dilution series was prepared with 9 standards named S1 to S9. DMEM/F-12 supplemented with 0.5% BSA was used as blank. 50µl of diluted (1x) coupled magnetic beads were added to each well of the 96-well assay plate. The plate was then placed on a magnet holder for 1 minute allowing the magnet to capture the magnetic beads and washed two times using the wash buffer supplied before aspirating and discarding the wash solution. Sample, standards, blanks and controls were vortexed and 50µl was added to each well. The plate was covered, protected from light and placed on a shaker at 850 rpm for 1 hour at room temperature. The plate was washed three times again using the magnet holder to capture the beads before discarding the wash solution. 25µl of diluted detection antibodies were added to the plate after which the plate was incubated in the dark for 30 minutes with shaking at 850 rpm at RT. This was followed by washing three times, adding 50µl of SA-PE was added to each well after which the plate was incubated in the dark for 10 minutes with shaking at 850 rpm at RT. The plate was washed thrice after which the beads were resuspended in 125µl assay buffer, shaken briefly at 850 rpm and then read using the Bio-Plex 100, 200 (Bio-Rad, Watford, UK) allowing for 50 reads per bead. The bead region and standard value for each analyte was set prior to reading the plate.

### 2.5.2 Proteome profiler™ Human Protease array

The Proteome profiler™ protease array (R and D Systems, Abingdon, UK) was performed to assess extracellularly released proteases. In brief, each pre-coated membrane was placed in each well of the 4-well multi dish supplied. Membranes were blocked in 2ml Array buffer 6 for 1 hour at room temperature on a rocking platform shaker. Samples were prepared and final volume was adjusted to 1.5ml using Array Buffer 6. 15µl of the detection antibody cocktail was added to each sample and incubated for 1 hour at room temperature. Following blocking samples were incubated with each membrane for an overnight period at 4°C on a rocking platform shaker.

The following day, membranes were washed 3 times for 10 minutes each in 20ml of wash buffer. This was followed by incubation with streptavidin-HRP (diluted 1:2000) for 30 minutes at RT on a rocking platform shaker and then washing 3 times for 10 minutes each. Dabbing off excess wash buffer, each membrane was placed on a flat plastic surface. 1ml of Chemi reagent mix was pipetted onto each membrane for 1 minute making sure the surface was coated evenly. Excess Chemi reagent mix was dabbed off and membranes were placed on a plastic tray taking care that no air bubbles were trapped underneath. The tray was placed in the LI-COR Odyssey® Fc Imaging System (LI-COR Biosciences UK Ltd, Cambridge, UK) for developing a dot blot image.

## 2.6 Microscopy and Image analyses

### 2.6.1 Microscopy and imaging

Fluorescence microscopy was carried out using the Improvision spinning disc confocal microscope and images were acquired using Volocity 3D image analysis software V6.3 (Perkin Elmer, MA, USA). Images were merged using ImageJ (Rasband, 1997-2016). Histology and brightfield images were acquired using the Nikon Diaphot 300 Inverted Microscope (Nikon UK Limited, UK). Immunohistochemical images were also acquired using the NanoZoomer and NDP.view.2 viewing software (Hamamatsu Photonics, Hertfordshire, UK)

### 2.6.2 Densitometry analysis

Dot blot images acquired using LI-COR Odyssey® Fc Imaging System (LI-COR Biosciences UK Ltd, Cambridge, UK). Images were imported into the Image Studio™ Lite version 5.2 software (LI-COR Biosciences UK Ltd, Cambridge, UK). Each duplicate dot on the blot represented a distinct protein sample. Under the analysis tab, the 'draw ellipse' tool was selected and an ellipse was drawn around each dot. The 'local background' subtraction was selected to eliminate background noise within the ellipse drawn. Mean pixel density readings generated by the software were exported to an Excel document and data was plotted.

## 2.7 Statistical Analyses

All data were processed using Microsoft Excel 2010 (Microsoft Corporation, USA). Unless otherwise stated, n=3 experimental data were presented with ± standard deviation (SD) and statistical analyses were performed for datasets using the GraphPad PRISM version 7.01 software (GraphPad Software Inc., La Jolla, CA, USA)

### 2.7.1 Analysis of variance

Tests were carried out to identify the variance occurring between groups compared. When comparing two independent samples either a Student's t-test or Multiple t-tests using a Bonferroni-Dunn post-hoc analysis was performed. When variance was investigated across 3 or more samples either a one-way ANOVA or a two-way ANOVA was performed. Post-hoc tests were carried out in order to confirm where the differences occurred between groups. A post-hoc Bonferroni correction was performed which takes into account the expected number of Type I errors and tests each individual hypothesis at a lower significance level. A Dunnet's post-hoc test was performed when all samples were compared to a selected control sample. All tests were carried out as two-tailed, where the null hypothesis is rejected when the value of the test statistic was less than 0.05 ($p<0.05$).

### 2.7.2 Linear regression and correlation analysis

Regression analysis was used to model the relationship between two or more variables using a straight line. Linear regression fits a straight line through the data to calculate the best fit value of the slope and intercept. Correlation analysis was used to calculate a correlation coefficient (r) which is a measure of the strength and direction of a linear relationship between two variables. Where x and y have a strong positive linear correlation (as values for x increases, values for y also increase) r is close to +1. Where r is close to -1 this indicates x and y have a strong negative correlation. Correlations in this thesis are non-normal (non-parametric) datasets therefore the non-parametric version of the statistical tool (Spearman's Correlation) was used.

# 3 CHAPTER 3: *In vitro* Modelling of Lymphangioleiomyomatosis

## 3.1 Introduction

### 3.1.1 Background

Laboratory models are an invaluable tool to investigate disease development in ways that are not possible in humans. The establishment of the Eker rat model first paved the way for subsequently better, genetically engineered mouse models and xenograft models to study LAM (Kwiatkowski, 2010, Clements et al., 2010). Although these models develop *TSC*$^{-/-}$tumours and are still widely used, they do not develop pulmonary LAM (Kwiatkowski, 2010). *In vitro* models based on human cells are therefore now being explored.

*In vivo* cells take cues from each other via the cell-cell contacts and extracellular matrix (ECM). As opposed to a 2-dimentional (2D) culture where cells grow in a monolayer, a true 3-dimensional (3D) conformation and the ECM components are required for most cells to form relevant physiological structures *in vitro* (Griffith and Swartz, 2006). The ECM provides physical support to the tissues and cells enmeshed therein, which is required for their normal functioning. The ECM in the lung plays an important role in influencing cell behaviour in both health and disease The pulmonary interstitium consists of non-cellular components, collagen primarily, and elastin fibres interspersed with the most commonly identified cellular component, fibroblasts, which are mainly responsible for ECM turnover (Dunsmore and Rannels, 1996, White, 2015). The parenchyma of a LAM lung consists of a heterogeneous population of cells

that aggregate to form nodules, within which only an estimated 20% of cells are associated with a bi-allelic inactivation of TSC2 (Pacheco-Rodriguez et al., 2007, Clements et al., 2015). This suggests that the remaining 80% of the cell population in a nodule is wild type with respect to TSC2. Histological examination of a LAM nodule shows the existence of at least two distinct populations of cells with a large number cells being spindle-shaped (Henske and McCormack, 2012) that are known to express mesenchymal cell markers such as vimentin, desmin and α-smooth muscle actin (Zhe and Schuger, 2004). It is therefore possible that these cells are of a fibroblastic phenotype.

The origin of these fibroblasts is unknown, however, it has been suggested that bone-marrow derived mesenchymal progenitors known as fibrocytes are the main contributors to new populations of fibroblasts and myofibroblasts as part of a stromal reaction to tumour development (Bellini and Mattoli, 2007). Another concept of fibroblast origin suggested a more local generation of fibroblasts from organ epithelium via epithelial-mesenchymal transition (EMT) (Iwano et al., 2002, Ogawa et al., 2006). Studies using bone marrow chimera mice have been consistent with the finding that pulmonary fibroblasts are derived from circulating fibrocytes via cytokine/chemokine recruitment. However it is not clear what phenotype of the fibroblast-like cell is recruited (Hashimoto et al., 2004, Schmidt et al., 2003, Phillips et al., 2004). *In vivo,* fibroblasts are relatively undifferentiated cells and, given the right stimulus, they are able to embark onto a path of differentiation acquiring features of other mesenchymal cells (Schmitt-Gräff et al., 1994). For example fibroblasts

can be activated by Transforming Growth Factor-beta (TGF-β) to give rise to the alpha-Smooth Muscle Actin (α-SMA) expressing fibroblast, known as the myofibroblast (Ogawa et al., 2006, Phan, 2008). Distinguishing between these two cell types, however is difficult.

Human lung fibroblasts have been known to be heterogeneous with respect to surface marker expression, proliferation and collagen production. This heterogeneity may arise from activation or differentiation processes taking place in the cells (Koumas et al., 2003). Thy-1 or Cluster of Differentiation 90 (CD90) that has been known to identify and phenotypically characterise fibroblasts into their distinct subsets (Baglole et al., 2005). This antibody was selected as our commercially bought normal human lung fibroblasts (NHLFs) have been characterised as $CD90^{+}$ cells (Promocell, 2015).

Fibroblast Activation Protein-alpha (FAP-α) has been shown to be expressed by reactive stromal fibroblasts and also in fibroblasts from Idiopathic Pulmonary Fibrosis (Acharya et al., 2006, Scanlan et al., 1994). This antibody was selected to determine if there was a difference in FAP-α expression between fibroblast-like cells isolated from LAM lung and NHLFs.

### 3.1.2 Aims & Objectives

The aims of this part of the study were to establish a working three-dimensional co-culture model of LAM consisting of the two main cell types identified in LAM nodules. This focused on the selection of the appropriate model, ECM substrate, cell number and cell ratio. In parallel the model was validated for markers of LAM, viability and proliferation.

## 3.2 Methods

### 3.2.1 Embedding Cells in Extracellular Matrix (ECM Gel)

NHLFs and 621-101 cells were cultured in DMEM/F-12 supplemented with 10% FCS as described which was replaced with DMEM/F-12 without FCS overnight. The cells were then labelled using CellTracker™ dyes as described in section 2.2.8 after which the cells were detached, pelleted and resuspended in DMEM/F-12. NHLFs, 621-101 cells or a 1:1, 5:1 and 10:1 mixture of NHLFs and 621-101 cells were counted to a total of $10^4$, $5x10^4$ and $10^5$ cells/well and were maintained at 4°C. The ECM gel (Sigma, Dorset, UK) was thawed overnight at 4°C and the cold liquid ECM gel was added to the cells in media at a concentration of 4 mg/ml (diluted from a stock concentration of 10 mg/ml). 500µl of the resulting co-culture and mono-culture solutions were added gently to each well of a pre-warmed (1 hour at 37°C) 24-well plate and the plate was maintained at 37°C and 5% $CO_2$ for 1 hour for the gels to set after which gels were overlaid with 500µl media to prevent drying out and put back into the incubator. Three NHLF donors were used and at least three wells per condition were set up. Gels were monitored for 7 days with images of cells taken on days 1, 3 and 7 using the Improvision spinning disc confocal microscope using Volocity 3D image analysis software V6.3 (Perkin Elmer, MA, USA).

### 3.2.2 Embedding Cells in Culturex® Basement Membrane Extract (BME) Gel

Fibroblasts (NHLFs and LAFs) and 621-101 cells were cultured, labelled, detached and resuspended in DMEM/F-12 as described in sections 2.2.4 and 2.2.8. A total of $5x10^4$ fibroblasts, 621-101 cells or a 10:1 mixture of fibroblasts and 621-101 cells were counted and maintained at 4°C. Culturex® BME gel (Trevigen, AMSBiotechnology, Abingdon UK) was thawed overnight at 4°C and was initially diluted from a stock concentration of 15.64mg/ml to 7.5mg/ml using DMEM/F-12 without FCS and maintained at 4°C. The diluted BME gel solution was added to the co-culture and mono-culture cell suspensions at a final concentration of 3.75mg/ml. For a 7.5mg/ml gel concentration, cells were added directly to the stock. 400µl of the resulting gel solution were gently added to each well of a pre-warmed 48-well plate (1 hour at 37°C) and the plate was maintained at 37°C and 5% $CO_2$ for 1 hour for the gels to set after which gels were overlaid with 400µl media to prevent drying out and put back into the incubator. Three NHLF and four LAF donors were used and at least three wells per condition were set up. Gels were monitored for 7 days with images of cells taken on days 1, 3 and 7 using the Improvision spinning disc confocal microscope using Volocity 3D image analysis software V6.3.

### 3.2.3 Spheroid (LAM Spheroid) Culture

Fibroblasts (NHLFs or LAFs) and 621-101 cells were cultured, labelled using CellTracker dyes, detached and resuspended using DMEM/F-12 as

described in section 2.3.4 and 2.2.8. Fibroblasts, 621-101 cells or a 10:1 mixture of fibroblasts and 621-101 cells were counted such that each spheroid contained $2x10^3$, $5x10^3$ or $10^4$ cells per spheroid. 100µl of this cell suspension was expelled into each well of the Lipidure-COAT® ULA 96-well U-bottomed plate (AMSBiotechnology, Abingdon, UK) and placed in the incubator at 37°C and 5% $CO_2$. Spheroids were formed spontaneously within 48 to 72 hours. Spheroids were imaged on days 1, 4 and 7 using the Improvision spinning disc confocal microscope using Volocity 3D image analysis software V6.3.

### 3.2.4 Organoid (LAMosphere) Culture

Fresh LAM lung tissue removed at the time for transplantation was obtained and cut into 1.2cm x 1.2cm pieces. Tissue was then teased apart using a scalpel and needle making cuts in the tissue to aid dissociation. A 0.5mg/ml Collagenase (*Clostridium histolyticum, type II,* Sigma, Dorset, UK) solution was prepared in DMEM/F-12, and tissue was submerged in and put placed at 37°C and 5% $CO_2$ for 3 to 4 hours. Digested tissue was then washed twice in DMEM/F-12 to get rid of tissue debris after which remaining tissue pellet containing cells was suspended in DMEM/F-12 supplemented with 10% FCS and plated onto 100mm tissue culture-treated culture dishes offering a low adhesive surface to cells. LAMospheres were formed after 24 hours and images were taken using a Nikon Diaphot 300 inverted microscope.

### 3.2.5 Measuring Spheroid and Organoid Size

Images of spheroids and organoids acquired using either a Nikon Diaphot Inverted microscope or an Improvision spinning-disc confocal microscope using Volocity 3D image analysis software V6.3 were imported into the ImageJ software (Rasband, 1997-2016). Here the scale of the images was set based on the magnification and known pixels and distance in μm of each objective. Once the scale was set, the line tool was selected and a horizontal, vertical and diagonal line was drawn across the longest diameter of the spheroid or organoids. The length of each line drawn was measured and the average of the three diameters was taken to be the diametric size of the spheroid or organoid.

### 3.2.6 Embedding Spheroids and Organoids

A 20mm x 25mm nylon mould consisting of 6 x 11 3mm diameter paraboloid-shaped pegs was 3D printed and kindly gifted by Dr Delyan Ivanov (Figure 3.2.1 (a)). The technique was adapted from (Ivanov and Grabowska, 2017). To make the spheroid and organoid embedding casket, 2ml of a 2% agarose solution (Sigma, Dorset, UK) was expelled into a 30mm x 24mm base mould (Simport, SLS, Nottingham, UK). The nylon mould was placed in the agarose solution and the base mould was kept at room temperature for 2 minutes and then at -20°C for 2 minutes for the agarose gel to set. Once set, the nylon mould was removed carefully which had now formed 3mm diameter holes into which the spheroids and organoids were expelled (Figure 3.2.1 (b)) and the base moulds were

centrifuged to allow settling. 1ml of 2-hydroxyethylagarose, type VII (Sigma, Dorset, UK), a low gelling temperature agarose was pipetted over the spheroids to cover the embedded area and the base mould was kept at room temperature for 1 minute and another minute at -20°C to set. This formed an agarose gel plug containing spheroids and organoids embedded within (Figure 3.2.1 (c)) which was then embedded in paraffin and formalin fixed paraffin (FFPE) embedded block sectioned at 4μm thickness.

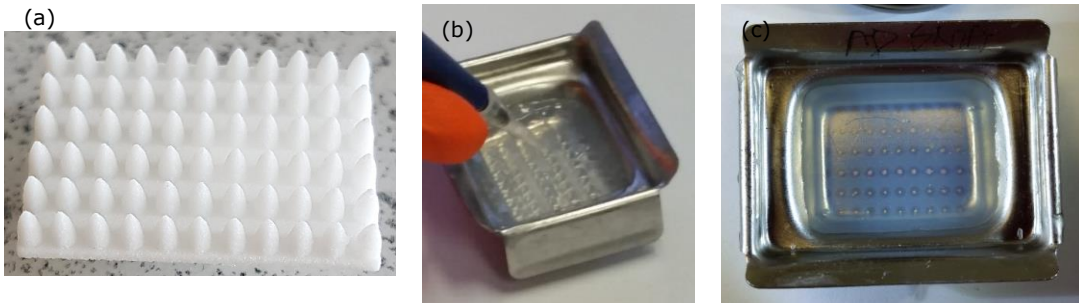



**Figure 3.2.1** ***Spheroid mould and agarose embedding of spheroids.*** *(A) Shows the nylon mould consisting 66 paraboloid-shaped pegs on a single plane. (B) Agarose gel after the mould-maker has been removed and spheroids are being cast. (C) Multiple spheroids embedded in a single agarose array.*

## 3.3 Results

To establish the 3-D co-culture model several new techniques needed to be established and optimised. The following sections demonstrate the process of developing this model and the results obtained therein.

### 3.3.1 Characterisation of Isolated Fibroblast-Like Cells via Immunofluorescent Detection of Fibroblast Markers

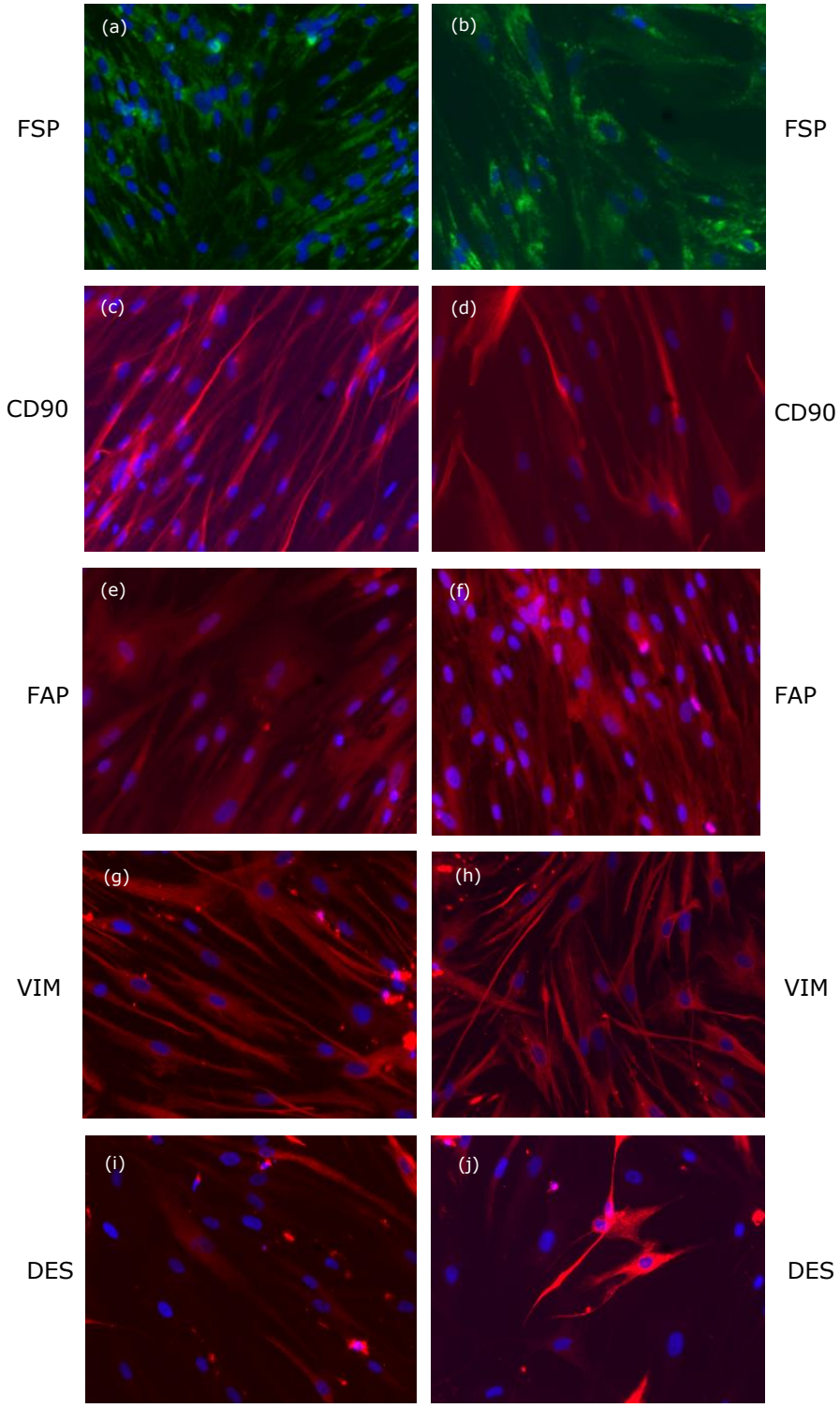


**Figure 3.3.1** ***Images of NHLFs and fibroblast-like cells (FLCs) showing presence of fibroblast markers.*** *All cells were cultured in media with the absence of FCS and are stained with DAPI (nuclei, blue). NHLFs and FLCs were stained with anti-fibroblast surface protein (FSP, clone 1B10, green), anti-CD90 (Thy-1), anti-FAP-α (FAP), anti-vimentin (VIM) and anti-desmin (DES) (red). Panels A, C, E, G and I show distinct expression patterns of the selected fibroblast markers in NHLFs as compared to FLCs (panels B, D, F, H and J). Images of cells taken at 20x using an Improvision spinning-disc confocal microscope.*

Cells released from the enzymatic tissue digest were cultured in DMEM supplemented with 10% FCS. Initial culture gave rise to a mixed population of cells consisting of both spindle shaped and epithelioid cells. Subsequent cell populations yielded homogeneous populations of adherent, proliferative fibroblast-like cells from all four donors. These fibroblast-like cells (FLCs) morphologically resembled primary human lung fibroblasts and could not be distinguished from commercially available normal human lung fibroblasts (NHLFs).

Immunocytochemistry was performed using an early passage of the fibroblast-like cells isolated from LAM lung tissue to ascertain their phenotype. Immunoreactivity of antibodies against established fibroblast markers was compared in both NHLFs and the isolated fibroblast-like cells. A similar staining pattern for FSP was observed in both the NHLFs and FLCs with expression of the antigen centred around the nucleus of the cell in a speckled pattern.

NHLFs exhibited extensive staining for Thy-1 or CD90 (Figure 3.3.1 (c)) showing strong immunoreactivity to anti-CD90 clearly along the cell membrane. The isolated FLCs however showed a weaker immunoreactivity with a few cells showing almost no membranous expression (Figure

3.3.1(d)). The expression pattern of Thy-1 or CD90 was therefore found to be consistent in the NHLFs but quite varied yet present among the FLCs.

Fibroblasts of a more reactive phenotype such as stromal fibroblasts or cancer-associated fibroblasts are known to express FAP-α (Brennen et al., 2012). A granular pattern of FAP-α staining was apparent in the fibroblast-like cells (Figure 3.3.1(f)). The NHLFs on the other hand, showed weaker staining for FAP-α (Figure 3.3.1(e)) suggesting that the derived fibroblast-like cells might have a more reactive phenotype.

Vimentin and desmin are known to be expressed by spindle-shaped cells in LAM nodules (Grzegorek et al., 2013) and the expression of mesenchymal marker vimentin (VIM), also used routinely for the identification of fibroblasts was visibly similar in both NHLFs and FLCs (Figure 3.3.1 (g) and (h)). The expression of desmin (DES) however was negligible in the NHLFs (Figure 3.3.1 (i)) with few FLCs (Figure 3.3.1 (g)) showing positive reaction to anti-desmin antibody again suggesting a more activated phenotype. Isotype controls were performed per donor for each antibody which were clean with little background staining. A representative image is shown in Appendix I.

A further characterisation study of the derived fibroblast-like cells was carried out to distinguish them from the other most abundantly found cells in the lung, normal airway smooth muscle cells (normal ASM, HASM), using α-SMA as the marker with cells cultured in the presence and absence of 10% FCS.

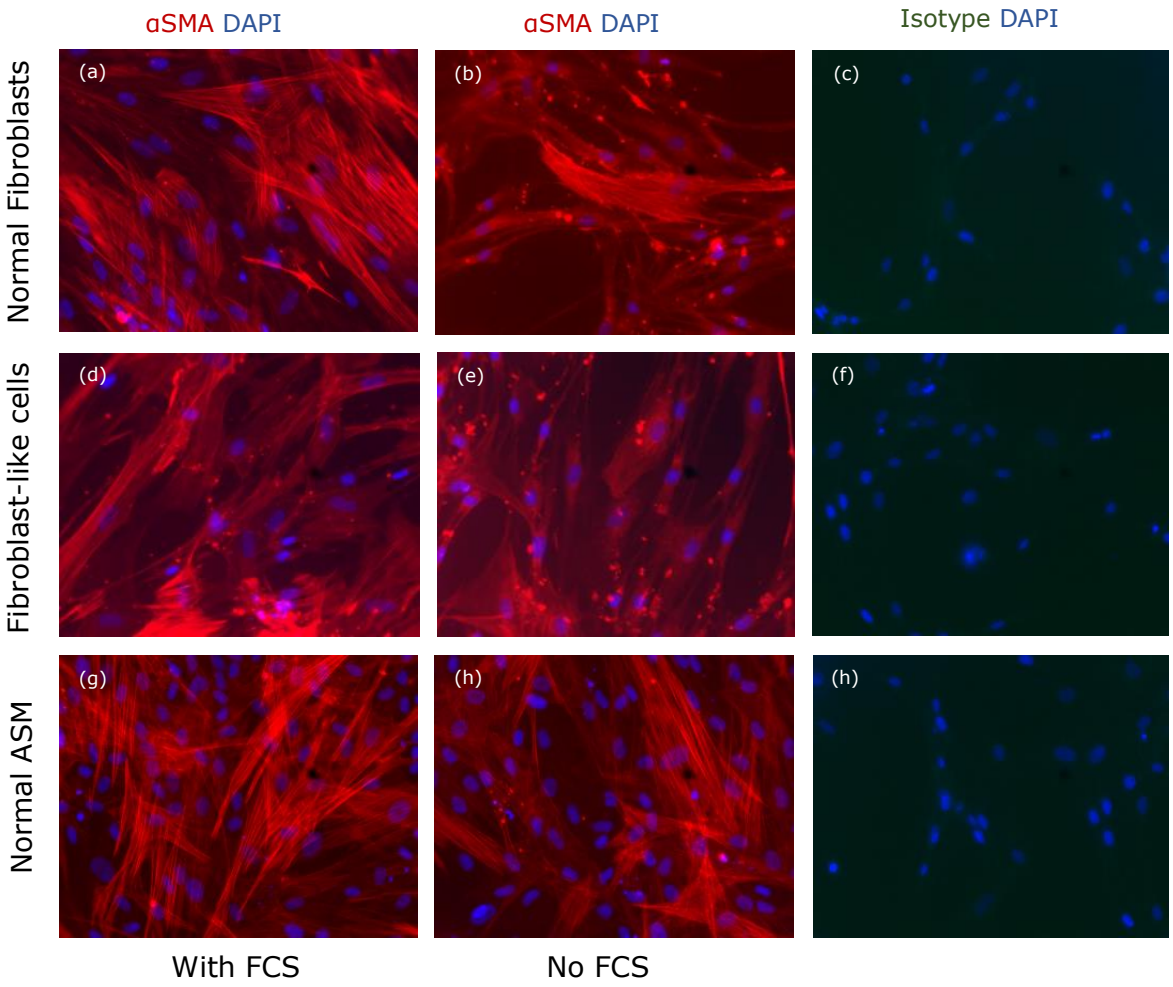



**Figure 3.3.2** ***Immunofluorescent images showing αSMA expression in NHLFs, FLCs and normal airway smooth muscle (normal ASM) cells.*** *Cells are immunostained with anti α-SMA (red), fluorophore-conjugated isotype (Alexa Fluor 488, green) and DAPI, (nuclei, blue). Panels A and D show NHLFs and FLCs respectively cultured in media containing FCS showing aligned actin filaments. Panels B and E show NHLFs and FLCs respectively cultured in media without FCS showing very few actin filaments. Panel G and H show normal ASM cells cultured in media with and without FCS showing actin filaments regardless of culturing condition. Panels C, F and I show isotypes for NHLFs, FLCs and ASM cells respectively. Images of cells taken at x20 using an Improvision spinning-disc confocal microscope.*

Figure 3.3.2 shows immunocytochemical staining performed for α-SMA to further characterise the fibroblast-like cells isolated from LAM lungs. Normal ASM cells, whether cultured continually in media containing FCS or serum starved for 48 hours showed stable expression of αSMA with the actin filaments being organised along the polar axis (Figure 3.3.2 (g and

h)). Similar expression of α-SMA was observed in the both the NHLFs and fibroblast-like cells cultured in media containing FCS (Figure 3.3.2 (a and d)) and both showed the presence of aligned actin filaments. The possible presence of growth factors in FCS provides an appropriate stimulus to the fibroblasts to acquire a more myofibroblastic phenotype displaying the presence of aligned actin filaments. However, the fibroblasts showed a more spindle-shaped morphology. On the other hand both types of fibroblasts when serum starved for 48 hours showed the presence of α-SMA showing positive red staining, but, exhibited very few to none actin stress fibres within their cytoskeleton (Figure 3.3.2 (b and e)) suggesting the presence of a large subset of an undifferentiated fibroblast population possibly due to the lack of activating factors from FCS. Immunostaining for all the selected fibroblast markers was performed in 3 LAF and 2 NHLF donors showing the same results as described. Isotype controls were clean with little background staining (Figure 3.3.2 (c, f and h)).

Using the markers selected, it can be concluded that the derived fibroblast-like cells, all showing a spindle-shaped morphology, were more similar to commercially bought control fibroblasts than to ASM cells. These fibroblast-like cells will therefore from here be described as **L**AM-**A**ssociated **F**ibroblasts or LAFs.

### 3.3.2 Extracellular Matrix (ECM) Gel as a Three Dimensional Scaffold

ECM gel (Sigma) an Engelbreth-Holm Swarm (EHS) murine tumour derived extracellular matrix offered a potentially useful biologically active scaffold for 3D cell culture. The main components of this extracted matrix are type IV collagen, laminin and a heparin sulphate-containing proteoglycan, perlecan which are important components of extracellular matrix and are required for proper adhesion of cells. The matrix solution which is liquid at 4°C forms a strong clear gel when warmed to 37°C. A growth factor reduced variant of the ECM gel (Kleinman and Martin, 2005) was also used.

#### 3.3.2.1 Determining Appropriate Cell Number and Ratio

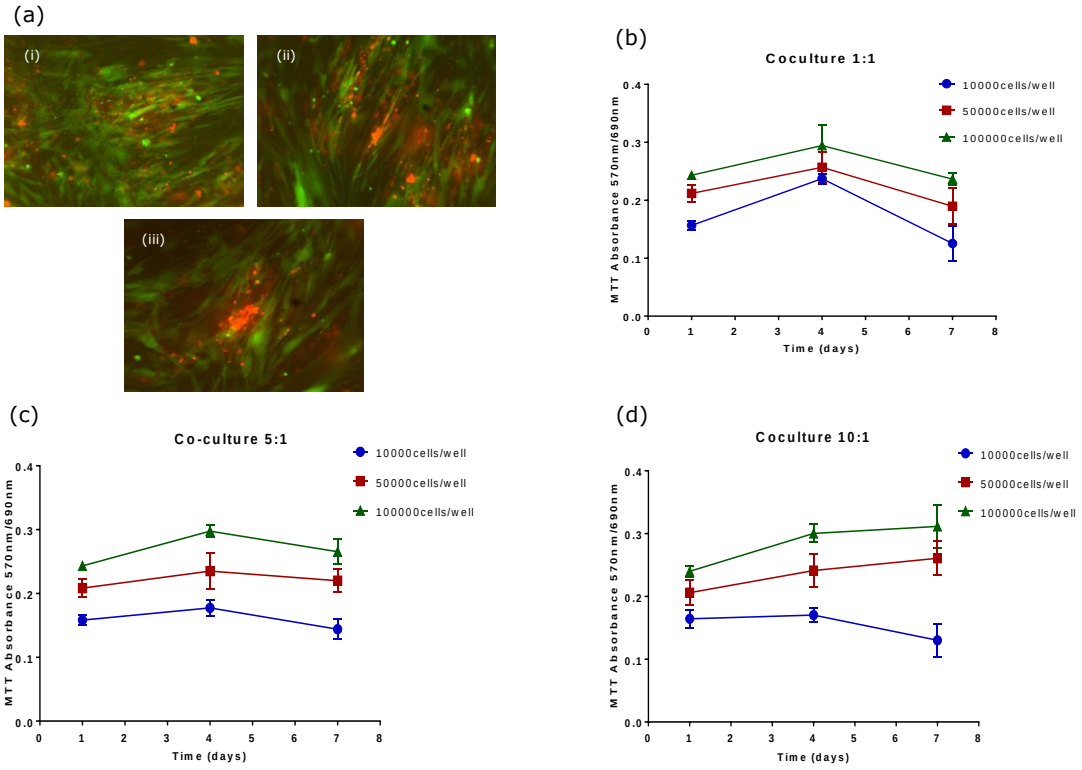



**Figure 3.3.3** ***Optimisation of cell number and ratio for 3D co-culture model.*** *Panels B, C and D show MTT readings obtained from NHLFs and 621-101 cells in co-culture at three different ratios 1:1, 5:1 and 10:1 respectively at three different cell densities. Panel A (i), (ii) and (iii) shows images of co-culture model at 10,000 cells/well in a 1:1, 5:1 and 10:1 ratio respectively. Values are mean ±SD (n=3 NHLF donors). Images of cells taken at x10 magnification using an Improvision spinning-disc confocal microscope. Labelled NHLFs and 621-101 cell images were merged using ImageJ software.*

For co-culture of fibroblasts with 621-101 cells, three different cell ratios (1:1, 5:1 and 10:1) and three different cell numbers ($10^4$, $5x10^4$ and $10^5$ cells/well) were assessed for viability for 7 days in the 3D BME gel via MTT reduction assay. NHLFs (n=3) were used to optimise culturing conditions suitable for the 3D LAM model. Figure 3.3.3 (b) shows both cells types cultured in a 1:1 ratio at different cell numbers. An initial increase in MTT assay signal at all three cell numbers was noted at day 4, however, by day 7 the signal reduced drastically suggesting a possible decrease in viable cells. This may be because cells in co-culture at a 1:1 ratio most likely become overcrowded due to the high proliferative capacity of 621-101 cells. At a 5:1 co-culture ratio, MTT reduction signal measured from cells at all three cell numbers showed a similar trend. Cells seeded at a $5x10^4$ cells per well however, showed a relatively more gradual decrease in MTT signal by day 7. This too could be attributed to overgrowth and a subsequent lack of nutrients. Figure 3.3.3 (a (ii)) shows a representative image of NHLFs and 621-101 cells in co-culture in a 5:1 ratio at a density of $10^5$ cells/well.

At a 10:1 co-culture ratio; $10^4$ cells/well showed a decrease in MTT signal at day 7. The MTT signal showed a linear increase when cells were seeded at $5x10^4$ cells/well, however when seeded at $10^5$ cells/well viability reached a plateau by day 7. Co-culturing NHLFs and 621-101 cells at both $5x10^4$ and $10^5$ cells/per well in a 10:1 ratio showed a steady MTT signal and therefore stable viable population of cells to maintain the model for 7 days. With an aim to have adequate number of viable cells, whilst avoiding overgrowth of cells, an initial seeding density of $10^5$ cells/well of a 24-well

plate was selected. Figure 3.3.3 (a (iii)) shows a representative image of NHLFs and 621-101 cells in co-culture in a 10:1 ratio at a density of $10^5$ cells/well.

Based on the MTT assay results a 10:1 co-culture ratio was selected for the model. This was also suitable to avoid overgrowth and overcrowding of cells due to the high proliferative capacity of the 621-101 cells compared to NHLF. The 10:1 ratio consisting of a larger population of wild type fibroblasts in our model also appeared to fit in with conditions *in vivo* as within a LAM nodule only 20% of cells express CD9 and CD44v6, markers that have been associated with bi-allelic inactivation of *TSC2* (Pacheco-Rodriguez et al., 2007).

### 3.3.2.2 Selection of the Appropriate Type of ECM Gel for 3D LAM Model Using Appropriate Cell Number and Cell Ratio

Cells were seeded in growth factor-reduced ECM gel (Sigma Aldrich, Cat #E6909) and in ECM gel containing full growth factors and phenol red (Sigma Aldrich, Cat #E1270) and were observed and imaged over a 7 day period. Cells were seeded in a 500µl gel plug in a 24-well plate at a density of $10^5$ cells/well.

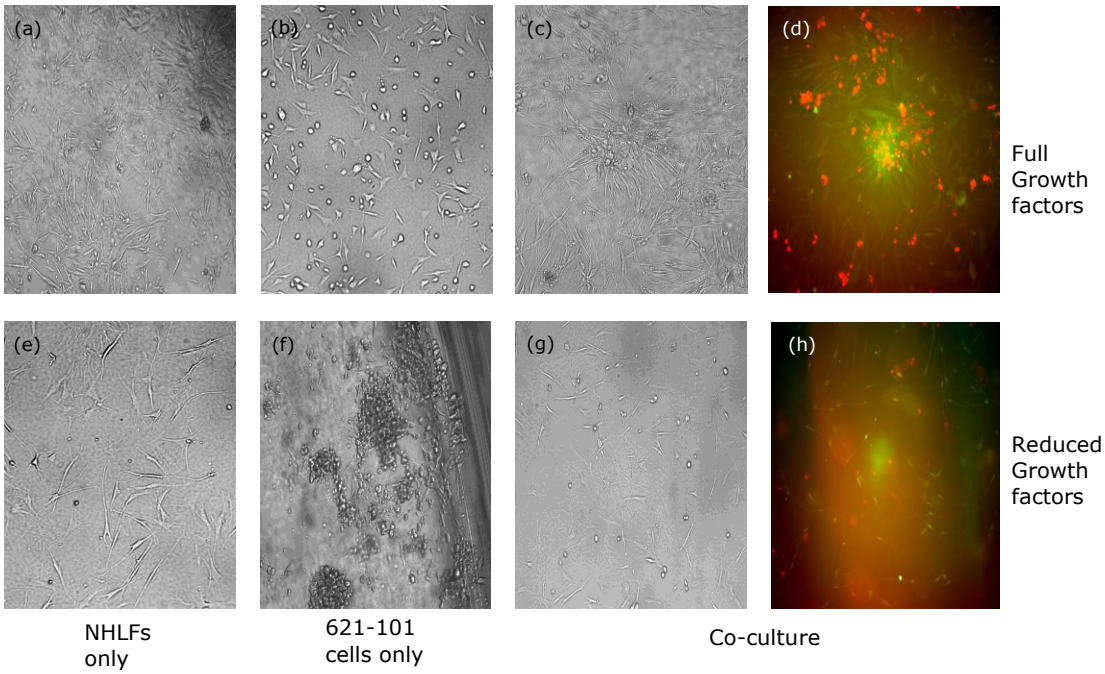



**Figure 3.3.4** ***Cells in co-culture and mono-culture embedded in ECM gel.*** *Images taken at day 3 show the NHLFs and 621-101 cells in co-culture (C, D and G, H) and mono-culture (A, B and E, F). Panels C (black and white) and D (coloured dye, NHLFs-green, 621-101 cells-red) show cells aggregating in full growth factor ECM gel. Panels G (black and white) and H (coloured dye, NHLFs-green, 621-101 cells-red) show reduced growth factor ECM gels with no aggregates. Images are taken at a x10 magnification using a Nikon Diphot Inverted microscope with epifluorescence.*

Figure 3.3.4 shows 8 representative images of NHLFs and 621-101 cells embedded in co-culture and mono-culture in ECM gel. Although 1x $10^5$ cells were seeded per well, the ECM gels with reduced growth factors showed a sparse scattering of cells in mono-culture with the 621-101 cells

only surviving on the edges of the well (Figure 3.3.4 (f)). In the full growth factor containing gel however, the cells were more viable and were seen in ample numbers. The two cell types in co-culture come together to spontaneously aggregate forming clumps containing both cell types. This phenomenon was not observed in the growth factor reduced gel condition where most cells did not survive well and remained apart.

Although the ECM gel initially showed promising results for modelling LAM in 3D, the results observed here were not reproducible as the gels did not consistently set within the same batch. A lot of batch variation was observed, as the exact concentration of the gelling components contained per batch in the ECM gel was unknown.

### 3.3.3 Culturex® Basement Membrane Extract (BME) Gel as a Three Dimensional Scaffold

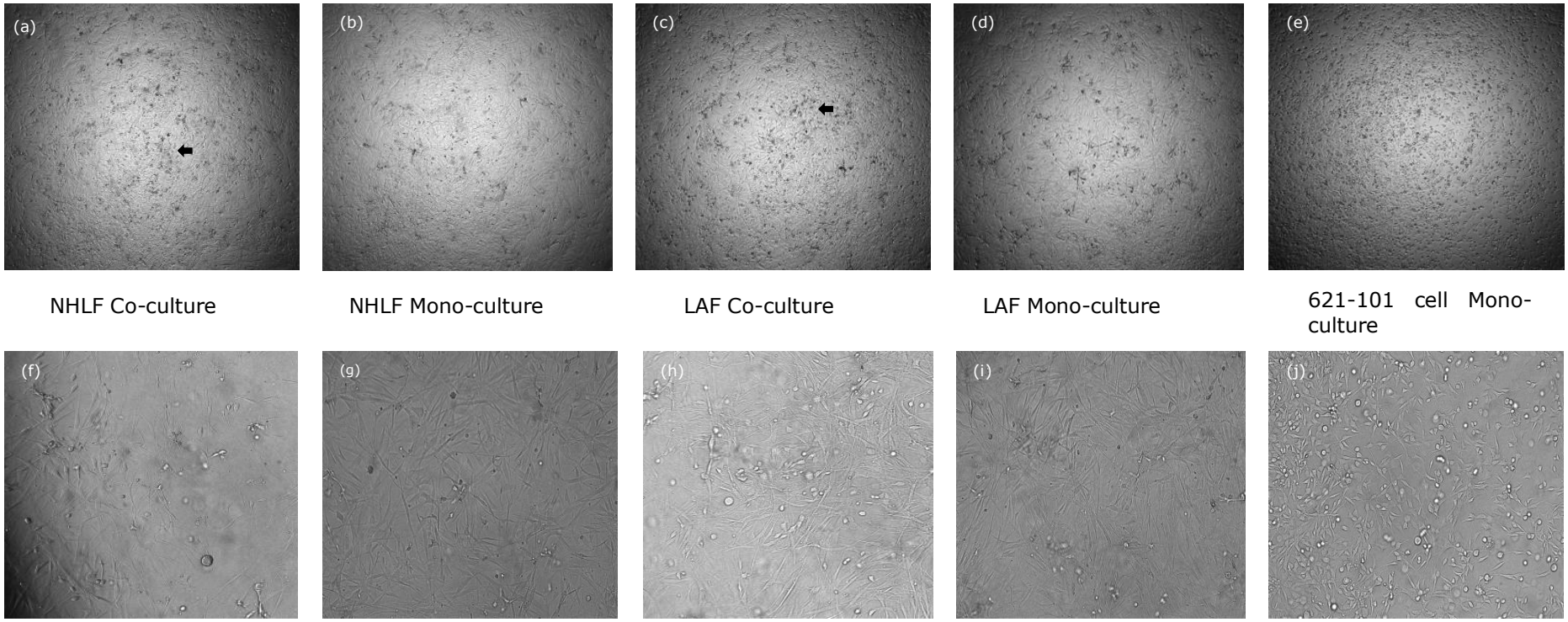



**Figure 3.3.5** ***NHLFs and LAFs in co-culture and mono-culture embedded in BME gel.*** *Images taken at day 3 show NHLFs and LAFs in co-culture and mono-culture. Panels A to E show x4 magnified images of gels in the in culture plate with co-culture showing formation of aggregates of both cell types (arrows, black). Panels F to J show x10 magnified images of cells embedded in gels showing a well spread out morphology. Images are taken using a Nikon Diaphot Inverted phase microscope.*

As the ECM gel was deemed unsuitable for use as a 3D scaffold due to its erratic gelling nature, Culturex® BME1 gel, was trialled which like ECM gel has been derived from the murine EHS tumour. The gel was diluted to 7.5mg/ml and 3mg/ml in which the cells were embedded. Gels formed using a 7.5mg/ml concentration were stiff due to which cells embedded in them did not survive beyond day 2. After initial optimisation using NHLFs, LAFs were used in the 3D models. Both NHLFs and LAFs behaved in the same manner when embedded within the 3mg/ml gel showing a well spread out spindle-shaped morphology (Figure 3.3.5 (b, g and d, i)) and in co-culture conditions are seen intertwined with 621-101 cells so as to form aggregates by day 3 (Figure 3.3.5 (a and c)). 621-101 cells on the other hand showed a more epithelioid-shaped morphology (Figure 3.3.5 (e and j)). The gels were set in a 48-well plate giving them a smaller surface area to set compared to a 24-well plate. The cell number was also therefore reduced to $5x10^4$ cells per well. The preferable features of this BME gel over the ECM gel are enlisted in Table 3.3.1.

| | Culturex® BME1 PathClear™ gel | ECM gel |
|---|---|---|
| **Advantages** | • Consistent gelling within a batch of gel<br>• Possibility to batch test<br>• Total protein concentration 12-18mg/ml<br>• Gels within 30 minutes at 37°C | • Does not require a two-fold dilution before use |
| **Disadvantages** | • Requires testing each batch before use<br>• Requires a two-fold dilution before use | • No consistent gelling within a batch<br>• Not possible to batch test<br>• Total protein concentration 8-12mg/ml<br>• Takes longer than 30 minutes to form a gel |

**Table 3.3.1** ***Advantages and disadvantages of Culturex® BME1 gel and ECM gel***

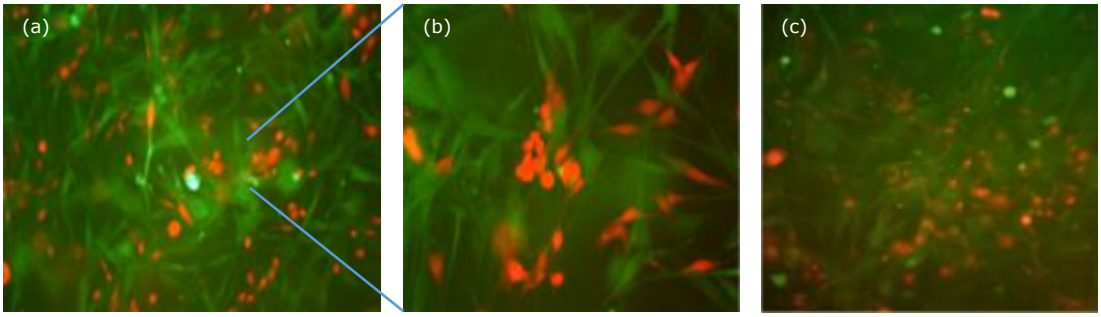



**Figure 3.3.6** ***LAFs in co-culture with 621-101 cells.*** *Panels A and C show 10x images of LAFs (green) and 621-101 cells (red) labelled with CellTracker™ dyes in co-culture. 621-101 cells were clumped together with LAFs at day 3. Panel B shows a x20 magnified image of a cell clump and Panel C show the 3D co-culture at day 7.*

Figure 3.3.6 shows three representative images of LAFs and 621-101 cells in co-culture embedded in Culturex® BME gel. LAFs and 621-101 cells show a viable morphology in the 3D gel and within 3 days the two cell types are aggregated forming clumps (Figure 3.3.6 (b)). All four LAF donors used behaved in the same manner with 621-101 cells. The gels were maintained for 7 days where the cells were still viable and identifiable by the dye, albeit, faded (Figure 3.3.6 (c)).

### 3.3.4 Assessment of Cellular Metabolic Activity via MTT Reduction Assay

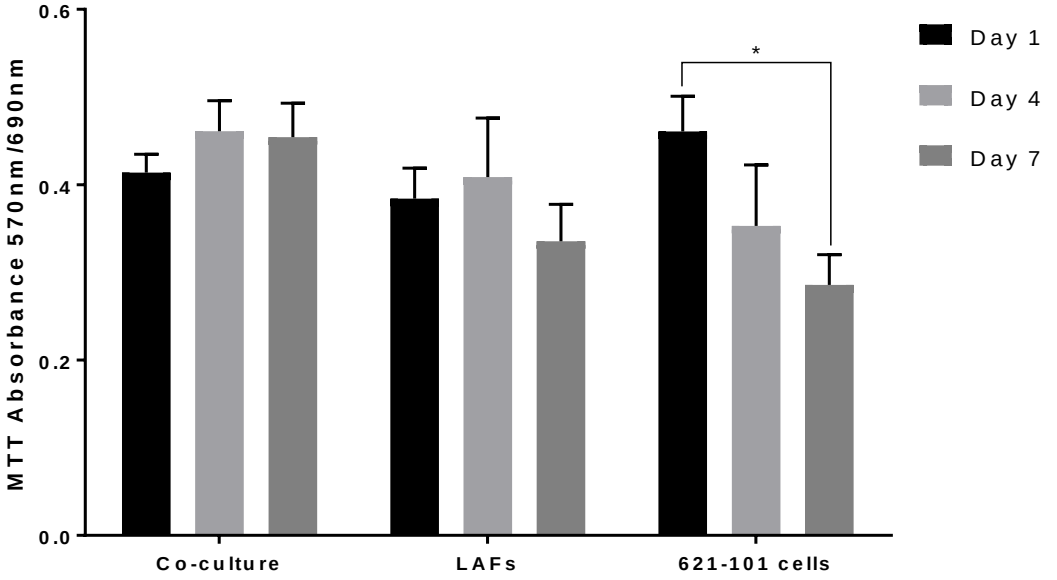



**Figure 3.3.7 *MTT reduction assay performed showing survival co-culture of model over 7 days.*** *Graph shows optical density readings obtained corresponding to number of surviving cells in the model. Cells in the co-culture gels survive over 7 days. LAFs (n=4) show a slight decrease at day 7 and 621-101 cells show a significant decrease in number by day 7. MTT readings are mean ±SD. Two-tailed Students t-test was performed, *p≤0.05.*

The MTT reduction assay was performed which measures cell metabolic activity reflecting the number of viable cells present in culture. This assay is a reflection of cellular mitochondrial activity which is constant for most viable cells. Therefore an increase or decrease in activity can be considered as an indicative of increase or decrease in cells (Berridge et al., 2005, van Meerloo et al., 2011). This assay was performed in order to assess the viability and an increase or decrease in cells of the 3D LAM model using Culturex® BME gel over a period of 7 days. Four LAF donors (n=4) were cultured with 621-101 cells and the co-culture model consisting of both cell types showed a non-significant ($p>0.05$) increase in the MTT signal and therefore, the number of cells in 4 days. Cells in the model were

consistently viable over 7 days. The viability of LAFs in mono-culture was comparable to that of cells in the co-culture model and is only slightly reduced by day 7. The 621-101 cells in mono-culture, showed a significant decrease (p=0.03) in MTT assay signal at day 7 suggesting that the 621-101 cells may require the support of LAFs in order to survive in a 3D environment.

### 3.3.5 Measuring Cell Viability Using Alamarblue® Viability Assay

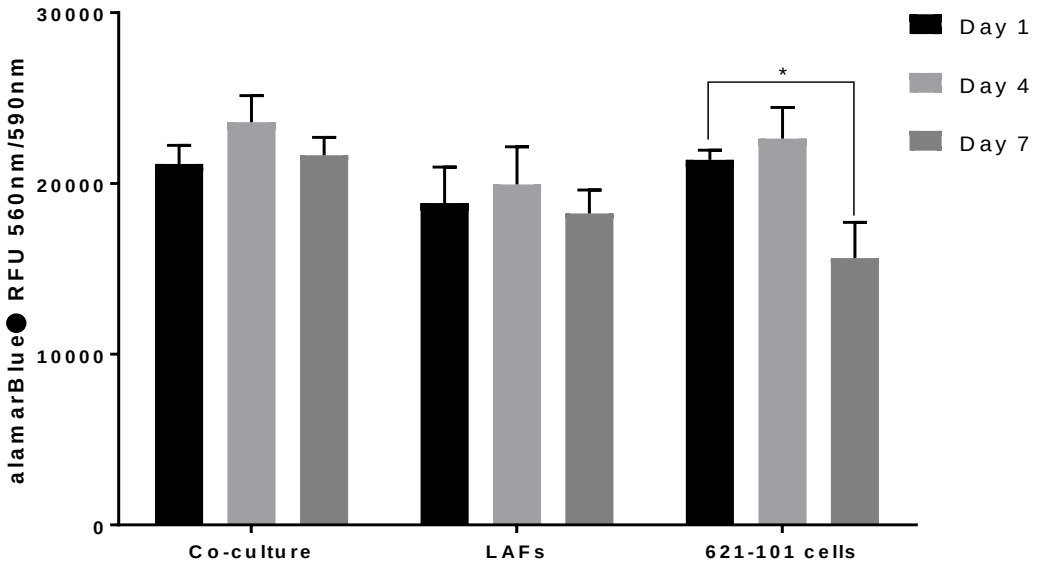



**Figure 3.3.8 *alamarBlue® assay performed showing survival co-culture of model over 7 days.*** *Graph shows relative fluorescence unit readings obtained corresponding to number of surviving cells in the model. Cells in the co-culture gels and LAFs (n=4 donors) in mono-culture gels survive over 7 days. 621-101 cells show a significant decrease in number by day 7. Fluorescence readings are mean ±SD. Two-tailed Student's t-test performed (*p≤0.05)*

The alamarBlue® assay was performed which measures the metabolic mitochondrial activity of cells based on the reduction of resazaurin to resorufin by mitochondrial enzymes. This assay was performed as another

measure of viability of the 3D LAM co-culture model using Culturex® BME gel and similar to MTT assay findings described in section 3.3.4, the 3D co-culture model is viable over a 7 day period. Viability of LAFs (n=4) in mono-culture was comparable to the cells in co-culture surviving well for 7 days, however, the 621-101 cells showed a significant decrease (p=0.041) in the fluorescent signal from day 1 to day 7. These findings were consistent with the MTT assay findings.

### 3.3.6 Gene Expression of Markers of A LAM Nodule and Fibroblast Specific Markers in the 3D BME Model

The aim of development of the 3D BME model was to recapitulate a LAM nodule in vitro, therefore the expression of melanocytic markers, hallmark of a LAM nodule were verified in the model.

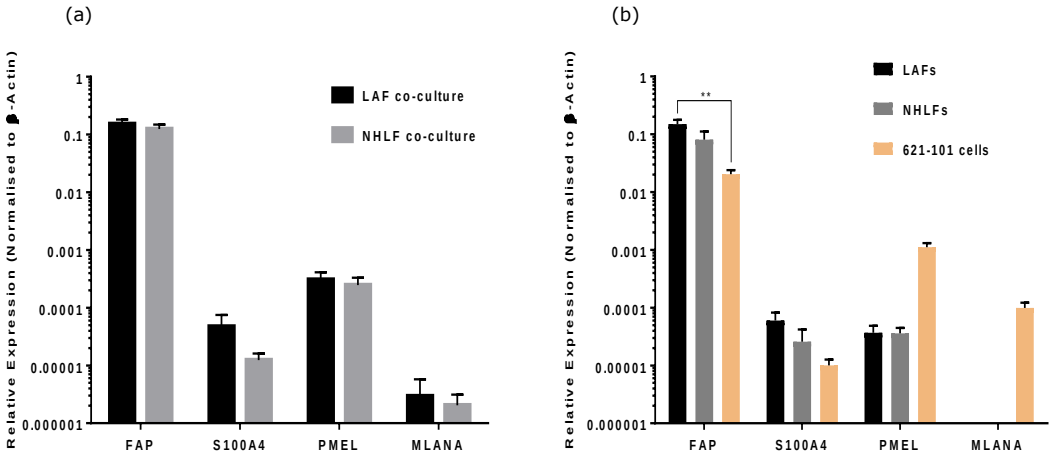



**Figure 3.3.9** ***Expression of markers of fibroblasts and melanocytic cells in NHLF and LAF 3D BME models.*** *Quantitative gene expression of markers of fibroblasts and melanocytic cells in three NHLF and four LAF donor 3D BME models, determined by quantitative real time PCR. One way ANOVA performed corrected for multiple comparisons using the Bonferroni correction method **p≤0.01.*

The transcriptional expression of melanocytic cell markers glycoprotein 100 (PMEL) and melan-A (MLANA) was very low to negligible in LAFs and NHLFs in mono-culture but was relatively high in 621-101 cell mono-culture. The expression of fibroblast marker FAP-α was significantly higher in LAFs ($n=4$, $p=0.0018$) as compared to its expression in 621-101 cells. Fibroblast-specific protein 1 (S100A4) mRNA was detected in both LAFs and NHLFs, however the expression was not significantly higher ($p<0.05$) than that found in 621-101 cells (Figure 3.3.9 (b)).

The co-culture models consisting of either LAFs or NHLFs with 621-101 cells recapitulating the LAM nodule maintained the expression of both markers of mesenchymal and melanocytic cells when analysed at day 4 (Figure 3.3.9 (a)). Expression for all four markers was detected in co-culture models with both cell types with no statistical difference between them.

### 3.3.7 Protein Expression of Markers of a LAM Nodule and Fibroblast Specific Markers in the 3D BME Model

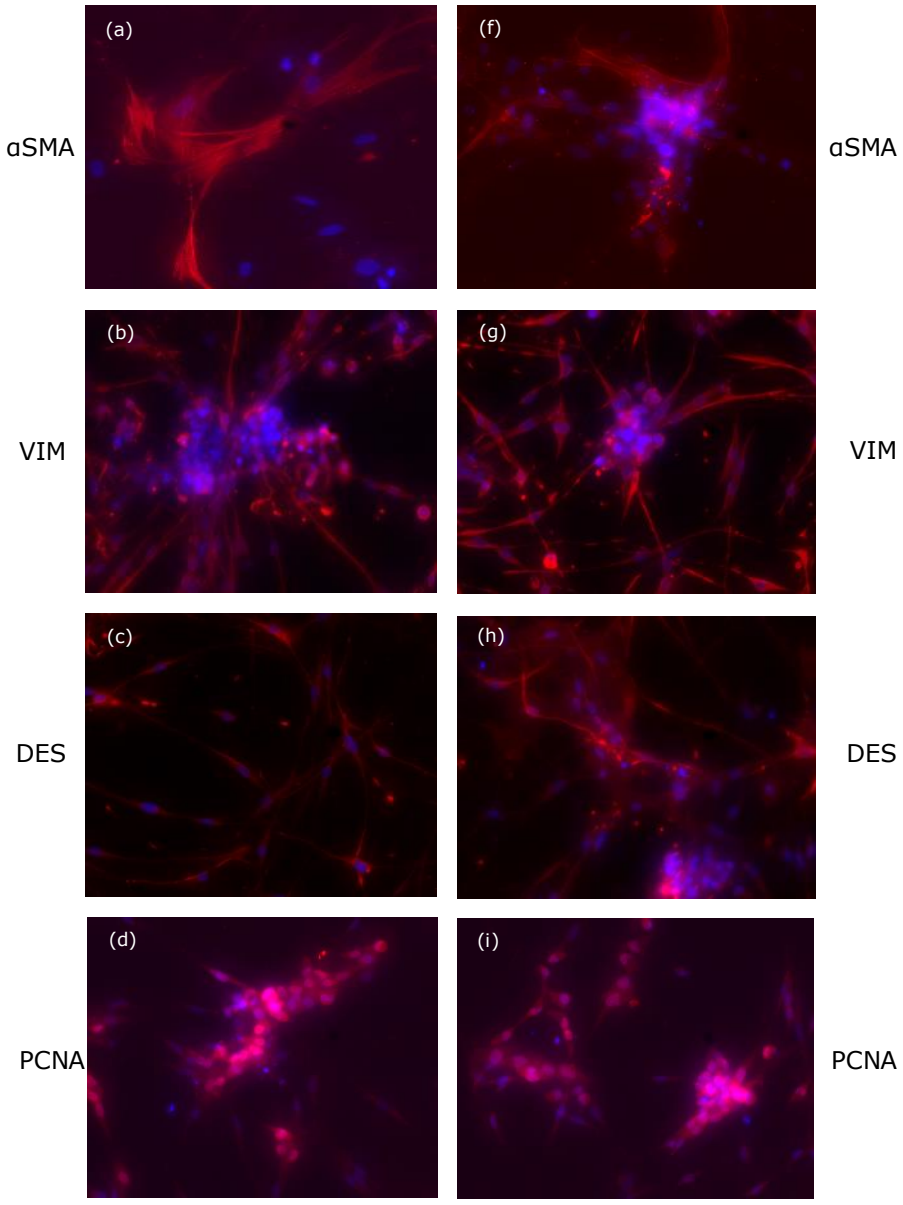



**Figure 3.3.10** ***LAF and NHLF co-cultures showing presence of LAM nodule-specific markers.*** *Images show clumps formed at day 4 from fibroblasts (n=4) and 621-101 cells in co-culture expressing markers of LAM nodules. Panels A-D show NHLF and E-H show LAF co-cultures stained for α-smooth muscle actin (α-SMA, red), vimentin (VIM, red), desmin (DES, red) and proliferating cell nuclear antigen (PCNA, red). Nuclei, blue (DAPI). Images of cells taken at x20 magnification using an Improvision spinning-disc confocal microscope.*

Both NHLFs (n=3) and LAFs (n=4) when cultured with 621-101 cells spontaneously formed clumps within 3 days that expressed markers specific to cells within LAM nodules thereby representing nodules *in vitro*. Figure 3.3.10 shows positive staining for α-SMA, vimentin and desmin in NHLF (Figure 3.3.10(a-c)) and LAF (Figure 3.3.10 (f-h)) co-cultures respectively. Positive nuclear staining for PCNA was also noted among several cells within the clumps (magenta coloured nucleus) (Figure 3.3.10 (d) and (i)).

This analysis has shown that fibroblasts and 621-101 cells in 3D BME gels form cell aggregates that express markers that identify a LAM nodule *in vivo*. However, it was not possible to assess the presence of melanocytic marker expression due to technical issues with the antibody. Although the two cell types within the clump cannot be distinguished from each other the analysis shows nonetheless that markers of a LAM nodule are present *in vitro*. Isotype controls were performed per donor for each antibody which were clean with little background staining. A representative image is shown in Appendix I.

### 3.3.8 Generation of Multicellular Co-Culture Spheroids - LAM Spheroids

A variety of features that are observed *in vivo* are absent in cell monolayers (2-dimensional culture). Multicellular spheroids are a 3-dimensional (3D) cell culture model that has become increasingly useful for the study of cell function as they satisfy the requirement for a more physiologically relevant model. Spheroids are capable of formation of a complex network of cell-cell contacts and are capable of producing depositing advanced extracellular matrix (ECM) (Froehlich et al., 2016, Jamieson et al., 2015). Conventionally spheroids have been generated from single-cell suspensions, co-culture multicellular spheroids (CMCS) were subsequently generated using various tumour cells and fibroblast mimicking tumour fibroblast interactions in order to study complex cell-to-cell and cell-to-matrix interactions, tumour-induced alterations in the fibroblast-specific ECM production and secretion and cancer cell to fibroblast cellular orientation within spheroids (Kunz-Schughart et al., 2001).

#### 3.3.8.1 Selection of Appropriate Technique for Spheroid Formation

A LAM nodule, although not a solid tumour, can be likened to a cancerous lesion as it presents with several typical hallmarks of cancer. The aim was to successfully generate co-culture multicellular spheroids using 621-101 cells and LAM-Associated fibroblasts to recapitulate their interactions within a LAM nodule *in vivo.* In order to do this the liquid overlay technique was incorporated by seeding cells in ultra-low attachment U-bottom plates to generate spheroids.

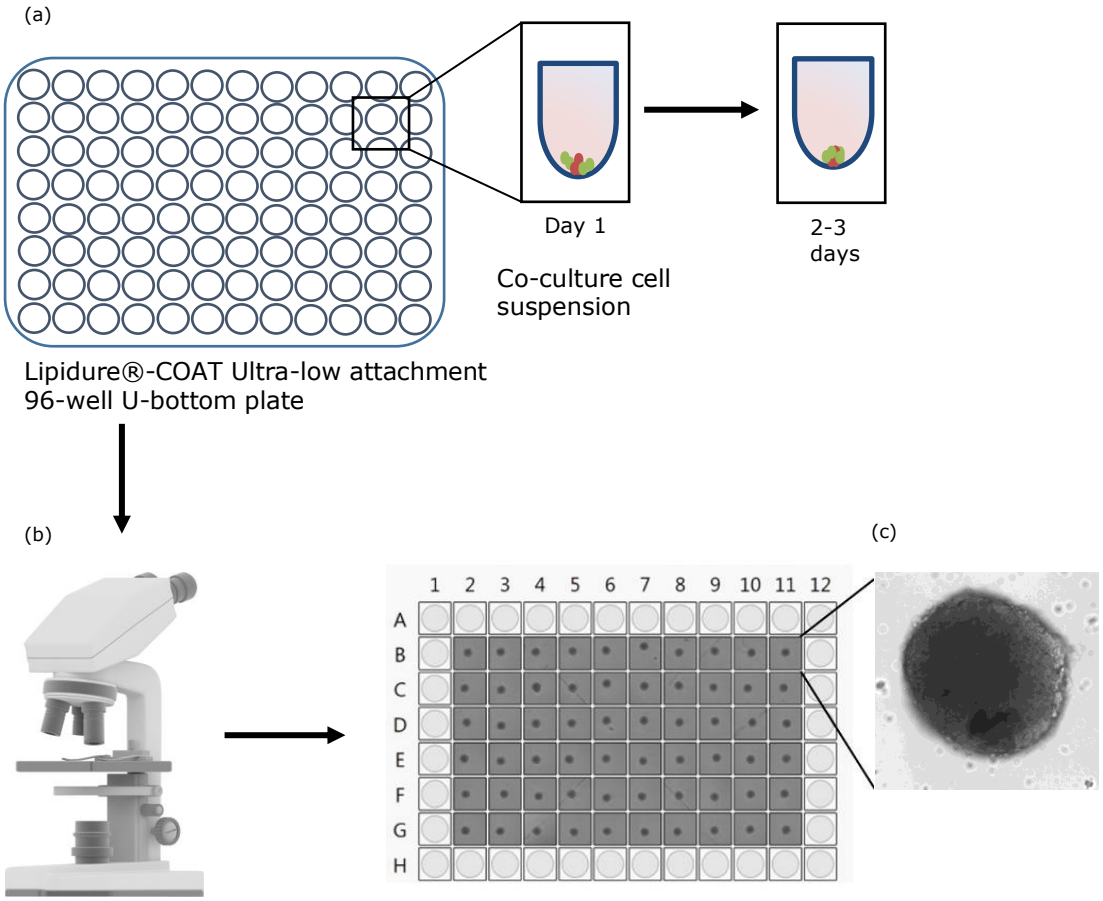



**Figure 3.3.11** ***Diagrammatic illustration of generation of spheroids using Lipidure-COAT ultra-low attachment U-bottom plate.*** *(a) Shows generation of spheroids using Ultra-low attachment (ULA) 96-well U-bottomed plates producing reproducibly sized, single spheroids in each well. (b) Spheroids were imaged at 10x magnification using a standard brightfield microscope. (c) Representative image of a single spheroid produced from a co-culture of NHLFs and 621-101 cells.*

Figure 3.3.11 shows an illustration of the method used to generate spheroids. The liquid overlay technique involves growing cells in plates with substrates that limit cell adhesion. The technique relies on the cell-cell adhesion being stronger than the cell-substrate adhesion. Lipidure-COAT® ULA plates are coated with a biocompatible polymer containing Phosphorylcholine (AMSBiotechnology, 2013) which encouraged the cells to aggregate and form spheroids enabling the formation of single CMCS of reproducible size.

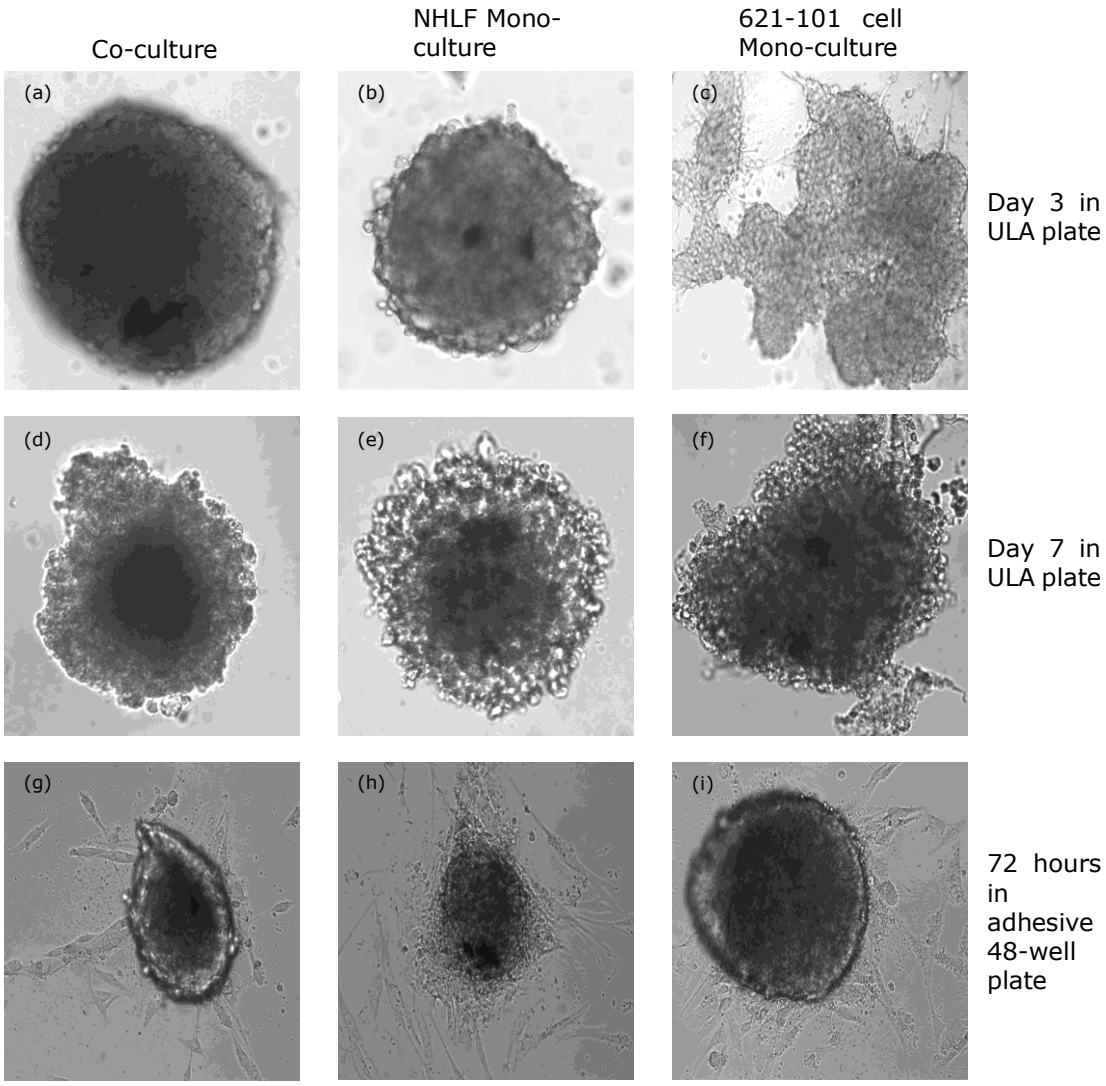



**Figure 3.3.12** ***Representative brightfield images of LAM spheroids generated using Lipidure-COAT® ULA 96-well U-bottomed plates.*** *Panels A-C show co-culture and mono-culture spheroids generated from NHLFs (n=3) and 621-101 cells on day 3 in an ULA plate. Panels D-F show the same spheroids on day 7 in the ULA plate. Panels G-I show cells disseminating out of 7-day old spheroids transferred on to each well of a standard tissue-culture treated (TC) 48-well culture plate. Images were taken at x20 magnification using a Nikon Diaphot Inverted microscope.*

In order to determine whether the Lipidure-COAT® ULA 96-well U-bottomed plates provided the appropriate conditions for the generation of LAM co-culture spheroids an initial seeding density of 10,000 cells per spheroid was chosen. Based on previous findings with regards to the BME co-culture model, a 10:1 cell ratio was maintained. As with earlier

technique optimisation studies in this chapter and due to the easier availability, NHLFs were used for this initial optimisation study.

Figure 3.3.12 shows single spheroids produced from NHLFs and 621-101 cells in suspension and the two cell types were able to aggregate to form compact spheroids within 48 to 72 hours (Figure 3.3.12 (a)). These spheroids were resistant to disruption by pipetting up and down. In mono-culture conditions, the NHLFs formed compact aggregates (Figure 3.3.12 (b)) however; the 621-101 cells formed very loosely packed aggregates. The spheroids were maintained in culture in the 96-well ULA plates for 7 days (Figure 3.3.12 (d-f)). The spheroids now showed the appearance of a darkened inner, possibly necrotic core, which was not visible before, and an outer layer of viable cells. When transferred to a standard tissue-culture treated plate cells from the spheroids disseminated and adhered on to the tissue culture plastic (Figure 3.3.12 (g-i)) suggesting that the cells from within the spheroid are still viable and proliferative.

This showed that the well shape promoted the formation of single, centrally located spheroids of reproducible size thereby showing that Lipidure-COAT® ULA plates provide the right conditions for the formation of LAM spheroids.

### 3.3.8.2 Determining Optimum Cell Number for LAM Spheroids

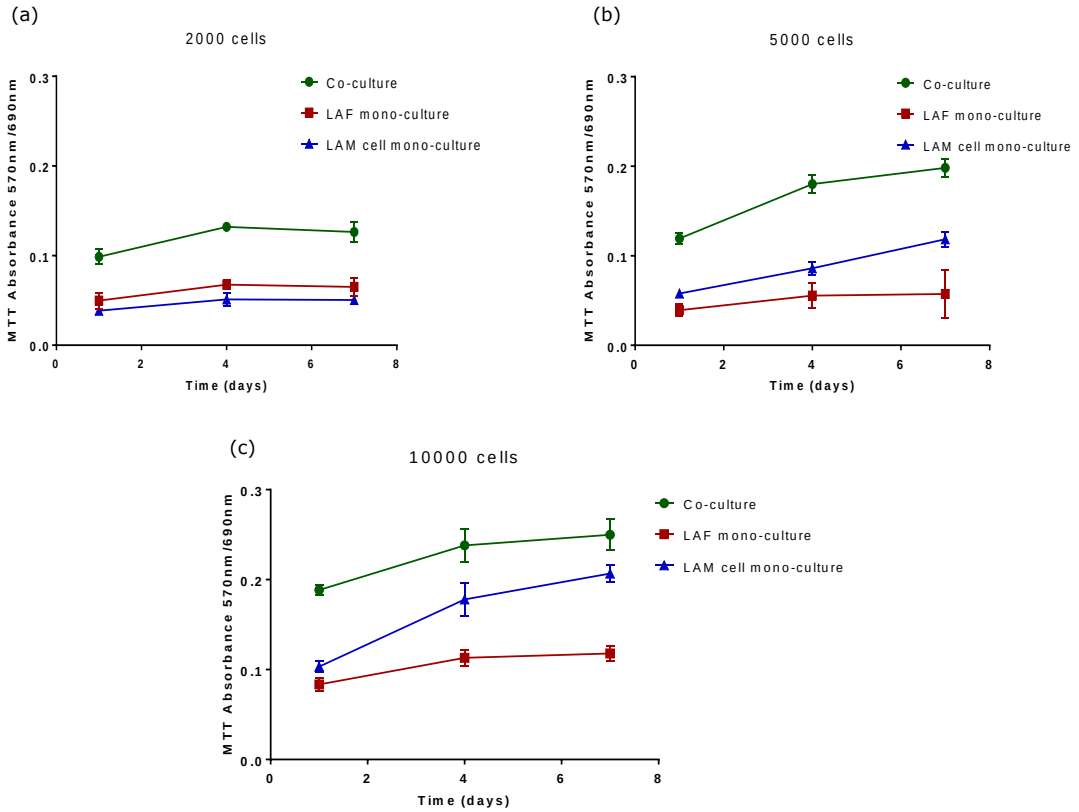


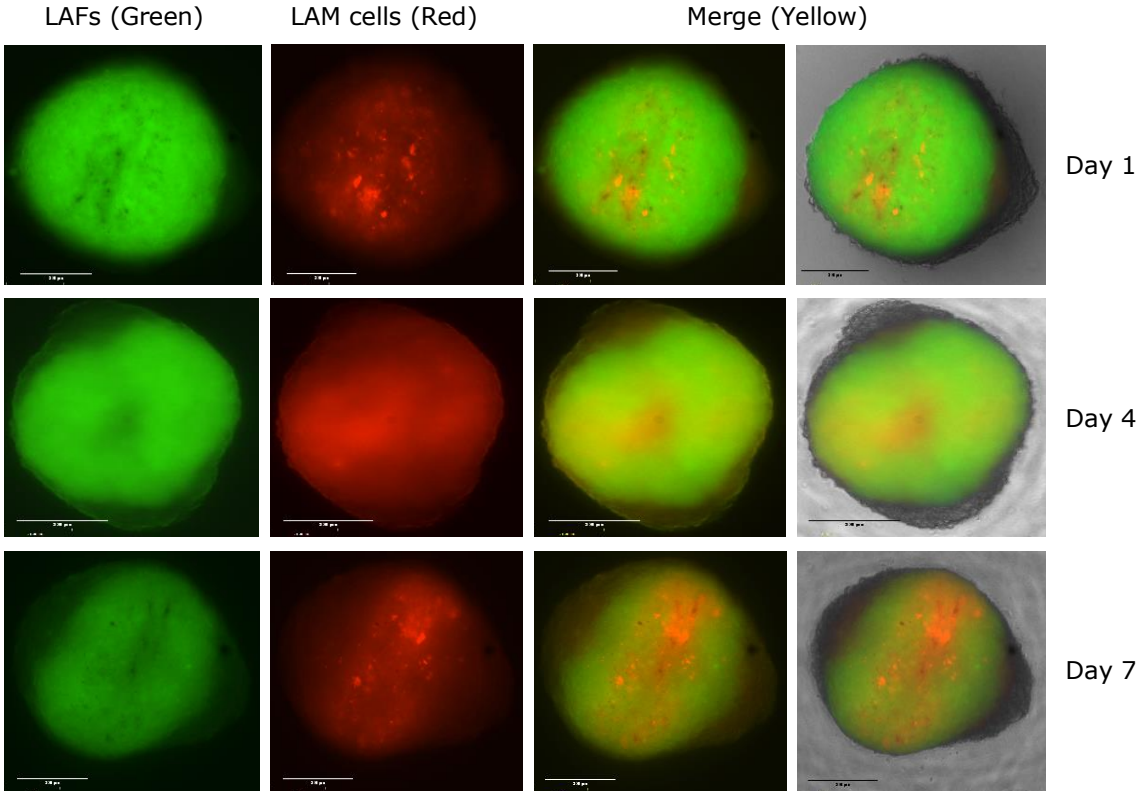

**Figure 3.3.13** ***Determining appropriate cell density for LAM spheroids.*** *Co-culture (10:1 ratio) and mono-culture spheroids for densities of (a) 2000 cells/well, (b) 5000 cells/well and (c) 10,000 cells/well were seeded in Lipidure-COAT® ULA 96-well plates. Viability was measured using MTT assay. Values are means ± SD, n=4 LAF donors.*

Once established that NHLFs and 621-101 cells were capable of forming compact spheroids, LAFs were then used to generate LAM spheroids. For the generation of LAM spheroids three different cell numbers were tested. The aim was to establish an optimal seeding density for both cell types in a 10:1 co-culture ratio such that each LAM spheroid fell within an appropriate diameter size range. Determining an optimum spheroid size and diameter range was important for initiating experimental studies without it being too necrotic in the centre (Vinci et al., 2012). Cultures were maintained by replacing 50% of the medium on days 1, 4 and 7. Co-

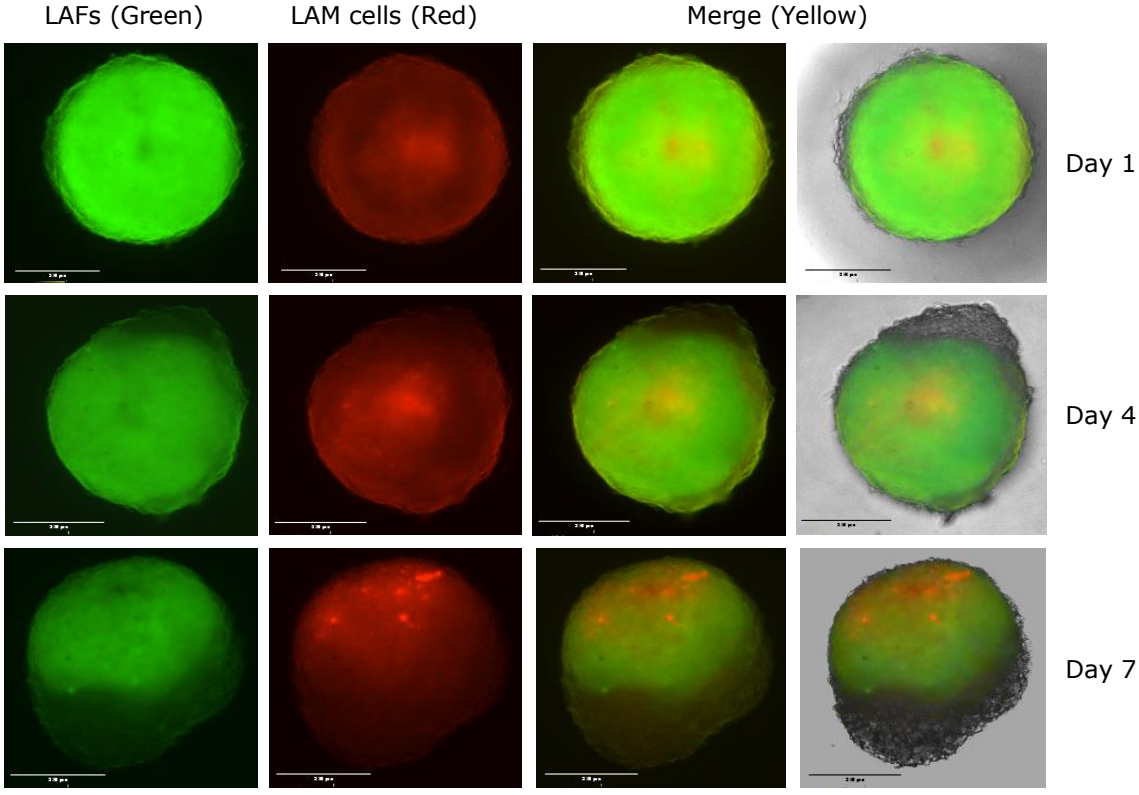
culture spheroids consisted of the LAFs and 621-101 cells seeded in a ratio of 10:1, as this was the optimum ratio determined previously using the 3D BME LAM model.

At a cell number of 2000 cells/well, both co-culture (LAM spheroids) and mono-culture spheroids showed a slight increase in MTT signal over 4 days and thereafter plateau. This may have been due to the fact that there were too few cells to form a compact spheroid leading the cells to die due to anoikis (Figure 3.3.13 (a)). At 5000 cells/well, the LAM spheroids showed an increase in MTT signal by day 4 after which a steady plateaued signal was observed. 621-101 cells in mono-culture showed a steady increase in MTT signal, on the other hand LAFs in mono-culture spheroids do not show an increased MTT signal over 7 days (Figure 3.3.13 (b)). At 10,000 cells/well the LAM spheroids showed a linear increase in MTT signal corresponding to cell viability or cell number over 7 days. 621-101 cells in mono-culture also appear to show a rapid increase in MTT assay signal at days 4 and 7 suggesting there may be an increase in number of cells. LAFs in mono-culture spheroids however, showed a marginal increase in assay signal at day 4 reaching a plateau thereafter (Figure 3.3.13 (c)).

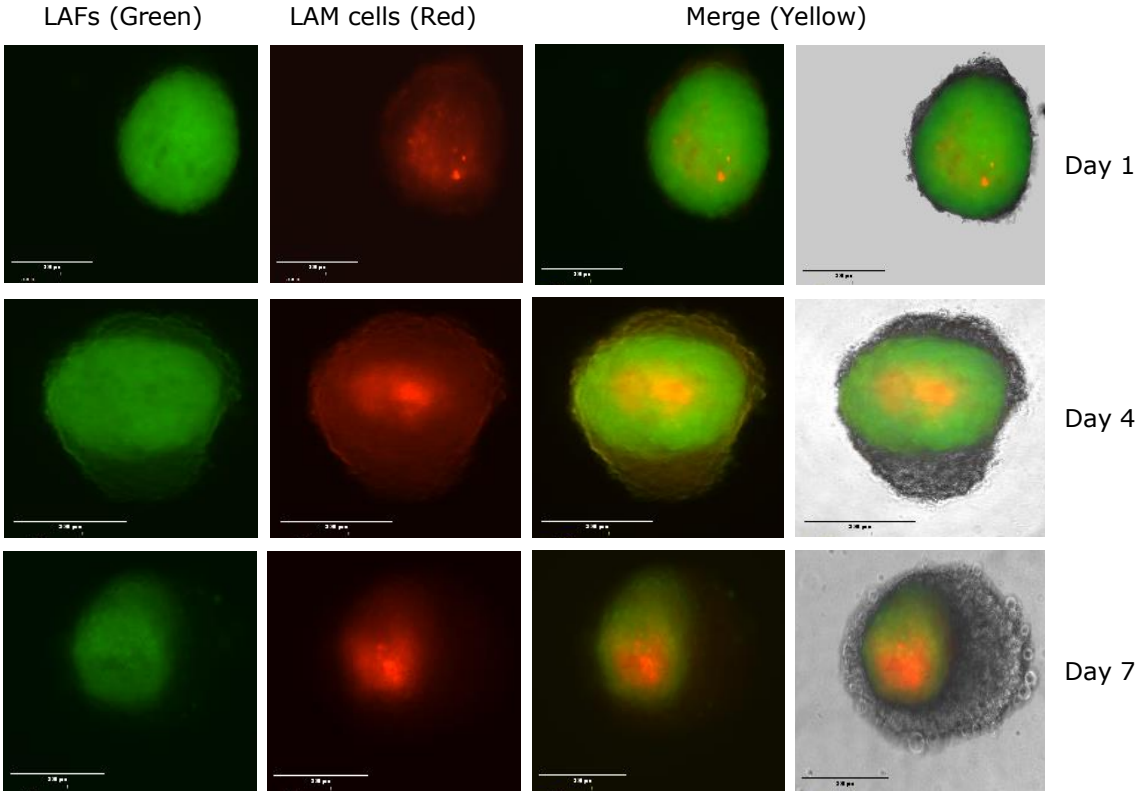
Panel A – 10,000 cells/well




Panel B – 5000 cells/well



Panel C – 2000 cells/well




Panel D – Average spheroid diameter over 7 days

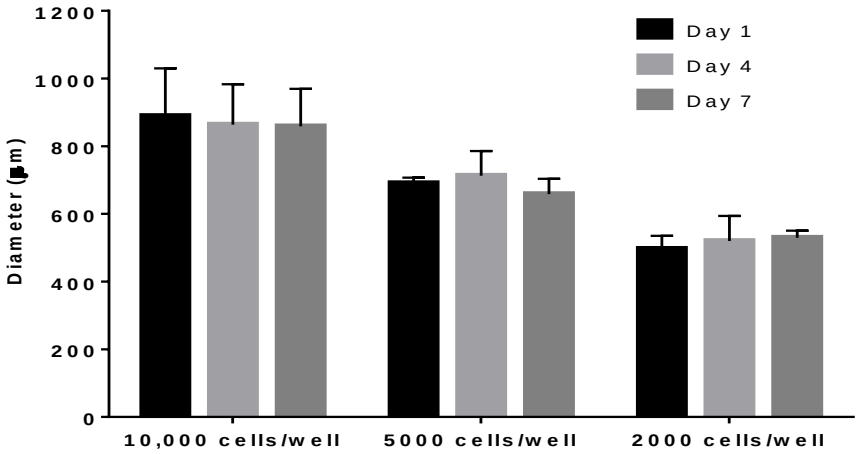



**Figure 3.3.14** ***Representative images of LAM spheroids at different cell numbers.*** *Image panel A, B and C show LAM spheroids generated from LAFs (green) and 621-101 cells (red) at 10,000, 5000 and 2000 cells/well respectively on days 1, 4 and 7. The left half of each panel shows the individual cells within a LAM spheroid while the right half shows the merged image (yellow). Scale bar 300µm. images acquired at x10 magnification using an Improvision spinning-disc confocal microscope. Image panel D shows the average diameter of LAM spheroids measured over 7 days to access for change in size Spheroid diameter was measured using ImageJ software. Values are means ±SD, n=4 LAF donors.*

Figure 3.3.14 shows single spheroids generated from LAFs and 621-101 cells. LAM spheroids generated of all three cell numbers, were strictly almost spherical in shape but became distorted by day 7. Initially showing a spheroid dominated by LAFs (almost green coloured merged image, Figure 3.3.14 Panels A, B and C, second to right image) at day 1, the 621-101 cells appear to infiltrate with LAFs by day 4 at all cell numbers resulting in yellow colouration (merged images). The perfectly spherical spheroids now appeared misshaped possibly due to slight proliferation of cells within the spheroids that appear faded as CellTracker dye gets diluted by cell division (Figure 3.3.14 Panels A, B and C, bright field merge, rightmost images).

By day 7 dye from all spheroids appeared faded. LAM spheroids consisting of 2000 cells showed a large outgrowth of cells that have lost their dye and only a few cells in the centre still containing the dye (Figure 3.3.14 Panel C, bright field merge, rightmost image). These spheroids however did not seem to show an increase in diameter, a measure of increase in cell number, from day 1 to 7 (Figure 3.3.14 Panel D). This suggested that cell death may be compensated by slight increase in cell proliferation. LAM spheroids of a 5000 cell density, despite forming perfectly shaped spheroids initially, also showed similar results as the 2000 cell density spheroids albeit, to a lesser extent.

LAM spheroids of a 10,000 cell density however, appeared to have far less cellular outgrowth and resisted a change in diameter over 7 days. Consisting of an average diameter of 900-1000μm (Figure 3.3.14 Panel D)

these spheroids were compact, had a well-rounded shape and were resistant to disruption by pipetting. The optimum cell density for LAM spheroids was therefore set at 10,000 cells/well as the both cell types in a 10:1 ratio formed compact, round spheroids that were resistant to disintegration and were easy to visualise by the naked eye.

### 3.3.9 Expression of Fibroblast and Melanocytic Markers in LAM Spheroids

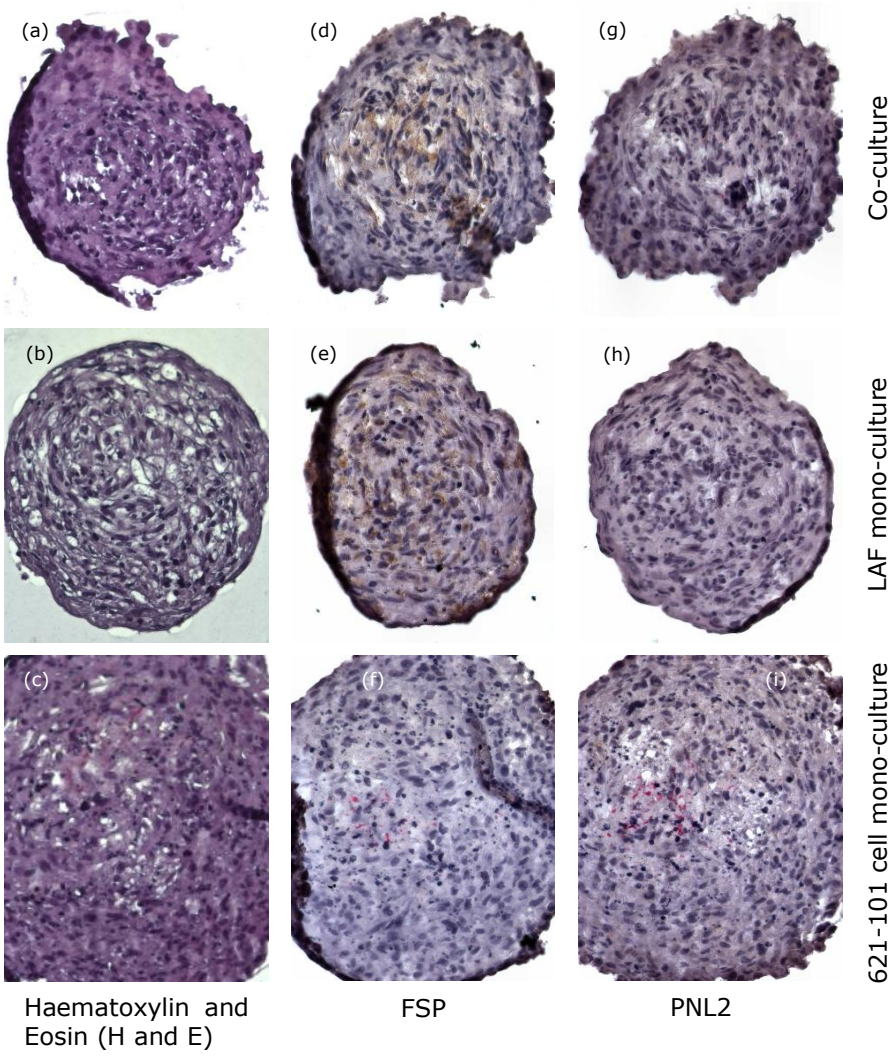



**Figure 3.3.15** ***Histomorphology of LAM spheroids generated.*** *Images show co-culture (LAM spheroids) and mono-culture spheroids generated from LAFs and 621-101 cells. Spheroids react with antibodies against fibroblast surface protein (FSP) and premelanosome protein (PNL2). Images are x40 magnified taken using a Nikon Diaphot Inverted microscope.*

LAM spheroids generated from a total of 10,000 LAFs (n=4) and 621-101 cells (10:1 ratio) in culture and their respective mono-culture spheroids were formalin fixed after 7 days in culture and embedded in paraffin. H and E staining (Figure 3.3.15 (a-c)) and immunohistochemistry was performed on resulting consecutive sections which were then assessed for

cellular organisation within spheroids and expression of specific markers. Figure 3.3.15 shows representative images of H and E and FSP (Figure 3.3.15 (d-f)) and PNL2 (Figure 3.3.15 (g-i)) stained spheroids. Expression of PNL2 was very faint to none but observed only in the 621-101 cell mono-culture spheroid and cells reacting to this antibody in the LAM spheroids appeared to be mainly organised around the periphery. FSP expression was exclusive to the LAF mono-culture spheroids and was present in 70% of cells. It appeared that the cells reacting to FSP in LAM spheroids were organised primarily in the centre. LAM nodules in vivo show the presence of spindle-shaped cells in the centre with epithelioid-shaped cells in the periphery. It appeared that in the LAM spheroids 621-101 cells had organised themselves around FSP positive LAFs. However, a more thorough analysis consisting of known LAM nodule markers as well as further LAF donors would be required to confirm this cellular arrangement in LAM spheroids.

### 3.3.10 Generation of LAM Lung Organoids – Tissue Derived LAMospheres

Virtually the best model to recapitulate diseased tissue and its microenvironment are tissue-derived tumourspheres (TDTS) as they are known to represent the parent tissue in terms of histological features, gene expression profiles and mutations (Kondo et al., 2011, Weiswald et al., 2013). Used initially only in human colon cancer studies, TDTS are now not only being used to study other types of cancers such as prostate, but have also been used to study non-neoplastic lung diseases (Weiswald et al., 2015, Young et al., 2013c, Henry et al., 2015). TDTS are generally derived by partial mechanical or enzyme dissociation of tissue followed by culture in non-adherent tissue culture-treated plastic in the presence of FCS (Weiswald et al., 2013).

This technique was therefore applied to LAM lung tissue obtained at the time of transplant and LAM tissue-derived LAMospheres were thereby generated which represented LAM in a dish.

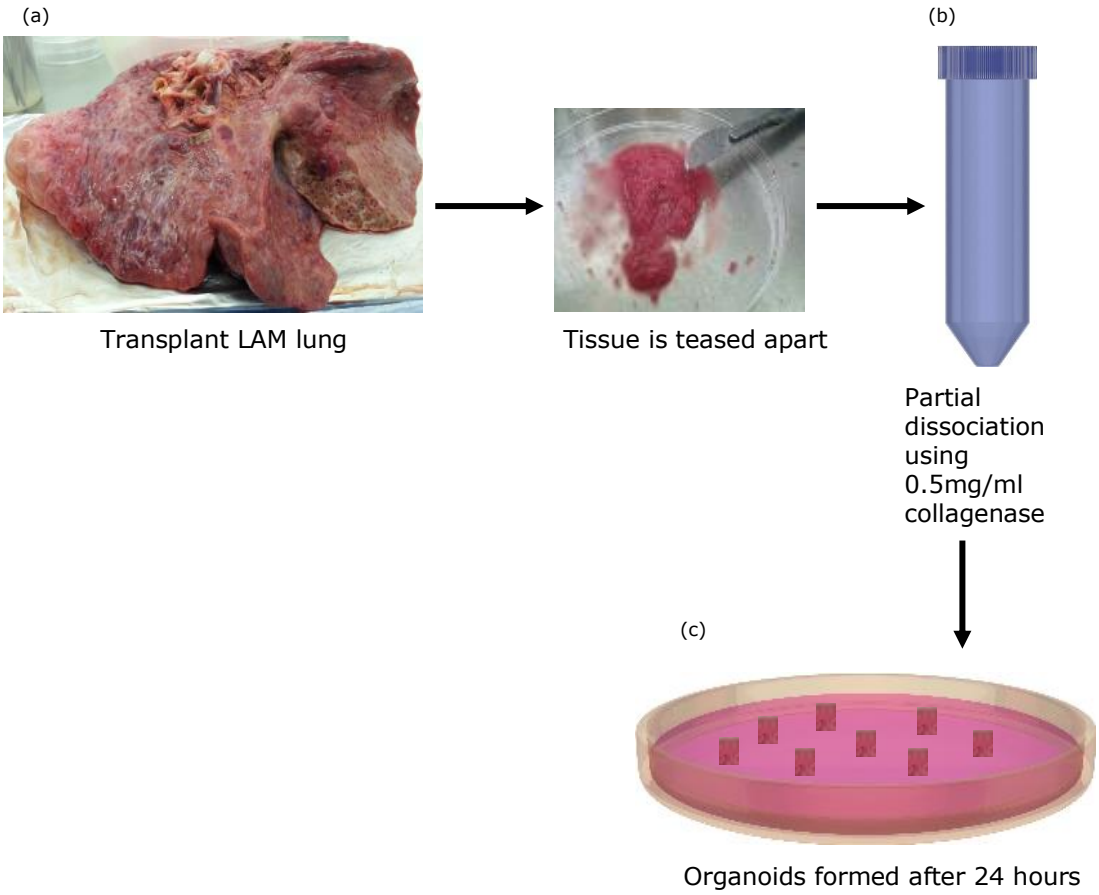



**Figure 3.3.16** ***Diagramatic representation of generation of LAM tissue-derived LAMospheres from transplant lung tissue.*** *(a) LAM lung tissue obtained at the time of transplant is cut into smaller pieces and teased apart using a scalpel. (b) Partial enzymatic dissociation of teased tissue using collagenase for 3-4 hours at 37°C and 5% $CO_2$. (c) LAMospheres fromed as a result are cultured in tissue culture-treated 100 mm petri dish.*

Figure 3.3.16 shows an illustration of the generation of LAMospheres from transplant lung tissue. Partial enzymatic digestion yielded a partially digested suspension of dead cells, tissue debris and tiny pieces of tissue representing the parent tissue which were the initial beginnings of organoids.

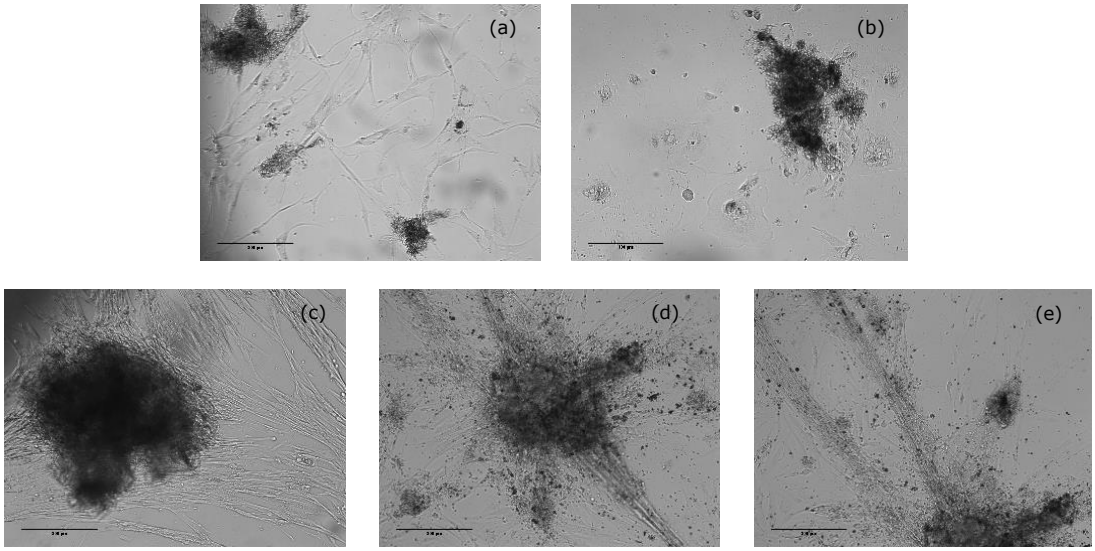



**Figure 3.3.17** ***Representative brightfield images of LAMospheres generated.*** *Panel A and B show initially isolated organoids on day 3. Panels C-E show cells disseminating out of 14 day old organoids transferred to each well of a standard tissue culture-treated 6-well plate. Scale bar 300µm. Images taken at x20 magnification using a Nikon Diaphot Inverted microscope.*

Figure 3.3.17 shows LAMospheres generated from partial enzymatic digestion of LAM lung which enables the maintenance of cell-cell contact between diseased cells. The resulting LAMospheres had an average diameter of between 100-600µm and when cultured in 100mm culture dishes, formation of LAMospheres occurred between days 1-3. These LAMospheres could be maintained in culture in growth media with FCS for more than 2 weeks. Some LAMospheres were transferred to standard adhesive tissue culture-treated 6-well plates and after 3 days in culture, a mixed cell population, largely consisting of proliferative spindle-shaped cells had emerged.

### 3.3.11 Expression of LAM-Specific Markers in LAMospheres

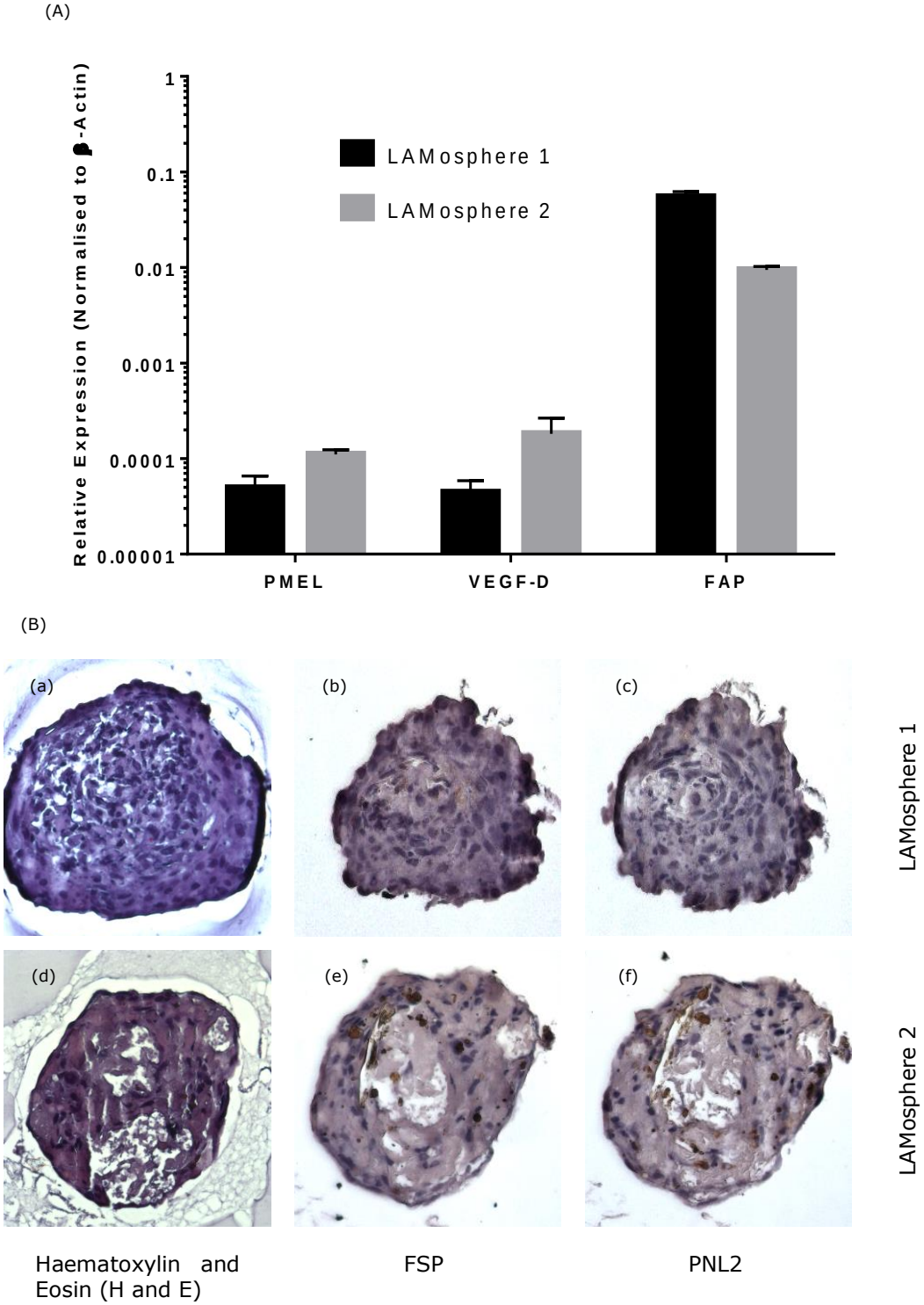



**Figure 3.3.18** ***Expression of LAM specific markers in LAMospheres.*** *Panel A shows gene expression of PMEL, VEGF-D and FAP in the cells dissemanated from LAMospheres. Panel B shows images of LAMospheres reacting positively to antibodies against FSP and premelanosome protein.*

To validate that LAMospheres were representative of a LAM nodule, expression of LAM specific markers were assessed via RT-PCR and immunohistochemistry. Figure 3.3.18 (a) shows the expression of gp100 (*PMEL*), *VEGF-D* and fibroblast specific markers *FAP* in two representative donor LAMospheres. As it was not possible to isolate enough RNA from the LAMospheres themselves, the LAMospheres were seeded onto standard tissue culture plastic 6-well plates, allowed to disseminate cells for four days in culture after which RNA was extracted and subjected to qRT-PCR as described in section 2.3.4. Comparable *PMEL* and *VEGF-D* expression was seen in both donors. Expression of *FAP* however was 175-fold and 288-fold more than *VEGF-D* and *PMEL* respectively. This suggested that the majority of proliferative cells contained within a LAMospheres were possibly fibroblasts. Immunohistochemical evaluation of LAMospheres showed a few but marked presence of FSP and PNL2 positive cells (Figure 3.3.18 (b)) Due to the initial lack of availability of embedding and processing LAMospheres, the organoids were in storage for long and had therefore slightly deteriorated. It was therefore difficult to assess whether the cellular arrangement was like that seen in vivo. However, the expression of LAM specific markers suggested that LAMospheres were indeed representative of LAM nodules in a dish expressing LAM specific markers. However, a more thorough analysis using more donors and other LAM nodule specific markers would be required to fully confirm this.

## 3.4 Discussion

This chapter describes the isolation and characterisation of fibroblasts from LAM lung tissue and their use thereafter in building *in vitro* 3-dimensional co-culture models to represent LAM. It was hypothesised that a large wild-type mesenchymal cell population exists within LAM nodules and Clements et al have previously shown that fibroblast–like cells isolated from LAM lung tissue morphologically resembled commercially bought normal fibroblasts and expressed fibroblast markers including anti-fibroblast marker, TE-7 and S100A4 (Clements et al., 2015). Positive identification of fibroblasts has been difficult to date; therefore, a panel of well-established fibroblast markers was required to confirm the presence of fibroblasts.

Comparable expression of well-established fibroblast markers FSP (1B10) and vimentin in both NHLFs and LAFs implied that the isolated cells were of mesenchymal lineage, specifically fibroblasts. Singer et al first reported that the anti-FSP, 1B10 antibody was fibroblast-specific and has been used since to identify quiescent dermal fibroblasts and lung fibroblasts (Singer et al., 1989, Goodpaster et al., 2008). Human lung fibroblasts consist of a mixed population of $CD90^{+}$ and $CD90^{-}$ subsets and the presence and absence of CD90 expression determines differentiation to a specific phenotype (Koumas et al., 2003). Varied expression of CD90 in LAFs suggests the presence of two distinct subsets of CD90 expression. Desmin expressed essentially in smooth muscle cells has been known to be expressed mostly by dermal fibroblasts (Goldring et al., 2002). Very low

to negligible expression of desmin in the isolated population of LAFs suggests a pure population of fibroblasts exists.

Fibroblasts can become 'activated' and activation can be induced by transforming growth factor-β during wound healing and fibrosis (Zeisberg et al., 2000). Similarly fibroblasts within the tumour stroma acquire a modified phenotype and such activated fibroblasts now known as cancer-associated fibroblasts (CAFs) are highly proliferative, secrete increased levels of ECM-degrading proteases and express α-SMA and FAP-α (Kalluri and Zeisberg, 2006). FAP-α expression in LAFs was therefore evidence that an activated fibroblast phenotype existed. The α-SMA-expressing fibroblasts are known as myofibroblasts and TGF-β is one of the main inducers of this phenotype. Myofibroblasts can lose their stress fibres and switch back into fibroblasts on withdrawal of stimulus and, work with animal models has given evidence of such phenotypic switching *in vivo* (Phan, 2008, Wicks et al., 2006). The expression of α-SMA and acquiring of aligned actin stress fibres in NHLFs and LAFs in the presence of FCS and the loss of these features when FCS was absent indicated a switch between phenotypes possibly due to the presence of TGF-β in FCS (Oida and Weiner, 2010). Thus, using the markers selected it can be concluded that the cells isolated from LAM lung are in fact fibroblasts that have an activated phenotype. These fibroblasts can exist as myofibroblasts in culture given the right stimulus, however they are highly unlikely to be smooth muscle cells.

Possessing very similar properties to Matrigel™ (BD Biosciences), the Culturex® BME gel is rich in several ECM proteins and growth factors and is one of the most commonly used ECMs for the study of non-malignant and malignant cells (Kleinman and Martin, 2005, Weigelt et al., 2014). The Culturex BME gel had a high protein concentration compared to ECM gel thereby enabling the final concentration to be adjusted based on the stiffness required. The average elastic modulus of Matrigel measured by atomic force microscopy (in Pascals, Pa) is 443±285 Pa (Soofi et al., 2009) whereas that of a normal human lung is between 1000–5000 Pa (Hinz, 2012). Taking into consideration that elasticity in a LAM lung is reduced due to the degradation of tissue matrix, the degree of stiffness provided by the Culturex® BME gel could be appropriate for the 3D BME model.

The Culturex® BME gel human cell model is physiologically relevant and eliminates species specific differences. The model shows that the two cell types can co-exist in a 3D conformation and subsequently clump akin to a LAM nodule. Cell clumping in the 3D model suggests that the two cell types are attracted to each other and aggregation subsequently supports cell growth. This was evidenced when cell viability was assessed using MTT reduction and alamarBlue® assays. LAFs and 621-101 cells in co-culture were viable for 7 days whereas 621-101 cells in mono-culture showed reduced cell viability by day 7.

In order to model a LAM nodule *in vitro*, another type of 3D model, co-culture multicellular spheroids (CMCS) were set up. Unlike the 3D BME gel model the CMCS model took advantage of the fact that no external ECM

was required to generate 3D spheroids thereby making it easier and less time consuming to set up. CMCS model can only be generated if the adhesive forces between the cells are greater than for the substrate they are plated on. The liquid-overlay technique prevents matrix deposition (Weiswald et al., 2015) and by using Lipidure®-COAT Ultra-low attachment 96-well U-bottom plates, 'LAM spheroids' were successfully generated using this technique. Cells subjected to the liquid-overlay technique can also form 'aggregates' which are often loose packages of cells that easily detach and disintegrate. However, compact spherical cultures or 'spheroids' are only formed when cell-cell adhesive forces are strong and can be easily manipulated or transferred without disintegrating (Mayer et al., 2001, Weiswald et al., 2015). LAM spheroids generated from all the LAF donors co-cultured with 621-101 cells formed compact spheres that could be easily transferred and manipulated. LAM spheroids consisting of 10,000 cells showed better viability over 7 days and were easy to visualise by naked eye. This suggested that strong attractive forces exist between LAFs and 621-101 cells. Our group has previously shown that LAFs migrate towards 621-101 cells and that this migration is reduced by 56% when treated with the CXCR4 receptor antagonist AMD3100 (Clements et al., 2015). Therefore, it is quite possible the two cell types spherically organise due to signalling via the CXCR4/CXCL12 axis and other adhesion mechanisms that may exist.

An appropriate spheroid diameter is important as spheroid cultures between diameters 200μm and 500μm begin to develop chemical

gradients (e.g. oxygen, nutrients and catabolites) and those that are >500μm begin to have a very hypoxic core (Hirschhaeuser et al., 2010). There is evidence to suggest that hypoxia-induced erythropoietin signalling exists within LAM lung lesions and Ikeda et al have also found the presence of hypoxia-inducible factor-2α (HIF-2α) in LAM lung nodules which is one of the transcription factors that plays a role in hypoxic response (Ikeda et al., 2011). These hypoxic regions may offer a selective advantage for abnormal LAM cells to grow similar to that seen in tumours (LaGory and Giaccia, 2016). Moreover by varying the size of spheroids for treatment, spheroid cultures are thus responsive to therapy-related studies with different emphasis focusing either on 3D cellular interactions and structure only or in combination with authentic pathophysiological environment conditions (Weiswald et al., 2015). Therefore, recapitulating this *in vivo* milieu in spheroid culture may be more representative of a LAM nodule *in vivo*.

Predictably the most relevant 3D *in vitro* LAM model was the tissue-derived LAMosphere model generated from parent tissue. Referred to as tissue-derived tumourspheres (TDTS) and primarily used in cancer studies, the TDTS model has now been used to successfully generate organotypic spheroids from both neoplastic and non-neoplastic tissue of colon, lung, bladder, prostate and melanoma (Morales and Alpaugh, 2009, Ham et al., 2016, Weiswald et al., 2013). The LAMospheres from LAM lung were formed by tissue remodelling and compaction after partial dissociation of tissue and remained compact and intact possibly due to strong cell-cell

interactions. These strong cell-cell interactions in colospheres, MARY-X spheroids and cancer-tissue derived spheroids enable them to escape anoikis and remain viable for several weeks. Similarly, the LAMospheres generated were able to survive for more than 2 weeks in culture and showed very slight volume of growth even after 15 days in culture. A potential reason for this could be that active cell proliferation is counterbalanced by extensive cell death and/or cell shedding (Kondo et al., 2011, Weiswald et al., 2015).

LAMospheres just like TDTS represent the parent tissue in terms of gene expression profiles and histological features. Organoids generated in this manner pave the way for individualised and patient-specific therapy. LAMospheres can therefore be generated from patient biopsies that contain a diverse population of cells such as those seen in a LAM nodule specific to the patient and the disease can thereon be tracked in real-time as it progresses in the patient. However, one of the challenge that this approach presents is preserving and sub-culturing LAMospheres successfully.

Three distinct 3D models were thus set up to best recapitulate LAM *in vitro*. However, each model had its own positive and negative features with regards to ease of use, relevance and reproducibility. Listed in Table 3.4.1 are the advantages and disadvantages of the three LAM models.

| | **Advantages** | **Disadvantages** |
|---|---|---|
| **3D BME model** | • Provides a biological ECM to cells<br>• Can be used to study influence of ECM on cell phenotype | • Requires time batch testing to set up each time<br>• Variable physical properties |

| | | |
|---|---|---|
| | • Provides right amount of stiffness as opposed to 2D plastic<br>• Can add other matrix components lacking in BME<br>• LAFs and 621-101 cells spontaneously aggregate together forming a clump akin to a LAM nodule<br>• Cells within the ECM can be visualised and distinguished<br>• IF can be performed | • Risks associated with biological material<br>• Gel formation not always reproducible resulting in cell death due to inappropriate matrix stiffness<br>• Difficult to manipulate as cell recovery is very low and the BME has to be taken into consideration during assays<br>• Number of cells required is high<br>• Imaging only possible using long focal length confocal microscopy |
| **LAM spheroid model** | • Does not require external addition of ECM<br>• Very easy to set up and single spherical spheroids are obtained using ULA 96-well U-bottomed plates<br>• LAFs and 621-101 cells are strongly attracted to from compact spheroids that can be easily manipulated and transferred<br>• LAFs and 621-101 cells spontaneously arranged themselves as *in vivo*<br>• Unlike on 2D plastic spheroid models develop gradients similar to conditions seen *in vivo*<br>• Size of spheroids can be manipulated for appropriate therapeutic response<br>• If required external matrix can be provided | • Imaging at a cellular level is difficult and requires more advanced forms of microscopy such as light sheet (Jamieson et al., 2015)<br>• Expression of cell distinguishing markers and proteins need to be assessed only via IHC which requires fixing and paraffin embedding of spheroids<br>• Exact responses of two cell types to drugs or stimuli cannot be distinguished<br>• A large necrotic core can develop within larger spheroids |
| **Tissue-derived LAMosphere model** | • Exact features of parent tissue<br>• Easy to generate once tissue is available<br>• Cells remain in their own 3D ECM right from the start thereby disallowing phenotypical changes | • Very hard to obtain especially for a rare disease like LAM due to lack of availability of diseased tissue<br>• Sub-culturing and preservation may not be easy |

| | | |
|---|---|---|
| | • LAMospheres can be maintained for weeks and do not grow substantially in size<br>• Can be used for individualised therapy and progress of disease can be tracked per patient | • LAMospheres are not consistent in size and may contain varying cell population and numbers resulting in disparity in responses<br>• Characterisation of each patient-specific LAMosphere is needed every time |

**Table 3.4.1** ***Advantages and disadvantages of three 3D LAM models designed.***

## 3.5 Conclusion

This chapter describes the isolation and characterisation of fibroblasts from LAM lung tissue and their use thereafter in building an *in vitro* 3-dimensional co-culture models to represent LAM. Although all of the models were designed and validated to resemble LAM nodules *in vivo*, each model had its own distinct applications and one particular model could not be used for all subsequent experimental manipulations. The LAM spheroid and LAMosphere models are fairly novel and are still a work in progress. Moreover, due to the additional consideration of a third dimension, the BME gel, assays normally designed for two dimensional (2D) cultures could not be applied to the 3D models. Therefore, although the use of the 3D models has been made further in this thesis, majority of the work was carried out using 2D co-culture models.

# 4 CHAPTER 4: Protease Profile for LAM: The Expression and Activity of Cathepsin K

## 4.1 Introduction

### 4.1.1 Background

Fibrillar collagens and elastins, proteins of the ECM, are the major contributors of tensile strength, viscoelasticity and structure to lung tissue. Other ECM proteins such as fibronectin, laminin and nidogen act as linking proteins (Vakonakis and Campbell, 2007). Remodelling of the ECM occurs effectively by the removal or breakdown of one or more of such components (Dunsmore and Rannels, 1996). Proteases are enzymes that play an essential role in many biological and pathological processes and whose main function is to perform proteolysis of the ECM which is an irreversible process that causes the catalytic cleavage of specific ECM substrates (Choi et al., 2012). In the healthy, lung proteases regulate processes such as regeneration and repair. However in disease conditions an imbalance between pulmonary proteases and anti-proteases often results in increased protease activity followed by extensive breakdown of ECM tissue substrates (Greene and McElvaney, 2009).

Human proteases consist of five broad classes, the largest class being matrix metalloproteinases (MMPs) followed by serine, cysteine, threonine and aspartic proteases. All 23 members of the MMP family of zinc dependent endopeptidases share a self-inhibitory pro-domain which needs to be removed by other proteases to render them enzymatically active (Page-McCaw et al., 2007). Capable of targeting a wide range of ECM

proteins MMPs-1, -8, -13 selectively degrade collagen, MMPs-2 and -9 degrade gelatin and MMP-12 prefers elastin (Cawston and Young, 2010). The MMPs are extremely pleotropic and are also involved in many biological processes including extra-cellular matrix turnover, inflammation, angiogenesis, metastasis, regulation of growth factor and chemokine activity (Ivanov and Grabowska, 2017). Serine proteases as the name suggests contain a serine moiety in catalytic site (Di Cera, 2009) and included under this class, proteases such as plasmin and urokinase-type plasminogen activator (uPA) are not only involved in tissue remodelling events themselves but also activate MMP precursors such as pro-MMP-3, MMP-9 and MMP-13 (Lijnen, 2001). Mammalian cysteine proteases mainly consist of 11 lysosomal cathepsins, namely cathepsins B, H, L, S, C, K, O, F, V, X and W, which are also synthesised inactive as proenzymes (McGrath, 1999, Van Noorden et al., 1997). Activation of these proteases requires an acidic environment and they are capable of degrading intracellular as well as extracellular ECM proteins (Green and Lund, 2005). In normal lung cysteine cathepsins not only play a role in matrix remodelling but also in antigen presenting and processing of surfactant proteins. However, overexpression of one or more members of this class of proteases has been implicated in asthma, bronchopulmonary dysplasia, COPD cystic fibrosis sarcoidosis and lung cancer (Sabeh et al., 2004).

*Protease – Anti-protease imbalance in LAM*

The mechanism of cyst formation in LAM is not well understood, although lung cysts are thought to arise as a result of LAM nodule derived matrix

degrading proteases (van Meerloo et al., 2011). Microscopic and immunohistochemical analysis of open lung biopsies by Fukuda et al revealed emphysema-like changes in the areas of cell accumulation that showed degraded collagen and elastic fibres which were believed to be caused by an imbalance of proteases such as collagenases and elastases (Fukuda et al., 1990). The expression of various abovementioned protease families has been described in LAM. LAM lung nodules express MMP-1, -2 and -14 (Hayashi et al., 1997, Matsui et al., 2000a, Ferri et al., 2004), MMP-2 is over expressed by *TSC2* knockout cells (Lee et al., 2009), and previous reports have shown that women with LAM have higher levels of MMP-2 and -9 in serum and MMP-9 in urine than healthy women (Chang et al., 2012, Odajima et al., 2009, Chang et al., 2013). However a recent study of MMP inhibition using doxycycline did not reduce decline in lung function despite suppression of MMP-9, suggesting other proteases could also be responsible for lung destruction (Chang et al., 2013). The serine proteases, uPA and plasmin are increased in LAM lung whilst the inhibitor, plasminogen activator inhibitor (PAI-1), is reduced suggesting activation of this protease axis (Zhe et al., 2005). Expression of cysteine protease cathepsin K was noted in LAM lung nodules and other PEC neoplasms (Martignoni et al., 2010, Chilosi et al., 2009). Cathepsin K is not present in normal lung tissue , but is classically expressed by osteoclasts as a bone remodelling protease (Zhao et al., 2009b) and by tumour stromal fibroblasts (Montgomery et al., 2012).

Identifying specific proteases overexpressed in LAM lung by screening candidate proteases from various protease families could provide a

reasonable initiation point to elucidate the functional role of the proteases involved. This would then shed light on and help confirm the main hypothesis that TSC2 null LAM cells and LAM lung fibroblasts synergistically cause lung destruction associated with LAM.

### 4.1.2 Aims & Objectives

The aims of this part of the study were to identify key proteases elevated in LAM known to play a role in the destruction of tissue with a view to identifying potentially novel drug targets. This was focused on the global screening of proteases in cell and tissue models and identification thereafter of a key potent protease expected to play a role in LAM lung destruction. In parallel the evidence of protease activity and crucial microenvironmental elements required for activation of the protease were also established.

## 4.2 Methods

### 4.2.1 Proteome Profiler – Protease Array

Expression of proteases in LAF/621-101 cell co-cultures and mono-cultures was assessed by the Proteome Profiler™ Array Human Protease Array kit. 6-well Boyden chamber Transwell cultures were set up. Polycarbonate membrane Transwell inserts (0.4µm pore size, Corning Life Sciences, SLS, Nottingham UK) were equilibrated for one hour at 37°C and 5% $CO_2$ prior to adding cells. Maintaining a 10:1 cell ratio, LAFs were seeded at $5x10^5$ cells per ml in the lower chamber and $5x10^4$ 621-101 cells (500µl) in the upper chamber. Mono-cultures of both cell types maintained the same cell number as co-cultures. Each condition per donor was set up as a duplicate, cultures were maintained for 96 hours after which supernatants were collected and clarified and assay was performed as described in section 2.5.2. After blocking the membranes, 500µl of supernatant samples were added to 1ml of Array buffer 6 making the final volume to 1.5ml. Membrane dot blot images were acquired using LI-COR Odyssey® Fc Imaging System. Densitometry performed on the dot blot image using the Image Studio™ Lite software. Each duplicate dot on the blot represented a distinct protease. An average of the six reference spots was calculated. Mean pixel density of the two dots was calculated by background subtraction and normalising to reference spots.

### 4.2.2 Double Chromogenic and Fluorescent Immunohistochemistry

For double chromogenic IHC, following first antibody staining and ImmPact DAB incubation, sections were blocked in 2.5% horse serum for 1 hour at room temperature followed by incubation with the second primary antibody for 1 hour at room temperature. Slides were then washed and incubated with secondary antibody for 1 hour at RT. Chromogenic detection for second antibody was performed using Vector Blue Alkaline Phosphatase Substrate (Vector Laboratories, Peterborough, UK). Levamisole (Vector Laboratories, Peterborough, UK) was added to block endogenous alkaline phosphatases. Sections were counterstained using Mayer's haematoxylin dehydrated through a series of graded alcohols through to Histoclear and then mounted using VectaMount permanent mounting medium. LAM lung tissue (x10) and LAM spheroids (x40) were imaged using the Nikon Diaphot 300 Inverted Microscope.

Double fluorescent IHC was performed on deparaffinised and hydrated sections which were epitope retrieved and blocked for non-specific binding as described in section 2.4.2. Sections were then sequentially incubated with primary antibodies against both antigens at 4°C overnight. The following day, sections were washed as described (section 2.4.2) after which they were incubated with both fluorophore conjugated secondary antibodies (pre-adsorbed against the other species) for 1 hour at RT. Sections were then washed, counterstained using DAPI (0.2µg/ml) for 10 minutes at room temperature and mounted using Fluorescent Mounting Medium.

### 4.2.3 Measurement of pH

A total of $5x10^4$ 621-101 cells were seeded onto 24-well standard tissue culture plastic in DMEM/F-12 for an overnight period to allow cells to adhere following which medium was replaced by unbuffered DMEM. Cells were maintained for 24 hours and pH was measured every 4 hours. Direct contact cultures were maintained in unbuffered DMEM for 48 hours. pH was measured every 4 hours until 24 hours and then once at the end of 48 hours.

Unbuffered medium was prepared by mixing 1 volume of 10x DMEM (Sigma, Dorset, UK) with 9 volumes of sterile deionised water and was supplemented with 0.584 gm/L L-glutamine and 0.004 gm/L folic acid (Sigma, Dorset, UK). As required, pH was adjusted using 2M sodium hydroxide solution and measured using an Oakton Waterproof pH Spear Pocket pH Tester (Cole-Parmer, London, UK) over 24 or 48 hours.

### 4.2.4 Intracellular Cathepsin K Activity – Magic Red®

Intracellular Cathepsin K activity was recorded in live cells using the Magic Red® substrate (ImmunoChemistry Technologies, 2B Scientific, Bicester, UK). Cultured LAFs and 621-101 cells were grown on 8-well chamber slides in DMEM/F-12 without serum for 24 hours at 37°C and 5% $CO_2$. Cells were then treated with unbuffered DMEM supplemented with 0.584 gm/L L-glutamine and 0.004 gm/L folic acid at pH 6.5 for 2 hours after which Magic Red substrate was added to the media at a 1:26 ratio in the presence and absence of Cathepsin K inhibitor L006235 (100nM), and cysteine protease

inhibitor E64 (10μM) (Tocris, Abingdon, UK). Each condition per donor was set up in triplicate. The cells were then incubated for 16 hours at 37°C and 5% $CO_2$. Cells were washed in PBS and labelled using 0.5% v/v Hoechst stain for 10 minutes at 37°C and 5% $CO_2$. Samples were then mounted using PBS.

### 4.2.5 Extracellular Cathepsin K activity assay

Extracellular cathepsin K activity assay was measured using a Fluorometric Cathepsin K Activity Assay Kit (Abcam, Cambridge, UK). 12-well Boyden chamber Transwell cultures were set up. Polycarbonate membrane Transwell inserts (0.4μm pore size) were equilibrated for one hour at 37°C and 5% $CO_2$ prior to adding cells. Maintaining a 10:1 cell ratio, LAFs were seeded at $5x10^5$ cells per ml in the lower chamber and $5x10^4$ 621-101 cells (500μl) in the upper chamber. Mono-cultures of both cell types maintained the same cell number as co-cultures. To assess the effect of inhibition of acid extruders on cathepsin K activity, in a 48-well standard tissue culture plate, $5x10^4$ LAFs, 621-101 cells or a mixture of 1:1 LAFs and 621-101 cells were cultured in direct contact cultures for 48 hours at 37°C and 5% $CO_2$. Cells were maintained in unbuffered DMEM supplemented with 0.584 gm/L L-glutamine and 0.004 gm/L folic acid at pH 6.0, 7.0 and 7.5 for 96 or 48 hours at 37°C and 5% $CO_2$. Each condition per donor was set up in triplicate. Media were then harvested, triplicates pooled, clarified and concentrated five-fold using Vivaspin 2 Centrifugal Concentrators (Sartorius, SLS, Nottingham, UK). 50μl of concentrated medium was

expelled into three wells each of a black-walled, clear-bottom 96-well assay plate and 50µl of kit supplied cathepsin K reaction buffer was added to the wells. 2µl of the cathepsin K substrate Ac-LR-AFC was added to each well of 96-well plate resulting in a final 200µM concentration. A substrate blank (no sample) and a buffer blank (no sample and substrate) were also set up. 2µl of cathepsin K inhibitor was added to inhibitor treated wells resulting in a final 20µM concentration. Samples were incubated for 16-18 hours protected from light at 37°C after which fluorescence was read at 400-nm excitation and 505-nm emission.

### 4.2.6 Cathepsin K ELISA

Cell supernatants collected from 48-well direct contact cultures after 48 hours of inhibition of proton pumps and membrane transporters were used to measure total cathepsin K. Media from donor replicates was pooled, clarified and concentrated five-fold using Vivaspin 2 Centrifugal Concentrators. Following this Human cathepsin K ELISA (LSBio, Source BioScience, Nottingham, UK) was performed as per manufacturer's instructions. In brief, 100µl of standards, substrate blank or concentrated supernatant samples were added per well of the pre-coated 96-well assay plate and incubated for 2 hours at 37°C. This was followed by incubation with Detection Reagent A for 1 hour at 37°C. The plate was washed 3 times adding approximately 350µl wash buffer per well for 2 minutes each time and then dried by tapping against absorbent paper. 100µl of Detection Reagent B was then added to each well and incubated for 60 minutes at 37°C. The plate was then washed 5 times as described above. Protected

from light, 90µl of TMB Substrate solution was then added to each well and incubated for 30 minutes at 37°C until blue colour develops. Finally, to stop the reaction, 50µl of Stop Solution was added to each well and optical density (OD value) for each well was determined at 450 nm using Flexstation 3. The standard curve set ranging from 300pmol/l to 1.172pmol/l and sample concentrations were back calculated using the SoftMax Pro version 5.4 software (Molecular devices, USA).

## 4.3 Results

To determine the protease profile for LAM several relevant proteases needed to be examined in *ex vivo* tissue and *in vitro* cellular models. The following sections demonstrate the process applied to screen various proteases and select relevant targets with a potential to be novel therapeutic avenues.

### 4.3.1 Literature Search and q RT-PCR Screen for Proteases Overexpressed in LAM

| Proteases | Gene symbol | Protease family | Disease elevated or expressed in | Reference |
|---|---|---|---|---|
| Matrix metalloproteinase-1 (MMP-1) | MMP1 | Metalloproteinases | LAM | (Hayashi et al., 1997) |
| Matrix metalloproteinase-2 (MMP-2) | MMP2 | Metalloproteinases | LAM serum | (Hayashi et al., 1997), (Matsui et al., 2000a), (Chang et al., 2012), (Odajima et al., 2009) |
| Matrix metalloproteinase-3 (MMP-3) | MMP3 | Metalloproteinases | LAM lung tissue, Mouse model of pulmonary LAM | (Hayashi et al., 1997), (Goncharova et al., 2012), (Atochina-Vasserman et al., 2014) |
| Matrix metalloproteinase-7 (MMP-7) | MMP7 | Metalloproteinases | LAM serum, Mouse model of pulmonary LAM | (Barnes et al., 2010), (Clements, 2009), (Goncharova et al., 2012), (Atochina-Vasserman et al., 2014) |
| Matrix metalloproteinase-9 (MMP-9) | MMP9 | Metalloproteinases | LAM serum and urine | (Hayashi et al., 1997), (Chang et al., 2012), (Odajima et al., 2009), (Pimenta et al., 2011) |
| Matrix metalloproteinase-12 (MMP-12) | MMP12 | Metalloproteinases | Mouse model of pulmonary LAM, Pulmonary sarcoidosis (PS) | (Goncharova et al., 2012), (Crouser et al., 2009) |
| Matrix metalloproteinase-13 (MMP-13) | MMP13 | Metalloproteinases | Bleomycin-induced IPF mouse model, Pulmonary sarcoidosis | (Henry et al., 2002), (Nkyimbeng et al., 2013) |
| Matrix metalloproteinase-14 (MMP-14) | MMP14 | Metalloproteinases | LAM tissue, spindle-shaped LAM cells | (Matsui et al., 2000a), (Glassberg et al., 2008) |
| Matrix metalloproteinase-15 (MMP-15) | MMP15 | Metalloproteinases | LAM lung tissue | (Matsui et al., 2000a) |
| Tissue inhibitor of metalloproteinases -1 (TIMP-1) | TIMP1 | Metalloproteinase inhibitor | LAM lung tissue | (Hayashi et al., 1997) |
| Tissue inhibitor of metalloproteinases -2 (TIMP-2) | TIMP2 | Metalloproteinase inhibitor | LAM lung tissue | (Hayashi et al., 1997) |

| | | | | |
|---|---|---|---|---|
| Tissue inhibitor of metalloproteinases -3 (TIMP-3) | TIMP3 | Metalloproteinase inhibitor | LAM lung tisse (absent), Interstitial lung diseases | (Zhe et al., 2003), (Edwards et al., 2005) |
| Extracellular matrix metalloproteinase inducer; Basigin (EMMPRIN) | BSG | Metalloproteinase inducer | LAM lung tisse, BAL from LAM patients | (Odajima et al., 2009, Odajima et al., 2010) |
| Cathepsin B | CTSB | Cysteine protease | Bleomycin-induced IPF mouse model, Airway smooth muscle cells, Lung fibroblasts | (Dong et al., 2016), (Faiz et al., 2013) |
| Cathepsin D | CTSD | Aspartic protease | Asthmatic airways, Langerhans cell histiocytosis, Cigarette smoke-induced COPD mouse | (Faiz et al., 2013), (Bracke et al., 2005), (Paulli et al., 1994) |
| Cathepsin E | CTSE | Aspartic protease | Langerhans cell histiocytosis | (Paulli et al., 1994) |
| Cathepsin H | CTSH | Cysteine protease | Asthmatic airways | (Faiz et al., 2013) |
| Cathepsin K | CTSK | Cysteine protease | LAM lung tissue, Angiomyolipomas, PEComas | (Chilosi et al., 2009, Martignoni et al., 2012) |
| Cathepsin L | CTSL | Cysteine protease | BAL fluid from emphysema patients, Airway smooth muscle cells, lung fibroblasts, bronchial epithelial cells | (Takeyabu et al., 1998), (Buhling et al., 2004c), (Faiz et al., 2013) |
| Cathepsin S | CTSS | Cysteine protease | Mouse model of sarcoidosis, ovalbumin-sensitised mice | (Fajardo et al., 2004), (Samokhin et al., 2011) |
| Urokinase-type plasminogen activator (uPA) | PLAU | Serine protease | LAM lung tisse | (Zhe et al., 2005) |
| Plasminogen activator inhibitor-1 (PAI-1) | SERPINE1 | Serine protease inhibitor | LAM lung tissue | (Zhe et al., 2005) |
| Urokinase receptor (uPAR) | PLAUR | Serine protease receptor | Serum from asthma and COPD patients, Asthamatic bronchial tissue | (Portelli et al., 2017, Portelli et al., 2014) |
| ADAM metallopeptidase domain 17 | ADAM17 | Disintegrin metalloproteinase | Several interstitial lung diseases including LAM | (Edwards et al., 2005) |
| ADAM like decysin 1 | ADAMDEC1 | Disintegrin metalloproteinase | Pulmonary sarcoidosis | (Crouser et al., 2009) |
| Chymase | CMA1 | Serine protease | LAM lung tissue, Interstitial lung | (Valencia et al., 2006), (Edwards et al., 2005) |

| | | | | |
|---|---|---|---|---|
| | | | diseases including LAM | |
| Renin | REN | Angiotensinogenase | LAM lung tissue | (Valencia et al., 2006) |
| Calpain-1 | CAPN1 | Non-lysosomal cysteine protease | Associated with Akt/mTOR signaling pathway in mouse asthma model, bleomycin-induced pulmonary fibrosis mouse model | (Rao et al., 2017), (Li et al., 2015) |
| Calpain-2 | CAPN2 | Non-lysosomal cysteine protease | Associated with Akt/mTOR signaling pathway and apoptosis | (Abeyrathna et al., 2016) |
| Lipocalin 2 (NGAL) | LCN2 | Transport protein | LAM patient urine | (Chang et al., 2014), (Moses et al., 2006) |

**Table 4.3.1** ***List of 30 proteases elevated in or expressed in LAM, other interstitial and airway lung diseases selected for screening in LAM lung tissue.***

A thorough literature search was conducted to identify key proteases that play a role in various respiratory conditions, mainly interstitial lung diseases. The search yielded a list of 30 candidate proteases comprising of various protease families. Endogenous protease inhibitors such as TIMPs and MMP inducer EMMPRIN were also included in the list. This identified list of proteases was then screened in LAM lung tissue using qRT-PCR. However, to determine whether the method applied was sensitive enough, the expression of the LAM markers was first compared.

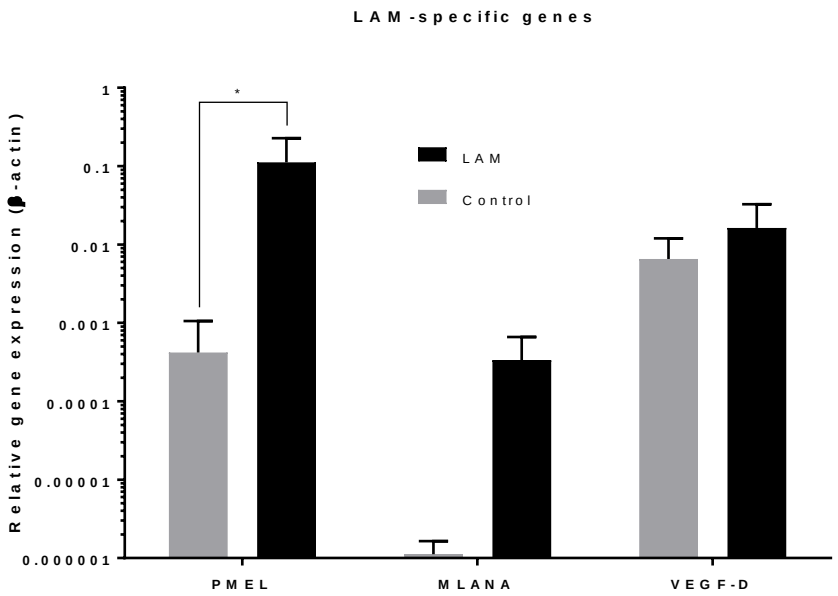



**Figure 4.3.1** ***Relative gene expression for LAM specific markers in human LAM and control lung tissue.*** *Figure shows expression markers of LAM (mean, ±standard deviation) analysed by q RT-PCR determined relative to β-actin using the $2^{-\Delta CT}$ method. Two-tailed Student's t-test performed, *p≤0.05.*

LAM lung tissue obtained at the time of diagnostic biopsy or lung transplant was received from UK transplant centres and the National Disease Research Interchange (NDRI). 200mg of fresh or OCT frozen tissue was homogenised following which RNA was isolated as described in section 2.3.1. Normal human total lung RNA was obtained from Ambion® (ThermoFisher Scientific) making sure that none of the donors had a history of any lung disease.

Figure 4.3.1 shows the expression of LAM markers Melan A *(MLANA)*, premelanosome protein *(PMEL)*, vascular endothelial growth factor D *(VEGF-D)* in LAM (n=6) and control (n=3) lung tissue. The transcriptional expression of *PMEL* was found to be significantly elevated in LAM lung (p=0.033) compared to control lung. Expression of MLANA and VEGF-D was found to be 267 and 2.47 fold respectively more abundant in LAM than

control lung tissue, however, these comparisons were not found to be statistically significant ($p>0.05$).

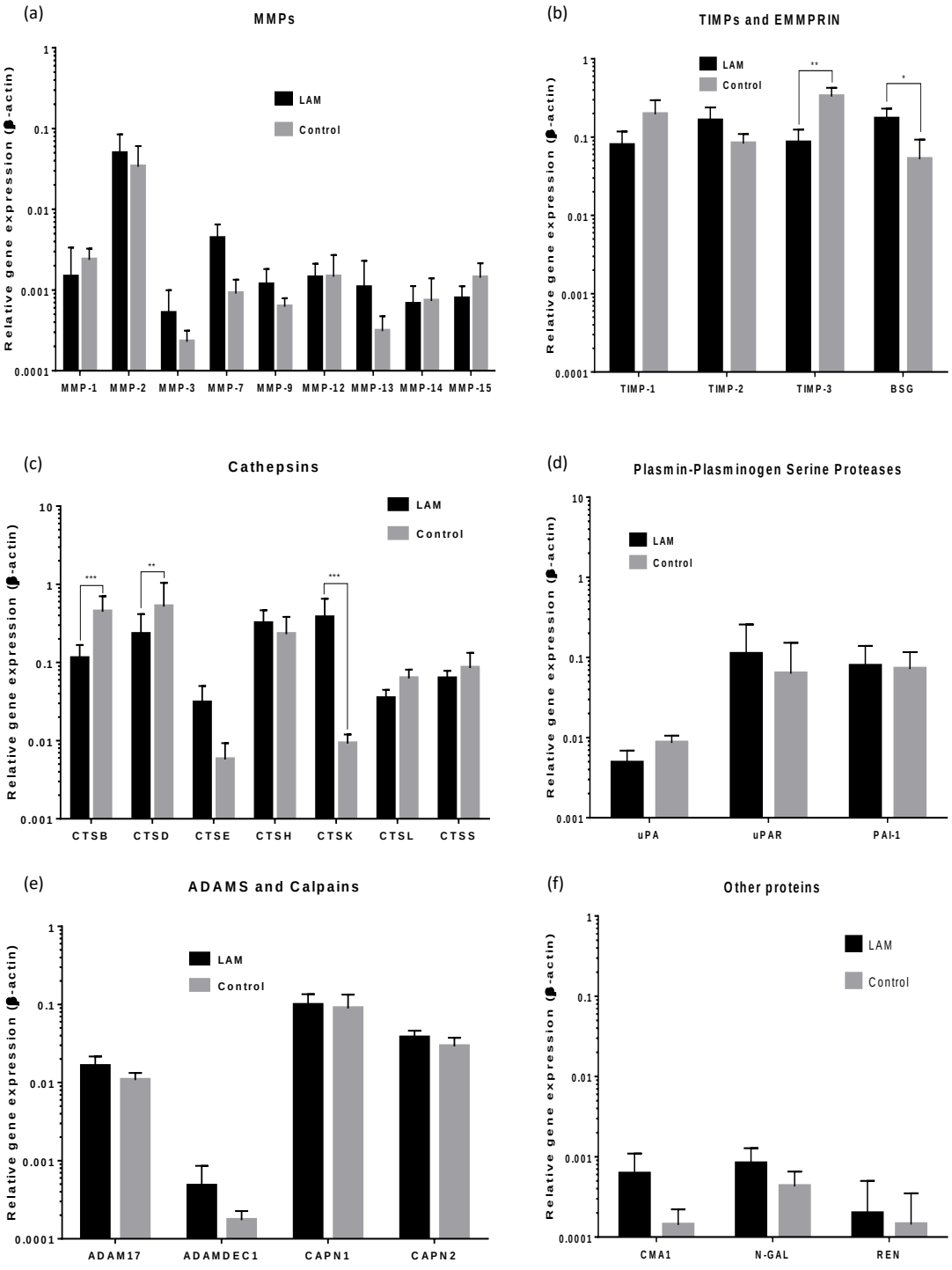


**Figure 4.3.2** ***Relative protease gene expression in human LAM and control lungs.*** *Whole lung RNA was extracted from 6 patients with LAM and 3 control patients without LAM. Protease gene expression was analysed by quantitative real time PCR. Figure shows mean (± standard deviation) protease gene expression determined relative to β-actin using the $2^{-\Delta CT}$ method. Multiple t-tests performed corrected for multiple comparisons using the Bonferroni-Dunn correction method. *p≤0.05, **p≤0.01, ***p≤0.001.*

mRNA for all proteases examined was detected in varying levels in LAM lung tissue. Transcript expression was variable between individual donors. Select members from different protease families namely matrix metalloproteinases (Figure 4.3.2 (a and e)) and their inhibitors (Figure 4.3.2 (b)) cysteine and aspartic proteases (Figure 4.3.2 (b and e)) and serine proteases (Figure 4.3.2 (d and f)). Transcripts for all 9 MMPs examined were detected in LAM lung tissue. Expression of *MMP-2* (1.5-fold), *MMP-3* (2.3-fold), *MMP-7* (4.5-fold), *MMP-9* (1.8-fold) and *MMP-13* (3.5-fold) was found to be elevated in LAM lung compared to control tissue while expression of others was unchanged. However, these comparisons were not found to be statistically significant ($p>0.05$). On the other hand, the endogenous MMP inhibitor *TIMP-3* was significantly reduced ($p=0.005$) and the expression of *TIMP-2* was 2.5-fold reduced in LAM lung tissue. Expression of MMP inducer *EMMPRIN (BSG)* was significantly ($p=0.019$) elevated in LAM lung compared to control lung tissue.

The most strongly expressed protease transcript in LAM lung was *CTSK* which was significantly increased 40-fold compared with normal tissue ($p<0.0001$). *CTSB* ($p<0.0001$) and *CTSD* ($p=0.0003$) were statistically significantly reduced in LAM. CTSH expression was 1.4-fold elevated whereas all other cysteine proteases were reduced in LAM lung tissue. These comparisons were not found to be statistically significant ($p>0.05$).

Transcriptional expression of serine protease *uPA* was slightly reduced in LAM tissue whereas that of its receptor, *uPAR* was slightly elevated (both, 1.7-fold) and expression of the inhibitor *PAI-1* was unchanged.

The mast cell serine protease *chymase* was 4.3-fold elevated while transport protein *lipocalin 2* was 2.0-fold elevated in LAM lung compared to control lung tissue. The rest of the comparisons were however, not found to be statistically significant ($p>0.05$).

### 4.3.2 Expression of Proteases in 2-Dimensional and 3-Dimensional Cell Cultures

Results from section 4.3.1 identified that four main groups, matrix metalloproteinases and their endogenous inhibitors and inducer, cathepsins, and serine proteases involved in plasmin-plasminogen protease axis showed variable expression in LAM lung and control tissue. Proteases belonging to these four groups were therefore examined in the 3D BME model. The ECM provides signalling cues to the cells enmeshed within that have an influence on the expression of ECM proteases. Gene expression of proteases in 2D and 3D models was therefore compared.

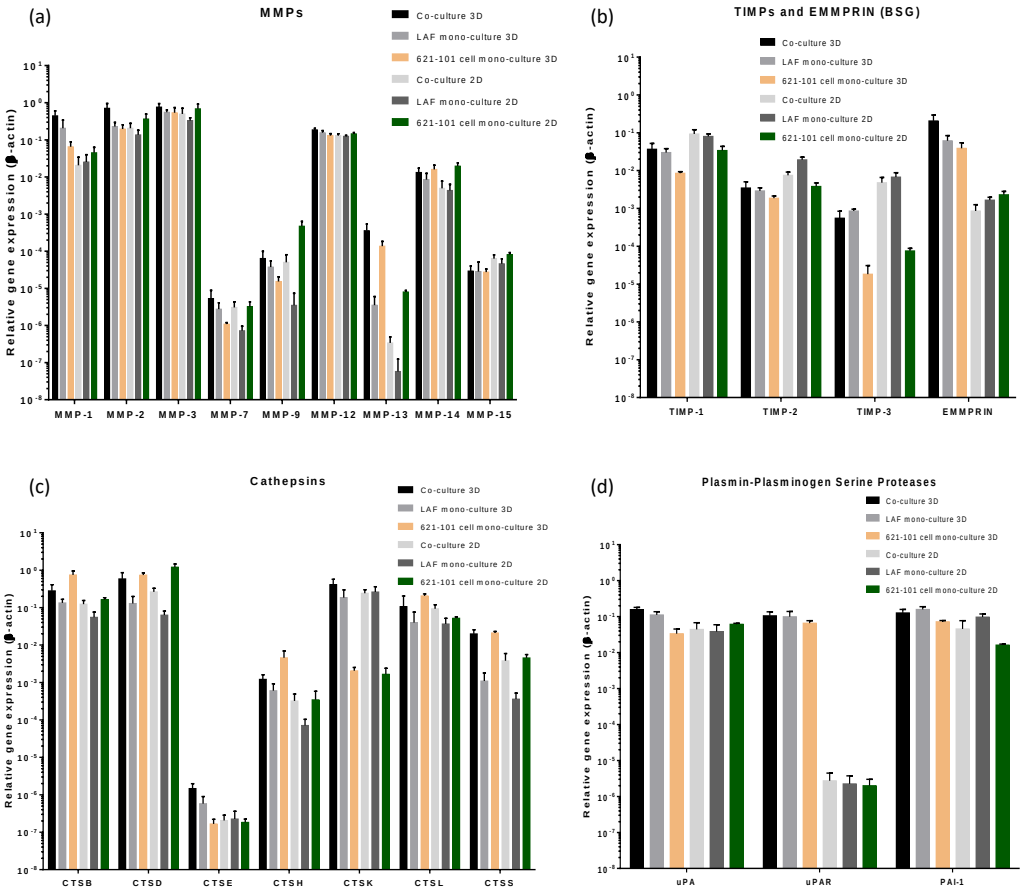



**Figure 4.3.3** ***Relative protease gene expression in LAF and 621-101 cell 2D and 3D cultures.*** *Total RNA was extracted from LAFs, 621-101 cells or a 10:1 mixture of LAFs and 621-101 cells cultured in 2D (standard tissue culture plastic) or 3D (BME gel cultures)*

*and protease gene expression was analysed by quantitative real-time PCR. Figure shows mean (± standard deviation) protease gene expression determined relative to β-actin using the $2^{-\Delta CT}$ method. Two-way ANOVA performed corrected for multiple comparisons using Bonferroni corection method.*

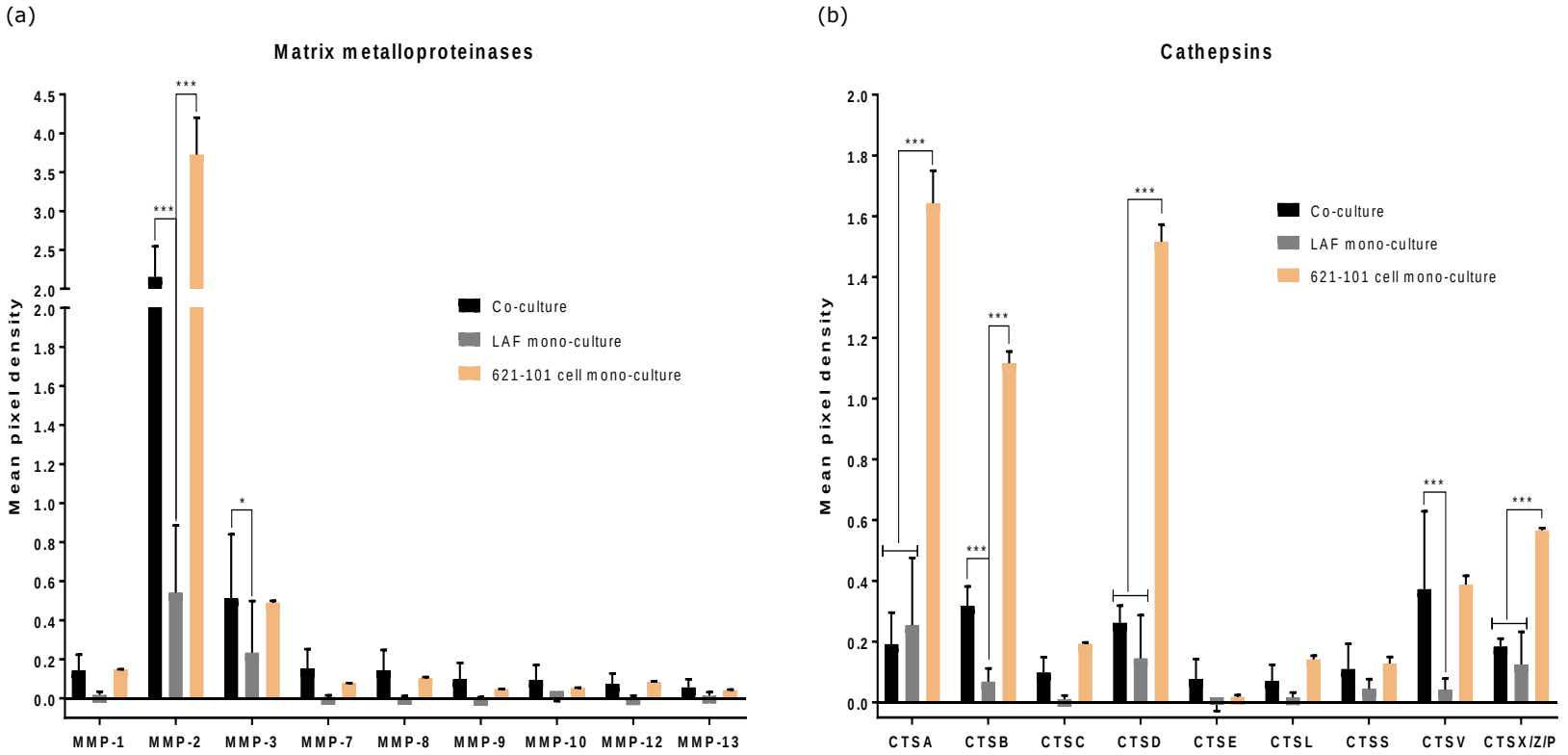
Varying expression of most proteases selected was detected in both 2D and 3D cultures (Figure 4.3.3). With the exception of the endogenous MMP inhibitors (*TIMPSs*), the expression of most proteases was elevated in the 3D BME gel LAM co-culture model as opposed to 2D cultures. Significant comparisons were as follows:

| **Protease type** | **Comparison** | **p value** |
|---|---|---|
| MMP-1 | Co-culture 3D vs. Co-culture 2D | p≤0.001 |
| MMP-2 | Co-culture 3D vs. Co-culture 2D | p≤0.001 |
| MMP-3 | Co-culture 3D vs. Co-culture 2D | p=0.003 |
| TIMP-1 | Co-culture 3D vs. Co-culture 2D | p=0.0066 |
| EMMPRIN (BSG) | Co-culture 3D vs. Co-culture 2D | p≤0.001 |
| CTSD | Co-culture 3D vs. Co-culture 2D | p≤0.001 |
| CTSK | Co-culture 3D vs. LAF mono-culture | p=0.0024 |
| | Co-culture 3D vs. 621-101 cell mono-culture 3D | p≤0.001 |
| uPA | Co-culture 3D vs. Co-culture 2D | p≤0.001 |
| uPAR | Co-culture 3D vs. Co-culture 2D | p≤0.001 |
| PAI-1 | Co-culture 3D vs. Co-culture 2D | p≤0.001 |

**Table 4.3.2** ***Significant protease gene expression comparisons between 2D and 3D cultures.***

Significantly elevated proteases in 3D co-cultures compared to 2D were *MMP-1, -2* and *-3, TIMP-1, EMMPRIN, CTSD, u PA, u PAR* and *PAI-1*. On the other hand, *CTSK* was elevated in both 3D and 2D cultures. Elevated *CTSK* expression was also detected in both 2D and 3D LAF mono-cultures. Expression of most proteases examined was detected in 621-101 cell mono-cultures, however, negligible expression of *CTSK* was detected in both 3D and 2D 621-101 cell mono-cultures.

### 4.3.3 Protein expression of proteases in non-contact Boyden chamber LAF and 621-101 cell cultures



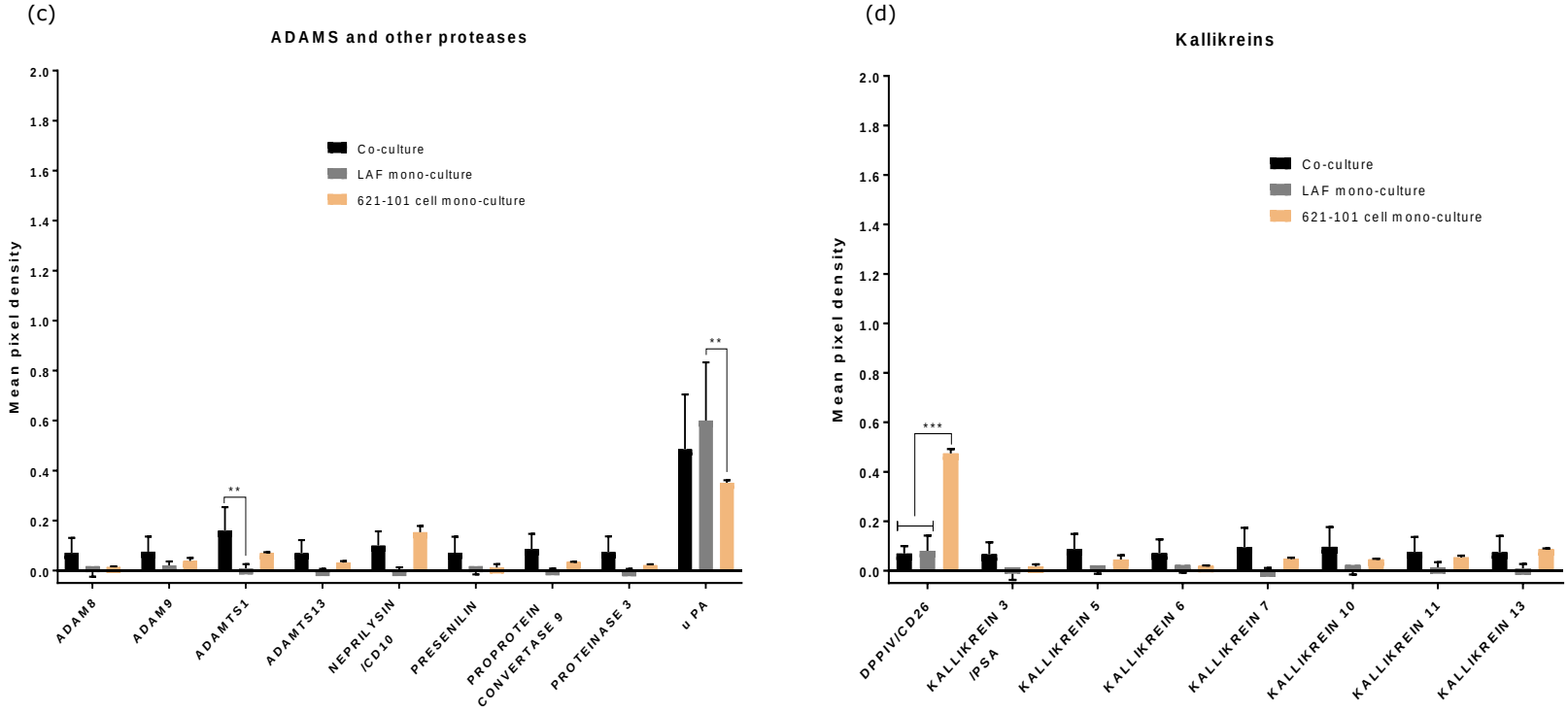



**Figure 4.3.4** ***Protein expression of proteases in LAF and 621-101 cell co-cultures and mono-cultures.*** *Expression of candidate proteases in LAF/621-101 cell co-cultures (n=3), LAF mono-cultures (n=3) and 621-101 cell mono-cultures. Figure shows the expression of (a) matrix metalloproteinases; (b) cathepsins; (c) ADAMS, neprilysin, presenilin, proprotein convertase 9, proteinase 3, urokinase-type plasminogen activator; (d) kallikreins and dipeptidyl peptidase-4. Expression was determined using the Proteome Profiler Human Protease Array Kit as mean pixel density (± standard deviation) compared to the reference standard and was plotted on the Y-axis. One-way ANOVA performed corrected for multiple comparisons using the Bonferroni correction method. *p≤0.05, **p≤0.01, ***p≤0.001.*

Following gene expression, protein expression of proteases was measured in the co-culture model using a pre-determined panel part of a protease array. Results obtained showed positive expression of matrix metalloproteinases (MMPs) (Figure 4.3.4 (a)); ADAM metalloproteinases (ADAMs 8 and 9), ADAM with thrombospondin motifs (ADAMTS 1 and 13), neprilysin, presenilin, proprotein convertase 9, proteinase 3, urokinase-type plasminogen activator (uPA) (Figure 4.3.4 (b)); cathepsins (CTS) (Figure 4.3.4 (c)) and kallikreins and dipeptidyl peptidase-4 (DPPIV/CD26) (Figure 4.3.4 (d)) in LAF/621-101 cell co-cultures and 621-101 cell mono-cultures. Protease expression was variable in the LAF donors. Both LAF/621-101 co-cultures and 621-101 cell mono-cultures showed significantly elevated MMP-2 protein compared to LAF mono-cultures ($p \leq 0.0001$) and MMP-3 was significantly elevated in co-cultures ($p=0.013$) compared to LAF mono-cultures. MMPs-13, -1, -12, -7, -8, -10 and -9 were increasingly elevated in LAF/621-101 cell co-cultures compared to LAF mono-cultures, however, these comparisons were not found to be statistically significant ($p>0.05$).

Expression of ADAM with thrombospondin motifs 1 (ADAMTS1) was significantly elevated ($p=0.0068$) in LAF/621-101 cell co-cultures compared to LAFs alone whereas serine protease, urokinase-type plasminogen activator (uPA) was elevated significantly elevated in LAF mono-cultures compared to 621-101 mono-cultures ($p=0.0012$). LAF/621-101 cell co-cultures showed elevated expression of ADAM metalloproteinases 8 (ADAM8) and 9 (ADAM9), ADAMTS13, neprilysin, presenilin, proprotein convertase 9 and proteinase 3 all of which were

negatively expressed in LAF mono-cultures. 621-101 cell mono-cultures showed more than 50% less expression of these proteases.

Expression of the kallikreins was elevated in co-culture however this was not found to be statistically significant compared to LAF and 621-101 cell mono-culture. Most kallikreins were negatively expressed in LAF mono-cultures. Again, 621-101 cell mono-cultures showed more than 30% less expression of most kallikreins compared to co-cultures. The 621-101 cell mono-cultures however, had significantly elevated levels of dipeptidyl peptidase-4 (DPPIV/CD26) compared to both co-culture and LAF mono-culture ($p \leq 0.0001$).

The expression of the panel of cathepsins however, was positively detected in all three conditions with the exception of cathepsin E (CTSE) being negatively expressed in LAF mono-cultures. Cathepsins A, B, D and X/Z/P were all significantly elevated in 621-101 mono-cultures compared to co-cultures and LAF mono-cultures ($p \leq 0.0001$). Expression of cathepsin V (CTSV) was however, significantly elevated in LAF/621-101 cell co-cultures compared to LAF mono-cultures ($p=0.0001$). Expression of cathepsins C, E, L and S was also elevated in co-cultures and 621-101 mono-cultures to a similar extent compared to LAF mono-cultures.

The above data suggested that although most proteases examined were elevated in LAF/621-101 co-cultures representing two key cell types in LAM nodule, *in vitro*, the most highly elevated were MMPs, mainly MMPs-2 and -3, uPA and the panel of 10 cathepsins. This suggested that the

cathepsins may be an important class of proteases involved in the destruction of the lung.

### 4.3.4 Cathepsin K Expression in *Ex Vivo* LAM Lung Tissue

On initial screening for elevated protease gene expression in LAM lung tissue, cathepsin K was identified as the most strongly expressed protease. Subsequent screening of gene and protein expression in LAF/621-101 co-cultures and mono-cultures identified that cathepsins were major group of proteases elevated in co-culture and that cathepsin K was almost exclusively expressed by the LAFs. Immunohistochemical expression of cathepsin K has previously been detected in LAM nodules (Chilosi et al., 2009). Cathepsin K expression was therefore assessed in the LAM lung tissue donors and was compared to fibroblast marker FSP.

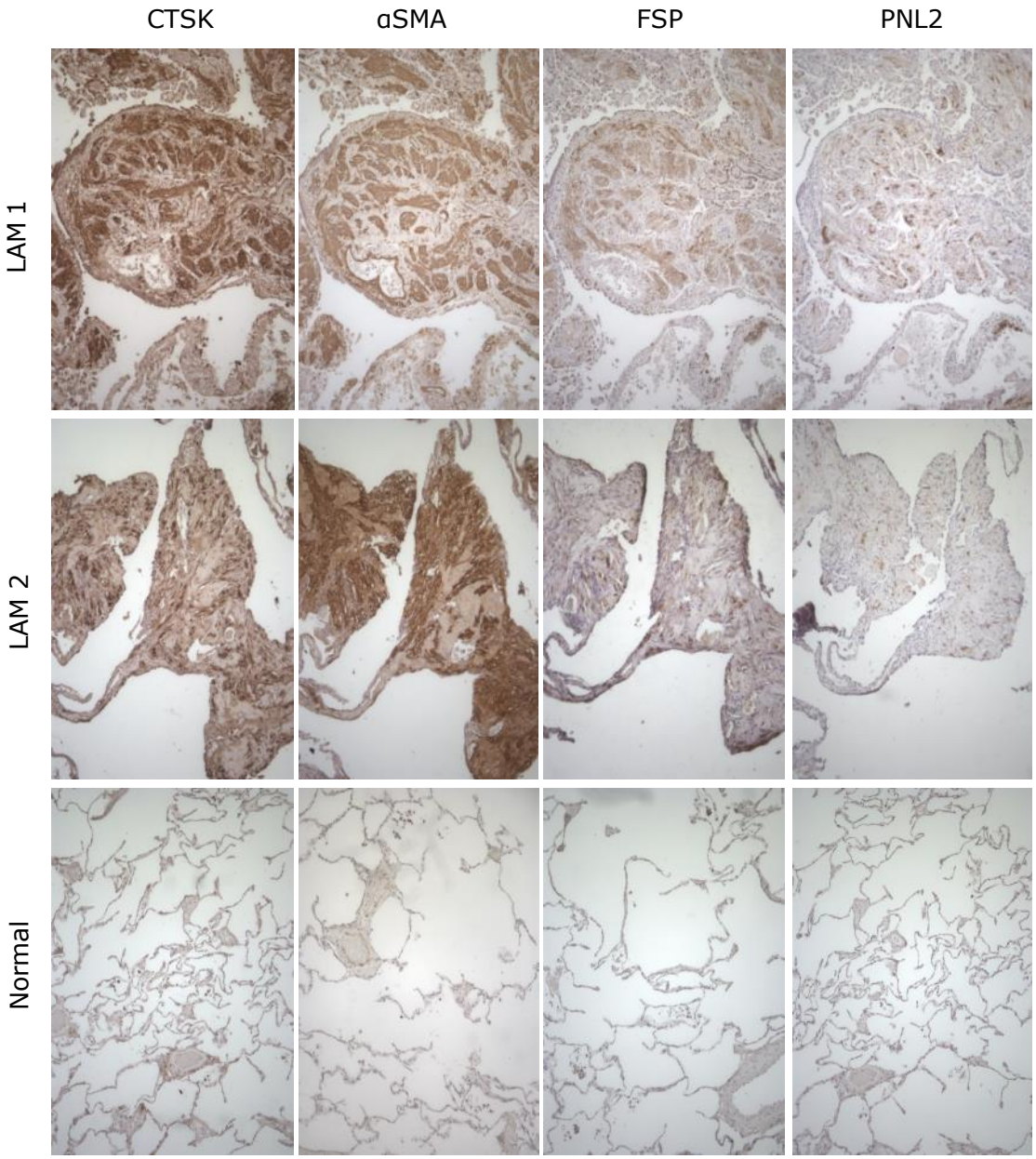



**Figure 4.3.5** ***Cathepsin K expression within LAM lung nodules.*** *Image shows immunohistochemical staining for cathepsin K (CTSK) α smooth muscle actin (α-SMA), fibroblast specific protein (FSP) and melanoma marker antibody (PNL2) in the nodules of two representative patients with LAM and normal lung tissue. x10 magnified images were taken using a Nikon Diphot Inverted microscope.*

Expression of cathepsin K was examined using immunohistochemistry in LAM lung tissue. Figure 4.3.5 shows comparative immunohistochemical staining in two representative LAM tissue donors and normal lung tissue. Cells within LAM nodules a showed strong immunoreactivity to the

cathepsin K antibody. Expression was particularly strong in the spindle-shaped cells within the nodules. These cells also strongly immunoreacted with α-SMA and fibroblast marker FSP expressed within the nodules. Punctate PNL2 expression was observed in rounded or epithelioid-shaped cells within the nodules which were distinct from the spindle-shaped areas within the nodules. Isotype controls were clean (Appendix I).

### 4.3.5 Cathepsin K Expression is Associated with LAM Nodules

As cathepsin K expression was found to be associated with LAM nodules, a further analysis was done to assess whether the nodular expression was associated with cystic destruction

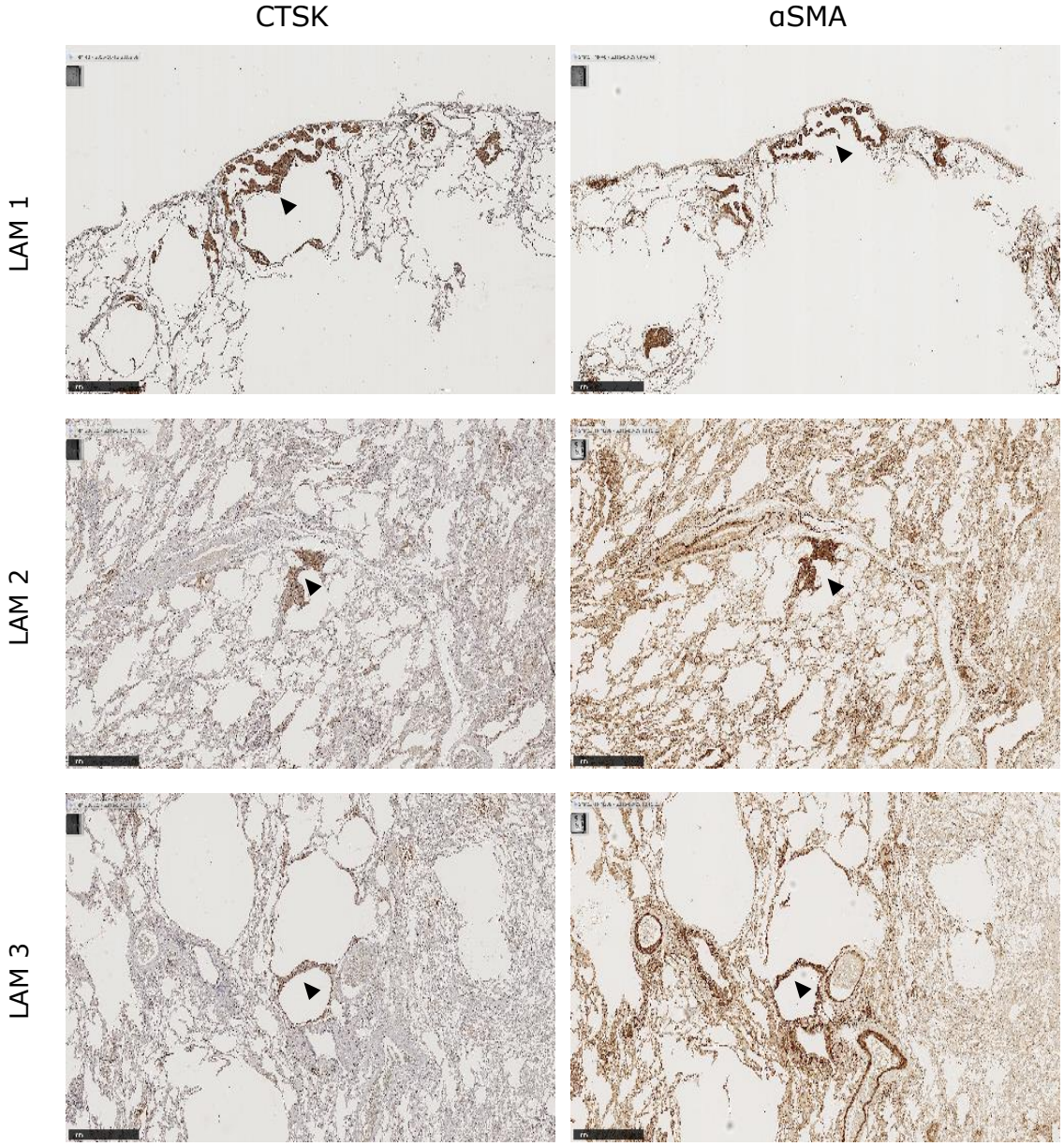



**Figure 4.3.6** ***Expression of Cathepsin K in LAM.*** *Immunohistochemical images of three representative LAM lung tissues. α-SMA identifies LAM nodules (black arrowhead) adjacent to cysts which have positive staining for cathepsin K. Magnification x2.5, scale bar 1mm.*

Six lung biopsy and seven transplant tissues from women with LAM were immunostained for cathepsin K. Nodules formed generally appear adjacent to cysts and immunostaining for α-SMA identified the nodules (black arrowhead) in three representative LAM donors presented. Cathepsin K staining was mainly localised to these nodules adjacent to cysts and was absent in the surrounding uninvolved lung tissue.

### 4.3.6 Effect of β-Estradiol (E2) and Rapamycin on CTSK Expression

*Cathepsin K* gene expression was then assessed in *ex vivo* LAM lung tissue. To determine whether expression in LAM lung was downstream of mTOR or oestrogen signalling, fresh LAM lung tissue pieces were treated with mTOR inhibitor rapamycin and β-estradiol. Due to the lack of availability of fresh LAM lung tissue, the experiment could be performed on two LAM donors only.

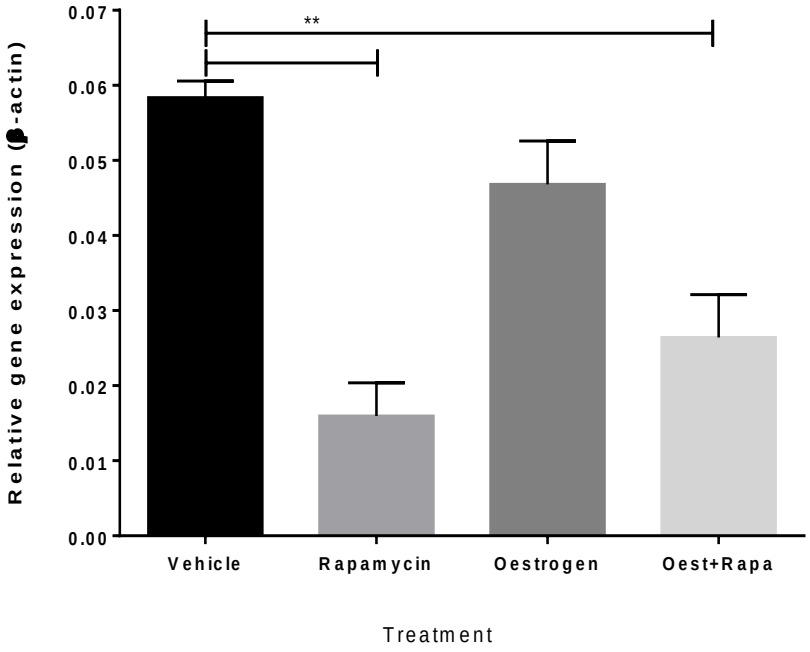



**Figure 4.3.7 *Cathepsin K gene expression in ex vivo LAM lung tissue*.** *Lung tissue was incubated for 48 hours with rapamycin (10nM), oestrogen (10nM), oestrogen and rapamycin or vehicle and gene expression measured by qRT-PCR. Figure shows mean (± standard deviation) CTSK gene expression determined relative to β-actin using the $2^{-\Delta CT}$ method. One-way ANOVA performed corrected for multiple comparisons using a post-hoc Dunnett's multiple comparisons test. **p≤0.01, n=12.*

Fresh pieces of LAM lung tissue were excised from six distinct areas of the lung parenchyma from two transplant lung donors. which showed variable expression possibly due to the variability of cells in each explant. Each of the six explants from both donors was treated with E2 and rapamycin

following which *cathepsin K* expression was measured making the number of replicates 12 (n=12). Therefore, a one-way ANOVA was performed to generate statistical differences.

*CTSK* gene expression was detected in all tissue explants. rapamycin (10nM) treatment reduced *CTSK* gene expression to around one quarter of vehicle control treated levels (p=0.0026). Treatment with E2 (10nM) had no significant effect upon *CTSK* levels. Additive treatment of E2 (10nM) and rapamycin (10nM) also resulted in signification reduction in CTSK gene levels (p=0.0077).

### 4.3.7 Expression of Cathepsin K (CTSK) in Cultured Cells

LAM nodules are heterogeneous structures with a complex mixture of cell types. To determine which cell types are responsible for cathepsin K expression the expression of the CTSK transcript was examined by qRT-PCR in LAFs, NHLFs and 621-101 cells.

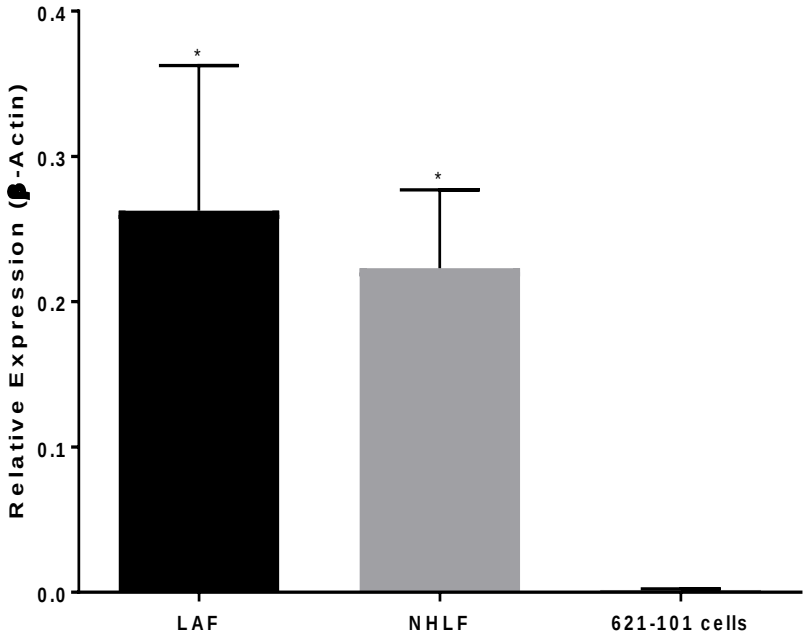



**Figure 4.3.8** ***Cathepsin K expression in fibroblasts and 621-101 cells.*** *Quantitative real-time PCR for cathepsin K in LAM associated fibroblasts (LAF, n=4), normal human lung fibroblasts (NHLF, n=3) and 621-101 cells. Figure shows mean (± standard deviation) CTSK gene expression determined relative to β-actin using the $2^{-\Delta CT}$ method. Two-tailed Students t-test was performed, *p≤0.05.*

CTSK transcript was present in both NHLFs and LAFs and was significantly elevated (p=0.045 and p=0.045 respectively) compared to 621-101 cells (Figure 4.3.8). Immunofluorescent expression of cathepsin K was then assessed in the LAFs, NHLFs and 621-101 cells detecting protein expression of this protease.

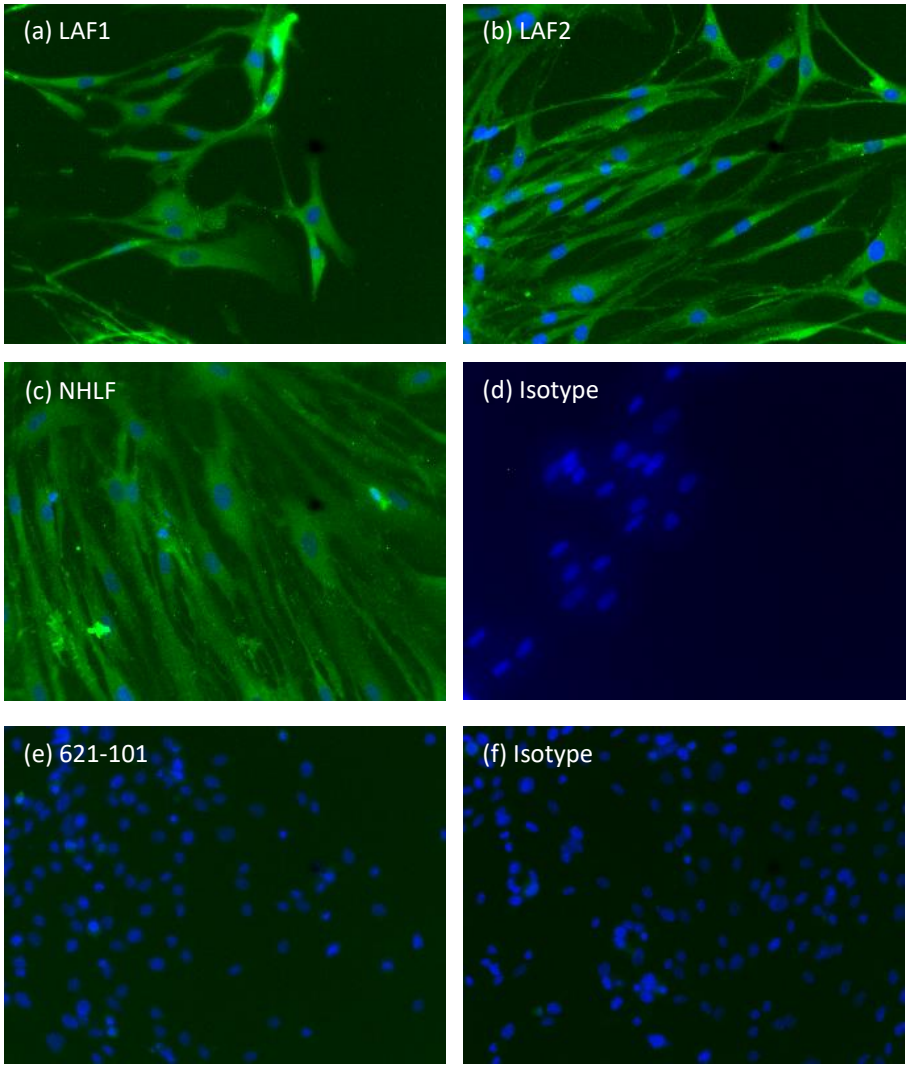



**Figure 4.3.9** ***Immunofluorescent detection of cathepsin K.*** *Image shows two LAF (A and B), NHLF (C) and 621-101 cells (E) stained using anti-CTSK antibody. Isotypes for fibroblasts (D) and 621-101 cells (F) were devoid of CTSK. Images taken at x20 using an Improvision spinning-disc confocal microscope.*

Two representative LAF donors (Figure 4.3.9 (a and b)) and one NHLF donor (Figure 4.3.9 (c)) are shown in the image above. Strong immunoreactivity to anti-CTSK was seen in both LAFs and NHLFs. All cells in culture showed an intra-cytoplasmic staining pattern and speckled granules suggested lysosomal presence of CTSK. However, the 621-101 cells (Figure 4.3.9 (e)) did not react with the CTSK antibody and were devoid of cathepsin K protein. Isotype controls for both fibroblasts and

621-101 cells were clean with little to no background staining (Figure 4.3.9 (d and f)).

### 4.3.8 Cathepsin K Expression in LAM Spheroids and LAMospheres

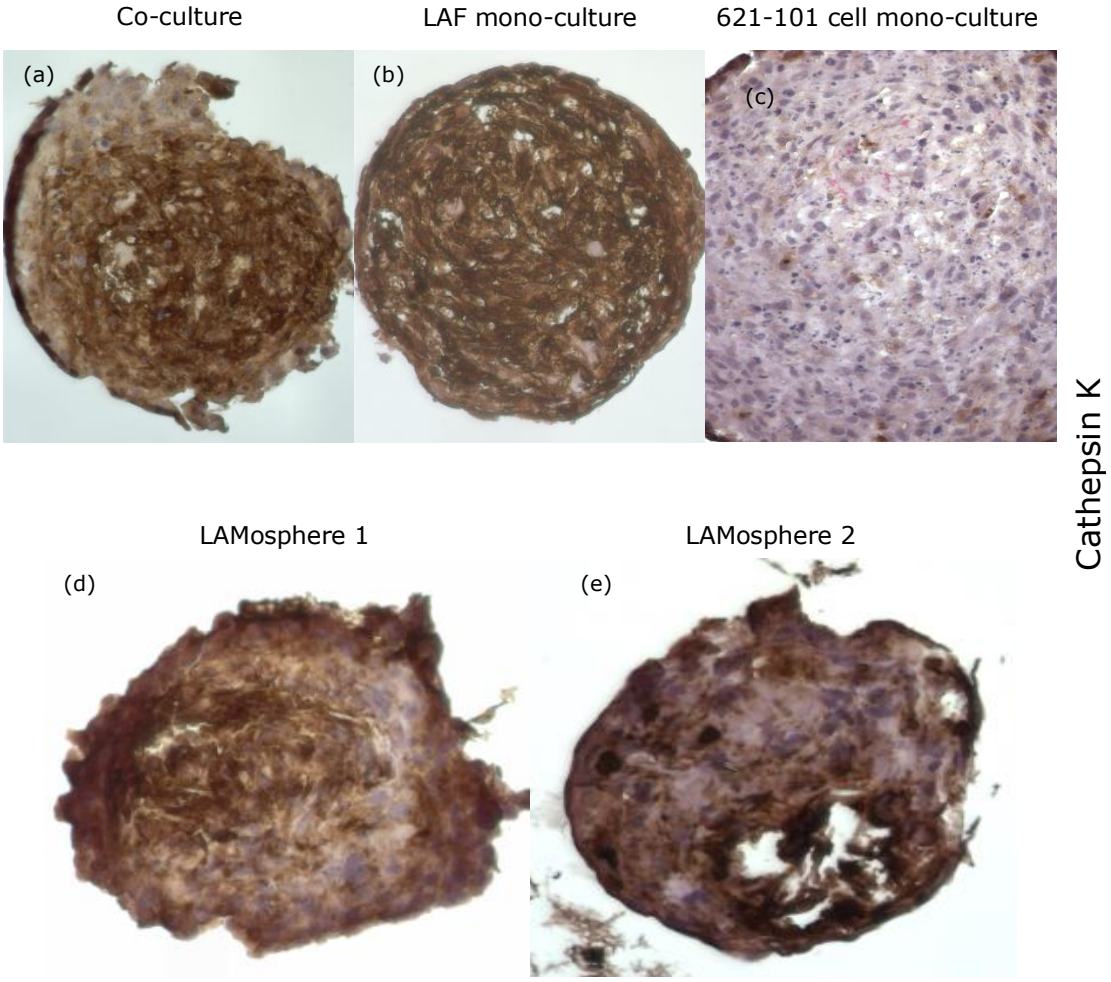



**Figure 4.3.10** ***Immunohistochemical expression of cathepsin K in LAM spheroids and LAMospheres.*** *Figure shows expression of cathepsin K in LAM spheroids and LAF and 621-101 cell mono-culture spheroids (panels A, B and C respectively) and LAMospheres obtained from two donors (panels D and E respectively). Images taken using Nikon Diaphot Inverted microscope at x40 magnification.*

Cathepsin K expression was found in both LAM spheroids and LAF mono-culture spheroids. Four independent LAF donors were examined all of which showed similar expression. LAF mono-culture spheroids showed strong immunoreactivity to the cathepsin K antibody (Figure 4.3.10 (b)). 621-101 cell mono-culture spheroid showed marginal expression of cathepsin K. Spheroids were imaged at x40 magnification however at the end of 7 days the loosely packed 621-101 cell mono-culture spheroids had

increased in size, did not fit in the area of focus and only 5-10% of the total cells expressed cathepsin K (Figure 4.3.10 (c)). Cathepsin K expression in the LAM spheroids however, was mainly observed in the centre of the spheroid (Figure 4.3.10 (a)). Cells in the periphery showed lower immunoreactivity to cathepsin K than those in the centre. This suggested that the positively reactive cells in the centre were LAFs surrounded by 621-101 cells in the periphery. LAMospheres from both LAM donors showed strong immunoreactivity to cathepsin K. Again, strong immunoreactivity was noted mainly in the centre of the LAMosphere surrounded by few negative cells in the periphery (Figure 4.3.10 (d and e)).

### 4.3.9 Magic Red® – Intracellular Cathepsin K Activity

Gene and protein expression of CTSK was detected in both LAFs and NHLFs (sections 4.3.2 and 4.3.7). However, since this study was based on the hypothesis that LAM cells recruit fibroblasts and possibly modify their phenotype all further experiments were carried out using LAFs alone. Although it was evident that LAFs expressed cathepsin K, activation of this protease is required to elicit its matrix degrading potential. The intracellular cathepsin K activity was therefore initially assessed in LAFs.

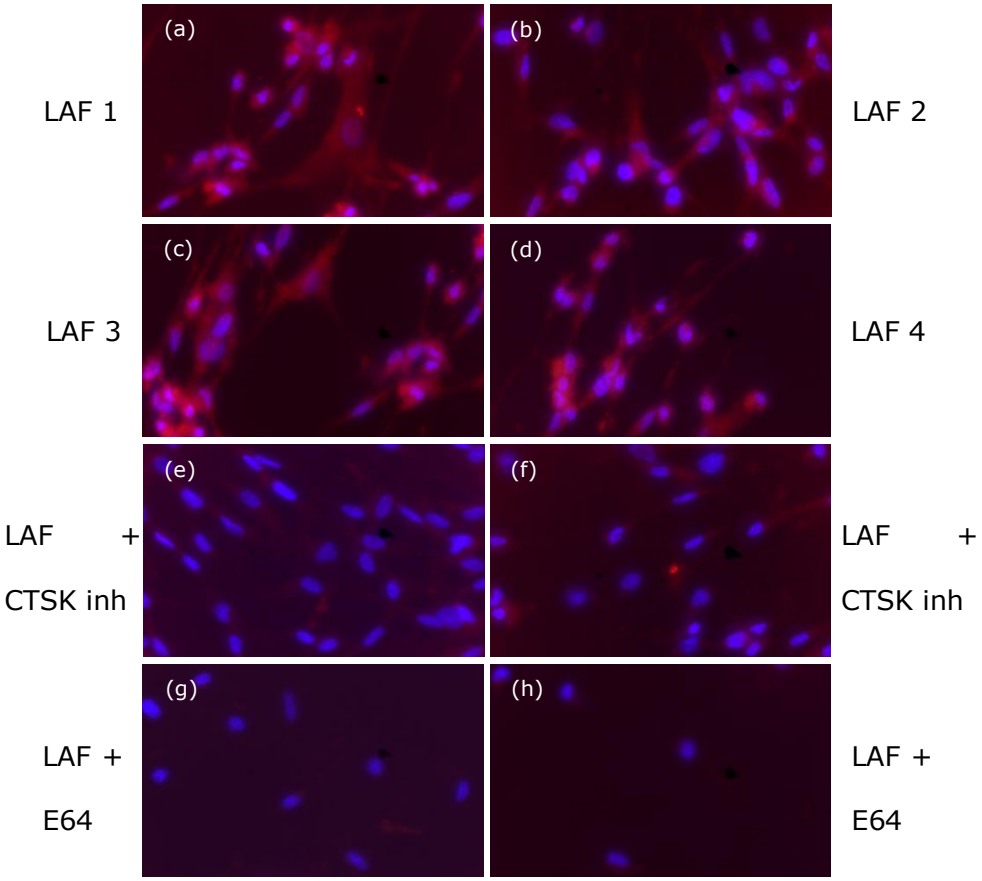



**Figure 4.3.11** ***Intracellular activity of cathepsin K measured using the Magic Red® substrate.*** *Intracellular cathepsin k activity is visible as red fluorescence in four LAF cultures (panels A-D) at pH 6.5. Fluorescence is reduced by the cathepsin K specific inhibitor L006235 (100nM) (panels E and F) and completely abrogated by the cysteine protease inhibitor E64 (10μM) (panels G and H). Magnification x20. Images acquired using Improvision spinning disc confocal microscope.*

To determine the presence of intracellular cathepsin K activity a synthetic substrate for cathepsin K was used. Magic Red makes use of a photo stable red fluorophore, cresyl violet that is bi-substituted via an amide linkage to two cathepsin k target peptide sequences such as (leucine-arginine)$_2$ (MR-(LR)$_2$). On enzymatic cleavage, the bi-substitution changes to a mono or non-substitution which causes cresyl violet to fluoresce and generate a red fluorescence when excited at 550-590nm (Van Noorden et al., 1997).

Fluorescence emitted by the cleaved cresyl violet substrate was imaged using a TRITC filter set on an Improvision spinning-disc confocal microscope. All four donors showed extensive intracellular CTSK activity (Figure 4.3.11 (a-d)) evidenced by the presence of red fluorescence. This activity was partially inhibited by highly specific and potent CTSK inhibitor, L006235 (Figure 4.3.11 (e and f)) and completely inhibited by the broad spectrum cysteine protease inhibitor E64 (Figure 4.3.11 (g and h)).

### 4.3.10 Association of Cathepsin K with Fibroblast-like Spindle-shaped cells in LAM nodules

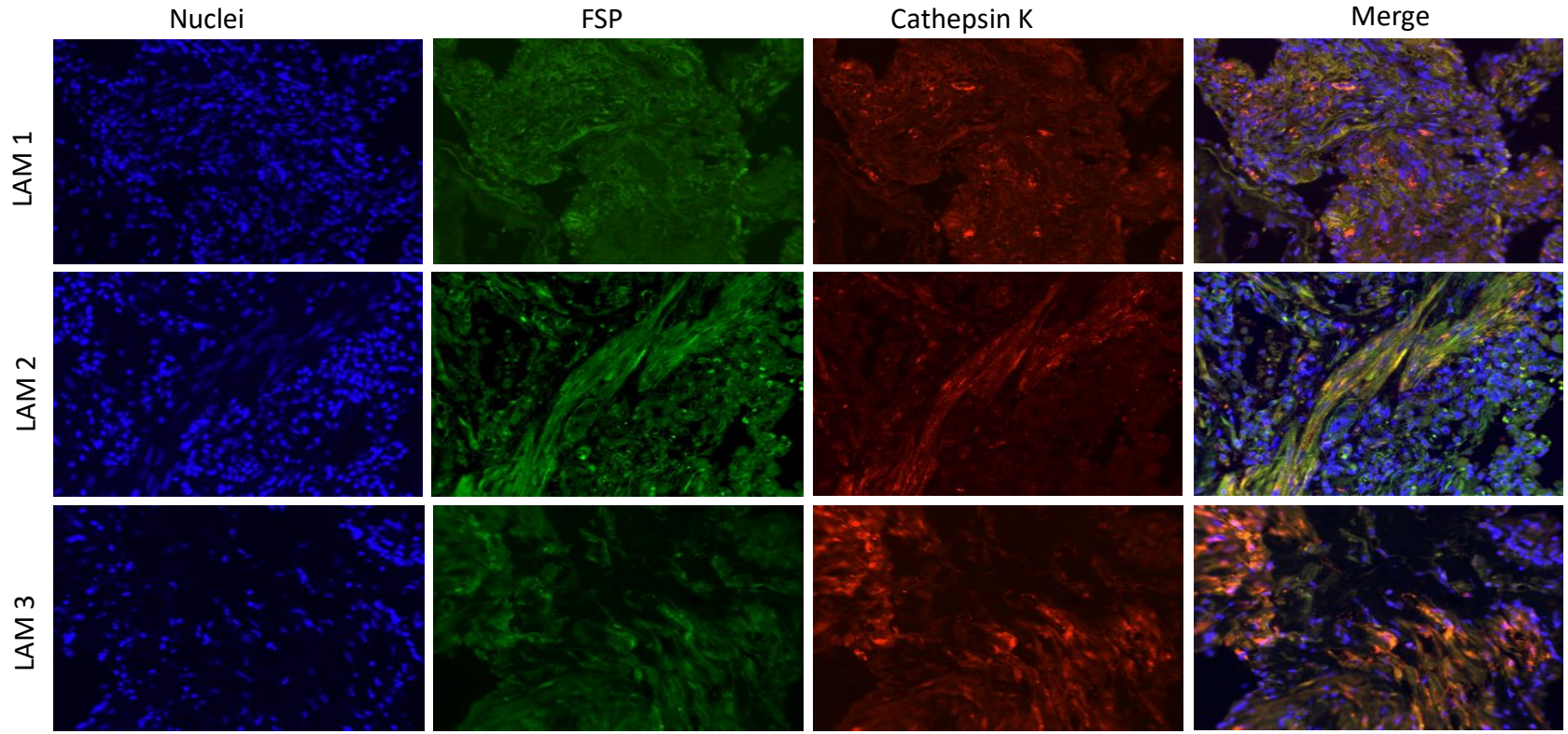



**Figure 4.3.12** ***Immunofluorescent (IHC-Fr) co-localisation of Fibroblast specific protein (FSP) and Cathepsin K in LAM lung nodules.*** *Image shows fluorescent immunohistochemical staining of LAM lung tissue from three donors. Individual panels show DAPI staining of nuclei (blue), fibroblast specific protein (FSP, green), cathepsin K (CTSK, red) and the overlay with co-localisation of FSP and CTSK (yellow). Cathepsin K and FSP are strongly co-localised, with only modest cathepsin K expression outside of LAM associated fibroblasts. Images x20 magnification.*

Clements et al. have previously shown the abundant presence of fibroblasts in LAM nodules (Clements et al., 2015). It is a well-known fact that fibroblasts express several proteolytic enzymes including several MMPs that have been known to participate in for tissue degradation (Sabeh et al., 2004, Sabeh et al., 2009). Therefore, to determine if the spindle-shaped cells, presumed to be LAFs, within the LAM nodules are the predominant source of cathepsin K, three LAM lung tissue donors were co-immunostained using fluorescently labelled antibodies against the fibroblast marker FSP and cathepsin K. Strong co-localisation of both cathepsin K and FSP expression was observed in the spindle-shaped cells in LAM nodules. The merging of green (FSP) and red (CTSK) fluorescent labels showed the appearance of yellow (merge) fluorescence in cells expressing both proteins (Figure 4.3.12) This was consistent with the expression of cathepsin K by LAM lung fibroblasts. A less intense cathepsin K staining could also be detected by immunofluorescence in FSP negative cells. Isotypes for both antibodies were clean with little or no background staining (Appendix I)

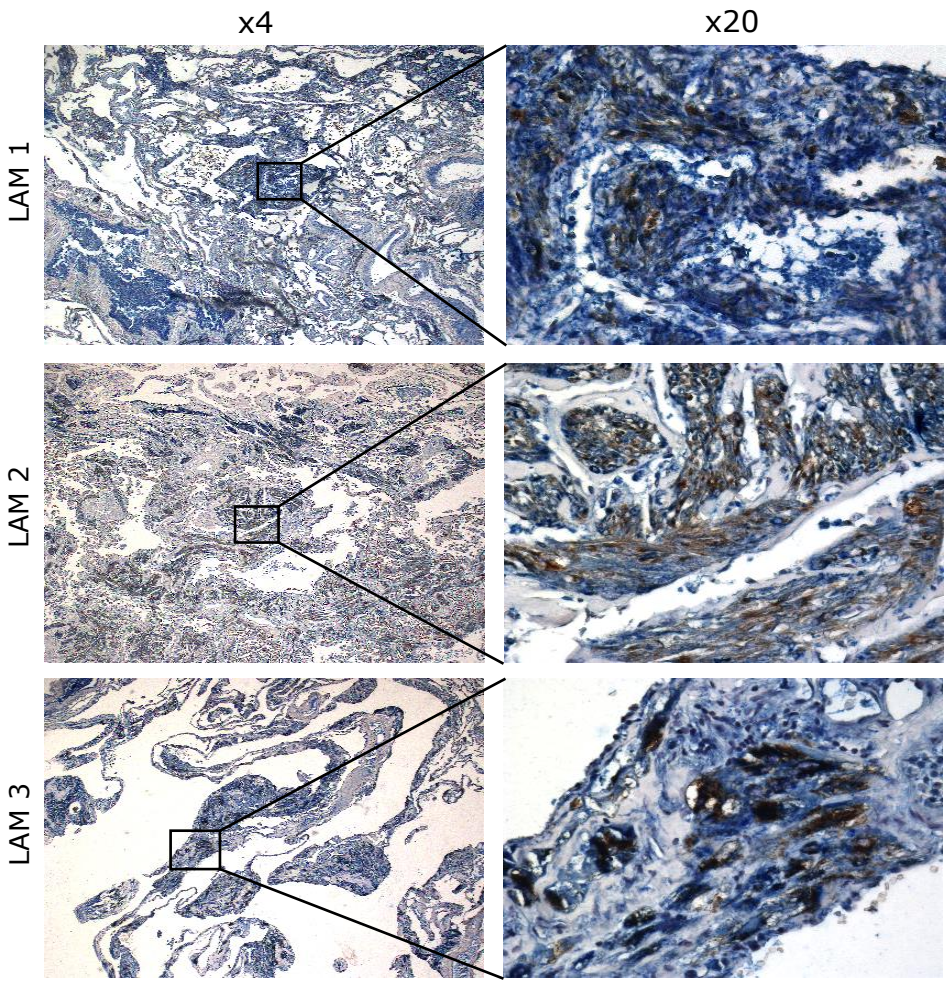



**Figure 4.3.13** ***Chromogenic immunohistochemical co-localisation of Fibroblast specific protein (FSP) and Cathepsin K in LAM lung nodules.*** *Dual chromogenic immunohistochemistry showing LAM nodules reacting with antibodies against both cathepsin K (blue) and fibroblast surface protein (brown). Left panels are x4 magnification and right are inset area at x40 taken from the same three representative donors. All donors showed spindle-shaped cells within nodules reacting with both antibodies.*

Dual chromogenic immunohistochemistry (IHC) was also performed to confirm the expression of cathepsin K in the spindle-shaped FSP-positive cells in LAM nodules. Cathepsin K (blue) was detected using Vector Blue alkaline phosphatase substrate and FSP (brown) detected using the ImmPact diaminobenzidine (DAB) substrate. Spindle-shaped cells within the nodules from all three donors reacted with both antibodies which was consistent with the IHC-Fr staining pattern. Cells expressing both proteins

appeared dark brown to black in colour (Figure 4.3.13). This was again consistent with the expression of cathepsin K by LAFs. Expression of cathepsin K was also noted in few surrounding FSP negative cells.

### 4.3.11 Extracellular Cathepsin K Activity

As it was established from section 4.3.10 that the FSP positive LAM-associated fibroblasts showed positive CTSK staining it was imperative to ascertain whether the CTSK expressed by LAFs *in vitro* was active extracellularly. Cathepsin K like most proteases requires activation from an inactive pro-form to elicit its potent matrix degrading activity (McQueney et al., 1997). This activation occurs in an acidic microenvironment therefore the extracellular activity of cathepsin K was measured at physiological and acidic pH. The fluorescent-based cathepsin K activity assay the preferred cathepsin K peptide substrate sequence leucine-arginine (LR) labelled with amino-4-trifluoromethyl coumarin (AFC). On cleavage of the peptide substrate the free released AFC can be measured at 400nm excitation and 505nm emission reflecting CTSK activity in samples.

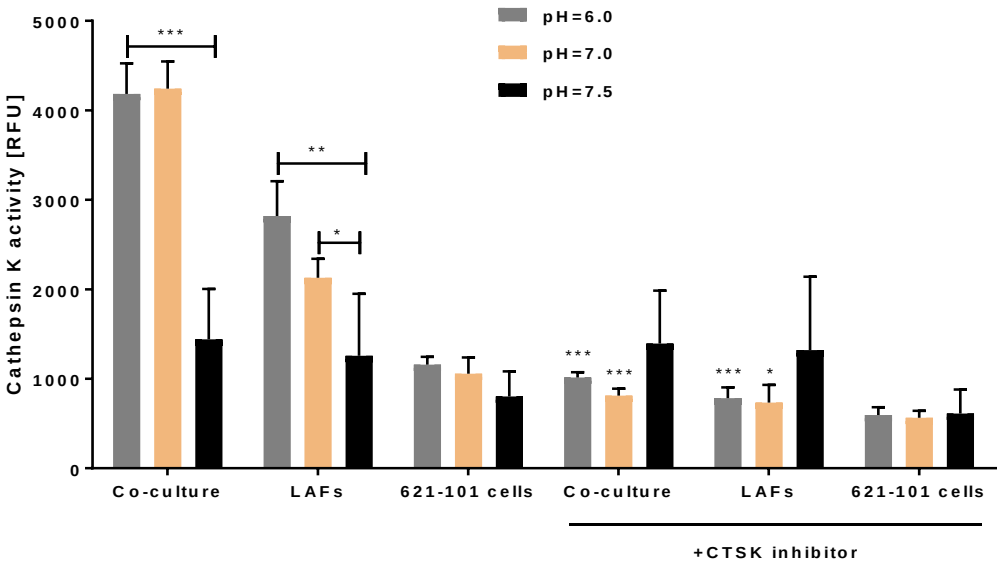



**Figure 4.3.14** ***Extracellular cathepsin K activity is pH dependant.*** *LAFs (n=4), 621-101 cells and LAF/621-101 cell co-cultures in a 10:1 ratio were grown in culture for 96 hours at a range of pH values. Cathepsin K activity was measured in in four LAF donors the presence and absence of CTSK inhibitor using the Cathepsin K activity assay (Abcam). Fluorescence was measured at 400nm excitation and 505nm emission and data were plotted as a mean (±standard deviation) of relative fluorescence units obtained from four donors per condition. Two-way ANOVA performed corrected for multiple comparisons using the Bonferroni correction method. *p≤0.05, ***p≤0.0001.*

Figure 4.3.14 shows *in vitro* cathepsin K activity examined using four separate LAF primary cultures (n=4) and 621-101 cells both separately as mono-cultures and combined in co-cultures (n=4). At physiological pH, cathepsin K activity was not significantly elevated above baseline values in any cell type or culture condition. However, at pH 7.0 and 6.0 LAF cathepsin K activity was 1.7 and 2.2-fold higher (p=0.044 and 0.0017 respectively) than at pH 7.5, and almost 3 fold higher (p≤0.0001) in co-cultures. Cathepsin K activity in 621-101 cell supernatants was low at all pH values.

Treatment with 20μM kit supplied CTSK inhibitor significantly reduced cathepsin K activity in LAFs at pH 6.0 (p≤0.0001) and 7.0 (p=0.0064). Activity was also significantly reduced in LAF/621-101 cell co-cultures

($p \leq 0.0001$) when treated with the inhibitor. Baseline cathepsin K activity was seen at physiological pH which remained unchanged despite inhibitor treatment.

### 4.3.12 Cell viability at low pH

Cell viability was assessed as a measure of MTT reduction as cells normally cultured at physiological pH were now treated with low pH medium.

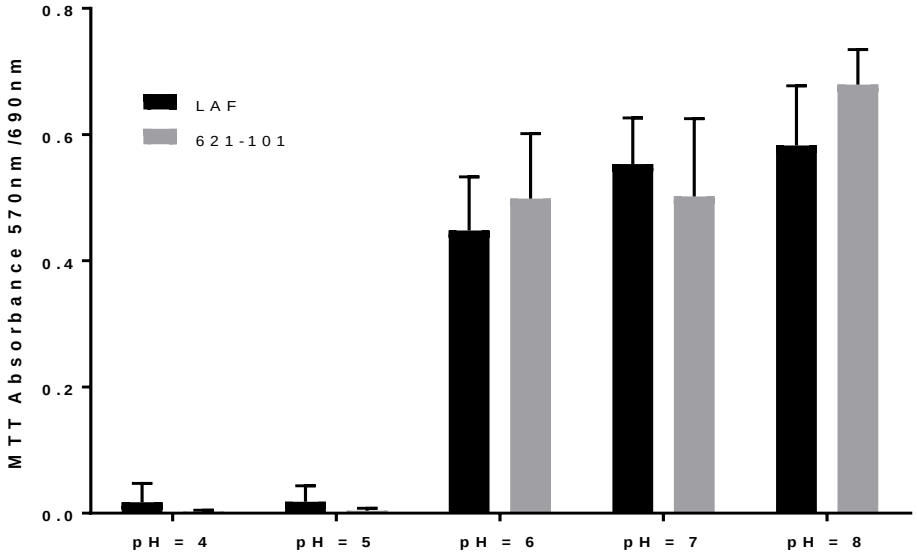



**Figure 4.3.15** ***LAFs and 621-101 cells survive at low pH.*** *Figure shows MTT (3-(4,5-Dimethylthiazol-2-Yl)-2,5-Diphenyltetrazolium Bromide) reduction by LAFs and 621-101 cells cultured for 24 hours in unbuffered DMEM at pH 4.0 – 8.0.*

Mitochondrial activity which reflected the number of viable cells measured after 96 hours in culture is seen in Figure 4.3.15. Both LAFs and 621-101 cells did not survive at pH 4.0 and 5.0. However, LAF viability increased more than 25-fold and 621-101 cell viability increased more than 125-fold when cultured at pH 6.0. Cell viability was increasingly higher at pH 7.0 and 8.0. Any resulting cell death was also confirmed by observation in

parallel with the MTT reduction assay. This suggested that cell viability was unimpaired at the low pH used for the activation of cathepsin K *in vitro*.

### 4.3.13 Acidification of Tissue Culture Medium by 621-101 Cells

Activation of cathepsin K requires an acidic pH. In the osteoclast where activation of this protease is best documented acidic conditions are provided by the microenvironment in the bone resorption pit (Everts et al., 2006). Therefore, to assess whether the *TSC2*$^{-/-}$ 621-101 cells could provide an environment conducive to LAF-derived cathepsin K activity their capability of lowering the pH of the culture medium was assessed over 24 hours *in vitro*.

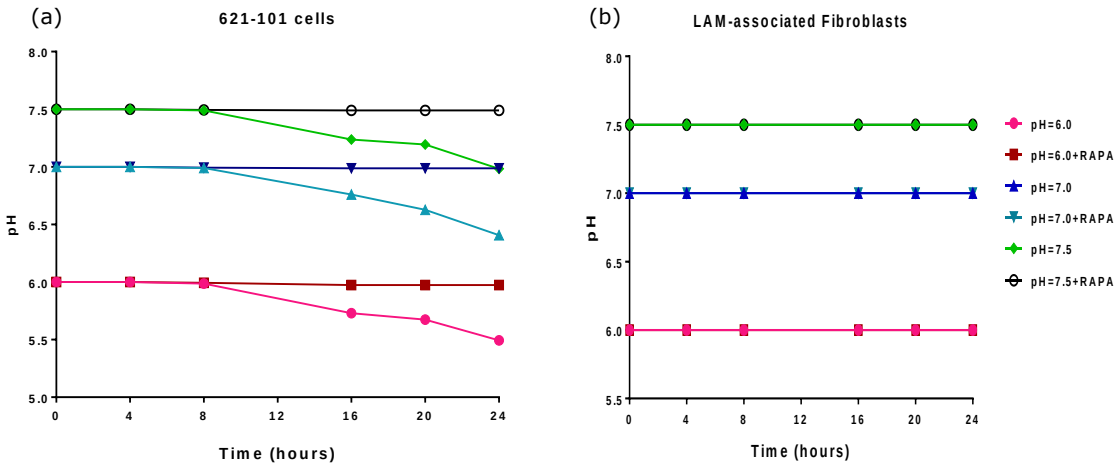



**Figure 4.3.16** ***Extracellular pH reduction by 621-101 cells.*** *(a) 621-101 cells and (b) LAFs (n=4) were cultured in unbuffered media for 24 hours at pH 7.5, 7.0 and 6.0 in the presence and absence of 10nM rapamycin. Culture medium pH was measured at the end of 24 hours using an Oakton Waterproof pH Spear Pocket pH tester.*

To establish this, *TSC2*$^{-/-}$ 621-101 cells and LAFs (n=4) were grown separately in unbuffered DMEM, adjusted to initial pH values of 7.5, 7.0 and 6.0. Both cell types were also treated with 10nM mTOR inhibitor

rapamycin and were maintained in culture for a period of 24 hours. All four LAF donors had no significant effect on culture medium pH over 24 hours and treatment with rapamycin did not alter their ability to maintain cell culture pH (Figure 4.3.16 (b)). Rapamycin treated 621-101 cells appeared to show no change in culture medium pH and could resist a change in pH over 24 hours. However, untreated 621-101 cells resulted in the acidification of culture medium pH which was independent of the starting pH.

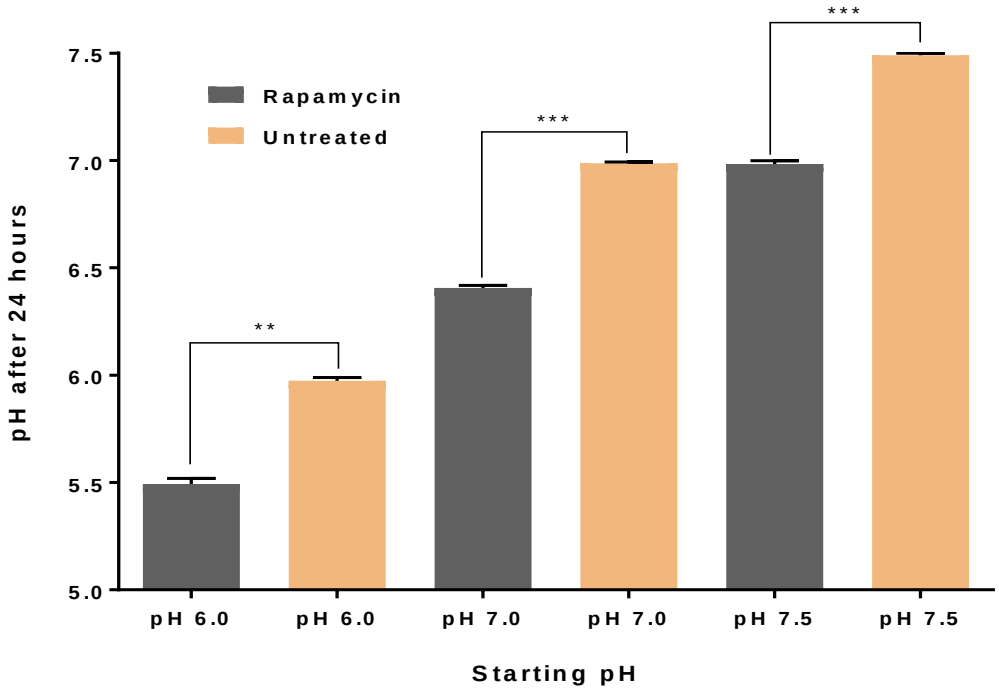



**Figure 4.3.17** ***621-101 cells rapidly reduced cell culture medium pH.*** *Figure shows the effect of rapamycin treatment on 621-101 cells in the absence of which, the cells rapidly reduced cell culture medium pH over 24 hours independent of starting pH. Two-tailed paired t-test performed, **p≤0.01, ***p≤0.001.*

Figure 4.3.17 shows 621-101 cell culture medium pH significantly reduced by 0.52 pH units from a starting pH of 7.5 ($p=0.0023$) and by 0.6 pH units from a starting pH of 7.0 ($p\leq0.0001$) and 6.0 ($p=0.0008$). The culture medium pH was initially noted to have reduced after 8 hours in culture and by the end of 24 hours, pH was 0.5 unit reduced independent of starting pH. All four LAF donors did not exhibit the ability to reduce extracellular pH whereas, in contrast, 621-101 cell culture resulted in a rapid decline in extracellular pH. This phenomenon was completely abrogated by the addition of mTOR inhibitor, rapamycin which suggested that the ability of 621-101 cells to acidify the extracellular environment was downstream of mTOR.

### 4.3.14 Expression of Membrane Proton Pumps and Transporters in 621-101 Cells

It was now established that $TSC2^{-/-}$ 621-101 cells were capable of acidifying the extracellular environment which was possibly a result of dysregulation of m TOR in these cells. Under normal circumstances, cells are capable of maintaining a physiological intracellular and extracellular pH by controlling the expression and activity of membrane proton pumps and transporters. An altered metabolism in tumour cells changes the normal regulation of such pumps and transporters resulting in an efflux of protons ($H^+$) to maintain an intracellular alkaline pH ($pH_i$) thus rendering the extracellular environment acidic ($pH_e$) (Damaghi et al., 2013, Huber et al., 2010). To determine the mechanism of extracellular acidification by

621-101 cells, expression of candidate membrane pumps and transporters was assessed in the 621-101 cells using qRT-PCR.

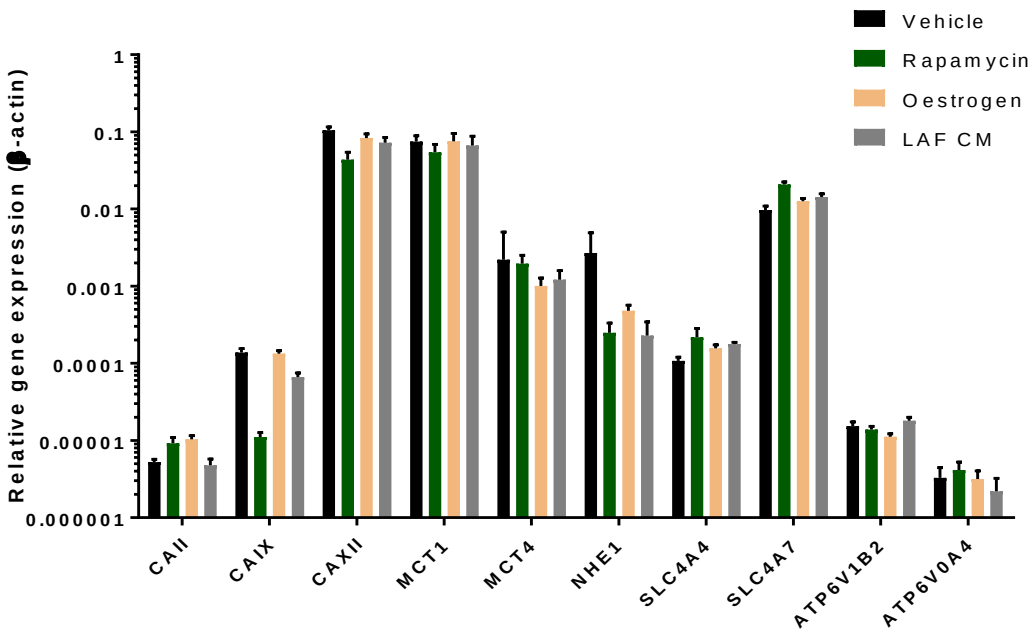



**Figure 4.3.18** ***Expression of membrane pumps and transporters in 621-101 cells.*** *Expression of carbonic anhydrase (CA) II, IX, XII, monocarboxylate transporter (MCT) 1, 4, sodium bicarbonate ($Na^+/HCO_3^-$) co-transporters (NBC) 1 / SLC4A4, 3 / SLC4A7, sodium $H^+$ ($Na^+/H^+$) exchanger (NHE) 1 / SLC9A1 and vacuolar-type $H^+$-ATPases (V-ATPases) ATP6V1B2 and ATP6V0A4 in 621-101 cells treated for 24 hours with either vehicle, rapamycin (10nM), oestrogen (10nM) or LAF conditioned medium (LAF CM) assessed via qRT-PCR. Figure shows mean (± standard deviation) gene expression determined relative to β-actin using the $2^{-\Delta CT}$ method.*

Figure 4.3.18 shows the expression of carbonic anhydrases *(CA), II, IX* and *XII*, monocarboxylate transporters *(MCT) 1* and *4*, sodium bicarbonate ($Na^+/HCO_3^-$) co-transporters, members of the NBC family *(NBC) 1 / SLC4A4* and *3 / SLC4A7*, sodium $H^+$ ($Na^+/H^+$) exchanger, member of the NHE family *(NHE) 1 / SLC9A1* and vacuolar-type $H^+$-ATPases *(V-ATPases) ATP6V1B2* and *ATP6V0A4* that were all found to be expressed in 621-101 cells. Incubation of 621-101 cells with rapamycin, oestrogen or LAF conditioned medium (LAF CM) did not significantly change the expression

of the candidate membrane pumps and transporters profiled ($p>0.05$). Gene expression of CAIX, CAXII and MCT1 however, was reduced in the presence of rapamycin by 12.5-fold, 2.4-fold and 1.3-fold respectively suggesting that the expression of these targets might be regulated by mTOR.

### 4.3.15 Expression of Membrane Pumps and Transporters in LAM Lung Tissue

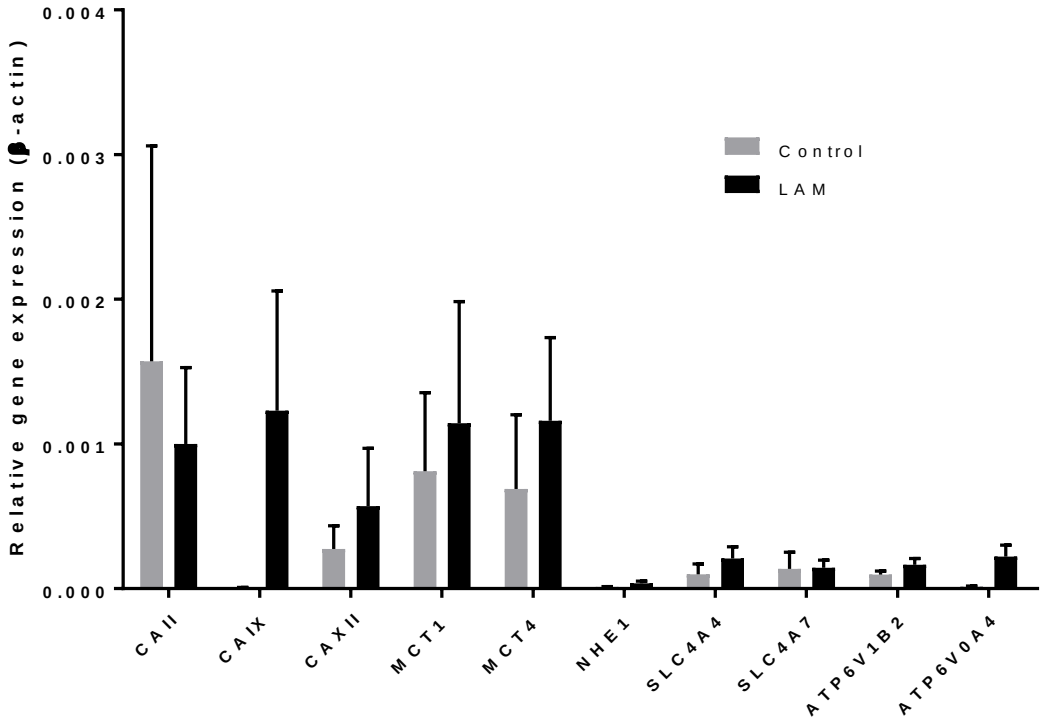



**Figure 4.3.19** ***Expression of $H^+$ ion transporters in LAM lung tissue.*** *Expression of CA II, IX, XII, MCT 1, 4, $Na^+/H^+$ exchanger, NHE1, $Na^+/HCO_3^-$ co-transporters SLC4A4, SLC4A7 and V-ATPases ATP6V1B2 and ATP6V0A4 in six LAM and three control patient derived lung tissues assessed via q RT-PCR. Figure shows mean (± standard deviation) gene expression determined relative to β-actin using the $2^{-\Delta CT}$ method.*

The expression of the candidate $H^+$ ion transporters was then measured in LAM and control lung tissue. Varying expression of all candidate membrane pumps and transporters was detected in six LAM and three control tissue donors. No significant changes were observed in the gene expression between LAM and control lung tissue ($p>0.05$). However, it is interesting to note that expression of *CAIX* was 283-fold upregulated in LAM lung tissue and was almost negligible in control tissue. Expression of all membrane pumps and transporters was elevated 2-fold or more in LAM lung tissue with the exception of *CAII* being expressed more in control tissue.

From the above results, it was evident that *CAIX* was the most highly expressed membrane transporter in LAM lung. CAIX and bicarbonate transporters such as SLC4A4 are known to form a metabolon which serves to enhance the hydration of $CO_2$ outside the cell and subsequent shuttling of $HCO_3^-$ ions into the cytosol. Therefore, the expression of these two candidate membrane transporters was assessed immunohistochemically in LAM lung tissue.

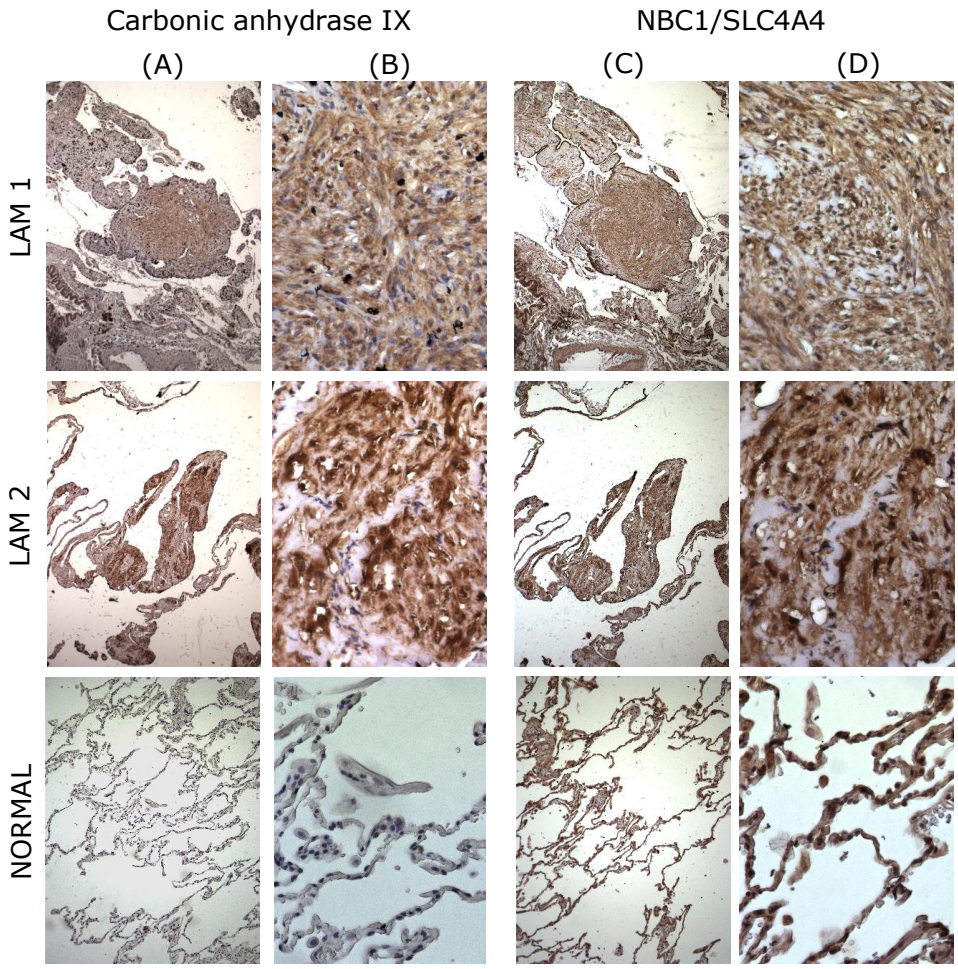



**Figure 4.3.20** ***Expression of CAIX and SLC4A4 in ex vivo LAM lung tissue.*** *Immunohistochemical staining of two representative LAM lung tissues showing positive staining in serial sections for CAIX and SLC4A4 within LAM nodules. Panels A and C show x4 images and B and D show x40 images of LAM and normal lung donors. Normal lung showed positive staining for SLC4A4 but not CA IX. Images taken using a standard brightfield Nikon Diaphot Inverted microscope.*

Figure 4.3.20 shows the expression of membrane transporter proteins CAIX and the $Na^+/HCO_3^-$ co-transporter SLC4A4 / NBC1 in two LAM lung and normal donor tissue. Both LAM donors showed strong immunoreactivity to CAIX and SLC4A4 antibodies. Expression of both CAIX and SLC4A4 was mainly observed in LAM nodules and it was interesting to note that expression was strong in the centre of the nodules. Slight expression of SLC4A4 was observed in normal lung tissue however, CAIX expression was completely absent.

### 4.3.16 Inhibition of Membrane Pumps and Transporters in 621-101 Cells

The expression of membrane pumps and transporters in 621-101 cells was established in section 4.3.14. All of these pumps and transporters are known $H^+$ ion transporters and net acid extruders (Damaghi et al., 2013). Therefore, in order to determine whether inhibition of these membrane pumps and transporters could inhibit extracellular acidification caused by 621-101 cells pharmacological inhibitors of these transporters were used.

As it has been postulated that similar to cancer cells a Warburg metabolism exists in LAM cells, one of the interesting targets for this study were monocarboxylate transporters (MCT) which are responsible for lactate shuttling. However, the universal MCT pharmacological inhibitor CHC (2-Cyano-3-(4-hydroxyphenyl)-2-propenoic acid) is itself an acid and when added to the pH adjusted unbuffered medium, rendered the medium acidic. Readjusting the medium pH did not help as the efficacy of the drug would be compromised and therefore due to these technical issues any results obtained using this inhibitor would be compromised and could not be considered.

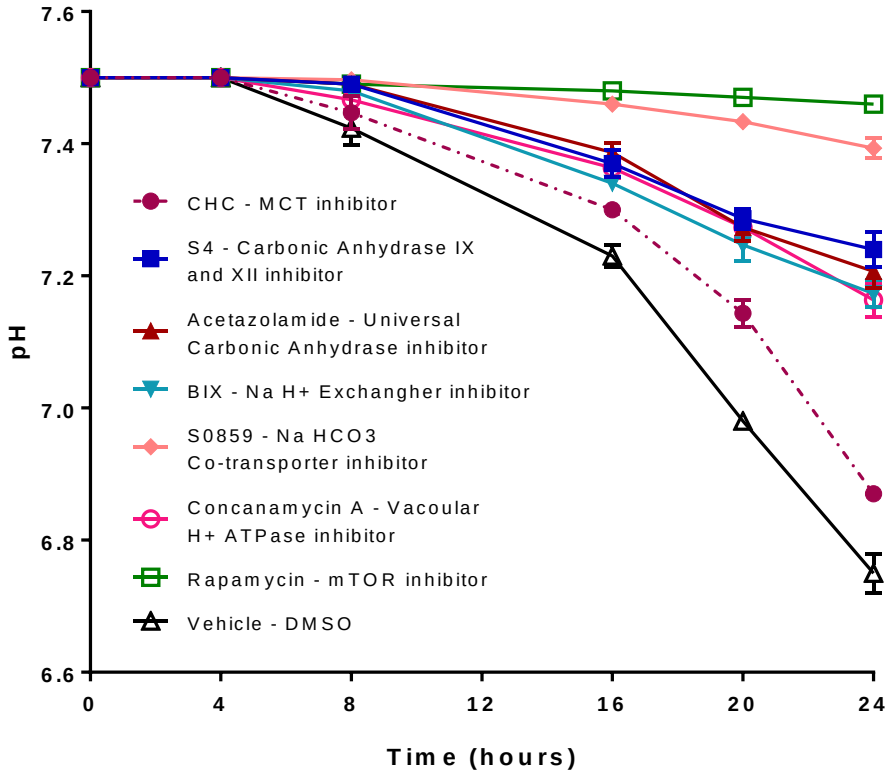



**Figure 4.3.21** ***Membrane pump and transporter inhibition in 621-101 cells.*** *Pharmacological inhibition of membrane pumps and transporters or mTOR inhibits extracellular acidification in 621-101 cell cultures. CHC (monocarboxylate transporter inhibitor) S4 and Acetazolamide (carbonic anhydrase inhibitors), BIX ($Na^+/H^+$ exchanger inhibitor), S0895 ($Na^+/HCO_3^-$ co-transporter inhibitor) and Concanamycin A (Vacuolar-type $H^+$-ATPase inhibitor).*

621-101 cells were cultured in unbuffered medium adjusted to pH 7.5 and were treated either with vehicle control or with the inhibitors of candidate net acid extruders described in section 2.1.4. Figure 4.3.21 shows 621-101 cells treated with vehicle control reduced extracellular pH by 0.75 pH units over 24 hours. Inhibition of CAs, $Na^+/H^+$ exchanger and V-ATPases blocked the extracellular acidification increasingly strongly and the least

resistant, inhibition of V-ATPases allowed reduction in pH by only 0.34 units.

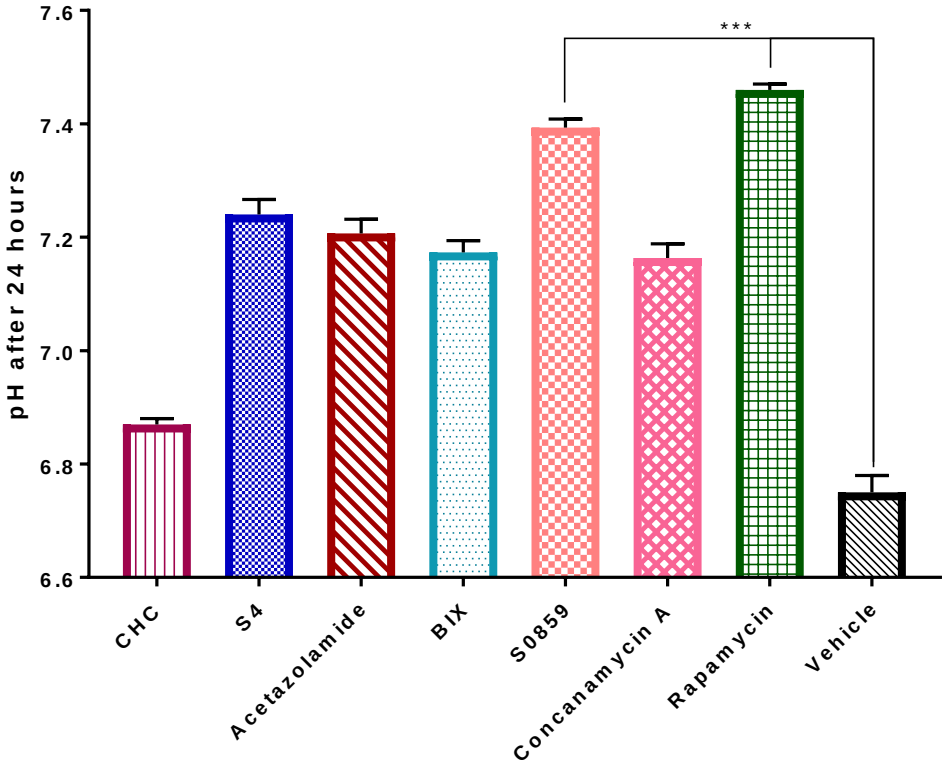



**Figure 4.3.22** ***24 hour inhibition of membrane pumps and transporters in 621-101 cells.*** *Figure shows the resulting culture medium pH after 24 hours of inhibition of membrane pumps and transporters in 621-101 cells. One-way ANOVA performed corrected for multiple comparisons using Dunnett's multiple comparisons test. ***p≤0.001*

However, inhibition of the $Na^+/HCO_3^-$ co-transporter significantly inhibited the reduction in culture medium pH (p=0.0003) over 24 hours (Figure 4.3.22). Interestingly the mTOR inhibitor rapamycin was more potent than any of the membrane transporter inhibitors and significantly abolished extracellular acidification (p=0.00019).

### 4.3.17 Effect of Inhibition of Membrane Pumps and Transporters on Cathepsin K Activity

It was established that optimum cathepsin K activity required a low pH environment (section 4.3.11). $TSC2^{-/-}$ 621-101 cells were capable of providing a low pH environment via the expression of membrane pumps and transporters. Inhibition of these candidate membrane pumps and transporters, mainly sodium bicarbonate co-transporters and carbonic anhydrases reduced the change in culture medium pH to an acidic pH by the 621-101 cells. Therefore, in order to recapitulate the LAM nodule environment it was important to examine whether the 621-101 cells were capable of acidifying their environment in the presence of LAF and whether this resulted in the inhibition of LAF-derived cathepsin K activity.

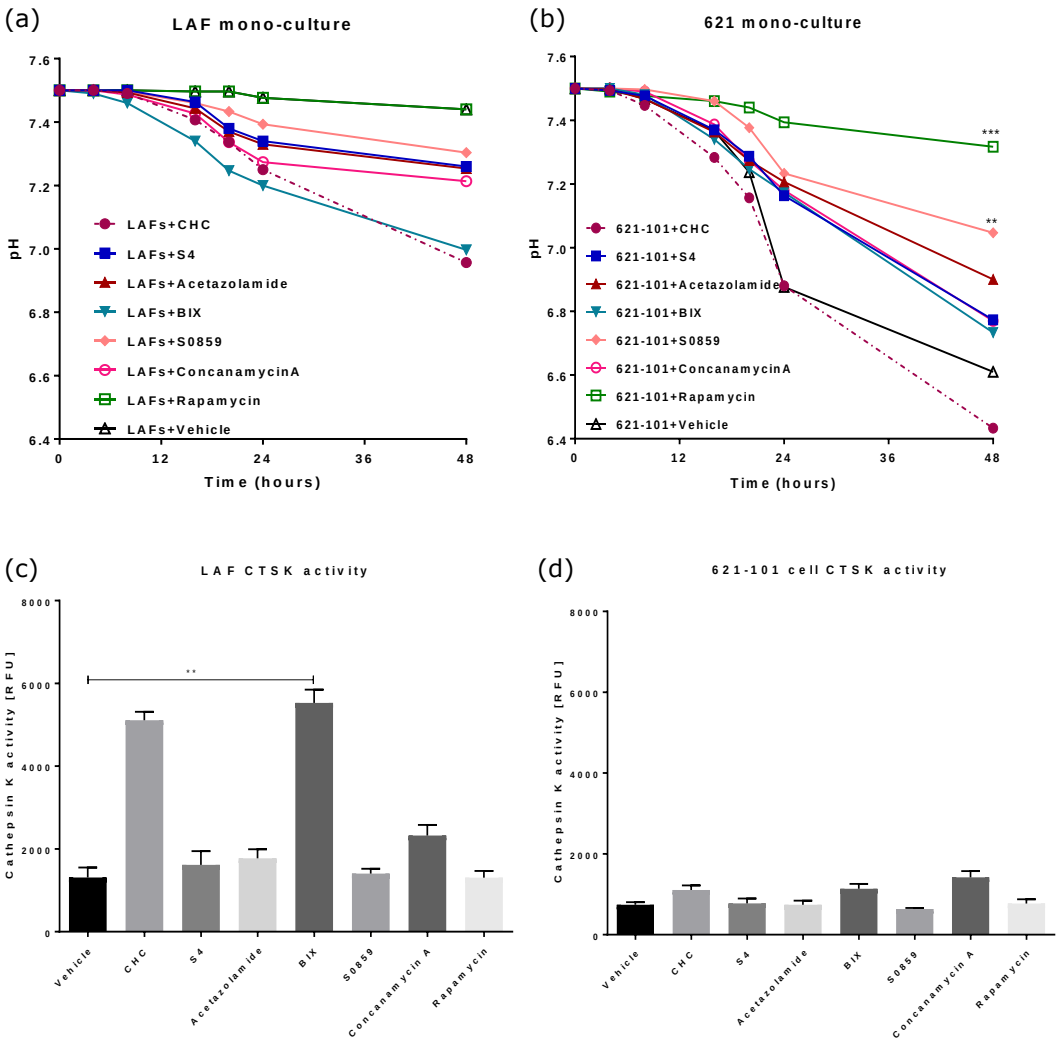



**Figure 4.3.23** ***Inhibition of membrane pumps and transporters and their effect on CTSK activity in LAFs and 621-101 cells.*** *LAFs (n=4) and 621-101 cells were grown as mono-cultures in unbuffered media in the presence of either vehicle control (DMSO) or CHC (MCT inhibitor), S4 (CAIX and CAXII inhibitor), acetazolamide (non-specific carbonic anhydrase inhibitor), BIX ($Na^+/H^+$ exchanger inhibitor), S0859 ($Na^+/HCO_3^-$ co-transporter inhibitor), concanamycin A (V-ATPase inhibitor) or rapamycin (mTOR inhibitor). Panels A and B show the measurement of pH after 48 hours of inhibitor treatment in LAFs and 621-101 cells respectively. Panels C and D show the cathepsin K activity measured after 48 hour inhibition of membrane transporters. One-way ANOVA performed corrected for multiple comparisons using the post-hoc Dunnett's test. **p≤0.01, ***p≤0.001.*

Vehicle and mTOR inhibitor treated LAFs (n=4) resisted pH change and did not result in a decrease in culture medium pH. Inhibition of membrane pumps and transporters in LAFs however, over 48 hours, caused a minimal reduction in extracellular pH (Figure 4.3.23 (a)). Inhibition of $Na^+/H^+$

exchanger, V-ATPases, carbonic anhydrases and $Na^+/HCO_3^-$ co-transporter caused reduced culture medium pH increasingly weakly. Again, on inhibition of MCT culture medium pH appeared reduced however this was due to the acidic properties of the inhibitor itself. The cathepsin K activity measured thereafter was complementary to the changes in pH obtained after 48 hours (Figure 4.3.23 (c)). As a decrease in pH was observed on inhibition of the $Na^+/H^+$ exchanger, cathepsin K activity was significantly high in LAFs treated with BIX compared to vehicle treated LAFs ($p=0.004$).

Inhibition of mTOR in 621-101 cells maintained a physiological extracellular pH which reduced by only 0.2 pH units at the end of 48 hours. Compared to rapamycin, vehicle treated 621-101 cells showed a significant reduction in pH ($p=0.0004$) over 48 hours of culture. Again, inhibition of $Na^+/HCO_3^-$ co-transporter significantly inhibited reduction in extracellular pH ($p=0.002$) (Figure 4.3.23 (b)). Inhibition of $Na^+/H^+$ exchanger, V-ATPases and carbonic anhydrases inhibited pH change increasingly strongly. It was interesting to note that despite a reduction in extracellular medium pH cathepsin K activity was very low to negligible (Figure 4.3.23 (d)). This was in keeping with the 621-101 cell activity measured in section 4.3.11.

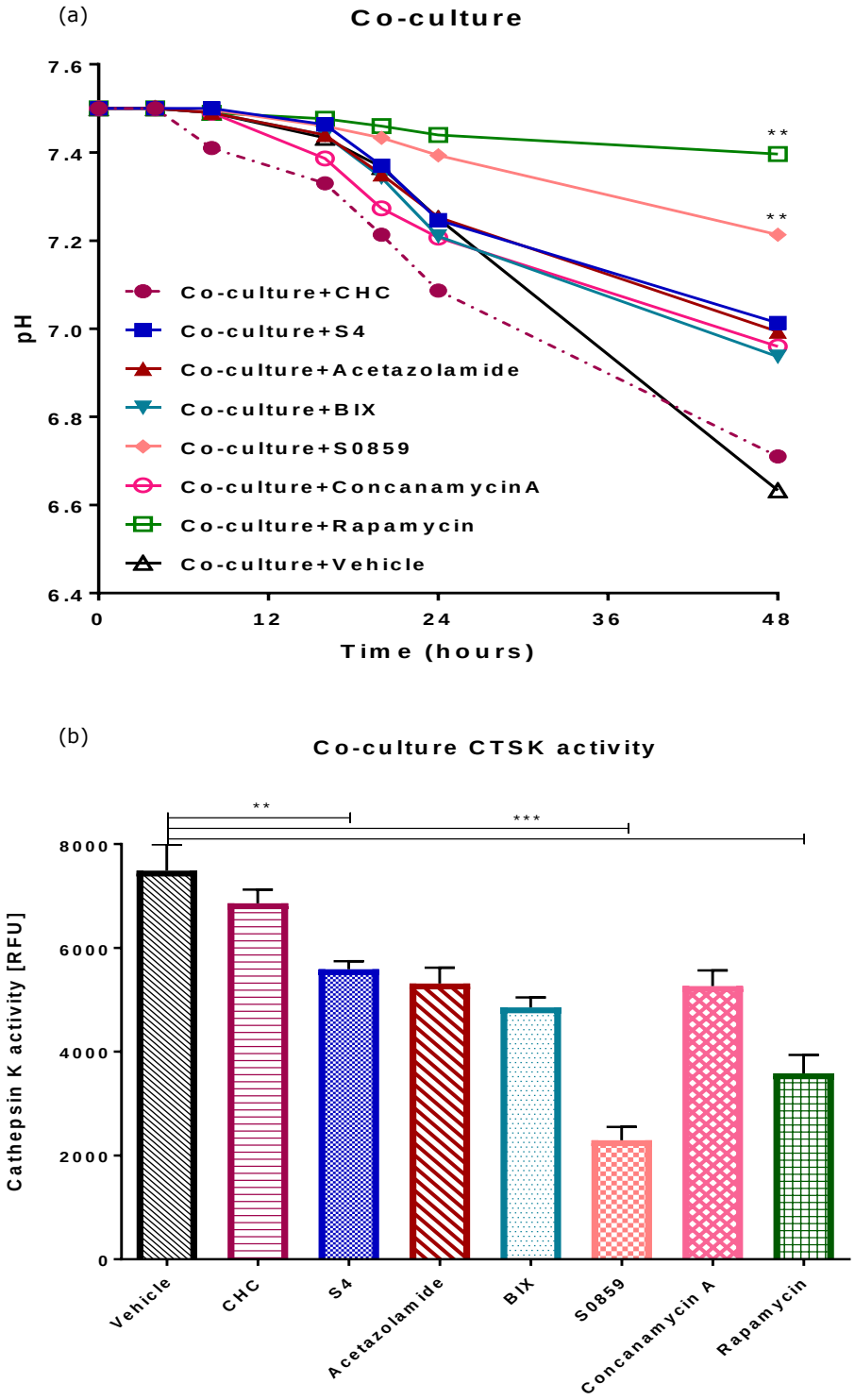



**Figure 4.3.24** ***Inhibition of membrane pumps and transporters and their effect on CTSK activity in LAF/621-101 co-cultures.*** *LAF/621-101 cell (n=4) co-cultures were grown in unbuffered media in the presence of either vehicle control (DMSO) or CHC (MCT inhibitor), S4 (CAIX and CAXII inhibitor), acetazolamide (non-specific carbonic anhydrase inhibitor), BIX (Na+/H+ exchanger inhibitor), S0859 (Na+/HCO3- co-transporter inhibitor), concanamycin A (V-ATPase inhibitor) or rapamycin (mTOR inhibitor). Panels A shows the measurement of pH after 48 hours of inhibitor treatment and panel B shows the cathepsin*

*K activity measured after 48 hour inhibition of membrane transporters in co-cultures. One-way ANOVA performed corrected for multiple comparisons using the Bonferroni correction method. **p≤0.01, ***p≤0.001.*

621-101 / LAF co-cultures acidified the extra-cellular space, which was associated with cathepsin K activity in the co-cultures (Figure 4.3.24 (a)). Vehicle treated 621-101 cells reduced the extracellular pH by almost 0.9 pH units over 48 hours. Membrane transporter inhibitors blocked extra-cellular acidification to the same degree as seen in 621-101 monocultures. Inhibition of both mTOR and $Na^+/HCO_3^-$ co-transporters significantly inhibited pH change compared to vehicle (p=0.007 and p=0.008 respectively). Inhibition of $Na^+/H^+$ exchanger, V-ATPases and carbonic anhydrases blocked extra-cellular acidification increasingly strongly. Again, inhibition of MCT showed a reduction in pH similar to vehicle treated 621-101 cells, however, this was possibly due to the acidic nature of the inhibitor itself.

Inhibition of pH change was also associated with reduced cathepsin K activity (Figure 4.3.24 (b)). Vehicle treated co-cultures showed the highest cathepsin K activity which was significantly reduced by the inhibition of carbonic anhydrases IX and XII (p=0.0021). Importantly, the $Na^+/HCO_3^-$ co-transporter inhibitor was the strongest inhibitor of both acidification and cathepsin K activity, significantly reducing activity by almost 75% (p=0.0001). Inhibitors with more modest effects on acidification had had lesser effects on cathepsin K activity. Again rapamycin was the strongest inhibitor of acidification and significantly reduced cathepsin K activity by around 50% (p=0.0001).

### 4.3.18 Effect of Inhibition of Membrane Pumps and Transporters on Cell Viability

To ensure that LAF and 621-101 cell viability was not affected by the inhibition of membrane pumps and transporters, an MTT reduction assay was carried out to asses these parameters.

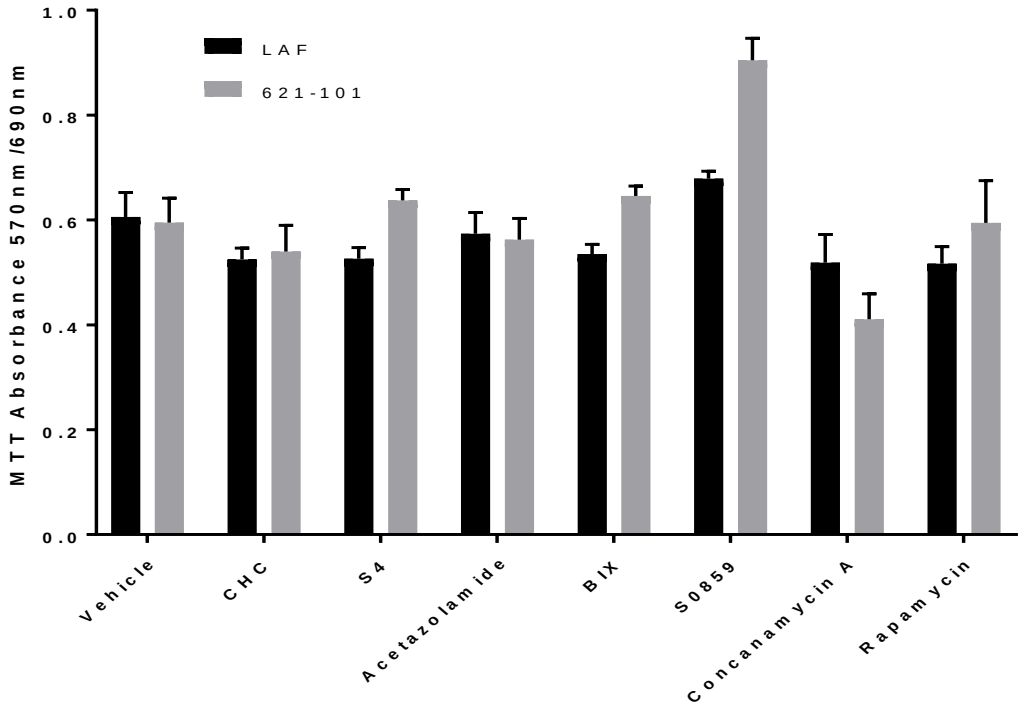



**Figure 4.3.25** ***Cell viability measured after inhibition of membrane pumps and transporters in LAFs and 621-101 cells.*** *Figure shows MTT reduction by LAFs (n=4) and 621-101 cells cultured for 48 hours in unbuffered media in the presence of either vehicle control or CHC (monocarboxylate transporter inhibitor), S4 (carbonic anhydrase IX, XII inhibitor), acetazolamide (universal carbonic anhydrase inhibitor), BIX ($Na^+/H^+$ exchanger inhibitor), S0859 ($Na^+/HCO_3^-$ co-transporter inhibitor), concanamycin A (V-ATPase inhibitor) or rapamycin (mTOR inhibitor).*

Cell viability was assessed as a measure of MTT reduction in LAFs and 621-101 cells treated with membrane pumps and transporters. Mitochondrial activity which reflected the number of viable cells measured after 48 hours in culture is seen in Figure 4.3.25. Both LAFs and 621-101 cells showed

similar viability over 48 hours regardless of inhibitor treatment. Inhibition of $Na^+/HCO_3^-$ co-transporters in the 621-101 cells resulted in a 1.3-fold increase in MTT signal compared to LAFs. This suggested that inhibition of membrane pumps and transporters did not reduce cell viability and that an increase in MTT signal by the 621-101 cells on inhibition of $Na^+/HCO_3^-$ co-transporters possibly increased 621-101 cell number reflected by an increase in mitochondrial activity.

### 4.3.19 Cathepsin K Activity Relates To Total Cathepsin K Expression in Cultured Cells

An elevated cathepsin K activity was detected in LAF/621-101 cell co-culture compared to their respective mono-cultures as a result of the activation mechanisms described above. Activity was inhibited to differing levels on the inhibition of membrane pumps and transporters. However, it was necessary to assess how this activity related to the total cathepsin K protein in LAFs and 621-101 cells. To quantify total cathepsin K in LAF/621-101 cell co-culture and LAF and 621-101 cell mono-cultures an ELISA was performed.

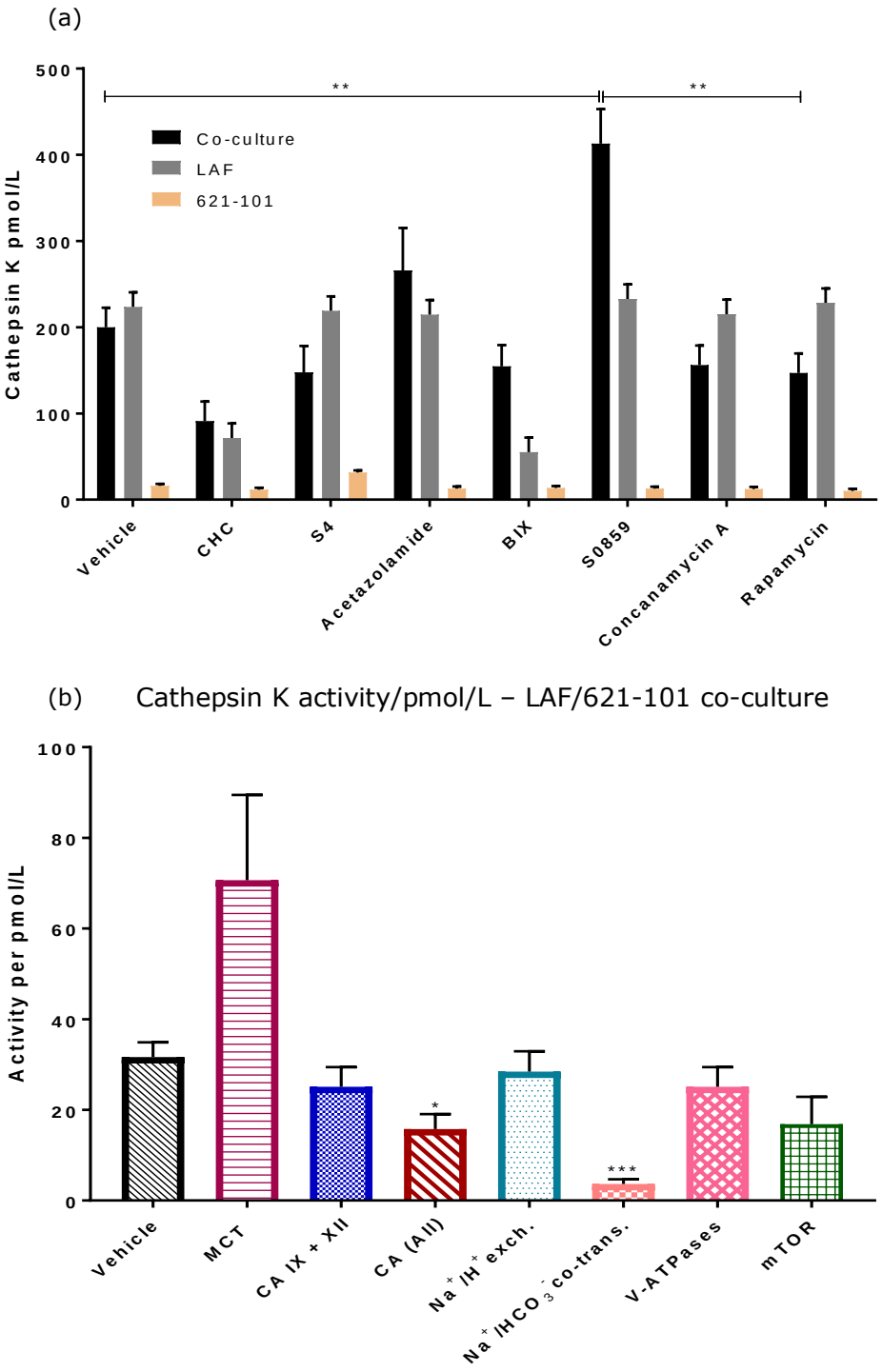



**Figure 4.3.26** ***Total cathepsin K protein measured in LAFs and 621-101 cells after inhibition of membrane pumps and transporters.*** *Panel A shows total cathepsin K protein simultaneously measured in LAFs (n=4), 621-101 cells or a 10:1 mixture of LAFs and 621-101 cells. Panel B shows cathepsin K activity per pmol/L in LAF/621-101 cell co-cultures. Activity and total protein were measured in culture supernatants collected after 48 hours of inhibition of membrane pumps and transporters. One-way ANOVA performed corrected for multiple corrections using Dunnett's multiple comparisons test. *p≤0.05, **p≤0.01, ***p≤0.001.*

Figure 4.3.26 (a) shows total cathepsin K protein measured in co-culture and mono-culture supernatants. Cathepsin K protein was significantly elevated in co-culture supernatants treated with S0859 compared to vehicle ($p=0.003$) and rapamycin ($p=0.0016$). Cathepsin K activity measured in co-cultures was compared to the total protein to assess the proportion of total protein that was active after inhibition of membrane pumps and transporters. Figure 4.3.26 (b) showed a significantly reduced activity per pmol/L of cathepsin K on inhibition of $Na^+/HCO_3^-$ co-transporter ($p=0.0002$) and carbonic anhydrases ($p=0.038$). mTOR inhibition by rapamycin resulted in an almost 2-fold decrease in activity per pmol/L however, this comparison was not found to be statistically significant ($p>0.05$). This suggested that while elevated protein levels were observed in co-cultures only a small proportion of this was active after treatment with S0859, acetazolamide and rapamycin.

## 4.4 Discussion

This chapter describes the screening of LAM tissue for elevated protease expression and selection of a key protease, cathepsin K, proposed to play a role in the lung destruction associated with LAM. This chapter has established the presence of cathepsin K in *ex vivo* tissue, cells *in vitro* and has also shown the intracellular and extracellular activation of cathepsin K. A plausible mechanism of activation of cathepsin K has then been illustrated in this chapter strengthening the hypothesis that fibroblasts and $TSC2^{-/-}$ LAM cells can synergistically cause destruction of the LAM lung.

Proteases not only mediate terminal protein degradation and ECM remodelling but also play a role in tumour cell invasion, angiogenesis, metastasis and can also activate other proteases and/or signalling molecules through cleavage of pro-peptides (Joyce and Pollard, 2009, Mason and Joyce, 2011). The elevated presence or absence of several MMPs, their endogenous inhibitors and inducer has been previously reported in LAM. The existence of the plasminogen protease axis, the presence of renin-angiotensin system along with the presence of mast cell chymases have all been briefly touched upon in LAM (see Table 4.3.1 for references). Thus, these proteases along with a few others associated with similar conditions and a new class of cathepsins were screened. From a panel of 30, the most strongly expressed protease transcript in LAM lung was cathepsin K.

Cathepsin K belongs to a class of cysteine proteases and is a potent collagenase and elastase. Primarily this protease has been known to play an important role in bone remodelling and is mainly expressed in

osteoclasts (Bromme et al., 1996). Expression of cathepsin K in LAM and other perivascular epithelioid tumours (PEComas) was first described by Chilosi and colleagues who also suggested cathepsin k expression may be mTOR dependent (Martignoni et al., 2012, Chilosi et al., 2009). A possible explanation for the significantly elevated protease expression in the 621-101 cells could probably be attributed to their genotype. The mTOR complex is a major regulator of cell metabolism including protein translation. Dysregulation of this regulator protein complex could possibly result in increased protein production suggesting that the elevated proteases could be downstream of m TOR signalling.

A large class of globular proteases that were initially described as intracellular peptide hydrolases are also now known to have several extracellular functions. The cysteine cathepsins have been known to play a role in the development of various pathological conditions, such as neurological disorders, cardiovascular diseases, obesity, inflammatory diseases, such as rheumatoid arthritis, and cancer, among others (Tan et al., 2013). Cysteine cathepsins B, L, K and S have been known to be expressed by various fibroblasts (Lemaire et al., 1997, Hou et al., 2002, Kasabova et al., 2014, Quintanilla-Dieck et al., 2009). In fact, genome-wide array analyses of invasive human melanomas showed an upregulation of cathepsins B and L in the stromal fibroblasts which aided enhanced melanoma cell invasion (Yin et al., 2012). An aspartic protease cathepsin D is overexpressed by human epithelial breast cancer cells and is closely correlated with poor prognosis in breast cancer. Studies have found that this overexpressed protease can be captured by the tumour-

fibroblasts resulting in increased ECM digestion, fibroblast motility and invasion (Masson et al., 2011, Heylen et al., 2002). Therefore, an upregulation of these proteases in co-culture suggests that the 621-101 cells confer upon the fibroblasts or the two cell types symbiotically produce and elevated protease phenotype in order to aid ECM digestion.

Nodular expression of cathepsin K which was found to be in the same areas as fibroblast marker FSP which suggested that cathepsin K was predominantly present in LAM nodules and was possibly expressed by fibroblasts indicating a role for cathepsin K in LAM lung tissue remodelling. To confirm that it was indeed the fibroblasts within LAM nodules that were responsible for majority of the cathepsin K expression, double fluorescent and chromogenic IHC was conducted. Well established marker for fibroblasts, fibroblast surface protein (FSP) was used which has been to show the presence of fibroblasts in LAM nodules (Clements et al., 2015) and been used to characterise LAFs obtained from LAM lung. Expression of cathepsin K in LAM nodules was almost exclusively associated with spindle-shaped cells within the nodule. Staining pattern obtained from both fluorescent and chromogenic IHC were consistent with the fact that FSP-positive fibroblasts were the major contributors of cathepsin K expression in LAM nodules.

Supressing mTOR with rapamycin in LAM lung tissue significantly supressed cathepsin K gene expression. In the osteoclast, cathepsin K expression is dependent on MITF, a helix-loop-helix transcription factor which regulates melanocyte development, cyclin dependent kinase and

anti-apoptotic gene expression (Levy et al., 2006). MITF binds three consensus sites in the cathepsin K promoter as a heterodimer with various partners including TFE3. In the osteoclast, cathepsin K mRNA and protein levels decreased after inhibition of mTOR and animal models demonstrated that inhibition of the mTOR pathway partially decreased bone resorption (Glantschnig et al., 2003, Kneissel et al., 2004). This raises the possibility that inhibition of mTOR and cathepsin K may have synergistic effects on inhibition of lung destruction in LAM. 48-hour treatment of LAM lung tissue explants with E2 did not significantly affect CTSK gene expression. However, prolonged treatment with oestrogen has been known to supress cathepsin K mRNA levels in osteoclasts and partially attenuate osteoporotic bone loss (Furuyama and Fujisawa, 2000).

Presence of cathepsin K expression has been found in various fibroblast types including dermal (Quintanilla-Dieck et al., 2009), synovial (Hou et al., 2002) and gingival (Beklen et al., 2015). Fibroblasts express several proteases including MMPs and cathepsins that are responsible for tissue degradation via collagenolytic and elastinolytic activity (as discussed previously). Cathepsin K expression can be regulated by or is downstream of various signalling molecules such as receptor activator of NF-κB (RANK) and its ligand, RANKL, nuclear factor of activated T-cells (NFAT), Mitf and p38/MAPK/AP-1 (mitogen-activated protein kinases/activator protein 1) (Troen, 2006, Matsumoto et al., 2004). The increased expression of cathepsin K in the fibroblasts and negligible expression at both mRNA and protein levels in 621-101 cells further supported the possibility that cathepsin K may be regulated by one or more of the abovementioned

factors and may not be downstream of mTOR signalling in the mTOR dysregulated 621-101 cells.

Cathepsin K has an optimum acidic pH within which it is most stable and displays limited stability in the mature (active) form at neutral pH (Bromme et al., 1996). In most mammalian cells, cysteine proteases are synthesized as precursors and are either secreted as a proenzyme or are transported via the mannose-6-phosphatase receptors to lysosomal compartments where they are processed into the mature active enzyme. In osteoclasts processing of the proenzyme form of cathepsin K to its mature form occurs just at the ruffled border where the pH is approximately 4.0 (Bossard et al., 1996). Thus, by providing an acidic environment intracellular lysosomal activity of cathepsin K was detected strongly in LAFs but not in 621-101 cells using the synthetic Magic Red® substrate. Although the LAFs were treated with a specific cathepsin K inhibitor, faint fluorescence was still observed since constitutively synthesized cysteine cathepsins besides cathepsin K, such as cathepsin B and L can target analogous amino acid sequences for proteolysis (Boonacker and Van Noorden, 2001). However, treatment with universal cysteine cathepsin inhibitor E64 completely abrogated the fluorescence confirming that it was indeed the work of cysteine cathepsins.

To elicit its matrix degrading activity, pro-cathepsin K requires activation and needs to remain in its active form. The requirement for low pH to activate cathepsin K is well described and although activation of cathepsin K in osteoclasts occurs at the ruffled border at pH 4.0, the site of cathepsin

K activity within the bone lacunae was found to have neutral pH (Dodds et al., 2001). This suggests that activation requires a low pH but the mature active form is stable enough to withstand neutral pH in order to exert its matrix degrading activity. Elevated cathepsin K activity was observed in LAF mono-cultures at pH 7.0 and below and activity is further elevated in LAF/621-101 cell co-cultures. As negligible cathepsin K activity was noted in 621-101 cell mono-cultures, elevated co-culture activity only suggested that the 621-101 cells elevated LAF-derived cathepsin K activity via some mechanism. It was clear that the activity was not a result of cell death as MTT readings showed both LAFs and 621-101 cells survive equally well at pH 6.0 above. In addition, 621-101 cells were capable of drastically lowering the extracellular pH ($pH_e$) in 24 hours regardless of starting pH a phenomenon which was completely abrogated by the treatment of these cells with m TOR inhibitor, rapamycin. Although the use of the *TSC2*$^{+/+}$ 621-103 cells was not possible for this study due to the culturing difficulties associated with these cells, Dongre et al have shown that *Tsc2*$^{+/+}$ mouse embryonic fibroblasts (MEFs) do not result in a change in extracellular pH, similar to rapamycin treated 621-101 cells, compared to *Tsc2*$^{-/-}$ MEFs which result in a drastic reduction in extracellular pH much like the *TSC2*$^{-/-}$ 621-101 cells (Dongre et al., 2017). This suggests that acidification of the $pH_e$ was a consequence of loss of TSC2 gene function and a subsequent dysregulation of mTOR.

Cancer cells contained within solid tumours can become increasingly distant from the basement membrane thereby encountering an oxygen poor environment due to which they undergo a metabolic switch towards

a more glycolytic phenotype (Gatenby and Gillies, 2004). Highly proliferative cancer cells produce a large number of protons ($H^+$) generated by increased glycolysis, glucose utilisation, lactic acid production and proton efflux. The cells continue to exhibit a glycolytic phenotype even in the presence of oxygen, resulting in an acidic extracellular environment. This phenomenon was proposed by Otto Warburg and is now known as the Warburg effect (Warburg, 1956, Potter et al., 2016). It has been proposed that while the acidic microenvironment can be toxic to normal cells, cancer cells by themselves being proton extruders have a selective advantage for survival. This way they maintain a slightly alkaline intracellular pH ($pH_i$) while the $pH_e$ is acidic.

Members of the well-known proton flux regulators, carbonic anhydrases, V-ATPases and the $Na^+/H^+$ exchangers that are known for their role in proton extrusion were all found to be expressed in varying levels in the 621-101 cells. In fact, in hypoxic conditions, carbonic anhydrases IX and XII have been known to be employed in cancers to maintain an extracellular acidic environment and an alkaline intracellular pH (Swinson et al., 2003). Although not responsible for direct proton extrusion, the $Na^+/HCO_3^-$ co-transporters facilitate movement of $HCO_3^-$ ions across the plasma membrane and can either acidify or alkalinise the $pH_e$. *SLC4A4*, the electrogenic co-transporter and SLC4A7, the electroneutral co-transporter, both expressed in the 621-101 cells are responsible for acid extrusion, proliferation and migration in colon and breast carcinoma cells and tissue (Boedtkjer et al., 2013, Parks and Pouyssegur, 2015). The acidic by-product of glycolysis, lactic acid, is shuttled in and out of cells by members

of the monocarboxylate transporters, *MCT1* and *MCT4* which were highly expressed in 621-101 cells. Overexpression of MCT1 and MCT4 has been reported in many tumours and has been linked to poor prognosis and disease progression in colorectal, ovarian, gastric and breast cancers (Chen et al., 2010, Pinheiro et al., 2010, Pinheiro et al., 2009). Gene expression of the acid extruders was also detected in LAM lung tissue most of which were upregulated in LAM and tissue expression of CAIX confirmed exclusive expression in LAM lung tissue.

Pharmacological inhibition of the proton pumps and membrane transporters inhibited a change in pH caused by the 621-101 cells. Inhibition of carbonic anhydrases, using both acetazolamide and S4, and $Na^+/HCO_3^-$ co-transporters, using high-affinity generic NBC inhibitor (Ch'en et al., 2008) was most potent in inhibiting a change from physiologic to acidic pH. One of the most well studied carbonic anhydrases, CAIX hydrolyses carbon dioxide to bicarbonate and a free proton that is released into the extracellular space. Researchers have hypothesised that the bicarbonate ion ($HCO_3^-$) at the cell surface is then recaptured by the $Na^+/HCO_3^-$ co-transporters in order to maintain an alkaline $pH_i$ (Swietach et al., 2009). Moreover, CAII enhances the transport capacity of SLCA4A by possibly forming a transport metabolon with the latter (Becker and Deitmer, 2007). This suggested that the two transporter groups work together and inhibiting either carbonic anhydrases or $Na^+/HCO_3^-$ co-transporters could alter the cellular metabolism from a more proton extruding phenotype thereby reducing the extracellular pH.

Strikingly, rapamycin completely and rapidly, abrogated acidification in culture despite only suppressing the transcription of *CAIX*, suggesting that the part of the effect may have been on 621-101 cell metabolism rather than exclusively on the transporters themselves. Constitutive activation of the mTOR pathway leads to an increase cell growth and division in turn leading to the activation of Warburg metabolism (Potter et al., 2016) and inhibiting the mTOR pathway has been shown to reduce lactic acid production in glioblastoma cell lines (Venkatesh et al., 2012). Therefore, it is possible that the mTOR inhibitor rapamycin indirectly inhibits general metabolism, supressing extracellular acidification.

There is evidence to suggest that extracellular acidity per se can intensify extracellular proteolytic activities and expression of pro-angiogenic factors. Extracellular acidification plays an important role in in digestion and remodelling of the ECM by not only facilitating the activity but also the release of secreted acidic proteases such as uPA (Kindzelskii et al., 2004), CTSD (Liaudet-Coopman et al., 2006), CTSB (Szpaderska and Frankfater, 2001) and CTSL (Mohamed and Sloane, 2006). Studies conducted by Punturieri et al showed that monocyte-derived macrophages acidify their pericellular milieu via V-ATPases thus enabling them to secrete cathepsin K and maintain the enzyme in its active form (Punturieri et al., 2000). Moreover, in osteoclasts cathepsin K activation occurs in the microenvironment of the bone resorbing lacunae at a low pH generated by membrane pumps and transporters such as carbonic anhydrases, V-

ATPases, $Na^+/H^+$ exchangers and chloride bicarbonate exchangers ($Cl^-/HCO_3^-$ exchanger) (Zhao et al., 2009a, Riihonen et al., 2007).

In LAF/621-101 cell co-cultures, the transporters acidified the extracellular space, whilst their inhibition, particularly the $Na^+/HCO_3^-$ co-transporters, blocked both extra-cellular acidification and protease activation. Also, when compared to the total CTSK protein levels measured, cathepsin K activity was significantly low in LAF/621-101 cell co-cultures treated with $Na^+/HCO_3^-$ inhibitor. Small molecule inhibitors of carbonic anhydrases and sodium bicarbonate co-transporters have been successfully used in several pre-clinical models of cancer (Kant et al., 2014, Lou et al., 2011) and to treat metabolic acidosis in the treatment of COPD (Heming et al., 2012). Again, inhibition of mTOR activity in LAF/621-101 cell co-cultures abrogated pH change and significantly decreased cathepsin K activity. Treatment of mantle cell lymphoma xenograft model with an mTOR inhibitor significantly increased $pH_e$ one day after administration similar to the effect observed in 24 hours in the $TSC2^{-/-}$ 621-101 cells however subsequent measurement showed a decrease in $pH_e$ (Akhenblit et al., 2016). This suggested that while an instant and rapid decrease in $pH_e$ was observed due to rapamycin treatment, further maintenance of neutral pH could be possible by inhibiting overexpressed membrane transporters. Thus, a combined therapy using both m TOR inhibitor rapamycin and a membrane transporter inhibitor could be most efficient in maintaining physiological pH and therefore inhibiting cathepsin K activity. Moreover, mTOR inhibitors which reduce lung function decline in LAM (McCormack et

al., 2011, Goldberg et al., 2015, Bee et al., 2015), may exert some of their protective action in the lung upon LAM cell related extracellular pH, cathepsin K activation and expression. The expression of transporters including the $Na^+/HCO_3^-$ co-transporter are downstream of mTORC1 / hypoxia inducible factor 1α (Kaluz et al., 2009, McIntyre et al., 2016). Further studies are required to understand, how mTOR activation and the expression of membrane transporters are related and whether inhibition of these transporters or cathepsin K activity will be of benefit in addition to mTOR inhibitors for LAM.

## 4.5 Conclusion

Taken together, the findings suggest that interactions between LAM cells and LAFs within LAM nodules could promote disease progression by protease activation in a similar manner to tumour cell and cancer associated fibroblast interactions in cancer. Although the 621-101 cells and LAFs in culture may not completely recapitulate the LAM nodule environment, this chapter describes that in addition to *in vitro* studies, the elements necessary to synthesise and activate cathepsin K are present in human lung tissue. Although there isn't direct evidence of an acidic environment in human LAM lung nodules, the presence of these components and the existence of an analogous situation in human cancers, suggest this is likely to be the case. These similarities are consistent with the idea that LAM is a low grade neoplastic disease, with a stroma similar to cancer(McCormack et al., 2012).

# 5 CHAPTER 5: Comparative transcriptional profiling of LAFs and NHLFs

## 5.1 Introduction

### 5.1.1 Background

Understanding cell-cell communication is a key to comprehending early signalling mechanisms that lead to aberrant cellular interactions and subsequent disease progression. These communications often involve soluble factors such as cytokines, chemokines and growth factors and recognition of these factors by their specific cell-surface receptors (Mittelbrunn and Sánchez-Madrid, 2012). Often abnormal or diseased cells such as malignant cells in within tumours or damaged alveolar epithelial cells in IPF, signal to fibroblasts via such paracrine signalling thereby recruiting them to the diseased area (Prasad et al., 2014). There is evidence to suggest that recruitment of fibroblasts in both IPF and LAM and in many cancers often takes place via the CXCR4/CXCL12 axis (Andersson-Sjoland et al., 2008, Clements et al., 2015, Teng et al., 2016, Orimo et al., 2005). These recruited fibroblasts undergo a phenotypic shift under the influence of diseased cells and become 'activated'. The activated fibroblasts can acquire a pro-inflammatory gene signature thereby broadcasting signals that can attract resident and non-resident immune cells (Kendall and Feghali-Bostwick, 2014). Interestingly, normal fibroblasts can be 'educated' by cancer cells to express pro-inflammatory genes and this 'education' seems to be reversible (Orimo et al., 2005).

*In vitro*, these cell-cell communications can only be studied if cells are cultured together in the right environment. Co-culturing normal lung

(NHLFs) or activated lung fibroblasts with diseased cells can result in fibroblasts showing altered responses. For example, NHLF and IPF fibroblasts when co-cultured with epithelial cells stimulate a differential epithelial repair response, and IPF fibroblasts show increased levels of bFGF and PDGF and faster wound healing rates (Prasad et al., 2014). Cancer-associated fibroblasts (CAFs), when cultured together with NCI-H358 cells induce EMT through direct contact, show an upregulated expression of α-SMA, TGF-β and FAP-α and are more potent in inducing collagen gel contraction compared to NHLFs (Choe et al., 2013, Horie et al., 2012). Fibroblasts co-cultured with $CD4^+$ T lymphocytes show a significant increase in $CD25^+$, IL-10 and TGF-β (Conte et al., 2013) and human bronchial fibroblasts from asthmatic patients when co-cultured with $CD4^+$ T cells show significantly elevated levels of IL-6, IL-17, IL-22, IL-1β, TGF-β and IL-23 (Loubaki et al., 2013). A wide range of signalling responses are therefore evoked in fibroblasts by different cells.

The microarray assay is a powerful tool that allows the simultaneous study of expression of several thousands of genes or their RNA products, thereby painting an accurate picture of gene expression in the cell at a particular point in time (Russo et al., 2003). A gene expression profile of a cell obtained in such a manner gives an insight into its function, phenotype and response to external stimuli. Such a global expression profile that can help elucidate cellular functions, biochemical pathways and regulatory mechanisms now termed as the 'transcriptome' (Su et al., 2002, Russo et al., 2003).

Microarray analyses are largely used to characterise diseased cells in comparison to healthy cells and to further characterise biological disease systems. There are few different types of microarray techniques of which oligonucleotide microarrays are increasingly the method of choice for many modern DNA microarray applications as they provide higher target specificity because they make use of shorter probe lengths (Jaluria et al., 2007). GeneChips® (Affymetrix, High Wycombe, UK) are the most widely used in situ-synthesised oligonucleotide arrays in which the oligonucleotide probes are synthesised directly on the surface of the microarray and consist of short (20 to 25 base pairs), multiple probes per target to improve sensitivity, specificity and statistical accuracy (Miller and Tang, 2009).

A lot is still unknown about the exact origin and lineage of LAM cells. The hypothesis was that LAM cells recruit fibroblasts, in doing so, the LAM cells could have an effect on their phenotype leading to altered signalling responses. Therefore co-culturing 621-101 cells with NHLFs or LAFs would help shed light onto a communication pattern between the cells and would also help expose any differences or similarities between NHLFs and LAFs. Comprised of more than 54,000 probe sets and capable of analysing the relative expression levels of more than 47,000 transcripts, the GeneChip® Human Genome U133 Plus 2.0 Array (Affymetrix, High Wycombe, UK) (Affymetrix, 2007) was selected for performing a microarray assay using RNA isolated from NHLFs and LAFs. Understanding these early mechanisms of cell-cell communication can give an idea of further cascading events leading to disease progression.

### 5.1.2 Aims and Objectives

The aims of this part of the study were to understand the early transcriptional consequences of 621-101 cells on the fibroblasts with a view to identifying a global gene signature for LAFs and NHLFs. This study set forth to find out how similar or different are the LAFs from the NHLFs with respect to the influence of LAM cells. This was focused on the microarray analyses to identify target genes showing changes in fibroblasts, validating the identified targets *in vitro* and in *ex vivo* samples and in parallel establishing a functional basis for the identified gene targets.

## 5.2 Methods

### 5.2.1 Boyden Chamber Transwell® Culture

Fibroblasts (LAFs and NHLFs) and 621-101 cells were cultured in DMEM/F-12 supplemented with 10% FCS, detached and resuspended in medium as described in section 2.2.4. Fibroblasts and 621-101 cells were counted using a haemocytometer and $5x10^4$ LAFs or NHLFs were seeded into each well of a standard tissue culture-treated 24-well plate with $5x10^3$ 621-101 cells seeded onto each 0.4µm pore size Transwell® insert, pre-coated with 10µg/ml Culturex® BME gel thus making up the lower and upper chambers respectively of a Boyden chamber. The cells were allowed to adhere overnight in the separate chambers after which the Transwell inserts were placed in the 24-well plates replacing the existing medium with fresh DMEM/F-12 without FCS. A LAF or NHLF mono-culture condition consisting of an empty pre-coated Transwell insert as the upper chamber was also set up. 10nM β-oestradiol (E2) was added to cells in both co-culture and mono-culture at the start of the experiment and cells were cultured for 96 hours with a fresh change of media containing 10nM β-estradiol every 48 hours. To assess the effect of E2, a second similar Boyden chamber Transwell culture was set up consisting of additional untreated LAF or NHLF co-cultures and mono-cultures. Three NHLF and LAF donors were used and each condition was tested either in triplicate or sets of six wells. Medium was replaced with fresh serum free DMEM/F-12 supplemented with 10nM E2 at the end of 48 hours. At the end of 96 hours, cell supernatants were collected and stored at -80°C. LAFs, NHLFs and 621-101 cells were washed

twice in PBS and cells were lysed using 250µl lysis buffer containing freshly added 2-mercaptoethanol. Lysates were stored at -80°C.

### 5.2.2 Chemotactic Mast Cell Migration Assay

Mast cell migration was examined using a 24-well microchemotaxis Boyden chamber assay. LAFs, 621-101 cells or a 5:1 mixture of LAFs and 621-101 cells were counted such that each well of 24-well (lower chamber) contained a total of $5x10^4$ cells per well cultured using IMDM. Prior to seeding, cells were conditioned using a 1:1 mixture of DMEM/F-12 and IMDM supplemented with 10% FCS. HMC-1 cells, were counted and $1x10^5$ cells were seeded onto each 5µm pore size Transwell® inserts (upper chamber) pre-coated with 10µg/ml fibronectin from human plasma and were cultured in IMDM. A CXCR2 inhibitor-treated (100nM SB225002,) tri-culture condition (LAFs and 621-101 cells in lower chamber and HMC-1 cells in upper chamber) and medium only control with HMC-1 cells alone were also setup. Cells were left to adhere in the separate chambers overnight after which the Transwell® inserts were placed in the 24-well plate. The chambers were incubated for 8 hours at 37°C and 5% $CO_2$. Non-migrated cells remaining in the upper chamber were then wiped off using a cotton bud and the migrated cells adhered to the bottom of the Transwell membrane were fixed using 4% formaldehyde (diluted from 37%) in PBS for 20 minutes at room temperature after which cell nuclei were stained using DAPI. Cell migration was measured by counting the number of cells attached to the lower surface of the Transwell membrane at a x10 magnification using a Nikon Diaphot 300 Inverted microscope with

epifluorescence. Each condition per donor was tested in triplicate and migration assay was carried out using three LAF donors. The results were expressed as the average number of migrating cells per three wells (±SD). The number of migrated cells obtained was normalised to the number of HMC-1 cells under the influence of gravity attached to the bottom of the Transwell® membrane.

### 5.2.3 Assessment of RNA Integrity Number (RIN)

RNA extracted from LAFs and NHLFs was adjusted to a concentration of 100ng/µl using elution solution, named as follows in Table 5.2.1 and was sent to Nottingham Arabidopsis Stock Centre (NASC) (Craigon et al., 2004) for quality assessment and generation of RIN.

Samples were designated as listed in Table 5.2.1.

| Condition | Sample name |
|---|---|
| LAF donor 1 (NC0914) + LAM cells Co-culture | LAM FB 1 |
| LAF donor 1 (NC0914) + empty Transwell Mono-culture | LAM FB 1C |
| LAF donor 2 (HF1014) + LAM cells Co-culture | LAM FB 2 |
| LAF donor 2 (HF1014) + empty Transwell Mono-culture | LAM FB 2C |
| LAF donor 3 (NC0913) + LAM cells Co-culture | LAM FB 3 |
| LAF donor 3 (NC0913) + empty Transwell Mono-culture | LAM FB 3C |
| NHLF donor 1 (HPF) + LAM cells Co-culture | NORM FB 1 |
| NHLF donor 1 (HPF) + empty Transwell Mono-culture | NORM FB 1C |
| NHLF donor 2 (RS11010) + LAM cells Co-culture | NORM FB 2 |
| NHLF donor 2 (RS11010) + empty Transwell Mono-culture | NORM FB 2C |

| | |
|---|---|
| NHLF donor 3 (NHLF34) + LAM cells Co-culture | NORM FB 3 |
| NHLF donor 3 (NHLF34) + empty Transwell Mono-culture | NORM FB 3C |

**Table 5.2.1** ***Extracted LAF and NHLF RNA designated with sample names for ease of use in further analyses.***

Assessment of RIN for extracted RNA samples was carried out using the Agilent 2100 Bioanalyzer instrument (Agilent Technologies, Stockport, UK). RIN was generated using the Agilent RNA 6000 Nano Kit (Agilent Technologies, Stockport, UK) by following the instructions provided by the manufacturer. The RNA chip was then run in the Agilent 2100 Bioanalyzer instrument to obtain the RIN score.

### 5.2.4 Labelling, Hybridisation and Generation of Transcriptional Expression Array using the Affymetrix U 133 Plus 2.0 GeneChip™

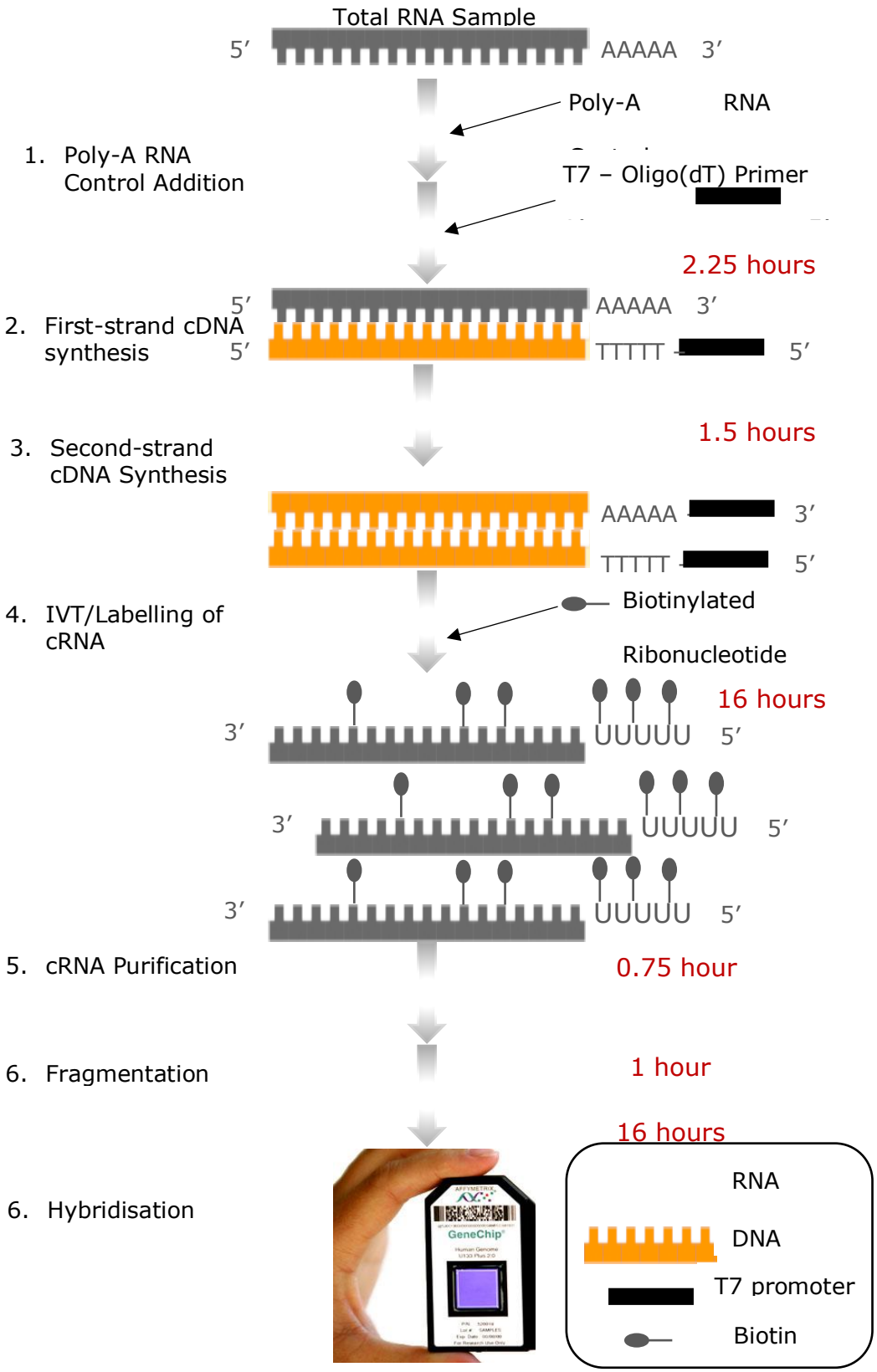



**Figure 5.2.1** ***Diagrammatic representation of assay workflow for amplification and labelling process.*** *Image shows 3′ IVT PLUS amplification and labelling process for*

*generation of GeneChip® Expression Arrays. Time taken per step in the protocol is denoted in red on the right hand side. Diagram adapted from GeneChip™ 3' Expression Arrays User Guide available at www.affymetrix.com (Affymetrix, 2017).*

Figure 5.2.1 shows a diagrammatic illustration of labelling, hybridisation and generation of the transcriptional expression which was performed as per standardised protocol available at (Affymetrix, 2017).

### 5.2.5 Measurement of Chemokine Protein Expression Using Bio-Plex® Multiplex Immunoassay

$5x10^4$ LAFs and $5x10^3$ 621-101 cells were seeded in the lower and upper chambers (pre-coated with 10µg/ml BME) respectively of a 24-well Boyden chamber. Respective LAF and 621-101 cell mono-cultures were also setup. Prior to seeding, 621-101 cells were treated with 10nM rapamycin for 24 hours following which existing media was removed and cells were washed thoroughly in several washes of medium to prevent any rapamycin carry over. At the start of the experiment appropriate 621-101 cell wells were treated with 10n M E2 which was replaced, at the end of 48 hours. Co-cultures and mono-cultures for each condition per donor were tested in triplicate and were maintained for 96 hours after which supernatants were collected and triplicates per condition were pooled. Supernatants generated from treating ex vivo tissue explants, LAM spheroids and mono-culture spheroids were collected and pooled.

Six replicates per donor per condition were set up. Bio-Plex Multiplex Immunoassay using a customised Bio-Plex® Pro Human Chemokine assay panel was carried out as described in section 2.5.1. Pooled supernatants were x2 diluted using DMEM/F-12 supplemented with 0.5% bovine serum

albumin (BSA). The bead region and standard value for each chemokine assessed was set as depicted in Table 5.2.2. The concentration of each chemokine in the pooled supernatants was calculated in pg/ml.

| Analyte | Bead region | Value for first standard (S1) pg/ml |
|---|---|---|
| CXCL1 | 61 | 55,942 |
| CXCL2 | 78 | 19,564 |
| CXCL5 | 73 | 195,500 |
| CXCL6 | 15 | 12,783 |
| CXCL8 | 54 | 8,332 |
| CXCL10 | 48 | 20,375 |
| CXCL12 | 22 | 160,868 |
| CCL2 | 53 | 4,172 |

**Table 5.2.2 Bead regions and first standard values (pg/ml) for chemokine analytes set for Bio-Plex 100,200 machine.**

### 5.2.6 Immune Cell Detection and Cell Counts

Immunohistochemical analysis to identify immune cells in LAM lung tissue was performed at the Histopathology department in Queens Medical Centre using the BenchMark ULTRA Automated IHC/ISH slide staining system (Ventana Medical Systems, Roche, Tuscon, AZ, USA). Heat-induced epitope retrieval was performed at pH 8.0-8.5 using tris-borate-EDTA buffer (Ultra CC1 buffer, Ventana Medical Systems, Roche, Tuscon, AZ, USA) and enzymatic retrieval was carried out using Protease 1 (Ventana Medical Systems, Roche, Tuscon, AZ, USA) an endopeptidase of the serine protease family. Finally, HRP-linked secondary antibody and chromogenic detection was carried out using either ultaView Universal DAB Detection Kit or OptiView DAB IHC Detection Kit (Ventana Medical Systems, Roche, Tuscon, AZ, USA). The primary antibody concentrations used and the specific conditions used were listed in Table 5.2.3.

| Primary antibody | Dilution | Antigen retrieval | Duration of primary | Host species | Supplier and |
|---|---|---|---|---|---|

| | | | antibody incubation | and Isotype | product code |
|---|---|---|---|---|---|
| CD4 | Ready to use | Ultra CC1 buffer for 64 minutes | 32 minutes at 37°C | Rabbit monoclonal IgG | Roche #790-4423 |
| CD10 | Ready to use | Ultra CC1 buffer for 40 minutes | 12 minutes at 37°C | Rabbit monoclonal IgG | Roche #790-4506 |
| CD68 | 1:2000 | Ultra CC1 buffer for 64 minutes | 32 minutes at 37°C | Mouse monoclonal IgG1, kappa | Dako, clone KP1 #M081401-2 |
| Mast cell tryptase | 1:500 | Protease 1 for 4 minutes | 32 minutes at 37°C | Mouse monoclonal IgG1, kappa | Dako, clone AA1 # M705229-2 |

**Table 5.2.3 Primary antibodies used to identify immune cells in LAM lung nodules**

Early and late LAM lung tissue stained for antibodies against CD4, CD10, CD68 and mast cell tryptase were imaged using the Hamamatsu Nanozoomer (Hamamatsu Photonics UK, Hertfordshire, UK). At least 3 nodules per donor were identified and tissue images, x5 magnified were used to draw a $1mm^2$ free-hand shape. Cells contained within this shape were counted per nodule and cell counts for early and late LAM donors were plotted.

## 5.3 Results

To understand the crosstalk between the $TSC2^{-/-}$ 621-101 cells and fibroblasts a global transcriptional array was performed. The following sections illustrate the process of gene expression analysis and selection and validation of chosen targets.

### 5.3.1 Experimental Design and Assessment of RNA Quality

Communication between the 621-101 cells and LAFs / NHLFs could be deciphered through soluble factors exchanged between cells. The LAFs or NHLFs were cultured with or without the 621-101 cells in a Boyden chamber Transwell to understand whether there were any similarities or differences between the LAFs and NHLFs and also whether the 621-101 cells evoked similar reactions in both type of fibroblasts.

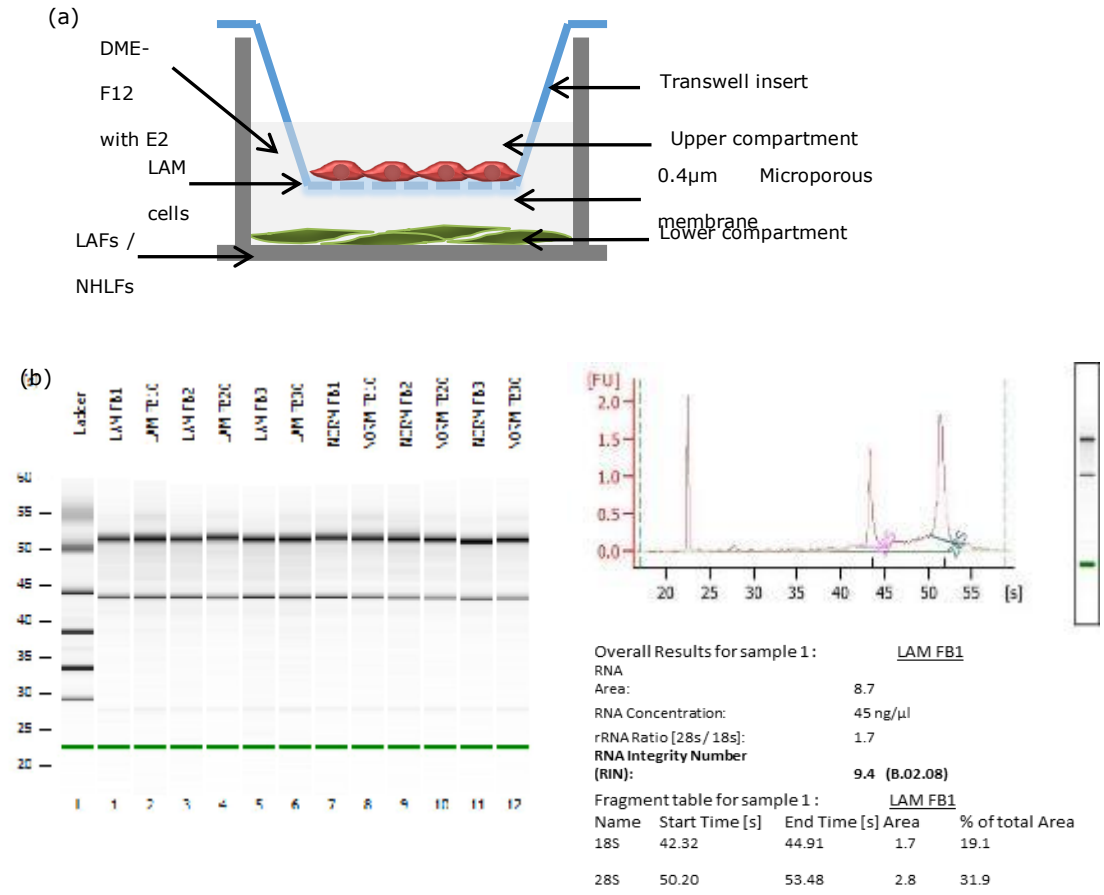



**Figure 5.3.1** ***Diagrammatic representation of experimental design and quality assessment of isolated RNA.*** *(a) Experimental setup illustration showing Boyden chamber culture of cells in each well of a 24-well plate. 621-101 cells were cultured in the upper compartment and LAFs or NHLFs in the lower compartment. (b) Electrophoresis gel showing the 18S and 28S bands for 3 LAM donors and their controls LAM FB1, LAM FB1C, LAM FB2, LAM FB2C, LAM FB3, LAM FB3C and 3 normal donors and their controls NORM FB1, NORM FB1C, NORM FB2, NORM FB2C, NORM FB3, NORM FB3C. Gel image is followed by representative individual graph for each sample showing 18S and 28S peaks with individual RNA integrity number (RIN, in bold).*

Figure 5.3.1 (a) shows the experimental design setup to understand and study cellular communication between 621-101 cells and LAFs or NHLFs. Cells were maintained in a 10:1 ratio and set up as a Boyden chamber culture as described in section 5.2.1. At the end of the time point, RNA from both fibroblasts in co-culture and mono-culture was isolated as described in 5.2.3.

Figure 5.3.1 (b) shows the QC report obtained from a representative RNA samples. The gel electrophoresis image (left hand side) showed all 12 samples displayed two ribosomal RNA (rRNA) bands, the 28S band, above and the 18S band, below. All 12 samples had a 28S/18S ratio of 1.6 to 1.8 which is known to result in excellent amplification results. Further, all the samples showed high peaks for 18S and 28S as is seen in the graphical data suggesting RNA was of very high quality which is proven by a high RIN of 9.3 to 10.0. After thorough QC analysis the high quality RNA was subjected to microarray analysis using a GeneChip® Human Genome U133 Plus 2.0 Array (Affymerix) analysed using the Affymetrix® GeneChip® Command Console®.

## 5.3.2 Normalisation of Data and Post-Import Quality Assessment / Quality Control (QA/QC) Reports Using Partek® Genomics Suite™ 6.6

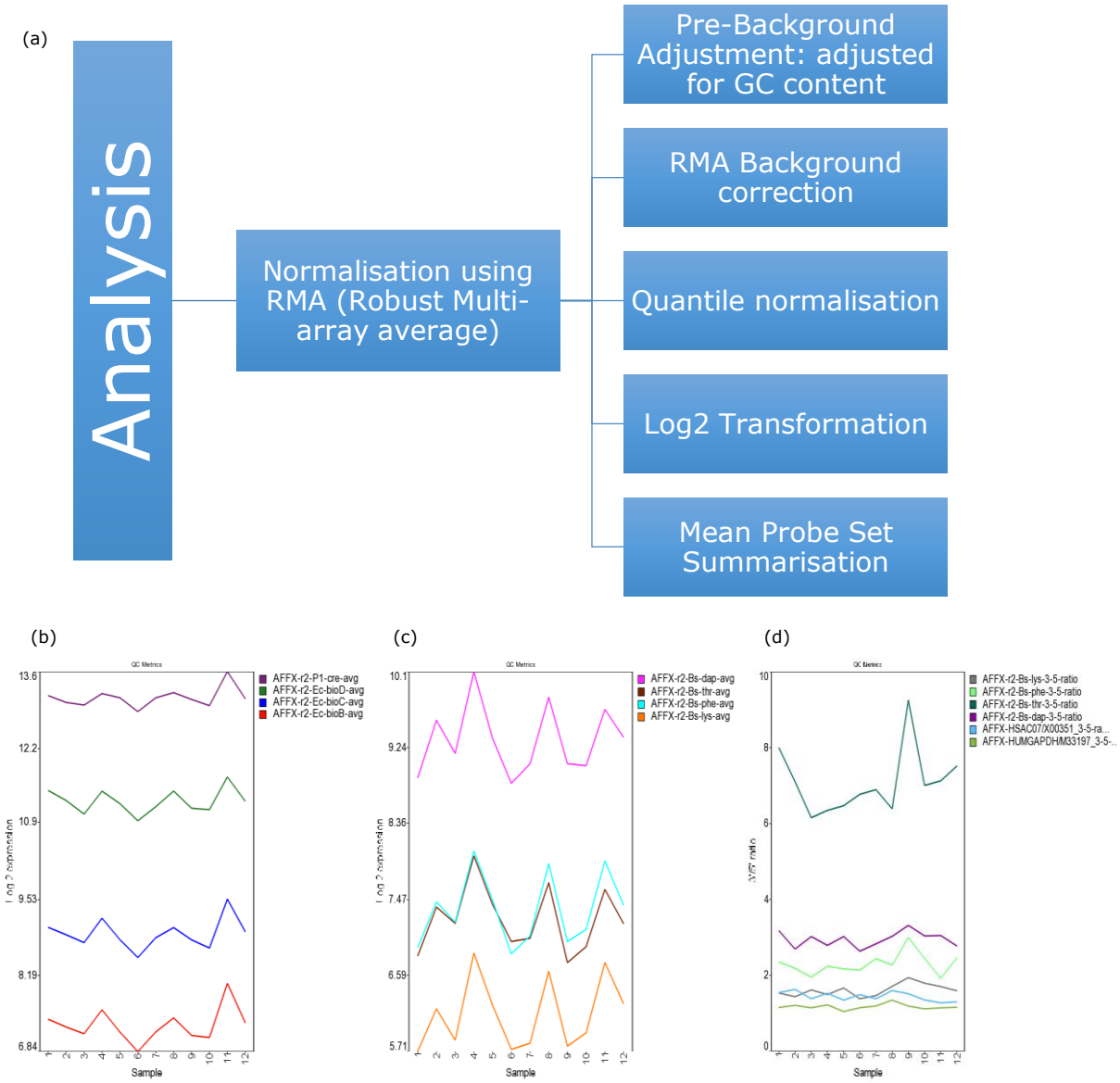



**Figure 5.3.2** ***Schematic representation of normalisation parameters applied and post-import QA/QC report.*** *Panel A shows a schematic representation of the normalisation parameters applied to the dataset which includes adjusting for GC content, RMA background correction, quantile normalisation, log2 transformation and mean probeset summarisation. Panels B, C and D show quality control parameters applied to the data including hybridisation controls, labelling controls and 3'/5' ratio metrics respectively.*

The analysis conducted using the Affymetrix® GeneChip® Command Console® and software yielded data in the form of CEL files which contained raw expression measurements. The data in the CEL format was

imported into the Partek software and a normalisation using a well-known technique, Robust Multi-Array Average (RMA), was used (Irizarry et al., 2003). The parameters included in this type of normalisation are shown in Figure 5.3.2 (a).

After normalisation, data was subjected to certain quality controls. These included hybridisation controls expected to be in an order from high to low: AFFX-rs-P1-cre-avg > AFFX-r2-Ec-bioD-avg > AFFX-r2-EcbioC-avg > AFFX-r2-Ec-bioB-avg. All 12 samples are on X axis in same order and the y-axis represents log2 values of the normalized spike in control probesets (Figure 5.3.2 (b)). The labelling controls should show increasing concentrations of four unlabelled polyA controls as, Lys<Phe<Thr<Dap. Again all 12 samples show the same order as predicted with the y-axis showing log2 values of the normalized spike in control probesets (Figure 5.3.2 (c)). PGS 6.6 calculates and plots the 3'/5' ratio of GAPDH, β-actin and all labelling controls used and displays under the 3'/5' tab after import of the arrays. The 3'/5' ratio compares the abundance of the signal at the 3' end over the abundance at the 5' end and a ratio of 3 or less is acceptable. As expected all samples showed a ratio of 3 or less for the housekeeping *GAPDH* and *β-actin* genes (Figure 5.3.2 (d)).

### 5.3.3 Assigning Sample Attributes and Principal Component Analysis Identifying Outliers and Overlapping Variables

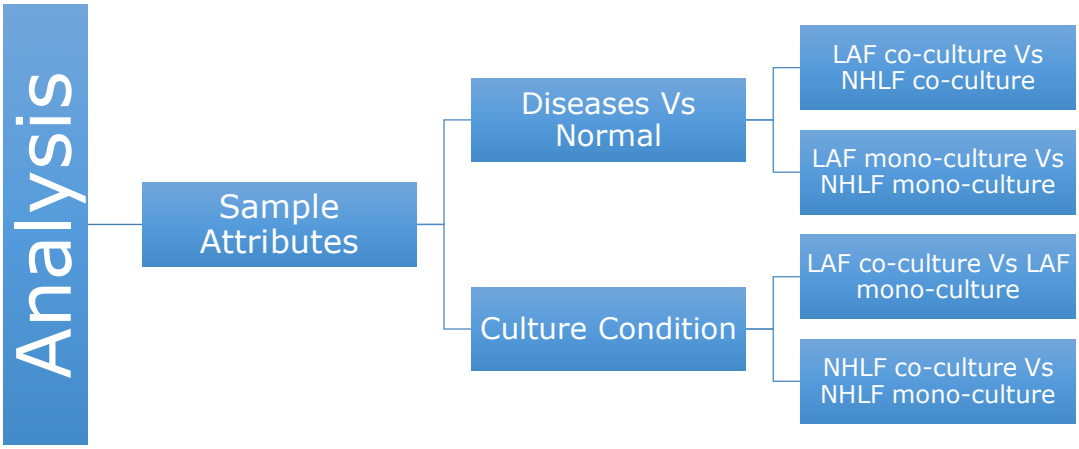



**Figure 5.3.3** ***Schematic representation of attributes assigned to samples.*** *Flow chart shows the attributes assigned to the samples to group them for comparative analyses.*

The 12 samples were assigned sample attributes to group them into specific lists for comparison of differentially expressed transcripts. This was done as depicted in Figure 5.3.3 and the exact sample assigned to each list is shown in Table 5.3.1.

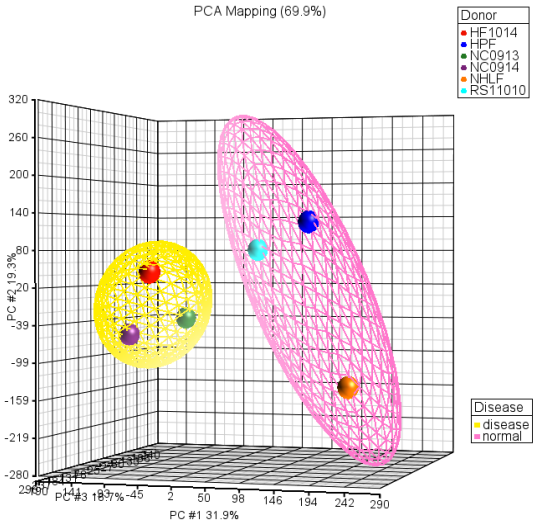
| Sample Attribute | Lists included | Samples included |
|---|---|---|
| Disease vs. Normal | LAF co-culture vs. NHLF co-culture | LAM FB 1, LAM FB 2, LAM FB 3 vs. NORM FB 1, NORM FB 2, NORM FB 3 |
| | LAF mono-culture vs. NHLF mono-culture | LAM FB 1C, LAM FB 2C, LAM FB 3C vs. NORM FB 1C, NORM FB 2C, NORM FB 3C |
| Culture condition | LAF co-culture vs. LAF mono-culture | LAM FB 1, LAM FB 2, LAM FB 3 vs. LAM FB 1C, LAM FB 2C, LAM FB 3C |
| | NHLF co-culture vs. NHLF mono-culture | NORM FB 1, NORM FB 2, NORM FB 3 vs. |

| | | |
|---|---|---|
| | | NORM FB 1C, NORM FB 2C, NORM FB 3C |

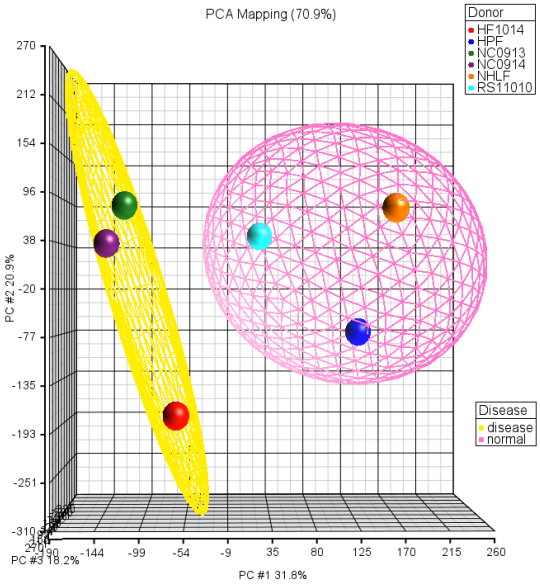
**Table 5.3.1** ***Samples included in each comparison list with appropriate attribute.***

The two main attributes or experimental factors were considered as disease (LAF) or normal (NHLF) and culturing conditions (co-culture vs. mono-culture). Further comparison lists based on these experimental factors were set up to decipher whether the 621-101 cells change the NHLF phenotype making them comparable to LAFs (disease) (LAF co-culture vs. NHLF co-culture) and to determine how similar or different diseased LAFs are to NHLFs without the influence of 621-101 cells (LAF mono-culture vs. NHLF mono-culture). The other comparison was made to understand the effect of culturing conditions on LAFs and NHLFs to determine cellular communications driving their phenotype.

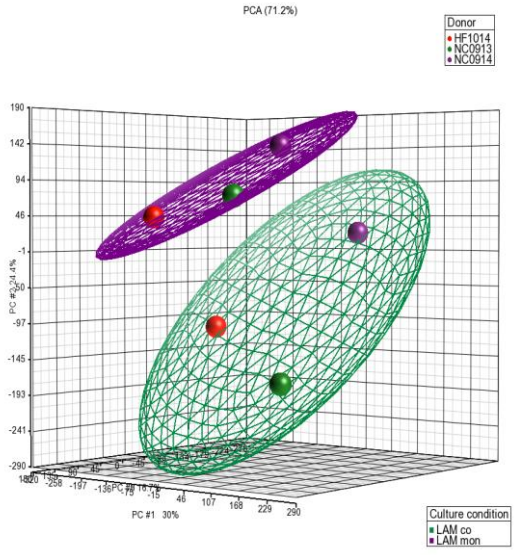
(a) LAF co-culture Vs NHLF co-culture




(b) LAF mono-culture Vs NHLF mono-culture




(c) LAF co-culture Vs LAF mono-culture




(d) NHLF co-culture Vs NHLF mono-culture

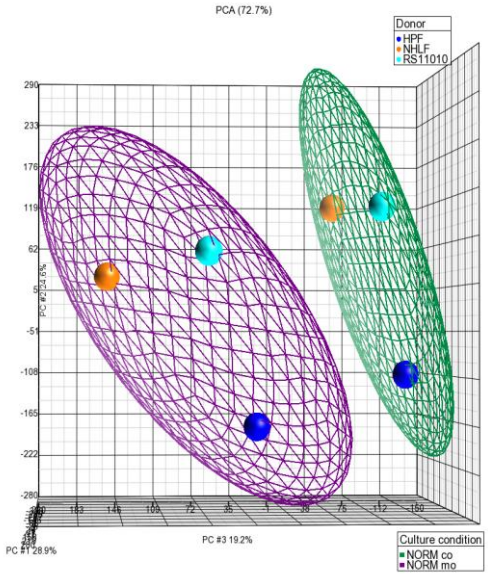



**Figure 5.3.4** ***Principal component analysis (PCA).*** *Panels A-D show four scatter plots with the PCA plot for each comparison. Each differently coloured dot in the PCA represents a donor clustered together based on the sample attribute.*

PCA plots were generated from each comparison list in the next step of exploratory data analysis to identify unexpected trends, outliers and batch effects that may influence this experiment. The PCA plots are a global

genome analysis and not an analysis of any gene in particular (Downey, 2006). PCA plot for LAF co-culture vs NHLF co-culture (Figure 5.3.4 (a)) showed a very tight clustering of the LAF donors grouped as 'disease' (yellow ellipsoid) whereas the NHLF donors were more spread out, grouped as 'normal' (pink ellipsoid). The total variation explained by PCs 1, 2 and 3 was 69.9%. In the LAF mono-culture vs. NHLF mono-culture comparison (Figure 5.3.4 (b)) however, both LAF and NHLF donors were clustered far apart suggesting that both groups have variable gene expression. The total variation explained by PCs 1, 2 and 3 was 70.9%. Clustering of all the donors was more spread out and comparable in the other two comparisons, LAF co-culture vs LAF mono-culture (Figure 5.3.4 (c)) and NHLF co-culture vs. NHLF mono-culture (Figure 5.3.4 (d)). This again suggested a variable expression was expected from both LAF and NHLF donors. The total variation explained by PCs 1, 2 and 3 was 71.2% and 72.7% respectively. None of the separate experimental factors or attributes, overlapped one another confirming that these factors were exclusive and independent of each other.

### 5.3.4 Differentially Expressed Genes and Sources of Variation

Differentially expressed genes for each comparison were generated by attributing an experimental factor as an analysis of variance (ANOVA) factor. The ANOVA is a powerful tool in identifying differentially expressed genes in a multi factor experiment. An initial ANOVA of differentially expressed genes for each was generated based on the ANOVA factors denoted in Table 5.3.2. This gave rise to a list of more than 54,000 differentially expressed genes along with their significance (p-value) and fold changes.

| Comparison list | Experimental factors | ANOVA factors | Contrast |
|---|---|---|---|
| LAF co-culture vs NHLF co-culture | • Disease<br>• Culture condition<br>• Donor | • Disease | LAM vs. NORMAL |
| LAF mono-culture vs. NHLF mono-culture | • Disease<br>• Culture condition<br>• Donor | • Disease | LAM vs. NORMAL |
| LAF co-culture vs. LAF mono-culture | • Culture condition<br>• Donor | • Culture condition<br>• Donor | LAM co-culture vs. LAM mono-culture |
| NHLF co-culture vs. NHLF mono-culture | • Culture condition<br>• Donor | • Culture condition<br>• Donor | NORM co-culture vs. NORM mono-culture |

**Table 5.3.2** ***ANOVA factors designated for each comparison list to generate initial list of transcripts*.**

In the first two comparison lists, namely LAF co-culture vs. NHLF co-culture and LAF mono-culture vs. NHLF mono-culture, the ANOVA factors considered were disease and an interaction disease*culture condition. This way, a two-way ANOVA could be performed. The following two comparisons took into account culturing conditions and donor effect and therefore again, a two-way ANOVA could be computed. The ANOVA

computation in PGS 6.6 only outputs a p-value and F ratio for each factor. Therefore, in order to get a fold change and a ratio between disease and normal or co-culture and mono-culture contrasts were set up as shown in Table 5.3.2.

After an initial expansive 54,000 plus transcript list, a further list was then generated by applying parameters for fold change and p-value. Transcript lists were generated by selecting targets that had a fold change of >2 or <-2 with an unadjusted p-value of 0.05 or less.

Within the realms of this study, the comparisons between Co-culture and Mono-culture (LAF and NHLF co-culture vs. LAF and NHLF mono-culture respectively) were analysed further. The results obtained from these comparisons were compelling enough to warrant a thorough analyses and therefore in the next sections only those will be presented and discussed.

#### 5.3.4.1 LAF Co-Culture vs. LAF Mono-Culture

| Gene Symbol | Gene Title | p-value (LAF co vs. LAF mono) | Fold-Change (LAF co vs. LAF mono) | Fold-Change (LAF co vs. LAF mono) (Description) |
|---|---|---|---|---|
| CXCL1 | chemokine (C-X-C motif) ligand 1 (melanoma growth stimulating activity, alpha) | 0.0093 | 36.98 | LAF co up vs LAF mono |
| CXCL6 | chemokine (C-X-C motif) ligand 6 (granulocyte chemotactic protein 2) | 0.0093 | 33.21 | LAF co up vs LAF mono |
| IFI44L | interferon-induced protein 44-like | 0.0099 | 32.81 | LAF co up vs LAF mono |
| SLC39A8 | solute carrier family 39 (zinc transporter), member 8 | 0.0047 | 21.71 | LAF co up vs LAF mono |

| | | | | |
|---|---|---|---|---|
| CXCL2 | chemokine (C-X-C motif) ligand 2 | 0.0188 | 21.34 | LAF co up vs LAF mono |
| CXCL8/IL8 | chemokine (C-X-C motif) ligand 8 (interleukin 8) | 0.0354 | 18.55 | LAF co up vs LAF mono |
| IFI6 | interferon, alpha-inducible protein 6 | 0.0125 | 17.28 | LAF co up vs LAF mono |
| CMPK2 | cytidine monophosphate (UMP-CMP) kinase 2, mitochondrial | 0.0296 | 15.75 | LAF co up vs LAF mono |
| SLC39A8 | solute carrier family 39 (zinc transporter), member 8 | 0.0044 | 15.50 | LAF co up vs LAF mono |
| CFB | complement factor B | 0.0130 | 15.17 | LAF co up vs LAF mono |
| IFIT1 | interferon-induced protein with tetratricopeptide repeats 1 | 0.0478 | 12.55 | LAF co up vs LAF mono |
| SOD2 | superoxide dismutase 2, mitochondrial | 0.0037 | 11.82 | LAF co up vs LAF mono |
| CXCL5 | chemokine (C-X-C motif) ligand 5 | 0.0333 | 11.30 | LAF co up vs LAF mono |
| GCH1 | GTP cyclohydrolase 1 | 0.0336 | 11.05 | LAF co up vs LAF mono |
| CXCL3 | chemokine (C-X-C motif) ligand 3 | 0.0336 | 10.44 | LAF co up vs LAF mono |
| ISG15 | ISG15 ubiquitin-like modifier | 0.0101 | 10.38 | LAF co up vs LAF mono |
| HERC6 | hect domain and RLD 6 | 0.0133 | 9.96 | LAF co up vs LAF mono |
| IFI27 | interferon, alpha-inducible protein 27 | 0.0155 | 9.06 | LAF co up vs LAF mono |
| OAS3 | 2'-5'-oligoadenylate synthetase 3, 100kDa | 0.0073 | 9.01 | LAF co up vs LAF mono |
| EPSTI1 | epithelial stromal interaction 1 (breast) | 0.0251 | 8.83 | LAF co up vs LAF mono |
| IL6 | interleukin 6 (interferon, beta 2) | 0.0280 | 8.44 | LAF co up vs LAF mono |
| NAMPT | nicotinamide phosphoribosyltransferase | 0.0040 | 8.28 | LAF co up vs LAF mono |
| IFIT3 | interferon-induced protein with tetratricopeptide repeats 3 | 0.0134 | 7.89 | LAF co up vs LAF mono |
| CLDN1 | claudin 1 | 0.0113 | 7.47 | LAF co up vs LAF mono |
| TNFAIP3 | tumor necrosis factor, alpha-induced protein 3 | 0.0035 | 7.16 | LAF co up vs LAF mono |
| TNFAIP6 | tumor necrosis factor, alpha-induced protein 6 | 0.0288 | 6.53 | LAF co up vs LAF mono |

| | | | | |
|---|---|---|---|---|
| ICAM1 | intercellular adhesion molecule 1 | 0.0008 | 5.25 | LAF co up vs LAF mono |
| VCAM1 | vascular cell adhesion molecule 1 | 0.0500 | 4.64 | LAF co up vs LAF mono |
| CCL2 | chemokine (C-C motif) ligand 2 | 0.0323 | 3.81 | LAF co up vs LAF mono |
| CXCL10 | chemokine (C-X-C motif) ligand 10 | 0.0289 | 2.45 | LAF co up vs LAF mono |
| DEPDC6 | DEP domain containing 6 | 0.0197 | -2.58 | LAF co down vs LAF mono |
| AK5 | adenylate kinase 5 | 0.0438 | -2.55 | LAF co down vs LAF mono |
| RASSF2 | Ras association (RalGDS/AF-6) domain family member 2 | 0.0115 | -2.26 | LAF co down vs LAF mono |
| COL21A1 | collagen, type XXI, alpha 1 | 0.0309 | -2.17 | LAF co down vs LAF mono |
| ANO3 | anoctamin 3 | 0.0076 | -2.15 | LAF co down vs LAF mono |
| GDF10 | growth differentiation factor 10 | 0.0252 | -2.15 | LAF co down vs LAF mono |
| COL5A3 | collagen, type V, alpha 3 | 0.0442 | -2.13 | LAF co down vs LAF mono |
| HTR2B | 5-hydroxytryptamine (serotonin) receptor 2B | 0.0486 | -2.01 | LAF co down vs LAF mono |
| SLC6A6 | solute carrier family 6 (neurotransmitter transporter, taurine), member 6 | 0.0209 | -2.01 | LAF co down vs LAF mono |
| STOX2 | storkhead box 2 | 0.0032 | -2.00 | LAF co down vs LAF mono |

**Table 5.3.3** ***Top 41 differentially expressed transcripts between LAF co-culture and LAF mono-culture.*** *Selected based on fold change >2 or <-2 with an unadjusted p-value of 0.05 or less.*

LAF co-culture when compared to LAF mono-culture yielded a list of 242 differentially expressed transcripts of which 11 were downregulated in LAF co-culture. Table 5.3.3 shows top 30 upregulated and top 11 downregulated transcripts in this list sorted by descending order of fold change. Interestingly, significantly upregulated in LAF co-culture were C-X-C motif type chemokines namely CXCL1, 2, 3, 5, 6, 8, 10. CXCL1 was the most upregulated transcript showing a 36.9-fold change (p=0.0092) whereas DEPDC6 was most downregulated, -2.5-fold (p=0.019) in LAF co-

culture when compared to LAF mono-culture. Adhesion molecules ICAM1 and VCAM1 were also significantly upregulated (5.2-fold, p=0.0008 and 4.6-fold, p=0.049 respectively) in LAF co-culture.

5.3.4.2 NHLF Co-Culture vs. NHLF Mono-Culture

| Gene Symbol | Gene Title | p-value (NHLF co vs. NHLF mono) | Fold-Change (NHLF co vs. NHLF mono) | Fold-Change (NHLF co vs. NHLF mono) (Description) |
|---|---|---|---|---|
| CXCL1 | chemokine (C-X-C motif) ligand 1 (melanoma growth stimulating activity, alpha) | 0.0034 | 50.32 | NHLF co up vs NHLF mono |
| CXCL8/IL8 | chemokine (C-X-C motif) ligand 8 (interleukin 8) | 0.0022 | 39.53 | NHLF co up vs NHLF mono |
| CXCL2 | chemokine (C-X-C motif) ligand 2 | 0.0002 | 36.28 | NHLF co up vs NHLF mono |
| CXCL6 | chemokine (C-X-C motif) ligand 6 (granulocyte chemotactic protein 2) | 0.0230 | 32.99 | NHLF co up vs NHLF mono |
| IFI44L | interferon-induced protein 44-like | 0.0120 | 25.39 | NHLF co up vs NHLF mono |
| C3 | complement component 3 | 0.0038 | 24.70 | NHLF co up vs NHLF mono |
| CXCL3 | chemokine (C-X-C motif) ligand 3 | 0.0079 | 22.17 | NHLF co up vs NHLF mono |
| SLC39A8 | solute carrier family 39 (zinc transporter), member 8 | 0.0060 | 19.51 | NHLF co up vs NHLF mono |
| IFI6 | interferon, alpha-inducible protein 6 | 0.0052 | 18.34 | NHLF co up vs NHLF mono |
| CXCL5 | chemokine (C-X-C motif) ligand 5 | 0.0025 | 17.01 | NHLF co up vs NHLF mono |
| IFI27 | interferon, alpha-inducible protein 27 | 0.0088 | 16.69 | NHLF co up vs NHLF mono |
| CMPK2 | cytidine monophosphate (UMP-CMP) kinase 2, mitochondrial | 0.0473 | 16.55 | NHLF co up vs NHLF mono |
| TDO2 | tryptophan 2,3-dioxygenase | 0.0111 | 15.13 | NHLF co up vs NHLF mono |
| CFB | complement factor B | 0.0007 | 14.18 | NHLF co up vs NHLF mono |
| IFIT1 | interferon-induced protein with tetratricopeptide repeats 1 | 0.0118 | 13.04 | NHLF co up vs NHLF mono |
| GCH1 | GTP cyclohydrolase 1 | 0.0011 | 11.21 | NHLF co up vs NHLF mono |

| | | | | |
|---|---|---|---|---|
| SOD2 | superoxide dismutase 2, mitochondrial | 0.0092 | 9.62 | NHLF co up vs NHLF mono |
| ISG15 | ISG15 ubiquitin-like modifier | 0.0267 | 9.35 | NHLF co up vs NHLF mono |
| NAMPT | Nicotinamide phosphoribosyltransferase | 0.0007 | 8.89 | NHLF co up vs NHLF mono |
| IFIT3 | interferon-induced protein with tetratricopeptide repeats 3 | 0.0216 | 8.58 | NHLF co up vs NHLF mono |
| NAMPT | nicotinamide phosphoribosyltransferase | 0.0036 | 8.27 | NHLF co up vs NHLF mono |
| CLDN1 | claudin 1 | 0.0027 | 8.08 | NHLF co up vs NHLF mono |
| TNFAIP6 | tumor necrosis factor, alpha-induced protein 6 | 0.0062 | 6.42 | NHLF co up vs NHLF mono |
| TNFAIP3 | tumor necrosis factor, alpha-induced protein 3 | 0.0047 | 5.72 | NHLF co up vs NHLF mono |
| ICAM1 | intercellular adhesion molecule 1 | 0.0015 | 4.74 | NHLF co up vs NHLF mono |
| CCL7 | chemokine (C-C motif) ligand 7 | 0.0039 | 4.20 | NHLF co up vs NHLF mono |
| CXCL10 | chemokine (C-X-C motif) ligand 10 | 0.0021 | 3.70 | NHLF co up vs NHLF mono |
| CCL8 | chemokine (C-C motif) ligand 8 | 0.0125 | 3.62 | NHLF co up vs NHLF mono |
| CCL2 | chemokine (C-C motif) ligand 2 | 0.0014 | 3.36 | NHLF co up vs NHLF mono |
| GDF10 | growth differentiation factor 10 | 0.0449 | -3.16 | NHLF co down vs NHLF mono |
| ANO1 | anoctamin 1, calcium activated chloride channel | 0.0287 | -3.05 | NHLF co down vs NHLF mono |
| ALDH1A1 | aldehyde dehydrogenase 1 family, member A1 | 0.0087 | -3.02 | NHLF co down vs NHLF mono |
| IGF1 | insulin-like growth factor 1 (somatomedin C) | 0.0232 | -3.00 | NHLF co down vs NHLF mono |
| SLC6A6 | solute carrier family 6 (neurotransmitter transporter, taurine), member 6 | 0.0253 | -2.88 | NHLF co down vs NHLF mono |
| DEPDC6 | DEP domain containing 6 | 0.0024 | -2.82 | NHLF co down vs NHLF mono |
| RASSF2 | Ras association (RalGDS/AF-6) domain family member 2 | 0.0354 | -2.76 | NHLF co down vs NHLF mono |
| FGF18 | fibroblast growth factor 18 | 0.0342 | -2.68 | NHLF co down vs NHLF mono |
| PALMD | palmdelphin | 0.0222 | -2.64 | NHLF co down vs NHLF mono |
| IGF1 | insulin-like growth factor 1 (somatomedin C) | 0.0317 | -2.61 | NHLF co down vs NHLF mono |

| | | | | |
|---|---|---|---|---|
| SCN7A | sodium channel, voltage-gated, type VII, alpha | 0.0114 | -2.42 | NHLF co down vs NHLF mono |
| IL17RD | interleukin 17 receptor D | 0.0025 | -2.40 | NHLF co down vs NHLF mono |

**Table 5.3.4** ***Top 41 differentially expressed transcripts between NHLF co-culture and NHLF mono-culture.*** *Selected based on fold change >2 or <-2 with an unadjusted p-value of 0.05 or less.*

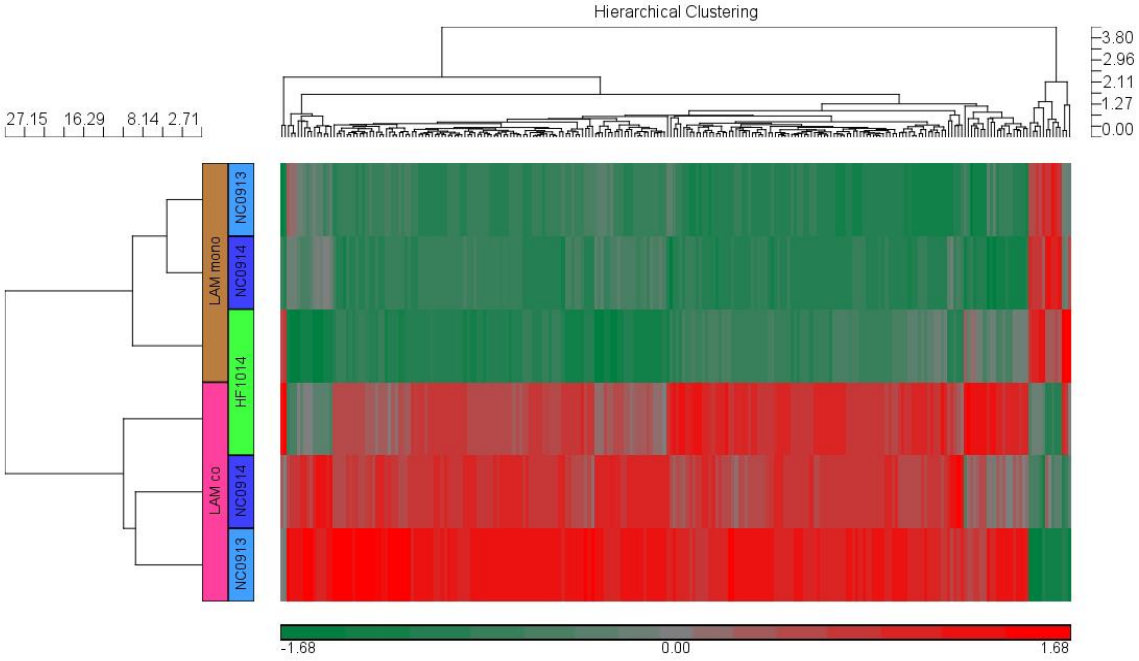
A similar transcript signature to the LAF co-cultures was observed in the NHLF co-cultures. NHLF co-culture vs. NHLF mono-culture yielded a list of 219 transcripts of which 29 transcripts were downregulated in NHLF co-cultures. Table 5.3.4 shows top 30 upregulated and top 11 downregulated transcripts in this list sorted by descending order of fold change. The same C-X-C motif chemokines were upregulated in NHLF co-cultures along with a few C-C motif chemokines, namely CCL2, 7 and 8. Again CXCL1 was the most upregulated transcript with a fold-change of 50.3 (p=0.0034) and GDF10 the most downregulated transcript (-3.1-fold, p=0.044) in NHLF co-cultures. Although ICAM1 was 4.7-fold (p=0.0015) upregulated in NHLF co-cultures, VCAM1 was not significantly changed in this comparative list.

### 5.3.5 Visualising Differentially Expressed Genes by Hierarchical Clustering

Agglomerative hierarchical clustering is a tool used to group similar objects into 'clusters'. Two most similar groups are combined into clusters and continue to combine until all objects form the same cluster thereby producing a tree (dendrogram) showing hierarchy of the clusters. This type of tool enables visualisation of how the microarrays group together based on similarity of features (Partek, 2017b, D'Haeseleer, 2005). Hierarchical clustering was therefore conducted on the transcript lists generated from

the comparative ANOVA applying the same parameters of p-value <0.05 and a fold difference of >2 or <-2.

(a) LAF co-culture (LAM co) Vs LAF mono-culture (LAF mono)




(b) NHLF co-culture (NORM co) Vs NHLF mono-culture (NORM mono)

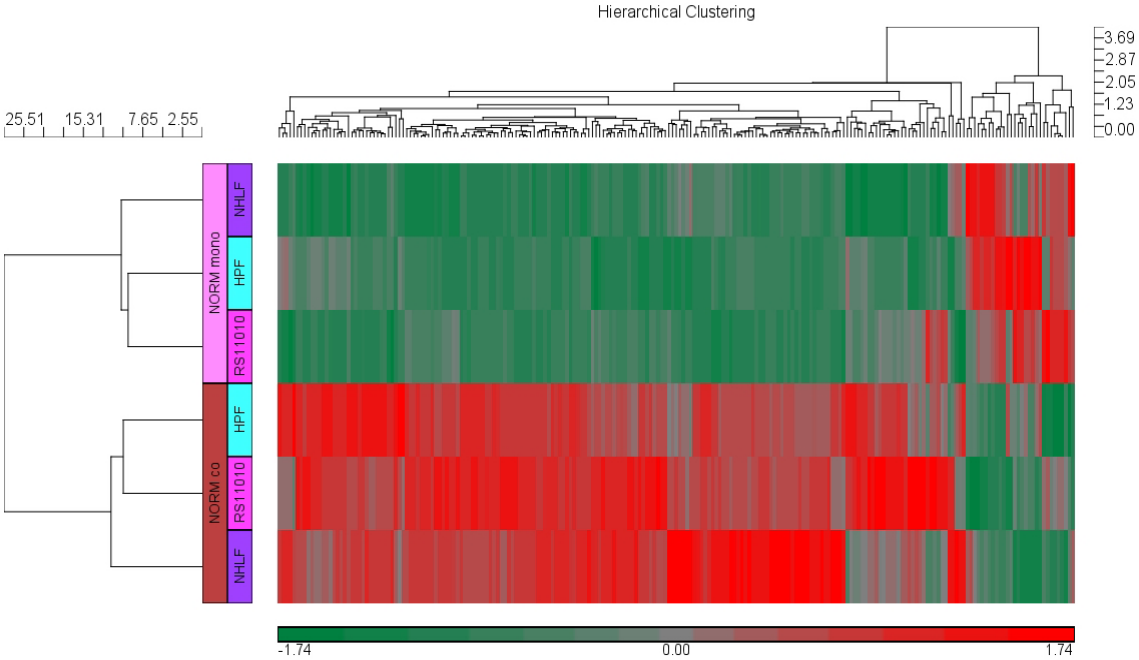



**Figure 5.3.5** ***Hierarchical clustering of all differentially expressed transcripts in co-culture vs. mono-culture comparison.*** *Panel A shows hierarchical clustering of all candidate differentially expressed transcripts in LAF co-culture vs. LAF mono-culture. Panel B shows hierarchical clustering of all candidate differentially expressed transcripts in NHLF co-culture vs. NHLF mono-culture. Each column represents a single probe and each row represents each different donor. Title legend for hierarchical tree is on the left of the cluster diagram. Red colour indicates high-level expression or upregulation, green indicates low-level expression or downregulation and grey areas are no change in expression.*

Unsupervised hierarchical clustering of all 242 and 219 differentially expressed transcripts in LAF co-culture vs LAF mono-culture and NHLF co-culture vs NHLF mono-culture respectively was undertaken (Figure 5.3.5). The default setting in the PGS 6.6 software set the gene expression standardised to mean 0 and standard deviation of 1. Unchanged genes were displayed as a value of 0 coloured grey. Upregulated genes had positive values displayed as red and downregulated genes had negative values displayed as green. The cluster analyses yielded differential expression patterns exhibited by the LAF and NHLF donors. Cluster analysis of the list comparing LAF co-culture to LAF mono-culture showed that again LAF donors NC0913 and NC0914 had comparable expression patterns and clustered together. However, clustering the NHLF co-culture vs mono-culture transcript list revealed that all 3 donors showed quite different red and green expression patterns. Although PGS 6.6 has clustered NHLF donors HPF and RS11010 together it was evident from the heat map that the 3 donors were quite different in terms of their gene expression. It was interesting to note however, that in both comparisons only 5%-10% of transcripts were significantly downregulated in co-culture.

### 5.3.6 Comparing Gene Lists Using Venn Diagrams

Venn diagrams enable comparison of two lists resulting similarities and differences between the lists. To understand the effect of 621-101 cells on both fibroblasts in culture the two lists obtained after an ANOVA were compared. The intersecting region between two comparative lists thus yielded a list of transcripts that changed in both fibroblasts when cultured with 621-101 cells.

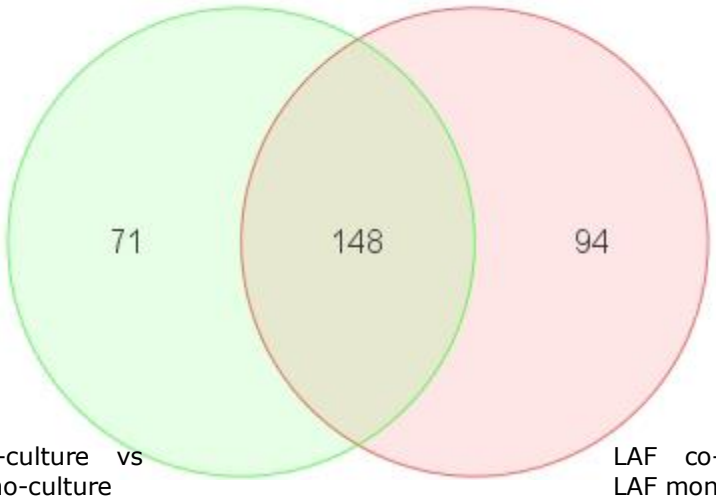



**Figure 5.3.6** ***Venn diagram comparing individual lists; LAF co-culture vs LAF mono-culture and NHLF co-culture vs NHLF mono-culture.*** *Each circle depicts each list. Green circle shows NHLF co-culture vs NHLF mono-culture (219 candidates) and pink circle shows LAF co-culture vs LAF mono-culture (242 candidates). The intersecting region between both circles identifies 148 transcripts that are differentially expressed among all group comparisons.*

Comparison of candidate transcript lists obtained from LAF co-culture vs LAF mono-culture and NHLF co-culture vs NHLF mono-culture visualised using a Venn diagram is shown in Figure 5.3.6. The Venn diagram illustrated significant differences specific to each set of individual comparisons (within a circle) versus those shared in more than one of the

statistical comparisons (intersecting region between circles). Comparing the two lists gave rise to 71 significantly altered transcripts in NHLFs (green circle) and 94 significantly different candidates exclusive to LAFs (pink circle). The intersecting region however, yielded a list of 148 transcripts that were common to both lists and were significantly different in both LAFs and NHLFs when cultured with 621-101 cells. Some of the significantly changed transcripts obtained from the intersecting list are listed in Table 5.3.5.

| | | **LAF co-culture vs LAF mono-culture** | | **NHLF co-culture vs NHLF mono-culture** | |
|---|---|---|---|---|---|
| **Gene Symbol** | **Gene Title** | **p-value (LAF co vs. LAF mono)** | **Fold-Change (LAF co vs. LAF mono)** | **p-value (NHLF co vs. NHLF mono)** | **Fold-Change (NHLF co vs. NHLF mono)** |
| CXCL1 | chemokine (C-X-C motif) ligand 1 (melanoma growth stimulating activity, alpha) | 0.0093 | 36.98 | 0.0034 | 50.32 |
| CXCL6 | chemokine (C-X-C motif) ligand 6 (granulocyte chemotactic protein 2) | 0.0093 | 33.21 | 0.0230 | 32.99 |
| CXCL2 | chemokine (C-X-C motif) ligand 2 | 0.0188 | 21.34 | 0.0002 | 36.28 |
| IL8 | interleukin 8 | 0.0354 | 18.55 | 0.0022 | 39.53 |
| SOD2 | superoxide dismutase 2, mitochondrial | 0.0037 | 11.82 | 0.0092 | 9.62 |
| CXCL5 | chemokine (C-X-C motif) ligand 5 | 0.0333 | 11.30 | 0.0025 | 17.01 |
| CXCL3 | chemokine (C-X-C motif) ligand 3 | 0.0336 | 10.44 | 0.0079 | 22.17 |
| IL6 | interleukin 6 (interferon, beta 2) | 0.0280 | 8.44 | 0.0134 | 7.29 |
| TNFAIP3 | tumor necrosis factor, alpha-induced protein 3 | 0.0035 | 7.16 | 0.0047 | 5.72 |
| TNFAIP6 | tumor necrosis factor, alpha-induced protein 6 | 0.0288 | 6.53 | 0.0062 | 6.42 |
| ICAM1 | intercellular adhesion molecule 1 | 0.0008 | 5.25 | 0.0015 | 4.74 |
| TNFAIP2 | tumor necrosis factor, alpha-induced protein 2 | 0.0146 | 4.09 | 0.0261 | 2.83 |

| | | | | | |
|---|---|---|---|---|---|
| CCL2 | chemokine (C-C motif) ligand 2 | 0.0323 | 3.81 | 0.0014 | 3.36 |
| PTGFR | prostaglandin F receptor (FP) | 0.0182 | 3.18 | 0.0028 | 3.29 |
| TNFSF10 | tumor necrosis factor (ligand) superfamily, member 10 | 0.0343 | 2.67 | 0.0455 | 2.50 |
| SERPINB 2 | serpin peptidase inhibitor, clade B (ovalbumin), member 2 | 0.0039 | 2.45 | 0.0163 | 2.98 |
| CXCL10 | chemokine (C-X-C motif) ligand 10 | 0.0289 | 2.45 | 0.0021 | 3.70 |
| PARP14 | poly (ADP-ribose) polymerase family, member 14 | 0.0003 | 2.44 | 0.0368 | 2.44 |
| PARP9 | poly (ADP-ribose) polymerase family, member 9 | 0.0027 | 2.21 | 0.0367 | 2.24 |
| MMP1 | matrix metallopeptidase 1 (interstitial collagenase) | 0.0370 | 2.09 | 0.0183 | 2.00 |
| SLC2A6 | solute carrier family 2 (facilitated glucose transporter), member 6 | 0.0132 | 2.09 | 0.0376 | 2.05 |
| RASSF2 | Ras association (RalGDS/AF-6) domain family member 2 | 0.0115 | -2.26 | 0.0354 | -2.76 |
| GDF10 | growth differentiation factor 10 | 0.0252 | -2.15 | 0.0449 | -3.16 |
| SLC6A6 | solute carrier family 6 (neurotransmitter transporter, taurine), member 6 | 0.0209 | -2.01 | 0.0095 | -2.79 |

**Table 5.3.5** ***24 out of the 148 differentially expressed in both fibroblasts when co-cultured***

A list of top 24 differentially expressed transcripts from a list of 148 commonly shared transcripts is listed in Table 5.3.5. This list obtained from the intersecting region of the Venn diagram (Figure 5.3.6) comparison generated a list of transcripts that were common to both comparisons and significantly change in both LAFs and NHLFs when cultured together with 621-101 cells. Contained in this list were several C-X-C motif chemokine ligands namely *CXCL1 (GRO-α), CXCL2 (GRO-β), CXCL3 (GRO-γ), CXCL5 (ENA-78), CXCL6 (GCP-2), CXCL8 (IL-8)* and *CXCL10 (IP-10). IL-6* and a

C-C motif chemokine, *CCL2* were also upregulated more than 7-fold and 3-fold respectively in a co-culture condition.

As our study was to determine what cellular communication exists between 621-101 cells and fibroblasts and also to identify whether LAFs were different to NHLFs the intersecting region lists from both comparisons were focused on and all further analyses were performed using these lists.

### 5.3.7 Analysis of Genetic Networks within the Acquired Lists Using Gene Ontology Enrichment Analysis

Genes that are known and studied are defined and annotated by gene ontology (GO). A specific annotation (term) is assigned to each gene in a GO structure within three independent domains: molecular function, biological process and cellular component. With an aim to identify statistically significant biological processes or pathways, transcripts obtained within a microarray analysis are routinely annotated using GO (Ashburner et al., 2000). A gene ontology analysis was therefore performed on the list of targets obtained from the intersect regions of the Venn diagram comparison lists in order to annotate a function for the genes.

*(LAF co-culture vs. LAF mono-culture) VS. (NHLF co-culture vs. NHLF mono-culture)*

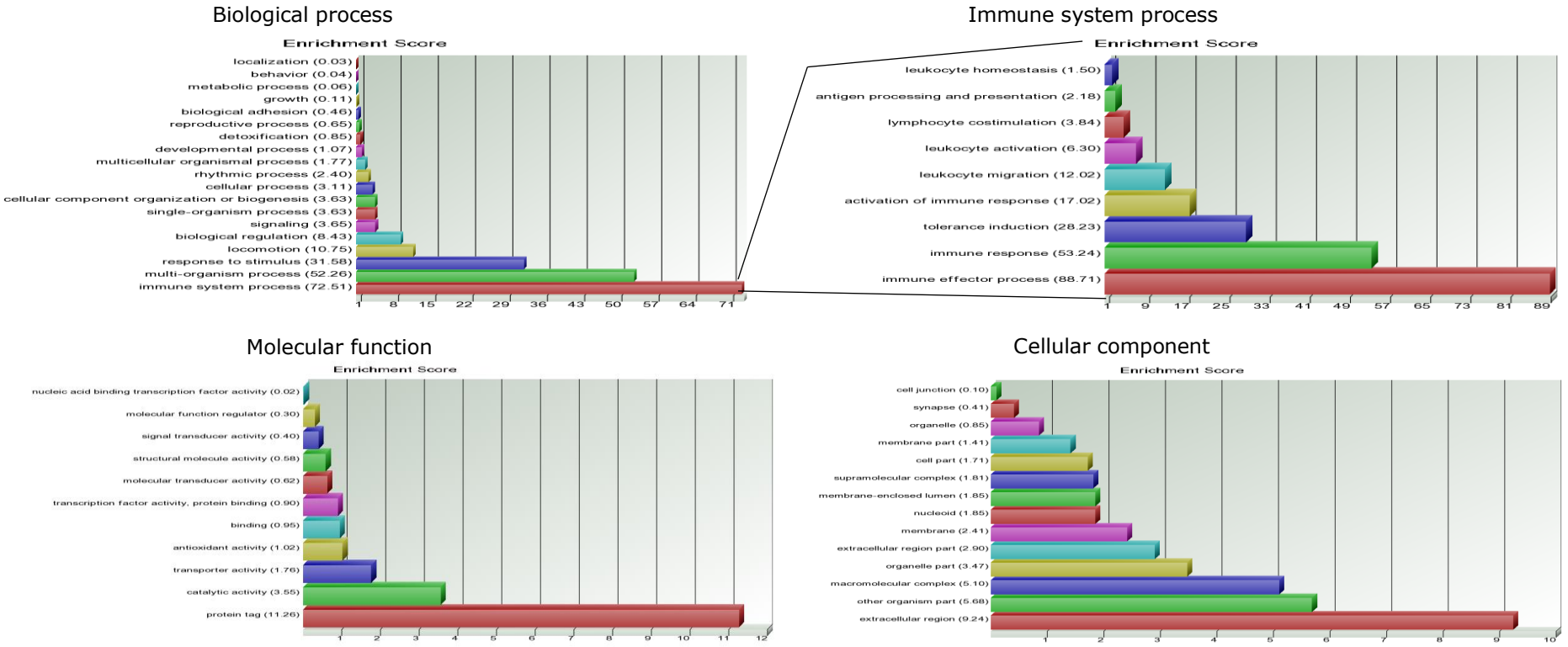



**Figure 5.3.7** ***GO Enrichment analysis performed on the list obtained from the Venn diagram comparison of LAF co-culture vs. LAF mono-culture VS. NHLF co-culture vs. NHLF mono-culture.*** *Image shows the biological process, molecular function and cellular component of the enriched gene targets in the comparative list, arranged in increasing order of their enrichment score. GO Enrichment analysis was performed on the list of transcripts obtained from the intersecting Venn diagram region comparing the two comparative lists. A Chi-squared test was applied to the transcript list and analysis was restricted to functional groups with more than 2 genes. Library file obtained from geneontology.org.*

The enrichment score reflects the degree to which a set of genes, which consist of a biological process, is abnormally overrepresented at the extremes (upregulated or downregulated) in the entire transcript list (Subramanian et al., 2005). Thus, a high enrichment score in the GO analysis meant that there was an increased likelihood that the gene function, defined by the group of elevated transcripts was involved in the phenomena under study.

Figure 5.3.7 shows annotated independent domains obtained from the GO analysis arranged in ascending order of their enrichment score. In this analysis, immune system process showed the highest enrichment score (72.51) under the biological process component. Expanding the immune system process function showed the type of functions involved under this annotation which included immune effector process (88.71) and leukocyte migration (12.02). Most enriched molecular functions were protein tag (11.26) and catalytic activity (3.56) which include protein sequestration, transport or degradation and enzyme-substrate binding reactions respectively (Carbon et al., 2008). Lastly, the most enriched cellular component was again extracellular region (9.24). These highly-enriched gene ontologies suggested that in a co-culture condition, LAFs and NHLFs acquired a pro-inflammatory phenotype.

| Function | Type | Enrichment Score | Enrichment p-value | % genes in group that are present | # genes in list, in group |
|---|---|---|---|---|---|
| type I interferon signalling pathway | biological process | 335.18 | 2.71E-146 | 25.81 | 16 |

| | | | | | |
|---|---|---|---|---|---|
| CXCR chemokine receptor binding | molecular function | 253.52 | 7.88E-111 | 43.75 | 7 |
| 2'-5'-oligoadenylate synthetase activity | molecular function | 189.01 | 8.24E-83 | 75.00 | 3 |
| cytokine-mediated signalling pathway | biological process | 156.38 | 1.22E-68 | 6.89 | 31 |
| response to interferon-alpha | biological process | 148.28 | 4.01E-65 | 30.00 | 6 |
| defence response to virus | biological process | 142.11 | 1.92E-62 | 10.83 | 17 |
| negative regulation of viral genome replication | biological process | 139.08 | 3.95E-61 | 19.15 | 9 |
| response to virus | biological process | 134.90 | 2.60E-59 | 8.54 | 21 |
| response to external biotic stimulus | biological process | 127.10 | 6.36E-56 | 5.07 | 36 |
| response to biotic stimulus | biological process | 121.30 | 2.09E-53 | 4.88 | 36 |

**Table 5.3.6** ***Top 10 enriched GO functions annotated to transcripts on comparison of LAF co-culture vs. LAF mono-culture VS NHLF co-culture vs. NHLF mono-culture.***

GO enrichment analysis yielded 2752 annotated gene functions of the 148 transcripts obtained from this comparison. Table 5.3.6 shows the top 10 highly enriched gene functions arranged by descending order of enrichment score. The most enriched molecular function was CXCR chemokine receptor binding (253.52) followed by chemokine activity (109.52). Highly enriched biological processes also included type I interferon signalling pathway (335.17) and cytokine-mediated signalling pathway (156.38). These data suggested that majority of the upregulated genes in LAFs and NHLFs as a result of co-culture cause an immune response.

### 5.3.8 Pathway Analysis Using Partek Pathway™

Unlike GO analysis, pathway analysis is more specific and detailed which associates a pathway, which comprises of a set of functionally related genes to a disease phenotype (Curtis et al., 2005). The Partek Pathway™

software is able to analyse an aggregation of genes that are clustered together functionally with the help of a predetermined biological knowledge database such as Kyoto Encyclopaedia of Genes and Genomes (KEGG) available at http://www.genome.jp/kegg/ (Partek, 2017c).

*Pathway analysis of intersect list obtained from comparing LAF co-culture vs. LAF mono-culture VS. NHLF co-culture vs. NHLF mono-culture*

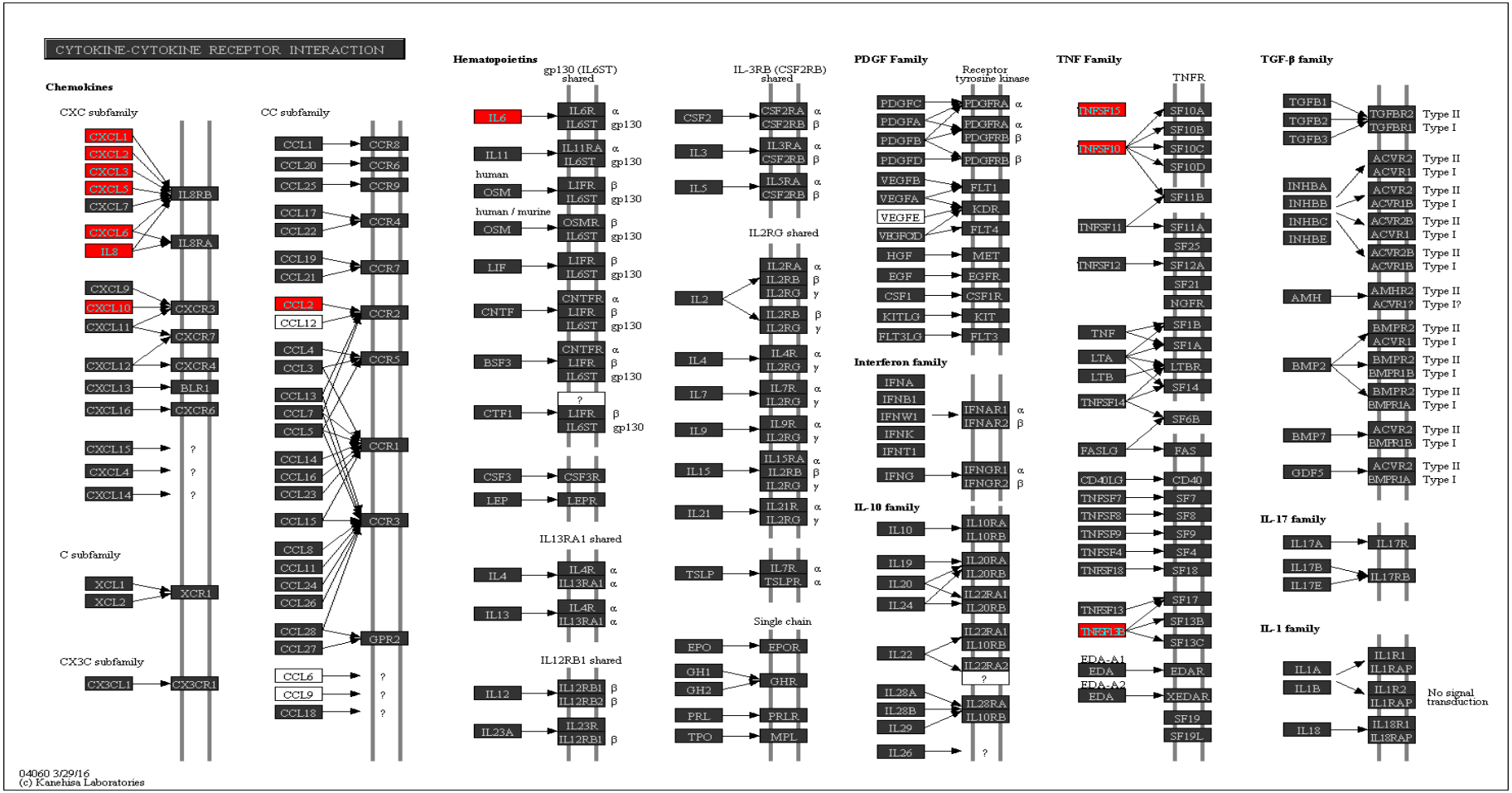
| Pathway Name | Enrichment Score | Enrichment p-value | Culture condition score | # genes in list, in pathway |
|---|---|---|---|---|
| Cytokine-cytokine receptor interaction | 20.15 | 1.77E-09 | 14.33 | 19 |
| TNF signalling pathway | 27.65 | 9.84E-13 | 10.53 | 16 |
| NOD-like receptor signalling pathway | 21.27 | 5.79E-10 | 3.22 | 16 |
| Influenza A | 16.29 | 8.46E-08 | 3.41 | 14 |
| Herpes simplex infection | 12.03 | 5.98E-06 | 3.91 | 12 |
| Chemokine signalling pathway | 11.86 | 7.08E-06 | 11.82 | 12 |
| Metabolic pathways | 0.07 | 0.932619 | 14.02 | 12 |
| Measles | 13.16 | 1.93E-06 | 3.88 | 11 |
| NF-kappa B signalling pathway | 14.61 | 4.51E-07 | 6.06 | 10 |
| Rheumatoid arthritis | 12.54 | 3.58E-06 | 5.93 | 9 |
| Hepatitis C | 9.70 | 6.11E-05 | 4.07 | 9 |
| Pathways in cancer | 2.39 | 0.0918417 | 15.67 | 9 |
| Legionellosis | 14.24 | 6.57E-07 | 5.14 | 8 |
| Toll-like receptor signalling pathway | 7.50 | 0.0006 | 5.60 | 7 |
| RIG-I-like receptor signalling pathway | 7.92 | 0.0004 | 1.92 | 6 |

**Table 5.3.7** ***Pathway analysis of 148 commonly shared transcripts between LAF co-culture vs. LAF mono-culture and NHLF co-culture vs. NHLF mono-culture.*** *Top 15 pathways enlisted arranged in descending order of number of genes in list, in pathway. The enrichment score is the negative natural log of the enrichment p-value derived from the contingency table, Fisher's exact test. The culture condition score is a separate score calculated for the initially considered ANOVA factor and is derived from the negative log (base 10) of the average p-value for the genes within the pathway for each factor respectively (Partek, 2017c).*

Pathway analysis conducted on the Venn diagram intersect yielded a list of 161 pathways. The Partek Pathway™ software with the help of the KEGG database clustered the transcripts from the list into functionally related

genes to a disease phenotype. The top 15 pathways are enlisted in Table 5.3.7 and are arranged in descending order for number of genes in list in pathway. The higher the culture condition score, the lower the p-value for the transcripts that fall into the pathway i.e., they display a greater degree of differential expression. The cytokine-cytokine receptor interaction pathway showed the highest culture condition score of 14.32 and consisted of the highest number of genes from list. The most enriched pathway was the TNF signalling pathway with an enrichment score of 27.64 ($p<0.0001$). This was followed by NOD-like receptor pathway, 21.27 ($p<0.0001$) and chemokine signalling pathway, 11.85 ($p<0.0001$). Other pathways such as NF-kappa B signalling pathway, Pathways in cancer, Toll-like receptor signalling pathway and RIG-I-like receptor signalling pathway were also highly enriched and consisted of at least 6-10 genes from the list.

(a)


CYTOKINE-CYTOKINE RECEPTOR INTERACTION
Chemokines
CXC subfamily
CC subfamily
C subfamily
CX3C subfamily
Hematopoietins
gp130 (IL6ST) shared
IL-3RB (CSF2RB) shared
IL2RG shared
IL13RA1 shared
IL12RB1 shared
Single chain
human
human / murine
PDGF Family
Receptor tyrosine kinase
Interferon family
IL-10 family
TNF Family
TNFR
TGF-β family
IL-17 family
IL-1 family
No signal transduction
04060 3/29/16
(c) Kanehisa Laboratories

(b)

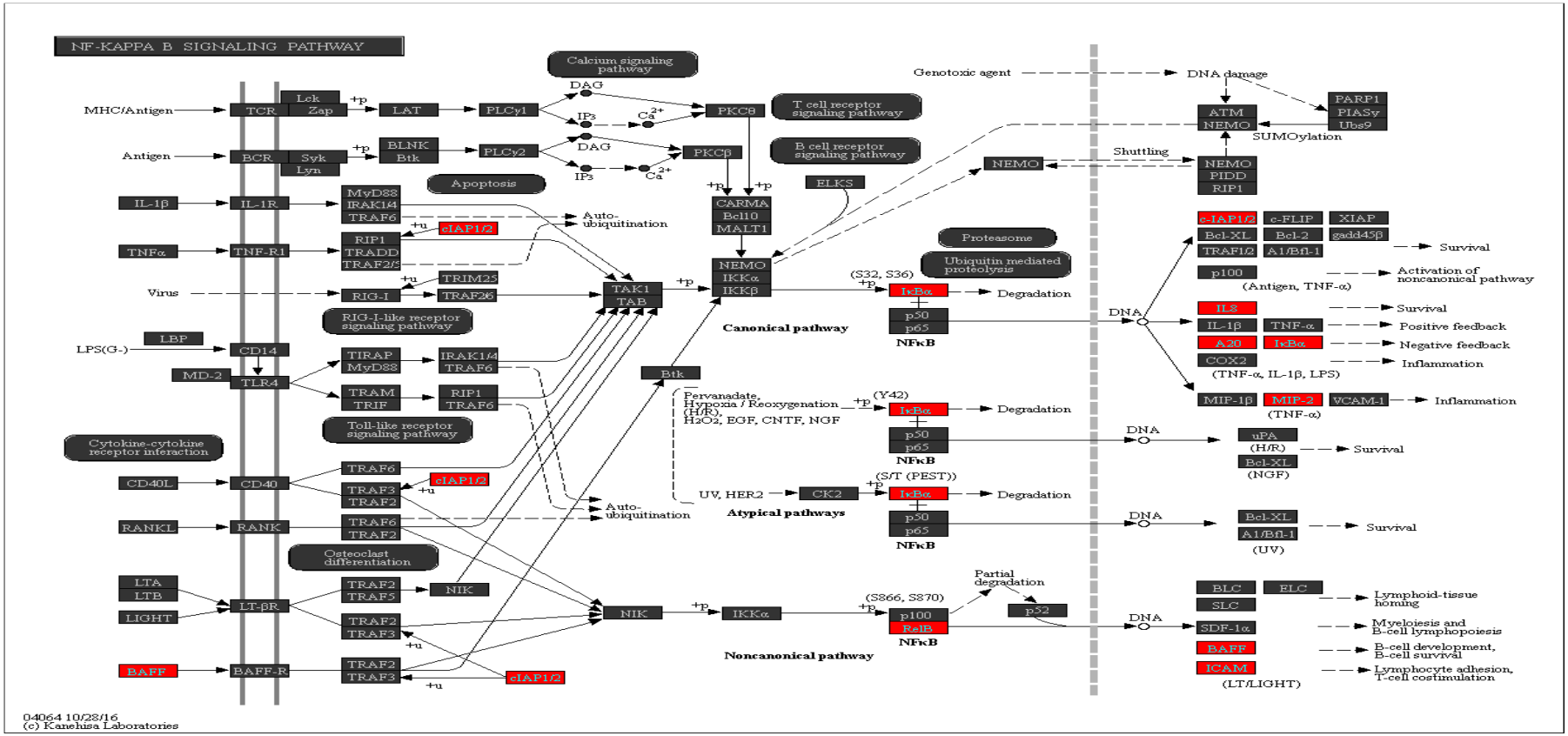



**Figure 5.3.8** ***Diagrammatic illustration of the top 2 most enriched pathways from the comparison list generated by Partek Pathway™.*** *Illustrations of pathways generated using Partek Pathway™ sorted by fold change >2 or <-2. Genes are denoted by gene symbol. Red colour depicts upregulated targets and green colour denotes downregulated targets. Genes in black or white were not present in the list of transcripts obtained. Panel A shows cytokine-cytokine receptor interaction pathway, panel B shows NF-kappa B signalling pathway.*

Figure 5.3.8 shows diagrammatic representations of most enriched pathways from the list. Several chemokines including *CXCL1, CXCL2, CXCL3, CXCL5, CXCL6, CXCL8 (IL8), CXCL10* and *CCL2* were upregulated in the cytokine-cytokine receptor interaction pathway (Figure 5.3.8 (a)) whereas none of the genes from the list were downregulated in this pathway. Upregulated in the NF-kappa B signalling pathway (Figure 5.3.8 (b)) were *ICAM1, NFKBIA* and *TNFSF13b.* All of these top pathways contained almost no downregulated genes from the lists which was in keeping with the heat maps discussed in section 5.3.5 showing several upregulated genes in a co-culture condition and very few downregulated genes.

| Gene Symbol | Gene name | Pathway Name |
|---|---|---|
| CCL2 | chemokine (C-C motif) ligand 2 | Cytokine-cytokine receptor interaction / Chemokine signalling pathway / TNF signalling pathway / NOD-like receptor signalling pathway |
| CXCL1 | chemokine (C-X-C motif) ligand 1 (melanoma growth stimulating activity, alpha) | Cytokine-cytokine receptor interaction / Chemokine signalling pathway / TNF signalling pathway / NOD-like receptor signalling pathway |
| CXCL2 | chemokine (C-X-C motif) ligand 2 | Cytokine-cytokine receptor interaction / Chemokine signalling pathway / TNF signalling pathway / NOD-like receptor signalling pathway |
| CXCL3 | chemokine (C-X-C motif) ligand 3 | Cytokine-cytokine receptor interaction / Chemokine signalling pathway / TNF signalling pathway / NOD-like receptor signalling pathway |
| CXCL5 | chemokine (C-X-C motif) ligand 5 | Cytokine-cytokine receptor interaction / Chemokine signalling pathway / TNF signalling pathway |
| CXCL6 | chemokine (C-X-C motif) ligand 6 | Cytokine-cytokine receptor interaction / Chemokine signalling pathway |

| | | |
|---|---|---|
| CXCL8 | chemokine (C-X-C motif) ligand 8 | Cytokine-cytokine receptor interaction / Chemokine signalling pathway / TNF signalling pathway / NOD-like receptor signalling pathway |
| CXCL10 | chemokine (C-X-C motif) ligand 10 | Cytokine-cytokine receptor interaction / Chemokine signalling pathway / TNF signalling pathway |
| IL6 | interleukin 6 | Cytokine-cytokine receptor interaction / TNF signalling pathway / NOD-like receptor signalling pathway |
| TNFSF10 | tumour necrosis factor (ligand) superfamily, member 10 | Cytokine-cytokine receptor interaction |
| TNFSF13B | tumour necrosis factor (ligand) superfamily, member 13b | Cytokine-cytokine receptor interaction / NF-kappa B signalling pathway |
| TNFSF15 | tumour necrosis factor (ligand) superfamily, member 15 | Cytokine-cytokine receptor interaction |
| ICAM1 | intercellular adhesion molecule 1 | TNF signalling pathway / NF-kappa B signalling pathway |
| MAP3K8 | mitogen-activated protein kinase 8 | TNF signalling pathway / MAPK signalling pathway |
| NFKBIA | nuclear factor of kappa light polypeptide gene enhancer in B-cells inhibitor, alpha | TNF signalling pathway / NF-kappa B signalling pathway |
| TNFAIP3 | tumour necrosis factor, alpha-induced protein 3 | TNF signalling pathway / NF-kappa B signalling pathway / NOD-like receptor signalling pathway |

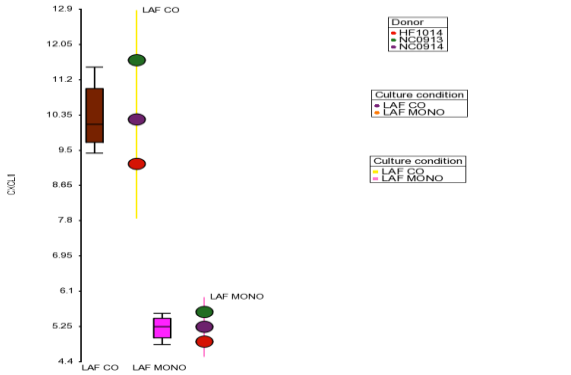
**Table 5.3.8** ***Specific genes from list involved in different highly enriched pathways.***

Functional pathways such as cytokine-cytokine receptor interaction, TNF signalling pathway, NOD-like receptor pathway, chemokine signalling pathway, NF-kappa B signalling pathway, and few others all suggested the existence of a pro-inflammatory disease phenotype. Several upregulated C-X-C chemokines from the comparative gene list, listed in Table 5.3.8 were involved in various inflammatory signalling pathways. As there was such a strong involvement of these chemokines, most of which signalled through the same C-X-C receptor, they were thus chosen to further validate in *in vitro* and *ex vivo* systems.

## 5.3.9 Visualisation of Distribution of Selected Gene Intensities Using Dot Plots and Box and Whiskers Plots

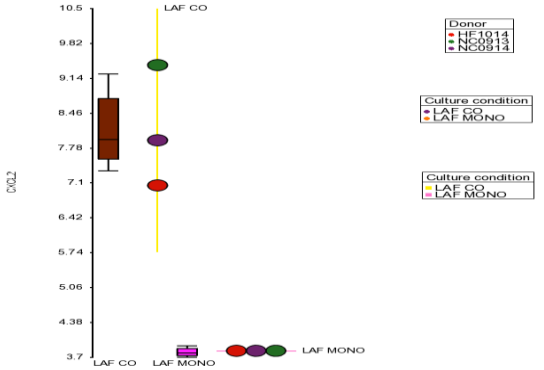
CXCL1

(a)



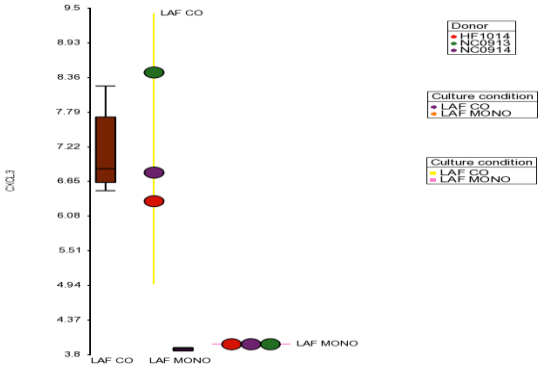

CXCL2

(b)



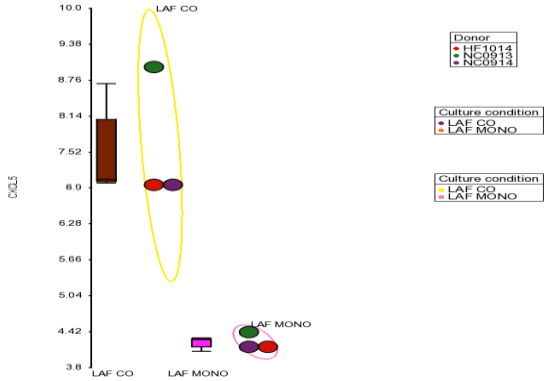

CXCL3

(c)



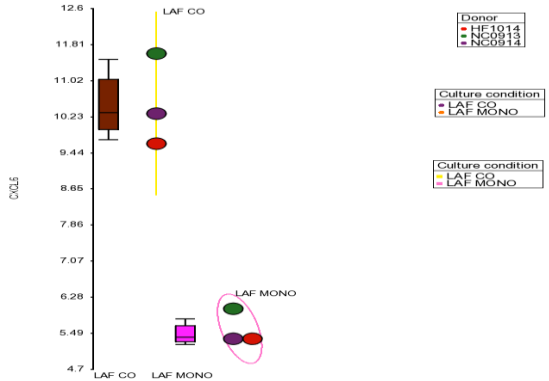

CXCL5

(d)



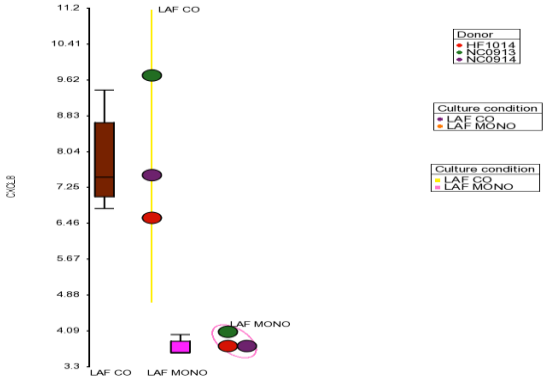

CXCL6

(e)




CXCL8

(f)



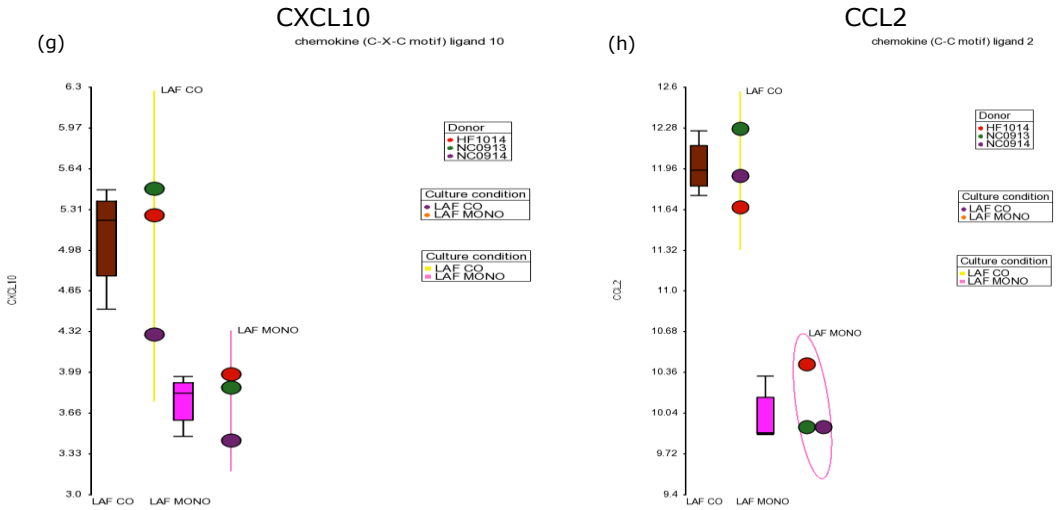
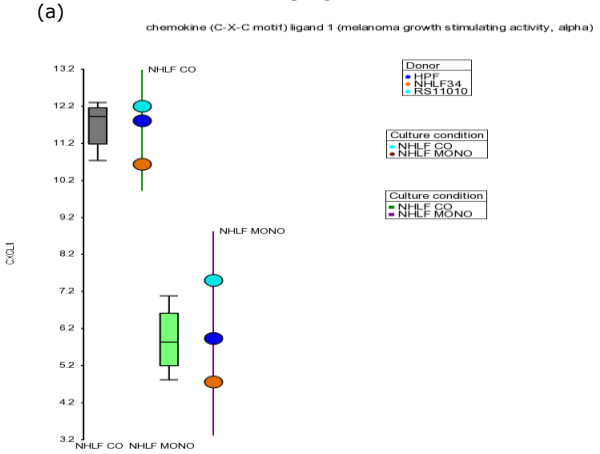


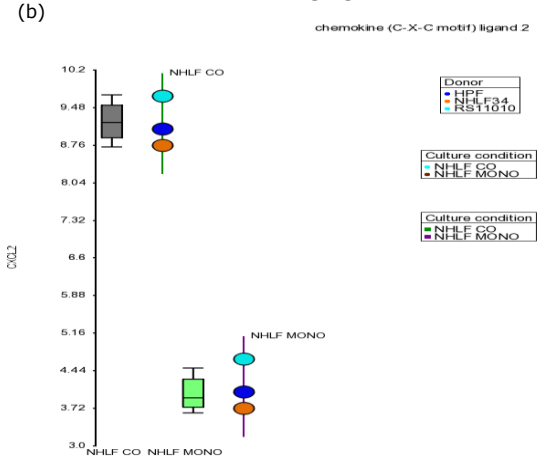

**Figure 5.3.9** ***Dot and box and whiskers plots showing distribution of genes intensities of selected targets in LAFs.*** *Dot and box plots were generated using Partek Genomics Suite™ 6.6. Plots show differential probe (set) / gene intensities of selected chemokines in LAF co-culture (LAF co) and LAF mono-culture (LAF mono). Panels A to H show the intensities of CXCL1, CXCL2, CXCL3, CXCL5, CXCL6, CXCL8, CXCL10 and CCL2 respectively. Probe set intensities are plotted on the Y-axis. Each different colour dot denotes a different LAF donor. Brown box shows LAF co-culture and pink box shows LAF mono-culture.*

Figure 5.3.9 (a to h) shows the differential gene intensities of CXCL1, CXCL2, CXCL3, CXCL5, CXCL6, CXCL8, CXCL10 and CCL2 respectively in LAF co-culture and LAF mono-culture. It was evident from the intensities that in a mono-culture condition, all LAF donors were clustered close together and showed minimal intensity for the selected chemokine targets (pink ellipsoids and pink box plot). However, on co-culturing with 621-101 cells, the donors were more spread out in their intensities (yellow ellipsoids and brown box plot) and one donor in particular, NC0913 (green dot) showed the highest probe intensity for most chemokines. The other two donors, HF1014 (red dot) and NC0914 (purple dot) showed similar yet increased gene intensities.

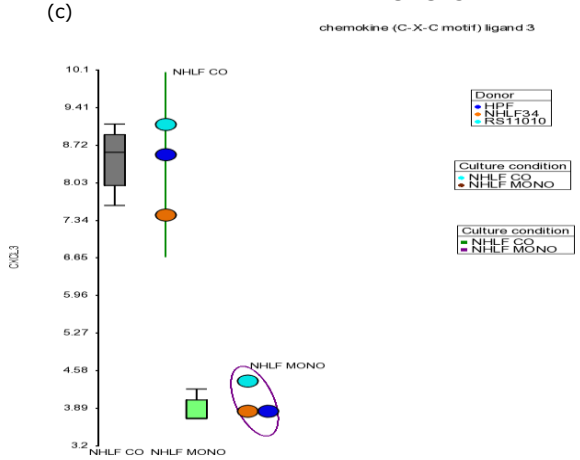
CXCL1



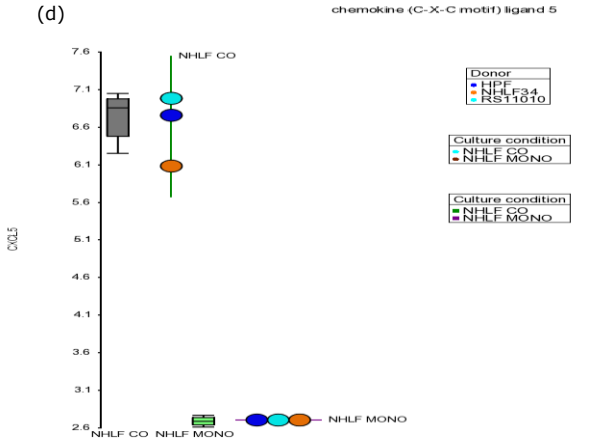

CXCL2



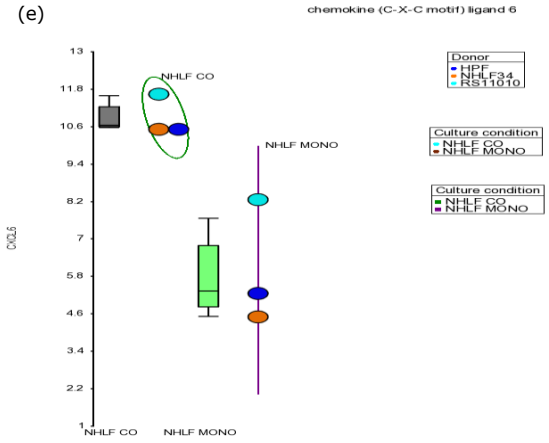

CXCL3



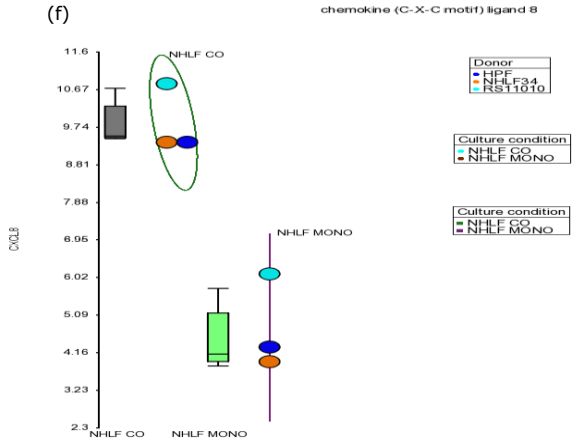

CXCL5




CXCL6




CXCL8



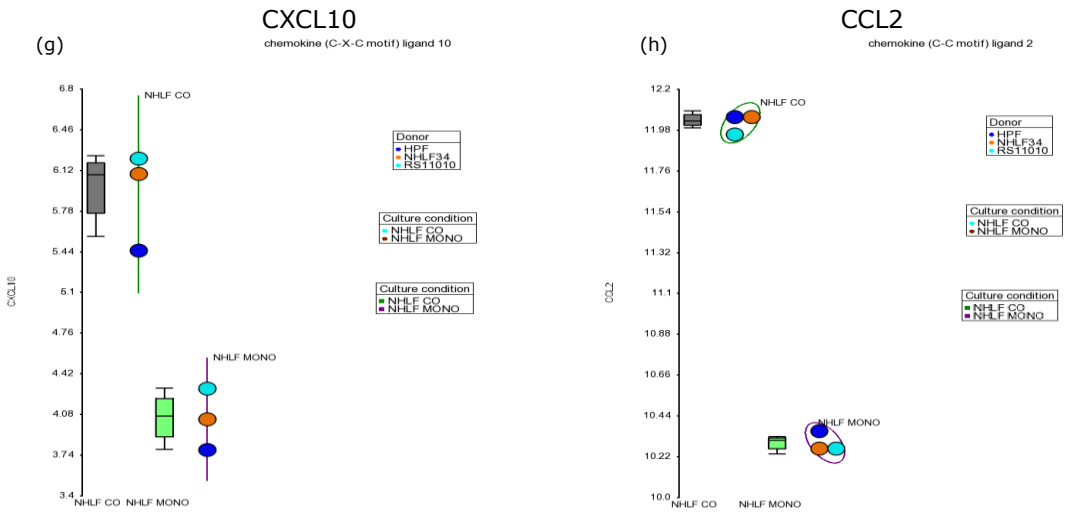



**Figure 5.3.10** ***Dot and box and whiskers plots showing distribution of genes intensities of selected targets in NHLFs.*** *Dot and box plots were generated using Partek Genomics Suite™ 6.6. Plots show differential probe (set) / gene intensities of selected chemokines in NHLF co-culture (NHLF co) and NHLF mono-culture (NHLF mono). Panels A to H show the intensities of CXCL1, CXCL2, CXCL3, CXCL5, CXCL6, CXCL8, CXCL10 and CCL2 respectively. Probe set intensities are plotted on the Y-axis. Each different colour dot denotes a different LAF donor. Grey box shows NHLF co-culture and green box shows NHLF mono-culture.*

Figure 5.3.10 (a to h) shows the differential gene intensities of *CXCL1, CXCL2, CXCL3, CXCL5, CXCL6, CXCL8, CXCL10* and *CCL2* respectively in NHLF co-culture and NHLF mono-culture. Unlike the LAFs, all the NHLF donors showed a degree of variation in the mono-culture condition (pink ellipsoids and green box plots). Although close clustering in a mono-culture condition of the donors was observed in the intensities of *CXCL3, CXCL5* and *CCL2*, the other chemokines showed variable intensities. NHLFs showed very close clustering in both co-culture and mono-culture gene intensities for *CCL2*. The mono-culture gene intensities for *CXCL1, CXCL2, CXCL6, CXCL8* and *CXCL10* however were different in all donors. Donor RS11010 (light blue dot) showed highest intensities for most chemokines while the other two, HPF (dark blue dot) and NHFL34 (orange dot) were mostly similar to each other.

### 5.3.10 Quantitative Real-Time PCR (qRT-PCR) Validation of Selected Gene Targets in LAFs and NHLFs

There is no single best way to validate microarray data, however, qRT-PCR is generally considered the 'gold standard' assay for measuring gene expression and is used by most biologists to confirm microarray data findings (Qin et al., 2006). qRT-PCR analysis was therefore performed using the same RNA sample set for LAFs and NHLFs and using an independent experimental RNA sample set for the same to evaluate consistency between the techniques.

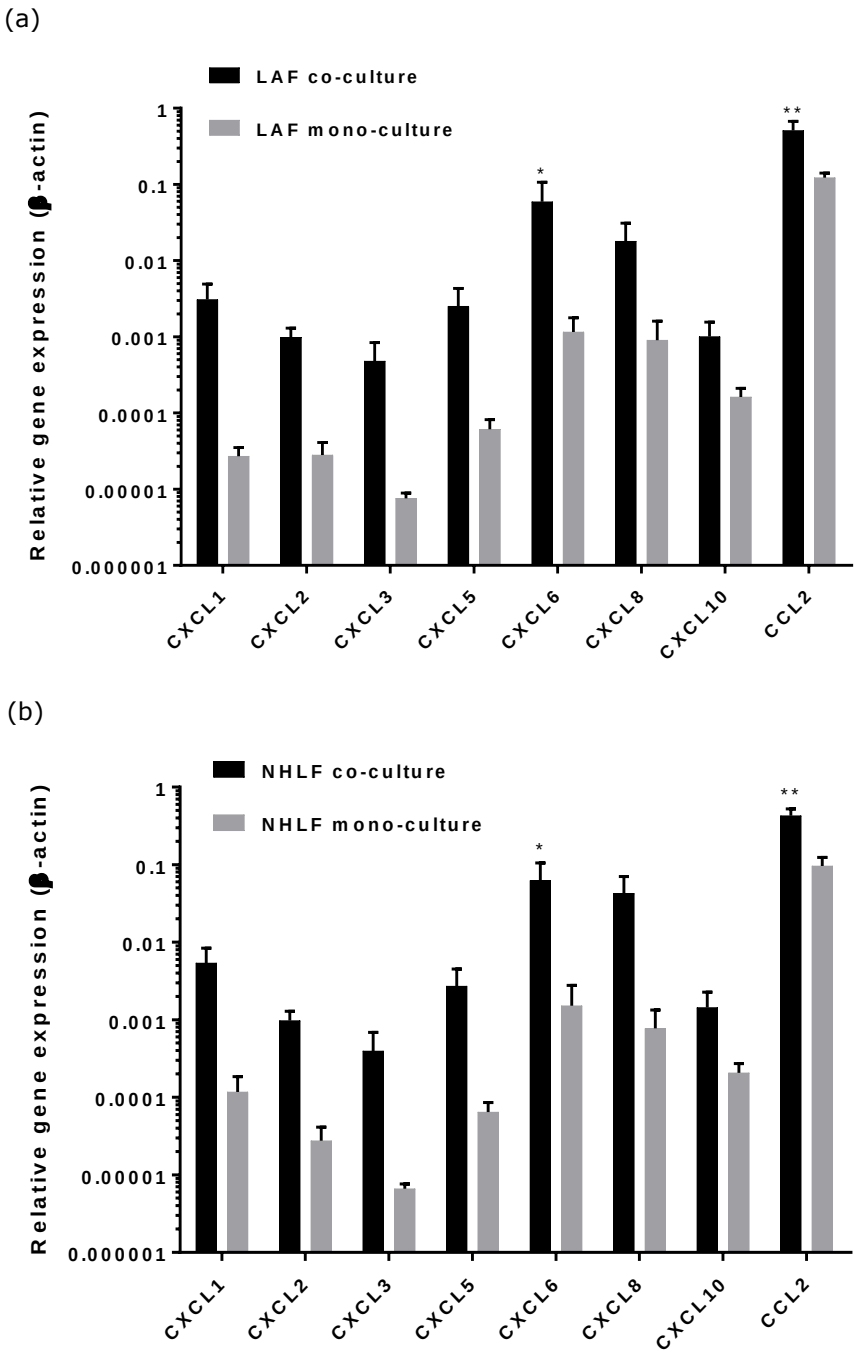



**Figure 5.3.11** ***Initial qRT-PCR validation of selected chemokine targets in LAFs and NHLFs.*** *Quantative gene expression for selected chemokine targets in (a) LAFs (n=3) and (b) NHLFs (n=3). Logarithmic ($log_{10}$) values of expression of target genes were determined relative to β-actin using the $2^{-\Delta CT}$ method and plotted on Y-axis (mean ± SD). Two-tailed Students t-test was performed. *p≤0.05, **p≤0.001.*

Gene expression data from each replicate was combined from both sets of experiments and plotted as shown in Figure 5.3.11. Expression of all the

chemokines was elevated in both LAFs (Figure 5.3.11 (a)) and NHLFs (Figure 5.3.11 (b)) when they were co-cultured with 621-101 cells. This was consistent with the results obtained from the microarray data and also reflected the same trend as that shown by the dot plots discussed in the previous section. *CXCL6* and *CCL2* gene expression was significantly upregulated in both LAFs ($p=0.049$ and $p=0.009$ respectively) and NHLFs ($p=0.0396$ and $p=0.0067$ respectively) in co-culture. Expression of all other chemokines, although elevated in co-culture, did not show a statistically significant change in co-culture compared to mono-culture ($p>0.05$). Expression of C-X-C chemokines in LAF and NHLF mono-culture was found to be marginal compared to their respective co-cultures. All of the upregulated chemokines analysed via qRT-PCR had fold changes greater than 2, consistent with the microarray data. These are denoted in Table 5.3.9.

| Gene name | Fold change increase in LAF co-culture | Fold change increase in NHLF co-culture |
|---|---|---|
| CXCL1 | 93.14 | 189.33 |
| CXCL2 | 35.11 | 35.34 |
| CXCL3 | 42.65 | 59.82 |
| CXCL5 | 33.10 | 42.03 |
| CXCL6 | 48.42 | 110.08 |
| CXCL8 | 21.90 | 65.89 |
| CXCL10 | 6.11 | 6.99 |
| CCL2 | 4.91 | 4.66 |

**Table 5.3.9** ***Fold change increase of chemokine expression in LAF and NHLF co-culture compared to mono-culture.*** *Table shows fold increase of chemokine expression calculated using the* $2^{-\Delta\Delta CT}$ *method.*

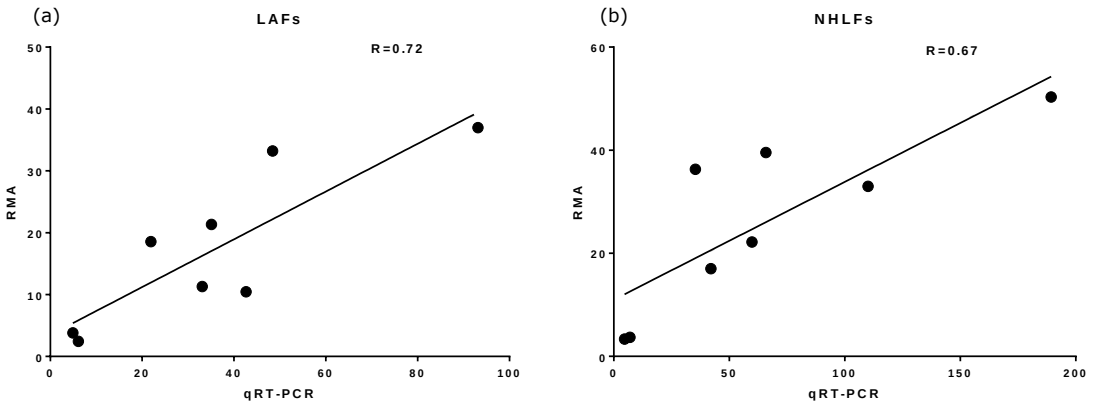



**Figure 5.3.12** ***Spearmans's correlations between fold-change obtained for gene of interest assessed by RMA and qRT-PCR.*** *Graphs show Spearman's correlations between average gene expression levels for (a) LAFs and (b) NHLFs between subsets of interest assessed by RMA and q RT-PCR for the 8 chemokines of interest.*

Figure 5.3.12 shows a Spearman's correlation analysis conducted between the mean fold changes obtained using both the RMA (microarray analysis) and qRT-PCR expression analyses. A significant and strong positive correlation was found between the fold-changes obtained by RMA and qRT-PCR for selected chemokines in LAFs (r=0.81, p=0.021) and NHLFs (r=0.82, p=0.013). Fold change values recorded by q RT-PCR were significantly higher than those obtained from the microarray analysis for the chemokines.

Therefore, based on the fact that each chemokine selected was expressed by LAFs and NHLFs, showed the exact trend as depicted in the microarray data (elevated in co-culture) and showed a fold change of greater than 2, the gene expression changes of the selected targets were considered validated.

## 5.3.11 Effect of β-estradiol (E2) on Gene Expression of Chemokines

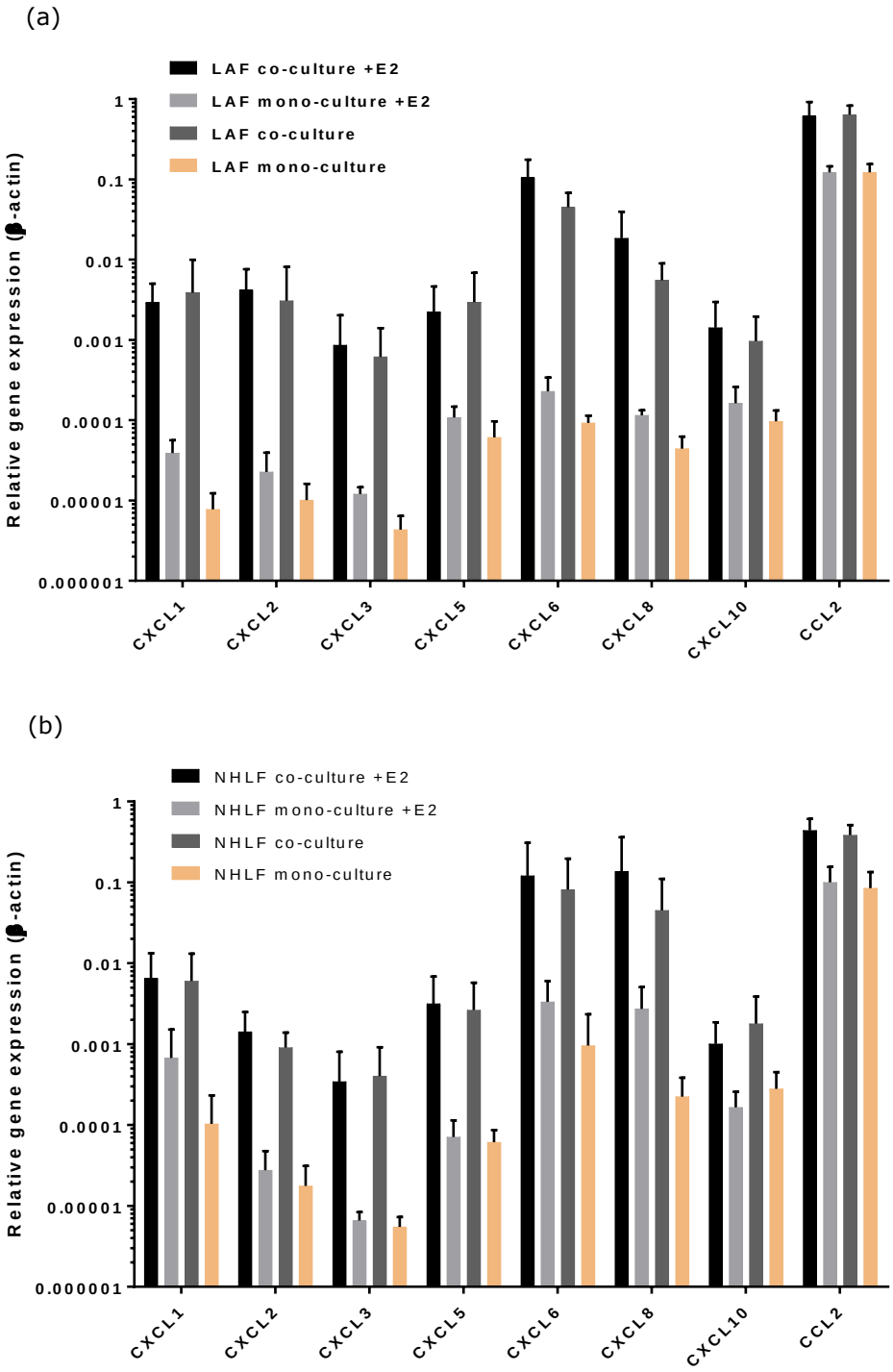



**Figure 5.3.13** ***Second gene expression analysis: Effect of β-estradiol on expression of chemokines in LAFs and NHLFs.*** *Quantitative gene expression of selected chemokines in (a) LAFs (n=3) and (b) NHLFs (n=3) in the presence and absence of E2. Logarithmic ($log_{10}$) values of expression of chemokines were determined relative to β-actin using the $2^{-\Delta CT}$ method and plotted on Y-axis (mean ± SD). Two-tailed Students t-test was performed, no comparisons were found to be significant (p>0.05).*

The initial co-culture experiment was set up with β-estradiol (E2). The subsequent microarray data and initial gene expression analyses were done in the presence of this hormone as the aim was to mimic the *in vivo* environment for LAM. Therefore, in order to assess the effect of E2 on the gene expression of chemokines another similar Boyden chamber experiment was performed.

Expression of selected chemokines in both LAFs (Figure 5.3.13 (a)) and NHLFs (Figure 5.3.13 (b)) did not change in the presence or absence of E2. Chemokine expression remained elevated in co-culture even in the absence of E2 suggesting that the gene expression of selected chemokines was independent of E2. Expression of *CXCL6* was 2.3-fold and 1.5-fold respectively and *CXCL8* was 3.2-fold and 3-fold elevated in LAF and NHLF co-cultures treated with E2 compared to untreated co-cultures. However, none of these comparisons was significant ($p>0.05$). Again, expression of most C-X-C chemokines in LAF and NHLF mono-culture was found to be quite low. Expression of *CXCL1 (5-6.5 fold), CXCL6 (2.5-3.5 fold)* and *CXCL8 (2.6-12 fold)* was slightly elevated in E2-treated LAF and NHLF mono-cultures compared to untreated mono-cultures.

### 5.3.12 Validation of Protein Expression of Selected Chemokines in LAFs

From the microarray and qRT-PCR analyses described in the previous sections, it was evident that the LAFs and NHLFs were very similar in their phenotype and responses to 621-101 cells. It was therefore important to ascertain whether chemokine protein expression followed the same trend as gene expression. This was measured only in the LAFs (n=3) using the Bio-Plex® Pro Human Chemokine Immunoassay system.

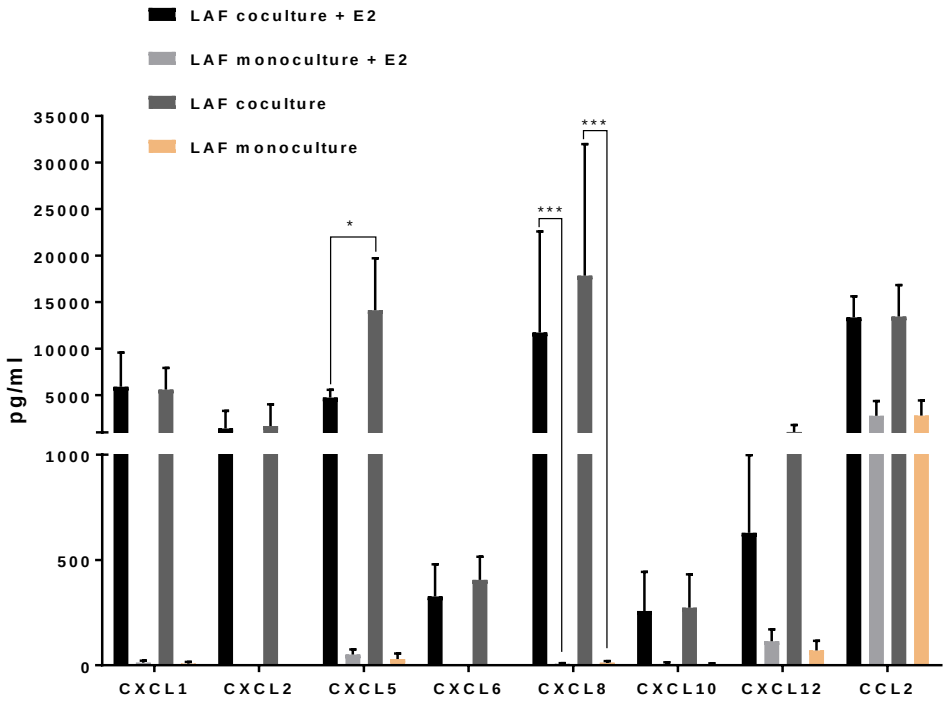



**Figure 5.3.14** ***Protein expression of selected chemokines assessed by Bio-Plex® Multiplex Immunoassay System.*** *Graphical image shows the level of CXCL1, CXCL2, CXCL5, CXCL6, CXCL8, CXCL10, CXCL12 and CCL2 protein expression in LAF culture supernatants. LAF co-culture and LAF mono-culture in the presence and absence of β-estradiol (E2) were assessed and protein levels recorded in pg/ml were plotted on Y-axis (mean ± SD). Two-tailed Students t-test was performed. n=3, *p≤0.05, ***p≤0.001.*

Figure 5.3.14 shows the level of protein expression of chemokines CXCL1, CXCL2, CXCL5, CXCL6, CXCL8, CXCL10, CXCL12 and CCL2 in LAFs. Consistent with gene expression, the expression of all chemokines measured was highly elevated in LAF co-culture compared with LAF mono-

culture. Again, E2 did not show any additive effect on the expression of chemokines reflecting gene expression data. Expression of CXCL1 was elevated more than 500-fold in LAF co-cultures with and without E2 treatment compared their respective mono-cultures. Expression of CXCL2 and CXCL6 was undetectable within the sensitivity of immunoassay. Expression of CXCL5 was significantly elevated ($p=0.011$) in LAF co-cultures without E2 compared to LAF co-cultures treated with E2. Expression of CXCL8 was significantly increased in both LAF co-cultures with ($p=0.0008$) and without ($p<0.0001$) E2 compared to the corresponding LAF mono-cultures. Although CXCL12 was not part of the Venn diagram intersect lists and had appeared only expressed by LAF co-culture, the expression of this chemokine was assessed as it has been suggested that *in vivo*, fibroblasts may be recruited via the CXCR4/CXCL12 axis (Clements et al., 2015, Clements et al., 2010). Again, similar to the other chemokines, CXCL12 expression was 5.5-fold elevated in LAF co-culture with E2 and almost 15-fold upregulated in LAF co-culture without E2 when compared to their corresponding mono-cultures. This increase in CXCL12 however, was not statistically significant ($p>0.05$). Expression of all other chemokines although elevated in both E2 and non-E2 co-culture conditions, did not show a statistically significant change when compared to mono-culture ($p>0.05$). Expression of most C-X-C chemokines was found to be very low.

The expression pattern described in sections 5.3.10 and 5.3.11 where elevated chemokine gene expression was observed in LAFs and NHLFs when co-cultured with 621-101 cells and the analogous protein expression

pattern observed both suggested that the 621-101 cells induce a chemokine signature in LAFs and NHLFs at both gene and protein level. Therefore, in the next section 621-101 cells and the effect of E2 on Rapamycin on their chemokine expression was assessed via the multiplex immunoassay.

5.3.13 Effect of E2 and Rapamycin on 621-101 Cell Chemokine Expression

It was evident that 621-101 cells induced chemokine gene and protein expression in the LAFs and NHLFs. Therefore, in order to determine whether this was due to their lack of TSC2 and therefore dysregulation of mTOR or the effect of oestrogen signalling due to the fact that 621-101 cells like LAM cells express oestrogen receptor α (ERα) (Yu et al., 2004), 621-101 cells were pre-treated with 10nM rapamycin or 10nM β-estradiol

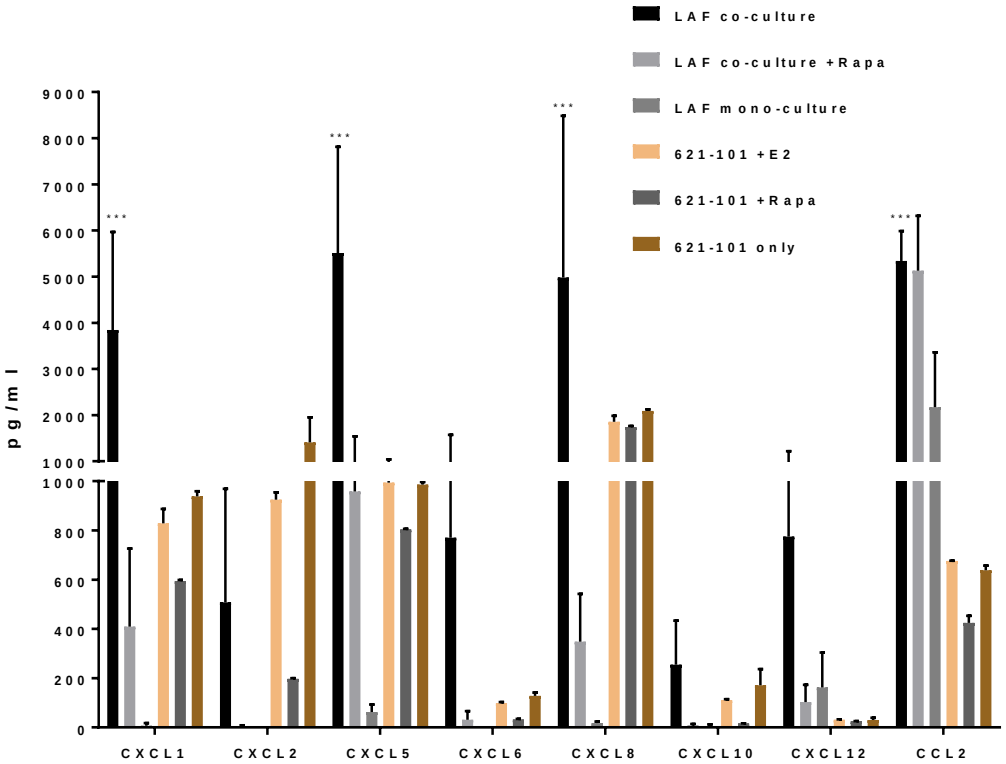



**Figure 5.3.15** ***Expression of chemokines in LAF co-culture, LAF mono-culture and 621-101 cell mono-culture assessed by Bio-Plex® Multiplex Immunoassay System.*** *Graphical image shows the level of CXCL1, CXCL2, CXCL5, CXCL6, CXCL8, CXCL10, CXCL12 and CCL2 protein expression culture supernatants. Chemokine expression levels in LAF co-culture, LAFs co-cultured with 621-101 pre-treated with rapamycin, LAF mono-culture and 621-101 cells treated with E2 and rapamycin were measured and protein levels (pg/ml) were plotted on the Y-axis (mean ± SD). Two-way ANOVA performed corrected for multiple comparisons using the Bonferroni correction method. n=3, ***p≤0.001.*

Figure 5.3.15It was evident that 621-101 cells induced chemokine gene and protein expression in the LAFs and NHLFs. Therefore, in order to determine

whether this was due to their lack of TSC2 and therefore dysregulation of mTOR or the effect of oestrogen signalling due to the fact that 621-101 cells like LAM cells express oestrogen receptor α (ERα) (Yu et al., 2004), 621-101 cells were pre-treated with 10nM rapamycin or 10nM β-estradiol

***Figure 5.3.15*** shows the expression of selected chemokines in LAF co-cultures, LAF co-cultures + rapamycin (LAFs + rapamycin pre-treated 621-101 cells), LAF mono-cultures, 621-101 cells + E2, rapamycin pre-treated 621-101 cell mono-cultures and untreated 621-101 cells. Chemokine responses measured (pg/ml) from the 621-101 cells in mono-culture were therefore normalised to their ratio within the co-culture, i.e., each response was divided by 10 after which data were plotted as seen. Expression of CXCL1, CXCL5, CXCL8 and CCL2 were significantly elevated ($p<0.0001$, $n=3$) in LAF co-cultures compared to 621-101 cell mono-cultures untreated and treated with E2 and rapamycin. Expression of CXCL6, CXCL10 and CXCL12 was more than 6-fold, 1.5-fold and 26-fold respectively elevated in LAF co-cultures compared to 621-101 cell mono-cultures. However, this was not found to be a statistically significant change ($p>0.05$). Unlike the expression of other chemokines, CXCL2 expression was 1.8 and 2.8-fold higher in 621-101 cell mono-cultures treated with E2 and rapamycin respectively compared to LAF co-cultures. Compared to LAF co-cultures expression CXCL1, CXCL5 and CXCL8 was significantly reduced ($p<0.0001$, $n=3$) in LAF and rapamycin pre-treated 621-101 cell co-cultures. Expression of CXCL2 and CXCL10 was almost completely abrogated in LAFs co-cultured with rapamycin pre-treated 621-101 cells whereas CCL2 expression remained unaffected by rapamycin pre-

treatment in co-cultures. Except for the expression of CXCL8 and CXCL12 expression of all other chemokines reduces by at least 20% in 621-101 cell mono-cultures pre-treated with rapamycin. Again, similar to LAF co-cultures and mono-cultures, E2 did show any added effect on chemokine expression in 621-101 cells.

All of the above data suggested that chemokine expression in LAFs was induced by 621-101 cells and this expression was possibly mTOR dependant but not downstream of oestrogen signalling, as pre-treatment of 621-101 cells with rapamycin reduced the expression of selected chemokines in LAF co-cultures.

### 5.3.14 Measuring Protein Expression of Selected Chemokines in *Ex Vivo* LAM Lung Tissue via Bio-Plex® Multiplex Immunoassay System and Immunohistochemistry

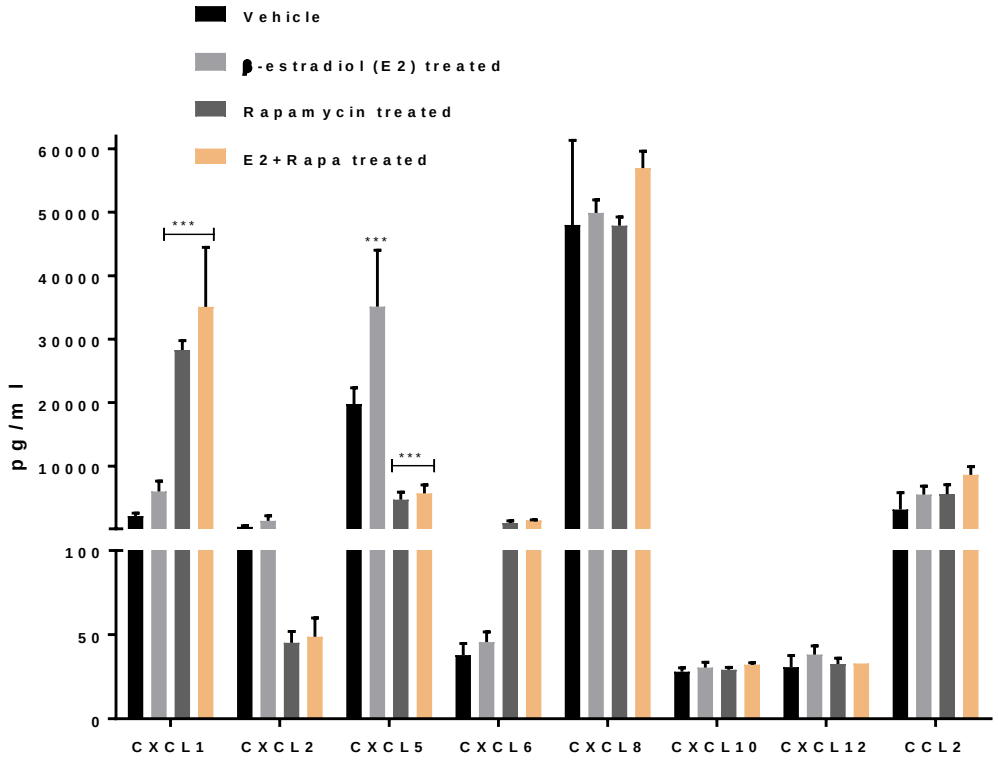



**Figure 5.3.16** ***Expression of selected chemokines in treated LAM lung tissue assessed by Bio-Plex® Multiplex Immunoassay System.*** *Protein levels of selected chemokines measured in culture supernatants obtained from LAM lung tissue treated with vehicle (DMSO), 10nM β-estradiol (E2), 10nM Rapamycin and a combination of 10nM E2 and Rapamycin. Two-way ANOVA performed corrected for multiple comparisons using the Dunnett's multiple comparisons method. ***p≤0.001, n=12.*

LAM lung tissue explants were generated from transplant lung tissue from two donors as described in section 2.2.7. Tissue supernatants were collected and expression of chemokines was measured using the Bio-Plex® Pro Human Chemokine assay panel. Expression of CXCL5 was found to be significantly elevated (p=0.0003) in all parenchymal areas in both donors (Figure 5.3.16) when treated with E2 compared to vehicle treated tissue. CXCL5 expression was significantly decreased when tissue was treated

with rapamycin ($p=0.0004$) and a combination of E2 and rapamycin ($p=0.0009$). On the contrary, expression of CXCL1 however, increased significantly when tissue was treated with rapamycin and with a combination of E2 and rapamycin (both $p<0.0001$). Like CXCL5, expression of CXCL2 was almost 19-fold elevated in vehicle and E2 treated tissue compared to rapamycin treated and combination of E2 and rapamycin, however the increase in expression was not statistically significant ($p>0.05$). CXCL6 expression pattern was like that of CXCL1, 30-fold elevated in rapamycin and combination of E2 and rapamycin treated tissue. Expression of all other chemokines in tissue was unaffected by either E2 or rapamycin or a combination of both.

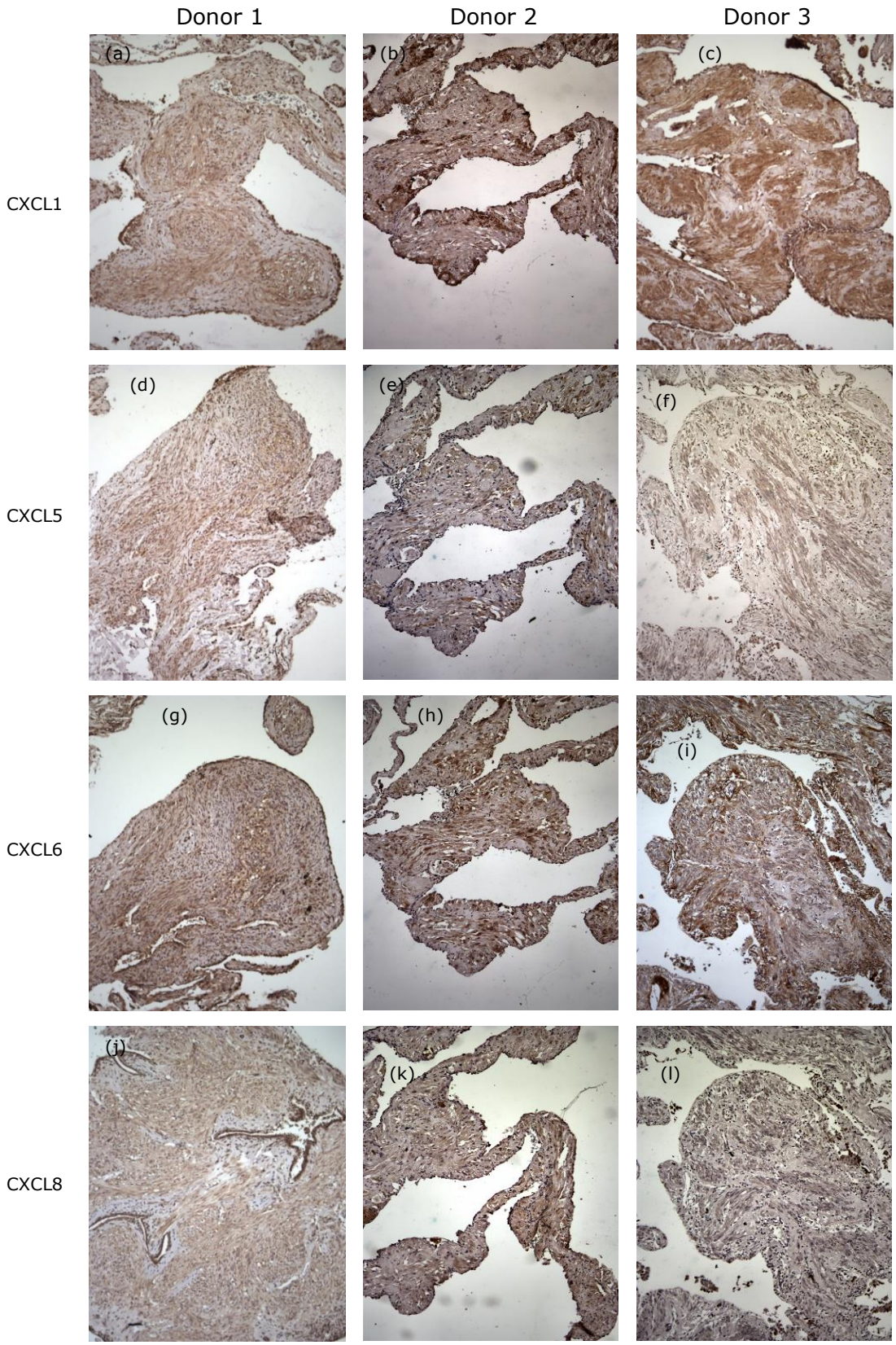



**Figure 5.3.17** ***Chemokine expression in LAM nodules.*** *Image shows nodules from three LAM lung tissue donors (n=3) reacting positively with antibodies against CXCL1 (a-c), CXCL5 (d-f), CXCL6 (g-i) and CXCL8 (j-l). Images are x10 magnified taken using a Nikon Diaphot 300 Inverted Phase microscope.*

To investigate whether chemokines were expressed in LAM nodules immunohistochemistry was used with antibodies against the selected chemokines concentrations of which are detailed in Table 2.1.3. Figure 5.3.17 shows the expression of these chemokines in LAM nodules present in tissue from three transplant LAM donors. Expression of CXCL1 was mainly seen in and around the spindle-shaped cells within the nodules in all three donors. Strong immunoreactivity to CXCL1 antibody (Figure 5.3.17 (a-c)) was also seen in the cells lining the nodules, possibly type II pneumocytes. Similar to the expression of CXCL1, CXCL5 (Figure 5.3.17 (d-f)), CXCL6 (Figure 5.3.17 (g-h)) and CXCL8 (Figure 5.3.17 (j-l)) was mainly observed in and around the spindle-shaped cells within the nodules. Like CXCL1, CXCL6 was also expressed by the type II pneumocytes lining the nodules. Expression of CXCL8 was faint in the LAM donors, possibly attributed to low antibody affinity. However, strong immunoreactivity to the CXCL8 antibody was also detected in the cells lining possibly the lymphatic vessels within the nodules.

All of the above observations suggested that the expression of selected chemokines was detected in LAM nodules and these chemokines are likely to be expressed mainly by spindle-shaped cells within the nodules. A shortcoming of this study however, was the lack of availability of normal matched donors and the lack of a normal equivalent of a LAM nodule for comparison of chemokine expression.

### 5.3.15 Expression of Selected Chemokines in 3D Culture Model – LAM Spheroids

In order to further validate the LAM spheroid model generated, chemokine protein expression was measured in the resulting LAM spheroids and co-culture supernatants to assess whether cells in both 2D and 3D cultures behaved in the same manner with regards to chemokine protein expression.

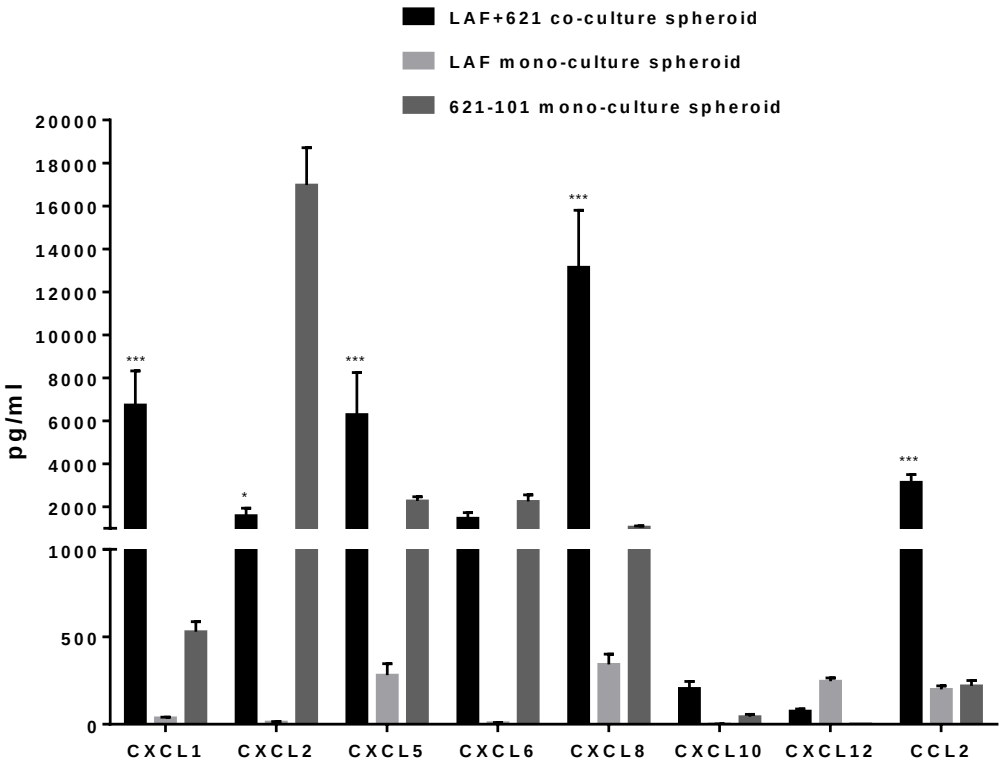



**Figure 5.3.18** ***Expression of selected chemokines in 3D LAM spheroid model assessed by Bio-Plex® Multiplex Immunoassay System.*** *Graph shows protein levels of chemokines measured in culture supernatants obtained from co-culture and mono-culture LAM spheroids (n=3) (mean ± SD). Two-way ANOVA performed corrected for multiple comparisons using the Dunnett's multiple comparisons method. n=3, *p≤0.05, ***p≤0.001.*

Six spheroids per donor per condition were set up and the spheroids were maintained in culture for 4 days after which supernatants were collected and chemokine expression was measured. Chemokine responses measured (pg/ml) from the 621-101 cells in mono-culture were normalised

to their ratio within the co-culture, i.e., each response was divided by 10 after which data were plotted.

Figure 5.3.18 shows the expression of selected panel of chemokines in LAM spheroids. Similar to 2-dimensional (tissue culture plastic) culture (Figure 5.3.14 and Figure 5.3.15), the expression of most chemokines was elevated in co-culture compared to LAF mono-culture. Expression of CXCL1, CXCL5 and CXCL8 was significantly elevated in LAF+621 co-culture spheroids (LAM spheroids, $p<0.0001$). CXCL2 expression was also significantly increased in LAM spheroids ($p=0.05$), however, 621-101 mono-culture spheroids showed a 10-fold increase in CXCL2 compared to LAM spheroids. This pattern was reflective of that seen in 2D culture (Figure 5.3.15) where CXCL2 expression was 2.8-fold higher in 621-101 cell mono-culture. Expression of CCL2 was also significantly increased in LAM spheroids compared to LAF mono-culture and 621-101 cell mono-culture spheroids ($p=0.0002$). CXCL12 expression on the other hand was negligible in 621-101 mono-culture spheroids but 3.3-fold increased in LAF mono-culture spheroids when compared to LAM spheroids. The expression of CXCL6 and CXCL10 although elevated in LAM spheroids was not found to be statistically significant.

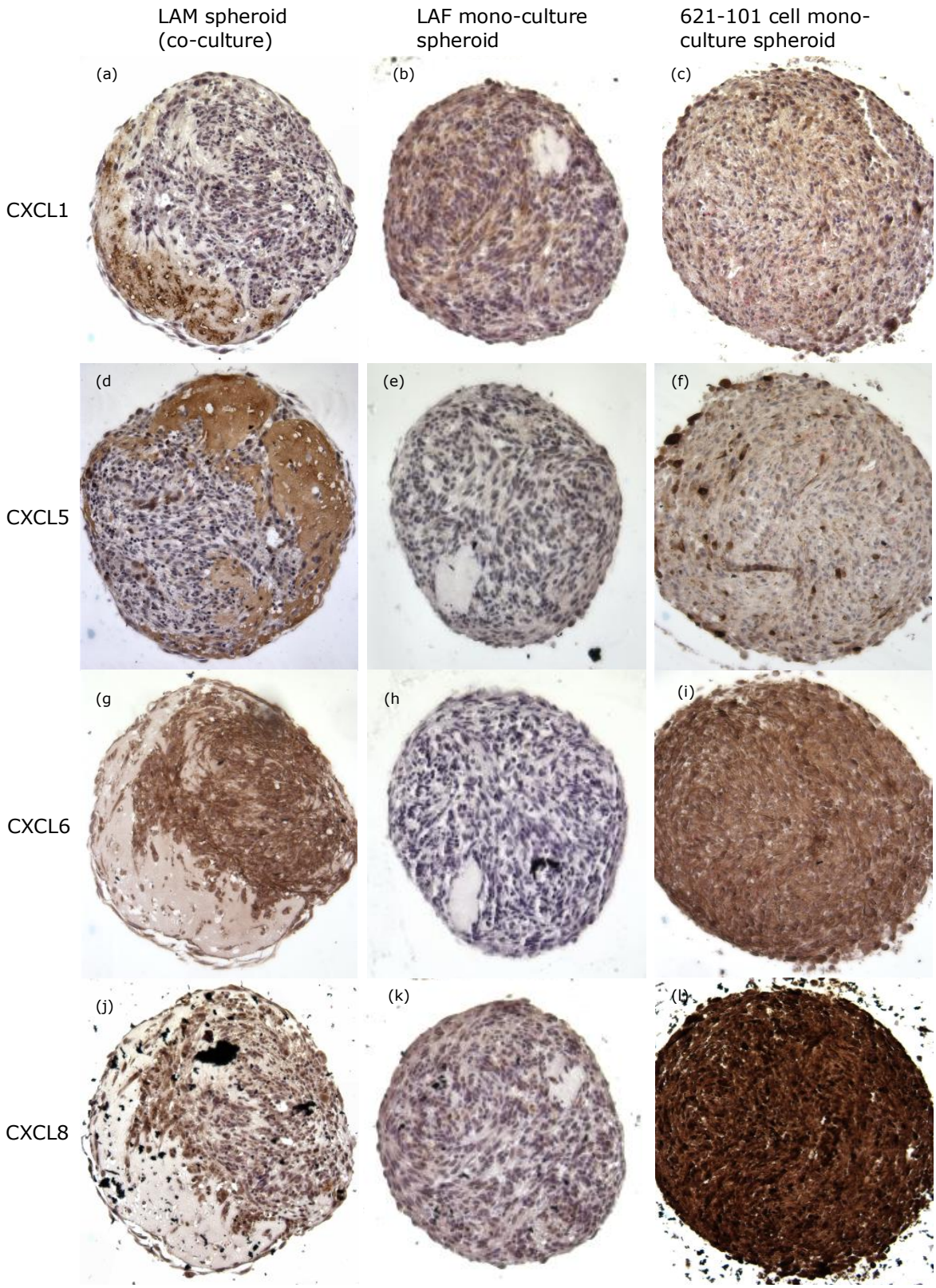



**Figure 5.3.19** ***Expression of C-X-C chemokines in LAM spheroids assessed via immunohistochemistry.*** *Image shows LAM spheroids and mono-culture spheroids showing a positive reaction to antibodies against chemokines CXCL1 (panels A-C), CXCL5 (panels D-F), CXCL6 (panels G-I) and CXCL8 (panels J-L). Images are x20 magnified and taken using a Nikon Diaphot 300 Inverted Phase microscope.*

LAM spheroids and LAF and 621-101 cell mono-culture spheroids consisting of a total of $10^5$ cells were fixed, embedded and sectioned as described in section 3.2.8. Spheroid sections were then immunostained with antibodies against CXCL1, CXCL5, CXCL6 and CXCL8, concentrations of which are detailed in Table 2.1.3.

Figure 5.3.19 shows the expression of CXCL1 (a-c), CXCL5 (d-f), CXCL6 (g-i) and CXCL8 (j-l) in LAM spheroids and LAF and 621-101 cell mono-culture spheroids generated from 4 LAF donors. LAM spheroids showed expression of all C-X-C chemokines. Although CXCL1 was present in the cells in the centre of the LAM spheroid (Figure 5.3.19 (a)), it was seen more in the periphery of the spheroid. This may be attributed to the angle at which the spheroids were embedded. LAF and 621-101 cell mono-culture spheroids (Figure 5.3.19 (b and c)) both showed moderate level of CXCL1 expression.

Like CXCL1, expression of CXCL5 was seen in few centrally located cells and was stronger immunoreactivity was seen in the cells located in the periphery of the LAM spheroids (Figure 5.3.19 (d)). LAF mono-culture spheroids showed negligible to no expression of this chemokine whereas moderate expression of CXCL5 was seen in the 621-101 cell mono-culture spheroids (Figure 5.3.19 (e and f)). Cells within the LAM spheroids (Figure 5.3.19 (g)) reacted strongly to the CXCL6 antibody showing a positive reaction in both centrally and peripherally located cells. LAFs in the mono-culture spheroids did not react positively with CXCL6 antibody, whereas, 621-101 cell mono-culture spheroids showed a strong positive reaction to

the CXCL6 antibody (Figure 5.3.19 (h and i)). This expression pattern was also detected by the Bio-Plex® Pro Human Chemokine assay panel where in fact, 2-D 621-101 mono-culture showed 1.5-fold increase in CXCL6 expression than LAM spheroids.

CXCL8 (Figure 5.3.19 (d)) was expressed in 70-80% of the cells within the LAM spheroid and was seen mainly in the cells within the centre of the spheroid. LAF mono-culture spheroids (Figure 5.3.19 (e)) showed very faint presence of CXCL8 with very few cells expressing this ligand. This was reflective of the immunoassay results obtained CXCL8 where expression was very low in LAF mono-culture. CXCL8 was highly expressed in 621-101 mono-culture spheroids (Figure 5.3.19 (f)). High CXCL8 expression in 621-101 cell mono-culture was also detected by the Bio-Plex® Pro Human Chemokine assay panel.

5.3.16 Expression of C-X-C Motif Chemokine Receptor 2 (CXCR2) in LAM

From the panel of chemokine ligands selected, the C-X-C motif ligands, CXCL1, CXCL2, CXCL3, CXCL5, CXCL6 and CXCL8 all had the same binding receptor, CXCR2 (Lazennec and Richmond, 2010). It was therefore essential to discern whether the LAFs themselves expressed this receptor giving rise to an autocrine signalling loop or the 621-101 cells expressed this receptor leading to paracrine signalling between these cells. Another important point to consider was whether the 621-101 cells show elevated expression of this receptor when co-cultured with LAFs. Data from the transcriptomic analysis had already shed light upon the fact that the LAFs did not show elevated expression of CXCR2 when co-cultured with 621-101 cells. Therefore, RNA isolated from LAFs (n=4) and 621-101 cells in mono-culture and 621-101 cells when co-cultured with LAFs (n=4 donors) was analysed via qRT-PCR.

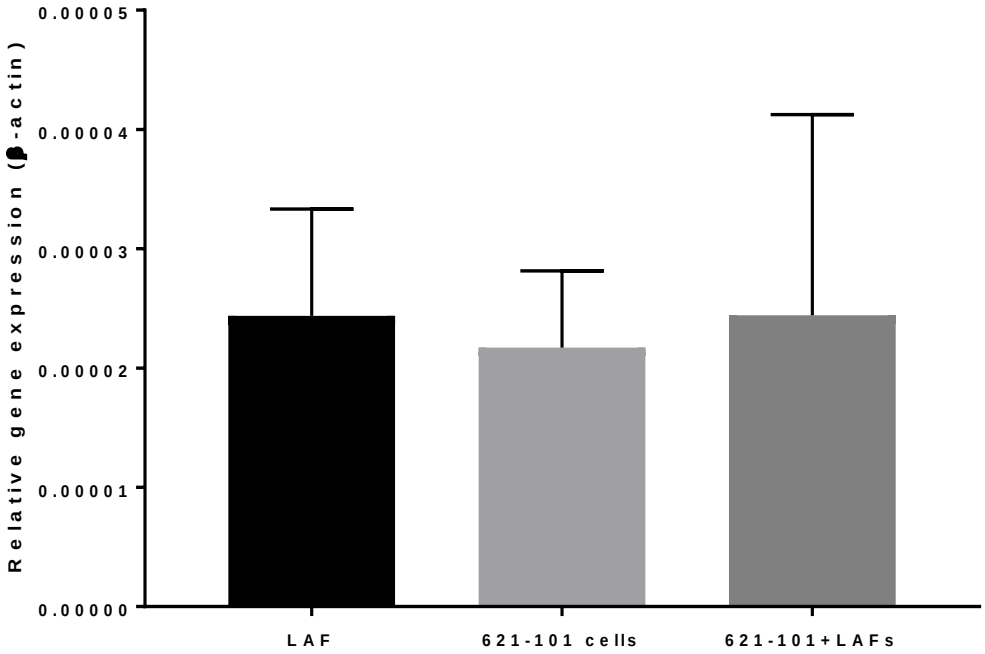



**Figure 5.3.20** ***qRT-PCR analysis for the expression of CXCR2 in LAFs and 621-101 cells.*** *Expression of CXCR2 analysed in LAFs (n=4), 621-101 cells and in 621-101 cells co-*

*cultured with LAFs (n=4) (mean ± SD). Expression levels of CXCR2 was determined relative to a housekeeping gene β-actin using the comparative $C_T$ ($2^{-\Delta C_T}$) method.*

As was evident from Figure 5.3.20, expression of *CXCR2* was extremely low in both LAFs and 621-101 cells. $C_T$ values obtained for both cell types were high suggesting very low to negligible expression of *CXCR2*. The expression of *CXCR2* did not appear elevated in 621-101 cells co-cultured with LAFs and also showed high $C_T$ values similar to LAFs and 621-101 cells in mono-culture.

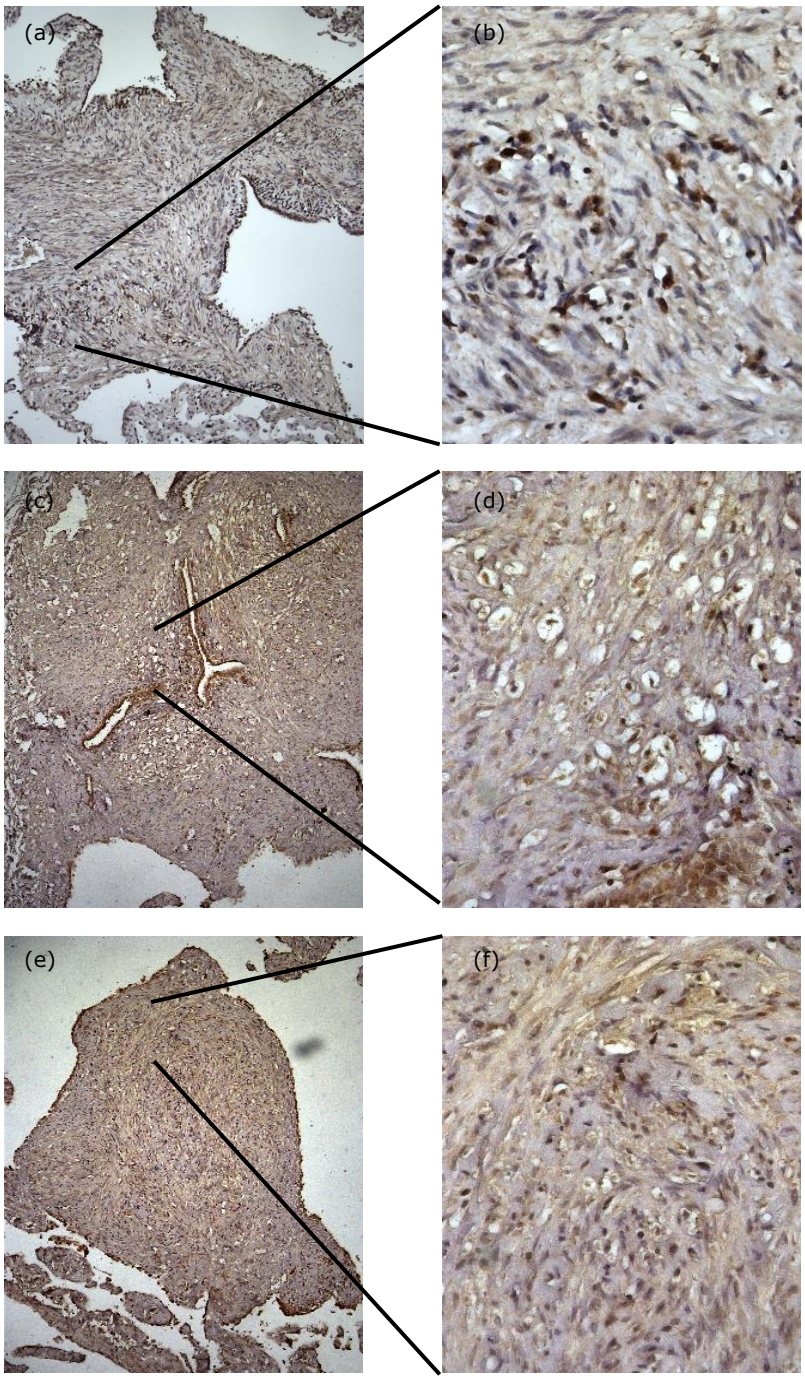



**Figure 5.3.21** ***Immunohistochemical detection of CXCR2 in LAM lung tissue.*** *Image shows the presence of CXCR2 protein in cells within the LAM nodules. Panels A, C, and E depict a LAM nodule magnified x10 and panels B, D and F show a x40 magnification of the cells within the nodule expressing CXCR2. Images were taken using a standard brightfield microscope Nikon Diaphot 300 Inverted Phase microscope.*

From Figure 5.3.20 it was clear that neither of the cells in question expressed the CXCR2 receptor. However, a significant upregulation of the abovementioned chemokines in the LAFs meant there could be other cell

types within the LAM nodule expressing this receptor. An immunohistochemical analysis was therefore performed using three LAM tissue donors to assess the presence of this receptor. Sub-populations of cells within the LAM nodules reacted with anti-CXCR2 antibody (Figure 5.3.21 (a, c and e)). It was interesting to note that the CXCR2 expressing cells had a more rounded appearance and were mostly seen centred near spindle-shaped cells (Figure 5.3.21 (b, d and f)).

### 5.3.17 Presence of Immune Cells in LAM Lung

Although the elevated expression C-X-C chemokine ligands was noted in LAFs in co-culture, an elevated expression of their receptor CXCR2 was not observed in either the LAFs or 621-101 cells. However, the presence of a sub-population of CXCR2 expressing cells in LAM nodules gave rise to the notion that other CXCR2 expressing cell types such as immune cells may be recruited to the LAM nodule via a chemokine signalling mechanism. The chemokine receptor CXCR2 is expressed by various immune cells, including, T cells (Lippert et al., 2004), neutrophils (Hu et al., 2011), macrophages (Patterson et al., 2002) and mast cells (Juremalm and Nilsson, 2005). An immunohistochemical analysis was therefore carried out using marker antibodies against surface antigens expressed by these cells to identify their presence in LAM nodules.

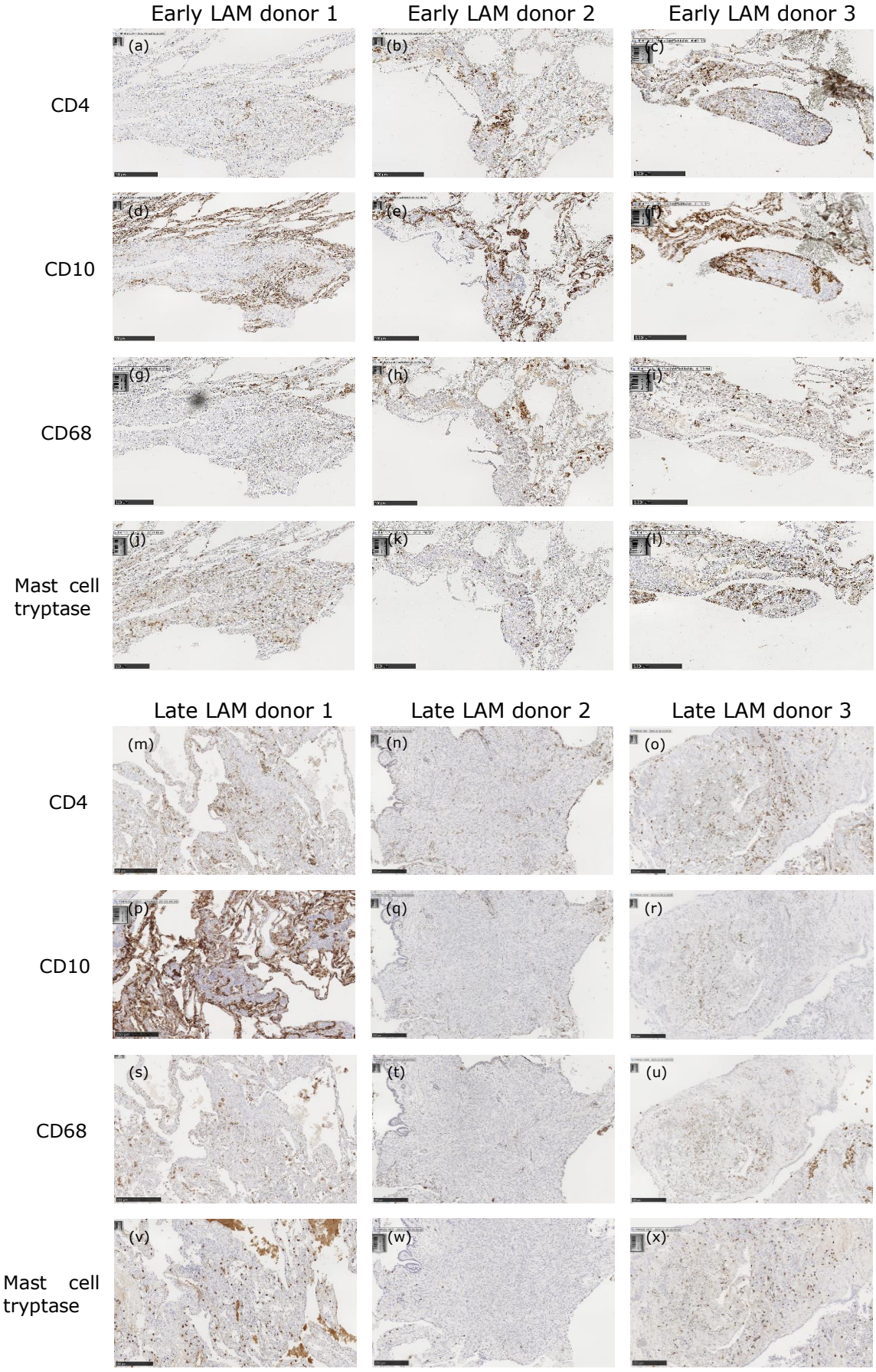

Early LAM donor 1
Early LAM donor 2
Early LAM donor 3
CD4
CD10
CD68
Mast cell tryptase
(a)
(b)
(c)
(d)
(e)
(f)
(g)
(h)
(i)
(j)
(k)
(l)
Late LAM donor 1
Late LAM donor 2
Late LAM donor 3
CD4
CD10
CD68
Mast cell tryptase
(m)
(n)
(o)
(p)
(q)
(r)
(s)
(t)
(u)
(v)
(w)
(x)

**Figure 5.3.22** ***Expression of markers of immune cells in LAM nodules in early and late LAM patients.*** *Image shows the immunohistochemical expression of markers identifying immune cells in nodules of early (top panel) and late (bottom panel) LAM patients. Cells expressing CD4 (helper T cells, panels a-c and m-o), CD10 (neutrophils, panels (d-f and p-r), CD68 (macrophages, panels (g-i) and (s-u) and mast cell tryptase (mast cells, panels (j-l) and (v-x) were identified in LAM nodules. Images were taken using the Hamamatsu Nanozoomer x10 magnified.*

Expression of markers of immune cells, namely, helper T cells, neutrophils, macrophages and mast cells were assessed in both early and late LAM donors. LAM lung tissue obtained at the time of a diagnostic biopsy was considered as early LAM while tissue obtained at the time of lung transplant was considered as late LAM. Four early and four late LAM donors, three of which are discussed here, were assessed using established immune cell markers cluster of differentiation 4 (CD4), cluster of differentiation 10 (CD10), cluster of differentiation 68 (CD68) and mast cell tryptase (MCT) as described in section 5.2.8.

Both early and late LAM donors showed immune cell infiltration within nodules Figure 5.3.22. Presence of helper T cells (CD4) within the nodules was evident in both early and late LAM donors (Figure 5.3.22(a-c) and (m-o)). The CD4 positive T cells were mainly seen accumulated within the nodules and few were also seen in the periphery lining the nodule. It was interesting to note that in the late LAM donors, these CD4 positive cells were mainly seen in areas adjacent to spindle-shaped cells within the nodule. Comparatively fewer cells were seen in the alveolar walls surrounding the LAM nodules.

The presence of neutrophils was also seen in both early and late LAM donors. All the early LAM donors (Figure 5.3.22(d-f)) showed similar CD10

expression but expression in late LAM donors (Figure 5.3.22(p-r)) was very variable. Late LAM donor 1 showed higher infiltration of CD10 positive neutrophils compared to donors 2 and 3. Neutrophils were mainly seen in the periphery of the nodules and a reasonable presence of neutrophils was seen in the alveolar walls.

Presence of CD68 positive macrophages was very low to none in the LAM nodules of both early (Figure 5.3.22(g-i)) and late LAM donors (Figure 5.3.22(s-u)). Macrophages were seen more in the surrounding tissue than within the nodules. However, late LAM donors did show a marginal presence of macrophages within the nodules, these cells were almost absent in the early donor nodules.

Abundant presence of mast cells was seen in both early (Figure 5.3.22(j-l)) and late donors (Figure 5.3.22(v-x)). Tryptase positive mast cells showed large infiltration of nodules and were diffuse throughout the nodule. Few mast cells were also seen in the alveolar walls surrounding the nodules. To determine the amount of immune cell infiltration within the LAM nodules, number of cells per milimeter$^2$ (mm$^2$) per nodule were counted in all four the early and late LAM donors.

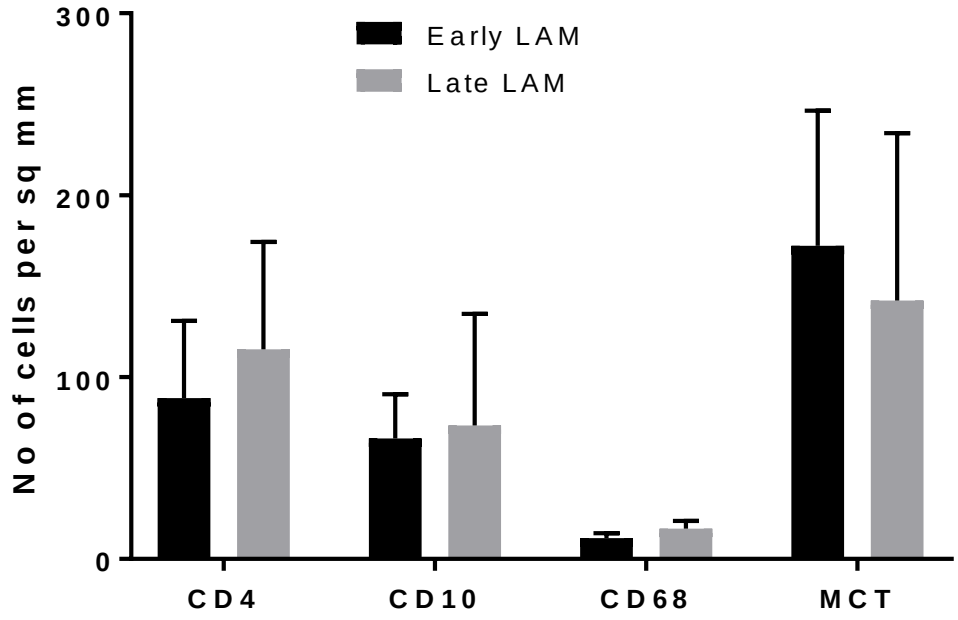



**Figure 5.3.23** ***Number of immune cells per mm² identified by specific markers.*** *Number of immune cells counted per mm² per nodule in early and late LAM donors (n=4) plotted on the Y-axis (mean ± SD). The cells counted were neutrophils, T cells, macrophages and mast cells.*

Figure 5.3.23 shows the number of CD4, CD10, CD68 and MCT positive cells counted per $mm^2$ per nodule. Three different nodules were counted in all the early and late donors. The number of cells per $mm^2$ was then plotted on the Y-axis. The number of CD4 positive T cells were 1.3-fold higher in late LAM donor nodules compared to early LAM donors. Similarly, CD10 positive neutrophils were 1.1-fold higher in late LAM. Macrophage infiltration (CD68 positive) in both early and late LAM donors was negligible. However, tryptase positive mast cells, unlike other immune cells infiltrations, were 1.2-fold higher in early LAM donors than late LAM donors. However, none of these comparisons were statistically significant ($p>0.05$) and several more LAM donors will be required in each group to drawn any confirmed conclusions.

### 5.3.18 Chemotactic Directional Migration of Mast Cells – Boyden Chamber Transwell® Migration Assay

Judging from the number of mast cells counted that infiltrate the nodules, it was postulated that *in vivo*, the TSC2 null cells invoke an elevated expression of C-X-C chemokines ligands. These chemokines, all of which signal through the same receptor, recruit CXCR2 expressing mast cells to the nodules. Although normal matched normal lung controls were not assessed for presence of mast cells in this study, it is a well-known fact that in normal lung the number of mast cells is low. To test this theory, the HMC-1 cell line, derived from a patient with mast cell leukaemia which exhibits a phenotype similar to that of human mast cells (Nilsson et al., 1994) was used. The HMC-1 cells, placed in the upper compartment of a Boyden chamber were allowed to migrate towards LAFs and 621-101 cells in co-culture and mono-culture.

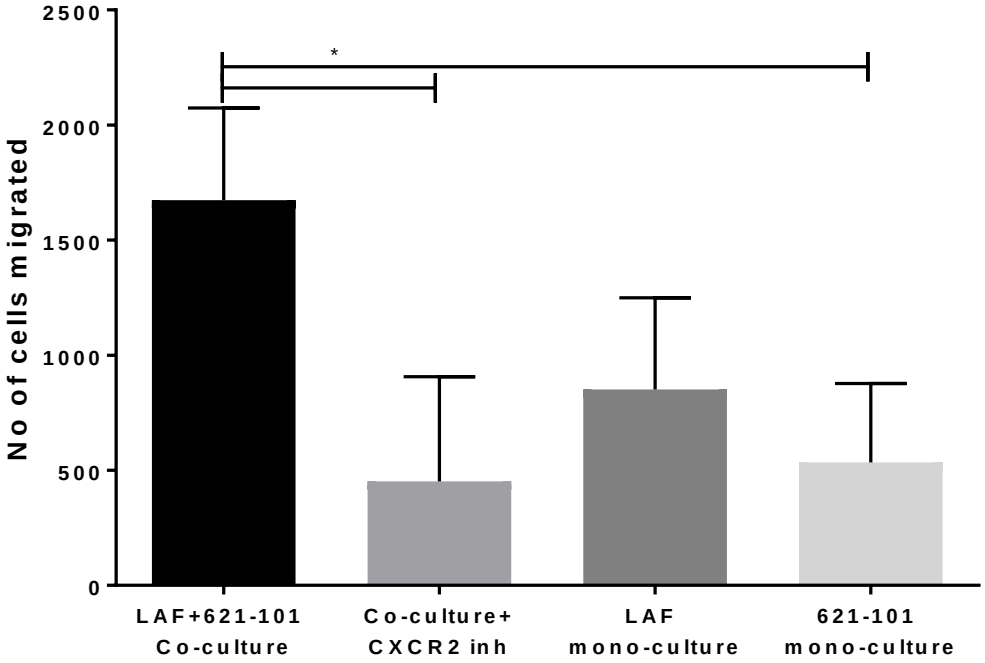


**Figure 5.3.24** ***Chemotactic migration of HMC-1 cells towards LAFs and 621-101 cells in co-culture and mono-culture.*** *Graphical image shows the number of migrated HMC-1 cells migrated towards LAF+621-101 cell co-cultures, Co-cultures treated with 100nM CXCR2 inhibitor (SB225002) and LAF (n=4) (mean ± SD) and 621-101 cell mono-cultures normalised number of cells under gravitational influence normalised to media only control. One-way ANOVA performed corrected for multiple comparisons using the Dunnett's multiple comparisons method. n=4, *p≤0.05.*

Figure 5.3.24 shows the number of HMC-1 cells migrated via a chemotactic gradient. More than 1600 HMC-1 cells migrated towards LAF and 621-101 cell co-cultures over a period of 8 hours. Directional migration was significantly reduced (p=0.035) on treatment of cells with 100nM CXCR2 inhibitor, SB225002. A 50% reduction in HMC-1 cell migration was seen towards LAF mono-cultures and migration significantly reduced (p=0.05) towards 621-101 cell mono-cultures. These data suggested that HMC-1 cells selectively migrated towards C-X-C chemokines released by cells in co-culture via their expression of the CXCR2 receptor.

## 5.4 Discussion

This chapter describes distinct profiles obtained from the LAF and NHLF transcriptomes, selection of the most significant and relevant gene targets obtained thereof and the successful validation of these targets in 2D and 3D LAM models along with *ex vivo* LAM lung tissue. The initial hypothesis that a large mesenchymal cell population exists within LAM nodules and that these cells are wild-type could only be confirmed if LAFs and NHLFs were compared. A comparative transcriptomic analysis thus performed was able to answer two main questions:

- Were LAFs and NHLFs similar or different to each other (essentially the same cell type) and if similar, how similar?
- Does the presence of TSC2 null 621-101 cells have phenotypic implications on LAFs and NHLFs?

The Boyden chamber experimental design was chosen to perform the analyses as this setup took advantage in the fact that both LAFs and NHLFs could communicate with the 621-101 cells via soluble factors and when required could be separated from each other to perform distinct analyses, and β-estradiol was added to mimic the cellular environment *in vivo*.

In the GeneChip® Human Genome U133 Plus 2.0 Array (Affymetrix) each gene is represented by one or more probe sets, each composed of 11-20 pairs of 25 base pairs long. Each of these pairs consists of a perfect match (PM) and a mismatch (MM), the mismatch created by changing the middle ($13^{th}$) base of the perfect match sequence. The mismatch is aimed at controlling experimental variation and nonspecific binding of other mRNA

with the probe (Affymetrix, 2007, Irizarry et al., 2003). The Partek Genomics Suite™ 6.6 (PGS 6.6) software offered quick and easy data normalisation options at the click of a button (Partek, 2017a). After adjusting for GC content to remove the effects of GC content on probe-level intensities the Robust Multi-Array Average (RMA) background correction was used on the dataset. An increasingly widely used method, this is a pre-processing procedure which exclusively makes use of the PM probes and ignores the MM probes and is among the best methods with respect to precision (Irizarry et al., 2003, Heber and Sick, 2006). In most principal component analysis comparisons, the LAF donors clustered close together compared to NHLF donors. This was possibly due to the fact that, while all the LAF donors were isolated and characterised in the same manner, the NHLF donors were commercially bought from two different suppliers and the third donor obtained from another department. Therefore, it would be possible that their global gene probe set intensities were quite different from each other. LAF donors in mono-culture however were more spread out in their probe intensities. This suggested that it is possibly the effect 621-101 cells that imparts a more analogous global expression to the LAFs.

To identify the differentially expressed genes the categorical sample attributes assigned to the dataset were considered as ANOVA factors. Fixed effects were understandably assigned to disease or normal condition as this aspect of donor cells was unchangeable. Culture condition also was a fixed effect because if the experiment was to be repeated, the cells would be cultured in the same manner. However, the donor category was

assigned a random effect because on repeating the experiment, different donors could be used. The ANOVA model thus contained both fixed and random effects making it a 'mixed model ANOVA'.

Historically, differential gene expression was judged purely in terms of fold-change with a typical 2-fold change cut off (DeRisi et al., 1996, Schena et al., 1996). However, considering only fold-change cut-offs did not take into account variability nor did it guarantee reproducibility. Therefore, it has now become common practice to only consider differentially expressed genes that satisfy both a p-value and fold-change criteria simultaneously and where possible the false discovery rate (FDR) is controlled in the analyses (McCarthy and Smyth, 2009). Most researchers consider a statistical significance of $p \leq 0.01$ or $p \leq 0.05$ and then rank significant genes by fold-change with a cut-off of 1.3, 1.5 or 2 (Patterson et al., 2006, Huggins et al., 2008). Filtered gene lists were created from the initial two-way ANOVAs by considering a statistical significance of $p \leq 0.05$ and ranking the significant genes by fold-change with a cut-off of >2 and <-2. The FDR could not be applied as this reduced the list of differentially expressed gene to zero. However, good quality Affymetrix GeneChips® that pass the QA/QC parameters could increase the number of differentially expressed genes while automatically reducing the expected false discovery rate in the identified candidate list (Heber et al., 2006).

To find significant genes commonly shared between two comparative lists Venn diagram comparisons were carried out. The genes that fell into the intersecting region of the two comparative lists were then considered. The

comparison of two lists LAF co-culture vs. LAF mono-culture and NHLF co-culture vs. NHLF mono-culture consisted of genes that changed in both LAFs and NHLFs when cultured as a co-culture with 621-101 cells. The list of top 22 genes showed a majority of upregulated chemokines mainly of the C-X-C motif type. All of these chemokines except CXCL10 contained three amino acid residues (Glutamine-Leucine-Arginine) at the $NH_2$-terminus which confers upon them their chemotactic activity and proangiogenic activities (Clark-Lewis et al., 1993, Strieter et al., 2005). Interestingly the chemokines *CXCL1, CXCL2, CXCL3, CXCL5, CXCL6* and *CXCL8* are located in a short region (360KB) of chromosome 4 (4q21). Bieche et al. reported that all of these chemokines are upregulated in breast cancer due to them being co-regulated. This type of upregulation was observed in breast cancer cells and intratumoural fibroblasts and was found to be a consequence of increased transcriptional activity downstream of nuclear factor kappa-light-chain-enhancer of activated B cells (NFκB) signalling. These genes were also induced by TNFα and correlated with poor prognosis outcomes for breast cancer patients possibly due to increased chemoattractant activity. (Bieche et al., 2007). Therefore, it is possible that this kind of transcriptional activity is at play in this transcriptional analysis resulting in the co-upregulation of the related chemokines.

CCL2 or monocyte chemoattractant protein 1 (MCP-1) is another pro-fibrogenic cytokine that can recruit monocytes, memory T cells and dendritic cells (Carr et al., 1994, Xu et al., 1996). Chen et al. showed that by knocking out IL-17RA expression in mice exposed to cigarette smoke

reduced the induction of CCL2 related macrophage recruitment, MMP12 expression crucial to development of emphysema (Chen et al., 2011). CCL2 expression is elevated in serum starved IPF and normal lung fibroblasts treated with thrombin in a dose-dependent manner and is mediated by transcriptional factors NFκB and AP-1 (Deng et al., 2013). Moreover, CCL2 was found to partially block staurosporin-induced apoptosis of lung fibroblasts through the IL-6/STAT3 pathway thereby promoting fibrosis through anti-apoptotic mechanisms (Liu et al., 2007).

CXCL10 has been known to be significantly upregulated in patients with asthma and COPD and is a potent chemoattractant for activated T cells, natural killer cells and eosinophils (Saetta et al., 2002). Mast cell migration in asthmatic airways is mediated via CXCL10 and its cognate receptor CXCR3 (Brightling et al., 2005). In human lung fibroblasts, CXCL10 gene and protein expression is synergistically elevated by IL-27 and TNF-α which is mediated via NFκB signalling pathways (Dong et al., 2013). MMP1 also known as collagenase-1 is an interstitial collagenase capable of cleaving a broad range of matrix proteins. This protease is also transcriptionally activated by AP-1 (Vincenti et al., 1996). Increased MMP1 expression has been reported in LAM, IPF, asthma and COPD (Hayashi et al., 1997, Rogers et al., 2014, Ramos et al., 2001, Kim et al., 2004). Liu et al. found that co-culturing lung cancer cells with lung fibroblasts in 3D collagen gels significantly increased MMP1 protein levels which were almost undetectable in fibroblast mono-cultures gels (Liu et al., 2016).

The upregulation of all of the described genes majority of which were pro-inflammatory chemokine and cytokines elevated in several lung diseases and cancers suggested that both LAFs and NHLFs had acquired a pro-inflammatory phenotype when co-cultured with 621-101 cells. Such a change in phenotype has been reported in various diseases characterised by a large presence of fibroblasts capable of modulating various immune cells including stromal fibroblasts isolated from cancerous tumours, fibroblasts in fibrotic lung diseases and synovial fibroblasts in rheumatoid arthritis and osteoarthritis (Neumann et al., 2010, Madar et al., 2013, Kendall and Feghali-Bostwick, 2014). As described, fibroblasts either switch on or significantly elevate expression of pro-inflammatory genes upon activation of transcription factors requiring certain stimuli. In this study, therefore, the fact that a co-culture condition exhibits this profile it is quite likely that the 621-101 cells have provided a stimulus to invoke this reaction. Although not all of the abovementioned targets could be validated within the realms of this thesis, they nonetheless paint a comprehensive picture of the effect of 621-101 cells on the fibroblast phenotype.

List of GO annotations showed CXCR chemokine binding as the most enriched molecular function with more than 43% gene in group that were present in the comparative list. This was expected as a large group of C-X-C chemokine ligands that bind to C-X-C receptors were upregulated in LAF and NHLF co-culture. Most other biological processes annotated by GO were of an immune response type. Therefore, when the list of differently expressed genes were assigned functions by a well complied and widely

trusted database it was evident that the LAFs and NHLFs had acquired pro-inflammatory functions and responses as a result of co-culture.

The comparative list, LAF co-culture vs. LAF mono-culture VS NHLF co-culture vs. NHLF mono-culture gave rise to several highly-enriched pathways. A significantly enriched pathway consisting of several genes from the list was again cytokine-cytokine receptor interaction. It was clear that the TNF signalling pathway and the NFκB signalling pathway, both of which were known stimuli for elevated chemokine expression, were upregulated in LAF and NHLF co-culture. The 621-101 cells were therefore, through a soluble stimulus, capable of activating these pathways in LAFs and NHLFs which could in turn lead to expression of chemokines.

The pathway analysis thus clarified the transcriptomic analysis and narrowed it down to a set of gene candidates that could be crucial to LAM. Elevation of such a group of genes that were an important part of relevant biological processes could not be ignored and therefore as part of this study the chemokines CXCL1, CXCL2, CXCL3, CXCL5, CXCL6, CXCL8, CXCL10 and CCL2 were further analysed.

Quantitative real-time PCR, to date, had been the method of choice for validating microarray data mainly because it is rapid, sensitive and is a high throughput process that requires minimal quantities of test material (Dallas et al., 2005). Various studies have reported wide range of correlations between microarray and qRT-PCR data ranging from r=-0.48 to 0.94 (Etienne et al., 2004, Dallas et al., 2005). Due to such a large correlation variability Rajeevan et al. only considered a valid result if the

fold change measured by both techniques were ≥ 2 (Rajeevan et al., 2001). Selected chemokines assessed via qRT-PCR using the same RNA sample set use to conduct the microarray analysis further confirmed the results from the analysis. All of the selected chemokines were elevated in LAF and NHLF co-culture whereas mono-cultures showed negligible levels. These data corroborated with dot plot visualisations generated by PGS 6.6 for each individual gene. Gene intensities for all the C-X-C chemokines and CCL2 showed the same trend where both LAF and NHLF co-cultures showed high intensities and mono-cultures very low intensities for all chemokines. Fold-change differences obtained via qRT-PCR analysis were not the same as those seen in the microarray. Few studies have reported observing differences in fold-change between those obtained from a microarray analysis and a qRT-PCR analysis and consistent with the results of Dallas et al. and Yuen et al. fold-change results determined by qRT-PCR were significantly higher than those assessed for the same genes by microarray analysis in both LAFs and NHLFs (Dallas et al., 2005, Yuen et al., 2002).

Oestrogen has been implicated to play a role in the development and progression of LAM and immunohistochemical findings from isolated LAM tissue and AML tissue from women with LAM have shown that they express oestrogen and progesterone receptors (Matsui et al., 2000b, Logginidou et al., 2000). Oestrogen signalling is complex and involved two main receptors oestrogen receptor α (ERα) and β (ERβ). Moreover, the 621-101 cells express both ERα and ERβ (Yu et al., 2004) which also could have an indirect effect on LAFs and NHLFs in co-culture. Chemokine ligand

expression showed the same trend as the first q RT-PCR confirmation in the second experimental setup. This confirmed that gene expression of the selected chemokines had been validated. It was however clear from the qRT-PCR data obtained that E2 had no added effect on LAFs and NHLFs in either co-culture or mono-culture conditions. Moreover, nothing of prognostic value was found in the expression of chemokines CXCL2, CXCL5 and CXCL6 when 48 ERα positive breast cancer tumours were tested (Bieche et al., 2007). Both the LAF and NHLF did not express ERα and expressed very low levels of ERβ, therefore it is possible that elevation of chemokine expression was due to other signalling mechanisms independent of oestrogen receptor signalling. The pro-inflammatory chemokine profile also seemed to be independent of any indirect oestrogen signalling via the 621-101 cells as well.

Protein levels of the chemokine ligands also followed the same trend. LAFs and NHLFs had shown very similar responses as was evident in the microarray data analyses. A second similar independent experimental setup included the 621-101 cells in mono-culture to measure the contribution of these cells to the secreted chemokine protein levels. The second protein expression validation also showed the same trend. However, 621-101 cell mono-cultures also showed increased chemokine secretion levels of which only slightly reduced for most chemokines on treatment with rapamycin. Cells deficient in TSC2, when treated with rapamycin can continue to have a pro-inflammatory profile due to the suppression of IL-10 (Weichhart et al., 2008). Moreover, although rapamycin selective binds and inhibits the mTORC1 complex, only

prolonged exposure to Rapamycin can inhibit mTORC2 (Wullschleger et al., 2006). Therefore, it was possible that 621-101 cells continued to have elevated chemokine secretion through this mechanism. However, when LAFs were co-cultured with rapamycin pre-treated 621-101 secreted chemokine levels significantly reduced compared to those seen in untreated co-cultures. The induction of elevated levels of chemokines in LAFs by the 621-101 cells was possibly a result of one or more soluble factors capable of activating chemokines either via transcription factors such as NFκB and AP-1 or via other cytokines and chemokines. Pro-inflammatory cytokines IL-1β, IL-6 and TNFα can promote a pro-inflammatory environment either directly or indirectly leading to the activation of several other chemokines. Moreover TNFα signalling is also a known regulator of NFκB activation (Zhang and An, 2007). Thus, inhibition of rapamycin could lead to suppression of downstream signalling and therefore a decrease in chemokine secretion.

Expression of chemokines measured in *ex vivo* transplant lung tissue however was slightly different to that seen in cell cultures. Secreted levels of CXCL1, CXCL6, CXCL8 and CCL2 were actually elevated due to rapamycin treatment. mTOR inhibitors like rapamycin have been reported to show an immunnostimulatory effect in human transplant recipients. In fact studies have shown that rapamycin-treated transplant recipients showed activation of IL-12-induced signalling and increased inflammatory responses by blood leukocytes (Brouard et al., 2010, Gallon et al., 2015). Moreover, the whole human lung tissue explants consisted of different cell

types that might show different inflammatory profiles and may respond differently to rapamycin treatment in explant cultures.

Immunohistochemical expression of CXCL1, CXCL5, CXCL6 and CXCL8 in LAM lung tissue confirmed the tissue validation of selected chemokine targets. Strong immunoreactivity to antibodies against CXCL1, 5, 6 and 8 was found mainly around spindle-shaped cell bundles within the LAM nodules in all donors. This suggested that the spindle-shaped cells most likely to be fibroblasts showed strong immunoreactivity to the antibodies against the selected chemokines. Pacheco-Rodriguez et al. have reported elevated levels of CXCL1 and CXCL5 in bronchoalveolar lavage fluid from LAM patients and only weak staining of C-C chemokines in LAM cells within the nodules with antibodies against CCL2, CCL27 and CCL28 (Pacheco-Rodriguez et al., 2009). Therefore, expression of the selected panel of chemokines in the spindle-shaped cells within LAM nodules has been reported for the first time in the study and had confirmed the *in vitro* finding in *ex vivo* LAM lung tissue.

Further validation in 3D LAM spheroid model showed the same trend in chemokine expression as the Boyden chamber 2D cultures. All the previously reported findings were the result of paracrine signalling between fibroblasts and 621-101 cells. Establishing direct contact co-cultures such as the LAM spheroid model would give an idea of the effect of juxtacrine signalling on the expression of chemokines. Studies have shown that during tumour formation and growth, cancer cells come into contact with the stroma providing the perfect microenvironment. This

leads to a sudden increase in pro-inflammatory factors and angiogenesis (Rowe and Weiss, 2009). Moreover, heterotypic cell-cell contacts are formed through adhesion molecules which in turn can promote a pro-inflammatory environment (Etzioni, 1996). Considering the fact LAM spheroids contained 5-fold fewer cells chemokine expression was elevated in LAM spheroids compared to LAF and 621-101 cell Boyden chamber. Juxtacrine signalling therefore might promote a more elevated inflammatory signature not only through soluble factors and signalling molecules, but also through direct contact adhesion molecules and intra-spheroid gradients.

Reflection of multiplex immunoassay system results in the immunohistochemical analysis of the LAM spheroids confirmed that the paracrine and juxtacrine signalling was in sync with each other. It was interesting to note that barring slight expression of CXCL1, no other chemokine expression was found in the LAF mono-culture spheroids which was also in keeping with the results obtained from the multiplex immunoassay in both 2D and 3D culture systems. This suggested that elevated chemokine expression in LAM spheroids was almost exclusively due to the presence of 621-101 cells. CXCL1 and CXCL5 immunoreactivity to what appears to be extracellular matrix possibly deposited by the fibroblasts was possibly due to the fact that both CXCL1 and CXCL5 when secreted, besides binding to their cognate receptor are also able to bind extracellular matrix glycosaminoglycans (GAGs) (Sepuru et al., 2014, Poluri et al., 2013). Strong reactivity of the 621-101 cell mono-culture spheroids to antibodies against CXCL6 and CXCL8 was possibly due to

different epitopes recognised by different antibodies used for the multiplex assay and IHC or a high accumulation of protein due to the cells being in a close conglomeration.

It was apparent that no autocrine (between the LAFs) or paracrine (between LAFs and 621-101 cells) CXCR2 signalling was at play in LAF and 621-101 cell co-cultures. Immunohistochemical staining with antibodies against several chemokine receptors including CXCR2 showed that more than 50% of smooth-muscle-like LAM cells were immunoreactive to CXCR2 (Pacheco-Rodriguez et al., 2009). Punctate expression of CXCR2 in the LAM nodules however, showed otherwise. Strong immunoreactivity was noted in the cytoplasm of specific sub-populations of cells within the nodules which interestingly were found near spindle-shaped cells in the nodules, presumably, fibroblasts in all three donors. In the lung, CXCR2 expression has been found in leukocytes, monocytes, bronchial epithelial cells, primary ASM cells, vascular endothelial cells and mast cells (Tomankova et al., 2015) and has been implicated in the recruitment of neutrophils and mast cells to the site of inflammation via one of its ligands (Sawant et al., 2015, Lippert et al., 1998). Therefore, detection of immune cell infiltration in LAM nodules and predominantly a large population of mast cells suggested that a CXCR2-dependent recruitment mechanism might be at play.

Mast cells are classified by the major proteins they store and secrete, namely tryptases and chymases. Cells can either contain tryptic enzymes making them tryptase positive or chymotryptic enzymes making them

chymase positive cells with a few mast cells consisting of both chymase and tryptase. The tryptase positive mast cells, recognised by the mast cell tryptase antibody, are the most abundant type in the lung and it is this tryptic enzyme that confers upon them their pro-inflammatory property (Caughey, 2007). Moreover, abundant presence of tryptase positive activated mast cells was also detected in LAM lung compared to chymase positive cells (Edwards et al., 2005). Slightly elevated nodular infiltration of mast cells in the early LAM donors could suggest that the mast cells may be recruited to the nodules when the disease first sets in. However, none of the data were significant and a larger study with several more LAM donors would be required to confirm the inferences.

Potent, competitive and highly selective (>150-fold) CXCR2 receptor antagonist, SB225002 has been shown to selectively inhibit CXCL1 and CXCL8 mediated chemotaxis of CXCR2 expressing neutrophils both *in vitro* and *in vivo* (White et al., 1998, Costa et al., 2014). The ability of LAFs and 621-101 cells in co-culture to stimulate directional migration (chemotaxis) rather than random migration (chemokinesis) of the HMC-1 cells which was significantly reduced by blocking CXCR2, was evident from the results of the Boyden chamber migration assay. CXCR2 dependent migration of HMC-1 cells towards a secreted chemokine gradient generated by the LAFs and 621-101 cells in co-culture reduced by 73% on treatment with 100nM SB225002. This clearly implied that the HMC-1 migration towards cells in co-culture was mediated via CXCL8.

## 5.5 Conclusion

This chapter describes the transcriptomic characterisation of LAFs and NHLFs and phenotypic effects of TSC2 null 621-101 cells on their transcriptional profile. It was concluded that though the LAFs and NHLFs showed transcriptional differences, they were in fact similar in their responses to 621-101 cells. These TSC2 null cells had conferred upon both LAFs and NHLFs a pro-inflammatory profile and although the 621-101 cells were not a true 'LAM lung cell' they were the closest to a model human cell line. Moreover, a thorough literature search has proven that the gene expression signature seen in the LAFs and NHLFs was extremely consistent with other transcriptomic and proteomic expression analyses conducted using fibroblasts from the abovementioned disease conditions.

# 6 CHAPTER 6: General Discussion

## 6.1 General Overview

This thesis has described a multitude of aspects and novel mechanisms encompassing LAM. The mainstay hypothesis of this study was that there exists a synergy between $TSC2^{-/-}$ LAM cells and fibroblasts and together these cells contribute to the destruction of lung parenchyma. The overall aim of therefore was to identify key mechanisms that directly or indirectly lead to lung destruction associated with LAM. The means to do this was by designing suitable *in vitro* 2D and 3D models which could recapitulate a LAM nodule in a culture dish.

The present study is the first to have described the design and validation of various *in vitro* models 2D and 3D which are versatile and can be used with differing outcomes. Although LAM nodules consist of a heterotypic population of cells only two studies conducted have used co-culture models, both of which were based on lymphatic endothelial cells (Kumasaka et al., 2015, Ikeda et al., 2003). The 2D and 3D *in vitro* co-culture models designed in this study thus shed light on the fact that LAM is a heterocellular disease and it takes more than one cell type to fully understand the complex mechanisms involved in LAM. The co-culture models therefore not only represented LAM nodules but could also be used successfully in the further aspects of this study.

Cathepsin K expression has been detected previously in LAM nodules and has since been speculated to be involved in destruction of the lung matrix mainly due to its potent proteolytic activity (Chilosi et al., 2009, van Meerloo et al., 2011). The exact mechanism of activation of this protease was still an unknown. However, the present study has been the first to show that cathepsin K expression in LAM is mainly dependent on the presence of fibroblasts within LAM nodules. The findings thus showed that cell-cell interactions within the LAM nodule stroma can generate conditions in which proteolytic lung damage may occur.

The present study has described a novel microarray analysis that led to the finding that $TSC2^{-/-}$ 621-101 cells altered the fibroblast phenotype towards a pro-inflammatory one. The expression of a few C-X-C and C-C motif type chemokines has been detected in LAM nodules and BAL fluid

and the presence of mast cells has been found in LAM nodules (Pacheco-Rodriguez et al., 2009, Coussens and Werb, 2002). However, the mechanisms involved in mast cell recruitment had not yet been explored. The models thus designed have provided a strong functional basis of the synergism between $TSC2^{-/-}$ 621-101 cells and LAFs in mechanisms examined, to be involved in the pathogenesis of LAM.

## 6.2 *In Vitro* Models

The 2D and 3D models incorporated two main cell types present in the LAM nodule hypothesised to be the key players in the pathogenesis of LAM. The present study has drawn from the hypothesis that fibroblasts may be recruited by $TSC2^{-/-}$ LAM cells to the nodule, akin to cancer cell recruitment of the stroma. *In vitro* co-culture models using cancer and stromal cells are now being increasingly used as unlike relying only on a cell line, the former approach takes into account the stroma and non-neoplastic cells involved. Similarly, in LAM research, most researchers have relied on the use of human or animal derived cell lines alone. It is now evident that a varying cell population exists within a LAM nodule and only a small percentage of cells is $TSC2^{-/-}$ therefore using a multicellular *in vitro* model can provide a clearer picture. This was evident when Transwell co-cultures showed elevated levels of chemokines. Moreover, expression of several MMPs and cathepsins was elevated in the 3D BME gel model supporting the fact that the ECM influences cellular responses.

## 6.3 Activated Fibroblast Phenotype in LAM

An important finding in this thesis was the presence and the level of involvement of fibroblasts in disease progression. The presence of fibroblasts in LAM lung has previously been showing a study conducted by Inoue et al which described the presence of α-SMA expressing myofibroblast-like cells within the LAM nodules. These cells were suspected to be myofibroblast-like as they expressed fibroblast growth factor receptors 1 and 2, however expression of these receptors was also found in other cells such as epithelial cells within the nodules (Ingram et al., 1997). On the other hand this thesis has described the isolation and characterisation of early passage LAM associated fibroblasts and Clements et al were the first to use fibroblast-specific markers to identify fibroblasts present in LAM nodules (Clements et al., 2015). Moreover, expression of FAP-α and the dynamic expression of αSMA suggested that the LAFs can acquire an activated phenotype given the right stimulus. Evidence of fibroblast activation was further confirmed by the elevated expression of pro-inflammatory chemokines and other factors in LAFs/621-101 cell co-cultures compared to respective mono-cultures. Cancer cells serve to modify the properties of fibroblasts recruited to the stroma resulting in the latter being known as cancer associated fibroblasts (CAFs) (Kalluri and Zeisberg, 2006). The term LAM associated fibroblasts has therefore been coined as a namesake as data from this thesis has made it evident that the LAFs are the stromal fibroblasts associated with this low-grade neoplasm.

Expression of several C-X-C and C-C motif pro-inflammatory chemokines has been documented in CAFs and activated fibroblasts. Such an expression signature is induced by the neighbouring cancer cells and has been attributed to be under the transcriptional control of NF-κB and cyclooxygenase 2 (COX-2) (Sasaki et al., 1984). Undoubtedly the presence of an extensive number of chemotactic chemokines enables the fibroblasts to assist in the activation and migration of resident and circulating immune cells such as macrophages, neutrophils and mast cells (Kendall and Feghali-Bostwick, 2014). Results within this thesis have shown the evidence of such a mechanism orchestrated by the 621-101 cell-induced activation of LAFs and have subsequently provided the basis of mast cell recruitment to the LAM nodules.

## 6.4 Recruitment of Mast cells

Mast cells originate from their progenitors which are few in number in normal lung physiology. Their numbers significantly increase during pulmonary inflammation and they are actively recruited to the site of inflammation (Watz* et al., 2007). Mast cells can be recruited through few mechanisms however, chemotactic recruitment occurs primarily through the CXCR2 receptor. The existence of a CXCR2-mediated recruitment mechanism which is the result of crosstalk between 621-101 cells and LAFs in LAM nodules has been eloquently described as part of this thesis. The presence of mast cells in LAM nodules has been previously reported (Edwards et al., 2005, Ingram et al., 1997) however, their role in the

pathogenesis of LAM is yet to be elucidated. It is not known whether recruitment of mast cells is beneficial or detrimental to disease progression, however, the pro-inflammatory activities of recruited mast cells have been shown to sustain tumour microenvironment. Recruited mast cells can synthesize and secrete several cysteine proteases, MMPs, various cytokines (IL-6 and TNF-α) and several mitogens (platelet derived growth factor, PDGF, vascular endothelial growth factor, VEGF and TGF-β) (Kelm et al., 2003) which can provide favourable conditions for recruitment of other immune cells, invasion and cell proliferation. In, neurofibromatosis, a similar disease characterised multiple neufibromas (tumours) and by a Knudson two-hit LOH of the *Nf1* gene, mast cells selectively migrate into the tumours in a stem cell factor (SCF)-mediated manner. Here via the secretion of TGF-β, a mitogen for fibroblasts, mast cells are able to activate and cause proliferation of the resident fibroblasts. This also causes further migration of fibroblasts and increased fibroblast-mediated ECM remodelling thereby promoting disease progression (Staser et al., 2012). Moreover a growing body of evidence suggests the mast cell plays a role in the pathogenesis of diseases characterised by fibrosis such as sarcoidosis (Dangles et al., 1997), hypersensitivity pneumonitis and IPF (Dangles-Marie et al., 2007). In fact, mast cells secrete several pro-fibrotic factors including tryptase itself which increases IPF fibroblast proliferation. Furthermore, IPF fibroblasts when co-cultured with mast cells serve to enhance their survival and are pro-proliferative (Majety et al., 2015). Therefore, based on this evidence, fibroblasts and mast cells could have a

supportive relationship towards each other and may also be involved in the recruitment of one another in the LAM nodule.

## 6.5 Acidification of the LAM Nodule Microenvironment

Activated fibroblasts and CAFs are also known to secrete increased potent ECM degrading proteases such as MMPs and cathepsins. These proteases become activated in the tumour or disease microenvironment where proteases such as cathepsins are activated in an acidic environment thereby aiding invasion and disease progression (Yin et al., 2012, Konur et al., 1996). The finding that cathepsin K was the most highly transcriptionally expressed protease in both LAFs and LAM tissue donors, the activity of which was elevated in LAF/621-101 cell co-cultures compared to mono-cultures lead the present study to the finding that an acidic environment could exist within the LAM nodules. Induced by low oxygen levels, the transcription factor hypoxia-inducible factor 1α (HIF1α) drives Warburg metabolism which can persist in cancer cells even in the presence of oxygen. Similarly in LAM despite aerobic conditions, constitutively active mTOR pathway elevates HIF1α transcription (Duvel et al., 2010) which provides a basis for the existence of the Warburg metabolism, a distinctive feature of neoplastic growth. Although the inhibition of monocarboxylate transporters, responsible for membranous lactate shuttling, was not possible due to technical issues, the expression of hypoxia driven MCT1 and MCT4 (Weiswald et al., 2009) in both $TSC2^{-/-}$

621-101 cells and LAM lung tissue support the existence of such a metabolism in LAM.

The other metabolic pathways parallel to glycolysis can significantly contribute to microenvironment acidification via the indirect release of $H^+$ protons. Oestrogen driven pentose phosphate pathway (PPP) resulting in enhanced glucose transport via GLUT1 and GLUT4 and uptake has been shown to exist in the $TSC2^{-/-}$ LAM cells (Sun et al., 2014). $CO_2$ a highly significant contributor to acidity is also a major by-product of the PPP. $CO_2$ can then be hydrated to produce $H^+$ and bicarbonate ($HCO_3^-$) by the combined activities of carbonic anhydrases (II, IX and XII) and $Na^+/HCO_3^-$ co-transporters with the latter shuttling $HCO_3^-$ back into the cell resulting in net acid export into the extracellular milieu (Ye et al., 2013, Uhlen et al., 2005). The finding that this very mechanism exists in the 621-101 cells suggests that the $TSC2^{-/-}$ LAM cells, akin to cancer cells, have undergone a metabolic shift that render the nodular microenvironment acidic aiding in the activation of proteases such as cathepsin K. Chapter 4 has therefore described that inhibition of the $Na^+/HCO_3^-$ co-transporters and to a lesser extent, the carbonic anhydrases resulted in significant reduction of cathepsin K activity in LAF/621-101 cell co-cultures.

## 6.6 Cathepsin K and Inflammation

Tissue-specific activated fibroblast derived expression of active cathepsin K has been described in various diseases where the main role of this potent collagen-elastin degrading protease has been proteolytic destruction of

tissue (van den Brule et al., 2005, Neumann et al., 2010, Beklen et al., 2015). As described in the introduction to this thesis (section 1.14), cathepsin K activity in cells is tightly regulated and an elevated activity of this protease can primarily mean proteolytic destruction of ECM. Therefore, although the present study has not elucidated active cathepsin K-mediated destruction of LAM lung tissue all of the elements necessary for this 'perfect storm' are present within the LAM nodule. Pro-inflammatory stimuli related to Toll-like receptor signalling (TLR) has been known to induce production of cytokines such as TNF-α and interleukin-1β (IL-1β) which in turn upregulate RANKL, a direct regulator of cathepsin K expression (Ferri et al., 2004, Lee et al., 2009). Moreover, cathepsin K deficient animal models for rheumatoid arthritis and periodontitis (both diseases believed to also show active fibroblast-derived cathepsin K activity) showed a radical reduction in bone erosion and TLR-4, 5 and 9-medaited inflammation (Beklen et al., 2015, Chang et al., 2013, Hou et al., Montgomery et al., 2012). Cathepsin K was therefore proposed to have an osteoimmune function which also suggested the presence of a feedback loop between cathepsin K and TLR signalling-mediated inflammation. Moreover, pathway analysis performed in chapter 5 (section 5.3.8) has also highlighted upregulated TLR-signalling in cells in co-culture. Finally, a recent study by Repnik et al, showed that cysteine cathepsins such as cathepsin K can proteolytically process ELR (glutamate-leucine-arginine) C-X-C chemokines such as CXCL1, 2, 3, 5 and 8 thereby elevating chemokine activity and regulating immune cell recruitment. In fact, in the presence of GAGs compared to cathepsins L and S, cathepsin K increasingly processed

the abovementioned chemokines N terminally to the ELR motif thus suggesting another pro-inflammatory role for this protease (Issaka et al., 2009).

## 6.7 Clinical applications of findings

This study has designed three distinct 3D models that can be used depending on the phenomena at study and the level of quantitation required. For example, the LAM spheroid model would be particularly useful for drug testing studies and can be used in high-throughput studies providing a high level of quantification. The LAM spheroid model can be tailored to be patient-specific where a patient's own cells derived from biopsy tissue can be used to generate LAM spheroids. The LAMosphere model is a direct donor representative which consists of the multiple cell types found in the LAM lung and may best represent LAM. Due to the rarity of LAM a very small number of patients can be recruited in clinical studies. Moreover, LAM patients are quite variable and respond differently to therapy. The LAM spheroids and LAMosphere models therefore can be used to bridge this gap by using them as a means of personalised therapy in drug studies and studying the responses of each patient individually.

Initially trialled mainly as anti-osteoporotic drugs, cathepsin K inhibitors have now been trialled in prostate cancer and breast cancer to prevent bone metastasis (ClinicalTrials.gov). Therefore, an already established drug target inhibitors targeting cathepsin K activity described in section 1.14.5 have reached Phase III trials in humans making cathepsin K a very

druggable target. Following successful preclinical studies, a clinical trial to assess the efficacy of cathepsin K inhibitors in reducing proteolytic lung destruction and decreasing airspace enlargement.

Another avenue targeting protease-mediated lung destruction described in the present study was the inhibition of net acid extruders responsible for the acidification of the nodular microenvironment. Carbonic anhydrase inhibitors acetazolamide and metazolamide have been trialled in the treatment of pulmonary hypoxia and to decrease tumour microenvironment pH in cervical cancer (ClinicalTrials.gov) and small molecule inhibitors of both carbonic anhydrase IX and sodium bicarbonate inhibitors have been used in preclinical cancer models (Kant et al., 2014, Lou et al., 2011). Therefore, acid extruder inhibitors alone or in combination with cathepsin K inhibitors warrant a potential clinical trial.

The role of mast cell infiltration in LAM lung nodules is still an unknown and it could be seen as benevolent or malevolent. However, in neurofibromas, treatment with tyrosine-kinase inhibitor Imatinib disrupts stem cell factor (SCF)/c-Kit-mediated mast cell cytopoesis and inflammation (Staser et al., 2012). Therefore, if mast cell infiltration is detrimental to LAM patients inhibiting their migration can also be achieved by CXCR2 inhibition. In fact, GlaxoSmithKline has just begun a Phase II trial using Danirixin, a selective CXCR2 antagonist as an anti-inflammatory for the treatment of COPD (ClinicalTrials.gov). Therefore, as another already druggable target, CXCR2 inhibition could reduce mast cell infiltration and thereby inhibit any downstream adverse events.

## 6.8 Strengths and weaknesses

This study has successfully isolated and characterised LAM associated fibroblasts from LAM lung donors using a wide panel of established fibroblast markers. Further these fibroblasts have been successfully used with 621-101 cells to design and build 2D and 3D co-culture models in order to represent LAM nodules in vitro. Although the 3D BME model was thoroughly validated for the expression of markers of a LAM nodule, due to the fact that the tools for generation and embedding were only developed towards the end of the study the exact histomorphometry and a full validation of the LAM spheroids and LAMospheres was not possible. Moreover, due to the lack of donors, any confirmed conclusions could not be drawn regarding the cellular arrangement of LAFs and 621-101 cells in LAM spheroids. Also, the level of disintegration of the LAMospheres made it difficult to assess for further LAM markers. In most studies 3 NHLF and 4 LAF donors were used.

The has also shown that LAFs are almost exclusively responsible for cathepsin K expression in vitro and that expression in ex vivo LAM lung tissue has been associated with FSP expression confirming that fibroblasts are responsible for nodular cathepsin K expression. The findings in chapter 4 have also shown the existence of an altered metabolism in the 621-101 cells which directly results in the activation of acidophilic proteases such as cathepsin K *in vitro*. Although it has been shown that ability of 621-101 cells to acidify the microenvironment could be partially downstream of

mTOR, it was not possible to use the 621-103 TSC2+/+ cells as a control due to culturing difficulties associated with these cells. However, a rapamycin treated control has been shown to behave similar to Tsc2+/+ MEFs. Also, it was not possible to prove the existence of Warburg effect in the 621-101 cells due to technical issues with the inhibition of MCTs.

This study has described a first of its kind transcriptomic analysis and has identified a distinct pro-inflammatory signature acquired by the LAFs influenced by the 621-101 cells. All of the chemokine targets identified in the analysis were validated on gene and protein level in 2D and 3D in vitro LAM models and also in ex vivo LAM lung tissue. Further, a potential mechanism for the recruitment of immune cells via a chemokine signalling axis was established when infiltration of mast cells was found in LAM nodules and finally functional studies done showed the recruitment of mast cells by LAF/621-101 cell co-culture via the CXCL8/CXCR2 axis.

Microarray analysis performed could not take into consideration false discovery rate when generating the ANOVA lists as none of the targets passed through this parameter. Despite this, all of the chosen gene targets were successfully validated making the analysis biologically relevant. Also, due to LAM being a rare disease this study could only use a small sample size of n=3 or 4 and for this reason deviation from the mean was used instead of standard error of the mean to plot variability from mean.

## 6.9 Final conclusion

Taken together the findings within this thesis suggest that a symbiotic relationship exists between the LAFs and LAM cells which results in the interplay of several mechanisms that are pro-fibrotic, pro-inflammatory and pro-proteolytic thereby promoting disease progression in a manner similar to cancer cell and CAF interactions in cancer. These similarities are consistent with the idea that LAM is indeed a low grade malignant neoplasm.

# 7 CHAPTER 7: Future work

## 7.1 Preclinical *in vivo* studies

Results obtained from 2D and 3D *in vitro* models are relevant and compelling. For the next stage, preclinical *in vivo* studies using the relevant animal model representing LAM could shed light on proteolytic airspace enlargement and immune cell recruitment *in vivo*. The use of a homograft model would be suitable for this purpose as it would allow the injection of cultured spheroids and genetically modified labelled cells. The animals treated with appropriate protease and pro-inflammatory inhibitors can be immunohistochemically assessed for tissue histology to assess immune cell infiltration into LAM nodules, measurement of enlarged airspace which can be related to nodular expression of cathepsin K and whether inhibition of cathepsin K decreases cyst formation. *In vivo* fluorescent pH indicators such as 5-(and-6)-Carboxy SNARF™-1 (Invitrogen) could give an idea of the *in vivo* lung pH and whether inhibition of net acid extruders results in increase in pH thereby preventing activation of proteases.

## 7.2 Establishing the proteolytic role of cathepsin K and the Warburg effect using *in vitro* models

A current field of great interest, especially in regenerative medicine, is that of tissue scaffold-based models. Further utilisation of the 3D disease models would be to decellularise lung tissue and subsequently seed the ECM scaffold with 621-101 cells and LAFs from LAM donor patients, creating a nodular microenvironment. The cells in co-culture would be

allowed to acidify the pH and activate cathepsin K as described in sections 4.3.10 and 4.3.12 followed by assessment of breakdown products of collagen such as C-terminal telopeptide (CTX) a result of cathepsin K-mediated proteolytic destruction.

To confirm the presence of the Warburg metabolism in 621-101 cells siRNA mediated knockdown of *MCT4* gene, one of the main lactate shuttling membrane bound transporter and subsequent measurement of lactate increase in culture. CRISPR-Cas9 deletion of MCT4 can also be performed. Further to assess whether the altered metabolism is a consequence of a hypoxic environment, hypoxic and normoxic culture of 621-101 cells would allow assessment of constitutively active and hypoxia-sensitive downstream signals.

## 7.3 Tailoring 2D and 3D *in vitro* models to LAM

The 2D and 3D models described in this thesis can be considered as a constant work in progress. With further knowledge about the different cell types found within a LAM nodule, these models can be further modified. A parallel study is being currently conducted in which immunohistochemical staining for various carefully selected LAM biomarkers is being correlated with lung function. This will enable our group to identify which cell types within the LAM nodules contribute to disease progression. Once identified, the models designed can be modified to incorporate these cells enabling recreation of an entire LAM nodule *in vitro*.

## 7.4 Identifying mechanisms of cell recruitment

The BME gel model and the LAM spheroid model described in sections 3.3.4 and 3.3.8 respectively both describe attractive forces between LAFs and 621-101 cells visualised by cell clumping and the formation of compact spheroids. These attractive forces could be the driving force of cell recruitment and although the CXCL12/CXCR4 recruitment has been partly implicated in cell recruitment, other chemotactic or adhesive forces have not been explored. Microarray studies performed described in chapter 5 have highlighted the upregulation of cellular adhesion molecules in LAF/621-101 cell co-cultures which could be involved in recruitment. These recruitment mechanisms can be studied in the LAM spheroid model by combining immunocytochemistry and light sheet fluorescence microscopy a technique which provides excellent optical sectioning capabilities at high speed. This would allow for visualisation at a single cell level correct spatial visualisation of adhesive forces as the cells would be in a 3D conformation. This technique could be extended to LAMospheres as well which would be more representative of the *in vivo* situation. Identifying and targeting the recruitment mechanisms between LAM cells and LAFs would reduce fibroblast infiltration thereby reducing proteolytic destruction in LAM.

# 8 Appendix

## 8.1 Appendix I: Isotype controls

Isotype controls for immunofluorescence

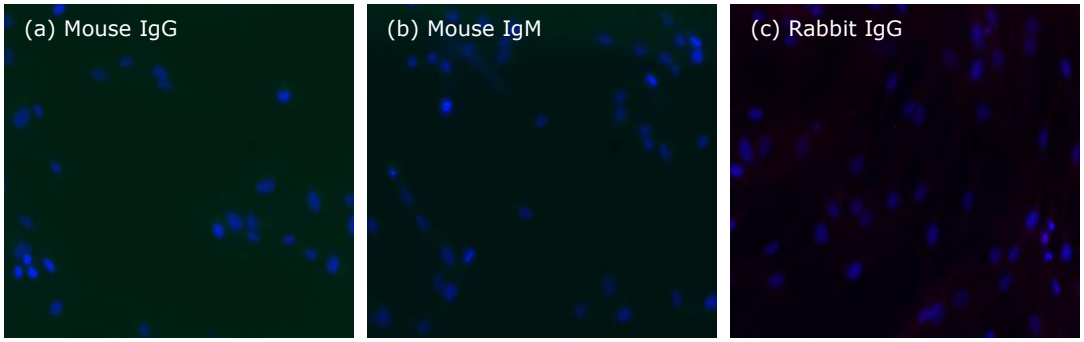



**Figure 1** ***shows the isotype controls for immunofluorescent staining***

Isotype controls for double IHC-Fr

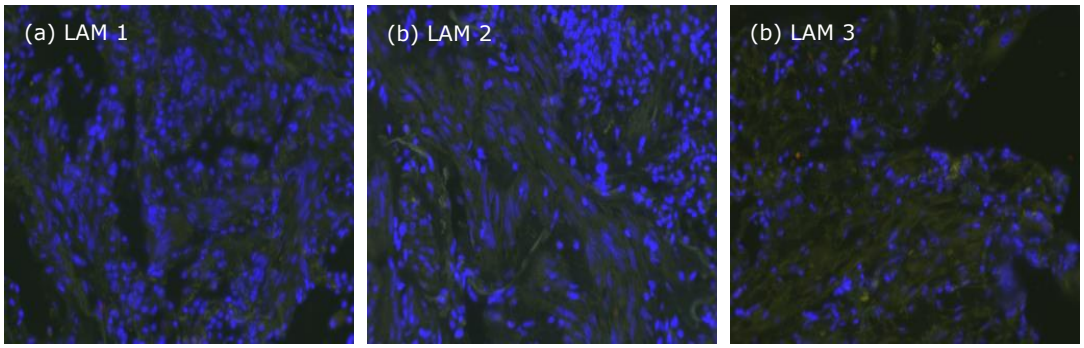



**Figure 2** ***shows the isotype controls for double fluorescent immunohistochemistry on three LAM donors.*** *Sections were incubated with mouse IgM and rabbit IgG isotypes sequentially.*

Isotype controls for double IHC

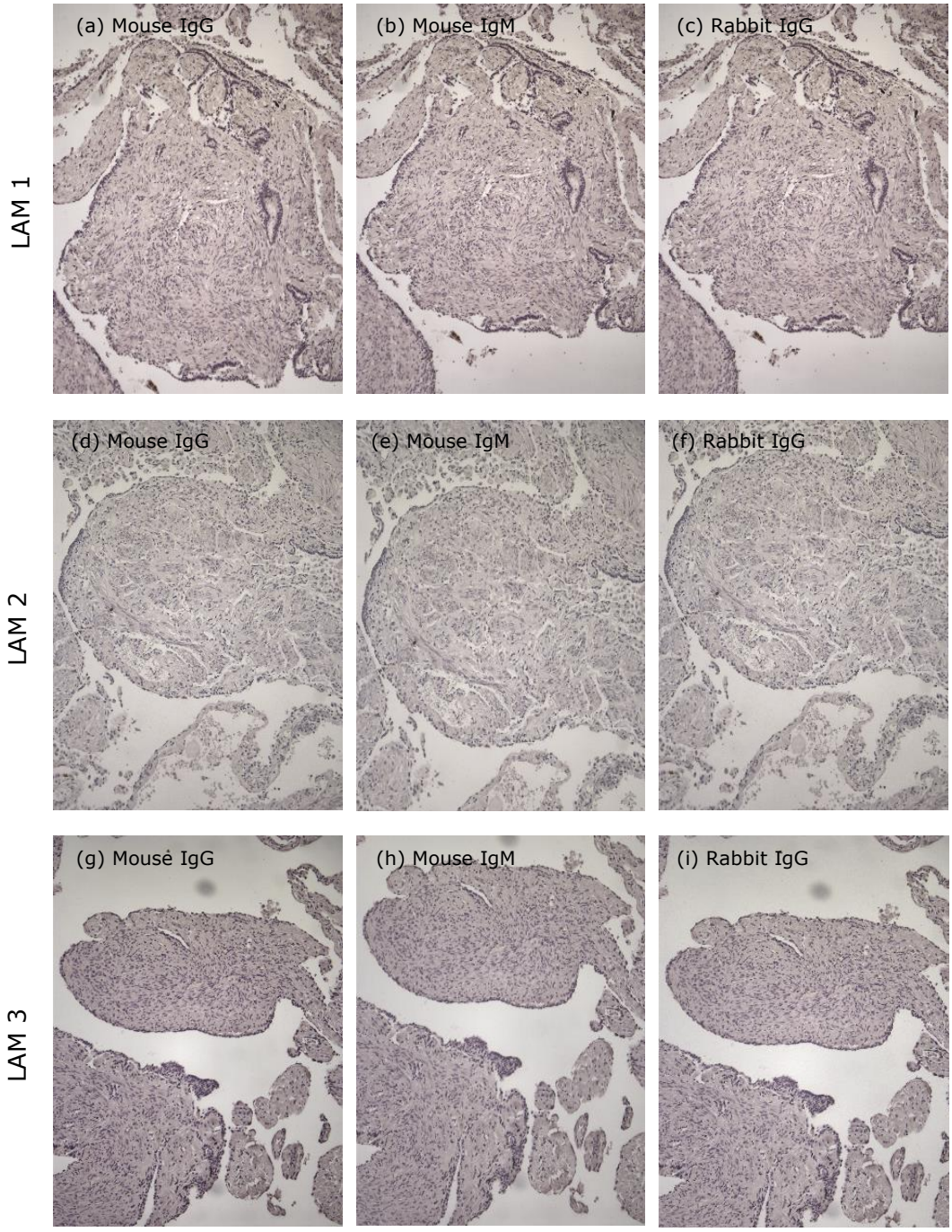



**Figure 3** ***shows isotype controls for IHC LAM donors for (A-C) mouse IgG (D-F) Mouse IgM and (G-I) Rabbit IgG***

# 9 Bibliography


*alamarBlue® Cell Viability Assay Protocol* [Online]. Available: https://www.thermofisher.com/uk/en/home/references/protocols/cell-and-tissue-analysis/cell-profilteration-assay-protocols/cell-viability-with-alamarblue.html.

ClinicalTrials.gov. U.S. National Institutes of Health.

*Understanding the Epidemiology of LAM* [Online]. Available: http://www.thelamfoundation.org/.

2014. *Rare Disease UK* [Online]. Available: http://www.raredisease.org.uk.

ABEYRATHNA, P. K., KOVACS, L. & SU, Y. 2016. Calpain-2 Activates Akt via TGFβ1-mTORC2 Pathway in Pulmonary Artery Smooth Muscle Cells. *The FASEB Journal,* 30**,** 719.8.

ACHARYA, P. S., ZUKAS, A., CHANDAN, V., KATZENSTEIN, A. L. & PURE, E. 2006. Fibroblast activation protein: a serine protease expressed at the remodeling interface in idiopathic pulmonary fibrosis. *Hum Pathol,* 37**,** 352-60.

ADAMSON, J., HASWELL, L. E., PHILLIPS, G. & GAÇA, M. D. 2011. In Vitro Models of Chronic Obstructive Pulmonary Disease (COPD). *In:* MARTIN-LOECHES, I. (ed.) *Bronchitis.* Rijeka: InTech.

AFFYMETRIX 2007. GeneChip® Human Genome U133 Arrays. *In:* AFFYMETRIX (ed.). Santa Clara, CA.

AFFYMETRIX. 2017. *GeneChipTM 3' IVT PLUS Reagent Kit*

*Manual Target Preparation for GeneChipTM 3' Expression*

*Arrays User Guide* [Online]. Carlsbad, CA, USA: Thermo Fisher Scientific. Available: http://tools.thermofisher.com/content/sfs/manuals/3_IVT_PLUS_Reagent_Kit_User_Manual.pdf.

AKHENBLIT, P. J., HANKE, N. T., GILL, A., PERSKY, D. O., HOWISON, C. M., PAGEL, M. D. & BAKER, A. F. 2016. Assessing Metabolic Changes in Response to mTOR Inhibition in a Mantle Cell Lymphoma Xenograft Model Using AcidoCEST MRI. *Molecular imaging,* 15**,** 10.1177/1536012116645439 1536012116645439.

ALMEIDA, P. C., NANTES, I. L., CHAGAS, J. R., RIZZI, C. C., FALJONI-ALARIO, A., CARMONA, E., JULIANO, L., NADER, H. B. & TERSARIOL, I. L. 2001. Cathepsin B activity regulation. Heparin-like glycosaminogylcans protect human cathepsin B from alkaline pH-induced inactivation. *J Biol Chem,* 276**,** 944-51.

AMSBIOTECHNOLOGY. 2013. *Lipidure®-COAT Plates* [Online]. Available: http://www.amsbio.co.uk/Lipidure-Coat.aspx.

ANDERSSON-SJOLAND, A., DE ALBA, C. G., NIHLBERG, K., BECERRIL, C., RAMIREZ, R., PARDO, A., WESTERGREN-THORSSON, G. & SELMAN, M. 2008. Fibrocytes are a potential source of lung fibroblasts in idiopathic pulmonary fibrosis. *Int J Biochem Cell Biol,* 40**,** 2129-40.

ANDO, K., FUJINO, N., MITANI, K., OTA, C., OKADA, Y., KONDO, T., MIZOBUCHI, T., KURIHARA, M., SUZUKI, K., HOSHIKA, Y., EBANA,

H., KOBAYASHI, E., TAKAHASHI, K., KUBO, H. & SEYAMA, K. 2016. Isolation of individual cellular components from lung tissues of patients with lymphangioleiomyomatosis. *Am J Physiol Lung Cell Mol Physiol,* 310**,** L899-908.

ANWAY, M. D., WRIGHT, W. W., ZIRKIN, B. R., KORAH, N., MORT, J. S. & HERMO, L. 2004. Expression and localization of cathepsin k in adult rat sertoli cells. *Biol Reprod,* 70**,** 562-9.

ARBISER, J. L., YEUNG, R., WEISS, S. W., ARBISER, Z. K., AMIN, M. B., COHEN, C., FRANK, D., MAHAJAN, S., HERRON, G. S., YANG, J., ONDA, H., ZHANG, H. B., BAI, X., UHLMANN, E., LOEHR, A., NORTHRUP, H., AU, P., DAVIS, I., FISHER, D. E. & GUTMANN, D. H. 2001. The generation and characterization of a cell line derived from a sporadic renal angiomyolipoma: use of telomerase to obtain stable populations of cells from benign neoplasms. *Am J Pathol,* 159**,** 483-91.

ASHBURNER, M., BALL, C. A., BLAKE, J. A., BOTSTEIN, D., BUTLER, H., CHERRY, J. M., DAVIS, A. P., DOLINSKI, K., DWIGHT, S. S., EPPIG, J. T., HARRIS, M. A., HILL, D. P., ISSEL-TARVER, L., KASARSKIS, A., LEWIS, S., MATESE, J. C., RICHARDSON, J. E., RINGWALD, M., RUBIN, G. M. & SHERLOCK, G. 2000. Gene ontology: tool for the unification of biology. The Gene Ontology Consortium. *Nat Genet,* 25**,** 25-9.

ASTRINIDIS, A., KHARE, L., CARSILLO, T., SMOLAREK, T., AU, K. S., NORTHRUP, H. & HENSKE, E. P. 2000. Mutational analysis of the tuberous sclerosis gene TSC2 in patients with pulmonary lymphangioleiomyomatosis. *Journal of Medical Genetics,* 37**,** 55-57.

ATLEY, L. M., MORT, J. S., LALUMIERE, M. & EYRE, D. R. 2000. Proteolysis of human bone collagen by cathepsin K: characterization of the cleavage sites generating by cross-linked N-telopeptide neoepitope. *Bone,* 26**,** 241-7.

ATOCHINA-VASSERMAN, E. N., GUO, C.-J., ABRAMOVA, E., GOLDEN, T. N., SIMS, M., JAMES, M. L., BEERS, M. F., GOW, A. J. & KRYMSKAYA, V. P. 2014. Surfactant Dysfunction and Lung Inflammation in the Female Mouse Model of Lymphangioleiomyomatosis. *American Journal of Respiratory Cell and Molecular Biology,* 53**,** 96-104.

AUBRY, M. C., MYERS, J. L., RYU, J. H., HENSKE, E. P., LOGGINIDOU, H., JALAL, S. M. & TAZELAAR, H. D. 2000. Pulmonary lymphangioleiomyomatosis in a man. *American Journal of Respiratory and Critical Care Medicine,* 162**,** 749-752.

AVILA, N. A., DWYER, A. J., RABEL, A. & MOSS, J. 2007. Sporadic lymphangioleiomyomatosis and tuberous sclerosis complex with lymphangioleiomyomatosis: comparison of CT features. *Radiology,* 242**,** 277-85.

AVILA, N. A., KELLY, J. A., CHU, S. C., DWYER, A. J. & MOSS, J. 2000. Lymphangioleiomyomatosis: abdominopelvic CT and US findings. *Radiology,* 216**,** 147-53.

BAGLOLE, C. J., REDDY, S. Y., POLLOCK, S. J., FELDON, S. E., SIME, P. J., SMITH, T. J. & PHIPPS, R. P. 2005. Isolation and phenotypic characterization of lung fibroblasts. *Methods Mol Med,* 117**,** 115-27.

BARNES, E. A., KENERSON, H. L., MAK, B. C. & YEUNG, R. S. 2010. The loss of tuberin promotes cell invasion through the ss-catenin pathway. *Am J Respir Cell Mol Biol,* 43**,** 617-27.

BECKER, H. M. & DEITMER, J. W. 2007. Carbonic anhydrase II increases the activity of the human electrogenic Na+/HCO3- cotransporter. *J Biol Chem,* 282**,** 13508-21.

BEE, J., BHATT, R., MCCAFFERTY, I. & JOHNSON, S. R. 2015. A 4-year prospective evaluation of protocols to improve clinical outcomes for patients with lymphangioleiomyomatosis in a national clinical centre. *Thorax,* 70**,** 1202.

BEKLEN, A., AL-SAMADI, A. & KONTTINEN, Y. T. 2015. Expression of cathepsin K in periodontitis and in gingival fibroblasts. *Oral Dis,* 21**,** 163-9.

BELLINI, A. & MATTOLI, S. 2007. The role of the fibrocyte, a bone marrow-derived mesenchymal progenitor, in reactive and reparative fibroses. *Lab Invest,* 87**,** 858-70.

BENTON, G., ARNAOUTOVA, I., GEORGE, J., KLEINMAN, H. K. & KOBLINSKI, J. 2014. Matrigel: from discovery and ECM mimicry to assays and models for cancer research. *Adv Drug Deliv Rev,* 79-80**,** 3-18.

BENTON, G., KLEINMAN, H. K., GEORGE, J. & ARNAOUTOVA, I. 2011. Multiple uses of basement membrane-like matrix (BME/Matrigel) in vitro and in vivo with cancer cells. *Int J Cancer,* 128**,** 1751-7.

BERRIDGE, M. V., HERST, P. M. & TAN, A. S. 2005. Tetrazolium dyes as tools in cell biology: new insights into their cellular reduction. *Biotechnol Annu Rev,* 11**,** 127-52.

BIECHE, I., CHAVEY, C., ANDRIEU, C., BUSSON, M., VACHER, S., LE CORRE, L., GUINEBRETIERE, J. M., BURLINCHON, S., LIDEREAU, R. & LAZENNEC, G. 2007. CXC chemokines located in the 4q21 region are up-regulated in breast cancer. *Endocr Relat Cancer,* 14**,** 1039-52.

BIO-PLEX. 2017. *Bio-Plex Pro Human Chemokine Assays* [Online]. Available: http://www.bio-rad.com/webroot/web/pdf/lsr/literature/10031990.pdf.

BISSELL, M. J. 1981. The Differentiated State of Normal and Malignant Cells or How to Define a "Normal" Cell in Culture. *In:* G.H. BOURNE, J. F. D. & JEON, K. W. (eds.) *International Review of Cytology.* Academic Press.

BISSLER, J. J., KINGSWOOD, J. C., RADZIKOWSKA, E., ZONNENBERG, B. A., FROST, M., BELOUSOVA, E., SAUTER, M., NONOMURA, N., BRAKEMEIER, S., DE VRIES, P. J., WHITTEMORE, V. H., CHEN, D., SAHMOUD, T., SHAH, G., LINCY, J., LEBWOHL, D. & BUDDE, K. 2013. Everolimus for angiomyolipoma associated with tuberous sclerosis complex or sporadic lymphangioleiomyomatosis (EXIST-2): a multicentre, randomised, double-blind, placebo-controlled trial. *Lancet,* 381**,** 817-24.

BISSLER, J. J., MCCORMACK, F. X., YOUNG, L. R., ELWING, J. M., CHUCK, G., LEONARD, J. M., SCHMITHORST, V. J., LAOR, T., BRODY, A. S., BEAN, J., SALISBURY, S. & FRANZ, D. N. 2008. Sirolimus for

angiomyolipoma in tuberous sclerosis complex or lymphangioleiomyomatosis. *N Engl J Med,* 358**,** 140-51.
BJERKVIG, R., TONNESEN, A., LAERUM, O. D. & BACKLUND, E. O. 1990. Multicellular tumor spheroids from human gliomas maintained in organ culture. *J Neurosurg,* 72**,** 463-75.
BLACK, J. L., GE, Q., BOUSTANY, S., JOHNSON, P. R., PONIRIS, M. H., GLANVILLE, A. R., OLIVER, B. G., MOIR, L. M. & BURGESS, J. K. 2005. In vitro studies of lymphangioleiomyomatosis. *European Respiratory Journal,* 26**,** 569-76.
BLOM, R. A. M., ERNI, S. T., KREMPASKÁ, K., SCHAERER, O., VAN DIJK, R. M., AMACKER, M., MOSER, C., HALL, S. R. R., VON GARNIER, C. & BLANK, F. 2016. A Triple Co-Culture Model of the Human Respiratory Tract to Study Immune-Modulatory Effects of Liposomes and Virosomes. *PLOS ONE,* 11**,** e0163539.
BOEDTKJER, E., MOREIRA, J. M., MELE, M., VAHL, P., WIELENGA, V. T., CHRISTIANSEN, P. M., JENSEN, V. E., PEDERSEN, S. F. & AALKJAER, C. 2013. Contribution of Na+,HCO3(-)-cotransport to cellular pH control in human breast cancer: a role for the breast cancer susceptibility locus NBCn1 (SLC4A7). *Int J Cancer,* 132**,** 1288-99.
BONNANS, C., CHOU, J. & WERB, Z. 2014. Remodelling the extracellular matrix in development and disease. *Nat Rev Mol Cell Biol,* 15**,** 786-801.
BOONACKER, E. & VAN NOORDEN, C. J. 2001. Enzyme cytochemical techniques for metabolic mapping in living cells, with special reference to proteolysis. *J Histochem Cytochem,* 49**,** 1473-86.
BOOTH, A. J., HADLEY, R., CORNETT, A. M., DREFFS, A. A., MATTHES, S. A., TSUI, J. L., WEISS, K., HOROWITZ, J. C., FIORE, V. F., BARKER, T. H., MOORE, B. B., MARTINEZ, F. J., NIKLASON, L. E. & WHITE, E. S. 2012. Acellular normal and fibrotic human lung matrices as a culture system for in vitro investigation. *Am J Respir Crit Care Med,* 186**,** 866-76.
BORIS, T., DUSAN, T. & GUY, S. S. 2002. Regulating Cysteine Protease Activity: Essential Role of Protease Inhibitors As Guardians and Regulators. *Current Pharmaceutical Design,* 8**,** 1623-1637.
BOSSARD, M. J., TOMASZEK, T. A., THOMPSON, S. K., AMEGADZIE, B. Y., HANNING, C. R., JONES, C., KURDYLA, J. T., MCNULTY, D. E., DRAKE, F. H., GOWEN, M. & LEVY, M. A. 1996. Proteolytic activity of human osteoclast cathepsin K. Expression, purification, activation, and substrate identification. *J Biol Chem,* 271**,** 12517-24.
BOYDEN, S. 1962. THE CHEMOTACTIC EFFECT OF MIXTURES OF ANTIBODY AND ANTIGEN ON POLYMORPHONUCLEAR LEUCOCYTES. *The Journal of Experimental Medicine,* 115**,** 453-466.
BRACKE, K., CATALDO, D., MAES, T., GUEDERS, M., NOEL, A., FOIDART, J. M., BRUSSELLE, G. & PAUWELS, R. A. 2005. Matrix metalloproteinase-12 and cathepsin D expression in pulmonary macrophages and dendritic cells of cigarette smoke-exposed mice. *Int Arch Allergy Immunol,* 138**,** 169-79.

BRENNEN, W. N., ISAACS, J. T. & DENMEADE, S. R. 2012. Rationale behind targeting fibroblast activation protein-expressing carcinoma-associated fibroblasts as a novel chemotherapeutic strategy. *Mol Cancer Ther,* 11**,** 257-66.

BRIGHTLING, C. E., AMMIT, A. J., KAUR, D., BLACK, J. L., WARDLAW, A. J., HUGHES, J. M. & BRADDING, P. 2005. The CXCL10/CXCR3 Axis Mediates Human Lung Mast Cell Migration to Asthmatic Airway Smooth Muscle. *American Journal of Respiratory and Critical Care Medicine,* 171**,** 1103-1108.

BROMME, D. & LECAILLE, F. 2009. Cathepsin K inhibitors for osteoporosis and potential off-target effects. *Expert Opin Investig Drugs,* 18**,** 585-600.

BROMME, D., LI, Z., BARNES, M. & MEHLER, E. 1999. Human cathepsin V functional expression, tissue distribution, electrostatic surface potential, enzymatic characterization, and chromosomal localization. *Biochemistry,* 38**,** 2377-85.

BROMME, D., OKAMOTO, K., WANG, B. B. & BIROC, S. 1996. Human cathepsin O2, a matrix protein-degrading cysteine protease expressed in osteoclasts. Functional expression of human cathepsin O2 in Spodoptera frugiperda and characterization of the enzyme. *Journal of Biological Chemistry,* 271**,** 2126-32.

BROMME, D., RINNE, R. & KIRSCHKE, H. 1991. Tight-binding inhibition of cathepsin S by cystatins. *Biomed Biochim Acta,* 50**,** 631-5.

BRÖMME, D. & WILSON, S. 2011. Role of Cysteine Cathepsins in Extracellular Proteolysis. *In:* PARKS, W. C. & MECHAM, R. P. (eds.) *Extracellular Matrix Degradation.* Berlin, Heidelberg: Springer Berlin Heidelberg.

BROUARD, S., PUIG-PEY, I., LOZANO, J. J., PALLIER, A., BRAUD, C., GIRAL, M., GUILLET, M., LONDONO, M. C., OPPENHEIMER, F., CAMPISTOL, J. M., SOULILLOU, J. P. & SANCHEZ-FUEYO, A. 2010. Comparative transcriptional and phenotypic peripheral blood analysis of kidney recipients under cyclosporin A or sirolimus monotherapy. *Am J Transplant,* 10**,** 2604-14.

BROWN, E. J., ALBERS, M. W., SHIN, T. B., ICHIKAWA, K., KEITH, C. T., LANE, W. S. & SCHREIBER, S. L. 1994. A mammalian protein targeted by G1-arresting rapamycin-receptor complex. *Nature,* 369**,** 756-8.

BUHLING, F., PEITZ, U., KRUGER, S., KUSTER, D., VIETH, M., GEBERT, I., ROESSNER, A., WEBER, E., MALFERTHEINER, P. & WEX, T. 2004a. Cathepsins K, L, B, X and W are differentially expressed in normal and chronically inflamed gastric mucosa. *Biol Chem,* 385**,** 439-45.

BUHLING, F., ROCKEN, C., BRASCH, F., HARTIG, R., YASUDA, Y., SAFTIG, P., BROMME, D. & WELTE, T. 2004b. Pivotal role of cathepsin K in lung fibrosis. *Am J Pathol,* 164**,** 2203-16.

BUHLING, F., WALDBURG, N., REISENAUER, A., HEIMBURG, A., GOLPON, H. & WELTE, T. 2004c. Lysosomal cysteine proteases in the lung: role in protein processing and immunoregulation. *Eur Respir J,* 23**,** 620-8.

BURNETT, P. E., BARROW, R. K., COHEN, N. A., SNYDER, S. H. & SABATINI, D. M. 1998. RAFT1 phosphorylation of the translational regulators p70 S6 kinase and 4E-BP1. *Proc Natl Acad Sci U S A,* 95**,** 1432-7.

CAGLIC, D., PUNGERCAR, J. R., PEJLER, G., TURK, V. & TURK, B. 2007. Glycosaminoglycans facilitate procathepsin B activation through disruption of propeptide-mature enzyme interactions. *J Biol Chem,* 282**,** 33076-85.

CAI, X., PACHECO-RODRIGUEZ, G., FAN, Q. Y., HAUGHEY, M., SAMSEL, L., EL-CHEMALY, S., WU, H. P., MCCOY, J. P., STEAGALL, W. K., LIN, J. P., DARLING, T. N. & MOSS, J. 2010. Phenotypic characterization of disseminated cells with TSC2 loss of heterozygosity in patients with lymphangioleiomyomatosis. *Am J Respir Crit Care Med,* 182**,** 1410-8.

CAMP, J. T., ELLOUMI, F., ROMAN-PEREZ, E., REIN, J., STEWART, D. A., HARRELL, J. C., PEROU, C. M. & TROESTER, M. A. 2011. Interactions with fibroblasts are distinct in Basal-like and luminal breast cancers. *Mol Cancer Res,* 9**,** 3-13.

CARBON, S., IRELAND, A., MUNGALL, C. J., SHU, S., MARSHALL, B. & LEWIS, S. 2008. AmiGO: online access to ontology and annotation data. *Bioinformatics,* 25**,** 288-289.

CARELLI, S., LESMA, E., PARATORE, S., GRANDE, V., ZADRA, G., BOSARI, S., DI GIULIO, A. M. & GORIO, A. 2007. Survivin expression in tuberous sclerosis complex cells. *Mol Med,* 13**,** 166-77.

CARR, M. W., ROTH, S. J., LUTHER, E., ROSE, S. S. & SPRINGER, T. A. 1994. Monocyte chemoattractant protein 1 acts as a T-lymphocyte chemoattractant. *Proc Natl Acad Sci U S A,* 91**,** 3652-6.

CARSILLO, T., ASTRINIDIS, A. & HENSKE, E. P. 2000. Mutations in the tuberous sclerosis complex gene TSC2 are a cause of sporadic pulmonary lymphangioleiomyomatosis. *Proc Natl Acad Sci U S A,* 97**,** 6085-90.

CASTRO, M., SHEPHERD, C. W., GOMEZ, M. R., LIE, J. T. & RYU, J. H. 1995. Pulmonary tuberous sclerosis. *Chest,* 107**,** 189-95.

CATANIA, M. G., JOHNSON, M. W., LIAU, L. M., KREMEN, T. J., DEVELLIS, J. S. & VINTERS, H. V. 2001. Hamartin expression and interaction with tuberin in tumor cell lines and primary cultures. *J Neurosci Res,* 63**,** 276-83.

CAUGHEY, G. H. 2007. Mast cell tryptases and chymases in inflammation and host defense. *Immunological reviews,* 217**,** 141-154.

CAWSTON, T. E. & YOUNG, D. A. 2010. Proteinases involved in matrix turnover during cartilage and bone breakdown. *Cell Tissue Res,* 339**,** 221-35.

CH'EN, F. F., VILLAFUERTE, F. C., SWIETACH, P., COBDEN, P. M. & VAUGHAN-JONES, R. D. 2008. S0859, an N-cyanosulphonamide inhibitor of sodium-bicarbonate cotransport in the heart. *Br J Pharmacol,* 153**,** 972-82.

CHANG, H. Y., CHI, J.-T., DUDOIT, S., BONDRE, C., VAN DE RIJN, M., BOTSTEIN, D. & BROWN, P. O. 2002. Diversity, topographic differentiation, and positional memory in human fibroblasts.

*Proceedings of the National Academy of Sciences of the United States of America,* 99**,** 12877-12882.
CHANG, W. Y., CANE, J. L., BLAKEY, J. D., KUMARAN, M., POINTON, K. S. & JOHNSON, S. R. 2012. Clinical utility of diagnostic guidelines and putative biomarkers in lymphangioleiomyomatosis. *Respir Res,* 13**,** 34.
CHANG, W. Y., CANE, J. L., KUMARAN, M., LEWIS, S., TATTERSFIELD, A. E. & JOHNSON, S. R. 2014. A 2-year randomised placebo-controlled trial of doxycycline for lymphangioleiomyomatosis. *European Respiratory Journal,* 43**,** 1114-23.
CHANG, W. Y., CLEMENTS, D. & JOHNSON, S. R. 2010. Effect of doxycycline on proliferation, MMP production, and adhesion in LAM-related cells. *Am J Physiol Lung Cell Mol Physiol,* 299**,** L393-400.
CHANG, W. Y. C., CANE, J. L., KUMARAN, M., LEWIS, S., TATTERSFIELD, A. E. & JOHNSON, S. R. 2013. A two year randomised placebo controlled trial of doxycycline for lymphangioleiomyomatosis. *Eur Resp J,* In press.
CHAUHAN, S. S., POPESCU, N. C., RAY, D., FLEISCHMANN, R., GOTTESMAN, M. M. & TROEN, B. R. 1993. Cloning, genomic organization, and chromosomal localization of human cathepsin L. *J Biol Chem,* 268**,** 1039-45.
CHEEMA, U., YANG, S. Y., MUDERA, V., GOLDSPINK, G. G. & BROWN, R. A. 2003. 3-D in vitro model of early skeletal muscle development. *Cell Motil Cytoskeleton,* 54**,** 226-36.
CHEN, H., WANG, L., BERETOV, J., HAO, J., XIAO, W. & LI, Y. 2010. Co-expression of CD147/EMMPRIN with monocarboxylate transporters and multiple drug resistance proteins is associated with epithelial ovarian cancer progression. *Clin Exp Metastasis,* 27**,** 557-69.
CHEN, K., POCIASK, D. A., MCALEER, J. P., CHAN, Y. R., ALCORN, J. F., KREINDLER, J. L., KEYSER, M. R., SHAPIRO, S. D., HOUGHTON, A. M., KOLLS, J. K. & ZHENG, M. 2011. IL-17RA Is Required for CCL2 Expression, Macrophage Recruitment, and Emphysema in Response to Cigarette Smoke. *PLoS ONE,* 6**,** e20333.
CHILOSI, M., PEA, M., MARTIGNONI, G., BRUNELLI, M., GOBBO, S., POLETTI, V. & BONETTI, F. 2009. Cathepsin-k expression in pulmonary lymphangioleiomyomatosis. *Mod Pathol,* 22**,** 161-6.
CHOE, C., SHIN, Y. S., KIM, S. H., JEON, M. J., CHOI, S. J., LEE, J. & KIM, J. 2013. Tumor-stromal interactions with direct cell contacts enhance motility of non-small cell lung cancer cells through the hedgehog signaling pathway. *Anticancer Res,* 33**,** 3715-23.
CHOI, K. Y., SWIERCZEWSKA, M., LEE, S. & CHEN, X. 2012. Protease-activated drug development. *Theranostics,* 2**,** 156-78.
CHOO, A. Y., YOON, S. O., KIM, S. G., ROUX, P. P. & BLENIS, J. 2008. Rapamycin differentially inhibits S6Ks and 4E-BP1 to mediate cell-type-specific repression of mRNA translation. *Proc Natl Acad Sci U S A,* 105**,** 17414-9.
CHOTTANAPUND, S., VAN DUURSEN, M. B., NAVASUMRIT, P., HUNSONTI, P., TIMTAVORN, S., RUCHIRAWAT, M. & VAN DEN BERG, M. 2013. Effect of androgens on different breast cancer cells co-cultured with

or without breast adipose fibroblasts. *J Steroid Biochem Mol Biol,* 138**,** 54-62.
CHU, S. C., HORIBA, K., USUKI, J., AVILA, N. A., CHEN, C. C., TRAVIS, W. D., FERRAND, V. J. & MOSS, J. 1999. Comprehensive evaluation of 35 patients with lymphangioleiomyomatosis. *Chest,* 115**,** 1041-1052.
CIRRI, P. & CHIARUGI, P. 2011. Cancer associated fibroblasts: the dark side of the coin. *American Journal of Cancer Research,* 1**,** 482-497.
CLARK-LEWIS, I., DEWALD, B., GEISER, T., MOSER, B. & BAGGIOLINI, M. 1993. Platelet factor 4 binds to interleukin 8 receptors and activates neutrophils when its N terminus is modified with Glu-Leu-Arg. *Proceedings of the National Academy of Sciences,* 90**,** 3574-3577.
CLEMENTS, D., ASPREY, S. L., MCCULLOCH, T. A., MORRIS, T. A., WATSON, S. A. & JOHNSON, S. R. 2009. Analysis of the oestrogen response in an angiomyolipoma derived xenograft model. *Endocr Relat Cancer,* 16**,** 59-72.
CLEMENTS, D., DONGRE, A., KRYMSKAYA, V. P. & JOHNSON, S. R. 2015. Wild type mesenchymal cells contribute to the lung pathology of lymphangioleiomyomatosis. *PLoS One,* 10**,** e0126025.
CLEMENTS, D., GLASGOW, C. G., MAGOWAN, L., CHANG, W. Y. C., MOSS, J., JOHNSON, S. R. 2009. Matrilysin/MMP−7 Expression in Lymphangioleiomyomatosis (LAM). *Am J Respir Crit Care Med* 179.
CLEMENTS, D., MARKWICK, L. J., PURI, N. & JOHNSON, S. R. 2010. Role of the CXCR4/CXCL12 axis in lymphangioleiomyomatosis and angiomyolipoma. *J Immunol,* 185**,** 1812-21.
CLINICALTRIALS.GOV.
CODOGNO, P. & MEIJER, A. J. 2005. Autophagy and signaling: their role in cell survival and cell death. *Cell Death Differ,* 12 Suppl 2**,** 1509-18.
COHEN, M. M., FREYER, A. M. & JOHNSON, S. R. 2009. Pregnancy experiences among women with lymphangioleiomyomatosis. *Respiratory Medicine,* 103**,** 766-772.
COHEN, M. M., POLLOCK-BARZIV, S. & JOHNSON, S. R. 2005. Emerging clinical picture of lymphangioleiomyomatosis. *Thorax,* 60**,** 875-9.
CONTE, E., GILI, E., FRUCIANO, M., FAGONE, E. & VANCHERI, C. 2013. Human lung fibroblasts increase CD4(+)CD25(+)Foxp3(+) T cells in co-cultured CD4(+) lymphocytes. *Cell Immunol,* 285**,** 55-61.
COSTA, K. M., MACIEL, I. S., KIST, L. W., CAMPOS, M. M. & BOGO, M. R. 2014. Pharmacological Inhibition of CXCR2 Chemokine Receptors Modulates Paraquat-Induced Intoxication in Rats. *PLOS ONE,* 9**,** e105740.
COUSSENS, L. M. & WERB, Z. 2002. Inflammation and cancer. *Nature,* 420**,** 860-867.
CRAIGON, D. J., JAMES, N., OKYERE, J., HIGGINS, J., JOTHAM, J. & MAY, S. 2004. NASCArrays: a repository for microarray data generated by NASC's transcriptomics service. *Nucleic Acids Res,* 32**,** D575-7.
CROUSER, E. D., CULVER, D. A., KNOX, K. S., JULIAN, M. W., SHAO, G., ABRAHAM, S., LIYANARACHCHI, S., MACRE, J. E., WEWERS, M. D., GAVRILIN, M. A., ROSS, P., ABBAS, A. & ENG, C. 2009. Gene

expression profiling identifies MMP-12 and ADAMDEC1 as potential pathogenic mediators of pulmonary sarcoidosis. *Am J Respir Crit Care Med,* 179**,** 929-38.

CUDZILO, C. J., SZCZESNIAK, R. D., BRODY, A. S., RATTAN, M. S., KRUEGER, D. A., BISSLER, J. J., FRANZ, D. N., MCCORMACK, F. X. & YOUNG, L. R. 2013. Lymphangioleiomyomatosis screening in women with tuberous sclerosis. *Chest,* 144**,** 578-85.

CUNNINGHAM, J. T., RODGERS, J. T., ARLOW, D. H., VAZQUEZ, F., MOOTHA, V. K. & PUIGSERVER, P. 2007. mTOR controls mitochondrial oxidative function through a YY1-PGC-1alpha transcriptional complex. *Nature,* 450**,** 736-40.

CURTIS, R. K., OREŠIČ, M. & VIDAL-PUIG, A. 2005. Pathways to the analysis of microarray data. *Trends in Biotechnology,* 23**,** 429-435.

D'HAESELEER, P. 2005. How does gene expression clustering work? *Nat Biotech,* 23**,** 1499-1501.

DABORA, S. L., JOZWIAK, S., FRANZ, D. N., ROBERTS, P. S., NIETO, A., CHUNG, J., CHOY, Y. S., REEVE, M. P., THIELE, E., EGELHOFF, J. C., KASPRZYK-OBARA, J., DOMANSKA-PAKIELA, D. & KWIATKOWSKI, D. J. 2001. Mutational analysis in a cohort of 224 tuberous sclerosis patients indicates increased severity of TSC2, compared with TSC1, disease in multiple organs. *Am J Hum Genet,* 68**,** 64-80.

DALLAS, P. B., GOTTARDO, N. G., FIRTH, M. J., BEESLEY, A. H., HOFFMANN, K., TERRY, P. A., FREITAS, J. R., BOAG, J. M., CUMMINGS, A. J. & KEES, U. R. 2005. Gene expression levels assessed by oligonucleotide microarray analysis and quantitative real-time RT-PCR – how well do they correlate? *BMC Genomics,* 6**,** 59-59.

DAMAGHI, M., WOJTKOWIAK, J. W. & GILLIES, R. J. 2013. pH sensing and regulation in cancer. *Front Physiol,* 4**,** 370.

DANGLES-MARIE, V., POCARD, M., RICHON, S., WEISWALD, L.-B., ASSAYAG, F., SAULNIER, P., JUDDE, J.-G., JANNEAU, J.-L., AUGER, N., VALIDIRE, P., DUTRILLAUX, B., PRAZ, F., BELLET, D. & POUPON, M.-F. 2007. Establishment of Human Colon Cancer Cell Lines from Fresh Tumors versus Xenografts: Comparison of Success Rate and Cell Line Features. *Cancer Research,* 67**,** 398.

DANGLES, V., FÉMÉNIA, F., LAINÉ, V., BERTHELEMY, M., LE RHUN, D., POUPON, M. F., LEVY, D. & SCHWARTZ-CORNIL, I. 1997. Two- and three-dimensional cell structures govern epidermal growth factor survival function in human bladder carcinoma cell lines. *Cancer Research,* 57**,** 3360-3364.

DARLING, T. N., PACHECO-RODRIGUEZ, G., GORIO, A., LESMA, E., WALKER, C. & MOSS, J. 2010. Lymphangioleiomyomatosis and TSC2-/- cells. *Lymphat Res Biol,* 8**,** 59-69.

DAVIES, D. M., DE VRIES, P. J., JOHNSON, S. R., MCCARTNEY, D. L., COX, J. A., SERRA, A. L., WATSON, P. C., HOWE, C. J., DOYLE, T., POINTON, K., CROSS, J. J., TATTERSFIELD, A. E., KINGSWOOD, J. C. & SAMPSON, J. R. 2011. Sirolimus therapy for angiomyolipoma in tuberous sclerosis and sporadic lymphangioleiomyomatosis: a phase 2 trial. *Clin Cancer Res,* 17**,** 4071-81.

DAVIES, D. M., JOHNSON, S. R., TATTERSFIELD, A. E., KINGSWOOD, J. C., COX, J. A., MCCARTNEY, D. L., DOYLE, T., ELMSLIE, F., SAGGAR, A., DE VRIES, P. J. & SAMPSON, J. R. 2008. Sirolimus therapy in tuberous sclerosis or sporadic lymphangioleiomyomatosis. *N Engl J Med,* 358**,** 200-3.

DAVIS, J. M., HYJEK, E., HUSAIN, A. N., SHEN, L., JONES, J. & SCHUGER, L. A. 2013. Lymphatic Endothelial Differentiation in Pulmonary Lymphangioleiomyomatosis Cells. *Journal of Histochemistry & Cytochemistry,* 61**,** 580-590.

DE WEVER, O. & MAREEL, M. 2003. Role of tissue stroma in cancer cell invasion. *J Pathol,* 200**,** 429-47.

DENG, X., XU, M., YUAN, C., YIN, L., CHEN, X., ZHOU, X., LI, G., FU, Y., FEGHALI-BOSTWICK, C. A. & PANG, L. 2013. Transcriptional regulation of increased CCL2 expression in pulmonary fibrosis involves nuclear factor-κB and activator protein-1. *The International Journal of Biochemistry & Cell Biology,* 45**,** 1366-1376.

DERISI, J., PENLAND, L., BROWN, P. O., BITTNER, M. L., MELTZER, P. S., RAY, M., CHEN, Y., SU, Y. A. & TRENT, J. M. 1996. Use of a cDNA microarray to analyse gene expression patterns in human cancer. *Nat Genet,* 14**,** 457-60.

DESURMONT, S., BAUTERS, C., COPIN, M. C., DEWAILLY, D., TONNEL, A. B. & WALLAERT, B. 1996. [Treatment of pulmonary lymphangioleiomyomatosis using a GnRH agonist]. *Revue Des Maladies Respiratoires,* 13**,** 300-4.

DEYOUNG, M. P., HORAK, P., SOFER, A., SGROI, D. & ELLISEN, L. W. 2008. Hypoxia regulates TSC1/2-mTOR signaling and tumor suppression through REDD1-mediated 14-3-3 shuttling. *Genes Dev,* 22**,** 239-51.

DI CERA, E. 2009. Serine Proteases. *IUBMB life,* 61**,** 510-515.

DODDS, R. A., JAMES, I. E., RIEMAN, D., AHERN, R., HWANG, S. M., CONNOR, J. R., THOMPSON, S. D., VEBER, D. F., DRAKE, F. H., HOLMES, S., LARK, M. W. & GOWEN, M. 2001. Human osteoclast cathepsin K is processed intracellularly prior to attachment and bone resorption. *J Bone Miner Res,* 16**,** 478-86.

DOKE, S. K. & DHAWALE, S. C. 2015. Alternatives to animal testing: A review. *Saudi Pharmaceutical Journal,* 23**,** 223-229.

DONG, J., YU, X., PORTER, D. W., BATTELLI, L. A., KASHON, M. L. & MA, Q. 2016. Common and distinct mechanisms of induced pulmonary fibrosis by particulate and soluble chemical fibrogenic agents. *Archives of toxicology,* 90**,** 385-402.

DONG, S., ZHANG, X., HE, Y., XU, F., LI, D., XU, W., WANG, H., YIN, Y. & CAO, J. 2013. Synergy of IL-27 and TNF-α in Regulating CXCL10 Expression in Lung Fibroblasts. *American Journal of Respiratory Cell and Molecular Biology,* 48**,** 518-530.

DONGRE, A., CLEMENTS, D., FISHER, A. J. & JOHNSON, S. R. 2017. Cathepsin K in Lymphangioleiomyomatosis: LAM Cell–Fibroblast Interactions Enhance Protease Activity by Extracellular Acidification. *The American Journal of Pathology,* 187**,** 1750-1762.

DOWNEY, T. 2006. Analysis of a multifactor microarray study using Partek genomics solution. *Methods Enzymol,* 411**,** 256-70.

DUNSMORE, S. E. & RANNELS, D. E. 1996. Extracellular matrix biology in the lung. *Am J Physiol,* 270**,** L3-27.

DUVEL, K., YECIES, J. L., MENON, S., RAMAN, P., LIPOVSKY, A. I., SOUZA, A. L., TRIANTAFELLOW, E., MA, Q., GORSKI, R., CLEAVER, S., VANDER HEIDEN, M. G., MACKEIGAN, J. P., FINAN, P. M., CLISH, C. B., MURPHY, L. O. & MANNING, B. D. 2010. Activation of a metabolic gene regulatory network downstream of mTOR complex 1. *Mol Cell,* 39**,** 171-83.

EBISUI, C., TSUJINAKA, T., MORIMOTO, T., KAN, K., IIJIMA, S., YANO, M., KOMINAMI, E., TANAKA, K. & MONDEN, M. 1995. Interleukin-6 induces proteolysis by activating intracellular proteases (cathepsins B and L, proteasome) in C2C12 myotubes. *Clin Sci (Lond),* 89**,** 431-9.

ECK, S. M., COTE, A. L., WINKELMAN, W. D. & BRINCKERHOFF, C. E. 2009. CXCR4 and matrix metalloproteinase-1 are elevated in breast carcinoma-associated fibroblasts and in normal mammary fibroblasts exposed to factors secreted by breast cancer cells. *Mol Cancer Res,* 7**,** 1033-44.

EDMONDSON, R., BROGLIE, J. J., ADCOCK, A. F. & YANG, L. 2014. Three-dimensional cell culture systems and their applications in drug discovery and cell-based biosensors. *Assay Drug Dev Technol,* 12**,** 207-18.

EDWARDS, S. T., CRUZ, A. C., DONNELLY, S., DAZIN, P. F., SCHULMAN, E. S., JONES, K. D., WOLTERS, P. J., HOOPES, C., DOLGANOV, G. M. & FANG, K. C. 2005. c-Kit immunophenotyping and metalloproteinase expression profiles of mast cells in interstitial lung diseases. *Journal of Pathology,* 206**,** 279-90.

EKER, R. 1954. Familial renal adenomas in Wistar rats; a preliminary report. *Acta Pathol Microbiol Scand,* 34**,** 554-62.

EKER, R., MOSSIGE, J., JOHANNESSEN, J. V. & AARS, H. 1981. Hereditary renal adenomas and adenocarcinomas in rats. *Diagn Histopathol,* 4**,** 99-110.

EL-HASHEMITE, N., WALKER, V., ZHANG, H. & KWIATKOWSKI, D. J. 2003. Loss of Tsc1 or Tsc2 induces vascular endothelial growth factor production through mammalian target of rapamycin. *Cancer Research,* 63**,** 5173-7.

ETIENNE, W., MEYER, M. H., PEPPERS, J. & MEYER, R. A., JR. 2004. Comparison of mRNA gene expression by RT-PCR and DNA microarray. *Biotechniques,* 36**,** 618-20, 622, 624-6.

ETZIONI, A. 1996. Adhesion Molecules-Their Role in Health and Disease. *Pediatr Res,* 39**,** 191-198.

EUROPEAN CHROMOSOME 16 TUBEROUS SCLEROSIS, C. 1993. Identification and characterization of the tuberous sclerosis gene on chromosome 16. *Cell,* 75**,** 1305-15.

EVERITT, J. I., GOLDSWORTHY, T. L., WOLF, D. C. & WALKER, C. L. 1992. Hereditary renal cell carcinoma in the Eker rat: a rodent familial cancer syndrome. *J Urol,* 148**,** 1932-6.

EVERITT, J. I., WOLF, D. C., HOWE, S. R., GOLDSWORTHY, T. L. & WALKER, C. 1995. Rodent model of reproductive tract leiomyomata. Clinical and pathological features. *Am J Pathol,* 146**,** 1556-67.

EVERTS, V., HOU, W. S., RIALLAND, X., TIGCHELAAR, W., SAFTIG, P., BROMME, D., GELB, B. D. & BEERTSEN, W. 2003. Cathepsin K deficiency in pycnodysostosis results in accumulation of non-digested phagocytosed collagen in fibroblasts. *Calcif Tissue Int,* 73**,** 380-6.

EVERTS, V., KORPER, W., HOEBEN, K. A., JANSEN, I. D. C., BROMME, D., CLEUTJENS, K. B. J. M., HEENEMAN, S., PETERS, C., REINHECKEL, T., SAFTIG, P. & BEERTSEN, W. 2006. Osteoclastic Bone Degradation and the Role of Different Cysteine Proteinases and Matrix Metalloproteinases: Differences Between Calvaria and Long Bone. *Journal of Bone and Mineral Research,* 21**,** 1399-1408.

FAIZ, A., TJIN, G., HARKNESS, L., WECKMANN, M., BAO, S., BLACK, J. L., OLIVER, B. G. & BURGESS, J. K. 2013. The expression and activity of cathepsins D, H and K in asthmatic airways. *Plos One,* 8**,** e57245.

FAJARDO, I., SVENSSON, L., BUCHT, A. & PEJLER, G. 2004. Increased Levels of Hypoxia-sensitive Proteins in Allergic Airway Inflammation. *American Journal of Respiratory and Critical Care Medicine,* 170**,** 477-484.

FENG, Z., ZHANG, H., LEVINE, A. J. & JIN, S. 2005. The coordinate regulation of the p53 and mTOR pathways in cells. *Proc Natl Acad Sci U S A,* 102**,** 8204-9.

FERRI, N., CARRAGHER, N. O. & RAINES, E. W. 2004. Role of Discoidin Domain Receptors 1 and 2 in Human Smooth Muscle Cell-Mediated Collagen Remodeling: Potential Implications in Atherosclerosis and Lymphangioleiomyomatosis. *Am J Pathol,* 164**,** 1575-1585.

FONOVIC, M. & TURK, B. 2014. Cysteine cathepsins and extracellular matrix degradation. *Biochim Biophys Acta,* 1840**,** 2560-70.

FOSTER, D. A. 2009. Phosphatidic acid signaling to mTOR: signals for the survival of human cancer cells. *Biochim Biophys Acta,* 1791**,** 949-55.

FRIAS, M. A., THOREEN, C. C., JAFFE, J. D., SCHRODER, W., SCULLEY, T., CARR, S. A. & SABATINI, D. M. 2006. mSin1 is necessary for Akt/PKB phosphorylation, and its isoforms define three distinct mTORC2s. *Curr Biol,* 16**,** 1865-70.

FRIEDRICH, J., SEIDEL, C., EBNER, R. & KUNZ-SCHUGHART, L. A. 2009. Spheroid-based drug screen: considerations and practical approach. *Nat. Protocols,* 4**,** 309-324.

FROEHLICH, K., HAEGER, J. D., HEGER, J., PASTUSCHEK, J., PHOTINI, S. M., YAN, Y., LUPP, A., PFARRER, C., MROWKA, R., SCHLEUSSNER, E., MARKERT, U. R. & SCHMIDT, A. 2016. Generation of Multicellular Breast Cancer Tumor Spheroids: Comparison of Different Protocols. *J Mammary Gland Biol Neoplasia*.

FUKUDA, Y., KAWAMOTO, M., YAMAMOTO, A., ISHIZAKI, M., BASSET, F. & MASUGI, Y. 1990. Role of elastic fiber degradation in emphysema-like lesions of pulmonary lymphangiomyomatosis. *Human Pathology,* 21**,** 1252-61.

FUKUMOTO, S. & YAMADA, Y. 2005. Review: extracellular matrix regulates tooth morphogenesis. *Connect Tissue Res,* 46**,** 220-6.
FURUYAMA, N. & FUJISAWA, Y. 2000. Regulation of collagenolytic cysteine protease synthesis by estrogen in osteoclasts. *Steroids,* 65**,** 371-8.
GALLON, L., TRAITANON, O., SUSTENTO-REODICA, N., LEVENTHAL, J., ANSARI, M. J., GEHRAU, R. C., ARIYAMUTHU, V., DE SERRES, S. A., ALVARADO, A., CHHABRA, D., MATHEW, J. M., NAJAFIAN, N. & MAS, V. 2015. Cellular and molecular immune profiles in renal transplant recipients after conversion from Tacrolimus to Sirolimus. *Kidney international,* 87**,** 828-838.
GANLEY, I. G., LAM DU, H., WANG, J., DING, X., CHEN, S. & JIANG, X. 2009. ULK1.ATG13.FIP200 complex mediates mTOR signaling and is essential for autophagy. *Journal of Biological Chemistry,* 284**,** 12297-305.
GARAMI, A., ZWARTKRUIS, F. J., NOBUKUNI, T., JOAQUIN, M., ROCCIO, M., STOCKER, H., KOZMA, S. C., HAFEN, E., BOS, J. L. & THOMAS, G. 2003. Insulin activation of Rheb, a mediator of mTOR/S6K/4E-BP signaling, is inhibited by TSC1 and 2. *Mol Cell,* 11**,** 1457-66.
GARCIA-MARTINEZ, J. M. & ALESSI, D. R. 2008. mTOR complex 2 (mTORC2) controls hydrophobic motif phosphorylation and activation of serum- and glucocorticoid-induced protein kinase 1 (SGK1). *Biochem J,* 416**,** 375-85.
GATENBY, R. A. & GILLIES, R. J. 2004. Why do cancers have high aerobic glycolysis? *Nat Rev Cancer,* 4**,** 891-9.
GAUTHIER, J. Y., CHAURET, N., CROMLISH, W., DESMARAIS, S., DUONG, L. T., FALGUEYRET, J.-P., KIMMEL, D. B., LAMONTAGNE, S., LÉGER, S., LERICHE, T., LI, C. S., MASSÉ, F., MCKAY, D. J., NICOLL-GRIFFITH, D. A., OBALLA, R. M., PALMER, J. T., PERCIVAL, M. D., RIENDEAU, D., ROBICHAUD, J., RODAN, G. A., RODAN, S. B., SETO, C., THÉRIEN, M., TRUONG, V.-L., VENUTI, M. C., WESOLOWSKI, G., YOUNG, R. N., ZAMBONI, R. & BLACK, W. C. 2008. The discovery of odanacatib (MK-0822), a selective inhibitor of cathepsin K. *Bioorganic & Medicinal Chemistry Letters,* 18**,** 923-928.
GINGRAS, A. C., RAUGHT, B. & SONENBERG, N. 2001. Regulation of translation initiation by FRAP/mTOR. *Genes Dev,* 15**,** 807-26.
GLACE, L., GRYGIELKO, E. T., BOYLE, R., WANG, Q., LAPING, N. J., SULPIZIO, A. C. & BRAY, J. D. 2009. Estrogen-induced stromal cell-derived factor-1 (SDF-1/Cxcl12) expression is repressed by progesterone and by Selective Estrogen Receptor Modulators via estrogen receptor alpha in rat uterine cells and tissues. *Steroids,* 74**,** 1015-24.
GLANTSCHNIG, H., FISHER, J. E., WESOLOWSKI, G., RODAN, G. A. & RESZKA, A. A. 2003. M-CSF, TNFalpha and RANK ligand promote osteoclast survival by signaling through mTOR/S6 kinase. *Cell Death Differ,* 10**,** 1165-77.
GLASGOW, C. G., STEAGALL, W. K., TAVEIRA-DASILVA, A., PACHECO-RODRIGUEZ, G., CAI, X., EL-CHEMALY, S., MOSES, M., DARLING, T. & MOSS, J. 2010. Lymphangioleiomyomatosis (LAM): molecular

insights lead to targeted therapies. *Respir Med,* 104 Suppl 1**,** S45-58.

GLASSBERG, M. K., ELLIOT, S. J., FRITZ, J., CATANUTO, P., POTIER, M., DONAHUE, R., STETLER-STEVENSON, W. & KARL, M. 2008. Activation of the estrogen receptor contributes to the progression of pulmonary lymphangioleiomyomatosis via matrix metalloproteinase-induced cell invasiveness. *Journal of Clinical Endocrinology & Metabolism,* 93**,** 1625-1633.

GOERS, L., FREEMONT, P. & POLIZZI, K. M. 2014. Co-culture systems and technologies: taking synthetic biology to the next level. *J R Soc Interface,* 11.

GOLDBERG, H. J., HARARI, S., COTTIN, V., ROSAS, I. O., PETERS, E., BISWAL, S., CHENG, Y., KHINDRI, S., KOVARIK, J. M., MA, S., MCCORMACK, F. X. & HENSKE, E. P. 2015. Everolimus for the treatment of lymphangioleiomyomatosis: a phase II study. *Eur Respir J,* 46**,** 783-94.

GOLDRING, K., JONES, G. E., SEWRY, C. A. & WATT, D. J. 2002. The muscle-specific marker desmin is expressed in a proportion of human dermal fibroblasts after their exposure to galectin-1. *Neuromuscul Disord,* 12**,** 183-6.

GOLOVATCH, P., MERCER, B. A., LEMAITRE, V., WALLACE, A., FORONJY, R. F. & D'ARMIENTO, J. 2009. Role for cathepsin K in emphysema in smoke-exposed guinea pigs. *Exp Lung Res,* 35**,** 631-45.

GONCHAROVA, E. A., GONCHAROV, D. A., CHISOLM, A., SPAITS, M. S., LIM, P. N., CESARONE, G., KHAVIN, I., TLIBA, O., AMRANI, Y., PANETTIERI, R. A., JR. & KRYMSKAYA, V. P. 2008. Interferon beta augments tuberous sclerosis complex 2 (TSC2)-dependent inhibition of TSC2-null ELT3 and human lymphangioleiomyomatosis-derived cell proliferation. *Molecular Pharmacology,* 73**,** 778-88.

GONCHAROVA, E. A., GONCHAROV, D. A., ESZTERHAS, A., HUNTER, D. S., GLASSBERG, M. K., YEUNG, R. S., WALKER, C. L., NOONAN, D., KWIATKOWSKI, D. J., CHOU, M. M., PANETTIERI, R. A., JR. & KRYMSKAYA, V. P. 2002. Tuberin regulates p70 S6 kinase activation and ribosomal protein S6 phosphorylation. A role for the TSC2 tumor suppressor gene in pulmonary lymphangioleiomyomatosis (LAM). *Journal of Biological Chemistry,* 277**,** 30958-67.

GONCHAROVA, E. A., GONCHAROV, D. A., FEHRENBACH, M., KHAVIN, I., DUCKA, B., HINO, O., COLBY, T. V., MERRILEES, M. J., HACZKU, A., ALBELDA, S. M. & KRYMSKAYA, V. P. 2012. Prevention of alveolar destruction and airspace enlargement in a mouse model of pulmonary lymphangioleiomyomatosis (LAM). *Science Translational Medicine,* 4**,** 154ra134.

GOODPASTER, T., LEGESSE-MILLER, A., HAMEED, M. R., AISNER, S. C., RANDOLPH-HABECKER, J. & COLLER, H. A. 2008. An immunohistochemical method for identifying fibroblasts in formalin-fixed, paraffin-embedded tissue. *J Histochem Cytochem,* 56**,** 347-58.

GREEN, K. A. & LUND, L. R. 2005. ECM degrading proteases and tissue remodelling in the mammary gland. *Bioessays,* 27**,** 894-903.

GREENE, C. M. & MCELVANEY, N. G. 2009. Proteases and antiproteases in chronic neutrophilic lung disease - relevance to drug discovery. *Br J Pharmacol,* 158**,** 1048-58.
GRIFFITH, L. G. & SWARTZ, M. A. 2006. Capturing complex 3D tissue physiology in vitro. *Nat Rev Mol Cell Biol,* 7**,** 211-24.
GRZEGOREK, I., DROZDZ, K., PODHORSKA-OKOLOW, M., SZUBA, A. & DZIEGIEL, P. 2013. LAM cells biology and lymphangioleiomyomatosis. *Folia Histochem Cytobiol,* 51**,** 1-10.
HAECKEL, C., KRUEGER, S., BUEHLING, F., BROEMME, D., FRANKE, K., SCHUETZE, A., ROESE, I. & ROESSNER, A. 1999. Expression of cathepsin K in the human embryo and fetus. *Dev Dyn,* 216**,** 89-95.
HAJI-KARIM, M. 1978. Proliferation and Viability in Cellular Spheroids of Human Origin. *Cancer Research,* 38**,** 1457-1464.
HAM, S. L., JOSHI, R., THAKURI, P. S. & TAVANA, H. 2016. Liquid-based three-dimensional tumor models for cancer research and drug discovery. *Exp Biol Med (Maywood),* 241**,** 939-54.
HAMMES, S. R. & KRYMSKAYA, V. P. 2013. Targeted Approaches toward Understanding and Treating Pulmonary Lymphangioleiomyomatosis (LAM). *Hormones & Cancer,* 4**,** 70-77.
HANEMAAIJER, R., VISSER, H., KOOLWIJK, P., SORSA, T., SALO, T., GOLUB, L. M. & VAN HINSBERGH, V. W. 1998. Inhibition of MMP synthesis by doxycycline and chemically modified tetracyclines (CMTs) in human endothelial cells. *Adv Dent Res,* 12**,** 114-8.
HARA, K., MARUKI, Y., LONG, X., YOSHINO, K., OSHIRO, N., HIDAYAT, S., TOKUNAGA, C., AVRUCH, J. & YONEZAWA, K. 2002. Raptor, a binding partner of target of rapamycin (TOR), mediates TOR action. *Cell,* 110**,** 177-89.
HARARI, S., CASSANDRO, R., CHIODINI, I., TAVEIRA-DASILVA, A. M. & MOSS, J. 2008. Effect of a gonadotrophin-releasing hormone analogue on lung function in lymphangioleiomyomatosis. *Chest,* 133**,** 448-54.
HARARI, S., TORRE, O., CASSANDRO, R. & MOSS, J. 2015. The changing face of a rare disease: lymphangioleiomyomatosis. *European Respiratory Journal,* 46**,** 1471-1485.
HARARI, S., TORRE, O., MOSS, J. 2011. Lymphangioleiomyomatosis: what do we know and what are we looking for? *Eur Respir Rev.,* 20**,** 34-44.
HARKNETT, E. C., CHANG, W. Y. C., BYRNES, S., JOHNSON, J., LAZOR, R., COHEN, M. M., GRAY, B., GEILING, S., TELFORD, H., TATTERSFIELD, A. E., HUBBARD, R. B. & JOHNSON, S. R. 2011. Use of variability in national and regional data to estimate the prevalence of lymphangioleiomyomatosis. *Qjm-an International Journal of Medicine,* 104**,** 971-979.
HASHIMOTO, N., JIN, H., LIU, T., CHENSUE, S. W. & PHAN, S. H. 2004. Bone marrow–derived progenitor cells in pulmonary fibrosis. *Journal of Clinical Investigation,* 113**,** 243-252.
HATHERELL, K., COURAUD, P.-O., ROMERO, I. A., WEKSLER, B. & PILKINGTON, G. J. 2011. Development of a three-dimensional, all-human in vitro model of the blood–brain barrier using mono-, co-,

and tri-cultivation Transwell models. *Journal of Neuroscience Methods,* 199**,** 223-229.
HAY, N. & SONENBERG, N. 2004. Upstream and downstream of mTOR. *Genes Dev,* 18**,** 1926-45.
HAYASHI, T., FLEMING, M. V., STETLER-STEVENSON, W. G., LIOTTA, L. A., MOSS, J., FERRANS, V. J. & TRAVIS, W. D. 1997. Immunohistochemical study of matrix metalloproteinases (MMPs) and their tissue inhibitors (TIMPs) in pulmonary lymphangioleiomyomatosis (LAM). *Human Pathology,* 28**,** 1071-8.
HEBER, S., HOWARD, B., PSARROS, M. & SICK, B. Automatic Quality Assessment of Affymetrix GeneChip Data. 44th Annual ACM Southeast Conference, 2006 Melbourne, FL, USA. 411-416.
HEBER, S. & SICK, B. 2006. Quality assessment of Affymetrix GeneChip data. *Omics,* 10**,** 358-68.
HEIDER, K. H., KUTHAN, H., STEHLE, G. & MUNZERT, G. 2004. CD44v6: a target for antibody-based cancer therapy. *Cancer Immunol Immunother,* 53**,** 567-79.
HEMING, N., URIEN, S. & FAISY, C. 2012. Acetazolamide: a second wind for a respiratory stimulant in the intensive care unit? *Crit Care,* 16**,** 318.
HENEWEER, M., MUUSSE, M., DINGEMANS, M., DE JONG, P. C., VAN DEN BERG, M. & SANDERSON, J. T. 2005. Co-culture of Primary Human Mammary Fibroblasts and MCF-7 Cells as an In Vitro Breast Cancer Model. *Toxicological Sciences,* 83**,** 257-263.
HENRY, E., CORES, J., HENSLEY, M. T., ANTHONY, S., VANDERGRIFF, A., DE ANDRADE, J. B. M., ALLEN, T., CARANASOS, T. G., LOBO, L. J. & CHENG, K. 2015. Adult Lung Spheroid Cells Contain Progenitor Cells and Mediate Regeneration in Rodents With Bleomycin-Induced Pulmonary Fibrosis. *Stem Cells Translational Medicine,* 4**,** 1265-1274.
HENRY, M. T., MCMAHON, K., MACKAREL, A. J., PRIKK, K., SORSA, T., MAISI, P., SEPPER, R., FITZGERALD, M. X. & O'CONNOR, C. M. 2002. Matrix metalloproteinases and tissue inhibitor of metalloproteinase-1 in sarcoidosis and IPF. *Eur Respir J,* 20**,** 1220-7.
HENSKE, E. P. 2003. Metastasis of benign tumor cells in tuberous sclerosis complex. *Genes Chromosomes Cancer,* 38**,** 376-81.
HENSKE, E. P. & MCCORMACK, F. X. 2012. Lymphangioleiomyomatosis - a wolf in sheep's clothing. *J Clin Invest,* 122**,** 3807-16.
HEYLEN, N., VINCENT, L. M., DEVOS, V., DUBOIS, V., REMACLE, C. & TROUET, A. 2002. Fibroblasts capture cathepsin D secreted by breast cancer cells: possible role in the regulation of the invasive process. *Int J Oncol,* 20**,** 761-7.
HINZ, B. 2012. Mechanical Aspects of Lung Fibrosis. *Proceedings of the American Thoracic Society,* 9**,** 137-147.
HIRSCHHAEUSER, F., MENNE, H., DITTFELD, C., WEST, J., MUELLER-KLIESER, W. & KUNZ-SCHUGHART, L. A. 2010. Multicellular tumor spheroids: an underestimated tool is catching up again. *J Biotechnol,* 148**,** 3-15.

HODGES, L. C., HOUSTON, K. D., HUNTER, D. S., FUCHS-YOUNG, R., ZHANG, Z., WINEKER, R. C. & WALKER, C. L. 2002. Transdominant suppression of estrogen receptor signaling by progesterone receptor ligands in uterine leiomyoma cells. *Mol Cell Endocrinol,* 196**,** 11-20.

HOLLIDAY, D. L., BROUILETTE, K. T., MARKERT, A., GORDON, L. A. & JONES, J. L. 2009. Novel multicellular organotypic models of normal and malignant breast: tools for dissecting the role of the microenvironment in breast cancer progression. *Breast Cancer Research : BCR,* 11**,** R3-R3.

HOLT, D. J., CHAMBERLAIN, L. M. & GRAINGER, D. W. 2010. Cell-cell signaling in co-cultures of macrophages and fibroblasts. *Biomaterials,* 31**,** 9382-94.

HOLZ, M. K. 2012. The role of S6K1 in ER-positive breast cancer. *Cell Cycle,* 11**,** 3159-65.

HOON, V., THUNG, S. N., KANEKO, M. & UNGER, P. D. 1994. HMB-45 reactivity in renal angiomyolipoma and lymphangioleiomyomatosis. *Archives of Pathology & Laboratory Medicine,* 118**,** 732-4.

HORIE, M., SAITO, A., MIKAMI, Y., OHSHIMA, M., MORISHITA, Y., NAKAJIMA, J., KOHYAMA, T. & NAGASE, T. 2012. Characterization of human lung cancer-associated fibroblasts in three-dimensional in vitro co-culture model. *Biochem Biophys Res Commun,* 423**,** 158-63.

HOSOKAWA, N., HARA, T., KAIZUKA, T., KISHI, C., TAKAMURA, A., MIURA, Y., IEMURA, S., NATSUME, T., TAKEHANA, K., YAMADA, N., GUAN, J. L., OSHIRO, N. & MIZUSHIMA, N. 2009. Nutrient-dependent mTORC1 association with the ULK1-Atg13-FIP200 complex required for autophagy. *Mol Biol Cell,* 20**,** 1981-91.

HOU, W.-S., LI, Z., GORDON, R. E., CHAN, K., KLEIN, M. J., LEVY, R., KEYSSER, M., KEYSZER, G. & BRÖMME, D. Cathepsin K Is a Critical Protease in Synovial Fibroblast-Mediated Collagen Degradation. *The American Journal of Pathology,* 159**,** 2167-2177.

HOU, W. S., LI, W., KEYSZER, G., WEBER, E., LEVY, R., KLEIN, M. J., GRAVALLESE, E. M., GOLDRING, S. R. & BROMME, D. 2002. Comparison of cathepsins K and S expression within the rheumatoid and osteoarthritic synovium. *Arthritis Rheum,* 46**,** 663-74.

HOWE, S. R., GOTTARDIS, M. M., EVERITT, J. I., GOLDSWORTHY, T. L., WOLF, D. C. & WALKER, C. 1995. Rodent model of reproductive tract leiomyomata. Establishment and characterization of tumor-derived cell lines. *Am J Pathol,* 146**,** 1568-79.

HSU, H., LACEY, D. L., DUNSTAN, C. R., SOLOVYEV, I., COLOMBERO, A., TIMMS, E., TAN, H. L., ELLIOTT, G., KELLEY, M. J., SAROSI, I., WANG, L., XIA, X. Z., ELLIOTT, R., CHIU, L., BLACK, T., SCULLY, S., CAPPARELLI, C., MORONY, S., SHIMAMOTO, G., BASS, M. B. & BOYLE, W. J. 1999. Tumor necrosis factor receptor family member RANK mediates osteoclast differentiation and activation induced by osteoprotegerin ligand. *Proc Natl Acad Sci U S A,* 96**,** 3540-5.

HU, N., WESTRA, J., RUTGERS, A., DOORNBOS-VAN DER MEER, B., HUITEMA, M. G., STEGEMAN, C. A., ABDULAHAD, W. H., SATCHELL, S. C., MATHIESON, P. W., HEERINGA, P. & M KALLENBERG, C. G.

2011. Decreased CXCR1 and CXCR2 expression on neutrophils in anti-neutrophil cytoplasmic autoantibody-associated vasculitides potentially increases neutrophil adhesion and impairs migration. *Arthritis Research & Therapy,* 13**,** R201.

HUBER, V., DE MILITO, A., HARGUINDEY, S., RESHKIN, S. J., WAHL, M. L., RAUCH, C., CHIESI, A., POUYSSEGUR, J., GATENBY, R. A., RIVOLTINI, L. & FAIS, S. 2010. Proton dynamics in cancer. *J Transl Med,* 8**,** 57.

HUDSON, C. C., LIU, M., CHIANG, G. G., OTTERNESS, D. M., LOOMIS, D. C., KAPER, F., GIACCIA, A. J. & ABRAHAM, R. T. 2002. Regulation of hypoxia-inducible factor 1alpha expression and function by the mammalian target of rapamycin. *Mol Cell Biol,* 22**,** 7004-14.

HUGGINS, C. E., DOMENIGHETTI, A. A., RITCHIE, M. E., KHALIL, N., FAVALORO, J. M., PROIETTO, J., SMYTH, G. K., PEPE, S. & DELBRIDGE, L. M. 2008. Functional and metabolic remodelling in GLUT4-deficient hearts confers hyper-responsiveness to substrate intervention. *J Mol Cell Cardiol,* 44**,** 270-80.

HUTCHINSON, L. & KIRK, R. 2011. High drug attrition rates--where are we going wrong? *Nat Rev Clin Oncol,* 8**,** 189-90.

HYNES, R. O. 2009. Extracellular matrix: not just pretty fibrils. *Science (New York, N.Y.),* 326**,** 1216-1219.

HYNES, R. O. & NABA, A. 2012. Overview of the matrisome--an inventory of extracellular matrix constituents and functions. *Cold Spring Harb Perspect Biol,* 4**,** a004903.

IKEDA, R. K., MILLER, M., NAYAR, J., WALKER, L., CHO, J. Y., MCELWAIN, K., MCELWAIN, S., RAZ, E. & BROIDE, D. H. 2003. Accumulation of peribronchial mast cells in a mouse model of ovalbumin allergen induced chronic airway inflammation: modulation by immunostimulatory DNA sequences. *J Immunol,* 171**,** 4860-7.

IKEDA, Y., TAVEIRA-DASILVA, A. M., PACHECO-RODRIGUEZ, G., STEAGALL, W. K., EL-CHEMALY, S., GOCHUICO, B. R., MAY, R. M., HATHAWAY, O. M., LI, S., WANG, J. A., DARLING, T. N., STYLIANOU, M. & MOSS, J. 2011. Erythropoietin-driven proliferation of cells with mutations in the tumor suppressor gene TSC2. *Am J Physiol Lung Cell Mol Physiol,* 300**,** L64-72.

INAOKA, T., BILBE, G., ISHIBASHI, O., TEZUKA, K., KUMEGAWA, M. & KOKUBO, T. 1995. Molecular cloning of human cDNA for cathepsin K: novel cysteine proteinase predominantly expressed in bone. *Biochem Biophys Res Commun,* 206**,** 89-96.

INGRAM, M., TECHY, G. B., SAROUFEEM, R., YAZAN, O., NARAYAN, K. S., GOODWIN, T. J. & SPAULDING, G. F. 1997. Three-dimensional growth patterns of various human tumor cell lines in simulated microgravity of a NASA bioreactor. *In Vitro Cell Dev Biol Anim,* 33**,** 459-66.

INOKI, K., LI, Y., XU, T. & GUAN, K. L. 2003a. Rheb GTPase is a direct target of TSC2 GAP activity and regulates mTOR signaling. *Genes Dev,* 17**,** 1829-34.

INOKI, K., LI, Y., ZHU, T., WU, J. & GUAN, K. L. 2002. TSC2 is phosphorylated and inhibited by Akt and suppresses mTOR signalling. *Nat Cell Biol,* 4**,** 648-57.

INOKI, K., OUYANG, H., ZHU, T., LINDVALL, C., WANG, Y., ZHANG, X., YANG, Q., BENNETT, C., HARADA, Y., STANKUNAS, K., WANG, C. Y., HE, X., MACDOUGALD, O. A., YOU, M., WILLIAMS, B. O. & GUAN, K. L. 2006. TSC2 integrates Wnt and energy signals via a coordinated phosphorylation by AMPK and GSK3 to regulate cell growth. *Cell,* 126**,** 955-68.

INOKI, K., ZHU, T. & GUAN, K. L. 2003b. TSC2 mediates cellular energy response to control cell growth and survival. *Cell,* 115**,** 577-90.

IRIZARRY, R. A., HOBBS, B., COLLIN, F., BEAZER-BARCLAY, Y. D., ANTONELLIS, K. J., SCHERF, U. & SPEED, T. P. 2003. Exploration, normalization, and summaries of high density oligonucleotide array probe level data. *Biostatistics,* 4**,** 249-64.

ISSAKA, R. B., OOMMEN, S., GUPTA, S. K., LIU, G., MYERS, J. L., RYU, J. H. & VLAHAKIS, N. E. 2009. Vascular Endothelial Growth Factors C and D Induces Proliferation of Lymphangioleiomyomatosis Cells through Autocrine Crosstalk with Endothelium. *The American Journal of Pathology,* 175**,** 1410-1420.

IVANOV, D. P. & GRABOWSKA, A. M. 2017. Spheroid arrays for high-throughput single-cell analysis of spatial patterns and biomarker expression in 3D. 7**,** 41160.

IWANO, M., PLIETH, D., DANOFF, T. M., XUE, C., OKADA, H. & NEILSON, E. G. 2002. Evidence that fibroblasts derive from epithelium during tissue fibrosis. *J Clin Invest,* 110**,** 341-50.

JACINTO, E., LOEWITH, R., SCHMIDT, A., LIN, S., RUEGG, M. A., HALL, A. & HALL, M. N. 2004. Mammalian TOR complex 2 controls the actin cytoskeleton and is rapamycin insensitive. *Nat Cell Biol,* 6**,** 1122-8.

JALURIA, P., KONSTANTOPOULOS, K., BETENBAUGH, M. & SHILOACH, J. 2007. A perspective on microarrays: current applications, pitfalls, and potential uses. *Microbial Cell Factories,* 6**,** 4.

JAMIESON, L. E., HARRISON, D. J. & CAMPBELL, C. J. 2015. Chemical analysis of multicellular tumour spheroids. *Analyst,* 140**,** 3910-20.

JI, R. C. 2006. Lymphatic endothelial cells, lymphangiogenesis, and extracellular matrix. *Lymphat Res Biol,* 4**,** 83-100.

JOHNSON, M. W., EMELIN, J. K., PARK, S. H. & VINTERS, H. V. 1999. Co-localization of TSC1 and TSC2 gene products in tubers of patients with tuberous sclerosis. *Brain Pathol,* 9**,** 45-54.

JOHNSON, M. W., KERFOOT, C., BUSHNELL, T., LI, M. & VINTERS, H. V. 2001. Hamartin and tuberin expression in human tissues. *Mod Pathol,* 14**,** 202-10.

JOHNSON, S. R. 2006. Lymphangioleiomyomatosis. *European Respiratory Journal,* 27**,** 1056-65.

JOHNSON, S. R. 2010. The ERS guidelines for LAM: trying a rationale approach to a rare disease. *Respir Med,* 104 Suppl 1**,** S33-41.

JOHNSON, S. R., CORDIER, J. F., LAZOR, R., COTTIN, V., COSTABEL, U., HARARI, S., REYNAUD-GAUBERT, M., BOEHLER, A., BRAUNER, M., POPPER, H., BONETTI, F. & KINGSWOOD, C. 2010. European

Respiratory Society guidelines for the diagnosis and management of lymphangioleiomyomatosis. *European Respiratory Journal,* 35**,** 14-26.
JOHNSON, S. R., LAZOR, R., CORDIER, J.F. 2004. Lymphangioleiomyomatosis. *Orphanet Encyclopaedia.* Orphanet.
JOHNSON, S. R. & TATTERSFIELD, A. E. 1999. Decline in lung function in lymphangioleiomyomatosis: relation to menopause and progesterone treatment. *Am J Respir Crit Care Med,* 160**,** 628-33.
JOHNSON, S. R. & TATTERSFIELD, A. E. 2000. Clinical experience of lymphangioleiomyomatosis in the UK. *Thorax,* 55**,** 1052-7.
JOYCE, J. A. & POLLARD, J. W. 2009. Microenvironmental regulation of metastasis. *Nat Rev Cancer,* 9**,** 239-52.
JUREMALM, M. & NILSSON, G. 2005. Chemokine receptor expression by mast cells. *Chem Immunol Allergy,* 87**,** 130-44.
JUVET, S. C., MCCORMACK, F. X., KWIATKOWSKI, D. J. & DOWNEY, G. P. 2007. Molecular pathogenesis of lymphangioleiomyomatosis: lessons learned from orphans. *Am J Respir Cell Mol Biol,* 36**,** 398-408.
KAFIENAH, W., EL, BRÖMME, D., BUTTLE, D. J., CROUCHER, L. J. & HOLLANDER, A. P. 1998. Human cathepsin K cleaves native type I and II collagens at the N-terminal end of the triple helix. *Biochemical Journal,* 331**,** 727.
KAIZUKA, T., HARA, T., OSHIRO, N., KIKKAWA, U., YONEZAWA, K., TAKEHANA, K., IEMURA, S., NATSUME, T. & MIZUSHIMA, N. 2010. Tti1 and Tel2 are critical factors in mammalian target of rapamycin complex assembly. *Journal of Biological Chemistry,* 285**,** 20109-16.
KALLURI, R. & ZEISBERG, M. 2006. Fibroblasts in cancer. *Nat Rev Cancer,* 6**,** 392-401.
KALUZ, S., KALUZOVA, M., LIAO, S. Y., LERMAN, M. & STANBRIDGE, E. J. 2009. Transcriptional control of the tumor- and hypoxia-marker carbonic anhydrase 9: A one transcription factor (HIF-1) show? *Biochim Biophys Acta,* 1795**,** 162-72.
KANT, S., KUMAR, A. & SINGH, S. M. 2014. Bicarbonate transport inhibitor SITS modulates pH homeostasis triggering apoptosis of Dalton's lymphoma: implication of novel molecular mechanisms. *Mol Cell Biochem,* 397**,** 167-78.
KARBOWNICZEK, M., ASTRINIDIS, A., BALSARA, B. R., TESTA, J. R., LIUM, J. H., COLBY, T. V., MCCORMACK, F. X. & HENSKE, E. P. 2003. Recurrent lymphangiomyomatosis after transplantation: genetic analyses reveal a metastatic mechanism. *Am J Respir Crit Care Med,* 167**,** 976-82.
KASABOVA, M., JOULIN-GIET, A., LECAILLE, F., GILMORE, B. F., MARCHAND-ADAM, S., SAIDI, A. & LALMANACH, G. 2014. Regulation of TGF-β1-Driven Differentiation of Human Lung Fibroblasts: Emerging Roles of Cathepsin B and Cystatin C. *Journal of Biological Chemistry*.
KATT, M. E., PLACONE, A. L., WONG, A. D., XU, Z. S. & SEARSON, P. C. 2016. In Vitro Tumor Models: Advantages, Disadvantages,

Variables, and Selecting the Right Platform. *Frontiers in Bioengineering and Biotechnology,* 4.
KELM, J. M., TIMMINS, N. E., BROWN, C. J., FUSSENEGGER, M. & NIELSEN, L. K. 2003. Method for generation of homogeneous multicellular tumor spheroids applicable to a wide variety of cell types. *Biotechnology and Bioengineering,* 83**,** 173-180.
KENDALL, R. T. & FEGHALI-BOSTWICK, C. A. 2014. Fibroblasts in fibrosis: novel roles and mediators. *Frontiers in Pharmacology,* 5.
KENERSON, H., DUNDON, T. A. & YEUNG, R. S. 2005. Effects of rapamycin in the Eker rat model of tuberous sclerosis complex. *Pediatr Res,* 57**,** 67-75.
KENERSON, H. L., AICHER, L. D., TRUE, L. D. & YEUNG, R. S. 2002. Activated mammalian target of rapamycin pathway in the pathogenesis of tuberous sclerosis complex renal tumors. *Cancer Research,* 62**,** 5645-50.
KIM, D. H., SARBASSOV, D. D., ALI, S. M., KING, J. E., LATEK, R. R., ERDJUMENT-BROMAGE, H., TEMPST, P. & SABATINI, D. M. 2002. mTOR interacts with raptor to form a nutrient-sensitive complex that signals to the cell growth machinery. *Cell,* 110**,** 163-75.
KIM, D. H., SARBASSOV, D. D., ALI, S. M., LATEK, R. R., GUNTUR, K. V., ERDJUMENT-BROMAGE, H., TEMPST, P. & SABATINI, D. M. 2003a. GbetaL, a positive regulator of the rapamycin-sensitive pathway required for the nutrient-sensitive interaction between raptor and mTOR. *Mol Cell,* 11**,** 895-904.
KIM, H., LIU, X., KOHYAMA, T., KOBAYASHI, T., CONNER, H., ABE, S., FANG, Q., WEN, F. Q. & RENNARD, S. I. 2004. Cigarette smoke stimulates MMP-1 production by human lung fibroblasts through the ERK1/2 pathway. *Copd,* 1**,** 13-23.
KIM, J. E. & CHEN, J. 2004. regulation of peroxisome proliferator-activated receptor-gamma activity by mammalian target of rapamycin and amino acids in adipogenesis. *Diabetes,* 53**,** 2748-56.
KIM, N. R., CHUNG, M. P., PARK, C. K., LEE, K. S. & HAN, J. H. 2003b. Pulmonary lymphangioleiomyomatosis and multiple hepatic angiomyolipomas in a man. *Pathology International,* 53**,** 231-235.
KINDZELSKII, A. L., AMHAD, I., KELLER, D., ZHOU, M. J., HAUGLAND, R. P., GARNI-WAGNER, B. A., GYETKO, M. R., TODD, R. F., 3RD & PETTY, H. R. 2004. Pericellular proteolysis by leukocytes and tumor cells on substrates: focal activation and the role of urokinase-type plasminogen activator. *Histochem Cell Biol,* 121**,** 299-310.
KITAICHI, M., NISHIMURA, K., ITOH, H. & IZUMI, T. 1995. Pulmonary lymphangioleiomyomatosis: a report of 46 patients including a clinicopathologic study of prognostic factors. *Am J Respir Crit Care Med,* 151**,** 527-33.
KLEINMAN, H. K. & MARTIN, G. R. 2005. Matrigel: basement membrane matrix with biological activity. *Semin Cancer Biol,* 15**,** 378-86.
KLEINMAN, H. K., MCGARVEY, M. L., LIOTTA, L. A., ROBEY, P. G., TRYGGVASON, K. & MARTIN, G. R. 1982. Isolation and characterization of type IV procollagen, laminin, and heparan sulfate proteoglycan from the EHS sarcoma. *Biochemistry,* 21**,** 6188-6193.

KNEISSEL, M., LUONG-NGUYEN, N. H., BAPTIST, M., CORTESI, R., ZUMSTEIN-MECKER, S., KOSSIDA, S., O'REILLY, T., LANE, H. & SUSA, M. 2004. Everolimus suppresses cancellous bone loss, bone resorption, and cathepsin K expression by osteoclasts. *Bone,* 35**,** 1144-56.

KNIGHT, E. & PRZYBORSKI, S. 2015. Advances in 3D cell culture technologies enabling tissue-like structures to be created in vitro. *Journal of Anatomy,* 227**,** 746-756.

KNUDSON, A. G. 2001. Two genetic hits (more or less) to cancer. *Nat Rev Cancer,* 1**,** 157-62.

KOBAYASHI, T., HIRAYAMA, Y., KOBAYASHI, E., KUBO, Y. & HINO, O. 1995. A germline insertion in the tuberous sclerosis (Tsc2) gene gives rise to the Eker rat model of dominantly inherited cancer. *Nat Genet,* 9**,** 70-4.

KOBAYASHI, T., MINOWA, O., KUNO, J., MITANI, H., HINO, O. & NODA, T. 1999. Renal carcinogenesis, hepatic hemangiomatosis, and embryonic lethality caused by a germ-line Tsc2 mutation in mice. *Cancer Research,* 59**,** 1206-11.

KOBAYASHI, T., MINOWA, O., SUGITANI, Y., TAKAI, S., MITANI, H., KOBAYASHI, E., NODA, T. & HINO, O. 2001. A germ-line Tsc1 mutation causes tumor development and embryonic lethality that are similar, but not identical to, those caused by Tsc2 mutation in mice. *Proc Natl Acad Sci U S A,* 98**,** 8762-7.

KONDO, J., ENDO, H., OKUYAMA, H., ISHIKAWA, O., IISHI, H., TSUJII, M., OHUE, M. & INOUE, M. 2011. Retaining cell-cell contact enables preparation and culture of spheroids composed of pure primary cancer cells from colorectal cancer. *Proc Natl Acad Sci U S A,* 108**,** 6235-40.

KONUR, A., KREUTZ, M., KNUCHEL, R., KRAUSE, S. W. & ANDREESEN, R. 1996. Three-dimensional co-culture of human monocytes and macrophages with tumor cells: analysis of macrophage differentiation and activation. *Int J Cancer,* 66**,** 645-52.

KOPITZ, C., ANTON, M., GANSBACHER, B. & KRUGER, A. 2005. Reduction of experimental human fibrosarcoma lung metastasis in mice by adenovirus-mediated cystatin C overexpression in the host. *Cancer Res,* 65**,** 8608-12.

KOUMAS, L., SMITH, T. J., FELDON, S., BLUMBERG, N. & PHIPPS, R. P. 2003. Thy-1 Expression in Human Fibroblast Subsets Defines Myofibroblastic or Lipofibroblastic Phenotypes. *The American Journal of Pathology,* 163**,** 1291-1300.

KRISTOF, A. S. 2010. mTOR signaling in lymphangioleiomyomatosis. *Lymphat Res Biol,* 8**,** 33-42.

KUESTER, D., LIPPERT, H., ROESSNER, A. & KRUEGER, S. 2008. The cathepsin family and their role in colorectal cancer. *Pathology - Research and Practice,* 204**,** 491-500.

KUMAR, S., DARE, L., VASKO-MOSER, J. A., JAMES, I. E., BLAKE, S. M., RICKARD, D. J., HWANG, S. M., TOMASZEK, T., YAMASHITA, D. S., MARQUIS, R. W., OH, H., JEONG, J. U., VEBER, D. F., GOWEN, M., LARK, M. W. & STROUP, G. 2007. A highly potent inhibitor of

cathepsin K (relacatib) reduces biomarkers of bone resorption both in vitro and in an acute model of elevated bone turnover in vivo in monkeys. *Bone,* 40**,** 122-31.

KUMASAKA, T., HOSHIKA, Y., KOBAYASHI, E., MITANI, K., OKURA, M. K., HONG, Y. K., TAKAHASHI, K. & SEYAMA, K. 2015. A Model of Lymphangioleiomyomatosis in a Three-Dimensional Culture System. *Lymphatic Research and Biology,* 13**,** 248-252.

KUMASAKA, T., SEYAMA, K., MITANI, K., SOUMA, S., KASHIWAGI, S., HEBISAWA, A., SATO, T., KUBO, H., GOMI, K., SHIBUYA, K., FUKUCHI, Y. & SUDA, K. 2005. Lymphangiogenesis-mediated shedding of LAM cell clusters as a mechanism for dissemination in lymphangioleiomyomatosis. *American Journal of Surgical Pathology,* 29**,** 1356-66.

KUNZ-SCHUGHART, L. A., HEYDER, P., SCHROEDER, J. & KNUECHEL, R. 2001. A heterologous 3-D coculture model of breast tumor cells and fibroblasts to study tumor-associated fibroblast differentiation. *Exp Cell Res,* 266**,** 74-86.

KWIATKOWSKI, D. J. 2010. Animal models of lymphangioleiomyomatosis (LAM) and tuberous sclerosis complex (TSC). *Lymphat Res Biol,* 8**,** 51-7.

KWIATKOWSKI, D. J., ZHANG, H., BANDURA, J. L., HEIBERGER, K. M., GLOGAUER, M., EL-HASHEMITE, N. & ONDA, H. 2002. A mouse model of TSC1 reveals sex-dependent lethality from liver hemangiomas, and up-regulation of p70S6 kinase activity in Tsc1 null cells. *Human Molecular Genetics,* 11**,** 525-34.

LAGORY, E. L. & GIACCIA, A. J. 2016. The ever-expanding role of HIF in tumour and stromal biology. *Nat Cell Biol,* 18**,** 356-365.

LAITALA-LEINONEN, T., RINNE, R., SAUKKO, P., VAANANEN, H. K. & RINNE, A. 2006. Cystatin B as an intracellular modulator of bone resorption. *Matrix Biol,* 25**,** 149-57.

LAMB, R. F., ROY, C., DIEFENBACH, T. J., VINTERS, H. V., JOHNSON, M. W., JAY, D. G. & HALL, A. 2000. The TSC1 tumour suppressor hamartin regulates cell adhesion through ERM proteins and the GTPase Rho. *Nat Cell Biol,* 2**,** 281-7.

LAPLANTE, M. & SABATINI, D. M. 2012. mTOR signaling in growth control and disease. *Cell,* 149**,** 274-93.

LAZENNEC, G. & RICHMOND, A. 2010. Chemokines and chemokine receptors: new insights into cancer-related inflammation. *Trends Mol Med,* 16**,** 133-44.

LECAILLE, F., BROMME, D. & LALMANACH, G. 2008. Biochemical properties and regulation of cathepsin K activity. *Biochimie,* 90**,** 208-26.

LECAILLE, F., KALETA, J. & BRÖMME, D. 2002. Human and Parasitic Papain-Like Cysteine Proteases: Their Role in Physiology and Pathology and Recent Developments in Inhibitor Design. *Chemical Reviews,* 102**,** 4459-4488.

LEE, D. F., KUO, H. P., CHEN, C. T., HSU, J. M., CHOU, C. K., WEI, Y., SUN, H. L., LI, L. Y., PING, B., HUANG, W. C., HE, X., HUNG, J. Y., LAI, C. C., DING, Q., SU, J. L., YANG, J. Y., SAHIN, A. A., HORTOBAGYI, G. N., TSAI, F. J., TSAI, C. H. & HUNG, M. C. 2007. IKK beta

suppression of TSC1 links inflammation and tumor angiogenesis via the mTOR pathway. *Cell,* 130**,** 440-55.

LEE, P.-S., TSANG, S. W., MOSES, M. A., TRAYES-GIBSON, Z., HSIAO, L.-L., JENSEN, R., SQUILLACE, R. & KWIATKOWSKI, D. J. 2009. Rapamycin-insensitive Up-regulation of MMP2 and Other Genes in TSC2-deficient LAM-like Cells. *Am. J. Respir. Cell Mol. Biol.***,** 2009-0050OC.

LEE, P. S., TSANG, S. W., MOSES, M. A., TRAYES-GIBSON, Z., HSIAO, L. L., JENSEN, R., SQUILLACE, R. & KWIATKOWSKI, D. J. 2010. Rapamycin-insensitive up-regulation of MMP2 and other genes in tuberous sclerosis complex 2-deficient lymphangioleiomyomatosis-like cells. *Am J Respir Cell Mol Biol,* 42**,** 227-34.

LEMAIRE, R., HUET, G., ZERIMECH, F., GRARD, G., FONTAINE, C., DUQUESNOY, B. & FLIPO, R. M. 1997. Selective induction of the secretion of cathepsins B and L by cytokines in synovial fibroblast-like cells. *Br J Rheumatol,* 36**,** 735-43.

LESMA, E., GRANDE, V., ANCONA, S., CARELLI, S., DI GIULIO, A. M. & GORIO, A. 2008. Anti-EGFR antibody efficiently and specifically inhibits human TSC2-/- smooth muscle cell proliferation. Possible treatment options for TSC and LAM. *Plos One,* 3**,** e3558.

LESMA, E., GRANDE, V., CARELLI, S., BRANCACCIO, D., CANEVINI, M. P., ALFANO, R. M., COGGI, G., DI GIULIO, A. M. & GORIO, A. 2005. Isolation and growth of smooth muscle-like cells derived from tuberous sclerosis complex-2 human renal angiomyolipoma: epidermal growth factor is the required growth factor. *Am J Pathol,* 167**,** 1093-103.

LEVY, C., KHALED, M. & FISHER, D. E. 2006. MITF: master regulator of melanocyte development and melanoma oncogene. *Trends Mol Med,* 12**,** 406-14.

LI, F.-Z., CAI, P.-C., SONG, L.-J., ZHOU, L.-L., ZHANG, Q., RAO, S.-S., XIA, Y., XIANG, F., XIN, J.-B., GREER, P. A., SHI, H.-Z., SU, Y., MA, W.-L. & YE, H. 2015. Crosstalk between calpain activation and TGF-β1 augments collagen-I synthesis in pulmonary fibrosis. *Biochimica et Biophysica Acta (BBA) - Molecular Basis of Disease,* 1852**,** 1796-1804.

LI, S., OGAWA, W., EMI, A., HAYASHI, K., SENGA, Y., NOMURA, K., HARA, K., YU, D. & KASUGA, M. 2011. Role of S6K1 in regulation of SREBP1c expression in the liver. *Biochem Biophys Res Commun,* 412**,** 197-202.

LI, Z., YASUDA, Y., LI, W., BOGYO, M., KATZ, N., GORDON, R. E., FIELDS, G. B. & BRÖMME, D. 2004. Regulation of Collagenase Activities of Human Cathepsins by Glycosaminoglycans. *Journal of Biological Chemistry,* 279**,** 5470-5479.

LIAUDET-COOPMAN, E., BEAUJOUIN, M., DEROCQ, D., GARCIA, M., GLONDU-LASSIS, M., LAURENT-MATHA, V., PREBOIS, C., ROCHEFORT, H. & VIGNON, F. 2006. Cathepsin D: newly discovered functions of a long-standing aspartic protease in cancer and apoptosis. *Cancer Lett,* 237**,** 167-79.

LIJNEN, H. R. 2001. Plasmin and matrix metalloproteinases in vascular remodeling. *Thromb Haemost,* 86**,** 324-33.
LINNEVERS, C., SMEEKENS, S. P. & BRÖMME, D. 1997. Human cathepsin W, a putative cysteine protease predominantly expressed in CD8+ T-lymphocytes. *FEBS Letters,* 405**,** 253-259.
LIPPERT, U., ARTUC, M., GRÜTZKAU, A., MÖLLER, A., KENDERESSY-SZABO, A., SCHADENDORF, D., NORGAUER, J., HARTMANN, K., SCHWEITZER-STENNER, R., ZUBERBIER, T., HENZ, B. M. & KRÜGER-KRASAGAKES, S. 1998. Expression and Functional Activity of the IL-8 Receptor Type CXCR1 and CXCR2 on Human Mast Cells. *The Journal of Immunology,* 161**,** 2600-2608.
LIPPERT, U., ZACHMANN, K., HENZ, B. M. & NEUMANN, C. 2004. Human T lymphocytes and mast cells differentially express and regulate extra- and intracellular CXCR1 and CXCR2. *Exp Dermatol,* 13**,** 520-5.
LIU, J., SUKHOVA, G. K., SUN, J. S., XU, W. H., LIBBY, P. & SHI, G. P. 2004. Lysosomal cysteine proteases in atherosclerosis. *Arterioscler Thromb Vasc Biol,* 24**,** 1359-66.
LIU, X.-Q., KIEFL, R., ROSKOPF, C., TIAN, F. & HUBER, R. M. 2016. Interactions among Lung Cancer Cells, Fibroblasts, and Macrophages in 3D Co-Cultures and the Impact on MMP-1 and VEGF Expression. *PLOS ONE,* 11**,** e0156268.
LIU, X., DAS, A. M., SEIDEMAN, J., GRISWOLD, D., AFUH, C. N., KOBAYASHI, T., ABE, S., FANG, Q., HASHIMOTO, M., KIM, H., WANG, X., SHEN, L., KAWASAKI, S. & RENNARD, S. I. 2007. The CC Chemokine Ligand 2 (CCL2) Mediates Fibroblast Survival through IL-6. *American Journal of Respiratory Cell and Molecular Biology,* 37**,** 121-128.
LIVAK, K. J. & SCHMITTGEN, T. D. 2001. Analysis of relative gene expression data using real-time quantitative PCR and the 2(-Delta Delta C(T)) Method. *Methods,* 25**,** 402-8.
LOGGINIDOU, H., AO, X., RUSSO, I. & HENSKE, E. P. 2000. Frequent estrogen and progesterone receptor immunoreactivity in renal angiomyolipomas from women with pulmonary lymphangioleiomyomatosis. *Chest,* 117**,** 25-30.
LOU, Y., MCDONALD, P. C., OLOUMI, A., CHIA, S., OSTLUND, C., AHMADI, A., KYLE, A., AUF DEM KELLER, U., LEUNG, S., HUNTSMAN, D., CLARKE, B., SUTHERLAND, B. W., WATERHOUSE, D., BALLY, M., ROSKELLEY, C., OVERALL, C. M., MINCHINTON, A., PACCHIANO, F., CARTA, F., SCOZZAFAVA, A., TOUISNI, N., WINUM, J. Y., SUPURAN, C. T. & DEDHAR, S. 2011. Targeting tumor hypoxia: suppression of breast tumor growth and metastasis by novel carbonic anhydrase IX inhibitors. *Cancer Res,* 71**,** 3364-76.
LOUBAKI, L., HADJ-SALEM, I., FAKHFAKH, R., JACQUES, E., PLANTE, S., BOISVERT, M., AOUDJIT, F. & CHAKIR, J. 2013. Co-Culture of Human Bronchial Fibroblasts and CD4+ T Cells Increases Th17 Cytokine Signature. *PLOS ONE,* 8**,** e81983.

LU, P., TAKAI, K., WEAVER, V. M. & WERB, Z. 2011. Extracellular matrix degradation and remodeling in development and disease. *Cold Spring Harb Perspect Biol,* 3.

LUDWIG, K., TSE, E. S. & WANG, J. Y. 2013. Colon cancer cells adopt an invasive phenotype without mesenchymal transition in 3-D but not 2-D culture upon combined stimulation with EGF and crypt growth factors. *BMC Cancer,* 13**,** 221.

LUTEMBACHER, R. 1918. Dysembryomes metatypiques des reins. Carcinose sublimiare aigue du poumon avec emphyseme generalise et double pneumothorax [Atypical kidney dysembryoma. Acute submiliary lung carcinomatosis with generalised emphysema and double pneumothorax]. *Ann Med,* 5**,** 435.

MA, L., CHEN, Z., ERDJUMENT-BROMAGE, H., TEMPST, P. & PANDOLFI, P. P. 2005. Phosphorylation and functional inactivation of TSC2 by Erk implications for tuberous sclerosis and cancer pathogenesis. *Cell,* 121**,** 179-93.

MA, X. M. & BLENIS, J. 2009. Molecular mechanisms of mTOR-mediated translational control. *Nat Rev Mol Cell Biol,* 10**,** 307-18.

MADAR, S., GOLDSTEIN, I. & ROTTER, V. 2013. 'Cancer associated fibroblasts'--more than meets the eye. *Trends Mol Med,* 19**,** 447-53.

MAHESHWAR, M. M., SANDFORD, R., NELLIST, M., CHEADLE, J. P., SGOTTO, B., VAUDIN, M. & SAMPSON, J. R. 1996. Comparative analysis and genomic structure of the tuberous sclerosis 2 (TSC2) gene in human and pufferfish. *Human Molecular Genetics,* 5**,** 562.

MAJETY, M., PRADEL, L. P., GIES, M. & RIES, C. H. 2015. Fibroblasts Influence Survival and Therapeutic Response in a 3D Co-Culture Model. *PLOS ONE,* 10**,** e0127948.

MAKOVSKI, V., HAKLAI, R. & KLOOG, Y. 2012. Farnesylthiosalicylic acid (salirasib) inhibits Rheb in TSC2-null ELT3 cells: a potential treatment for lymphangioleiomyomatosis. *Int J Cancer,* 130**,** 1420-9.

MANNING, B. D., TEE, A. R., LOGSDON, M. N., BLENIS, J. & CANTLEY, L. C. 2002. Identification of the tuberous sclerosis complex-2 tumor suppressor gene product tuberin as a target of the phosphoinositide 3-kinase/akt pathway. *Mol Cell,* 10**,** 151-62.

MARTIGNONI, G., BONETTI, F., CHILOSI, M., BRUNELLI, M., SEGALA, D., AMIN, M. B., ARGANI, P., EBLE, J. N., GOBBO, S. & PEA, M. 2012. Cathepsin K expression in the spectrum of perivascular epithelioid cell (PEC) lesions of the kidney. *Mod Pathol,* 25**,** 100-11.

MARTIGNONI, G., PEA, M., REGHELLIN, D., GOBBO, S., ZAMBONI, G., CHILOSI, M. & BONETTI, F. 2010. Molecular Pathology of Lymphangioleiomyomatosis and Other Perivascular Epithelioid Cell Tumors. *Archives of Pathology & Laboratory Medicine,* 134**,** 33-40.

MASON, S. D. & JOYCE, J. A. 2011. Proteolytic networks in cancer. *Trends Cell Biol,* 21**,** 228-37.

MASSON, O., PRÉBOIS, C., DEROCQ, D., MEULLE, A., DRAY, C., DAVIAUD, D., QUILLIOT, D., VALET, P., MULLER, C. & LIAUDET-COOPMAN, E. 2011. Cathepsin-D, a Key Protease in Breast Cancer, Is Up-

Regulated in Obese Mouse and Human Adipose Tissue, and Controls Adipogenesis. *PLOS ONE,* 6**,** e16452.
MATHUR, S., MATHUR, R. S., GOUST, J. M., WILLIAMSON, H. O. & FUDENBERG, H. H. 1977. Sex steroid hormones and circulating IgE levels. *Clin Exp Immunol,* 30**,** 403-7.
MATSUI, K., TAKEDA, K., YU, Z. X., TRAVIS, W. D., MOSS, J. & FERRANS, V. J. 2000a. Role for activation of matrix metalloproteinases in the pathogenesis of pulmonary lymphangioleiomyomatosis. *Archives of Pathology & Laboratory Medicine,* 124**,** 267-75.
MATSUI, K., TAKEDA, K., YU, Z. X., VALENCIA, J., TRAVIS, W. D., MOSS, J. & FERRANS, V. J. 2000b. Downregulation of estrogen and progesterone receptors in the abnormal smooth muscle cells in pulmonary lymphangioleiomyomatosis following therapy. An immunohistochemical study. *Am J Respir Crit Care Med,* 161**,** 1002-9.
MATSUI, K., TATSUGUCHI, A., VALENCIA, J., YU, Z., BECHTLE, J., BEASLEY, M. B., AVILA, N., TRAVIS, W. D., MOSS, J. & FERRANS, V. J. 2000c. Extrapulmonary lymphangioleiomyomatosis (LAM): clinicopathologic features in 22 cases. *Human Pathology,* 31**,** 1242-8.
MATSUI, K., W, K. R., HILBERT, S. L., YU, Z. X., TAKEDA, K., TRAVIS, W. D., MOSS, J. & FERRANS, V. J. 2000d. Hyperplasia of type II pneumocytes in pulmonary lymphangioleiomyomatosis. *Archives of Pathology & Laboratory Medicine,* 124**,** 1642-8.
MATSUMOTO, M., KOGAWA, M., WADA, S., TAKAYANAGI, H., TSUJIMOTO, M., KATAYAMA, S., HISATAKE, K. & NOGI, Y. 2004. Essential Role of p38 Mitogen-activated Protein Kinase in Cathepsin K Gene Expression during Osteoclastogenesis through Association of NFATc1 and PU.1. *Journal of Biological Chemistry,* 279**,** 45969-45979.
MAYER, B., KLEMENT, G., KANEKO, M., MAN, S., JOTHY, S., RAK, J. & KERBEL, R. S. 2001. Multicellular gastric cancer spheroids recapitulate growth pattern and differentiation phenotype of human gastric carcinomas. *Gastroenterology,* 121**,** 839-852.
MAZIAK, D. E., KESTEN, S., RAPPAPORT, D. C. & MAURER, J. 1996. Extrathoracic angiomyolipomas in lymphangioleiomyomatosis. *European Respiratory Journal,* 9**,** 402-405.
MCCARTHY, D. J. & SMYTH, G. K. 2009. Testing significance relative to a fold-change threshold is a TREAT. *Bioinformatics,* 25**,** 765-771.
MCCORMACK, F. X. 2008. Lymphangioleiomyomatosis: a clinical update. *Chest,* 133**,** 507-16.
MCCORMACK, F. X., INOUE, Y., MOSS, J., SINGER, L. G., STRANGE, C., NAKATA, K., BARKER, A. F., CHAPMAN, J. T., BRANTLY, M. L., STOCKS, J. M., BROWN, K. K., LYNCH, J. P., 3RD, GOLDBERG, H. J., YOUNG, L. R., KINDER, B. W., DOWNEY, G. P., SULLIVAN, E. J., COLBY, T. V., MCKAY, R. T., COHEN, M. M., KORBEE, L., TAVEIRA-DASILVA, A. M., LEE, H. S., KRISCHER, J. P. & TRAPNELL, B. C. 2011. Efficacy and safety of sirolimus in lymphangioleiomyomatosis. *N Engl J Med,* 364**,** 1595-606.

MCCORMACK, F. X., TRAVIS, W. D., COLBY, T. V., HENSKE, E. P. & MOSS, J. 2012. Lymphangioleiomyomatosis: calling it what it is: a low-grade, destructive, metastasizing neoplasm. *Am J Respir Crit Care Med,* 186**,** 1210-2.

MCGRATH, M. E. 1999. The lysosomal cysteine proteases. *Annu Rev Biophys Biomol Struct,* 28**,** 181-204.

MCINTYRE, A., HULIKOVA, A., LEDAKI, I., SNELL, C., SINGLETON, D., STEERS, G., SEDEN, P., JONES, D., BRIDGES, E., WIGFIELD, S., LI, J.-L., RUSSELL, A., SWIETACH, P. & HARRIS, A. L. 2016. Disrupting Hypoxia-Induced Bicarbonate Transport Acidifies Tumor Cells and Suppresses Tumor Growth. *Cancer Research,* 76**,** 3744-3755.

MCQUENEY, M. S., AMEGADZIE, B. Y., D'ALESSIO, K., HANNING, C. R., MCLAUGHLIN, M. M., MCNULTY, D., CARR, S. A., IJAMES, C., KURDYLA, J. & JONES, C. S. 1997. Autocatalytic activation of human cathepsin K. *Journal of Biological Chemistry,* 272**,** 13955-60.

MEIER, C., MEINHARDT, U., GREENFIELD, J. R., DE WINTER, J., NGUYEN, T. V., DUNSTAN, C. R. & SEIBEL, M. J. 2006. Serum cathepsin K concentrations reflect osteoclastic activity in women with postmenopausal osteoporosis and patients with Paget's disease. *Clin Lab,* 52**,** 1-10.

MELLOR, G. W., THOMAS, E. W., TOPHAM, C. M. & BROCKLEHURST, K. 1993. Ionization characteristics of the Cys-25/His-159 interactive system and of the modulatory group of papain: resolution of ambiguity by electronic perturbation of the quasi-2-mercaptopyridine leaving group in a new pyrimidyl disulphide reactivity probe. *Biochem J,* 290 ( Pt 1)**,** 289-96.

MERRILEES, M. J., HANKIN, E. J., BLACK, J. L. & BEAUMONT, B. 2004. Matrix proteoglycans and remodelling of interstitial lung tissue in lymphangioleiomyomatosis. *Journal of Pathology,* 203**,** 653-60.

MI, R., MA, J., ZHANG, D., LI, L. & ZHANG, H. 2009. Efficacy of combined inhibition of mTOR and ERK/MAPK pathways in treating a tuberous sclerosis complex cell model. *J Genet Genomics,* 36**,** 355-61.

MIKI, Y., ONO, K., HATA, S., SUZUKI, T., KUMAMOTO, H. & SASANO, H. 2012. The advantages of co-culture over mono cell culture in simulating in vivo environment. *J Steroid Biochem Mol Biol,* 131**,** 68-75.

MILLER, M. B. & TANG, Y.-W. 2009. Basic Concepts of Microarrays and Potential Applications in Clinical Microbiology. *Clinical Microbiology Reviews,* 22**,** 611-633.

MITANI, K., KUMASAKA, T., TAKEMURA, H., HAYASHI, T., GUNJI, Y., KUNOGI, M., AKIYOSHI, T., TAKAHASHI, K., SUDA, K. & SEYAMA, K. 2009. Cytologic, immunocytochemical and ultrastructural characterization of lymphangioleiomyomatosis cell clusters in chylous effusions of patients with lymphangioleiomyomatosis. *Acta Cytol,* 53**,** 402-9.

MITTELBRUNN, M. & SÁNCHEZ-MADRID, F. 2012. Intercellular communication: diverse structures for exchange of genetic information. *Nat Rev Mol Cell Biol,* 13**,** 328-335.

MOGNETTI, B., MONTAGNA, G. L., PERRELLI, M. G., PAGLIARO, P. & PENNA, C. 2013. Bone marrow mesenchymal stem cells increase motility of prostate cancer cells via production of stromal cell-derived factor-1α. *Journal of Cellular and Molecular Medicine,* 17**,** 287-292.

MOHAMED, M. M. & SLOANE, B. F. 2006. Cysteine cathepsins: multifunctional enzymes in cancer. *Nat Rev Cancer,* 6**,** 764-75.

MOIR, L. M., NG, H. Y., PONIRIS, M. H., SANTA, T., BURGESS, J. K., OLIVER, B. G. G., KRYMSKAYA, V. P. & BLACK, J. L. 2011. Doxycycline inhibits matrix metalloproteinase-2 secretion from TSC2-null mouse embryonic fibroblasts and lymphangioleiomyomatosis cells. *British Journal of Pharmacology,* 164**,** 83-92.

MONTGOMERY, N., HILL, A., MCFARLANE, S., NEISEN, J., O'GRADY, A., CONLON, S., JIRSTROM, K., KAY, E. & WAUGH, D. 2012. CD44 enhances invasion of basal-like breast cancer cells by upregulating serine protease and collagen-degrading enzymatic expression and activity. *Breast Cancer Research,* 14**,** R84.

MORALES, J. & ALPAUGH, M. L. 2009. Gain in cellular organization of inflammatory breast cancer: A 3D in vitro model that mimics the in vivo metastasis. *BMC Cancer,* 9**,** 462.

MOSES, M. A., HARPER, J. & FOLKMAN, J. 2006. Doxycycline treatment for lymphangioleiomyomatosis with urinary monitoring for MMPs. *N Engl J Med,* 354**,** 2621-2.

MOSS, J., AVILA, N. A., BARNES, P. M., LITZENBERGER, R. A., BECHTLE, J., BROOKS, P. G., HEDIN, C. J., HUNSBERGER, S. & KRISTOF, A. S. 2001a. Prevalence and clinical characteristics of lymphangioleiomyomatosis (LAM) in patients with tuberous sclerosis complex. *Am J Respir Crit Care Med,* 164**,** 669-71.

MOSS, J., DECASTRO, R., PATRONAS, N. J. & TAVEIRA-DASILVA, A. 2001b. Meningiomas in lymphangioleiomyomatosis. *JAMA,* 286**,** 1879-81.

MURTHY, V., STEMMER-RACHAMIMOV, A. O., HADDAD, L. A., ROY, J. E., CUTONE, A. N., BEAUCHAMP, R. L., SMITH, N., LOUIS, D. N. & RAMESH, V. 2001. Developmental expression of the tuberous sclerosis proteins tuberin and hamartin. *Acta Neuropathol,* 101**,** 202-10.

NAUMNIK, W., NIKLINSKA, W., OSSOLINSKA, M. & CHYCZEWSKA, E. 2009. Serum cathepsin K and cystatin C concentration in patients with advanced non-small-cell lung cancer during chemotherapy. *Folia Histochem Cytobiol,* 47**,** 207-13.

NELLIST, M., SANCAK, O., GOEDBLOED, M. A., ROHE, C., VAN NETTEN, D., MAYER, K., TUCKER-WILLIAMS, A., VAN DEN OUWELAND, A. M. & HALLEY, D. J. 2005. Distinct effects of single amino-acid changes to tuberin on the function of the tuberin-hamartin complex. *Eur J Hum Genet,* 13**,** 59-68.

NELLIST, M., VAN SLEGTENHORST, M. A., GOEDBLOED, M., VAN DEN OUWELAND, A. M., HALLEY, D. J. & VAN DER SLUIJS, P. 1999. Characterization of the cytosolic tuberin-hamartin complex. Tuberin

is a cytosolic chaperone for hamartin. *Journal of Biological Chemistry,* 274**,** 35647-52.
NEUMANN, E., LEFEVRE, S., ZIMMERMANN, B., GAY, S. & MULLER-LADNER, U. 2010. Rheumatoid arthritis progression mediated by activated synovial fibroblasts. *Trends Mol Med,* 16**,** 458-68.
NIIDA, Y., STEMMER-RACHAMIMOV, A. O., LOGRIP, M., TAPON, D., PEREZ, R., KWIATKOWSKI, D. J., SIMS, K., MACCOLLIN, M., LOUIS, D. N. & RAMESH, V. 2001. Survey of somatic mutations in tuberous sclerosis complex (TSC) hamartomas suggests different genetic mechanisms for pathogenesis of TSC lesions. *Am J Hum Genet,* 69**,** 493-503.
NILSSON, G., BLOM, T., KUSCHE-GULLBERG, M., KJELLEN, L., BUTTERFIELD, J. H., SUNDSTROM, C., NILSSON, K. & HELLMAN, L. 1994. Phenotypic characterization of the human mast-cell line HMC-1. *Scand J Immunol,* 39**,** 489-98.
NISHIMURA, Y., KAWABATA, T., FURUNO, K. & KATO, K. 1989. Evidence that aspartic proteinase is involved in the proteolytic processing event of procathepsin L in lysosomes. *Arch Biochem Biophys,* 271**,** 400-6.
NISHIMURA, Y., KAWABATA, T. & KATO, K. 1988. Identification of latent procathepsins B and L in microsomal lumen: characterization of enzymatic activation and proteolytic processing in vitro. *Arch Biochem Biophys,* 261**,** 64-71.
NISSLER, K., KREUSCH, S., ROMMERSKIRCH, W., STRUBEL, W., WEBER, E. & WIEDERANDERS, B. 1998. Sorting of non-glycosylated human procathepsin S in mammalian cells. *Biol Chem,* 379**,** 219-24.
NKYIMBENG, T., RUPPERT, C., SHIOMI, T., DAHAL, B., LANG, G., SEEGER, W., OKADA, Y., D'ARMIENTO, J. & GUNTHER, A. 2013. Pivotal role of matrix metalloproteinase 13 in extracellular matrix turnover in idiopathic pulmonary fibrosis. *PLoS One,* 8**,** e73279.
NOEL, A., MUNAUT, C., BOULVAIN, A., CALBERG-BACQ, C. M., LAMBERT, C. A., NUSGENS, B., LAPIERE, C. M. & FOIDART, J. M. 1992. Modulation of collagen and fibronectin synthesis in fibroblasts by normal and malignant cells. *J Cell Biochem,* 48**,** 150-61.
NOVINEC, M., KOVAČIČ, L., LENARČIČ, B. & BAICI, A. 2010. Conformational flexibility and allosteric regulation of cathepsin K. *Biochemical Journal,* 429**,** 379.
OCHI, Y., YAMADA, H., MORI, H., NAKANISHI, Y., NISHIKAWA, S., KAYASUGA, R., KAWADA, N., KUNISHIGE, A., HASHIMOTO, Y., TANAKA, M., SUGITANI, M. & KAWABATA, K. 2014. Effects of eight-month treatment with ONO-5334, a cathepsin K inhibitor, on bone metabolism, strength and microstructure in ovariectomized cynomolgus monkeys. *Bone,* 65**,** 1-8.
ODAJIMA, N., BETSUYAKU, T., NASUHARA, Y., INOUE, H., SEYAMA, K. & NISHIMURA, M. 2009. Matrix metalloproteinases in blood from patients with LAM. *Respir Med,* 103**,** 124-9.
ODAJIMA, N., BETSUYAKU, T., YOSHIDA, T., HOSOKAWA, T. & NISHIMURA, M. 2010. High levels of extracellular matrix

metalloproteinase inducer are expressed in lymphangioleiomyomatosis. *Human Pathology,* 41**,** 935-43.
OGAWA, M., LARUE, A. C. & DRAKE, C. J. 2006. Hematopoietic origin of fibroblasts/myofibroblasts: Its pathophysiologic implications. *Blood,* 108**,** 2893-6.
OIDA, T. & WEINER, H. L. 2010. Depletion of TGF-β from fetal bovine serum. *Journal of Immunological Methods,* 362**,** 195-198.
ONDA, H., LUECK, A., MARKS, P. W., WARREN, H. B. & KWIATKOWSKI, D. J. 1999. Tsc2(+/-) mice develop tumors in multiple sites that express gelsolin and are influenced by genetic background. *J Clin Invest,* 104**,** 687-95.
OPRESCU, N., MCCORMACK, F. X., BYRNES, S. & KINDER, B. W. 2013. Clinical predictors of mortality and cause of death in lymphangioleiomyomatosis: A population-based registry. *Lung,* 191**,** 35-42.
ORIMO, A., GUPTA, P. B., SGROI, D. C., ARENZANA-SEISDEDOS, F., DELAUNAY, T., NAEEM, R., CAREY, V. J., RICHARDSON, A. L. & WEINBERG, R. A. 2005. Stromal Fibroblasts Present in Invasive Human Breast Carcinomas Promote Tumor Growth and Angiogenesis through Elevated SDF-1/CXCL12 Secretion. *Cell,* 121**,** 335-348.
ORKIN, R. W., GEHRON, P., MCGOODWIN, E. B., MARTIN, G. R., VALENTINE, T. & SWARM, R. 1977. A murine tumor producing a matrix of basement membrane. *The Journal of Experimental Medicine,* 145**,** 204.
PACHECO-RODRIGUEZ, G., KUMAKI, F., STEAGALL, W. K., ZHANG, Y., IKEDA, Y., LIN, J. P., BILLINGS, E. M. & MOSS, J. 2009. Chemokine-enhanced chemotaxis of lymphangioleiomyomatosis cells with mutations in the tumor suppressor TSC2 gene. *J Immunol,* 182**,** 1270-7.
PACHECO-RODRIGUEZ, G. & MOSS, J. 2010. The role of chemokines in migration of metastatic-like lymphangioleiomyomatosis cells. *Crit Rev Immunol,* 30**,** 387-94.
PACHECO-RODRIGUEZ, G., STEAGALL, W. K., CROOKS, D. M., STEVENS, L. A., HASHIMOTO, H., LI, S., WANG, J. A., DARLING, T. N. & MOSS, J. 2007. TSC2 loss in lymphangioleiomyomatosis cells correlated with expression of CD44v6, a molecular determinant of metastasis. *Cancer Research,* 67**,** 10573-81.
PAGE-MCCAW, A., EWALD, A. J. & WERB, Z. 2007. Matrix metalloproteinases and the regulation of tissue remodelling. *Nat Rev Mol Cell Biol,* 8**,** 221-33.
PARKS, S. K. & POUYSSEGUR, J. 2015. The Na(+)/HCO3(-) Co-Transporter SLC4A4 Plays a Role in Growth and Migration of Colon and Breast Cancer Cells. *J Cell Physiol,* 230**,** 1954-63.
PARTEK. 2017a. Available: www.partek.com.
PARTEK. 2017b. *Partek Genomics Suite Resources - Microarray* [Online]. Available: http://www.partek.com/pgs-resources-microarray.
PARTEK. 2017c. *Partek Pathway* [Online]. Available: http://www.partek.com/partekpathway.

PATTERSON, A. M., SCHMUTZ, C., DAVIS, S., GARDNER, L., ASHTON, B. A. & MIDDLETON, J. 2002. Differential binding of chemokines to macrophages and neutrophils in the human inflamed synovium. *Arthritis Research,* 4**,** 209-214.

PATTERSON, T. A., LOBENHOFER, E. K., FULMER-SMENTEK, S. B., COLLINS, P. J., CHU, T. M., BAO, W., FANG, H., KAWASAKI, E. S., HAGER, J., TIKHONOVA, I. R., WALKER, S. J., ZHANG, L., HURBAN, P., DE LONGUEVILLE, F., FUSCOE, J. C., TONG, W., SHI, L. & WOLFINGER, R. D. 2006. Performance comparison of one-color and two-color platforms within the MicroArray Quality Control (MAQC) project. *Nat Biotechnol,* 24**,** 1140-50.

PAULLI, M., FELLER, A. C., BOVERI, E., KINDL, S., BERTI, E., ROSSO, R., MERZ, H., FACCHETTI, F., GAMBINI, C., BONETTI, F. & ET AL. 1994. Cathepsin D and E co-expression in sinus histiocytosis with massive lymphadenopathy (Rosai-Dorfman disease) and Langerhans' cell histiocytosis: further evidences of a phenotypic overlap between these histiocytic disorders. *Virchows Arch,* 424**,** 601-6.

PEARCE, L. R., HUANG, X., BOUDEAU, J., PAWLOWSKI, R., WULLSCHLEGER, S., DEAK, M., IBRAHIM, A. F., GOURLAY, R., MAGNUSON, M. A. & ALESSI, D. R. 2007. Identification of Protor as a novel Rictor-binding component of mTOR complex-2. *Biochem J,* 405**,** 513-22.

PENG, T., GOLUB, T. R. & SABATINI, D. M. 2002. The immunosuppressant rapamycin mimics a starvation-like signal distinct from amino acid and glucose deprivation. *Mol Cell Biol,* 22**,** 5575-84.

PERDEREAU, C., GODAT, E., MAUREL, M. C., HAZOUARD, E., DIOT, E. & LALMANACH, G. 2006. Cysteine cathepsins in human silicotic bronchoalveolar lavage fluids. *Biochim Biophys Acta,* 1762**,** 351-6.

PETERSON, T. R., LAPLANTE, M., THOREEN, C. C., SANCAK, Y., KANG, S. A., KUEHL, W. M., GRAY, N. S. & SABATINI, D. M. 2009. DEPTOR is an mTOR inhibitor frequently overexpressed in multiple myeloma cells and required for their survival. *Cell,* 137**,** 873-86.

PHAM, C. T. & LEY, T. J. 1999. Dipeptidyl peptidase I is required for the processing and activation of granzymes A and B in vivo. *Proc Natl Acad Sci U S A,* 96**,** 8627-32.

PHAN, S. H. 2008. Biology of Fibroblasts and Myofibroblasts. *Proceedings of the American Thoracic Society,* 5**,** 334-337.

PHILLIPS, R. J., BURDICK, M. D., HONG, K., LUTZ, M. A., MURRAY, L. A., XUE, Y. Y., BELPERIO, J. A., KEANE, M. P. & STRIETER, R. M. 2004. Circulating fibrocytes traffic to the lungs in response to CXCL12 and mediate fibrosis. *J Clin Invest,* 114**,** 438-46.

PIMENTA, S. P., BALDI, B. G., ACENCIO, M. M., KAIRALLA, R. A. & CARVALHO, C. R. 2011. Doxycycline use in patients with lymphangioleiomyomatosis: safety and efficacy in metalloproteinase blockade. *Jornal Brasileiro De Pneumologia,* 37**,** 424-30.

PINHEIRO, C., ALBERGARIA, A., PAREDES, J., SOUSA, B., DUFLOTH, R., VIEIRA, D., SCHMITT, F. & BALTAZAR, F. 2010. Monocarboxylate

transporter 1 is up-regulated in basal-like breast carcinoma. *Histopathology,* 56**,** 860-7.
PINHEIRO, C., LONGATTO-FILHO, A., SIMOES, K., JACOB, C. E., BRESCIANI, C. J., ZILBERSTEIN, B., CECCONELLO, I., ALVES, V. A., SCHMITT, F. & BALTAZAR, F. 2009. The prognostic value of CD147/EMMPRIN is associated with monocarboxylate transporter 1 co-expression in gastric cancer. *Eur J Cancer,* 45**,** 2418-24.
PLANK, T. L., YEUNG, R. S. & HENSKE, E. P. 1998. Hamartin, the product of the tuberous sclerosis 1 (TSC1) gene, interacts with tuberin and appears to be localized to cytoplasmic vesicles. *Cancer Research,* 58**,** 4766-70.
POLURI, K. M., JOSEPH, P. R., SAWANT, K. V. & RAJARATHNAM, K. 2013. Molecular basis of glycosaminoglycan heparin binding to the chemokine CXCL1 dimer. *J Biol Chem,* 288**,** 25143-53.
PORSTMANN, T., SANTOS, C. R., GRIFFITHS, B., CULLY, M., WU, M., LEEVERS, S., GRIFFITHS, J. R., CHUNG, Y. L. & SCHULZE, A. 2008. SREBP activity is regulated by mTORC1 and contributes to Akt-dependent cell growth. *Cell Metab,* 8**,** 224-36.
PORTELLI, M. A., MOSELEY, C., STEWART, C. E., POSTMA, D. S., HOWARTH, P., WARNER, J. A., HOLLOWAY, J. W., KOPPELMAN, G. H., BRIGHTLING, C. & SAYERS, I. 2017. Airway and peripheral urokinase plasminogen activator receptor is elevated in asthma, and identifies a severe, nonatopic subset of patients. *Allergy,* 72**,** 473-482.
PORTELLI, M. A., SIEDLINSKI, M., STEWART, C. E., POSTMA, D. S., NIEUWENHUIS, M. A., VONK, J. M., NURNBERG, P., ALTMULLER, J., MOFFATT, M. F., WARDLAW, A. J., PARKER, S. G., CONNOLLY, M. J., KOPPELMAN, G. H. & SAYERS, I. 2014. Genome-wide protein QTL mapping identifies human plasma kallikrein as a post-translational regulator of serum uPAR levels. *FASEB J,* 28**,** 923-34.
POTTER, C. J., PEDRAZA, L. G. & XU, T. 2002. Akt regulates growth by directly phosphorylating Tsc2. *Nat Cell Biol,* 4**,** 658-65.
POTTER, M., NEWPORT, E. & MORTEN, K. J. 2016. The Warburg effect: 80 years on. *Biochem Soc Trans,* 44**,** 1499-1505.
PRASAD, S., HOGABOAM, C. M. & JARAI, G. 2014. Deficient repair response of IPF fibroblasts in a co-culture model of epithelial injury and repair. *Fibrogenesis & Tissue Repair,* 7**,** 7.
PRIZANT, H., SEN, A., LIGHT, A., CHO, S. N., DEMAYO, F. J., LYDON, J. P. & HAMMES, S. R. 2013. Uterine-specific loss of Tsc2 leads to myometrial tumors in both the uterus and lungs. *Mol Endocrinol,* 27**,** 1403-14.
PROMOCELL. 2015. *Human Pulmonary Fibroblasts (HPF)* [Online]. Available: http://www.promocell.com/products/human-primary-cells/fibroblasts/human-pulmonary-fibroblasts-hpf/.
PUNTURIERI, A., FILIPPOV, S., ALLEN, E., CARAS, I., MURRAY, R., REDDY, V. & WEISS, S. J. 2000. Regulation of Elastinolytic Cysteine Proteinase Activity in Normal and Cathepsin K–Deficient Human Macrophages. *The Journal of Experimental Medicine,* 192**,** 789-800.

QIN, L.-X., BEYER, R. P., HUDSON, F. N., LINFORD, N. J., MORRIS, D. E. & KERR, K. F. 2006. Evaluation of methods for oligonucleotide array data via quantitative real-time PCR. *BMC Bioinformatics,* 7**,** 23.

QIN, W., BAJAJ, V., MALINOWSKA, I., LU, X., MACCONAILL, L., WU, C. L. & KWIATKOWSKI, D. J. 2011. Angiomyolipoma Have Common Mutations in TSC2 but No Other Common Genetic Events. *Plos One,* 6.

QUINTANILLA-DIECK, M. J., CODRIANSKY, K., KEADY, M., BHAWAN, J. & RUNGER, T. M. 2009. Expression and regulation of cathepsin K in skin fibroblasts. *Exp Dermatol,* 18**,** 596-602.

RADZIKOWSKA, E., JAGUŚ, P., SOBIECKA, M., CHOROSTOWSKA-WYNIMKO, J., WIATR, E., KUŚ, J. & ROSZKOWSKI-ŚLIŻ, K. 2015. Correlation of serum vascular endothelial growth factor-D concentration with clinical presentation and course of lymphangioleiomyomatosis. *Respiratory Medicine,* 109**,** 1469-1475.

RAJEEVAN, M. S., RANAMUKHAARACHCHI, D. G., VERNON, S. D. & UNGER, E. R. 2001. Use of real-time quantitative PCR to validate the results of cDNA array and differential display PCR technologies. *Methods,* 25**,** 443-51.

RAKOWSKI, S. K., WINTERKORN, E. B., PAUL, E., STEELE, D. J., HALPERN, E. F. & THIELE, E. A. 2006. Renal manifestations of tuberous sclerosis complex: Incidence, prognosis, and predictive factors. *Kidney Int,* 70**,** 1777-82.

RAMA-ESENDAGLI, D., ESENDAGLI, G., YILMAZ, G. & GUC, D. 2014. Spheroid formation and invasion capacity are differentially influenced by co-cultures of fibroblast and macrophage cells in breast cancer. *Mol Biol Rep,* 41**,** 2885-92.

RAMOS, C., MONTANO, M., GARCIA-ALVAREZ, J., RUIZ, V., UHAL, B. D., SELMAN, M. & PARDO, A. 2001. Fibroblasts from idiopathic pulmonary fibrosis and normal lungs differ in growth rate, apoptosis, and tissue inhibitor of metalloproteinases expression. *Am J Respir Cell Mol Biol,* 24.

RAMPERSAD, S. N. 2012. Multiple Applications of Alamar Blue as an Indicator of Metabolic Function and Cellular Health in Cell Viability Bioassays. *Sensors (Basel, Switzerland),* 12**,** 12347-12360.

RAO, S. S., MU, Q., ZENG, Y., CAI, P. C., LIU, F., YANG, J., XIA, Y., ZHANG, Q., SONG, L. J., ZHOU, L. L., LI, F. Z., LIN, Y. X., FANG, J., GREER, P. A., SHI, H. Z., MA, W. L., SU, Y. & YE, H. 2017. Calpain-activated mTORC2/Akt pathway mediates airway smooth muscle remodelling in asthma. *Clinical & Experimental Allergy,* 47**,** 176-189.

RAPA, I., VOLANTE, M., CAPPIA, S., ROSAS, R., SCAGLIOTTI, G. V. & PAPOTTI, M. 2006. Cathepsin K Is Selectively Expressed in the Stroma of Lung Adenocarcinoma but Not in Bronchioloalveolar CarcinomaA Useful Marker of Invasive Growth. *American Journal of Clinical Pathology,* 125**,** 847-854.

RASBAND, W. S. 1997-2016. *ImageJ* [Online]. Bethesda, Maryland, USA: U. S. National Institutes of Health. Available: https://imagej.nih.gov/ij/.

RAVI, M., PARAMESH, V., KAVIYA, S. R., ANURADHA, E. & SOLOMON, F. D. P. 2015. 3D Cell Culture Systems: Advantages and Applications. *Journal of Cellular Physiology,* 230**,** 16-26.

REISER, J., ADAIR, B. & REINHECKEL, T. 2010. Specialized roles for cysteine cathepsins in health and disease. *The Journal of Clinical Investigation,* 120**,** 3421-3431.

RIEMAN, D. J., MCCLUNG, H. A., DODDS, R. A., HWANG, S. M., HOLMES, M. W., JAMES, I. E., DRAKE, F. H. & GOWEN, M. 2001. Biosynthesis and processing of cathepsin K in cultured human osteoclasts. *Bone,* 28**,** 282-9.

RIEMSMA, R., FORBES, C. A., KESSELS, A., LYKOPOULOS, K., AMONKAR, M. M., REA, D. W. & KLEIJNEN, J. 2010. Systematic review of aromatase inhibitors in the first-line treatment for hormone sensitive advanced or metastatic breast cancer. *Breast Cancer Res Treat,* 123**,** 9-24.

RIESE, R. J. & CHAPMAN, H. A. 2000. Cathepsins and compartmentalization in antigen presentation. *Curr Opin Immunol,* 12**,** 107-13.

RIIHONEN, R., SUPURAN, C. T., PARKKILA, S., PASTOREKOVA, S., VAANANEN, H. K. & LAITALA-LEINONEN, T. 2007. Membrane-bound carbonic anhydrases in osteoclasts. *Bone,* 40**,** 1021-31.

ROGERS, N. K., CLEMENTS, D., DONGRE, A., HARRISON, T. W., SHAW, D. & JOHNSON, S. R. 2014. Extra-cellular matrix proteins induce matrix metalloproteinase-1 (MMP-1) activity and increase airway smooth muscle contraction in asthma. *PLoS One,* 9**,** e90565.

ROOD, J. A., VAN HORN, S., DRAKE, F. H., GOWEN, M. & DEBOUCK, C. 1997. Genomic organization and chromosome localization of the human cathepsin K gene (CTSK). *Genomics,* 41**,** 169-76.

ROWE, R. G. & WEISS, S. J. 2009. Navigating ECM barriers at the invasive front: the cancer cell-stroma interface. *Annu Rev Cell Dev Biol,* 25**,** 567-95.

ROZENCHAN, P. B., CARRARO, D. M., BRENTANI, H., DE CARVALHO MOTA, L. D., BASTOS, E. P., E FERREIRA, E. N., TORRES, C. H., KATAYAMA, M. L., ROELA, R. A., LYRA, E. C., SOARES, F. A., FOLGUEIRA, M. A., GOES, J. C. & BRENTANI, M. M. 2009. Reciprocal changes in gene expression profiles of cocultured breast epithelial cells and primary fibroblasts. *Int J Cancer,* 125**,** 2767-77.

RUBINFELD, B., CROSIER, W. J., ALBERT, I., CONROY, L., CLARK, R., MCCORMICK, F. & POLAKIS, P. 1992. Localization of the rap1GAP catalytic domain and sites of phosphorylation by mutational analysis. *Mol Cell Biol,* 12**,** 4634-42.

RUBINFELD, B., MUNEMITSU, S., CLARK, R., CONROY, L., WATT, K., CROSIER, W. J., MCCORMICK, F. & POLAKIS, P. 1991. Molecular cloning of a GTPase activating protein specific for the Krev-1 protein p21rap1. *Cell,* 65**,** 1033-42.

RUSSO, G., ZEGAR, C. & GIORDANO, A. 2003. Advantages and limitations of microarray technology in human cancer. *Oncogene,* 22**,** 6497-507.

RYU, J. H., MOSS, J., BECK, G. J., LEE, J. C., BROWN, K. K., CHAPMAN, J. T., FINLAY, G. A., OLSON, E. J., RUOSS, S. J., MAURER, J. R., RAFFIN, T. A., PEAVY, H. H., MCCARTHY, K., TAVEIRA-DASILVA, A., MCCORMACK, F. X., AVILA, N. A., DECASTRO, R. M., JACOBS, S. S., STYLIANOU, M. & FANBURG, B. L. 2006. The NHLBI lymphangioleiomyomatosis registry: characteristics of 230 patients at enrollment. *Am J Respir Crit Care Med,* 173**,** 105-11.

SABATINI, D. M., ERDJUMENT-BROMAGE, H., LUI, M., TEMPST, P. & SNYDER, S. H. 1994. RAFT1: a mammalian protein that binds to FKBP12 in a rapamycin-dependent fashion and is homologous to yeast TORs. *Cell,* 78**,** 35-43.

SABEH, F., LI, X. Y., SAUNDERS, T. L., ROWE, R. G. & WEISS, S. J. 2009. Secreted versus membrane-anchored collagenases: relative roles in fibroblast-dependent collagenolysis and invasion. *J Biol Chem,* 284**,** 23001-11.

SABEH, F., OTA, I., HOLMBECK, K., BIRKEDAL-HANSEN, H., SOLOWAY, P., BALBIN, M., LOPEZ-OTIN, C., SHAPIRO, S., INADA, M., KRANE, S., ALLEN, E., CHUNG, D. & WEISS, S. J. 2004. Tumor cell traffic through the extracellular matrix is controlled by the membrane-anchored collagenase MT1-MMP. *J Cell Biol,* 167**,** 769-81.

SAETTA, M., MARIANI, M., PANINA-BORDIGNON, P., TURATO, G., BUONSANTI, C., BARALDO, S., BELLETTATO, C. M., PAPI, A., CORBETTA, L., ZUIN, R., SINIGAGLIA, F. & FABBRI, L. M. 2002. Increased Expression of the Chemokine Receptor CXCR3 and Its Ligand CXCL10 in Peripheral Airways of Smokers with Chronic Obstructive Pulmonary Disease. *American Journal of Respiratory and Critical Care Medicine,* 165**,** 1404-1409.

SAFTIG, P. & KLUMPERMAN, J. 2009. Lysosome biogenesis and lysosomal membrane proteins: trafficking meets function. *Nat Rev Mol Cell Biol,* 10**,** 623-35.

SAMOKHIN, A. O., GAUTHIER, J. Y., PERCIVAL, M. D. & BRÖMME, D. 2011. Lack of cathepsin activities alter or prevent the development of lung granulomas in a mouse model of sarcoidosis. *Respiratory Research,* 12**,** 13.

SAMPSON, J. R. & HARRIS, P. C. 1994. The molecular genetics of tuberous sclerosis. *Human Molecular Genetics,* 3 Spec No**,** 1477-80.

SANCAK, Y., BAR-PELED, L., ZONCU, R., MARKHARD, A. L., NADA, S. & SABATINI, D. M. 2010. Ragulator-Rag complex targets mTORC1 to the lysosomal surface and is necessary for its activation by amino acids. *Cell,* 141**,** 290-303.

SARBASSOV, D. D., ALI, S. M., KIM, D. H., GUERTIN, D. A., LATEK, R. R., ERDJUMENT-BROMAGE, H., TEMPST, P. & SABATINI, D. M. 2004. Rictor, a novel binding partner of mTOR, defines a rapamycin-insensitive and raptor-independent pathway that regulates the cytoskeleton. *Curr Biol,* 14**,** 1296-302.

SARBASSOV, D. D., ALI, S. M., SENGUPTA, S., SHEEN, J. H., HSU, P. P., BAGLEY, A. F., MARKHARD, A. L. & SABATINI, D. M. 2006. Prolonged rapamycin treatment inhibits mTORC2 assembly and Akt/PKB. *Mol Cell,* 22**,** 159-68.

SARBASSOV, D. D., GUERTIN, D. A., ALI, S. M. & SABATINI, D. M. 2005. Phosphorylation and regulation of Akt/PKB by the rictor-mTOR complex. *Science,* 307**,** 1098-101.

SASAKI, T., YAMAMOTO, M., YAMAGUCHI, T. & SUGIYAMA, S. 1984. Development of multicellular spheroids of HeLa cells cocultured with fibroblasts and their response to X-irradiation. *Cancer Res,* 44**,** 345-51.

SAWANT, K. V., XU, R., COX, R., HAWKINS, H., SBRANA, E., KOLLI, D., GAROFALO, R. P. & RAJARATHNAM, K. 2015. Chemokine CXCL1-Mediated Neutrophil Trafficking in the Lung: Role of CXCR2 Activation. *J Innate Immun,* 7**,** 647-58.

SCANLAN, M. J., RAJ, B. K., CALVO, B., GARIN-CHESA, P., SANZ-MONCASI, M. P., HEALEY, J. H., OLD, L. J. & RETTIG, W. J. 1994. Molecular cloning of fibroblast activation protein alpha, a member of the serine protease family selectively expressed in stromal fibroblasts of epithelial cancers. *Proceedings of the National Academy of Sciences of the United States of America,* 91**,** 5657-5661.

SCHENA, M., SHALON, D., HELLER, R., CHAI, A., BROWN, P. O. & DAVIS, R. W. 1996. Parallel human genome analysis: microarray-based expression monitoring of 1000 genes. *Proceedings of the National Academy of Sciences,* 93**,** 10614-10619.

SCHIEKE, S. M., PHILLIPS, D., MCCOY, J. P., JR., APONTE, A. M., SHEN, R. F., BALABAN, R. S. & FINKEL, T. 2006. The mammalian target of rapamycin (mTOR) pathway regulates mitochondrial oxygen consumption and oxidative capacity. *Journal of Biological Chemistry,* 281**,** 27643-52.

SCHMIDT, M., SUN, G., STACEY, M. A., MORI, L. & MATTOLI, S. 2003. Identification of circulating fibrocytes as precursors of bronchial myofibroblasts in asthma. *J Immunol,* 171**,** 380-9.

SCHMITT-GRÄFF, A., DESMOULIÈRE, A., GABBIANI, G., SCHMITT-GRÄFF, A. & DESMOULIÈRE, A. 1994. Heterogeneity of myofibroblast phenotypic features: an example of fibroblastic cell plasticity. *Virchows Archiv,* 425**,** 3-24.

SCHRODER, B. A., WROCKLAGE, C., HASILIK, A. & SAFTIG, P. 2010. The proteome of lysosomes. *Proteomics,* 10**,** 4053-76.

SEIDL, P., HUETTINGER, R., KNUECHEL, R. & KUNZ-SCHUGHART, L. A. 2002. Three-dimensional fibroblast-tumor cell interaction causes downregulation of RACK1 mRNA expression in breast cancer cells in vitro. *Int J Cancer,* 102**,** 129-36.

SEPURU, K. M., POLURI, K. M. & RAJARATHNAM, K. 2014. Solution Structure of CXCL5 — A Novel Chemokine and Adipokine Implicated in Inflammation and Obesity. *PLOS ONE,* 9**,** e93228.

SERVEAU-AVESQUE, C., MARTINO, M. F., HERVE-GREPINET, V., HAZOUARD, E., GAUTHIER, F., DIOT, E. & LALMANACH, G. 2006. Active cathepsins B, H, K, L and S in human inflammatory bronchoalveolar lavage fluids. *Biol Cell,* 98**,** 15-22.

SETHI, K. K., YANNAS, I. V., MUDERA, V., EASTWOOD, M., MCFARLAND, C. & BROWN, R. A. 2002. Evidence for sequential utilization of

fibronectin, vitronectin, and collagen during fibroblast-mediated collagen contraction. *Wound Repair Regen,* 10**,** 397-408.

SHALHOUB, V., FAUST, J., BOYLE, W. J., DUNSTAN, C. R., KELLEY, M., KAUFMAN, S., SCULLY, S., VAN, G. & LACEY, D. L. 1999. Osteoprotegerin and osteoprotegerin ligand effects on osteoclast formation from human peripheral blood mononuclear cell precursors. *J Cell Biochem,* 72**,** 251-61.

SHEKHAR, M. P., WERDELL, J., SANTNER, S. J., PAULEY, R. J. & TAIT, L. 2001. Breast stroma plays a dominant regulatory role in breast epithelial growth and differentiation: implications for tumor development and progression. *Cancer Res,* 61**,** 1320-6.

SHI, G. P., BRYANT, R. A., RIESE, R., VERHELST, S., DRIESSEN, C., LI, Z., BROMME, D., PLOEGH, H. L. & CHAPMAN, H. A. 2000. Role for cathepsin F in invariant chain processing and major histocompatibility complex class II peptide loading by macrophages. *J Exp Med,* 191**,** 1177-86.

SHI, G. P., CHAPMAN, H. A., BHAIRI, S. M., DELEEUW, C., REDDY, V. Y. & WEISS, S. J. 1995. Molecular cloning of human cathepsin O, a novel endoproteinase and homologue of rabbit OC2. *FEBS Lett,* 357**,** 129-34.

SHINGLETON, W. D., HODGES, D. J., BRICK, P. & CAWSTON, T. E. 1996. Collagenase: a key enzyme in collagen turnover. *Biochem Cell Biol,* 74**,** 759-75.

SIEUWERTS, A. M., KLIJN, J. G., PETERS, H. A. & FOEKENS, J. A. 1995. The MTT tetrazolium salt assay scrutinized: how to use this assay reliably to measure metabolic activity of cell cultures in vitro for the assessment of growth characteristics, IC50-values and cell survival. *Eur J Clin Chem Clin Biochem,* 33**,** 813-23.

SINGER, K. H., SCEARCE, R. M., TUCK, D. T., WHICHARD, L. P., DENNING, S. M. & HAYNES, B. F. 1989. Removal of fibroblasts from human epithelial cell cultures with use of a complement fixing monoclonal antibody reactive with human fibroblasts and monocytes/macrophages. *J Invest Dermatol,* 92**,** 166-70.

SLINGERLAND, J. M., GROSSMAN, R. F., CHAMBERLAIN, D. & TREMBLAY, C. E. 1989. Pulmonary manifestations of tuberous sclerosis in first degree relatives. *Thorax,* 44**,** 212-4.

SMITH, G. N., JR., BRANDT, K. D. & HASTY, K. A. 1996. Activation of recombinant human neutrophil procollagenase in the presence of doxycycline results in fragmentation of the enzyme and loss of enzyme activity. *Arthritis Rheum,* 39**,** 235-44.

SMOLAREK, T. A., WESSNER, L. L., MCCORMACK, F. X., MYLET, J. C., MENON, A. G. & HENSKE, E. P. 1998. Evidence that lymphangiomyomatosis is caused by TSC2 mutations: chromosome 16p13 loss of heterozygosity in angiomyolipomas and lymph nodes from women with lymphangiomyomatosis. *Am J Hum Genet,* 62**,** 810-5.

SOBONYA, R. E., QUAN, S. F. & FLEISHMAN, J. S. 1985. Pulmonary lymphangioleiomyomatosis: quantitative analysis of lesions producing airflow limitation. *Human Pathology,* 16**,** 1122-8.

SON, B. R., MARQUEZ-CURTIS, L. A., KUCIA, M., WYSOCZYNSKI, M., TURNER, A. R., RATAJCZAK, J., RATAJCZAK, M. Z. & JANOWSKA-WIECZOREK, A. 2006. Migration of bone marrow and cord blood mesenchymal stem cells in vitro is regulated by stromal-derived factor-1-CXCR4 and hepatocyte growth factor-c-met axes and involves matrix metalloproteinases. *Stem Cells,* 24**,** 1254-64.

SOOFI, S. S., LAST, J. A., LILIENSIEK, S. J., NEALEY, P. F. & MURPHY, C. J. 2009. The elastic modulus of Matrigel™ as determined by atomic force microscopy. *Journal of structural biology,* 167**,** 216-219.

SRIVASTAVA, M., STEINWEDE, K., KIVIRANTA, R., MORKO, J., HOYMANN, H.-G., LÄNGER, F., BUHLING, F., WELTE, T. & MAUS, U. A. 2008. Overexpression of cathepsin K in mice decreases collagen deposition and lung resistance in response to bleomycin-induced pulmonary fibrosis. *Respiratory Research,* 9**,** 54.

STAMBOLIC, V., MACPHERSON, D., SAS, D., LIN, Y., SNOW, B., JANG, Y., BENCHIMOL, S. & MAK, T. W. 2001. Regulation of PTEN transcription by p53. *Mol Cell,* 8**,** 317-25.

STASER, K., YANG, F. C. & CLAPP, D. W. 2012. Pathogenesis of plexiform neurofibroma: tumor-stromal/hematopoietic interactions in tumor progression. *Annu Rev Pathol,* 7**,** 469-95.

STRIETER, R. M., BURDICK, M. D., GOMPERTS, B. N., BELPERIO, J. A. & KEANE, M. P. 2005. CXC chemokines in angiogenesis. *Cytokine Growth Factor Rev,* 16**,** 593-609.

SU, A. I., COOKE, M. P., CHING, K. A., HAKAK, Y., WALKER, J. R., WILTSHIRE, T., ORTH, A. P., VEGA, R. G., SAPINOSO, L. M., MOQRICH, A., PATAPOUTIAN, A., HAMPTON, G. M., SCHULTZ, P. G. & HOGENESCH, J. B. 2002. Large-scale analysis of the human and mouse transcriptomes. *Proc Natl Acad Sci U S A,* 99**,** 4465-70.

SUBRAMANIAN, A., TAMAYO, P., MOOTHA, V. K., MUKHERJEE, S., EBERT, B. L., GILLETTE, M. A., PAULOVICH, A., POMEROY, S. L., GOLUB, T. R., LANDER, E. S. & MESIROV, J. P. 2005. Gene set enrichment analysis: A knowledge-based approach for interpreting genome-wide expression profiles. *Proceedings of the National Academy of Sciences,* 102**,** 15545-15550.

SUKHOVA, G. K., SHI, G. P., SIMON, D. I., CHAPMAN, H. A. & LIBBY, P. 1998. Expression of the elastolytic cathepsins S and K in human atheroma and regulation of their production in smooth muscle cells. *Journal of Clinical Investigation,* 102**,** 576-583.

SUN, Y., GU, X., ZHANG, E., PARK, M. A., PEREIRA, A. M., WANG, S., MORRISON, T., LI, C., BLENIS, J., GERBAUDO, V. H., HENSKE, E. P. & YU, J. J. 2014. Estradiol promotes pentose phosphate pathway addiction and cell survival via reactivation of Akt in mTORC1 hyperactive cells. *Cell Death & Disease,* 5**,** e1231.

SUTHERLAND, R. M., INCH, W. R., MCCREDIE, J. A. 1970. A Multi-component Radiation Survival Curve Using an in Vitro Tumour Model. *International Journal of Radiation Biology and Related Studies in Physics, Chemistry and Medicine,* 18**,** 491-495.

SUTHERLAND, R. M., MCCREDIE, J. A. & INCH, W. R. 1971. Growth of multicell spheroids in tissue culture as a model of nodular carcinomas. *J Natl Cancer Inst,* 46**,** 113-20.

SUZUKI, S., SATO, M., SENOO, H. & ISHIKAWA, K. 2004. Direct cell-cell interaction enhances pro-MMP-2 production and activation in co-culture of laryngeal cancer cells and fibroblasts: involvement of EMMPRIN and MT1-MMP. *Exp Cell Res,* 293**,** 259-66.

SWIETACH, P., PATIAR, S., SUPURAN, C. T., HARRIS, A. L. & VAUGHAN-JONES, R. D. 2009. The Role of Carbonic Anhydrase 9 in Regulating Extracellular and Intracellular pH in Three-dimensional Tumor Cell Growths. *The Journal of Biological Chemistry,* 284**,** 20299-20310.

SWINSON, D. E., JONES, J. L., RICHARDSON, D., WYKOFF, C., TURLEY, H., PASTOREK, J., TAUB, N., HARRIS, A. L. & O'BYRNE, K. J. 2003. Carbonic anhydrase IX expression, a novel surrogate marker of tumor hypoxia, is associated with a poor prognosis in non-small-cell lung cancer. *J Clin Oncol,* 21**,** 473-82.

SZPADERSKA, A. M. & FRANKFATER, A. 2001. An intracellular form of cathepsin B contributes to invasiveness in cancer. *Cancer Res,* 61**,** 3493-500.

TAKEYABU, K., BETSUYAKU, T., NISHIMURA, M., YOSHIOKA, A., TANINO, M., MIYAMOTO, K. & KAWAKAMI, Y. 1998. Cysteine proteinases and cystatin C in bronchoalveolar lavage fluid from subjects with subclinical emphysema. *Eur Respir J,* 12**,** 1033-9.

TAN, G.-J., PENG, Z.-K., LU, J.-P. & TANG, F.-Q. 2013. Cathepsins mediate tumor metastasis. *World Journal of Biological Chemistry,* 4**,** 91-101.

TANG, H., HORNSTEIN, E., STOLOVICH, M., LEVY, G., LIVINGSTONE, M., TEMPLETON, D., AVRUCH, J. & MEYUHAS, O. 2001. Amino acid-induced translation of TOP mRNAs is fully dependent on phosphatidylinositol 3-kinase-mediated signaling, is partially inhibited by rapamycin, and is independent of S6K1 and rpS6 phosphorylation. *Mol Cell Biol,* 21**,** 8671-83.

TAVEIRA-DASILVA, A. M., HEDIN, C., STYLIANOU, M. P., TRAVIS, W. D., MATSUI, K., FERRANS, V. J. & MOSS, J. 2001. Reversible airflow obstruction, proliferation of abnormal smooth muscle cells, and impairment of gas exchange as predictors of outcome in lymphangioleiomyomatosis. *American Journal of Respiratory and Critical Care Medicine,* 164**,** 1072-1076.

TAVEIRA-DASILVA, A. M., STYLIANOU, M. P., HEDIN, C. J., HATHAWAY, A. & MOSS, J. 2004. Decline in lung function in patients with lymphangioleiomyomatosis treated with or without progesterone. *Chest,* 126**,** 1867-1874.

TAYLOR, J. R., RYU, J., COLBY, T. V. & RAFFIN, T. A. 1990. Lymphangioleiomyomatosis. Clinical course in 32 patients. *N Engl J Med,* 323**,** 1254-60.

TEE, A. R., FINGAR, D. C., MANNING, B. D., KWIATKOWSKI, D. J., CANTLEY, L. C. & BLENIS, J. 2002. Tuberous sclerosis complex-1 and -2 gene products function together to inhibit mammalian target of rapamycin (mTOR)-mediated downstream signaling. *Proc Natl Acad Sci U S A,* 99**,** 13571-6.

TEE, A. R., MANNING, B. D., ROUX, P. P., CANTLEY, L. C. & BLENIS, J. 2003. Tuberous sclerosis complex gene products, Tuberin and Hamartin, control mTOR signaling by acting as a GTPase-activating protein complex toward Rheb. *Curr Biol,* 13**,** 1259-68.

TENG, F., TIAN, W.-Y., WANG, Y.-M., ZHANG, Y.-F., GUO, F., ZHAO, J., GAO, C. & XUE, F.-X. 2016. Cancer-associated fibroblasts promote the progression of endometrial cancer via the SDF-1/CXCR4 axis. *Journal of Hematology & Oncology,* 9**,** 8.

THEDIECK, K., POLAK, P., KIM, M. L., MOLLE, K. D., COHEN, A., JENO, P., ARRIEUMERLOU, C. & HALL, M. N. 2007. PRAS40 and PRR5-like protein are new mTOR interactors that regulate apoptosis. *Plos One,* 2**,** e1217.

THERMOFISHERSCIENTIFIC. 2008. *alamarBlue Cell Viability Assay Protocol* [Online]. Available: https://www.thermofisher.com/uk/en/home/references/protocols/cell-and-tissue-analysis/cell-profilteration-assay-protocols/cell-viability-with-alamarblue.html.

TOMANKOVA, T., KRIEGOVA, E. & LIU, M. 2015. Chemokine receptors and their therapeutic opportunities in diseased lung: far beyond leukocyte trafficking. *Am J Physiol Lung Cell Mol Physiol,* 308**,** L603-18.

TOSCHI, A., LEE, E., XU, L., GARCIA, A., GADIR, N. & FOSTER, D. A. 2009. Regulation of mTORC1 and mTORC2 complex assembly by phosphatidic acid: competition with rapamycin. *Mol Cell Biol,* 29**,** 1411-20.

TROEN, B. R. 2006. The regulation of cathepsin K gene expression. *Ann N Y Acad Sci,* 1068**,** 165-72.

TURAN, S. 2014. Current research on pycnodysostosis. *Intractable & Rare Diseases Research,* 3**,** 91-93.

UHLEN, M., BJORLING, E., AGATON, C., SZIGYARTO, C. A., AMINI, B., ANDERSEN, E., ANDERSSON, A. C., ANGELIDOU, P., ASPLUND, A., ASPLUND, C., BERGLUND, L., BERGSTROM, K., BRUMER, H., CERJAN, D., EKSTROM, M., ELOBEID, A., ERIKSSON, C., FAGERBERG, L., FALK, R., FALL, J., FORSBERG, M., BJORKLUND, M. G., GUMBEL, K., HALIMI, A., HALLIN, I., HAMSTEN, C., HANSSON, M., HEDHAMMAR, M., HERCULES, G., KAMPF, C., LARSSON, K., LINDSKOG, M., LODEWYCKX, W., LUND, J., LUNDEBERG, J., MAGNUSSON, K., MALM, E., NILSSON, P., ODLING, J., OKSVOLD, P., OLSSON, I., OSTER, E., OTTOSSON, J., PAAVILAINEN, L., PERSSON, A., RIMINI, R., ROCKBERG, J., RUNESON, M., SIVERTSSON, A., SKOLLERMO, A., STEEN, J., STENVALL, M., STERKY, F., STROMBERG, S., SUNDBERG, M., TEGEL, H., TOURLE, S., WAHLUND, E., WALDEN, A., WAN, J., WERNERUS, H., WESTBERG, J., WESTER, K., WRETHAGEN, U., XU, L. L., HOBER, S. & PONTEN, F. 2005. A human protein atlas for normal and cancer tissues based on antibody proteomics. *Mol Cell Proteomics,* 4**,** 1920-32.

URBAN, T., LAZOR, R., LACRONIQUE, J., MURRIS, M., LABRUNE, S., VALEYRE, D. & CORDIER, J. F. 1999. Pulmonary

lymphangioleiomyomatosis. A study of 69 patients. Groupe d'Etudes et de Recherche sur les Maladies "Orphelines" Pulmonaires (GERM"O"P). *Medicine (Baltimore),* 78**,** 321-37.

VAKONAKIS, I. & CAMPBELL, I. D. 2007. Extracellular matrix: from atomic resolution to ultrastructure. *Curr Opin Cell Biol,* 19**,** 578-83.

VALENCIA, J. C., PACHECO-RODRIGUEZ, G., CARMONA, A. K., XAVIER, J., BRUNEVAL, P., RIEMENSCHNEIDER, W. K., IKEDA, Y., YU, Z. X., FERRANS, V. J. & MOSS, J. 2006. Tissue-specific renin-angiotensin system in pulmonary lymphangioleiomyomatosis. *Am J Respir Cell Mol Biol,* 35**,** 40-7.

VAN DEN BRULE, S., MISSON, P., BUHLING, F., LISON, D. & HUAUX, F. 2005. Overexpression of cathepsin K during silica-induced lung fibrosis and control by TGF-beta. *Respir Res,* 6**,** 84.

VAN MEERLOO, J., KASPERS, G. J. & CLOOS, J. 2011. Cell sensitivity assays: the MTT assay. *Methods Mol Biol,* 731**,** 237-45.

VAN NOORDEN, C. J., BOONACKER, E., BISSELL, E. R., MEIJER, A. J., VAN MARLE, J. & SMITH, R. E. 1997. Ala-Pro-cresyl violet, a synthetic fluorogenic substrate for the analysis of kinetic parameters of dipeptidyl peptidase IV (CD26) in individual living rat hepatocytes. *Anal Biochem,* 252**,** 71-7.

VAN NOORDEN, C. J. F. & EVERTS, V. 1991. Selective inhibition of cysteine proteinases by Z-Phe-AlaCH2F suppresses digestion of collagen by fibroblasts and osteoclasts. *Biochemical and Biophysical Research Communications,* 178**,** 178-184.

VAN SLEGTENHORST, M., DE HOOGT, R., HERMANS, C., NELLIST, M., JANSSEN, B., VERHOEF, S., LINDHOUT, D., VAN DEN OUWELAND, A., HALLEY, D., YOUNG, J., BURLEY, M., JEREMIAH, S., WOODWARD, K., NAHMIAS, J., FOX, M., EKONG, R., OSBORNE, J., WOLFE, J., POVEY, S., SNELL, R. G., CHEADLE, J. P., JONES, A. C., TACHATAKI, M., RAVINE, D., SAMPSON, J. R., REEVE, M. P., RICHARDSON, P., WILMER, F., MUNRO, C., HAWKINS, T. L., SEPP, T., ALI, J. B., WARD, S., GREEN, A. J., YATES, J. R., KWIATKOWSKA, J., HENSKE, E. P., SHORT, M. P., HAINES, J. H., JOZWIAK, S. & KWIATKOWSKI, D. J. 1997. Identification of the tuberous sclerosis gene TSC1 on chromosome 9q34. *Science,* 277**,** 805-8.

VAN SLEGTENHORST, M., NELLIST, M., NAGELKERKEN, B., CHEADLE, J., SNELL, R., VAN DEN OUWELAND, A., REUSER, A., SAMPSON, J., HALLEY, D. & VAN DER SLUIJS, P. 1998. Interaction between hamartin and tuberin, the TSC1 and TSC2 gene products. *Human Molecular Genetics,* 7**,** 1053-1057.

VENKATESH, H. S., CHAUMEIL, M. M., WARD, C. S., HAAS-KOGAN, D. A., JAMES, C. D. & RONEN, S. M. 2012. Reduced phosphocholine and hyperpolarized lactate provide magnetic resonance biomarkers of PI3K/Akt/mTOR inhibition in glioblastoma. *Neuro Oncol,* 14**,** 315-25.

VERBOVSEK, U., VAN NOORDEN, C. J. & LAH, T. T. 2015. Complexity of cancer protease biology: Cathepsin K expression and function in cancer progression. *Semin Cancer Biol,* 35**,** 71-84.

VINCENTI, M. P., WHITE, L. A., SCHROEN, D. J., BENBOW, U. & BRINCKERHOFF, C. E. 1996. Regulating expression of the gene for matrix metalloproteinase-1 (collagenase): mechanisms that control enzyme activity, transcription, and mRNA stability. *Crit Rev Eukaryot Gene Expr,* 6**,** 391-411.

VINCI, M., GOWAN, S., BOXALL, F., PATTERSON, L., ZIMMERMANN, M., COURT, W., LOMAS, C., MENDIOLA, M., HARDISSON, D. & ECCLES, S. A. 2012. Advances in establishment and analysis of three-dimensional tumor spheroid-based functional assays for target validation and drug evaluation. *BMC Biology,* 10**,** 29.

VON STOSSEL, E. 1937. Uber muskulare Cirrhose der Lunge (Muscular cirrhosis of the lung). *Beitr Klin Tuberk,* 90**,** 432–442.

WAHEDNA, I., COOPER, S., WILLIAMS, J., PATERSON, I.C., BRITTON, J.R., TATTERSFIELD, A.E. 1994. Relation of pulmonary lymphangio-leiomyomatosis to use of the oral contraceptive pill and fertility in the UK: a national case control study. *Thorax,* 49**,** 910-914.

WALKER, C., GOLDSWORTHY, T. L., WOLF, D. C. & EVERITT, J. 1992. Predisposition to renal cell carcinoma due to alteration of a cancer susceptibility gene. *Science,* 255**,** 1693-5.

WALKER, C. L., CESEN-CUMMINGS, K., HOULE, C., BAIRD, D., BARRETT, J. C. & DAVIS, B. 2001. Protective effect of pregnancy for development of uterine leiomyoma. *Carcinogenesis,* 22**,** 2049-52.

WALKER, C. L., HUNTER, D. & EVERITT, J. I. 2003. Uterine leiomyoma in the Eker rat: a unique model for important diseases of women. *Genes Chromosomes Cancer,* 38**,** 349-56.

WANG, B. T., DUCKER, G. S., BARCZAK, A. J., BARBEAU, R., ERLE, D. J. & SHOKAT, K. M. 2011. The mammalian target of rapamycin regulates cholesterol biosynthetic gene expression and exhibits a rapamycin-resistant transcriptional profile. *Proc Natl Acad Sci U S A,* 108**,** 15201-6.

WANG, L., HARRIS, T. E., ROTH, R. A. & LAWRENCE, J. C., JR. 2007. PRAS40 regulates mTORC1 kinase activity by functioning as a direct inhibitor of substrate binding. *Journal of Biological Chemistry,* 282**,** 20036-44.

WANG, X., LI, W., WILLIAMS, M., TERADA, N., ALESSI, D. R. & PROUD, C. G. 2001. Regulation of elongation factor 2 kinase by p90(RSK1) and p70 S6 kinase. *EMBO J,* 20**,** 4370-9.

WANG, Z., ZHENG, T., ZHU, Z., HOMER, R. J., RIESE, R. J., CHAPMAN, H. A., JR., SHAPIRO, S. D. & ELIAS, J. A. 2000. Interferon gamma induction of pulmonary emphysema in the adult murine lung. *J Exp Med,* 192**,** 1587-600.

WARBURG, O. 1956. On the origin of cancer cells. *Science,* 123**,** 309-14.

WATZ*, H., ENGELS*, K., LOESCHKE, S., AMTHOR, M., KIRSTEN, D., MAGNUSSEN, H. & MAGNUSSEN, H. 2007. Lymphangioleiomyomatosis—presence of receptor tyrosine kinases and the angiogenesis factor VEGF-A as potential therapeutic targets. *Thorax,* 62**,** 559-559.

WEICHHART, T., COSTANTINO, G., POGLITSCH, M., ROSNER, M., ZEYDA, M., STUHLMEIER, K. M., KOLBE, T., STULNIG, T. M., HORL, W. H.,

HENGSTSCHLAGER, M., MULLER, M. & SAEMANN, M. D. 2008. The TSC-mTOR signaling pathway regulates the innate inflammatory response. *Immunity,* 29**,** 565-77.

WEIGELT, B., GHAJAR, C. M. & BISSELL, M. J. 2014. The need for complex 3D culture models to unravel novel pathways and identify accurate biomarkers in breast cancer. *Adv Drug Deliv Rev,* 69-70**,** 42-51.

WEISWALD, L. B., BELLET, D. & DANGLES-MARIE, V. 2015. Spherical cancer models in tumor biology. *Neoplasia,* 17**,** 1-15.

WEISWALD, L. B., RICHON, S., MASSONNET, G., GUINEBRETIÈRE, J. M., VACHER, S., LAURENDEAU, I., COTTU, P., MARANGONI, E., NEMATI, F., VALIDIRE, P., BELLET, D., BIÈCHE, I. & DANGLES-MARIE, V. 2013. A short-term colorectal cancer sphere culture as a relevant tool for human cancer biology investigation. *British Journal of Cancer,* 108**,** 1720-1731.

WEISWALD, L. B., RICHON, S., VALIDIRE, P., BRIFFOD, M., LAI-KUEN, R., CORDELIERES, F. P., BERTRAND, F., DARGERE, D., MASSONNET, G., MARANGONI, E., GAYET, B., POCARD, M., BIECHE, I., POUPON, M. F., BELLET, D. & DANGLES-MARIE, V. 2009. Newly characterised ex vivo colospheres as a three-dimensional colon cancer cell model of tumour aggressiveness. *Br J Cancer,* 101**,** 473-482.

WERLE, B., SCHANZENBACHER, U., LAH, T. T., EBERT, E., JULKE, B., EBERT, W., FIEHN, W., KAYSER, K., SPIESS, E., ABRAHAMSON, M. & KOS, J. 2006. Cystatins in non-small cell lung cancer: tissue levels, localization and relation to prognosis. *Oncol Rep,* 16**,** 647-55.

WHITE, E. S. 2015. Lung Extracellular Matrix and Fibroblast Function. *Annals of the American Thoracic Society,* 12**,** S30-S33.

WHITE, J. R., LEE, J. M., YOUNG, P. R., HERTZBERG, R. P., JUREWICZ, A. J., CHAIKIN, M. A., WIDDOWSON, K., FOLEY, J. J., MARTIN, L. D., GRISWOLD, D. E. & SARAU, H. M. 1998. Identification of a Potent, Selective Non-peptide CXCR2 Antagonist That Inhibits Interleukin-8-induced Neutrophil Migration. *Journal of Biological Chemistry,* 273**,** 10095-10098.

WICKS, J., HAITCHI, H. M., HOLGATE, S. T., DAVIES, D. E. & POWELL, R. M. 2006. Enhanced upregulation of smooth muscle related transcripts by TGF beta2 in asthmatic (myo) fibroblasts. *Thorax,* 61**,** 313-9.

WIEDERANDERS, B., KAULMANN, G. & SCHILLING, K. 2003. Functions of propeptide parts in cysteine proteases. *Curr Protein Pept Sci,* 4**,** 309-26.

WILLSTÄTTER, R. & BAMANN, E. 1929. Über die Proteasen der Magenschleimhaut: Erste Abhandlung über die Enzyme der Leukocyten. *Hoppe-Seyler's Zeitschrift fur Physiologische Chemie,* 180**,** 127-143.

WILSON, C., IDZIASZCZYK, S., PARRY, L., GUY, C., GRIFFITHS, D. F., LAZDA, E., BAYNE, R. A., SMITH, A. J., SAMPSON, J. R. & CHEADLE, J. P. 2005. A mouse model of tuberous sclerosis 1 showing background specific early post-natal mortality and metastatic renal cell carcinoma. *Human Molecular Genetics,* 14**,** 1839-50.

WULLSCHLEGER, S., LOEWITH, R. & HALL, M. N. 2006. TOR signaling in growth and metabolism. *Cell,* 124**,** 471-84.
XU, K.-P., LI, X.-F. & YU, F.-S. X. 2000. Corneal Organ Culture Model for Assessing Epithelial Responses to Surfactants. *Toxicological Sciences,* 58**,** 306-314.
XU, L. L., WARREN, M. K., ROSE, W. L., GONG, W. & WANG, J. M. 1996. Human recombinant monocyte chemotactic protein and other C-C chemokines bind and induce directional migration of dendritic cells in vitro. *J Leukoc Biol,* 60**,** 365-71.
YASUDA, H., SHIMA, N., NAKAGAWA, N., YAMAGUCHI, K., KINOSAKI, M., MOCHIZUKI, S., TOMOYASU, A., YANO, K., GOTO, M., MURAKAMI, A., TSUDA, E., MORINAGA, T., HIGASHIO, K., UDAGAWA, N., TAKAHASHI, N. & SUDA, T. 1998. Osteoclast differentiation factor is a ligand for osteoprotegerin/osteoclastogenesis-inhibitory factor and is identical to TRANCE/RANKL. *Proc Natl Acad Sci U S A,* 95**,** 3597-602.
YATES, J. R. 2006. Tuberous sclerosis. *Eur J Hum Genet,* 14**,** 1065-73.
YE, Y., TIAN, H., LANGE, A. R., YEARSLEY, K., ROBERTSON, F. M. & BARSKY, S. H. 2013. The genesis and unique properties of the lymphovascular tumor embolus are because of calpain-regulated proteolysis of E-cadherin. *Oncogene,* 32**,** 1702-1713.
YEUNG, R. S., XIAO, G. H., EVERITT, J. I., JIN, F. & WALKER, C. L. 1995. Allelic loss at the tuberous sclerosis 2 locus in spontaneous tumors in the Eker rat. *Mol Carcinog,* 14**,** 28-36.
YEUNG, R. S., XIAO, G. H., JIN, F., LEE, W. C., TESTA, J. R. & KNUDSON, A. G. 1994. Predisposition to renal carcinoma in the Eker rat is determined by germ-line mutation of the tuberous sclerosis 2 (TSC2) gene. *Proc Natl Acad Sci U S A,* 91**,** 11413-6.
YIN, M., SOIKKELI, J., JAHKOLA, T., VIROLAINEN, S., SAKSELA, O. & HÖLTTÄ, E. 2012. TGF-β Signaling, Activated Stromal Fibroblasts, and Cysteine Cathepsins B and L Drive the Invasive Growth of Human Melanoma Cells. *The American Journal of Pathology,* 181**,** 2202-2216.
YIP, C. K., MURATA, K., WALZ, T., SABATINI, D. M. & KANG, S. A. 2010. Structure of the human mTOR complex I and its implications for rapamycin inhibition. *Mol Cell,* 38**,** 768-74.
YOUNG, L., LEE, H. S., INOUE, Y., MOSS, J., SINGER, L. G., STRANGE, C., NAKATA, K., BARKER, A. F., CHAPMAN, J. T., BRANTLY, M. L., STOCKS, J. M., BROWN, K. K., LYNCH, J. P., 3RD, GOLDBERG, H. J., DOWNEY, G. P., SWIGRIS, J. J., TAVEIRA-DASILVA, A. M., KRISCHER, J. P., TRAPNELL, B. C. & MCCORMACK, F. X. 2013a. Serum VEGF-D a concentration as a biomarker of lymphangioleiomyomatosis severity and treatment response: a prospective analysis of the Multicenter International Lymphangioleiomyomatosis Efficacy of Sirolimus (MILES) trial. *Lancet Respir Med,* 1**,** 445-52.
YOUNG, L. R., LEE, H.-S., INOUE, Y., MOSS, J., SINGER, L. G., STRANGE, C., NAKATA, K., BARKER, A. F., CHAPMAN, J. T., BRANTLY, M. L., STOCKS, J. M., BROWN, K. K., LYNCH, J. P., GOLDBERG, H. J.,

DOWNEY, G. P., SWIGRIS, J. J., TAVEIRA-DASILVA, A. M., KRISCHER, J. P., TRAPNELL, B. C. & MCCORMACK, F. X. 2013b. Serum VEGF-D concentration as a biomarker of lymphangioleiomyomatosis severity and treatment response: a prospective analysis of the Multicenter International Lymphangioleiomyomatosis Efficacy of Sirolimus (MILES) trial. *The lancet. Respiratory medicine,* 1**,** 445-452.

YOUNG, S. R., SAAR, M., SANTOS, J., NGUYEN, H. M., VESSELLA, R. L. & PEEHL, D. M. 2013c. Establishment and serial passage of cell cultures derived from LuCaP xenografts. *Prostate,* 73**,** 1251-62.

YU, J., ASTRINIDIS, A. & HENSKE, E. P. 2001. Chromosome 16 loss of heterozygosity in tuberous sclerosis and sporadic lymphangiomyomatosis. *Am J Respir Crit Care Med,* 164**,** 1537-40.

YU, J., ASTRINIDIS, A., HOWARD, S. & HENSKE, E. P. 2004. Estradiol and tamoxifen stimulate LAM-associated angiomyolipoma cell growth and activate both genomic and nongenomic signaling pathways. *Am J Physiol Lung Cell Mol Physiol,* 286**,** L694-700.

YU, J. & HENSKE, E. P. 2010. mTOR activation, lymphangiogenesis, and estrogen-mediated cell survival: the "perfect storm" of pro-metastatic factors in LAM pathogenesis. *Lymphat Res Biol,* 8**,** 43-9.

YU, J. J., ROBB, V. A., MORRISON, T. A., ARIAZI, E. A., KARBOWNICZEK, M., ASTRINIDIS, A., WANG, C., HERNANDEZ-CUEBAS, L., SEEHOLZER, L. F., NICOLAS, E., HENSLEY, H., JORDAN, V. C., WALKER, C. L. & HENSKE, E. P. 2009. Estrogen promotes the survival and pulmonary metastasis of tuberin-null cells. *Proceedings of the National Academy of Sciences of the United States of America,* 106**,** 2635-2640.

YUEN, T., WURMBACH, E., PFEFFER, R. L., EBERSOLE, B. J. & SEALFON, S. C. 2002. Accuracy and calibration of commercial oligonucleotide and custom cDNA microarrays. *Nucleic Acids Res,* 30**,** e48.

ZEIDAN, A. A., RÅDSTRÖM, P. & VAN NIEL, E. W. 2010. Stable coexistence of two Caldicellulosiruptor species in a de novo constructed hydrogen-producing co-culture. *Microbial Cell Factories,* 9**,** 102.

ZEISBERG, M., STRUTZ, F. & MULLER, G. A. 2000. Role of fibroblast activation in inducing interstitial fibrosis. *J Nephrol,* 13 Suppl 3**,** S111-20.

ZENG, Z., SARBASSOV DOS, D., SAMUDIO, I. J., YEE, K. W., MUNSELL, M. F., ELLEN JACKSON, C., GILES, F. J., SABATINI, D. M., ANDREEFF, M. & KONOPLEVA, M. 2007. Rapamycin derivatives reduce mTORC2 signaling and inhibit AKT activation in AML. *Blood,* 109**,** 3509-12.

ZHANG, H., CICCHETTI, G., ONDA, H., KOON, H. B., ASRICAN, K., BAJRASZEWSKI, N., VAZQUEZ, F., CARPENTER, C. L. & KWIATKOWSKI, D. J. 2003. Loss of Tsc1/Tsc2 activates mTOR and disrupts PI3K-Akt signaling through downregulation of PDGFR. *J Clin Invest,* 112**,** 1223-33.

ZHANG, H. H., HUANG, J., DUVEL, K., BOBACK, B., WU, S., SQUILLACE, R. M., WU, C. L. & MANNING, B. D. 2009. Insulin stimulates adipogenesis through the Akt-TSC2-mTORC1 pathway. *Plos One,* 4**,** e6189.

ZHANG, J.-M. & AN, J. 2007. Cytokines, Inflammation and Pain. *International anesthesiology clinics,* 45**,** 27-37.
ZHAO, Q., JIA, Y. & XIAO, Y. 2009a. Cathepsin K: a therapeutic target for bone diseases. *Biochem Biophys Res Commun,* 380**,** 721-3.
ZHAO, Q., JIA, Y. & XIAO, Y. 2009b. Cathepsin K: A therapeutic target for bone diseases. *Biochemical and Biophysical Research Communications,* 380**,** 721-723.
ZHE, X. & SCHUGER, L. 2004. Combined smooth muscle and melanocytic differentiation in lymphangioleiomyomatosis. *Journal of Histochemistry & Cytochemistry,* 52**,** 1537-42.
ZHE, X., YANG, Y., JAKKARAJU, S. & SCHUGER, L. 2003. Tissue inhibitor of metalloproteinase-3 downregulation in lymphangioleiomyomatosis: potential consequence of abnormal serum response factor expression. *Am J Respir Cell Mol Biol,* 28**,** 504-11.
ZHE, X., YANG, Y. & SCHUGER, L. 2005. Imbalanced plasminogen system in lymphangioleiomyomatosis: potential role of serum response factor. *Am J Respir Cell Mol Biol,* 32**,** 28-34.
ZHENG, T., ZHU, Z., WANG, Z., HOMER, R. J., MA, B., RIESE, R. J., JR., CHAPMAN, H. A., JR., SHAPIRO, S. D. & ELIAS, J. A. 2000. Inducible targeting of IL-13 to the adult lung causes matrix metalloproteinase- and cathepsin-dependent emphysema. *J Clin Invest,* 106**,** 1081-93.
ZHONG, H., CHILES, K., FELDSER, D., LAUGHNER, E., HANRAHAN, C., GEORGESCU, M. M., SIMONS, J. W. & SEMENZA, G. L. 2000. Modulation of hypoxia-inducible factor 1alpha expression by the epidermal growth factor/phosphatidylinositol 3-kinase/PTEN/AKT/FRAP pathway in human prostate cancer cells: implications for tumor angiogenesis and therapeutics. *Cancer Research,* 60**,** 1541-5.